THROUGH LIFE RELIABILITY OF A BULK CARRIER

By

Ioannis Tsarouchas, M.Sc.

Thesis submitted for the Degree of Doctor of Philosophy

Department of Naval Architecture and Ocean Engineering

University Of Glasgow

August 2001

ProQuest LLC.
789 East Eisenhower Parkway
P.O. Box 1346
Ann Arbor, MI 48106 – 1346

ACKNOWLEDGMENTS

The author is greatly obliged to his supervisor and head of the department, professor Nigel Barltrop for his idea to conduct this work, and for his valuable assistance and discussions during the time of this thesis, without which it would not have been possible to complete this study.

Many thanks also to professor P. K. Das for his helpful guidance and provision of excellent sources of reference.

The author also greatly appreciates the help and guidance of professor Vasilios Papazoglou, department of Naval Architecture and Marine Engineering, National Technical University of Athens, and for letting me work under his supervision and providing the necessary software and equipment.

Special thanks to Maureen and Thelma, for their tolerance and patience that showed to my constant trouble. I am also obliged to Mr. David Percival, for his valuable assistance in developing the code and for his software support.

I cannot forget Michael, the Janitor of James Watt Building, for all the friendly discussions we had and giving a different perspective to my typical stays in the office.

I need also to thank the many friends I had over my long stay in Glasgow, for the good time we had in and out of the office. Special thanks, to Iason Lambos and for all the great time we had, and by providing me with valuable information; to William Alifgragis for the nice company one summer and his friendship ever after; to Trym Tveitnes (kamaki) for the excellent time throughout the PhD years and his real friendship. Also to Dimitris Karathanos, for his friendship and expertise in technical matters regarding ship structures.

I am deeply and truly grateful to my family for their support by any means, my father Kostas and mother Liana, my two sisters Sophia and Gina , grand father Giorgos and grand mother Sophia. Also to my cousin Giorgos for the many long telephone conversations and by keeping my morale high.

TABLE OF CONTENTS

- List of Symbols -

a	:	Crack size, Crack depth
A	:	Weibull distribution scale parameter, Area
B	:	Weibull distribution shape parameter, Breadth
B_{cor}	:	Corrosion rate factor
C	:	Crack growth constant
E	:	Event, Modulus of elasticity
F	:	Plastic modulus, Traction forces
$F_x()$	:	Cumulative distribution function
$f_x()$	:	Probability density function
$f_{xx}()$	:	Joint probability density function
g	:	Acceleration of gravity
G	:	Elastic strain energy release rate, Shear modulus
$G()$	:	Limit state function, Threshold factor
H	:	Parameter similar to Y for elastic stress intensity factor
$h()$	:	Sampling density
H_s	:	Significant wave height
I	:	Second moment of area
$I[]$	:	Indicator
J_{mat}	:	Critical strain energy release rate for non-linear materials
K	:	Stress concentration factor, Stress intensity factor
K_c	:	Fracture toughness
K_I	:	Stress intensity factor
K_{mat}	:	Fracture toughness
K_r	:	Fracture ratio

L	:	Load, Length
m	:	Crack growth exponent, Slope of S-N curve
m_o, m_2, m_4	:	Spectral moments
N	:	Number of samples, Number of stress cycles
P()	:	Probability function
P_f	:	Probability of failure
POD	:	Probability of detection
q	:	Shear flow
R	:	Resistance, Stress ratio
r^*	:	Plastic zone radius
r_p	:	Plastic zone radius
S	:	Stress range
S()	:	Sea spectrum
SF	:	Safety factor
S_r	:	Plastic ratio
t	:	Thickness, Time
T	:	Time
T_z	:	Mean wave period, Mean zero crossing period
U	:	Strain energy
W	:	Work done, Strain energy
Y	:	Geometry factor, Vertical position
z	:	Depth, Thickness
α	:	Parameter in extreme Type I distribution
β	:	Reliability index, Parameter in extreme Type I distribution
γ	:	Acceleration, Fraction of time
ΔK	:	Stress intensity factor range

ΔK_{th}	:	Stress intensity factor range threshold
δ_{mat}	:	CTOD
$\Delta\sigma$	:	Stress range
ε	:	Error, Bandwidth parameter
θ	:	Wave heading, Angle
λ	:	Non-dimensional length of tensile region
μ	:	Proportion of time
ν	:	Poisson's ratio
ν_o	:	Mean zero crossing rate
ξ	:	Non-dimensional length
Π	:	Total energy
ρ	:	Density, Plasticity correction factor, Plastic zone length
σ	:	Standard deviation, Stress
σ_{eff}	:	effective stress range
σ_{eq}	:	Equivalent stress range
σ_f	:	Flow strength
σ_n	:	Net stress
σ_t	:	Tensile strength
σ_y	:	Yield stress
τ	:	Shear stress
Φ	:	Standard normal probability function
ω	:	Wave frequency
ω_e	:	Frequency of encounter

SUMMARY

A methodology for a through life structural assessment of a ship is proposed and applied to a bulk carrier. The objective of the analysis is to calculate the probability of failure of the corroding vessel, having many initial defects which grow through fatigue.

The assessment requires bringing together many different analyses. Loading is a key input in the analysis. There are two important loads that need to be considered: *1)* Fatigue loading, which causes cracks to grow. A fatigue analysis provides useful information on fatigue loading (stress ranges) on many different structural details found in a bulk carrier. The operational profile of the vessel is specified together with the loading conditions and the service speed. Modeling the wave environment is done using a sea scatter diagram. From the fatigue analysis a selection of details to consider for the analysis is possible (i.e. details with low fatigue lives). *2)* Extreme loading in conjunction with cracks causes fracture. Short-term statistical analysis on wave environment is performed to estimate extreme loads. Other loads are the still water loading and self-equilibrating stresses of which welding residual stresses have been included.

Fracture mechanics are used to perform the crack extension calculations. A simplified model based on Paris' law is used, modified to include threshold and corrosion effects. Suitable crack growth constants are selected that simulate crack extension in a corrosive environment with a reasonable accuracy.

Another fundamental part of the analysis is to establish a fracture criterion. A suitable criterion is based on a failure assessment diagram described in PD 6493. This accounts for the plastic zone which develops in front of the crack tip, in addition to the simplified fracture criterion based on linear elastic fracture mechanics. By using this method, the need to use non-linear analysis (*J-Integral* estimation) is avoided.

A bulk carrier has many possible structural details where initial welding defects can develop into cracks and propagate. Each crack will grow at a different rate. Crack growth parameters are used taken from published references. Information on the

stress intensity factors, for typical cracked details is obtained either from published references or by the use of FEA.

Most parameters that are modelled as random variables are specified and their uncertainty is described by a probability distribution defined by a mean value and a coefficient of variation and type of distribution.

Reliability analysis is performed using the Monte Carlo simulation method. This was selected because it is the most flexible method to perform complicated time-dependent reliability analysis (because of the crack propagation) and combine all necessary parts into one computer program. Because of the large number of locations to consider, (e.g. for a realistic case of a ship structure there are thousands of cracks present, and each crack must be treated separately in the simulation), there are limitations on the use of the simulation method (it requires a lot of computer memory and computational time). Because of these restrictions, the simulation is limited to approximately 100 cracks.

A real ship structure requires many thousands of cracks to be considered so a simplified methodology is established which uses results (load and strength distributions) from the simulation method (with a limited number of cracks), and is capable of evaluating the failure probability of the whole ship. For the purpose of demonstrating the methodology, simplified assumptions are made for the input parameters. Cracks are distributed over the entire vessel, subjected to different loading, having different material properties (for crack growth calculations). Loading variation along the structure is based on simplified assumptions. Results of the method are compared with the simulation (for a limited number of cracks) and with some actual statistical data available from various sources e.g. classification societies or other organizations related to ships.

Although the absolute values from the analysis may not be accurate (since simplified assumptions for the input data have been made), however the trend of the results are of interest and in reality the results are the best estimate available. By performing several analyses it is possible to study the effects of corrosion, inspection, sea route and loading conditions on the reliability of the vessel. At the design stage requirements and methods for inspection can be balanced against the provision of

additional steel, better details, better steel toughness grades. When more realistic data is available such a methodology can be used to schedule optimum inspection intervals, by maintaining the reliability levels to a specified target value. This will result in a more efficient, safe and economic way of vessel operation.

It is important for the application of the methodology to have a database of input parameters that can be used by consultants, ship owners, or classification societies when undertaking this type of analysis. This includes data on crack growth parameters, fracture toughness, corrosion rates, initial crack sizes and distribution of cracks.

Assumptions made on the physical models can also be improved, such as loading estimation (fatigue and extreme), crack propagation process, accuracy of the reliability method to refine the simplified method.

CHAPTER 1

THE PROBLEM OF CRACKING IN SHIP STRUCTURES AND WAYS OF CONTROL

1.1 Fracturing of Ship Structures: A Consistent and Persistent Problem

Cargo vessels are generally constructed by steel using welds to join the various parts together, a technique used over, at least, the last 40 years. Although there have been steel quality improvements to resist fracture, advances in welding techniques to minimise welding imperfections and more strict quality controls by shipyards and classification societies, defects cannot be eliminated completely from ship structures. Considering the enormous amount of welded connections in a ship structure and the physical size of these structures it is highly likely that defects will be present.

It would be economically unacceptable to design and build a crack free ship structure. It is therefore common practise to try and monitor the structural performance of the vessel with respect to fatigue and corrosion and minimise the risk of failure. Classification societies impose inspections and if necessary repairs, to ensure the structural safety of the vessels. However, it would be economically more attractive to schedule inspections and repairs based on the risk of failure at any time of individual ships. For example, for a low risk of failure the inspection can be postponed for a later time (i.e. save time and money), whereas for a ship with a high risk of failure the action would be immediate inspection (and possibly save the ship).

It is impossible to determine the exact risk of failure of an actual ship structure because of its complex construction, the loading to which is subjected, the uncertain state of corrosion and because of the many ways or modes of failure. Apart from fracture failure, other important modes of failure for a ship structure are buckling failure and plastic collapse failure. Each failure mode is associated with a different risk of failure. In many cases more than one failure mode can cause a failure or a combination of them. Which mode of failure is most important depends on the use of the vessel i.e. its intended functions, operational environment and loading conditions.

1.1.1 Development of an Approach to Determine the Risk of Failure

Over the last twenty years a new approach in design appeared, to assist making predictions for the risk or probability of failure of an engineering structure or equipment. This method is called 'Structural Reliability'. The principle use of the method is to determine an estimate for the failure probability of an engineering system under a particular failure mode. An estimate of the reliability of the engineering structure or system is then possible. This value is very important when considering the cost-profit relationship of the structure and can certainly decide whether the structure is economically efficient to operate or not.

The first attempts to adopt structural reliability theory in the decision making for inspection planning were made for fixed offshore platforms, e.g. Wirsching *et al* (1987). Because of the welds between the tubular members, fatigue cracks were a possible risk of failure, considering the extreme environmental conditions of the Northern North Atlantic which they were placed. Especially after the catastrophic failure of an accommodation platform, the Alexander Kielland semi-submersible, (Moan 1985), because of a single fatigue crack, efforts were made to design against fatigue and fracture failures as well as against extreme loading.

Hence a necessity arose to predict the risk of failure at any time so that inspections could be planned accordingly. Because the inspection of an offshore platform is a costly operation, some identification of when this was necessary could prove very important for economically maintaining the safety of the structure.

Models were then developed to predict the failure probability with respect to fatigue and fracture. There are numerous papers written on this subject. The first models considered only a single crack and fatigue as the failure mode e.g. Wirsching (1979 and 1987), Huang (1989), Zhao (1989), Connolly *et al* (1993). Shetty and Baker (1990), proposed a probabilistic approach for offshore structures based on fracture assessment. The methodology was further improved to estimate optimal inspection intervals so that maintaining an acceptable probability of failure throughout the life of the structure, Madsen *et al* (1987), Dalane *et al* (1990), Jiao (1992), MTD 92/100

report 1992, Sigurdson (1995), Florentino (1998). These earlier works were mainly concerned with estimating the failure probability of individual joints, and not for the whole structure.

The reliability of the structure however is a function of all of its components hence system effects are important. Shetty (1992), studied the probability of failure of a offshore structure considering system effects under fatigue. Oakley *et al* (1994), modelled an offshore structure using a finite element package which was interacting with a reliability code to calculate the reliability of a complete offshore platform including the effects of inspection. Faber *et al* (1992) and Moan *et al* (1998), have also studied system effects on the reliability of offshore structures and proposed methods for optimum inspection intervals. Faber (2000), has also proposed a risk based inspection planning scheme which can be applied to any engineering structure.

Ship structures could also benefit from such a methodology, to determine inspection intervals based on the probability of failure. Brooking and Barltrop (1992), proposed the application of a probabilistic methodology to ship structures. The method uses information on loading (fatigue and extreme), structural degradation (corrosion, general wear), material (fracture toughness, ultimate strength) and operation profile to constantly monitor the ships' structural condition and propose inspections and repairs when necessary.

Pegg *et al* (1992), have studied reliability methods that can be applied to ship structures with respect to fatigue. Guedes Soares *et al* (1996), have allowed for a time dependent section modulus in the fatigue reliability model. The same authors in Guedes Soares *et al* (1999) account for the effect of corrosion and multiple cracks. Fujimoto (1997) investigate the effect of different inspection methods on the fatigue reliability, however on a component level. A very good review of the method is also given by Thayamballi (1984) with particular attention in the crack propagation stage and useful information about crack growth parameters and stress intensity factors. Lotsberg *et al* (1999), have also studied the fatigue reliability of an FPSO vessel accounting for system effects.

A major work was by Bea *et al* (1995) and Bea *et al* (1997) at the University of Berkeley. The work was carried out in three phases, over a period of 5 years. Part of the work was to assess the fatigue performance of oil tankers including the effect of inspection and repair. In that work system effects were considered by allowing for a crack site distribution. Only cracks in welds where considered, each crack was subjected to identical loading and had identical material properties. The failure probability of the system is then simplified and reduced to the failure probability of the crack site with the largest defect size.

There is still a lot of work to be done before the reliability approach can be fully integrated into an optimised inspection-planning programme for ship structures. The complexity of the ship structure itself, the difficulty in loading and material properties estimation, and evaluation of when fracture occurs are all factors that make the estimation of the failure probability very uncertain. Furthermore, the ship should be examined as a system of crack sites, each one with its own individual characteristics (loading, material properties, geometry). The overall failure probability will then depend on every crack site, so that the contribution to the total failure probability of each crack must be considered.

1.1.2 Aims of the Thesis

As is evident, fatigue reliability of offshore and ship structures has been extensively studied. Based on the results of a reliability analysis, inspection intervals can be estimated that will assist in operating the structure in a more safe and efficient way. Failure in a simple fatigue reliability analysis is defined by one of the following ways; *a)* when the fatigue damage accumulation reaches a critical value, in which case Miner's rule is used to calculate the fatigue damage with respect to time, *b)* when the fatigue cracks exceeds a critical value, in which case fracture mechanics are used to calculate the crack growth with respect to time.

None of the above methods account for fracture failure, i.e. when the crack driving force, e.g. the stress intensity, exceeds the fracture toughness of the material. Since fatigue cracks can lead to fracture failure, as in the case of the Alexander Kielland platform, it is also important to assess the risk of fracture failure because of fatigue

cracks. The main objective of this thesis is to assess the risk of fracture failure because of fatigue cracks in a ship structure.

Of particular concern are vessels, that operating in extreme environments, are subjected to severe loading and hence have an increase risk of failure. Many bulk carriers operate in extreme environmental conditions, and carry heavy cargo (iron ore) which gives rise to very large stresses. Severe loading in combination with fatigue cracks can result in the loss of the structure because of fracture. Bulk carriers are also very prone to corrosion, which reduces the strength of the vessel and increase the risk of fracture. A bulk carrier is hence chosen for study in this thesis. The particular characteristics of the bulk carrier studied in this thesis are given in Table A.4 in appendix A.

Structural reliability will be used to determine the failure probability of a system of growing cracks in corroding structure, considering fracture. A more advanced treatment of the system of crack sites will be attempted. Instead of accounting only for the largest crack sizes in the system of crack sites as in Cramer *et al* (1995), every crack is treated individually and its contribution to the total system failure probability is estimated. Furthermore, loading and material properties are allowed to vary between crack sites, to model the effect of cracks being in different locations in the ship structure. It is then possible to investigate the contribution to the failure probability of cracks at the deck or keel subjected mainly to global bending and shear, and cracks at the side shell subjected to dynamic fluctuating stresses because of local hydrodynamic wave pressure forces and acceleration forces due to cargo. In addition, material constants for the crack propagation model will not be the same at every crack site. At the side and keel structure, plating will be subjected to corrosion which increases crack growth rates, whereas crack growth at the deck may be affected by corrosion to a lesser extent.

Another important effect is that of the correlation in loading. Since all the cracks belong to the same system, the same vessel, loading is likely to be correlated and not independent. For example, when the ship is subjected to large stresses it is very probable that all cracks will be experiencing large loading, and vice versa i.e.

positively correlated. It is then more realistic to account for correlation in loading and compare results with a case where loading is assumed independent.

The study is initially limited to a finite number of crack sites, because of limitations of computer speed and memory (for the simulations required to determine the failure probability, chapter 2 and 7). However, a real ship structure may contain thousands of cracks. Eventually, by studying the effect of multiple cracks on the system reliability of the vessel using a finite number of cracks (approximately 100), an approach to calculate the reliability of a whole ship structure with thousands of cracks is deduced, a subject tackled in chapter 7.

1.1.3 Necessary Tasks to Undertake Fracture Assessment

A probabilistic fracture assessment requires bringing together a very wide range of analyses. Many individual assessments should be carried out, to determine the various parameters necessary for a reliability-based fracture analysis.

Loading is one fundamental requirement for this analysis. Both fatigue and extreme loading are necessary for a fracture assessment. Fatigue cracks propagate because of stress fluctuations. In ship structures these stress fluctuations are caused primarily due to waves and to a lesser extent due to vibrations and mechanical equipment. Waves can cause fluctuations due to global ship bending e.g. stress fluctuations on the whole section due to global vertical and horizontal bending, or local stress fluctuations to some area due to dynamic wave pressure (e.g. at the side shell) or internal cargo accelerations (e.g. at double bottom or transverse bulkheads). These stress fluctuations or stress ranges are in magnitude equal to the difference between the maximum and minimum stress for every wave encounter or cycle. Hence the number of stress ranges experienced by the ship is approximately equal to the number of wave cycles for a given period of time the ship spends at sea.

It is usually rare to measure the stress ranges during the ship's voyage as this requires special instrumentation (stress gauges) and it is also difficult and time consuming to determine the stress ranges and cycles from this data, although there are techniques available (e.g. rainflow, reservoir). In an advanced fatigue analysis, from the ships'

operational profile, estimates are made for the wave environment by the use of scatter diagrams, which have been developed by statistical analysis and determine the probability of occurrence of a sea state (usually defined by significant wave height and mean zero crossing period).

A spectral analysis is the best way to calculate the response of the ship at a particular sea state. By combining the response of the ship to a unit wave height (Response Amplitude Operator) with a sea spectrum (which describes the spread of wave energy with respect to wave frequency) it is possible to estimate the response of the vessel to various sea states. The response amplitude operators (RAOs) are obtained using a response analysis programme utilising linear strip theory or a more advanced 3D-wave diffraction theory. The input to these codes usually consists of the geometric description of the vessel (offsets), load distribution (lightship weight, cargo weight, ballast and other loads), speed of the vessel and wave direction. The output consists of the RAOs of the various loading components with respect to the length of the ship; vertical and horizontal bending moments, vertical and horizontal shear forces, torsional moments and if possible, dynamic wave pressure forces at different locations.

When the RAOs are combined together with the sea spectrum, the response spectrum is available. From this, it is possible to find the mean of the response, e.g. the mean value of the vertical bending moment at a location for a particular sea state. By transforming the response spectra from bending moments, shear forces etc. into stress range response spectra, the mean value of the stress range can be estimated, and used in the fatigue analysis. In the same way, the extreme stress spectra are evaluated, which define the value of the extreme stress in a particular the sea state, by considering statistics of the extremes. Combining together all the extreme stress spectra for all the sea states, and accounting for the probabilities of occurrence of each sea state, the extreme stress distribution can be found. This distribution defines the probability of occurrence of an extreme stress within a particular time interval. The extreme stresses are very important for the fracture analysis which is discussed later in this section. Chapter 3 deals with all the aspects of fatigue and extreme loading,

and ways of estimation. Appendix A presents results from a simplified spectral fatigue analysis for selected locations in a bulk carrier.

When loading is defined, it is then necessary to estimate how much the cracks grow with respect to time. This requires the application of fracture mechanics. A semi empirical formula is used to determine the rate of crack growth with time. In its simplest form, this equation is called Paris' law and relates crack size to material properties and loading.

Crack propagation according to the above relationship depends on material properties and loading. Cracks grow under fluctuating loading which is discussed and defined in chapter 3. Material properties are the other parameters which must be determined for fracture mechanics application. Different material have different crack growth characteristics, therefore it is important that the appropriate values are used for the material the ship is built from. Another factor that crack growth depends on is the environment, e.g. a corrosive environment (typical in cargo holds of a bulk carrier) tends to accelerate crack propagation, so material properties should account for this effect. Material properties for crack growth analysis have been determined by testing and measurements and are available in many references, although there is a big degree of scatter on the results. This is discussed further in chapter 6.

There are other aspects that must be considered into the crack growth analysis, which affect crack propagation and are not taken explicitly in the crack growth equation. There is for example a value for stress intensity factor called the 'stress intensity factor threshold' under which there is no crack growth at all. Corrosion tends to decrease material thickness, hence increase stress levels and crack growth rate. Large mean stress, increases crack growth rate as well, e.g. when the stress fluctuations are about a large constant stress. Stress ratio, which is defined as the ratio of the minimum to the maximum stress, increases crack growth, which means that crack growth for the same magnitude of stress range is not equal. Interaction effects also play a role on crack growth. This is a very complicated phenomenon, which is responsible for crack growth retardation after the application of a large stress, when loading is variable. Residual stresses have also an effect on crack growth by

increasing the mean stress. All of these matters should ideally be given extra thought and taken into account in crack growth analysis, if they are important. In chapter 4, there is an extensive discussion on all of the above-mentioned phenomena, and justification of their inclusion or exclusion from the analysis.

Fatigue crack growth analysis can now be carried out, since loading and crack growth modelling have been defined. The next step is to perform fracture analysis, i.e. to determine if a crack has reached a critical size to cause fracture. A ship structure contains welding imperfections, which with time and under fatigue loading (stress fluctuations), develop into cracks, which consequently grow larger and larger with every stress fluctuation. Some of these cracks may have grown to a large size because of large stress ranges at that location, accelerated crack growth because of corrosion, large stress intensity because of crack geometry. So that it is possible when an extreme stress is applied, e.g. because of a big wave, in combination with a large still water loading and a large crack size, fracture failure occurs. That means that the material resistance to fracture has been exceeded.

A vital subject is to define when fracture failure occurs, i.e. to establish a fracture criterion. If during crack growth, the area close to the crack tip was behaving in an elastic manner, then when the elastic stress intensity factor exceeded the material fracture toughness that would constitute failure. However, the region in the proximity of the crack tip deforms plastically because of the stress singularity which gives rise to large stresses and allows the formation of a plastic region in front of the crack tip. Although this region is small enough to allow us to use linear elastic fracture mechanics for crack growth, it complicates matters for fracture assessment and we cannot use the above simple criterion for fracture. A more advanced treatment of the problem is found in the fracture criterion which is adopted in this thesis, and is described in PD 6493 a British Standards document. A more detailed description is given in chapter 4, but in simple terms this describes failure between two limiting cases: Brittle fracture and plastic collapse, using an interpolation formula based on the Dugdale solution for these intermediate situations.

As a ship contains many details, it is also important for the fracture mechanics analysis that stress intensity factors are defined for different geometries. Although, there are stress intensity factor handbooks which contain stress intensity factors for many geometry and loading configurations, these are simple cases when compared with actual details found in ship structures. Hence, actual ship details were modelled using finite elements to allow evaluation of actual stress intensity factors. Chapter 5 includes this analysis.

When all the necessary input parameters are defined and their mean values estimated, reliability analysis can be carried out to determine the risk or probability of failure. Reliability analysis can be performed in various ways and there are many techniques available, as discussed in chapter 2. However, not every method is suitable for every reliability analysis, and it is important that the best method is chosen for the analysis of interest. Reliability analysis of fracture assessment is a time dependent analysis since the crack sizes vary with time, and this complicates matters. A suitable method for this analysis is the simulation method, which is described in chapter 2.

Finally a method to account for system effects and consider the possibility of thousands of cracks being present in the structure is developed in chapter 7, which puts together all the separate analyses to determine the failure probability of the ship structure. Results from this chapter, are compared with actual statistical data on bulk carrier losses in chapter 8, and this gives some credibility to the results of the reliability analysis.

1.2 Historical Review on Fractures of Steel Structures and Development of Fracture Mechanics Theory

Metal ships have been fracturing since they become available about 150 years ago. Firstly, naval architects were concerned with understanding the failure modes of riveted ships. During the Second World War rivets were replaced by welding for the mass-produced Liberty ships. Fractures were observed in 25% of all-welded Liberty ships that were constructed in the United States, (Barsom 1977). Of the 4.694 ships that were constructed, 1.289 casualties (structural failure) were reported, 233 of which

being so serious that the ships were lost or considered unsafe. Between 1942 and 1952 more than 200 ships had sustained fractures classified as serious, and at least nine T-2 tankers and seven Liberty ships had broken completely into two as a result of brittle fracture, (Tetelman 1967). The majority of fractures in the Liberty ships started at square hatch corners, or square cut-outs at the top of the sheerstrake. Most of the fractures in the T-2 tankers originated in defects in the bottom-shell butt welds.

It was obvious that the experience gained for the riveted ships could no longer be used for welded ships. A better understanding of critical details, high stress concentration areas, residual stresses and fracture toughness was needed. However, in spite of design improvements, the increased use of crack arresters, improvements in quality of workmanship, and restrictions on the chemical composition of steels during the late 1940s, brittle fractures still occurred in ships in early 1950s. Between 1951 and 1953, two comparatively new all-welded cargo ships and a transversely framed welded tanker broke in two. In the winter of 1954, a longitudinally framed welded tanker constructed from improved steel quality using up-to-date concepts of good design and welding quality broke in two. The fracture of the 584 ft long Tank Barge I.O.S. 3301 in 1972, in which the 1-yr-old vessel suddenly broke almost completely in half while in port with calm seas, (Barsom 1977), shows that this type of failure can still occur.

Fracture theories based on crack extension require the mathematical concepts of stress and strain that were not forthcoming until given by Cauchy and other great French mathematicians/engineers of the 19^{th} century. The first person that made a quantitative connection between strength and crack size was A. A. Griffith, whose landmark work on glass fibres first appeared around 1920. However, while some additional work was subsequently contributed by Westergaard (1939), fracture remained for some time a scientific field that did not evolve into engineering design. One significant, but not the only, reason may be the apparent non-applicability of the Griffith theory to engineering materials such as steel, aluminium etc., since the theory was developed initially for glass.

This state existed until sometime after the Second World War, when, more than any other reason, the large number of sudden and catastrophic fractures that occurred in welded merchant ships gave the impetus for the development of fracture mechanics.

It was then that the next major contribution to the field was given by Irwin (1948), when he generalised Griffith's ideas for applicability to metals and other engineering materials. Another subsequent step in the evolution of fracture mechanics, to connect the stress intensity factor to Griffith's energy balance, was also performed by Irwin (1957).

The developments that immediately followed Irwin's work were almost entirely focused on linear elastic fracture mechanics, (LEFM). Then there was another distinct point in the history of fracture mechanics. This is when J. R. Rice developed the J-integral (1968), and explained the way such a concept can be used to describe directly the discrete and non-linear events involved in crack propagation. That methodology is usually referred to as *advanced fracture mechanics* and is used to solve problems of crack propagation with non-linear and dynamic behaviour, which is beyond linear elastic fracture mechanics theory.

It was then that engineers started the more intense study of fracture mechanics, with the Comet aircraft disasters, which failed catastrophically while at high altitudes (Bishop 1955), additionally spurring work in Europe. An exhaustive investigation indicated that the failures initiated from very small fatigue cracks originating from rivet holes near openings in the fuselage. The failures of F-111 aircraft were attributed to brittle fractures of members with pre-existing flaws. Also in the 1950s, several failures of steam turbines and generator rotors occurred that were explained using Fracture Mechanics, (Barsom 1977).

In 1962, the Kings Bridge in Melbourne failed by brittle fracture, at a temperature of 40°F. Poor details and fabrication resulted in cracks, which caused the failure. In 1967, the Point Pleasant bridge collapsed without warning, resulting in the loss of 46 lives,(Barsom 1977). Since the time of the Point Pleasant Bridge failure, other fractures have occurred in steel bridges, ships and other steel structures as a result of unsatisfactory fabrication methods, design details or material properties.

Fracture mechanics has shown that because of the *interrelation* among materials, design, and fabrication, fractures cannot be eliminated in structures merely by using materials with improved fracture toughness. The designer still has the fundamental responsibility for the overall safety and reliability of his structure. The science of fracture mechanics can be used to describe quantitatively the trade-offs among these three factors (stress, material toughness, flaw size), so that the designer can determine the relative importance of each of them preferably during *design* rather than during *failure* analysis.

Between 1960 and 1970, the size of an average bulk carrier and oil tanker increased by a factor of about six. This is a huge increase in size in a relatively short period of 10 years. At the same time, economic considerations for weight saving and optimised construction, imposed simplified details and reduced scantlings by the use of high strength steels. A typical example are the vessels that entered service in the Trans-Alaskan Pipeline Service (TAPS), (Sucharski 1997). Although new, these ships were fracturing severely. An important cause of these fractures was the use of high strength steel. It is ironic that technological advances in design and fabrication areas have led to problems associated with today's designs.

1.3 Recent Examples of Ship Related Cracking

In recent years, ships were designed under classification societies rules for being able to withstand, cargo loads while at pier with seaway loads while at sea. Weight savings considerations meant the use of higher strength steels where mild steel was used previously. The condition for such designs was that they were regularly and properly maintained. The life span for such vessels was approximately 25 years. In practice, in the last 10 to 20 years these conditions were not met. The result was frequent structural failures of vessels under loading much less than the design load. The most severe catastrophes were the sinking of 25 bulk carriers and the damage beyond repair of another 25 in the early 1990s. The majority of these failures were older vessels, operating under third, fourth or even fifth owner. The main cause of these failures was the improper maintenance, which lead to high corrosive degradation of the hull

structure. Because these vessels were built of high strength steel, reduction in thickness played a much more severe role in the final failure.

In the TAPS trade, very large crude carriers (VLCCs) evidenced fatigue cracking very early in their life. The use of high strength steel is one main cause for these fractures. Unfortunately, the use of high strength materials does not mean high resistance to fatigue. The other reason was the severe sea conditions that these vessels were experiencing. Reports (USCG 1990, Lacey & Chen 1993) present that the operating environmental conditions were 20% more severe than classification society North Atlantic design standards.

The conclusions are easy to make. Thinner sections if not regularly maintained and coated are more prone to corrosion. The inadequate attention in design and fabrication of critical joints can also lead to fatigue fractures in high stress concentration areas.

Conventional elastic analysis together with FEA has shown that most fractures in recent bulk carriers and tankers occurred under stress loading much less than yield, (NRC 1997). This result points out that the main cause of fracturing in these vessels is fatigue. Although the fractures in the modern vessels are not as severe as in the early design (Liberty ships), they can cause however costly repairs and frequent service disruptions, which can prove very uneconomical to ship owners.

1.3.1 Causes and Consequence of Cracking in Ship Structures

Every bulk carrier and oil tanker contains cracks. Even from the fabrication stage, small crack-like defects will be present as a result of welding. The life of a typical vessel subjected to dynamic random loading has three stages, in terms of fatigue failures, (NRC 1997):

1. The first stage, where failures per year, because of inherent defects from fabrication, reduce with time
2. The second stage, where the number of failures occur randomly, but are constant with time
3. The third or ageing stage, where the number of failures increases with time. Failures in this stage are mainly due to structural degradation

In a well-designed vessel, the third stage should occur after its useful economic life.

There are three main types of strength related failures. These are,

- Yielding, (plastic collapse)
- Buckling
- Fracture

Yielding implies the presence of plastic regions. Further increase of load will result in overall yield and when there is no further capacity (available path for the stress re-distribution), the structure will fail by plastic collapse. Yielding may occur with tension or compression loading.

Buckling is related to member failure under compressive loading, usually through a combination of elastic buckling and plastic effects.

Fracture occurs when the fracture toughness of the material is exceeded, by a combination of crack size and load. When the force due to the presence of the crack in the material and an applied load (which results in a driving force at the crack tip) exceeds the material capacity (the fracture toughness), the crack grows unstably until final fracture. The primary initiation sites for fracture in ship structures are fatigue cracks.

1.3.2 Cracking Trends in Bulk Carriers and Oil Tankers

Available studies based on inspection results have shown a general trend for cracking in structural connections (NRC 1997). Many cracks were found at bracket connections and cut-out details. This is not surprising since the stress concentration factors in these details are very high. A study from Schulte-Strauthaus (1991), based on 10 oil tankers, (2 double hull, 2 double bottom and 6 single hull) collected a database of 3,600 cracks. The study revealed that

- 40% of the cracks occurred at side shell longitudinals to transverse web frames or bulkheads
- 10% of the cracks being on bottom longitudinal-end connections

- 10% on horizontal stringers
- 10% on longitudinal bulkhead longitudinal-end connections
- The rest in various members 1% of which at deck longitudinal-end connections

There is also a tendency of cracking in the middle part of the ship with very few cracks at the fore and aft sections. Cracking in the side shell and at the bracket/bulkhead connections is significant from the point of view that oil spills or mixing between cargo can happen.

An ABS guide on bulk carriers indicates (ABS 1995), that cracking occurs in the following areas,

- At bracket toe frame connections to the upper and lower wing ballast tanks
- At transverse corrugated bulkhead intersections with topside structures
- At the intersection of inner bottom and hopper tanks
- At hatch corners and coamings

Cracking in bulk carriers can be very significant, not only for the environment but also for the vessel itself. The first type of cracking can result in the detachment of the web frames from the side shell plating, which results in a reduction in the load bearing capacity (in an area of high shear stress!). The second type of cracking can result in the detachment of the support of the bulkhead. Cracking at hatch corners can result in loss of water integrity, and crack propagation at the side shell with possible catastrophic results. Figure 1.1 shows typical crack locations in a bulk carrier. Table 1.1 also indicates locations prone to fatigue, corrosion and buckling damage.

1.3.3 Main Causes of Cracking

The amount of experience gained over the last 20 years has proved valuable in determining the most important reasons of cracking in ship structures. Research on fatigue and fracture of ship structures has also helped to understand better and

indicate why cracking takes place. The main causes of cracking in ship structures are (NRC 1997)

- *Pre-existence of defects in welds.* In welded structures, defects are very likely to exist because of welding procedures. The size, type and frequency of these flaws depend on the welding technique, quality and weld type. Defects can be surface or embedded. Generally, defects are formed because of notches in weldments. Notches can be internal or external, and exist because of changes in weld geometry or section, surface ripples, undercuts, lack of fusion porosity and inclusions.

  Dirt or scale on the surface of the material can create lack of fusion. Porosity is caused by gas entrapment during cooling of the weld metal.

  - In transversely loaded full penetration welds, frequently cracks initiate at the weld toe. Lack of fusion can also cause cracks. In longitudinally loaded welds, ripples on the surface are a common starting point for fatigue cracks or at starts/stops during changes of electrode in manual welding.

  - In transverse fillet welds, flaws exist at weld toes and in longitudinal at surface ripples.

  Figure 1.2 shows some typical cracks initiated at butt and fillet welds.

- *High local stresses.* Because fatigue damage is proportional to the cube of the stress range, a slight increase in stress level results in a significant reduction of fatigue life. High local stresses are caused by high stress concentration factor due to bad detail design, fabrication error, increased global loading and degradation (corrosion, wear).

- *Extreme operational conditions.* Some operational routes are more severe than others. The common basis for extreme load design is the North Atlantic wave environment. Certain service routes may possess even worst wave conditions than the North Atlantic wave environment. For bulk carriers we can think of one more

additional factor; the cargo. Certain cargoes accelerate wear and hence assist cracking, coal and other liquid cargoes for example contribute to accelerated corrosion. Iron ore and other heavy cargoes have been associated with increased risk of failure, probably as a result of increased stress.

- *Bad detailing in design stage.* This can be a cause of cracking or can make the consequences of cracking even worst. Bad detail design in conjunction with the use of high tensile steel enhances the risk of cracking. There are numerous examples of cracks being initiated from bad details and in some cases this even lead to the total loss of the structure (Alexander Kielland).

- *The use of High Tensile Steel (HTS).* Cost savings enforced the use of HTS which resulted in significant weight savings and hence less material been used, up to 20% less. However, thinner sections meant an increase in stress levels compared to mild steel vessels, by an amount of about 30 to 40% depending on the quality of the HTS used. Corrosion can significantly reduce more the even 'reduced' section scantlings (compared with mild steel sections). Undoubtedly corrosion was always present even in mild steel vessels, but to a less significant degree.

- *Dynamic fluctuating stresses.* The fatigue effects of external hydrodynamic wave pressure and internal liquid cargo pressure were not taken into account in the older designs, other than through experience based scantlings increase. Larger reserve strength of the older vessels and the large increase of size of bulk carriers and tankers in the 1960s resulted in a rather questionable experience base. Local cracking in areas of fluctuating loads such as side shell structure and transverse bulkheads, showed the importance of addressing these loads in the design process.

1.3.3.1 Corrosion

Corrosion leads to a loss of material thickness which decreases the ultimate strength at least in proportion to the thickness loss and by more than the thickness loss if buckling is important. Corrosion also increases the stress ranges and so decreases fatigue life e.g. with an S-N slope of 3 a 10% reduction in thickness because of corrosion, will result in a 33% increase ($1.1^3 - 1$) in the fatigue damage rate. There is

some possibility that corrosion might act as an initial defect for crack propagation. There is also the possibility that corrosion might remove initial defects but there is little evidence for either at present. It is known that a corrosive environment also increases crack growth rates, (as it will be shown in chapter 6).

The problem is significant in oil tankers where specific type of cargoes accelerate the corrosion rate. Oil itself tends to protect from corrosion (e.g. a protective film of oil), but any water trapped under the oil will corrode the material. In bulk carriers, the problem is even more severe. Bulk carriers carry at the same time iron ore and coal. Because coal contains sulphur, it reacts with water deposits in the cargo spaces, producing sulphuric acid that corrodes the steel. This, in conjunction with high stresses because of the iron ore cargo, may result in further crack initiation.

From the economic point of view, corrosion means to ship owners, steel renewals, if they wish to operate the vessel further (and get the vessel approved by classification societies). A study carried out by the Tanker Co-operative Forum, showed a large scatter in the steel renewal trends. For instance, for a specific amount of time, a coated vessel had no repairs at all, whereas another vessel operated in the tropical zone carrying heated cargoes required repairs of around 800 tonnes of steel. These can be significant economic considerations for ship operators and owners.

Corrosion is usually, present in various forms but the most common found in ship structures are

- General corrosion, which is the most common form of corrosion in ship structures. Its characteristics are general oxidation of the material, but it is more likely to develop over large areas rather than in depth, Figure 1.3a. The effect is a reduction in material thickness.

- Grooving corrosion, which is a more localised form. It usually occurs at structural intersections or welds where deposits like mud or scale collect or water flows, and corrodes the material at a higher rate, Figure 1.3b. Because of the relative small width of the corrosion zone, its effect is in depth rather in surface area. This is also called 'necking' effect.

- Pitting corrosion, which is also a localised effect. It usually occurs in bottom structures, horizontal surfaces and at local details that trap water. The residual water creates very localised corrosion in the form of deep small holes or pits, Figure 1.3c. These holes can then initiate cracks because of the large stress intensity factors in the local area. They can also lead to hull penetration and induce leakages.

Because of the large size of these vessels and the limited time available to the inspectors it is impossible to inspect every detail on the ship. A typical 250,000 t bulk carrier has tens of kilometres of longitudinal stiffeners and the total area to inspect is around 300,000 m^2! It is also difficult to say exactly to the inspectors 'where to look' at and 'what to look for', since each vessel is different, operated in different conditions and carrying different cargo. There are however typical 'suspect' areas for every ship, indicated by studies carried out by classification societies or other bodies like the Tanker Structure Co-operative Forum, consisting of owners, operators and classification societies. These are

- Ballast tank spaces. Problems in this area come from grooving corrosion due to exposure to seawater. High humidity air and a salty atmosphere cause also atmospheric corrosion. The longitudinals in this area are the most affected members.

- Cargo only spaces. Pitting corrosion in horizontal members is very often from acid water settling out from cargo oil. At the aft ends water usually accumulates because of the stern trim of the vessel.

- Cargo/clean water ballast. Generally less exposed to corrosion because of oil film deposits. However, tank washing can destroy this oil film and expose fresh steel to water. The result is pitting corrosion on flat and vertical surfaces because of water residuals.

Table 1.2 lists in detail areas subjected to corrosion and identifies also the risk of corrosion of these areas.

1.3.4 The Consequences of Cracking

When cracks start to appear, many problems appear as well. The effect of cracking varies in importance and depends on many factors. Generally, there are three main effects

1. Operational disruptions due to increase in maintenance and repairs
2. Environmental catastrophes due to pollution
3. Loss of cargo, vessel and lives due to structural failure

The third effect is the most serious and the first the less serious. The environmental effect can be serious and non-serious. For example, an environmental serious effect would be the spill of oil or dangerous chemicals into the sea, close to the shoreline.

1.3.4.1 Structural Failures

Fracture failures today are not very frequent and most importantly not as catastrophic as the failures of the early welded vessels (Liberty ships) during and after the Second World War. Nevertheless, statistics from classification societies and the International Maritime Organization (IMO), show that ship losses due to fracture still occur, (chapter 8). The ageing bulk and combination carriers (OBO), where fractures still happen even today are of more concern than other vessels. It is for this reason that this study concentrates on the risk of fracture failure in bulk carriers.

Where fractures still occur, usually it is the human factor to blame due to bad loading, grounding or even faulty design (see figures in chapter 8). An example of faulty design fracture failure can be considered the loss of the *Derbyshire,* which was lost without a trace, unable even to transmit a distress call, in 1980 in China Sea. The official inquiry decided simply to blame the overwhelming forces of nature, since the vessel was in the middle of a Typhoon. However, relatives of the victims believe the vessel was split in to two due to a faulty stiffener connection, cracking across the deck and separating the aft end (with the superstructure) from the rest of the ship. Video records taken from the wreckage for an official report show the vessel in fragments

scattered in a large area with the superstructure some miles away. In 1998 the case was re-examined and from the investigations carried out, a hatch cover failure was to blame (MV Derbyshire Surveys). A sister ship of the *Derbyshire,* the *Kowloon Bridge*, broke in two after running aground, which might indicate the faulty design of the vessels.

Another very serious incident of fracture failure, although not to a ship structure but to a floating offshore structure, was the loss of the *Alexander Kielland* platform, again due to a faulty designed member with a crack, (Moan 1985). In March 1980 a semi submersible operating in the North Sea, capsized. Of the 212 men onboard only 89 were rescued. After examination of the platform, investigators concluded that the accident was caused because of

A. Failure of one of the braces, due to a fatigue crack initiated in the fillet welds connecting the hydrophone support to the brace. Early growth of the fatigue crack was enhanced by pre-existing cracks in the fillet welds between the hydrophone support and the brace. As a result the crack propagated in both sides of the hydrophone support

B. Fracture failure of the brace, mainly in a brittle manner

C. Fractures of remaining braces due to overloading, in a ductile manner, i.e. with plastic deformations

The result was the detachment of one of the five columns from the rest of the structure, which caused heeling, progressive flooding and final capsize.

Structural failures that also involved human error, in a more indirect way, were the fatigue failures of nearly new oil tankers operating in the TAPS trade, (NRC 1997).

The existence of crack-like flaws cannot be precluded in a ship structure. At the same time, increasing demands for energy and material conservation are dictating that structures be designed with smaller safety margins. Consequently, accurate quantitative estimates of the flaw tolerance of structures are increasingly becoming of direct concern for the prevention of fracture in load-bearing components of all kinds.

This has not always be so. Prudent design procedures that avoided large stress concentration factors, together with immediate repair and/or retirement from service of components that exhibited cracks, have been effective methods of preventing failures. However, there is a combination of factors that have now emerged to oppose this approach.

First, the steels that are used from the shipbuilders have seen considerable improvement in their fracture toughness, which means that they are more resistant in fatigue and fracture. Second, improved quality control from shipbuilders, e.g. non-destructive evaluation (NDE) procedures have enabled defects to be found that would have gone unnoticed before. That means that very few cracks exist in the components of the new vessels, and even the presence of such cracks does not necessarily mean that a structural component is at the end of its useful life. Third, frequent inspections made from ship owners means that many cracks are detected and subsequently repaired before failures can occur. The cost of the repaired or replacement of a flawed component can therefore be balanced against the possibility that continued service could lead to disruptions or even failure. A fourth reason is the crack-arrest ability of the hull. Therefore, even if a crack grows there is a very high possibility that it will be arrested by the structure itself before reaching a critical size.

However, if fracture occurs there is a sequence before final failure. For example, cracks at the side shell frames tend to separate them from the side structure and this is a 'domino' effect. When enough side frames have been detached the shear stress carrying ability has reduced and buckling can take place. Luckily, the detachment of the side frames can easily be seen and they can be repaired at the first opportunity. There are other failures that are hard to detect before they happen and shown little sign of external damage. For example a failure scenario would be, progressive flooding of a cargo hold because of cracking in the side shell or hatch corner, collapse of transverse bulkheads at the ends of the flooded hold and hence loss of buoyancy, further hull girder collapse due to excessive loads, and final loss of the vessel.

1.3.4.2 Environmental Effects

Among the most serious environmental disaster ever are the oil spills. However, from the estimated 2.5 million tonnes of oil spilled into the sea from all sources (natural leaks, land-based and offshore activities, collision and grounding) tanker leaks because of cracking contribute very little. This is particularly because of the strict rules now imposed to oil tanker design and operation after major oil spill disasters, mainly due to human error (collision or grounding not structural failure).

For example one of the worst oil spill disasters that of the *Exxon Valdez* (Alaska 1989, the slick covered almost 1,450 sq. km. and killed thousands of sea animals), was due to navigational error and grounding. Although it ranks only tenth in the most serious oil spill disasters, the cleaning up operation cost in excess of $2 billion the highest up to date. Another recent grounding disaster was the running into rocks of the *Sea Empress,* before entering the British port of Milford Haven, with 72,000 tonnes spilled into the sea, (Karen Farrington 2000).

Apart from the legal costs that such incidents have, with typical payments of $30,000 to $100,000 per tonne spilled, the more serious threat is near term ecological harm to the environment. This has effect on the wildlife as well as to human life. The *Sea Empress* disaster for example had an affect on tourism and fishing was banned as a concern to public safety.

1.3.4.3 Operational Disruptions, Maintenance and Repair Costs

The other less serious effect of cracks (no loss of lives, vessel or environmental disaster) is the service disruptions and downtime with repair costs associated with. This effect can be a significant economic loss for the ship owner or operator. It is more serious for bulk carrier owners and operators that do not trade in specific routes like oil tankers, but in a more competitive worldwide trade business.

Apart from the downtime, that is the wastage of time, other costs involved are the steel renewals, dry dock charging, coatings and tank cleaning. Typical values for steel renewals per tanker per 20 year life-time, range from up to 70 tonnes for uncoated cargo spaces, up to 30 tonnes for coated cargo spaces, up to 400 tonnes for

uncoated ballast tank spaces and up to 200 tonnes for coated tanks. Most of steel renewals are because of corrosion, hence the reduced numbers for coated spaces. Unfortunately, there is no such data for bulk carriers, but the indications are that the numbers would be even higher because of the more rigorous use, and the abrasive and corrosion cargos. In oil tankers, the oil deposits some times retard the effect of corrosion.

1.4 Ways of Fracture Control for New Ships

Traditionally ships were built to withstand still water and wave shear stresses and bending moments, and to avoid buckling and yielding. Fatigue calculations were not normally undertaken. In the last 10 years however, bulk carriers and oil tankers have been designed against fatigue as well as for other failure modes e.g. buckling and yielding. To prevent fractures occurring in ship structures classification societies and shipbuilders have adopted new techniques, used new technology and have imposed more strict quality controls.

From the shipbuilder's side, the contribution against fracture failures comes from,

- Attention in detail design. Very large stresses can rise from poor detail design with high stress concentration and intensity factors. Many cracks are initiated from bad designed structural connections and joints. A lot of effort has put into providing smoother transfer of stresses and avoiding member misalignments.

- Use of tougher materials (high fracture toughness steels with more resistance to fracture). The steels used in the shipbuilding industry undergo changes in behaviour, from ductile to brittle, with changes in temperature and loads. In high toughness steels these changes in behaviour take place at different temperatures or loads.

- Quality control in welding. Welds are the most common places to find cracks. It is for this reason that in welded structures the fatigue initiation stage is neglected. Cracks are already present in the structure. Shipyards have now their own quality controls, and cracks that would once have escaped detection and gone into the

ship structure from the construction date, now are found. This is possible mainly due to the new techniques available like, ultrasonic inspection.

- Advanced structural design. By the use of modern technology and advanced engineering tools such as Finite Elements, stress analysis in a very detailed way is undertaken. Apart from the global structure, very local details can be modelled and the stresses are estimated. Optimisation of local joints is then possible to reduce any high stresses likely to cause fatigue cracks. Fatigue damage accumulation is also calculated by performing fatigue analysis. An advanced fatigue approach, that of the spectral method, requires information of the wave environment (wave scatter diagram), and determines the stress range transfer functions. By appropriately considering all the possible sea states the ship experiences (taking into account the probability of occurrence of each sea state), the stress range histogram is constructed, and the fatigue damage based on that, evaluated.

The classification societies try to control the fabrication tolerances such as misalignments in butt and fillet welds, weld undercuts, dimensions of sections, and straightness of stiffeners and plates.

1.5 Control of Cracking and Corrosion for Vessels in Service

It is very difficult to eliminate cracks from ships structures, especially from vessels already in service. Over the recent years economic pressures on the trading industry have increased by low freight rates and high competition. As a consequence, the number of new vessel ordered has decrease significantly with further consequence the ageing of the existing ships. In fact about 60 percent of the world tanker and 40 percent of the bulk carrier fleet are over 15 years old. In many cases bulk carriers operate under third, fourth or even fifth owner! This underlines even more the need for control and minimising the risk of potential failures.

Structural defects may exist in ships in service, but the incidence of cracking can be reduced and its consequences be contained. There are various methods for reducing the consequences of cracking, the most important are,

- Repair/redesign of localised structural joints
- Frequent surveys and repairs
- Fitness-for-Service assessment using probabilistic approach

These are now briefly discussed.

1.5.1 Repair/Redesign of Local Joints

This approach is based on experienced gained from the past. From past incidents of cracking that occurred in ship structures, the parts that exhibited cracks where repaired, strengthened or even modified. Typical members, for example, cracking frequently are longitudinals to bulkhead connections. There have been developments towards redesigning these details, which gave rise to large stress concentrations. Finite Elements Analysis (FEA) is usually applied to calculate the local stress fields and then propose modifications to assist in reducing the stress concentrations. It may be necessary to even strength the detail further by providing brackets or other supporting structural members to re-distribute the stresses.

The modifications may be required to only a few details or to all similar details. Therefore the cost may be relatively high, and repair time can be long. Unfortunately with this approach you must 'wait for defects to occur' and then take action. It would be of course more desirable to anticipate the occurrence of cracking from the design stage, and introduce modifications then, to avoid it.

1.5.2 Frequent Surveys and Repairs (for cracks and corrosion control)

1.5.2.1 Corrosion Control

The problems associated with corrosion were discussed in 1.3.3.1. To avoid or minimise these problems, corrosion protection systems are available. The most common corrosion protection systems used in ships are coatings, anodes and cathodic protection. To ensure that corrosion does not lead to structural failure, ship owners and classification societies also do frequent inspection and surveys. The interval of these surveys and inspections may vary according to,

- The cargo of the ship. Certain cargos accelerate corrosion and therefore such vessels should be inspected more frequently.
- The operating environment. High temperatures and high humidity air tends to increase corrosion rates. Tropical zones for example have such conditions.
- The type of the vessel. Bulk and combination carriers are more prone to corrosion than oil tankers, because of the different use.

It was not unusual in the past for shipbuilders to build ships with corrosion allowances in scantlings, e.g. using thicker scantlings than the rules would suggest. In some cases it can be more economical such an approach, i.e. allowing a margin for corrosion during the ship's economic life, than to repair and use coatings.

At some stage (early 1980s), Classification societies (e.g. Lloyd's Register) have even permitted the construction of ships to standard scantlings minus the tolerable corrosion margins, on the basis that ship owners would not allow corrosion to occur. These "Corrosion Control" (C.C.) ships became a major problem for their owners as they inevitably aged and corroded.

1.5.2.2 Control of Cracks

Probably the best way to confine the consequences of cracking and structural deterioration. Classification societies have imposed strict inspection and repair intervals (see next section), for oil tankers and bulk carriers. Cracks are repaired by

- Re-welding crack on original material. It is easy and cheap, but new weld crates new cracks
- Re-welding and add weld improvement. Cracks can be permanently removed and fatigue life extended significantly
- Cutting and replacing cracked plate
- Modifying design. Strengthen detail by adding e.g. a bracket to reduce stress concentrations
- Drilling a hole. Very temporary way to stop a crack, used only when ship is in service

1.5.2.3 Inspection Schemes

There are annual, intermediate, special surveys and dry-docking surveys, (Caridis 2000, Tanker Co-operative Forum 1992).

Annual inspections may be more general, and concentrate on larger areas of the ship (main deck, superstructure, bulkheads, cargo spaces, hatch corners), and part of the inspection is to check the hull condition for cracks and corrosion (machinery, piping systems, watertight integrity are among other things to check)

Intermediate surveys are held in place of the second or third annual inspection (depending on vessel age), and during these, more internal inspections are carried out (electrical systems, internal checking of all cargo spaces, and check mechanical systems, propeller and shaft, fire protection systems)

Special surveys (within 5-year periods) concentrate on specific areas of the ship that classification societies think have high risk of damage. Checking in areas of high

stress concentrations, of high corrosion rates, thickness measurements and internal inspection of cargo and tank spaces

Dry-docking surveys have to be performed every 36 months, inspecting outer hull for corrosion and contact damage, cracks and other machinery items.

There is of course the economic aspect. During inspections the vessels should be dry docked and possibly cleaned so that inspectors can easily access spaces. On top of that the ship's downtime increases. The physical size of the vessels itself is a restraining factor. The questions of 'where to inspect', 'what to inspect' and 'how often to inspect' arise given the limitation of time the ship stays in the dry dock.

The most efficient way to carry out inspections would be to assess the risk of failure of the ship, and if this risk exceeded a certain value, then carry out the inspections. By this way the time interval between inspection can be optimised and the economic life of the ship even extended. A balance is achieved, between the expected benefits of the inspection and repair and the economic costs.

Based on this principle is the third method that we discuss.

1.5.2.4 Inspection

Inspection and safety are two things very closely related. Without inspection, the safety of a structure would be at much greater risk. Consider the following example. A living organism is able to detect pain because it has sensors (nerves). A structure cannot detect by itself where there is some anomaly (cracks for example). The role the sensors have in a living organism is fulfilled by inspection in a structure. It is a diagnostic tool for structures.

Inspection tells us the condition of the structure, with respect to cracks, corrosion, and other possible sources of damage (wear, accidental damage because of loading/unloading, operational damages). After the diagnosis, it must be decided whether the damages found will be repaired, depending on the extend of damage.

The better the diagnosis, the better the actions to repair them will be, and the less the chance of the structure failing from structural causes afterwards. A perfect inspection implies that no damage has gone unnoticed, and all possible problems have been identified. In reality it is very difficult to perform a perfect inspection to ship structures for many reasons.

First, the physical size of ship structures is prohibiting for a perfect inspection. A bulk carrier of the Capesize type has approximately 58 km of welds. It would require weeks for a thorough inspection of such huge structure.

Second, not every part of the structure is accessible to the inspector. There are many parts of the structure that the inspector has no access to or visibility conditions are very poor, like double bottom structures (usually accessible), or structures under the deck (accessible only by scaffolding). Any defects (sometimes even medium sized cracks 100 – 300mm) in such areas will go unnoticed.

Thirdly, easily seen damage, like corrosion, has a higher chance of been identified. Cracks on the other hand, have less chance of been seen, specially very small cracks. The quality of the inspection technique here plays a most important role.

To make inspections more efficient, many guidelines have been proposed by classification societies based on experience (see previous section). These guidelines suggest where to look at and for what to look at, which shortens the time of inspection and increases efficiency (i.e. the probability of finding cracks, if any).

1.5.2.5 Crack Detection Techniques

There is a range of crack detection techniques available which enable a component to be examined without further damage (Parker 1981). Then actual size of the defect, which is likely to be detected, varies widely, even for a particular detection technique, and depends on operator experience, crack location, and orientation. An important prerequisite for non-destructive testing (NDT) examination is normally knowledge of critical locations likely to develop cracks during service. Some of the most common NDT methods are :

(a) Visual inspection. This depends on the use of the naked eye assisted only by visual magnifiers, mirrors and suitable lighting. User experience is required to detect even moderately short surface cracks. Accessibility is a particular problem, lightening conditions another.

(b) Dye-penetrant. This method is suitable for surface cracks only, involves the application of a liquid penetrant, which is subsequently wiped off the surface before application of a powdered 'developer'. Crack-like defects will produce a contrasting colored line on the developer.

(c) Magnetic anomalies. Fluorescent liquid containing iron particles in suspension is applied to component. When placed in a strong magnetic field and illuminated with ultraviolet light, disturbances in magnetic field induced by cracks and cutouts appear as a change in the field pattern. It is limited to magnetic materials only.

(d) Radiography. In the case of X-ray or gamma ray radiography, a portable source is used to irradiate the component, and the absorption assessed from the image, on a sensitive film, on the opposite side of the component from the source. Cracks, which absorb less radiation, appear as dark areas on the film. The method is sensitive, and may be used to detect internal cracks. However, poor crack orientation may produce inferior images.

(e) Ultrasonic. A probe emits a high frequency sound wave into the component, which is reflected by surfaces, including internal cracks. The time taken for transmission and reflection of a pulse is normally indicated on an oscilloscope. This may be interpreted as a distance through the component, and hence allows the crack to be properly located.

(f) Eddy current. A small coil induces eddy currents in the metal component. This re-induces a current in the coil. A change in the inductive 'fingerprint' of a component may indicate a crack or defect.

(g) Acoustic emission. stress or pressure waves are generated within components during dynamic material processes. the presence of cracks alters the load at

which plastic deformation begins, thus altering the acoustic emission pattern. The record obtained during loading can be used to assess the incidence and severity of the flaws.

1.5.3 Fitness-for-Service Assessment Using Probabilistic Approach

Degradation on ship structures will always exist in some degree, because of corrosion, fatigue cracks and structural wear. The objective of such an analysis is to indicate the 'risk of failure'. When fatigue cracks are considered, the analysis will indicate the 'risk' of a crack becoming 'unstable' namely, propagate under accelerating pace until the ship breaks.

If for example, a large crack were discovered, it would be of interest to assess the risk associated with this crack, and find out how long to wait (usually a few days or weeks) before repair action. On the other hand, it may be required to evaluate the annual risk of failure of a ship operating in a specific environment and loading condition. The latter usually requires a more complicated analysis because many more factors need to be taken into account.

A fitness-for-purpose analysis uses probabilistic methods to quantify the risk or probability of failure. Based on these results inspection and maintenance planning can be scheduled. Also such analysis produces more flexible designs than traditional safety factor approaches (since safety factors can be reduced), and vessels can be constructed to suit particular applications. For example, a vessel designed for frequent inspections can be constructed from low toughness steels so that higher degradation can be counteracted by frequent inspection intervals. A vessel built of higher toughness steel however, although requires higher capital cost, this can be offset by bigger inspection intervals.

The use of the results of a probabilistic approach can assist decisions relating to more efficient use of materials, evaluating optimum inspection intervals, and maintenance strategies. One important advantage that such an analysis has, is the ability to 'update', from information that becomes available during inspections, input

parameters and refine/optimise the initial estimates. For example, inspection intervals can increase if the actual deterioration of the structure is better than the estimated. Of course the opposite can happen, in which case it may signal the end of the useful economic life of the vessel.

Because of the various uncertainties, in the input parameters, the results represent only an estimate of the reliability of the structure, which can change, as more information becomes available. It is by no means a physical property of the structure.

Results from a probabilistic analysis are very easy to read and understand. Usually a graph shows the probability of failure versus time. On one graph we can show results of several analyses and the difference on the results is more easily seen. For example, the effect of including corrosion in the analysis can be more easily seen when compared with results with no corrosion effect. Also the effect of inspection and repair on the reliability of the structure can be seen when they occur. As stated in the previous paragraph, the results represent only an estimate with a possibility of a large error. However, they can show the general trend of the reliability and they can also present useful information.

As an example, we can consider the two cases; Results with no inspection, and results with inspection and repair (e.g. Figure 7.7). The reliability of the structure, in the first case, would decrease with time monotonically. The general trend can therefore be seen. In the second case, with inspection and repair included, the results would show the effect of inspection on the reliability. An increase on reliability after the inspection and repair is evident. From results with inspection and repair included in the analysis, the effect of inspection against the reliability can be seen and from there decide whether the advantages of inspection can balance the economic costs. If for example the reliability of the structure is high and the additional increase because of the inspection is low, then the ship owner may decide to wait before repairing until the second inspection interval. Important decisions can be made by simply observing a single graph and do not require advanced interpretation. Therefore, they can be presented to ship owners/operators directly and can easily be understood at every level.

A ship structure is made of many components, contains thousands of meters of welds, and hundreds of different types of joints. It is more appropriate for this reason to consider it as a system and not as one single unit. The reliability of a system is a function of the reliabilities of all of its components. Reliability analysis is capable of considering individual components and evaluating the overall reliability of the system based upon estimates of the reliabilities of individual members.

1.6 Overview of a Probabilistic Approach for Fracture Assessment

Generally, a probabilistic approach requires the use of reliability assessment. Reliability analysis methods are described in the next chapter, and a full probabilistic analysis is undertaken in chapter 7, so only a brief description of the method will be given. The required input for the analysis is dealt with more detail here. A flowchart of the method is shown in Figure 1.4.

In reliability analysis, variables are characterised as deterministic or random, (chapter 6).

As a first step, a failure mode should be considered, in this case the fracture failure mode. Next step is to estimate all the uncertain parameters and characterise them and assign them with a distribution, which might be deferred in terms of a mean value and a standard deviation. The more accurate this information, the more accurate the results of the analysis.

Fracture analysis consists of several parts. It is better understood in the flow chart of Figure 1.4. The input to the analysis is the loading, the material properties and the crack sizes of the defects. A further input can be the corrosion rates at various parts of the structure. Inspection interval and quality is also input in the analysis. A failure criterion must also be selected, namely a way to describe when failure occurs.

Results are obtained from the reliability method that is used, i.e. from the central box in the flow chart. Reliability analysis for complicated structural systems is difficult to carry out using other method than a simulation. Hence, the proposed method here is to

perform a time history simulation, which considers all the individual members of the system. A better description of the simulation method follows in the next chapter and a more detailed description of the analysis is given in chapter 6.

- *Material Properties.* Tensile and yield strength and fracture toughness are required for the fracture assessment. Paris' constants C and m for the fatigue crack growth. Stress threshold values may also be used in crack growth. Material property data is usually obtained from tests on laboratory specimens.

- *Loading.* Cyclic stress ranges due to global bending and shear and local dynamic wave pressure forces, are necessary for fatigue crack propagation. Extreme stresses for fracture assessment. The best possible way to obtain information on loading is to measure the actual stresses on the ship by on-board instrumentation and deduce the stress history of the structure. However, in most cases and certainly for older vessels, there is no equipment on board to measure actual stresses. In this case a spectral method may be employed to determine the stress history taking into account the ship's operational profile, i.e. sea route and probable sea states that it will face. In addition to the above loading, other loads may be required. Especially for fracture assessment, still water bending stresses are important which give rise to the total maximum stress. Residual stresses from welding are also important, especially the tensile part of them which, because of the high magnitude (very close to the yield stress), add to the total maximum stress and can facilitate fracture.

- *Corrosion.* Corrosion rates are necessary to model the effect of corrosion on fatigue crack growth rates. Corrosion rates are usually obtained from measurements but a certain degree of variability may be allowed. There is some data for oil tankers, but no enough data for bulk carriers.

- *Initial Defect Sizes.* Because of the large amount of welded connections and joints in ship structures, defects are very likely to be present even from the fabrication stage. The size, frequency and location of these cracks depend on welding procedure, quality and type. The mean value and variability of the crack sizes can largely affect the result of the reliability analysis. It is important to know, for

system effects, the number of defects per meter of weld. In a ship with many kilometres of welds, hundreds or thousands of defects may be present even before the ship enters service.

- *Fatigue crack propagation.* Fracture assessment requires a time dependent analysis of the crack growth of initial defects with respect to time. Crack sizes increase with time because of the repetitive cyclic loading due to waves. Fatigue crack propagation analysis is able to determine the crack sizes with respect to time. A crack growth equation is required, the simplest of which is Paris' law. More advanced forms exist but the complexities involved make their use very restrictive and only valid when enough data is available. Corrosion effects are introduced here. Stress intensity factors (SIF) are needed for the geometries involved. For simple geometries SIF solutions are readily available in handbooks. For more complicated geometric configuration subjected to complex loading the use of finite elements is necessary. There are many techniques available to determine SIF either using FE or other analytical solutions (e.g. weight functions).

- *Fracture assessment using reliability method (simulation).* A means of assessing failure is necessary. The current practise adopts the criterion for failure based on the Central Electricity Generating Board (CEGB) R6 diagram based on the strip-yield (Dugdale solution) model. Failure occurs between two limiting conditions: plastic collapse and brittle fracture. A British Standards document, PD 6493 (referenced in chapter 4), uses this criterion to assess failure of flaws in welded structures. Required parameters include,

    - Extreme stresses, due to bending, shear, dynamic wave pressure
    - Residual stresses
    - Still water bending stresses
    - Defect size
    - Fracture toughness

- Plastic capacity

- *Inspection.* Inspection is considered in detail in 6.4

For the reliability analysis statistical information of all the uncertain parameters is needed in the form of a probability distribution with a mean and a standard deviation value. Simulation techniques are then used to determine the probability of failure of the structure. A simulation analysis would generate random samples from the probability distribution of each random variable, and use this sample in the failure criterion. Normally, this requires a big sample size. In the simplest simulation method, the probability of failure is equal to the number of times the structure failed over the total sample size, assuming the sample size is large enough. The matter of course is complicated when a system is considered. Here, further examination is needed to understand when a system fails (chapter 2 has more on system failure definition). In chapter 7 all the assumptions for a reliability analysis of a bulk carrier are discussed and a methodology is described of how to include in the analysis the thousands of defects that are present in the structure. From the results of the analysis, decision making on inspection scheduling is then possible.

REFERENCES

- "Defect assessment in offshore structures- Procedure and commentary", Glasgow Marine Technology center report, 1992.
- A.S. Tetelman, "Fracture of structural materials", 1967
- ABS, 'Guide for dynamic based design and evaluation of bulk carrier structures', March 1995
- Barsom J. M. , Rolfe S. T. , 'Fracture and fatigue control in structures', Prentice Hall, 1977
- Bea R., Cramer E., Schulte-Strauthaus R., Mayoss R., Gallion K., Ma K., Holzman R., Demsetz L., 'Ship's maintenance project', phase 1, SSC 386 report, 1995
- Bea R., Xu T., Ma K., Schulte-Strauthaus R., 'Ship's maintenance project', phase 2 & 3, SSC 395 report, 1997
- Bishop T., 'Fatigue and the Comet disasters', Metal progress, p. 75, May 1955
- Brooking M., Barltrop N., 'Ship structural management for improved safety', RINA Transactions on 'Tankers & Bulk Carriers – The way ahead', 1992
- Connoly M, Hudak S, "A simple reliability model for the fatigue failure of repairable offshore structures", Fatigue & Fracture of Engineering Materials & Structures, Vol. 16, No. 2, pp. 137-150, 1993
- Dalane J. I., Skjong R., Lotsberg I., 'Optimal fatigue design of offshore structures', Proceedings of OMAE, 1990
- Faber M. H., 'Risk based inspection – The framework', Workshop on Risk and Reliability based inspection planning, Zurich, Switzerland, December 2000
- Faber M. H., Sorensen J. D., Kroon I. B., 'Optimal inspection strategies for offshore structural systems', Proceedings of OMAE, Calgary 1992

- Farrington K., 'Shipwrecks', Parkgate Books, 2000

- Florentino S., 'Optimal inspection scheduling methodology for fixed offshore structures basen on reliability analysis', Proceedings of OMAE, 1998

- Fujimoto Y., Sung C. K., Shintaka E., 'Sensitivity analysis on fatigue reliability and inspection of ship structural members', Proceedings of ISOPE, May 1997

- Griffith A. A., 'The phenomena of rupture and flow in solids', Philosophical Transcactions, Series A, Vol. 221, pp. 163-198, 1920

- Guedes Soares C., Garbatov Y., 'Fatigue reliability of the ship hull girder accounting for inspection and repair', Reliability Engineering and System Safety 51, 1996

- Guedes Soares C., Garbatov Y., 'Reliability of corrosion protected and maintained ship hulls subjected to corrosion and fatigue', Journal of Ship Research, Vol. 43, No. 2, pp. 65-78, June 1999

- Huang X, Hancock W J, "A reliability analysis of fatigue crack growth under random loading", Fracture engineering of materials & structures, vol.12, No 3, 1989, pp247-258.

- Huang X., Hancock J. W., 'A reliability analysis of fatigue crack growth under random loading', Fatigue and Fracture of Engineering Materials & Structures, Vol. 12, No. 3 pp. 247-258, 1989

- Irwin G. R., 'Analysis of stresses and strains near the end of a crack transversing a plate', Transactions ASME, Journal of Applied Mechanics, Vol. 24, pp. 361-364,1957

- Irwin G. R., 'Fracture Dynamics', Fracturing of Metals, American Society for Metals, Cleveland, pp. 147-166, 1948

- Jiao G., 'Reliability analysis of crack growth with inspection planning', Proceedings of OMAE, Vol. 2, 1992

- Kozin F, Bogdanoff J L, "A critical analysis of some probabilistic models for fatigue crack growth", Engineering fracture mechanics, vol. 14, 1981, pp59-89.

- Lacey P., Chen H., 'Improved passage planning using weather forecasting, maneuvering guidance and instrument feedback', Presented in SNAME meeting (Los Angeles section), November 1993

- Lotsberg I., Sigurdsson G., Wold P. T., 'Probabilistic inspection planning of the Asgard A FPSO hull structure with respect to fatigue', Proceedings, Offshore Mechanics and Arctic Engineering Conference, Newfoundland Canada, 1999

- M.H. Faber, J.D. Sorensen 'Aspects of inspection planning – Quality and quantity', Proceedings, ICASP 8, pp. 739-746, Sydney, Australia 1999

- Madsen H O, Tallin A, "Probabilistic updating of fatigue crack growth reliability", ASCE fall meeting, Boston, Mass., Oct. 1986.

- Moan T., 'The progressive structural failure of the Alexander L. Kielland platform', In Case Histories in Offshore Structures, Edited by G. G. .Maier, International Centre for Mechanical Sciences, Springer, 1985

- Moan T., Song R., 'Implication of inspection updating on system fatigue reliability of offshore structures', Proceedings of OMAE, Portugal 1998

- MTD Ltd., 'Probability based fatigue inspection planning", Report 92/100, 1992.

- MV Derbyshire Surveys, UK/EC Assessor's Report, DETR, 1998

- NRC, Symposium and Workshop on, 'Prevention of fracture in ship structures', Ship Structure Committee, SR-1363, February 1997

- Oakley A., Brown M., Barltrop N. D. P., 'Optimised inspection scheduling for offshore structures a probabilistic approach', BOSS 1994

- Parker,A.P. "The mechanics of fracture and fatigue" E.& F.N. SPON LTD, 1981

- Pegg N. G., Orisamolu I. R., Stredulinsky D. C., 'Fatigue reliability methods for ship structures', Proceedings of OMAE, Vol. 2, 1992

- Rice J. R., 'A path independent integral and the approximate analysis of strain concentration by notches and cracks', Transactions ASME, Journal of Applied Mechanics, Vol. 35, pp. 379-386, 1968

- Sagrilo L.V.S., deLima E.C.P., Henriques C.C.D., Rodriguez S.G.H., 'Using structural reliability analysis in inspection planning of offshore structures', Proceedings of the International Offshore and Polar Engineering, Vol. 4, pp. 174-178, 1997

- Schulte-Strauthaus R., 'Fatigue database development and analysis', Report No. SMP 1-1, Dept. of Naval Architecture, University of Berkeley, 1991

- Shetty K. N., Baker M. J., "Fatigue reliability of tubular joints in offshore structures: reliability analysis", Proceedings of OMAE, pp231-239, 1990

- Shetty K. N., Baker M. J., "Fatigue reliability of tubular joints in offshore structures: fatigue loading", Proceedings of OMAE, pp33-40, 1990

- Sigurdsson G. Torhaug R., 'Discussion of the fatigue crack model used as decision basis for probabilistic inspection planning', Journal of OMAE, May 1995

- Sucharski D., 'Crude oil tanker hull structure fracturing: An operator's perspective', in Prevention of Fracture in Ship Structure, NRC 1997

- Tait & Garret, "Fracture and fracture mechanics case studies", 1984

- Tanker Structure Co-operative Forum, 'Condition evaluation and maintenance of tanker structures',Whitherby, 1992

- Thayamballi A., Chen Y. K., Donald L., 'Fracture mechanics based assessment of fatigue reliability in ship structures', SNAME, in Ship Structures Symposium 1984

- USCG, 'Report on the TAPS tanker structural failure study', June 1990

- Westergaard H. M., 'Bearing pressures and cracks', Transactions of ASME, Journal Applied Mechanics, Vol. 6, pp. 49-53, 1939

- Wirsching, P. H., Chen, Y. N., 'Fracture mechanics fatigue model in a reliability formal', Proceedings of OMAE, Vol. 3, 1987

- Wirsching, P.H., "Reliability in Welded Joints of Offshore Structures", Offshore Technology Conference, OTC, 1979

- Wirsching, P.H., Chen, Y-N., "Considerations of Probability - Based Fatigue Design for Marine Structures" Journal Marine Structures, vol. 1, No. 1, 1988

- Zhao W., 'Reliability analysis of fatigue and fracture under random loading', PhD Thesis, Dept. of Civil Eng., Imperial College London, 1989

TYPICAL DEFECTS TYPES

Item	*Corrosion*	*Buckling*	*Cracks*
Longitudinal Material	– *Upper deck plating.* – *Upper deck longitudinals.* – *Weldment between structural elements, deck longitudinals to deck plating in particular. Scallops and openings for drainage.* – *Webs of longitudinals on longitudinal bulkheads, longitudinals, high rates and localized corrosion (grooving).* – *Flanges of bottom longs, pitting.* – *Bottom plating, pitting, erosion near suctions.* – *Longitudinal bulkhead plating (Rel. thin).*	– *Upper deck plating.* – *Upper deck longitudinals.* – *Bottom plating.* – *Bottom longitudinals.* – *Longitudinal Bulkhead plating middle and upper part.* – *Deck and bottom girders.*	– *At discontinuities.* – *At openings, notches.* – *At connections with transverse elements.*
Transverse Web Frames	– *Upper part, connection to deck.* – *Just below top coating.* – *Flanges of bottom transverses.*	– *Web plate (Shear).* – *Brackets.* – *Flanges.* – *Cross ties*	– *Connections with longitudinal elements.* – *Scallops in connection with longitudinals.* – *Bracket toes.* – *Holes and openings.* – *Crossing face flats.*
Transverse Bulkheads	– *Upper part, connection to deck.* – *Stringer webs.* – *Close to openings in stringers.* – *High stress locations, i.e. around bracket toes etc.*	– *Horizontal stringers, web plate (Shear).* – *Girder/stringer brackets.* – *Vertical girders, web plate (Shear).* – *Corrugated bulkhead plate.*	– *Connections with longitudinal elements.* – *Connection between girder systems.* – *Bracket toes.*
Swash Bulkheads	– *Upper part, connection to deck.* – *Stringer webs.* – *Close to openings in bulkhead plating.* – *High stress locations, i.e. around bracket toes.*	– *Horizontal stringers, web plate (Shear).* – *Vertical girders, web plate (Shear).* – *Girder/stringer brackets.* – *Bulkhead plating around openings.*	– *Connections with longitudinal elements.* – *Connections between girder systems.* – *Bracket toes.* – *At openings in bulkhead plating.*

Table 1.1 – *Locations susceptible to fatigue, corrosion and buckling damage* (Tanker Structure Co-operative Forum)

RISK OF CORROSION AND PITTING

Type of Tank	Fully Coated	Upper Part Coated	Upper + Lower Part	Anodes	None
Segregated Ballast	L	H+	H+	M-H	1) H++
Cargo/Clean Ballast (Arrival Ballast)	Lp	H	Hp	M	2) H+
Cargo/Dirty Ballast (Departure Ballast)	Lp	M	Mp	M-L	M-H
Cargo/Heavy Ballast	(L)	L	L	X	L-M
Cargo Only	X	L-	L-	X	L

H = High Risk H+ = Higher Risk X = Not Considered
M = Medium Risk
L = Low Risk L- = Lower Risk () = Negligible
p = Risk of Pittings

NOTES

1) *Especially exposed items:*
   - *Horizontal stringers.*
   - *Longitudinals on longitudinal bulkhead.*
   - *Longitudinal bulkhead plating.*
   - *Web frames upper part and close to longitudinal bulkheads.*
   - *Cross ties.*
   - *Transverse bulkhead plating, upper part.*

2) *Exposed to pitting:*
   - *Horizontal surface of stringers.*
   - *Bottom plating.*
   - *Bottom longitudinal face plates/flanges*

3) *Other factors contributing to the risk of corrosion:*
   - *Neighbouring tanks heated.*
   - *Local coating faults due to poor workmanship.*
   - *Unfavourable structural details from coating point of view.*
   - *High local stress areas (See Figure 3.1).*
   - *Areas with high flow rate, i.e. around openings, notches etc (see Figure 3.2).*
   - *Drip locations of cleaning guns.*

Table 1.2 – *Locations with risk of corrosion* (Tanker Structure Co-operative Forum)

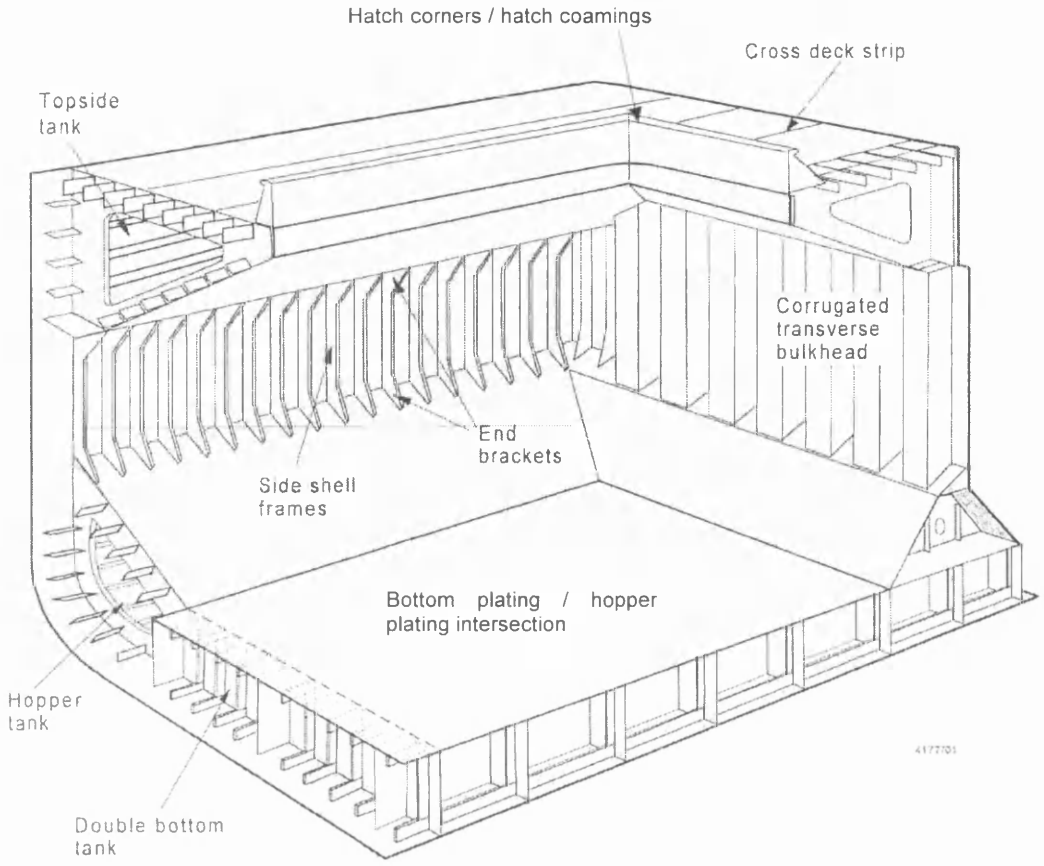

Figure 1.1 - *Crack locations in bulk carriers (ABS)*

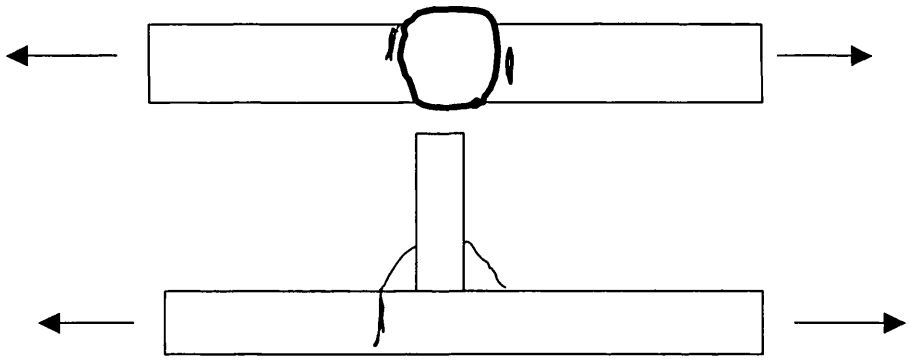

a) Transversely loaded welds

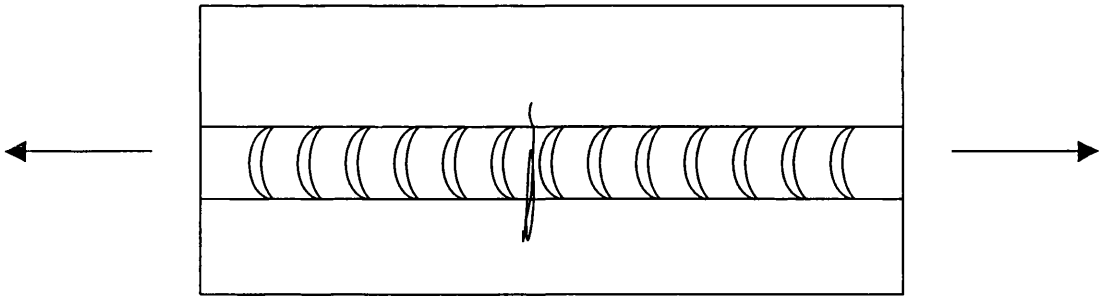

b) Longitudinally loaded weld (butt weld)

Figure 1.2 – *Initiation sites at fully penetrated welds*

a)

b)

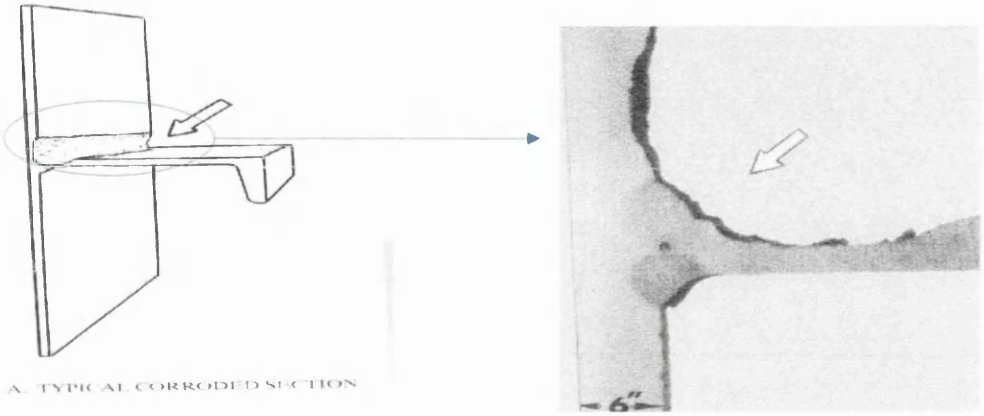

c)

Figure 1.3 – *Examples of corrosion forms* (Tanker Structure Co-operative Forum)

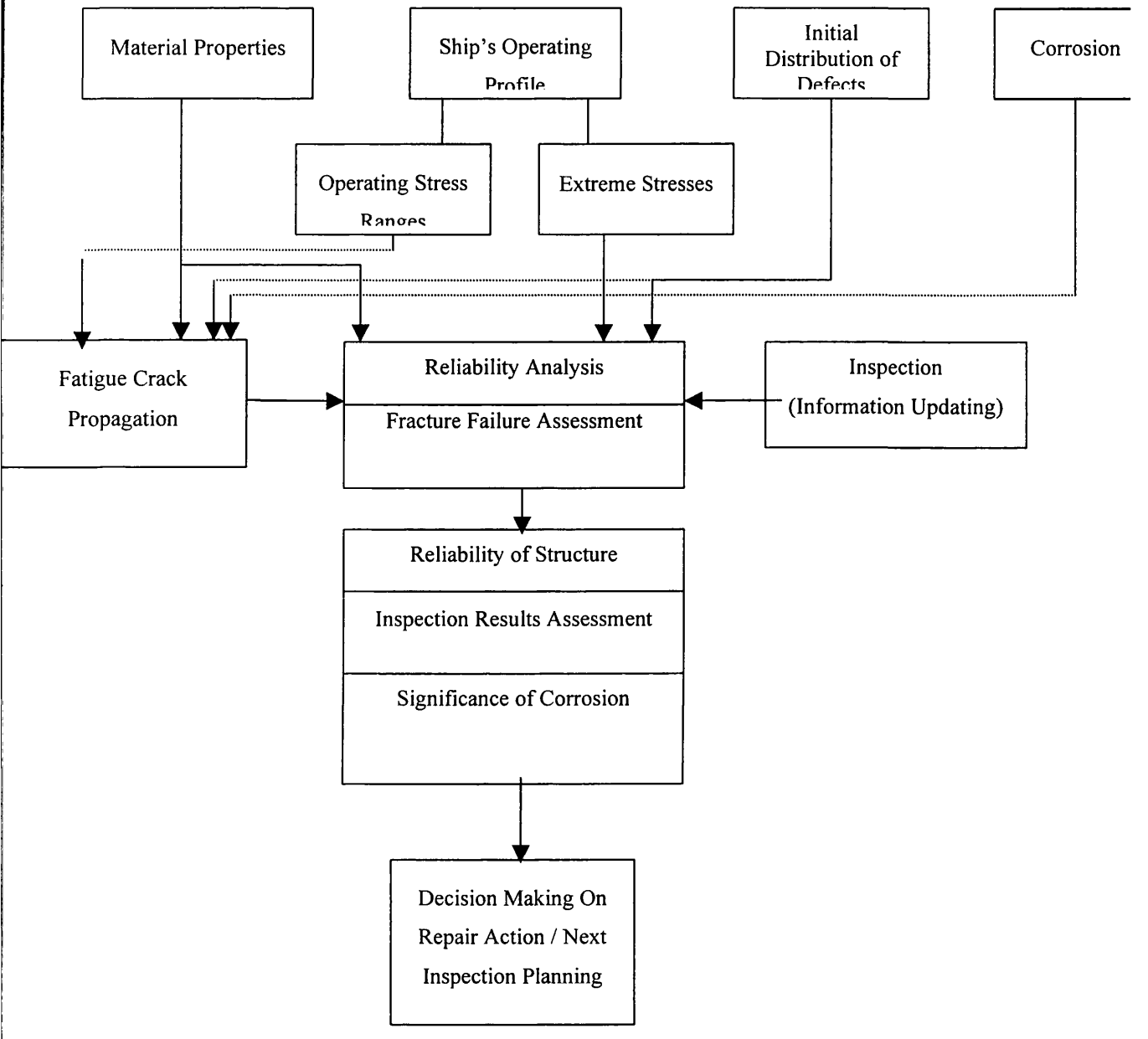

Figure 1.4 – *Flow chart of probabilistic fracture assessment*

CHAPTER 2

THE RELIABILITY APPROACH IN ENGINEERING DESIGN

2.1 Engineering and Risk

The engineering profession has a very challenging task: To design and build what has not existed before. From the very ancient periods up to the current time, engineers design and build systems that have not existed previously. One other responsibility of the engineers is to ensure the safety and function of their creations. However, the latter is generally a difficult problem particularly in engineering systems. A proof of that is the many failures of engineering systems throughout history, (buildings, bridges, ships, aeroplanes, spaceships are some typical examples of engineering systems that have failed to perform for various reasons). It is not wrong to assume that there is an inherent risk associated with every engineering system.

The primary cause of this risk is the lack of information during the design of engineering systems. This lack of information is transformed into uncertainty during design, consequently a risk of unacceptable performance is always possible. Under this condition of uncertainty it is not practically or economically possible to design an absolute safe system.

This risk can be associated with different things. For engineering structures, it is possible that this risk is associated with a failure. A collapsed building for example because of inadequate strength fails into this category (i.e. uncertainty in strength). A ship structure or a bridge failure because of extreme environmental loading (i.e. uncertainty in loading) is another example. In many instances such failures result in very serious consequences, which include environmental catastrophes, loss of structure even loss of lives.

In other instances the risk is associated with unacceptable service from engineering systems. Traffic system failure for example, does not mean loss of any structure, but can result in serious traffic chaos, which consequently may have an impact on human life and economy. Failure of an electric supply system affects the supply of a particular good, and when the supply is less than the demand, there is a problem.

2.1.1 Types of Uncertainty

In reality, every physical quantity is associated with a degree of uncertainty. In engineering structures for example, actual stresses are not known since they are not measured, deflections are rarely recorded, and actual strength cannot be determined since it cannot be measured without destroying the structure. But uncertainty does not only exist in physical quantities. Mathematical models possess also uncertainty, when they cannot describe reality exactly.

As a general reason of uncertainty we can consider the physical variability of the underlying quantity. Physical variability is associated with the variability that governs physical quantities such as loading, material properties and dimensions. Physical uncertainty can be quantified only by collection of data, i.e. measurements of actual values and using probability distributions to describe the data. This in effect gives rise to the first type of uncertainty.

1. *Statistical uncertainty*: This type of uncertainty arises because of limited amount of data and information. When data is collected, there is an attempt to find an appropriate probability distribution to describe it. But with a limited amount of data (often historic rather than future data) such a task unavoidably introduces uncertainty.

2. *Modelling uncertainty:* Engineering makes use of mathematical models that relate physical quantities one to each other, (stresses and deflections to bending moments, force to strain, for example). These models may have been developed from good understanding of the actual process or from experimental results and hence empirical formulas. Except in very few cases, it is very difficult to predict the response of a system to an input, hence there is a source of uncertainty because of modelling.

2.2 The Need for Reliability Approach

There is no dispute for the need of reliable products. We have all faced problems when things become unreliable or 'break down' like TV sets and cars. It is even more

serious when unreliable products cause big economic losses to organisations like airlines when planes are withdrawn from service for repairs and to shipping companies when ships are dry-docked for repairs. Even more serious considerations would be the loss of lives because of unreliable engineering systems.

The basic formulation of the problem can be deduced in a problem of 'demand' and 'supply'. For example in a service, if the supply is greater than the demand there is no problem. It is the same concept that applies in engineering as well. When the strength (capacity or supply) of a structure is greater than the load (demand) the structure is safe. Reliability is a measure of the ability of the structure to perform its intended function. Or in a more pessimistic way - the probability of not achieving the intended function.

Traditionally, because of the various uncertainties present (see 2.1.1), the reliability of the structure, if we limit the discussion to only engineering structures hence structural reliability, was achieved by the use of a safety 'margin' or 'factor', and adopting conservative estimates of important parameters such as load and strength. This is the so-called 'deterministic' approach. The traditional approach has worked reasonable well in the past, and is widely used mainly because of its simplicity and the ability to be adopted into codes, especially from classification societies. Safety factors can significantly vary between structures (buildings, ships, aeroplanes) and are usually determined from experience.

However, in today's very competitive environment there is a need for better use of resources (materials, workforce, and money) and more reliable, economic and efficient structures. As we mentioned earlier, safety is a 'supply' and 'demand' problem. When the supply is greater than the demand the structure is safe but not necessarily economic. To produce an economic structure, supply must not exceed too much demand i.e. use to large safety factors, but the supply (strength) must be close to demand (load) and at the same time must remain greater all the time. And it is the latter that causes the risk of a failure, since it is difficult to quantify the load without some degree of uncertainty.

Reliability approach is not different from the traditional approach, since in both methods the same uncertainties apply. However, reliability approach makes use of all the information available (in form of probability distribution of important parameters) and yield better estimates for the strength and load. Hence, a reduction in safety margin may be possible in case of a very low risk of failure, (i.e. more cost efficient structure because of less material used), or a better designed and strengthened structure if the probability of failure is not acceptable.

Probability of failure is a ratio, with a maximum value of one and a lowest value of zero. Quantifying what is an acceptable risk of failure is not an easy task, especially when loss of lives is possible. It all depends in finding a balance between economics and safety. Again the 'target reliability' varies between structures, the more serious the potential disaster the lower the target reliability value would be. For example nuclear reactors will have a lower probability of failure target value than ships.

Reliability analysis is capable of evaluating the time varying probability of failure of a structure. This is particularly important for structures where reliability is reducing with time because of structural degradation (e.g. a ship structure because of fatigue cracks, corrosion and ageing). By estimating the reliability of the structure with time it is possible to estimate optimum inspection and repair plans, which will make sure that the structure remains safe throughout its operational life. This concept was described in 1.5.3 and is used in this thesis to analyse the reliability of a bulk carrier susceptible to fatigue crack growth and corrosion. It would not be possible to do the same using a deterministic approach since it does not account for the variability and uncertainties of the various parameters.

Another important feature of reliability is that it updates results according to available information (e.g. during inspections when crack size and corrosion measurements are taken, and loading information from stress and strain gauges). Reliability makes use of this information and updates the initial estimates for a better and refined solution. In a reliability analysis the better the information the more 'reliable' the estimates.

These estimates however, only represent the belief of the engineer in the structure fulfilling its purpose. It is not an absolute measure and must be used with care and

consideration. A good application of reliability analysis would be to calibrate existing safety factors to obtain more uniform reliability over a wide range of coefficients. Nevertheless, the trend of these results is more important than the absolute values, and their correct interpretation is certainly to benefit the operational efficiency of the structure and probably the design of future structures.

2.3 Structural Reliability and Methods of Estimation

Most engineering systems, mechanical, electronic or electrical tend to deteriorate with time because of excessive use, temperature or chemical changes, overloading, fatigue and other reasons, and eventually fail. Structural systems on the other hand, deteriorate mainly due to fatigue and corrosion only, and in some cases even become stronger (concrete structures for example).

The reason why structures fail is the application of an extreme load, which exceeds the resistance of the structure and leads to failure. Failure can of course have various modes i.e. routes which to follow (also see section 1.3.1). In engineering structures the most important modes of failure are,

- Yielding, when applied stress exceeds yielding capacity
- Buckling, due to structural instability
- Fatigue, which leads to fracture when a crack has reached critical dimensions

It is therefore important to recognise the failure mode and establish a mathematical model which best describes it. The mathematical model is called the '*Limit State Function*' and relates the load and the strength/resistance parameters, i.e. the basic variables. Reliability analysis then determines a measure of the probability of the load to exceed the strength and hence the structure failing. As discussed in 2.2 the reliability is not a physical property and is only what the engineers believe for the risk associated with the structure.

2.3.1 The Basic Problem (Convolution Integral Method)

Structural reliability has to deal with load and strength parameters. The problem in structural reliability is very basic and deals with only two parameters: The Load (or Supply) and the Strength (or Resistance or Capacity). The probability of failure (P_f) is then defined as, 'The probability (P) of the load (L) exceeding the strength (R)', (Thoft-Christensen & Baker 1982). This can be written as

$$P_f = P(R \leq L) \qquad 2.1$$

The limit state function (G) is then written as

$$G = R - L \qquad 2.2$$

If each is described by a known probability density function (p.d.f.), (which must have the same units), then a measure of the probability of failure can be found. Let $f_L(x)$ be the p.d.f of the load, and $f_R(x)$ the p.d.f of the strength, the two distributions are seen in Figure 2.1. The probability of failure is estimated from the integration of the *joint probability density function* of the load and the resistance, over the failure region, i.e. (R < L)

$$P_f = \int\int f_{RL}(R,L)dR,dL \qquad 2.3$$

which accounts for all the combinations of the load being higher than the strength.

Generally the joint p.d.f is very difficult to estimate, but for statistically independent variables

$$f_x(x_1 \ldots x_n) = f(x_1) \cdot f(x_2) \cdot \ldots \cdot f(x_n) \qquad 2.4$$

where $f_x(x_1 \ldots x_n)$ is the joint p.d.f. of all the variables and $f(x)$ is the individual p.d.f. of each variable.

Hence equation 2.3 can be written as

$$P_f = \int\int f_R(R) \cdot f_L(L)dRdL \qquad 2.5$$

This needs to be integrated over the entire region that load and strength can take values. Namely

$$P_f = \int_0^{\infty} \int_0^{L>S} f_R(R) f_L(L) dR dL \qquad 2.6$$

The lower limit is zero since there is no physical meaning for negative strength and load. This however can introduce some errors if load and strength are modelled with a distribution which takes negative values. This is not an error associated with the method though.

The cumulative probability function of a variable X is given by

$$F_x(x) = P(X \le x^*) = \int_0^{x^*} f_x(x) dx \qquad 2.7$$

Equation 2.6 can then be written as

$$P_f = \int_0^{\infty} F_R(x) f_L(x) dx \qquad 2.8$$

Equation 2.8 is known as the '*Convolution Integral*', and gives the failure probability of the load exceeding the strength, (Melchers 1987). All possible events are considered:

The cumulative probability function of the strength describes the probability of the strength being less than some value x. The p.d.f. of the load represents the probability of the load in the interval $x+dx$. Hence, by considering all possible values of x, the failure probability is estimated, (Figure 2.2)

2.3.2 Methods of Reliability Estimation

Unfortunately, not every problem can be described by only two variables, as in the case described above. Limit state functions can be very complicated, depending on the nature of the problem. Many problems do have more than one limit states, which then need to be treated as a system. For cases where the limit state function cannot be

reduced in the basic problem i.e. in the load and strength variables, there are other methods to calculate the failure probability. There are numerous reference books available that describe in detail these methods (Thoft-Christensen 1982, Melchers 1987 and 1999, Madsen 1986)

In general the probability of failure, given a limit state function $G(\boldsymbol{x})$ where $\boldsymbol{x}$ is a vlector of the basic variables that constitute the limit state function, is given by

$$P_f = \int \cdots \int f_{x_1, x_2, \ldots x_n}(x_1, x_2, \ldots, x_n) dx_1, dx_2, \ldots, dx_n \qquad 2.9$$

with $f_{x_1, x_2, \ldots x_n}(x_1, x_2, \ldots, x_n)$ being the joint probability density function and $x_1, x_2, \ldots, x_n$ the vector of the basic variables of the limit state function.

The integral of equation 2.9 is very difficult to solve, and as stated earlier it is even more difficult to determine the joint p.d.f. and it requires information about the correlation coefficients between the basic variables. There are however methods available to determine the failure probability without the need to perform the integration.

Briefly, the most common methods are described below, with more emphasis given to the method used in this thesis, the simulation method which is described in section 2.4. Reliability methods are generally classified as level 1, 2, 3, and 4.

2.3.2.1 The First Moment Method or Level 1

This is also called the traditional approach, and the method is based on the concept of the safety factor. Safety is achieved by estimation of the safety factor which will allow a safety margin between the load and the strength of the structure. The safety factor is defined as

$$SF = \frac{L}{R} \qquad 2.10$$

Because uncertainties in the load and strength parameters are not considered at all, the results may be very conservative, which frequently leads to expensive and inefficient

designs. On the other hand, its simplicity makes it easy to adapt to codes and it is the preferred method of codes of practice and classification societies.

Safety factors are usually bigger than one (SF > 1), and they are usually determined from experience, and judgement of the engineer. The last decade however, increasingly, safety factors are based on some results of reliability analysis during the code development stage.

2.3.2.2 Second Moment Methods or Level 2

In this method use is made of the statistical properties of the basic variables. In particular the first and second moments are used i.e. the mean and variance. Under Level 2 methods there are a lot of variations, with some more sophisticated methods. Two of these methods will be described as more representative.

a. The First Order Second Moment (FOSM)

In this method the mean and variance of the limit state function *G(x)* are estimated. Use is made of the Taylor series expansion of *G(x)* about the mean of the basic variables and considering only the linear terms. This gives an estimate of the mean of *G(x)* and the variance as

$$\overline{G}(x) = g(\overline{x}_1,\ldots,\overline{x}_n), \text{ (mean)} \qquad 2.11$$

$$\sigma^2_{\overline{G}(x)} \cong \left[\sum_{i=1}^{n}\sigma^2_{xi}\left(\frac{\partial G(x)}{\partial x_i}\right)^2\right], \text{ (variance of independent parameters)} \qquad 2.12$$

The partial derivatives in equation 2.12 are evaluated at the mean of *G(x)*. When the mean and variance of the limit state function are known, a reliability index is calculated from

$$\beta = \frac{\overline{G}(x)}{\sigma_{G(x)}} \qquad 2.13$$

If all the variables of *G(x)* are normally distributed, hence *G(x)* itself is normally distributed, the probability of failure is given by

$$Pf = 1 - \Phi(\beta) \qquad 2.14$$

where Φ is the cumulative probability function of the standard normal variate and its values are tabulated.

A significant weakness of this method lies in the linearization of *G(x)*. When *G(x)* is not a linear function significant errors occur. The errors occur because linearization is done about the mean of *G(x)* which may not lie close to the failure surface. An additional disadvantage occurs from the fact that the reliability index depends on the form of the *G(x)* so even when the same function is expressed in a different way, i.e. mathematically different form of the same function, the reliability index will be different.

b. The Advanced First Order Second Moment (AFOSM)

This is an improvement to FOSM which addresses its disadvantages. In this method linearization takes place not at the mean but at a point called 'design point' which is on the failure surface. All the basic variables are transformed to standard variables and the calculation is done in a normalized coordinate system. In the new coordinate system, the shortest distance from the failure surface to the origin represents the reliability index β.

The calculation of β can be done in several ways, but generally, an iterative method is used, (Thoft-Christensen 1982). With this method, the problem of not all variables being normally distributed is solved, by using equivalent normal distributions.

The only disadvantage of the method is the complex equations that are used and that the partial derivatives that are required for the iterative solution of the method. Furthermore, when the number of the variables increase, so does the number of iterations necessary for convergence. There is also the possibility that convergence is not achieved if the limit state function is too irregular and its behavior in the vicinity

of the origin has many local minima. The solution is only exact when the limit state function is linear.

The advantages include good accuracy and that it does not use information about the probability distribution of the variables.

2.3.2.3 The Second Order Method (SORM) or Level 3

In this method the failure surface is represented by a second order curve and not a linear curve as in FORM. This however complicates further the analysis, since it is necessary to evaluate the eigenvalues of the second order derivative matrix. The calculation of the second order derivative matrix requires time and can introduce errors into the analysis, (Melchers 1987 and 1999)

2.3.2.4 Using FORM and SORM for Fracture Assessment

The fracture assessment of bulk carriers includes many analyses, as it was discussed in chapter 1. FORM and SORM could be used to perform the reliability analysis, but they would have to be incorporated in the total analysis as a separate part. The nature of the limit state function, as it will be shown in chapter 4, is very irregular and both methods would have problems of convergence. This was verified when two general purpose reliability packages where used to calculate an example case using the limit state function for fracture assessment, (CALREL, and STRUREL). FORM and SORM failed in both codes. However, the simulation method worked well in both codes and produced similar results, albeit it needed a lot of time. However, this proved that simulation techniques are the only method currently available to deal with very complicated analysis, (and for this reason they were chosen in this thesis).

The other factor that complicates even further the analysis apart from the complex limit state function, is the time varying nature of the problem, as it was again discussed in chapter 1. Crack size, which is an important input parameter to the analysis, varies with time (cracks grow under fatigue loading with respect to time). The mean value and variance (i.e. the first and second moments of the probability distribution which are used by FORM and SORM) of the crack size distribution are

both varying with time. Their estimation can only be done by performing a separate simulation analysis, since the crack size distribution is very difficult to describe with time (i.e. find a known distribution that fits the data well) and hence determine its mean value and variance, (see section 7.5).

Using simulation methods, all separate parts of the fracture analysis are treated in one big simulation process (see chapter 7), which simplifies the analysis (although the simulation process is quite complex). For this reason, a reliability code was written as part of this thesis, which deals with the time varying nature of the analysis.

2.3.2.5 The Fully Probabilistic Approach or Level 4

This method is 'exact' since it uses the joint p.d.f. to evaluate the probability of failure. Integration of equation 2.9 can be done either analytically if a close form solution exists and the joint p.d.f. is known (a rare case), or numerically using simulation techniques.

Simulation techniques will be discussed in the next section in more detail, since they will be used in this thesis to conduct reliability analysis.

2.4 The Simulation Method in Reliability Analysis

In the past limitation in computer speed prohibited the effective use of simulation. But the rapid advances in speed of computers now enables the use of simulation in many engineering fields. Simulation techniques are now very common and widespread and they are used to solve very complex engineering problems which cannot be solved analytically, (Rubinstein 1981, Melchers 1987)

In reliability analysis the simulation technique is associated with the generation of 'random' numbers. Hence, the name 'Monte Carlo' simulation method, because of the association of Monte Carlo the town with the casino and the roulette wheel, one of the simplest ways to generate random numbers.

2.4.1 The Monte Carlo Simulation Method and its Application to Structural Reliability Problems

Monte Carlo simulation is used to generate random numbers and estimate the probability of an event. Its application has three stages:

a. Generation of sample data set (i.e. one set of possible values defining the problem), by generating random numbers. This action is called simulation and is repeated many times

b. Use of sample data set in mathematical model of physical system

c. Statistical analysis of many results sets from the mathematical model, (one for each simulation)

Random numbers are generated for every basic variable of the physical model. In general, random numbers are generated from the uniform distribution with interval [0,1]. There are also many computer codes available to generate 'pseudo' random numbers from the uniform distribution. These are not really random since a mathematical model is used to generate them, and they start repeating themselves in the same order after a number of simulations, which is very big and does not cause any practical problem ($N > 10^{19}$).

This random number is used to create another random number according to a probability distribution. There are many techniques available to generate random numbers according to probability distributions, the most common is the inverse transform technique described in many references, (e.g. Rubinstein 1981), and is the method used in this thesis, because it is the simplest way to introduce correlation in the samples, which is very important for this analysis, (see chapter 7).

Other techniques to generate random numbers according to probability distributions directly are more time efficient and are available as standard subroutines in many computer-programming codes and produce random number directly from a probability distribution (e.g. Fortran).

Every sample data set that is generated is used/substituted into the physical model i.e. the limit state function, $G(x)$. There are only two possible outcomes from the simulation, a fail or a safe state. When $G(x) \leq 0$, this represents the fail state and when $G(x) > 0$, this represents the safe state. By repeating this process many times i.e. simulating it, it is possible to evaluate the probability distribution of $G(x)$.

The probability of failure is then estimated by one of the following methods

a. By fitting a cumulative probability function into the simulated results as shown in Figure 2.3. The probability of failure is then estimated from

$$P_f \approx F_G(G = 0) \qquad 2.15$$

where $F_G(G)$ is the fitted cumulative distribution function. It is also possible to fit several distributions if one does not describe very well the entire data. However, it is most important that the data is fitted well at the region where G becomes negative since that is the failure domain.

b. Using directly the statistics of the simulation process. This in terms of the simulation means counting the number of times the limit state function, G, failed during the simulation. The failure probability is given by

$$P_f = \int \ldots \int I[G(x) \leq 0] f_x(x) dx \qquad 2.16$$

where $f_x(x)$ is the joint p.d.f. and $\mathbf{x}$ is the random variable vector. I[...] is an indicator function which equals 1 if $G(x) \leq 0$ or equals 0 if $G(x) > 0$. From statistics we can estimate the probability of failure as

$$Pf \approx \frac{1}{N} \sum_{i=1}^{N} I[G(x) \leq 0] \qquad 2.17$$

in which the summation part is simply the number of failures encounter during the simulation i.e. number of times that $G(x) \leq 0$. The failure probability is then the ratio of the number of failures over the total number of simulations, N. The number of simulations, N, should be large enough so the volume under the joint

p.d.f. is uniformly sampled, i.e. samples are selected so that to represent completely the underlying joint p.d.f.

However, the results of Monte Carlo simulation greatly depend on the number of simulations and generally the accuracy increases as the number of trials increase. The variance of the results is given by

$$\sigma^2_{I(G(x)\le 0)} = \frac{1}{N-1}\left\{\left(\sum_{i=1}^{N} I^2[G(x)\le 0]\right) - N\left(\frac{1}{N}\sum_{i=1}^{N} I[G(x)\le 0]\right)^2\right\} \quad 2.18$$

It is often desirable to know the number of simulations required to obtain a certain accuracy. Melchers (1987) states that the confidence interval is given by

$$P(-\kappa\sigma < J - \mu < \kappa\sigma) = C \quad 2.19$$

where J is given by 2.17, and μ is the expected value of J ($\mu = E[I(G(x)\le 0)]$), and σ is the standard deviation of J. For C = 95%, $k = 1.96$. However σ is not known in advance. Melchers (1987) suggests that σ be approximated with $(Nqp)^{1/2}$, and μ with (Np), with $q = 1 - p$, and $p = pf$. The error, ε, then in the result would be (with $\varepsilon = (J - Np) / Np$ and substituting it in 2.19)

$$\varepsilon = k \cdot \left[\frac{(1-p)}{Np}\right]^{1/2} \quad 2.20$$

From equation 2.20 we can determine an approximate number of simulation for a given probability level. E.g. for a failure probability of 10^{-4}, and an error of less than 20% (with a confidence interval of 95%, k = 1.96), the number of simulations required is about 960,000.

Monte Carlo simulation has become a very powerful tool in the hands of engineers to help them solve complicated problems. And with the increase in the performance of the computers it is even more attractive. One very strong advantage is its simplicity. It can also tackle any kind of problem even the most irregular and non-linear functions. The main disadvantage is the large required number of simulations for a given probability, which when system effects come into the equation, becomes even more

significant. There are various techniques which try to reduce the variance (variance reduction techniques) and use much less simulations.

2.4.2 Variance Reduction Techniques

The aim of these methods is to reduce the variance of the Monte Carlo estimate using the same amount of simulations or with even less. There are various methods available that can be to reduce the variance of the simulation estimate, for a detailed description there are many references e.g. Rubinstein (1981), Melchers (1987), Ang (1984). The most widely used variance reduction technique is called 'Importance Sampling'.

As the name implies, this method concentrates sampling on the importance region i.e. the region close to the failure surface. However, the shortest distance from the failure surface to the origin (in the transformed co-ordinate system) determines the failure probability. This is called the design point. There are various schemes and search algorithms available to locate the design point.

The probability of failure is estimated by

$$Pf = \int\!\!\ldots\!\int I[G(\mathrm{x}) < 0] \frac{f(\mathrm{x})}{h(\mathrm{x})} h(\mathrm{x}) d(\mathrm{x}) \qquad 2.21$$

where **x** in this equation takes all possible values, some of which lead to failure i.e $G(\mathbf{x})<0$, $h(\mathbf{x})$ is the importance sampling density function, and $f(\mathbf{x})$ is the joint p.d.f. An unbiased estimate of Pf is given by

$$Pf = \frac{1}{N} \sum_{i=1}^{N} I[G(\mathrm{x}) < 0] \frac{f(\mathrm{x})}{h(\mathrm{x})} \qquad 2.22$$

where the sampling vector **x** is generated by uniformly sampling the volume under the importance sampling function $h(\mathbf{x})$.

An attempt was made to use variance reduction techniques to improve the efficiency of the simulation method. That would reduce the number of required simulations. In particular importance sampling was used with an adaptive search algorithm to

determine an approximate design point. However, there are a number of reasons that importance sampling failed to work.

The choice of the importance sampling function generally does not matter much, although some functions will lead to better estimates than others. However, It can be seen from equation 2.22 that information on the joint p.d.f. is required to estimate the failure probability. For an independent system the joint p.d.f. is given by the multiplication of the individual p.d.fs, but for a correlated system the joint p.d.f. is very difficult to estimate. Therefore, it would not be possible to use this technique for fracture assessment reliability calculations and account for correlation between members. The only joint p.d.f. that can be determined analytically is when all variables follow the normal distribution (or lognormal). Unfortunately this is not the case here.

The adaptive search algorithm requires information about the uncertainty of the variables in the form of the type of the probability distribution and the first moments e.g. mean value and standard deviation. It uses this information to locate an approximate design point. The problem arises for time-dependent variables when there is no exact model to describe their variability with time. For example crack size (and hence crack size distribution) varies with time and depends on fatigue loading, crack growth material constants, corrosion and the crack growth model. It is very difficult to find an exact analytical distribution that would describe the uncertainty in crack size with respect to time (the lognormal distribution is used and compared with the actual numerical distribution but is not a good fit, see chapter 7). And although the mean value and standard deviation can easily be found the form of the distribution cannot. The problem can be solved only if a numerical distribution is used. For this reason a separate simulation is needed to obtain the numerical crack size distribution and use it in conjunction with the search algorithm.

When the limit state function is too irregular there is also an additional problem. It is very likely that there are many local minima close to the origin and the search algorithm may fall into a trap, and search for minima which is not the design point.

2.5 Reliability of Structural Systems

Typically structures consist of many components. Each component may fail because of different failure mode than other components. Thus in a complete system, one has to examine all the structural members and the failure modes associated with them. The failure path i.e. the sequence of the various failures of the individual components is also very important to understand. System reliability evaluates the probability of failure of the system by considering all probable modes of failure of all members of the system. System reliability is discussed in detail by Melchers (1987 and 1999) and Madsen (1986)

From the above considerations, there are two important system effects to consider in a system reliability analysis. The first system effect comes from the different modes of failure. Even if only a single component is considered, the various possible failure modes associated with it, require a system approach to assess the risk of failure. The second system effect comes from the multiple components of a system. It may require more than one component to fail before the whole system fails. In this case, the failure path determines the sequence of the failures, which leads to the total failure of the system.

To identify all potential failure modes and their sequence a *fault tree* and *event tree* models are drawn. These are essentially a diagram which in the case of the fault tree, decomposes the main failure mode into unions and intersections of sub-events or combinations of them. The probability of each sub-event can then be calculated as a single failure mode event.

An important question to answer is the following. When does a system fail? There are two cases which could be considered as upper and lower bounds. The first case assumes failure of the system when 'any' of its members fail. This is called a 'weakest link' or series system and it is the lower bound. The second case considers system failure when 'all' members must fail, and is called a parallel system. In reality system failure may be a combination of series and parallel sub-systems. This depends mostly on the failure mode considered.

For example in a ship structure, when considering buckling failure, buckling of a single member (e.g. a stiffener) may not constitute failure of the ship. It might require several components to fail, which may be in series or parallel. On the other hand, a crack that leads to breaking in two or leakage (hence to environment pollution or mixing of cargoes) may be considered a system failure.

Another concern in system reliability analysis is the degree of dependency between variables of different members. Physical parameters between different members of the system may be *correlated* i.e. dependent on each other, and not independent. This is something that needs a lot of consideration when discussing a system. The degree of dependency should also be evaluated i.e. a measure of how strong the dependency or correlation is. Usually, statistical analysis is required to determine the correlation between parameters.

The probability of failure of a system is calculated in the same way as it is done for a single component. However, if more than one member is considered the number of random variables increases, since each member has its own set of random variables. The joint p.d.f. becomes even more complicated and difficult to estimate, and numerical techniques may be the only way to perform the integration. Furthermore, if more than one limit state function is considered, the integration must be carried out over the surface that all possible limit state functions become unsafe i.e. the domain of integration is the entire space where each limit state becomes zero or negative. Generally, for k failure modes and n random variables, the probability of failure is given by

$$Pf = \int \ldots \int f_x(x_1 \ldots x_n) dx_1 \ldots dx_n \quad , G_i(x) \leq 0,\ i=1,2 \ldots k \qquad 2.23$$

It is a very difficult task to perform the integration of equation 2.20, and it is almost impossible to evaluate analytically even when a close form solution exists for the joint p.d.f. When time dependent analysis is also required, the only suitable method to evaluate the integral is the numerical approach, i.e. Monte Carlo simulation, as it will be discussed in chapter 7.

2.5.1 Equation of Failure Probability for a Series System

A series system, as stated earlier, needs any one or more members to fail, for system failure. This type of system has no redundancy and is also known as a 'weakest link' system. The event of a series system of n members failing is given by

$$E_{system} = E_1 \cup E_2 \cup \ldots \cup E_n \qquad 2.24$$

Where $E_1 \ldots E_n$ is the event of a member failing. The symbol $\cup$ denotes the union of the events i.e. in this case the probability of any one or more members failing. The probability of failure of the system is given by

$$P(E_{system}) = P(E_1) \cup P(E_2) \cup \ldots \cup P(E_n) \qquad 2.25$$

When only two events are possible, equation 2.22 can be writen as

$$P(E_{system}) = P(E_1 \cup E_2) = P(E_1) + P(E_2) - P(E_1 \cap E_2) \qquad 2.26$$

Equation 2.23 gives the failure probability of a series system of two members. For more members this expression becomes very complicated and relates the conditional probabilities of all events, (Ang 1984, Ditlevesen 1996). The last term of equation 2.23 requires the knowledge of the conditional probabilities of all the events. This information is rarely available in real systems and is related to the correlation between the variables.

For an independent system equation 2.23 is simplified to

$$P(E_{system}) = P\left(\bigcup_{i=1}^{n} E_i\right) = 1 - P\left(\bigcap_{i=1}^{n} \overline{E}_i\right) = 1 - \prod_{i=1}^{n} (1 - P(E_i)) \qquad 2.27$$

Where $\overline{E}_i$ is called the complementary event i.e. the event that E_i does not occur. For small probability values equation 2.24 may be approximated by

$$P(E_{system}) \approx \sum_{i=1}^{n} P(E_i) \qquad 2.28$$

For positively correlated events, (Ang 1984)

$$P(E_{system}) \leq 1 - \prod_{i=1}^{n}[1 - P(E_i)] \qquad 2.29$$

For negative correlated events

$$P(E_{system}) \geq 1 - \prod_{i=1}^{n}[1 - P(E_i)] \qquad 2.30$$

Equation 2.26 is then a lower bound of the failure probability of a series system, and equation 2.27 an upper bound. Equation 2.26 also indicates that the failure probability of a positively correlated system is less than the failure probability of an independent system. This is a subject of study for chapter 7, where results from the simulation method are presented, and the effect of correlation in the system is studied. In chapter 7, the results from the simulation method for an independent system are also verified with equation 2.24, which can be used as a means to check the simulation results.

REFERENCES

- Ang A. H. S., Tang W. H., 'Probability concepts in engineering planning and design', Vol. 1, John Wiley, 1975

- Ang A. H. S., Tang W. H., 'Probability concepts in engineering planning and design', Vol. 2, John Wiley, 1984

- Chang P. Y., 'A state of the art review of the reliability approach and methodology for the design of aerospace and ocean systems', Marine Technology, Vol. 27, No. 5, September 1990

- Ditlevesen O., Madsen H. O., 'Structural reliability methods', Chichester, John Wiley & Sons, 1996

- Madsen M. J., Krenk S., Lind N. C., 'Methods of structural safety', Prentice Hall, 1986

- Melchers R. E., 'Structural reliability analysis and prediction', Ellis Horwood Chichester, 1987

- Melchers R. E., 'Structural reliability analysis and prediction', Ellis Horwood Chichester, (Third Edition), 1999

- Nikolaidis E., Kapania R. K., 'System reliability and redundancy of marine structures: A review of the state of the art', Journal of ship research, March 1990

- Rubinstein R. Y., 'Simulation and the Monte Carlo method', New York, Chichester, Wiley, 1981

- SSC-351, 'An introduction to structural reliability theory', Ship Structures Committee, 1990

- Stiansen S. G., Mansour A., Jan H. Y., Thayamballi A., 'Reliability methods in ship structures', RINA Transactions, 1979

- Thoft-Christensen P., Baker M.J., 'Structural reliability theory and its application', New York, 1982

- Thoft-Christensen P., Murotsu Y., 'Application of structural systems reliability', Springer-Verlag, 1986

- White G. J., Ayyub B. M., 'Reliability methods for ship structures', Naval Engineers Journal, May 1985

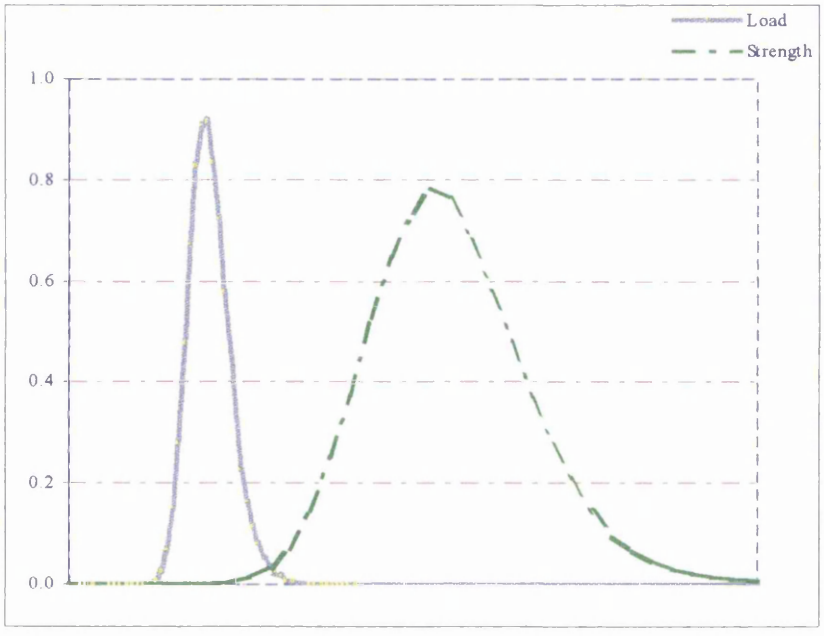

Figure 2.1 –*Load and Strength Probability Density Functions*

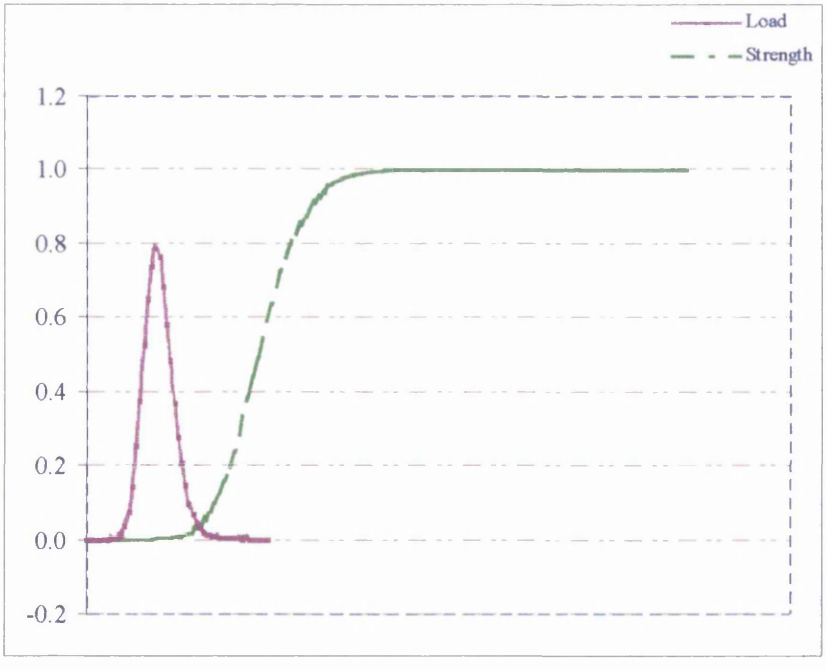

Figure 2.2 –*Load p.d.f. and Strength cumulative probability function used in the convolution integral*

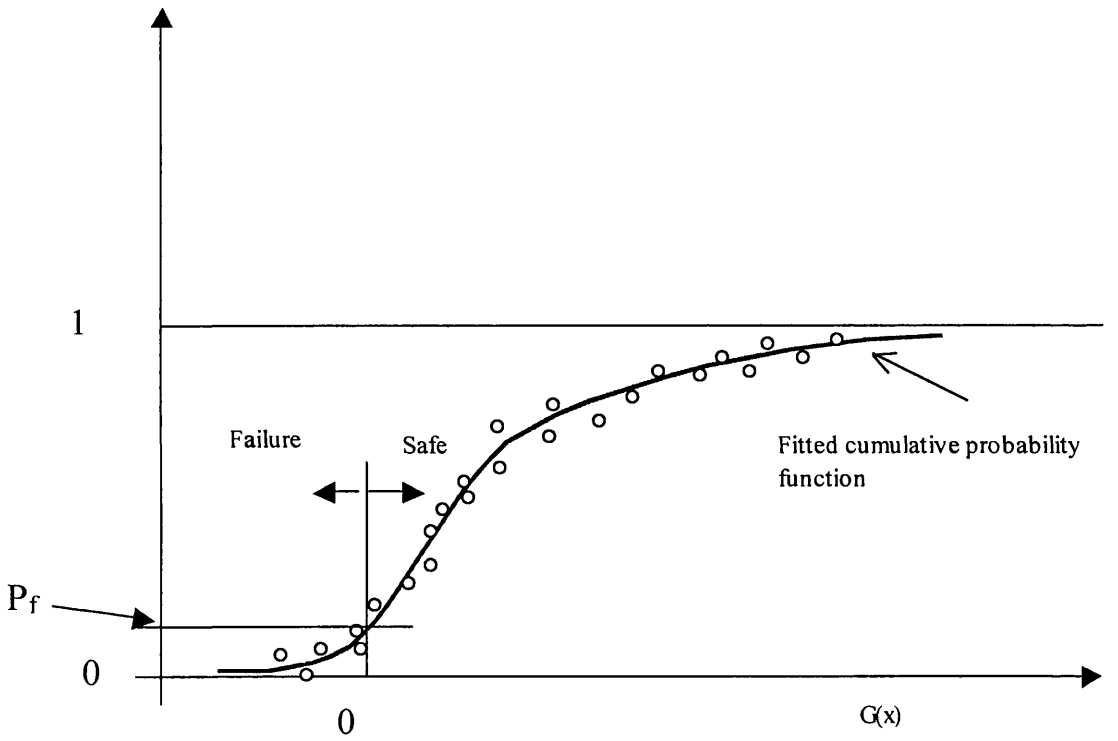

Figure 2.3 – *Cumulative function fitted to Monte Carlo simulation results*

CHAPTER 3

LOAD AND STRESS ANALYSIS FOR FATIGUE AND FRACTURE ASSESSMENT OF A SHIP STRUCTURE

3.1 Identification of Loads Relevant to Ship Structures

This section provides information on the various loads acting on a ship structure. The loading imposed on a ship, depends on several parameters such as climatic and environmental conditions, the way the ship's master responds in extreme conditions, the cargo it carries. For different analyses, different loading histories are required, and the period of interest may be a few hours up to the life of the ship.

There are various ways these loads are imposed on the ship. The primary way is by the waves. Other significant loads arise from the weight and bouyancy of the structure, the cargo loads, vibration loads from the engine, thermal loads and acceleration loads from liquids in tanks.

The study is investigating in particular cyclic loads that arise from waves and cause fatigue cracks to propagate. These can be generated in several ways. One of the most important mechanisms is via the hull girder bending. This loading can be characterized as global cyclic load with a period of a few seconds. Other forms of wave loading include more local effects such as wave pressure loads experienced at the side of the ship, between the transverse frames. Also acceleration loads from liquids stored in tanks, because of the ship motion. In some extreme sea conditions, slamming can occur which is a highly non-linear phenomenon and very difficult to quantify.

3.1.1 Load Categorization

The loads acting on a ship structure can be categorized as follows, (SSC 373)

1. Hull Girder or Global Loads

Still water loading, due to the ship's weight and bouyancy which causes vertical shear forces and bending moments.

Wave induced loading, which cause horizontal and vertical shear forces and bending moments

High frequency steady state wave excitation, also called springing, which induces vertical shear forces and bending moments.

The calculation of the still water loads is a relative straightforward procedure and involves little error. The low frequency steady state loads can be calculated using linear strip theory or 3D diffraction/radiation analysis.

2. Local Loads

These loads can again be categorized as:

Static loads, because of still water loads, weight of permanent equipment, ballast, or cargo

Low frequency wave loads, because of external hydrodynamic wave pressure acting locally

High frequency transient wave impact loading, resulting in slamming forces at the bow of the structure.

Cargo inertial loads, this is internal loads because of cargo acceleration

Liquid sloshing loads, again internal loads due to liquid impact in a tank

The calculation of the above loads, except in the static loads case, involves considerably greater uncertainty than the hull girder loads, and often complex analysis is required.

3. Fatigue Loads

Fatigue may be defined as a process of cycle-by-cycle accumulation of damage in a material undergoing fluctuating stresses. A significant feature of fatigue is that the load may not be large enough to cause immediate failure, but after a certain number of cycles the accumulated damage may have reached a critical level. Fatigue loads arise from:

- *Global bending of hull girder (global)*

- *Water pressure oscillations, (local)*

- *Acceleration forces due to cargo (local)*

Changes in still water bending moments, thermal stresses, vibration stresses are all possible source of cyclic loading. Still water bending moment and thermal stresses changes are usually infrequent and therefore do not contribute much to fatigue crack propagation, but they might have an effect on crack growth acceleration or retardation. Vibration stresses are mainly due to propeller or mechanical equipment and usually affect localized parts of the hull structure. Vibration is not considered in this work.

Fatigue damage at the deck and bottom structure of a ship (particularly in the midship region) is caused by global shear and bending. On the side shell structure, it is the local wave pressure fluctuations which contribute most. Because fatigue damage is typically proportional to the stress range cubed (from Miner's rule) a small error in stress range leads to a large error in fatigue life.

3.2 Load Definition for Fatigue and Fracture Assessment

There are two important loads that must be determined, for fatigue and fracture analysis. These are:

- Stress ranges, important for fatigue crack propagation

- Extreme loads, important for fracture

Both of these loads arise from the cyclic wave action experienced by the ship. The stress range determines the working stress levels experienced by the ship during the period of interest. The stress range calculation requires information of the route of the ship so that all necessary climatic and environmental conditions are accurately assumed. Fatigue damage accumulates with time; therefore, all stress ranges in the period of interest must be considered.

Extreme loads, are the loads that the ship will experience in extreme wave condition e.g. a severe storm. The probability of a ship facing a storm should be accounted for,

and the period the storm will last is also assumed, usually a few hours. Ocean statistics are then used to determine the extreme loads, based on the extreme wave height.

The importance of establishing both loads can be more easily understood in the case of a ship containing cracks. A ship will start its life containing cracks from the day it leaves the shipyard, due to imperfections during the manufacturing process, as discussed in chapter 1. Therefore, the ship possesses a certain strength capacity, which degrades with time as these cracks start to grow under the cyclic wave action. The crack propagation can only be determined with knowledge of the stress range spectrum the structure is subjected to. After some time, the cracks will have propagated to such an extent that the strength capacity is so low that any high (extreme) stress will cause fracture, i.e. failure of the ship. To make an assessment of the probability of the ship failing any time during its life, both the stress range spectrum and the extreme loading should be determined.

These loads can be determined in a *short-term* or in a *long-term* analysis. Short-term analysis is capable of providing estimates on extreme loads that will be experienced by the ship during a storm (which lasts a few hours), but only long-term analysis is able to provide information on the stress range spectrum necessary for crack growth analysis over longer periods. A description of how to determine these loads follows next.

3.3 Load Determination Using Theoretical Analysis

Loads can be calculated either experimentally or theoretically. For reliability analysis in this thesis the theoretical calculations are more suitable. Experimental results are useful when calibrating results from theory.

There are various methods to determine loads from theoretical calculations, from some very simple models, to other very advanced methods (e.g. spectral analysis or finite element analysis, a numerical method). In this report fatigue and extreme loads are determined by *spectral analysis* which is more suitable for reliability analysis. Finite element analysis is more rigorous, requires the creation of a model and is

suitable for very detailed local stress analysis usually in a deterministic analysis. Spectral analysis involves the following steps:

- Description of the service profile, including the loading conditions, the wave environment (wave scatter diagram), and duration of time of assessment
- Calculation of ship motions and hydrodynamic forces in a seaway, usually by linear strip or 3D diffraction theory.
- Calculation of the stress range transfer function by combining all important loads at location of interest
- Combining stress range transfer functions (RAO's) with sea spectrum for every combination of wave height and period defined in the scatter diagram to obtain the stress range response spectrum.
- The long-term stress range distribution is then obtained by combining the stress range response spectra by taking into account the probability of occurrence of each sea state, probability of wave heading, and loading condition

Spectral method of analysis assumes that the effects of different wave frequencies in a sea state can be combined by linear superposition. A detailed spectral fatigue analysis is presented in appendix A, and for selected structural details, the fatigue lives were computed.

3.3.1 Environmental Modeling

The sea surface is irregular and random and can only be described statistically. Naval architects, find it conveniently to divide the ocean into squares, known as Marsden squares, (Hogben 1967 and 1986). Each of these areas covers a particular geographic area over which the wave conditions are assumed to be similar. For each area, a scatter diagram is defined. The scatter diagram is a collection of joint probability of occurrences of wave parameters such as significant wave height, H_S, and mean zero-crossing period, T_Z, measured every one or three hours over a period of several years,

for each geographical zone. If the ship's route is known then the relative time the ship spends in each area can be estimated and the frequency of occurrence of different sea states is found as the weighted average of the wave statistics in the different areas

$$(H_S, T_Z)_{average} = \sum_{i=1}^{N} \mu_i (H_S, T_Z)_i \qquad 3.1$$

where μ_i is the proportion the ship spends in the *i'th* area.

In general, wave statistics change with time. In the past years, reports suggest (e.g. Storm Warning 1998), that significant wave heights have been increased, probably as a result of global warming. To account for this increase in significant wave heights the sea scatter must be expanded and updated to account for the higher probabilities. Methods of sea scatter expansion are described by Fang (1980). However, the area of operation of the specific bulk carrier (a more detailed description follows in appendix A), is the Central Atlantic Ocean, and the probability of occurrence of large waves (i.e big significant height) is seldom compared with the North Atlantic wave environment, hence there is no need to expand the sea scatter diagram (seen in Figure3.1).

3.3.1.1 Wave Spectrum

Each sea state contains wave energy which is distributed between the various frequencies. The energy distribution over a range of frequencies can be described by the wave spectrum. Wave spectra are estimated for particular locations, the North Atlantic being one of the areas of extensive research. There are many wave spectra available according to the area of interest, e.g. the Pierson-Moskowitz and the Bretschneider for open seas, the JONSWAP for severe sea states, or the I.S.S.C. specially developed for the North Atlantic, (Chen 1997)

The wave spectrum can be modelled, for a specified wave height and wave period, using theoretical models that have been fitted to real life environmental data from measurements over, usually, large periods of time (typically more than ten years).

A more complete description of the sea state would require to define also the spread of the energy with the direction of wave components, namely how much each of the

components of the sea, in different directions, contribute to the energy distribution (sea spectrum). Therefore a more realistic representation of the sea state would comprise a two dimensional directional spectrum, indicating the direction and the frequencies of the wave components. The directional spectrum, however, is difficult to calculate, and it is approximated by two independent functions (SSC-392)

$$S(\omega,\theta) = S(\omega)\mu(\theta) \qquad 3.2$$

where

$$\mu(\theta) = \begin{cases} k\cos^n\theta & for\ |\theta| \le \frac{\pi}{2} \\ 0 & for\ |\theta| > \frac{\pi}{2} \end{cases} \qquad 3.3$$

and

$$k = \frac{1}{\sqrt{\pi}} \frac{\Gamma(\frac{N}{2}+1)}{\Gamma(\frac{N}{2}+\frac{1}{2})} \qquad 3.4$$

with N being the number of load cycles, and n the spreading parameter (typically n = 2). For this report the I.S.S.C. sea spectrum was chosen (the form is given by equation A.4.1 in appendix A), typical for the North Atlantic, and account for directional spreading was also taken using equation 3.2.

3.3.2 Response Calculations

During the response analysis, the ship's motions (heave, pitch, surge, yaw, roll and sway), bending moments (vertical and horizontal), shear forces, torsion and (probably) wave pressure distribution, are determined. These are called the 'transfer functions' or 'Response Amplitude Operators' and describe the response of the ship to a regular sinusoidal wave, with unit amplitude, for different frequencies. The transfer function can be obtained, practically from towing tank experiments, or theoretically using wave response software.

The most commonly used theoretical methods are linear strip theory or the more advanced 3D diffraction theory. In linear strip theory the forces and moments acting on the ship are obtained by integration of forces and moments acting on the various 'strips' that model the ship (Salvensen *et al* 1970, Vugts 1971). The transfer functions are valid only for a specific ship speed, wave direction, and loading condition.

Some important restrictions on strip theory are (Salvensen 1990)

- Strip theory is better suited for high encounter frequency loading hence it is more applicable for head seas rather than following seas for a ship with forward speed

- The theory does not properly account for the interaction between the steady wave system and the oscillatory effects of ship motions. This particularly applies when the Froude number exceeds or is equal to 0.4. The Froude number of the vessel studied is 0.17

- The effects of slamming and green water are not taken into consideration

- Strip theory has shown questionable results when the length to beam ratio is low. However, the vessel considered is a Panamax bulk-carrier with a relatively high length to beam ratio.

Linear strip theory provides good agreement between theory and model predictions for wall sided structures in moderate seas, and for fatigue calculations the limitations of strip theory are not crucial, (SSC-402). Fatigue crack propagation usually occurs under the low-frequency oscillatory loads imposed by moderate seas since they are the most probable sea states, hence they cause the largest amount of stress ranges.

For the extreme loads however, where highly non-linear phenomena occur, such as slamming, and dynamic pressure loads, this assumption may not be true, especially in the case of fast cruise ships. In case extreme predictions in severe sea states are necessary, and the response is non-linear, further improvements should be applied, such as a second order strip theory method, 3D diffraction methods, or corrections on the linear strip theory (SSC-402).

The objective of the response analysis is to determine the ship response for a particular sea state. The input in the analysis is the sea state, and the output the ship response. In order to determine the ship response, first we have to make some assumptions for the behavior of the ship. This assumption states that the ship response to wave excitation is *linear* so that the total response can be described by superimposing the responses to individual regular wave components that consist the sea state.

The analytical computations of loads and motions use a simple theory based on linearity. In the case of a ship structure (the system), dynamic wave loading is applied (input) and the response (output) is computed. The conditions that should apply are that the input should be a statistically *ergodic* and *stationary* process, described in the next section, (SSC-351). Once these conditions are met, the response can be assumed linear (which in some cases may not be a good assumption, e.g. when calculating dynamic pressure at the side of the vessel, or when the vessel has a fine form). The input from many different sea states can be used and superimposed to yield an overall response of the system. Using the response output together with statistical analysis will provide information on both extreme loads and stress range spectrum.

The RAOs obtained from linear strip theory are responses due to a single loading mode, i.e. bending moment, shear force, wave pressure or torsion. It is necessary to combine them together to determine the total stress spectrum at the location of interest. First the loads must be translated into stresses, and the stresses must be appropriately combined to determine the total stress transfer function. The process of translating loads into stresses and combining them together is called stress analysis and is discussed in section 3.7.

It is now important to find the relationship between the sea spectrum and the response stress spectrum. Mansour (SSC-351), states that for linear systems this expression has the form

$$Response\ Spectrum = Sea\ spectrum \cdot |\ Transfer\ Function\ |^2 \qquad 3.5$$

3.3.3 Stress Response Spectrum

Equation 3.5 describes the input-output relation in the frequency domain, for linear systems. The response spectrum describes the response of the ship to a particular wave height, period, direction and loading condition (SSC-351). The statistical parameters of the response spectrum are of the most importance. The area under the response spectrum, denoted by m_0 gives the mean of the response. The square root of the area under the response spectrum is the root mean square (rms) of the response. The response statistics are fundamental properties of the response spectrum that are used in the calculation of the stress ranges that are necessary for a fatigue analysis, (Barltrop 1991).

For fatigue and fracture loads need to be translated into stresses. For fatigue the stress range is important, and for fracture analysis the stress amplitude. Hence, the load RAOs must be transformed into stress RAOs and combined together to calculate the total stress at the location of interest (using the procedure described in 3.7). The stress RAO is used as an input to the spectral analysis, and the stress response spectrum is determined.

A stress response spectrum is estimated for each sea state, wave heading and loading condition using equation 3.5. Each stress spectrum is associated with a probability accounting for the probability of each sea state, wave direction and loading condition. It is therefore important to establish the probability density function of the stress spectrum, which can then be used in a reliability analysis. To determine the stress probability density function, we must use statistical analysis and make some assumptions for the waves (or the sea surface). These are discussed in the next section.

3.4 Wave Response Statistics

Sea states are very difficult to predict and to describe. Stress variations are non-stationary, broad-banded and pseudo-random in nature, (SSC-363, Madsen 1983). However, for simplification reasons, sea states for use in fatigue crack propagation

analysis are characterized as, stationery, narrow-banded, ergodic, Gaussian processes (SSC-351, SSC-315).

Stationarity, for a short period (1~3 hours) a random process is assumed to be stationery if its distributions are invariant under a shift of time scale.

Narrow band process, i.e. if the distribution of waves has significant values only over a relatively small band or range of frequencies. A random process is wide band if its distribution has significant values over a wide band of frequencies.

Ergodic hypothesis, that is, a single sample distribution is typical of all other sample distributions.

Gaussian random process, namely, if the wave surface elevation follows a normal distribution.

Until further advances in this field, the above assumptions enable the estimation of the stress range/stress amplitude distribution by use of the spectral method, for different sea states and loading conditions. The long-term stress distribution over a specific period of time, is determined by combining all the short-term distributions, into a weighted average distribution, (section 3.4.3). An alternative way is to fit the long-term distribution into a theoretical distribution so that an analytical form is available, (section 3.5).

Sequence effect might also be important for fatigue crack propagation. Sequence of cyclic stresses cannot be constructed from the short-term or long-term stress range distributions. Simulation methods can be used but a lot of attention should be given to understanding the nature of stress histories, (a large trough usually follows a large peak, sea states develop gradually not randomly), (SSC-351). Sequence effects were not considered in this work, the reason explained in chapter 4.

The statistical description of an irregular sea state and the associated ship response can be categorized as a *short- term* or *long- term* response.

3.4.1 Short-Term Response Statistics

Under the assumptions of a *stationary, zero mean Gaussian* wave elevation, for each sea state, the response process for a linear system is also a stationary zero mean Gaussian process. Furthermore, if we assume that this response is *narrow banded* the probability distribution function for the peaks follow a Rayleigh distribution, (SSC-351), since each positive peak would correspond to a negative trough. The distribution and the probability density function are respectively given by

$$F(x) = 1 - e^{\left(-\frac{x^2}{2m_0}\right)} \qquad 3.6$$

$$f(x) = \frac{x}{m_o} e^{-\left(\frac{x^2}{2m_0}\right)} \qquad 3.7$$

The distribution function for the peaks is dependent on the form of the wave spectrum. In some cases, the narrow band assumption is not valid and the peaks do not follow a Rayleigh distribution. It has been shown by Rice (1944) , that for a *stationary, zero mean Gaussian* process but not necessarily narrow banded, the peak distribution has the form

$$F(x) = \Phi\left(\frac{x}{\varepsilon\sqrt{m_0}}\right) - \sqrt{1-\varepsilon^2}\, e^{\left(-\frac{x^2}{2m_0}\right)} \Phi\left(\frac{\sqrt{1-\varepsilon^2}}{\varepsilon}\frac{x}{\sqrt{m_0}}\right) \qquad 3.8$$

where

$$\Phi(x) = \int_{-\infty}^{x} \frac{1}{\sqrt{2\pi}} e^{-\frac{x^2}{2}} dx \qquad 3.9$$

is the standard normal distribution

$$\varepsilon^2 = 1 - \frac{m_2^2}{m_0 m_4} \qquad 3.10$$

with ε being the bandwidth parameter representing the relative width of the spectrum, (narrow band assumption is said to be valid for $\varepsilon \leq 0.6$).

$$m_i = \int_0^\infty \omega^i S(\omega) d\omega \qquad 3.11$$

is the i-th spectral moment, with i = 0,2,4. Also m_0 is equal to the variance of the spectrum, σ_χ^2. It also represents the area under the spectrum.

In the case where ε approaches zero, the process is becoming narrow banded and the distribution in equation 3.9 reduces to the Rayleigh distribution. In the case ε approaches one, equation 3.8 becomes the normal distribution, i.e. the peak distribution reduces to the distribution of the wave surface distribution.

From the spectral analysis carried out in this work (the report presented in appendix A) the bandwidth parameter was in the range of 0.2 ~ 0.45. Hence, the narrow band assumption is validated and the Rayleigh model for the wave elevation was adopted here. The Rice distribution is not much use for fatigue analysis since there is not a stress range for each peak, and a Dirlik distribution would be more appropriate (Barltrop 1991).

The number of peaks over a specified time period, for a narrow band process, is approximated by the zero crossing rate, v_0.

$$v_0 = \frac{1}{2\pi}\sqrt{\frac{m_2}{m_0}} \qquad 3.12$$

3.4.1.1 Stress Range Distribution

For a stationary, narrow band, Gaussian process each peak is associated with a trough with approximately the same amplitude, therefore the stress range is twice the peak amplitude. Obviously, the stress range cumulative distribution is the same as the peak cumulative distribution with amplitude equal the half of the stress range amplitude (SSC-392). It was discussed in the previous section that the distribution of the peaks follows a Rayleigh distribution. Hence the stress range distribution is the same as equation 3.6 with $S = 2x$ which leads to

$$F(S) = 1 - e^{\left(-\frac{S^2}{8m_0}\right)} \qquad 3.13$$

for the cumulative function and

$$f(S) = \frac{S}{4m_0} e^{-\frac{1}{2}\left(\frac{S^2}{4m_0}\right)} \qquad 3.14$$

for the probability density function.

Generally stress ranges evaluated using the narrow band assumption will be somewhat bigger and this will leads to conservative results, because narrow band assumption tends to ignore the effect of small amplitude, high frequency oscillations which reduce the peaks and hence the stress ranges, (SSC-315).

3.4.2 The Long-Term Stress Range Distribution

In a long term analysis the total response of the ship can be assumed as the sum of the short term responses weighted to account for the relative time of ship exposure in each sea state. The time the ship spends in every sea state is defined by the operational conditions and the probability of occurrence of each sea state is defined by the scatter diagram. Ii is also necessary to account for other probabilities such as the fraction of time the ship spends in a specific loading condition, the probability of wave direction, and the probability of a specific ship speed. As a simplification, it was assumed that each wave heading has equal probability of occurrence, and ship speed was assumed constant during the ship's route.

Assuming that in any sea state, direction, loading condition the response is a Rayleigh distribution with p.d.f. $P(S|H_S, T_Z, \Theta, L)$, $N(H_S, T_Z, \Theta, L)$ the number of cycles per unit time, and $\gamma(H_S, T_Z, \Theta, L)$ the probability of occurrence of each sea state, the long-term p.d.f. of stress ranges for all combinations, is given by

$$P(S) = \frac{\sum_{H_S}\sum_{T_Z}\sum_{\Theta}\sum_{L} P(S \mid H_S, T_Z, \Theta, L) \cdot N(H_S, T_Z, \Theta, L) \cdot \gamma(H_S, T_Z, \Theta, L)}{\sum_{H_S}\sum_{T_Z}\sum_{\Theta}\sum_{L} N(H_S, T_Z, \Theta, L)} \qquad 3.15$$

In the above equation the speed of the ship and the wave spectrum were assumed constant. If this is not the case the above equation should be modified to include additional summation of these extra variables as well.

The number of stress cycles N, over the period of interest per years, is calculated from

$$N = \sum_{H_S i}\sum_{T_Z}\sum_{\Theta}\sum_{L} \gamma(H_s, T_Z, \Theta, L)\, N(H_s, T_z, \Theta, L) \times T \times 3600 \text{ /years} \qquad 3.16$$

Equation 3.15 is very difficult to solve (numerically only), therefore fitting the expression to an equivalent long-term distribution is the method to follow. Mansour (1972) and Munse (SSC-318) have proposed that for fatigue analysis, a *Weibull* distribution is found to give good approximation of the actual long-term stress range distribution. The Weibull distribution has the following form

$$F(x) = 1 - e^{\left[-\left(\frac{x}{A}\right)^B\right]} \qquad 3.17$$

and the density function is given by

$$f(x) = \frac{B}{A}\left(\frac{x}{A}\right)^{B-1} e^{-\left(\frac{x}{A}\right)^B} \qquad 3.18$$

where A and B are the scale and shape parameters of the distribution respectively. The scale and shape parameters are calculated using a statistical fitting technique as discussed in 3.5.

3.5 Curve Fitting of Weibull Parameters

The long-term stress range distribution is approximated by a Weibull distribution. Hence, the scale and shape parameters of the Weibull distribution are required. In many cases it is difficult to achieve a perfect match of the actual stress distribution given by 3.15 and the Weibull distribution given by 3.17. For fatigue analysis, it is important that the part of the actual stress distribution that causes most of the fatigue damage is matched well with the Weibull distribution. Therefore, best fit is achieved

at that part of the stress distribution that causes the most damage, and not at the tail ends of the distribution, with low probability of occurring, stresses.

During the spectral fatigue analysis carried out in this thesis the long-term stress range distribution was calculated according to 3.15, i.e. combining together all sea states, wave headings, and loading conditions. The fatigue damage with respect to stress range was also calculated (the calculations were based on one year). A typical graph can be seen in Figure 3.3. From this graph, we are able to see which stress ranges cause more fatigue damage and then the Weibull distribution is best fitted in this region. The actual stress distributions and the corresponding fitted Weibull distributions can be seen in Figure 3.2. A summary of the shape and scale parameters of the details considered in the fatigue analysis is given in Tables A.1 and A.2 in appendix A. The shape parameter is particularly important since it controls the shape of the Weibull distribution and also the tail end. The tail end is very important for the extreme loads. The shape factors deduced from the spectral analysis agree well with empirical formulae for shape factors for ship structures given by classification societies e.g. in rules and codes of practice (ABS, DnV), see Table 3.2.

In order to make the fitting as accurate as possible certain conditions should be met. An important criterion for fatigue is the *effective fatigue stress range*, (Barltrop 1991). This stress range calculated from the actual stress distribution using the response statistics should match the mean value of the fitted Weibull distribution. To calculate the equivalent stress range, two methods are employed:

1. *The Analytical Method*

In this method the response spectrum statistics are used. For every response spectrum we calculate an effective stress range (Barltrop 1991), given by

$$\sigma_{eff} = 2\sqrt{2}m_0^{1/2}\left[\Gamma\left(1+\frac{m}{2}\right)\right]^{1/m} \qquad 3.19$$

The effective fatigue stress range is equal to

$$\sigma_{eq} = \sqrt[m]{\frac{\sum_{i=1}^{k} N_i \sigma_{eff_i}^{m}}{N}} \qquad 3.20$$

where k is the number of response spectra, σ_{eff} is the effective stress range for each response spectrum, N_i is the number of stress cycles of each effective stress range σ_{eff} in each response spectrum given by

$$N_i = \frac{365 \times 24 \times 60 \times 60}{T_z} \times \rho \qquad 3.21$$

where

$$T_z = \frac{1}{\nu_0} \qquad 3.22$$

is the zero-crossing period of the response, ν_o is the zero-crossing frequency, and ρ is the probability of occurrence of each sea state. 365 x 24 x 60 x 60 is the number of seconds in one year. N is the total number of stress cycles given by

$$N = \sum_{i=1}^{k} N_i \qquad 3.23$$

Finally σ_{eq} from equation 3.20 should be approximately equal to $E[\sigma]$ the effective fatigue stress from the Weibull distribution given by (SSC-351)

$$E[\sigma] = \sqrt[m]{A^m \cdot \Gamma\left[\frac{m}{B} + 1\right]} \qquad 3.24$$

2. *The Numerical Approach*

Under the assumption of a narrow band process the probability distribution of the short-term stress range distribution is assumed to follow a Rayleigh distribution. We can evaluate the probability of the stress ranges using the Rayleigh p.d.f. for ranges, (for every sea state (H_S, T_Z), wave direction (Θ), and loading condition (L))

$$f(\sigma) = \frac{\sigma}{4m_0} e^{\left(-\frac{\sigma^2}{8m_0}\right)} \qquad 3.25$$

The equivalent stress range can then be found from

$$\sigma_{eq} = \sqrt[m]{\sum_i f(\sigma) \cdot \sigma \cdot \delta\sigma} \qquad 3.26$$

where i represents a sea state, wave direction, loading combination and σ is the stress range.

Again we can compare the effective stress ranges evaluated using 3.26 to the one evaluated using equation 3.24, and both should be approximately equal to the stress of equation 3.20.

3.5.1 Example on Curve Fitting of Weibull Parameters

Table 3.1 shows an example of a curve fitting of the long-term stress distribution into a Weibull distribution. The detail considered is a deck longitudinal. In the first column is the stress range. In the second column are the long-term probability values from the stress range distribution calculated from spectral analysis.

The effective fatigue stress range is calculated using the numerical approach first. In the third column, the term inside the cube root in equation 3.26 is calculated. Finally the effective stress range is calculated by the sum of all the values in the third column and taking its cubic root. The equivalent stress range calculated by the analytical approach is also given, (it has been calculated during fatigue spectral analysis using a Fortran code). In the next column is the fatigue damage as calculated from spectral analysis for each stress range. When plotted against stress range, (Figure 3.3), it will give an indication of which stress ranges contribute the most to the fatigue damage. It is then important that the Weibull distribution is best fitted at these stress ranges. Figure 3.21 shows the fitted Weibull distribution (on a log-log scale), showing clearly that good fit is achieved between 0 – 100 N/mm^2, which is the stress ranges range with the maximum fatigue damage contribution.

The fitting method used is the least squares technique, and the Weibull scale and shape parameters which give the best fit into the region selected, are calculated.

3.6 Extreme Wave Loads

Extreme wave loads are the loads the ship will experience during a severe storm. These are loads much higher than the normal operational loads, and they can cause the structure to fail, under various modes, e.g. buckling, yielding or fracture. Hence, the determination of extreme loads is necessary for a failure analysis.

Prediction of extreme loads is done using extreme statistics theory, (e.g. Mansour 1972 and 1981, Ochi 1973, Barltrop 1991). Extreme theory of statistics determines the probability of occurrence of the extreme values (i.e. the smallest or largest values) in a population of samples, which is also called the '*parent*' probability distribution.

Suppose that the parent distribution, is the probability distribution of wave amplitudes during a sea state and for the reasons stated in a previous section it is assumed to follow a Rayleigh distribution. This distribution describes the probability of occurrence of each wave amplitude during a sea state (which normally lasts a few hours). However, if we require the probability distribution of the extreme values only, we must use the extreme value distribution for this information.

For fracture assessment, the largest values in the distribution are of interest. The extreme value distribution of the largest values is then required. First, the parent distribution must be established and then use the extreme statistics theory to determine the largest value distribution.

In computing extreme loads, we are not interested in the total range of the stress, but only in the amplitude that produces the highest values. Therefore, the stress amplitude distribution is now necessary. To obtain the stress amplitude distribution, the same procedure we followed for the stress ranges is used, but using the distribution of amplitudes instead of the distribution of ranges. The long-term distribution of stress amplitudes, is now fitted to a *Weibull* distribution and the scale and shape parameters need to be found again. The procedure is exactly the same as described in 3.4.2.

Fitting of the long-term stress amplitude distribution to the Weibull distribution however, requires different conditions to be met. In the stress amplitude distribution we are not interested in the low and medium stress ranges, which are not important for failure but at the extreme values with small probability of occurrence. It is this tail end of the actual distribution which must be fitted well to the Weibull distribution. For example, in Figure3.4, the tail end is important to be fitted well, which accounts for the large value, but low probability stress amplitudes occurring in one year. The probability level range which is important, can be estimated by taking the inverse of the number of stress cycles in one year and considering a probability range around this value. e.g. If the long-term stress amplitude distribution represents a period of one year, and the stress cycles are calculated from equation 3.16, then the probability of a stress amplitude occurring only once every year is equal to $p(f) = 1 / N$. The probability of exceedance is then $1 / N$ and this means

$$1 - F(S_a) = \frac{1}{N} \qquad 3.27$$

From the Weibull distribution we also have

$$F(S_a) = 1 - e^{\left[-\left(\frac{S_a}{A}\right)^B\right]} \qquad 3.28$$

So by solving for stress amplitude S_a we obtain

$$S_a = A\left\{-ln\left(\frac{1}{N}\right)\right\}^{\frac{1}{B}} \qquad 3.29$$

It is very important to know the shape of parent distribution. In particular, it is important to know the shape of the tail end of the parent distribution. From the shape of the tail end of the parent distribution, the extreme value distribution can be estimated.

The parent distribution of the stress amplitudes, is given by the Weibull distribution, and the tail end of the largest values has an exponential form. The extreme value distribution for an exponentially shaped tail end parent distribution, follows the

extreme type I distribution (Ang 1984), the cumulative function and p.d.f. of which are given by (for the largest values)

$$F_X(x) = exp\left(-e^{-\alpha(x-\beta)}\right) \qquad 3.30$$

$$f_X(x) = \alpha \cdot exp\left(-\alpha(x-\beta) - exp(\alpha(x-\beta))\right) \qquad 3.31$$

where α and β are parameters of the distribution. In particular,

$$\beta = A \cdot [ln(N)]^{1/B} \qquad 3.32$$

and

$$\alpha = N \cdot f_{parent}(\beta) \qquad 3.33$$

where A and B are the scale and shape parameters of the parent Weibull distribution, and $f_{parent}(\beta)$ is the value of the parent Weibull distribution at β, N is the number of stress cycles in one year. Figure 3.5 shows an example of a parent distribution (Weibull) and the largest extreme value distribution for $N = 10^5$ cycles. As the number of cycles increase the extreme distribution will move to the left. Extreme value theory is valid for long periods were the number of cycles is large (as in this case where one year is considered), but for very short periods it may not be very accurate.

3.7 Analysis Used to Determine Stresses from Loads

3.7.1 Load Considerations

The method for load estimation should depend on the degree of sophistication required in the analysis. In this thesis linear strip theory is used. Generally, as stated in 3.3.2 linear strip theory provides good estimates (especially for head and bow seas) for moderate sea states, where the response for boxed structures can be assumed linear with wave amplitude.

In sections 3.3 to 3.6 a method was described to establish the long-term stress range distribution, and the extreme stress distribution which are important parameters for the reliability assessment of fatigue and fracture. In section 3.3 a method to determine important loads (e.g. bending moments, shear forces, torsion) was discussed. In this section, the process of translating loads in stresses is described.

This needs the development of a stress analysis which relates the stresses needed for an the analysis to the loads acting on the ship. The most important loads on ships and their source, were discussed in section 3.1. For different ships, different loads are important. For example, for naval ships hull girder bending may not be significant because of the relative small and strengthened section. Slamming forces or impact loads may be more important for the design, Nevertheless, for large merchant vessels (e.g. oil tankers, bulk carriers) the resulting stresses are due to (SSC-373, Watson 1998)

- Global vertical and horizontal bending moments
- Global shear forces
- Torsional moments (global loads)
- External dynamic wave pressure (local)
- Internal acceleration forces due to cargo (local loads)

Depending on the location of interest, the importance of these loads varies. For fatigue and fracture analysis the important stress (range or amplitude) is the 'local' stress in the vicinity of the crack. However, this local stress may be a result of the loads described above. Some guidance on what type of load is important depending on the location and ship type is given below (Chen 1997)

- **Deck structure**

For closed deck structures in the mid-body region, stresses arise from uniaxial global vertical (and in a minor extend from horizontal) bending. These are typically deck

structures of oil tankers. In the forward/aft body green water effects may be important.

For open deck structures (e.g. bulk carriers, container-ships), in the mid-body, stresses arise from global bending and from torsion caused by waves (which gives rise to horizontal shear stresses). One mechanism for torsion induced stresses is due to the warping longitudinal stress (Hughes 1983, chen 1997) and is significant in places where rigid sections meet weaker sections (e.g. the first hatch opening forward of the aft deck house). Warping effects were not considered in this thesis (a detailed finite element analysis probably is needed). Another mechanism is due to excessive distortion of the hatch openings. Torsion stresses were introduced in this report as shear stresses (shear flow) due to torque.

- **Bottom Structure**

Fatigue stresses for bottom structures arise in a way similar to the deck structure i.e. global bending (vertical and in a lesser extend horizontal), and global shear forces. In particular cargo acceleration forces are important local loads (in a bulk carrier due to oil and granular cargo). Other loads include slamming loads at the fore end, especially important for high speed vessels.

- **Side Shell Structure**

Global bending is important; horizontal bending stresses are maximum at the side shell, because of largest distance from centreline and vertical bending stresses are important to the upper and lower end of the side shell (the region at the centre can be assumed close to the neutral axis where vertical bending stresses are low).

Shear forces are very important, since side shell structure is the main structure that supports the deck loads and transmits shear to the bottom structure. Also any changes in buoyancy (due to wave action) would result in shear stress ranges in the side shell.

Another primary mechanism of stress generation at the side shell is the external wave pressure fluctuations, particularly important for the submerged part of the side shell. Internal cargo pressure stresses may also add to the total stress.

3.7.1.2 Global Loading

Shear forces and bending moments come directly from the RAOs obtained from linear strip theory, for different wave headings and loading conditions, (Details for the analysis are given in appendix A), a typical set of the vertical bending moment RAOs is shown in Figure3.6. Similar RAOs are obtained for the horizontal bending, vertical and horizontal shear forces and torsion. Hogging and sagging will not be identical but for a wall-sided vessel (e.g. a bulk carrier) the difference is not large (Chen 1997).

Vertical bending moment is particularly large at head and following seas, and reducing as the wave direction moves towards beam seas. Horizontal bending and torsion become important at oblique seas. Torsion is maximum at the fore end of the structure (near the quarter length), whereas bending is maximum at the midship region. Vertical shear force is maximum in head and following seas and horizontal is maximum at oblique seas. A complete set of RAOs is given in Figures A.27 to A.29 in appendix A.

3.7.1.3 Local Loading

Local loading comprises the external dynamic wave pressure loads at the side shell structure, and internal inertial loads due to cargo accelerations.

The double bottom especially at the fore end of any large ship is affected by inertial cargo loading especially if the cargo transported is of high density ($\cong$ 3 t/m^3). In the following two sections, the procedure used for the calculation of the local loads is discussed. Side shell structure is also subjected to inertial loads because of cargo, and external pressure due to waves.

3.7.1.3.1 External Hydrodynamic Pressure due to Waves

Low frequency, dynamic, wave induced, pressure loads at the side of the ship hull are usually calculated using strip theory with some corrections made at the waterline level to account for the non-linearities (SSC-373). The other more accurate method is the 3D diffraction theory. Unfortunately, the computer codes available in the dept. of Naval Architecture & Ocean Engineering of the University of Glasgow, do not calculate wave pressure distributions. A methodology was adopted (Barltrop 1991) to

calculate the wave pressure distribution at the side shell structure and then calculate the corresponding stresses.

Two pressure components have been included in the analysis. The incident wave pressure due to the pressure exerted by the wave, and the hydrostatic pressure created due to the relative ship motions (heave, roll, pitch). The diffracted wave pressure due to the presence of the ship hull, and the radiated wave pressure due to the ship oscillations were not considered. The last two components can only be estimated using 3D diffraction/radiation theory, or by some simplified methods (Chen 1997).

In still water, the pressure increases hydrostatically following the formulae $p = -\rho gz$ were z is zero at the waterline and positive above. The introduction of waves alters the pressure distribution since at the wave crest, we have an increase of pressure, but at the wave trough a decrease.

Linear wave theory (Salvensen 1970) was selected to model the pressure distribution mainly because of its simplicity and applicability in wall-sided vessels, (e.g. bulk carriers). Linear wave theory is a regular wave theory simulating waves of the same form without changing the shape. The main disadvantage of the linear wave theory is that the procedure used to establish a mathematical relation between the potential function and the wave period, height and length assumes that the wave heights are small. This assumption restricts the theory only those waves with small wave height. This restriction can be avoided by assuming that the highest region in the pressure distribution is simulated by hydrostatic pressure.

The effect of the pressure fluctuations are of interest, so the procedure used to calculate the fluctuations, was to superimpose the pressure distribution when the wave reached the maximum and minimum wave height. The subtraction of the two pressure profiles gave us the pressure fluctuation. The pressure profiles and their equations are outlined in Figure 3.8 to 3.10. Pressure distribution is calculated for each sea state and then combined in the total stress transfer function using appropriate relationships, as discussed in 3.7.2.2.

3.7.1.4 Cargo Inertial Loads

For bulk carriers, if tanks are not empty, the cargo can create additional forces (hence stresses) due to the ship acceleration. Cargo creates two kinds of forces

- Hydrostatic, due to gravity. Hydrostatic load at the side structures vary with the height of the cargo, $P = \rho \cdot g \cdot h$ where ρ is the cargo density, g the gravitational acceleration, and h the depth of the cargo. At bottom structures, cargo is considered as a distributed load.

- Dynamic, due to accelerations. The load due to the acceleration is found from

$$p_i = \rho \cdot x_i \cdot \gamma_i \qquad 3.34$$

where p_i is the pressure, i is the acceleration direction (i.e. longitudinal, vertical, or transeverse), x is the distance of the location of interest from the center of motion, γ is the acceleration, ρ is the cargo density.

The accelerations were computed using the results of the motion amplitudes and phases leading to the distributed loading on the structure.

$$\gamma_v = -\omega_e^2 \cdot (heave_{amplitude} \cdot e^{heave_{phase}} - l \cdot pitch_{amplitude} \cdot e^{pitch_{phase}}) \qquad 3.35$$

$$\gamma_h = -\omega_e^2 \cdot (sway_{amplitude} \cdot e^{sway_{phase}} - l \cdot roll_{amplitude} \cdot e^{roll_{phase}}) \qquad 3.36$$

Where :

ω_e : Frequency of encounter

l : Distance from center of motion

γ_v : Vertical acceleration

γ_h : Horizontal acceleration

3.7.2 Calculation of Stresses from Load Components

The loads must be translated into stress RAOs for use in the spectral fatigue analysis. Again the sophistication of the method used depends on the part of the structure analysed, the structural geometry, and the load combinations. The two approaches used more often are:

- First principles method, based on beam theory
- Finite element analysis

First principles are used when the geometry is relatively simple, and beam theory can be used. A bulk carrier is considered a boxed structure, hence beam theory provides good results (Pedersen 1991), especially for the middle body of the structure (i.e. the cargo holds area) which is where the fatigue study in this thesis is performed. A study by Lambos (1998) on a bulk carrier, proves that first principles theory agree well with results from finite element analysis.

Finite element analysis provides results that are more accurate when difficult geometries are considered, and load combinations are important. However, to calculate stress ranges all dynamic loading components must be applied to the finite element model, with a phase angle so that a complete cycle is defined, (Chen 1997).

3.7.2.1 Stress Considerations

Classification society rules for fatigue assessment for bulk carriers (e.g. ABS) consider also the loadings described in 3.7. It is recommended that these loads be estimated either from FEA or by beam theory. When this is not possible empirical based formulas are given. The guide separates the stresses into primary (due to hull girder bending), secondary bending (due to bending of stiffened plates between transverse bulkheads), additional secondary bending (due to local bending of longitudinal stiffener between transverse supports), and tertiary (due to local bending of plating between longitudinal stiffeners). The total stress is the sum of the absolute values of these stresses.

ABS rules (ABS 1995) split the fatigue locations in three zones.

- Zone A, which consists of the deck and bottom structures, and side shell and longitudinal bulkheads within 10% D from the deck or bottom, where D is the ship's moulded depth. The total stress in the deck and bottom structures comprises the primary stress due to hull girder bending and for the side shell and longitudinal bulkheads also local pressures.

- Zone B, which consists of the side shell and longitudinal bulkheads. Primary stresses for this zone consist of vertical and horizontal bending stresses, secondary primary stresses consist of dynamic wave pressure stresses and inertial load stresses.

- Zone C, which is a transitional zone between zone A and B. Stresses here is a combination of stresses between zones A and B, calculated using interpolation formulae.

In this report, the structural details for fatigue study are mainly in the deck and bottom structure, with a few locations at the side shell (see Figure A.2 in appendix A). A detailed description of the stresses acting on each location is given in section A.7 in appendix A. However, as a general case the following considerations were made, which agree well with the proposals given in the ABS guide for fatigue assessment of bulk carriers and described above.

Locations in Deck Structure

Hull girder bending stresses were considered only (which agrees with the Zone A stress evaluation). A small exception was for hatch corner, where torsional stresses were also considered and compressive shear stresses due to wave pressure acting at the top end of the side shell.

Locations in Bottom Structure

Hull girder bending stresses mainly, together with local secondary stresses due to cargo acceleration forces on the top of the double bottom. Wave pressure at the keel, may also cause secondary local stresses, but because wave pressure distribution is not varying very much at the keel, these stresses are ignored.

Locations at the Side Shell

Greater importance here have the local stresses due to external dynamic wave pressure at the side shell. Shear stresses may be also important for this region.

3.7.2.2 Stress Combinations

The various load effects e.g. moments, forces, torsion cannot be combined together by simple addition. They must first be transformed into a common quantity, i.e. stress. Then, stress combinations, for fatigue crack growth, are dictated by, location and fatigue crack orientation (see section A.7 in appendix A). The transformation into stresses is done using beam theory, and the relationships are shown below, (Hughes 1995). One thing to note, is that the bending moments, shear forces and torsion calculated from the computer code are non dimensional parameters. The following dimensionalisation constants must be used

For bending moment and torsion

$N_{dim} = \rho g B L^2$

For shear forces

$N_{dim} = \rho g B L$

Force and moment RAOs are translated to stress RAOs using the relationships given below. Since RAOs are given in complex quantities (i.e. amplitude and phase) they are added together according to the phase angle. The total stress RAO is then obtained. The addition of the stress RAOs is not simply the algebraic sum of the individual stresses due to bending, torsion and shear. The addition is done using the stress transformation relationships (Young 1989).

$$\sigma_\theta = \sigma_x \cdot \cos^2\theta + \sigma_y \cdot \sin^2\theta + \tau_{xy} \cdot \sin 2\theta \qquad 3.37$$

$$\tau_\theta = \frac{1}{2}\left(\sigma_x - \sigma_y\right) \cdot \sin 2\theta - \tau_{xy} \cdot \cos 2\theta \qquad 3.38$$

as shown in Figure 3.7.

Finally, the total stress RAO is obtained. However, this is only valid for a particular sea state, wave direction and loading condition, i.e. there is one stress RAO for each sea state, wave heading, and loading condition. The process described in 3.3, i.e. spectral analysis, must be followed to combine all RAOs together.

The transformation relationships used to convert moments and loads into stresses are:

For global hull girder stresses

- *Vertical and Horizontal Bending Stresses*

The general expression for bending stress is given by:

$$\sigma_{Bend} = \frac{M}{I} \cdot y \cdot K_G \qquad 3.39$$

where

σ: Vertical or horizontal bending stress
M: Vertical or horizontal bending moment
I: Second moment of area about transverse (vertical bending), or vertical axis (horizontal bending)
y: Vertical distance from neutral axis (vertical bending), or transverse distance from vertical axis (horizontal bending)
K_G: Global stress concentration factor, to account for stress magnification (holes, notches)

- *Vertical and Horizontal Shear Stresses*

The shear stresses due to global shear forces are calculated using:

$$\tau = \frac{V}{t} \cdot q \cdot K_G \qquad 3.40$$

where

τ: Vertical or horizontal shear stress
V: Vertical or horizontal shear force
q: Vertical or horizontal shear flow per unit shear force
t: Thickness of plating at point of interest
K_G: Global stress concentration factor

- *Torsional Stresses*

The torsional stress is given by,

$$\tau_t = \frac{TM}{t} \cdot q_t \qquad 3.41$$

where

τ_t: Torsional shear stress
TM: Torsional moment
q_t: Shear flow per unit torque

For local pressure forces

Local pressure stresses due to external wave pressure or internal cargo pressure were calculated by first translating the pressures to the local bending moments, and then to local bending stresses.

3.8 Residual Stresses

During arc-welding, a highly localized region is heated above melting point and joined with filler material. The localized shrinkage associated with the cooling down of the hot weld metal is restrained by the cold surrounding metal, and this introduces the residual stresses. The formation of residual stresses therefore depends upon welding procedure and material. Residual stresses are self-equilibrating, and induce local plastic deformation. They do not cause plastic collapse themselves, but can contribute to both fracture and buckling, (Reemsnyder 1997).

One important characteristic of residual stresses is the *'shake down'* effect. This is the effect whereby residual stresses gradually disappear as a consequence of the cyclic stresses. When a very high stress amplitude is applied, due to extreme loading for example, residual stresses do not increase in magnitude, and the load is shared among the rest of the ligament which has not deformed plastically. When the load is removed, in order to maintain equilibrium, the load must also be removed from the plastic zone as well, which means a reduction in the magnitude of the residual

stresses. For the residual stresses to be further reduced, the next extreme load must be higher in magnitude than the last high load.

It is essential, to state some assumptions before further investigation on residual stresses can be made.

- Residual stresses from welding are considered only
- Effects of multi-pass welding is not accounted for

3.8.1 Residual Stress Distribution Fields in Butt Welds

Residual stresses will be present, in any weld joining together two steel plates, as illustrated in Figure 3.11. For such a configuration, along the weld region very high tensile stresses of yield stress magnitude are induced. As the distance from the weld increases, the tensile residual stresses drop off rapidly and become compressive at some point. The compressive stresses are again dropping off as we further move away from the weld. The transverse distribution of residual stresses is also shown. The distribution is symmetrical if the welding speed is relatively high compared to the rate of heat conduction of the material.

Many authors have investigated the longitudinal residual stress distribution. Terada (1976) was one of the first to establish a theoretical model for it. The distribution must satisfy certain conditions,

The residual stress is

- Self-balancing i.e. $\int_{-\infty}^{\infty} f(x)dx = 0$
- Symmetrical, $f(x) = f(-x)$
- Maximum at $x=0$
- Decreasing, as the distance from the weld x is increasing, $f(x)=0, (x = \pm\infty)$

- Having maximum value at $x=0$, then decreasing until it reaches a maximum negative value and increases again to zero with no fluctuations, with increasing x.

An equation satisfying the above requirements has the form

$$f_1(\xi) = \sigma_o e^{-0.5\xi^2}(1-\xi^2) \qquad 3.42$$

Where σ_o is the stress at $\xi=0$ usually taken as equal to the yield stress of the material, ξ is a non dimensional length (distance from center of weld over the length of the tensile region). Figure 3.12 shows the function together with experimental results obtained by Terada (1985). The function represents well the tensile region but overestimates the compressive region. Tada and Paris (1983) have developed another form of the residual stress distribution based on the conditions described by Terada

$$f_2(\xi) = \sigma_o \frac{(1-\xi^2)}{(1+\xi^4)} \qquad 3.43$$

This forms predicts the tensile region quite well but underestimates the compressive region. Smith (1985), has proposed a stress distribution which uses Tada and Paris function but with some appropriate positive constants chosen so that better accuracy is achieved. Tada and Paris emphasize that both of the above functions provide reasonable representation for experimentally measured stress distribution especially for the tensile region (which is more important for fracture analysis), as shown in Figure 3.12.

3.8.2 Shake Down of Residual Stresses

Because of cyclic wave loading, residual stresses diminish gradually. The shake down is caused by high overloads which induce plastic deformation where the stresses have exceeded the yield stress, and upon removal, they relieve the plastic region, and as a result reducing the residual stresses. This is explained with the help of Figure 3.13, and using a simplified residual stress distribution.

Assume the tensile region extends over a distance λ, and the width of the plate is equal to B. Also the compressive residual stress is equal to *10%* of the magnitude of the yield stress, whereas the tensile region is of yield magnitude.

Under the application of an applied stress $\sigma_{applied}$, the stress in the tensile region cannot increase further since it has already reached the yield stress. The stress in the plate, however, is increased. We have

$$\sigma_{Tensile\ region} = \sigma_y \qquad 3.44$$

$$\sigma_{Compressive\ region} = -10\%\sigma_y + \sigma_{applied}\frac{B}{B-\lambda} \qquad 3.45$$

Upon removal of this high stress, the remaining stresses are equal to

$$\sigma_{Tensile\ region} = \sigma_y - \sigma_{applied} \qquad 3.46$$

$$\sigma_{Compressive\ region} = -10\%\sigma_y + \sigma_{applied}\frac{B}{B-\lambda} - \sigma_{applied} \qquad 3.47$$

Obviously, the stress in the tensile region has been decreased. For a further decrease in the residual stress magnitude, an even higher overload than the previous one must be applied. The analysis showed (using simulation methods) that in areas of high applied stress the residual stresses reduced to 40~50 % of the yield stress in only 1 year. In areas of low applied stress, the residual stresses are hardly reduced over the lifetime of the structure.

REFERENCES

- 'An Approach to Conducting Timely Structural Fatigue Analysis of Large Tankers', SNAME, Technical & Research Report No. R-41, September 1992
- 'Storm warning: shipping slow to react', Fairplay, 4th June 1998
- ABS, 'Guide for dynamic based design and evaluation of bulk carrier structures', March 1995
- ABS, 'Guide for fatigue strength assessment for tankers', September 1993
- Ang A. H. S., Tang W. H., 'Probability concepts in engineering planning and design', Vol. 2, John Wiley, 1984
- Barltrop N. P. D., Adams A. J., 'Dynamics of fixed marine structures', Butterworth-Heinemann, 3rd Edition, London 1991
- Chen Y. N., Shin Y. S., 'Consideration of loads for fatigue assessment of ship structures', in Symposium and Workshop on the Prevention of Fracture in Ship Structure, NRC, 1997
- Cronin D. J., Godfrey P. S., Hook P. M., Wyatt T. A., 'Spectral fatigue analysis for offshore structures', in Numerical methods in Offshore Engineering, 1975
- DnV, 'Fatigue Strength Analysis for Mobile Offshore Units', Classification Note No. 30.2, August 1984
- Faltinsen O.M., 'Sea Loads on Ships and Offshore Structures', Cambridge University Press, 1990
- Fang, Z. S., Hogben, N., "Long term Statistics of wave heights and periods", The Naval Architect, 1980
- Hogben H., Dacunha N. M. C., Oliver G. F., 'Global Wave Statistics', BMT, 1986
- Hogben N., Lumb F. E., 'Ocean Wave Statistics', Her Majesty's stationery Office, 1967

- Hughes O., 'Ship structural design: a rationally based computer-aided optimisation approach', SNAME publication, 1995

- Lambos-Papageorgiou I., 'Aspects on structural assessment of a bulk carrier using first principles', M. Sc. Thesis, Dept. of Naval Architecture & Ocean Engineering, University of Glasgow, 1998

- Liapis N., Faltinsen O. M., "Diffraction of Waves around a Ship", Journal of Ship Research, SNAME, Vol. 24, No. 3, pp 147-155, Sept. 1980

- Madsen H O, "Probabilistic and deterministic models for predicting damage accumulation due to time varying loading", DIALOG 5-82, Danish engineering academy, Lyngby, Denmark, 1983.

- Mansour A., 'Probabilistic concepts in ship structural safety and reliability', Transactions SNAME, 1972

- Mansour A., 'Combining extreme environmental loads for reliability based designs', Proceedings SSC-SNAME, Extreme Loads Response Symposium, October 1981

- Mansour, A., Faulkner, "On Applying the Statistical Approach to Extreme Sea Loads and Ship Hull Strength", Trans. RINA, 1972

- Moskowitz, L., Pierson, W.J. and Mehr, E., 'Wave Spectra Estimated from Wave Records Obtained by the OWS Weather Explorer and OWS Weather Reporter', New York University, College of Engineering, (1962-1963)

- Moskowitz, L., Pierson, W.J., and Mehr, E., 'A Proposed Spectral Form for Fully Developed Wind Seas Based on the Similarity Theory of S.A. Kitaigorodskii', Technical Report for U.S. Naval Oceanographic Office, New York University, 1963

- Ochi M. K. 'Wave Statistics for the Design of Ships and Ocean Structures', Trans. SNAME, Vol. 86, pp.47-76, 1978

- Ochi M. K., 'On prediction of extreme values', Journal of Ship Research, March 1973

- Pedersen T., 'Beam theories for torsional-bending response of ship hulls', Journal of Ship Research, Vol. 35, 1991

- Reemsnyder H. S., 'Fatigue and fracture of ship structures', in Symposium and Workshop on the Prevention of Fracture in Ship Structure, NRC, 1997

- Rice S. O., 'Mathematical analysis of random noise', Bell System Technical Journal, Vol. 23, 1944

- Salvensen, N., Tuck, E.O., and Faltinsen, O., 'Ship Motions and Sea Loads', SNAME, Extreme Loads Symposium, November 1970

- Shetty K N, Baker M J, 'Fatigue reliability of tubular joints in offshore structures: fatigue loading', Proceedings OMAE, 1990

- Smith E., 'The stress intensity factor for a crack perpendicular to a longitudinal weld in a large plate', International Journal of Fracture, Vol. 27, pp. 75-79, 1985

- SSC-315, 'Fatigue Considerations in View of Measured Load Spectra', Ship Structure Committee, 1983

- SSC-318, 'Fatigue characterization of fabricated ship details for design', Ship Structure Committee, 1983

- SSC-351, 'An introduction to structural reliability theory', Ship Structures Committee, 1990

- SSC-363, 'Uncertainties in stress analysis of marine structures', Ship Structures Committee, 1991

- SSC-373, 'Probability based ship design; loads and load combinations', Ship Structures Committee report, 1994

- SSC-392, 'Probability based ship design; implementation of design guidelines', Ship Structures Committee report, 1996

- SSC-402, 'Guide to damage tolerance analysis of marine structures', Ship Structures Committee report, 1997

- Tada H., Paris P. C., 'The stress intensity factor for a crack perpendicular to the welding bead', International Journal of Fracture, Vol. 21, pp. 279-284, 1983

- Terada H., 'An analysis of the stress intensity factor of a crack perpendicular to the welding bead', Engineering Fracture mechanics, Vol. 8, pp. 441-444, 1976

- Terada H., Nakajima T., 'Analysis of stress intensity factor of a crack approaching welding bead', International Journal of Fracture, Vol. 27, pp. 83-90, 1985

- Vugts J. H., 'The hydrodynamic forces and ship motions in oblique waves', Netherlands Ship Research Center, Report 150 S, December 1971

- Watson D. G. M., 'Practical ship design', Elsevier, 1998

- Young C. W., 'Roark's formulas for stress and strain', McGraw-Hill, 6th edition, New York 1989

Heavy Ballast Deck Longitudinal			Scale parameter: Shape parameter:	10,134 0,822
Stress range	*Probability (Spectral)*	σ^3 *pf* $d\sigma$	*Damage*	*Probability (Weibull)*
0,1	9,503E-01	1,90E-03	8,118E-11	9,778E-01
0,3	9,427E-01	5,09E-03	6,099E-09	9,461E-01
0,5	9,289E-01	2,32E-02	4,088E-08	9,192E-01
0,7	9,114E-01	6,25E-02	1,302E-07	8,948E-01
0,9	8,921E-01	1,30E-01	2,887E-07	8,723E-01
1,1	8,725E-01	2,32E-01	5,237E-07	8,512E-01
1,3	8,531E-01	3,75E-01	8,451E-07	8,312E-01
1,5	8,341E-01	5,63E-01	1,264E-06	8,122E-01
1,7	8,155E-01	8,01E-01	1,788E-06	7,941E-01
1,9	7,974E-01	1,09E+00	2,416E-06	7,768E-01
3,9	6,462E-01	7,67E+01	1,415E-05	6,337E-01
5,9	5,379E-01	2,21E+02	3,315E-05	5,267E-01
7,9	4,556E-01	4,49E+02	6,079E-05	4,427E-01
9,9	3,876E-01	7,52E+02	9,760E-05	3,749E-01
11,9	3,303E-01	1,11E+03	1,404E-04	3,194E-01
13,9	2,817E-01	1,51E+03	1,861E-04	2,735E-01
15,9	2,408E-01	1,94E+03	2,317E-04	2,350E-01
17,9	2,062E-01	2,37E+03	2,757E-04	2,027E-01
19,9	1,770E-01	2,79E+03	3,170E-04	1,753E-01
21,9	1,522E-01	3,20E+03	3,553E-04	1,520E-01
26,9	1,052E-01	1,02E+04	4,339E-04	1,074E-01
31,9	7,352E-02	1,19E+04	4,847E-04	7,679E-02
36,9	5,191E-02	1,30E+04	5,085E-04	5,541E-02
41,9	3,706E-02	1,36E+04	5,099E-04	4,030E-02
46,9	2,678E-02	1,38E+04	4,952E-04	2,950E-02
51,9	1,959E-02	1,37E+04	4,704E-04	2,173E-02
56,9	1,450E-02	1,34E+04	4,403E-04	1,608E-02
61,9	1,085E-02	1,29E+04	4,082E-04	1,196E-02
66,9	8,190E-03	1,23E+04	3,764E-04	8,934E-03
71,9	6,233E-03	1,16E+04	3,460E-04	6,699E-03
76,9	4,773E-03	1,09E+04	3,173E-04	5,040E-03
81,9	3,670E-03	1,01E+04	2,904E-04	3,805E-03
86,9	2,831E-03	9,29E+03	2,650E-04	2,881E-03
91,9	2,186E-03	8,48E+03	2,411E-04	2,188E-03
96,9	1,689E-03	7,68E+03	2,183E-04	1,666E-03
101,9	1,304E-03	6,90E+03	1,966E-04	1,271E-03
106,9	1,006E-03	6,15E+03	1,760E-04	9,728E-04
111,9	7,749E-04	5,43E+03	1,564E-04	7,459E-04
116,9	5,957E-04	4,76E+03	1,381E-04	5,732E-04
121,9	4,571E-04	4,14E+03	1,211E-04	4,413E-04
131,9	2,676E-04	6,14E+03	9,112E-05	2,631E-04
141,9	1,555E-04	4,44E+03	6,680E-05	1,579E-04
151,9	8,976E-05	3,15E+03	4,782E-05	9,540E-05
161,9	5,160E-05	2,19E+03	3,350E-05	5,798E-05
171,9	2,961E-05	1,50E+03	2,304E-05	3,542E-05
181,9	1,701E-05	1,02E+03	1,559E-05	2,175E-05
191,9	9,832E-06	6,95E+02	1,043E-05	1,342E-05
201,9	5,738E-06	4,72E+02	6,934E-06	8,320E-06
211,9	3,396E-06	3,23E+02	4,605E-06	5,178E-06
221,9	2,043E-06	2,23E+02	3,074E-06	3,236E-06
241,9	7,775E-07	2,20E+02	1,421E-06	1,278E-06
261,9	3,106E-07	1,12E+02	6,964E-07	5,113E-07
281,9	1,259E-07	5,64E+01	3,540E-07	2,072E-07
301,9	5,021E-08	2,76E+01	1,795E-07	8,492E-08
321,9	1,934E-08	1,29E+01	8,794E-08	3,517E-08

Stress range from numerical approach:	**24,3**
Stress range from analytical approach:	22,5
Stress range from Weibull distribution:	**24,6**

Table 3.1 – *Example calculation of Weibull scale and shape parameters*

ABS

$B = 1.40 - 0.036\alpha L^{1/2}$ for $190 < L \leq 305$

$B = 1.40 - 0.044\alpha^{0.8} L^{1/2}$ for $L > 305$

L : Ship's length

$\alpha = 1.0$ for deck longitudinals, includind side shell within 0.15D from deck

$= 0.93$ for bottom structure and side shell structure within 0.15D from bottom

$= 0.86$ for side shell within 0.7D of did - depth region

$= 0.80$ for transverse bulkhead structures

DnV

$B = B_o$	for deck longitudinals
$B = B_o + 0.05\ (D-z)/(D-T)$	for side structure above WL
$B = B_o + 0.05$	for side structure at WL
$B = B_o + 0.05\ z/T - 0.005(T-z)$	for side structure below WL
$B = B_o - 0.05\ T$	for bottom longitudinals
$B = B_o - 0.05$	for deck longitudinals 0.15D from deck or bottom

D : Ship's depth

T : Ship's draft

z : Vertical position

Table 3.2 – *Rule based shape factors for ship structures*

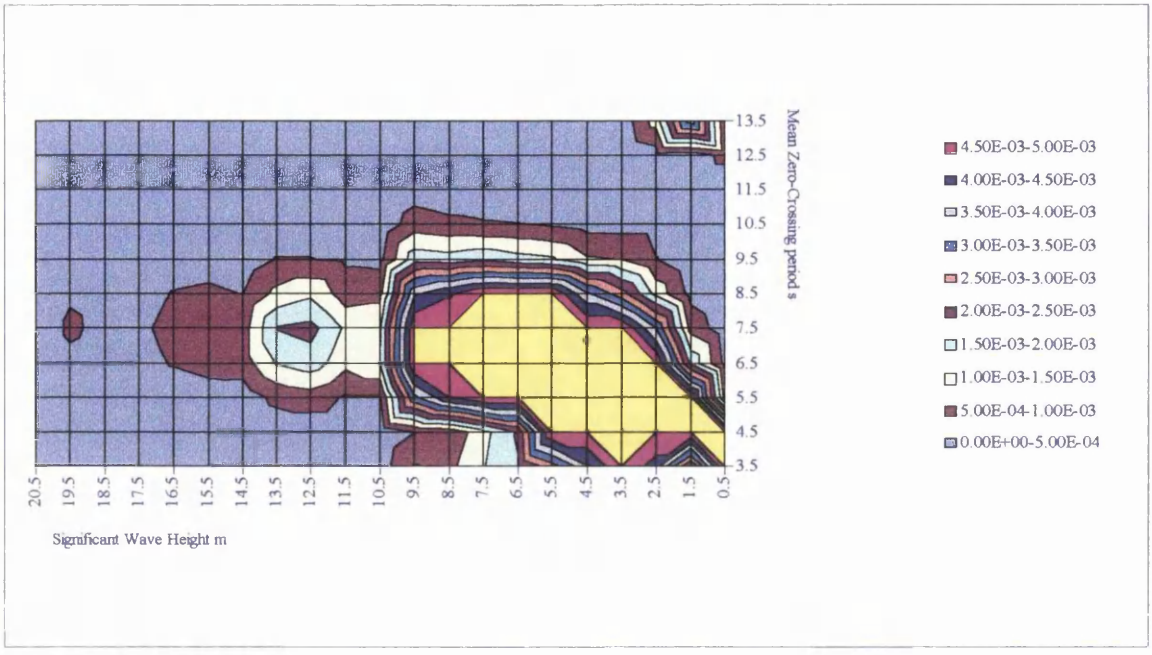

Figure 3.1 – *Sea scatter diagram for selected regions of the Atlantic Ocean*

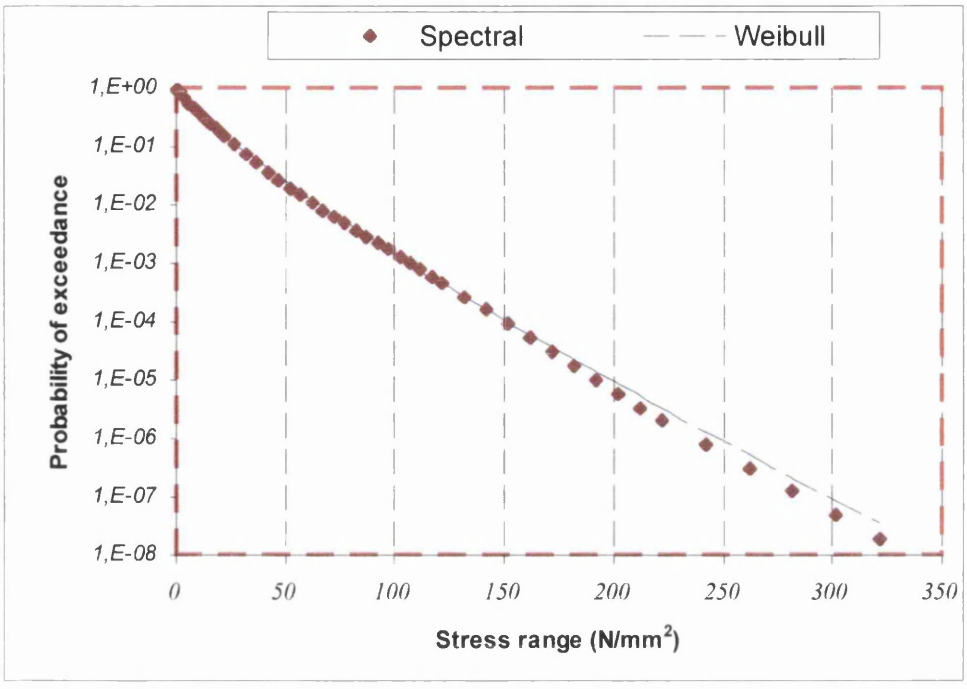

Figure 3.2 – *Example of Weibull fit to actual stress data*

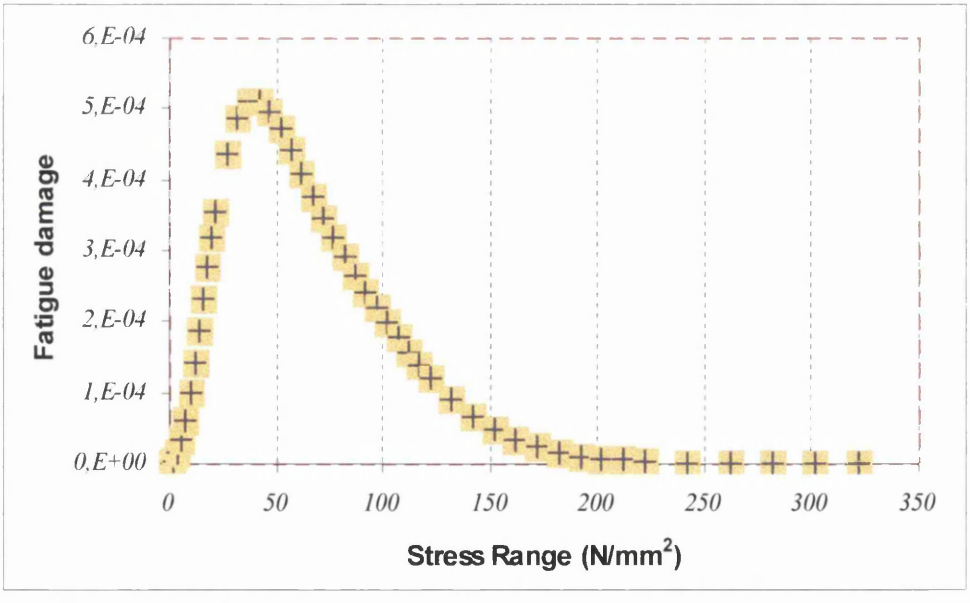

Figure 3.3 – *Fatigue damage versus stress range*

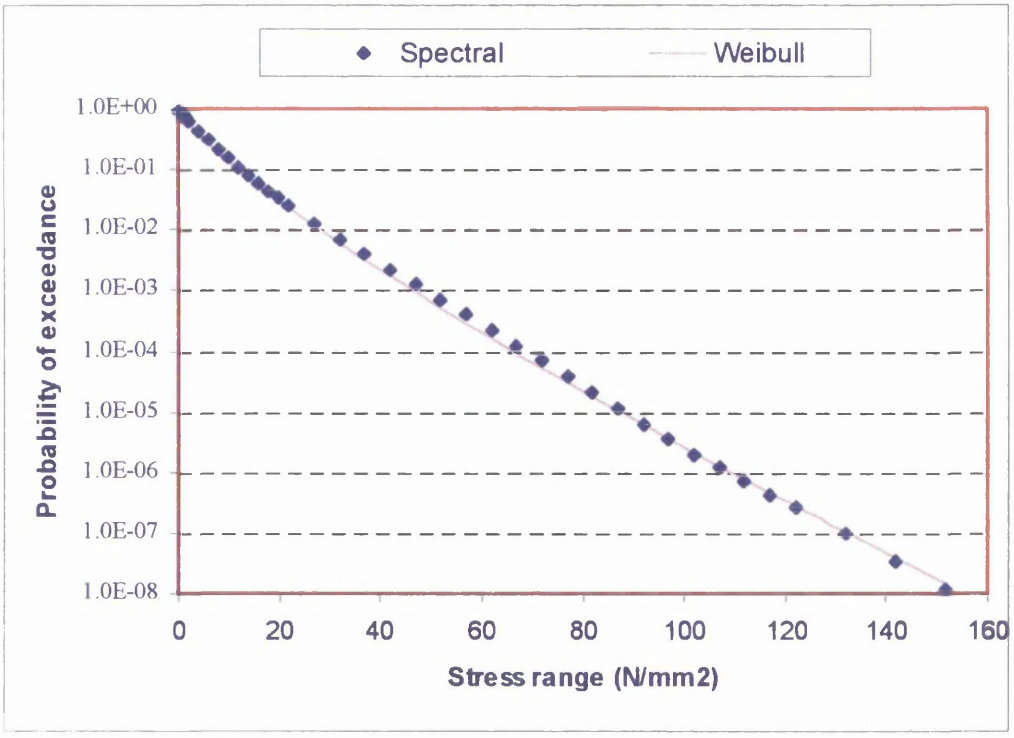

Figure 3.4 – *Weibull fit to stress amplitude data (fit at the tail end)*

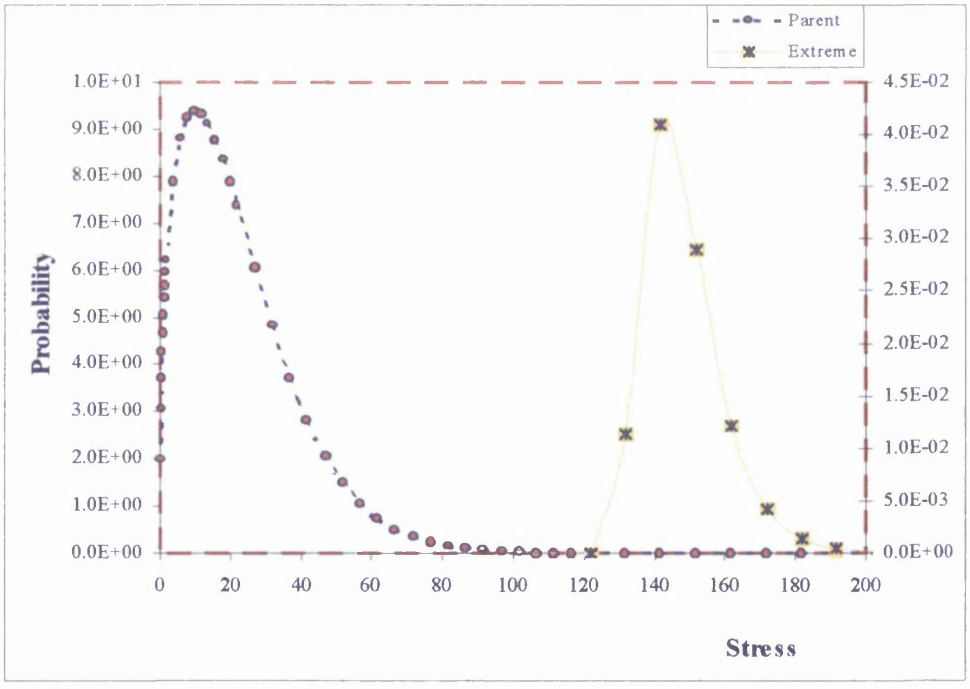

Figure 3.5 – *Parent and extreme value distributions for* $N = 10^5$

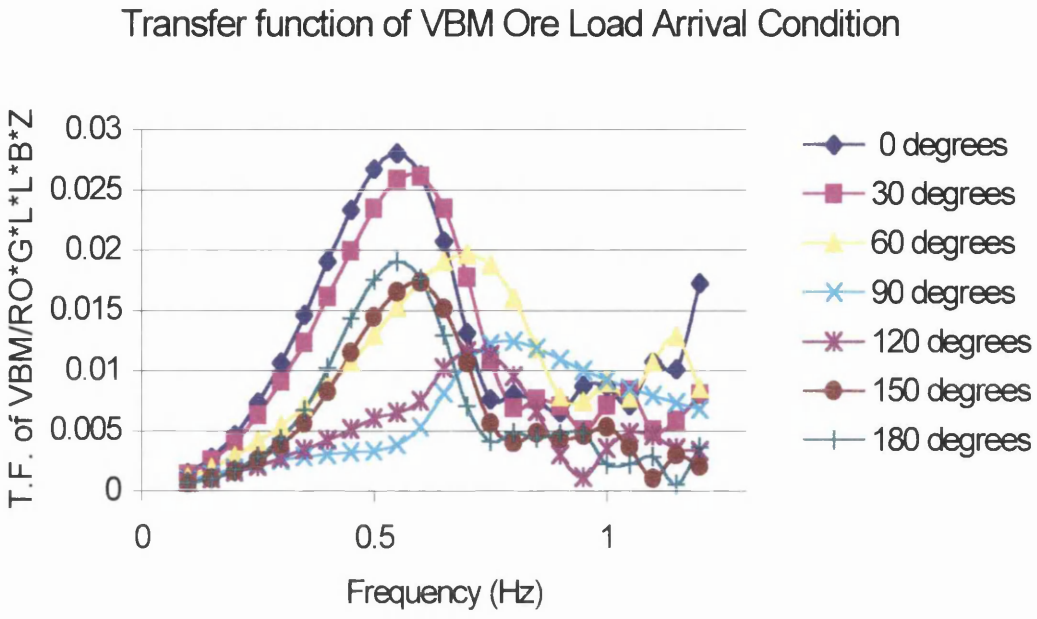

Figure 3.6 – *Typical vertical bending moment RAOs*

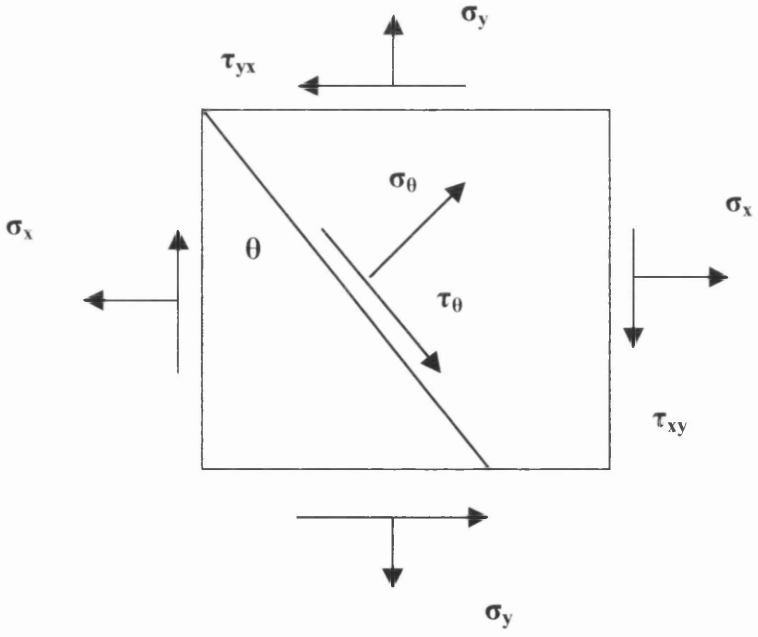

Figure 3.7 – *Stresses in a plane*

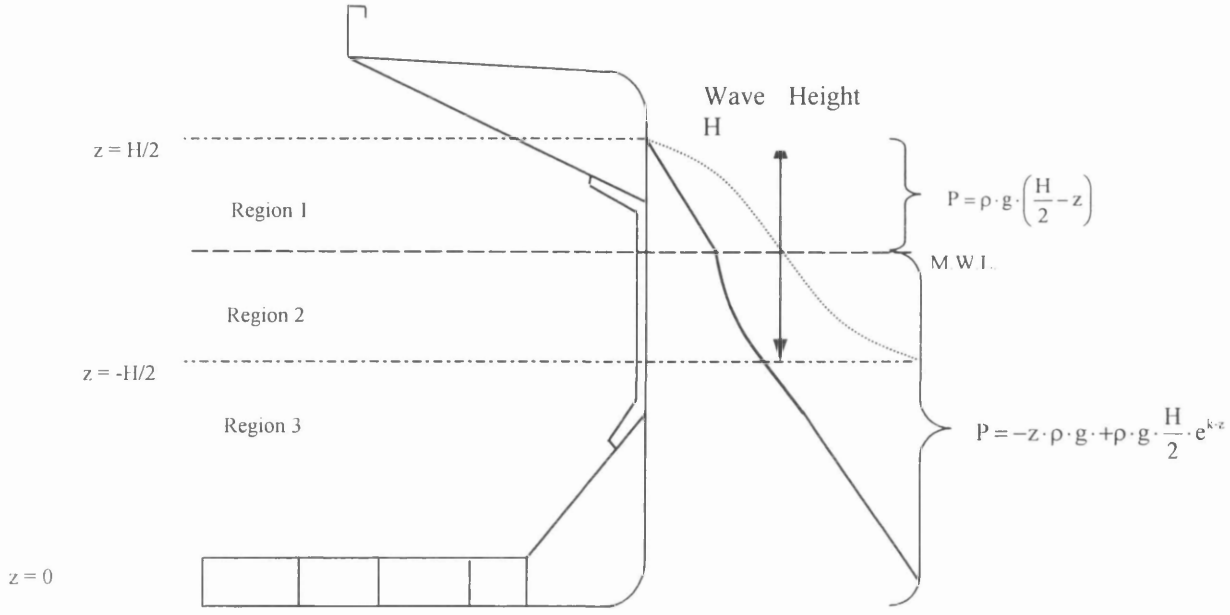

Figure 3.8 - *Pressure distribution when the wave reaches the maximum height*

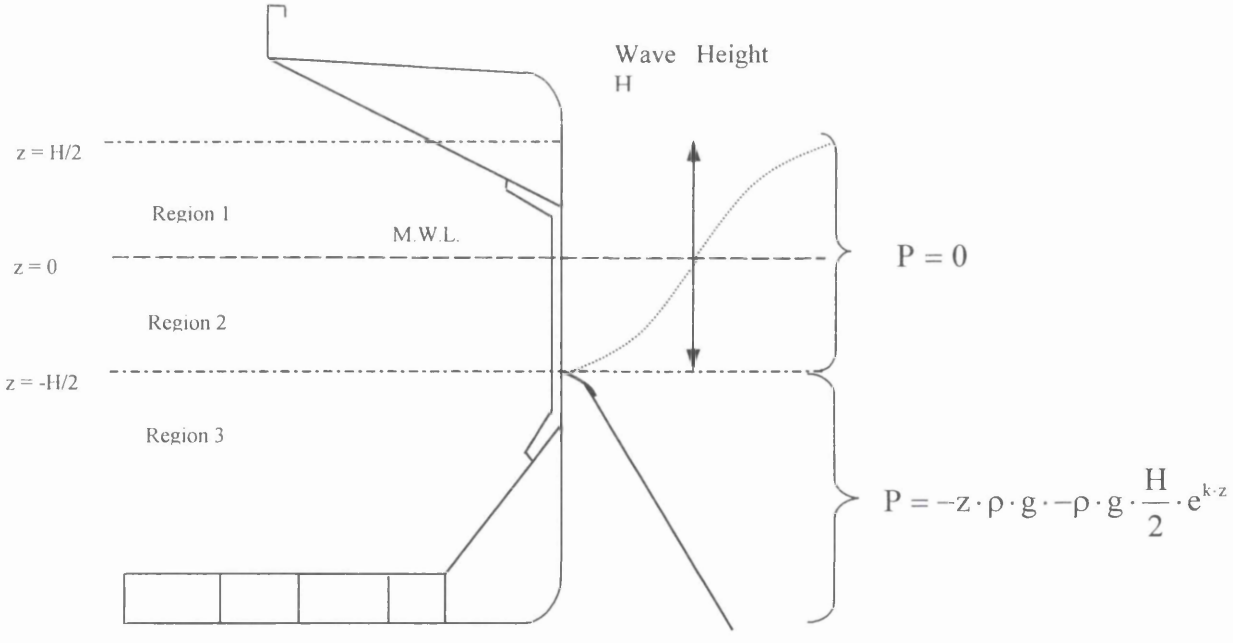

Figure 3.9 – *Pressure distribution when wave at trough*

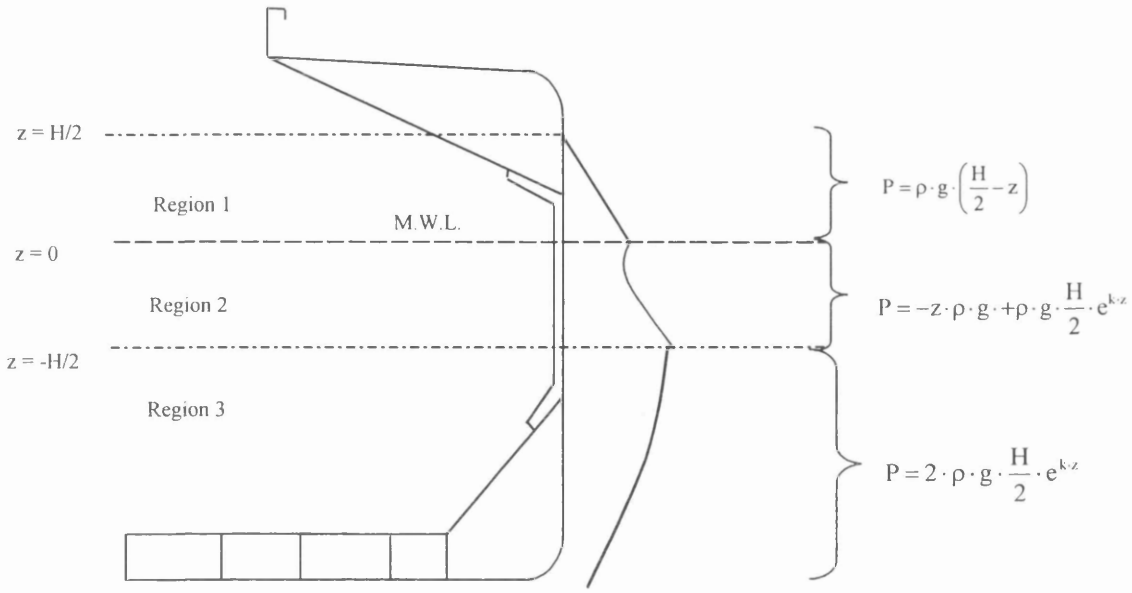

Figure 3.10 – *Pressure distribution obtained from difference between cases described in figures 3.8 and 3.9*

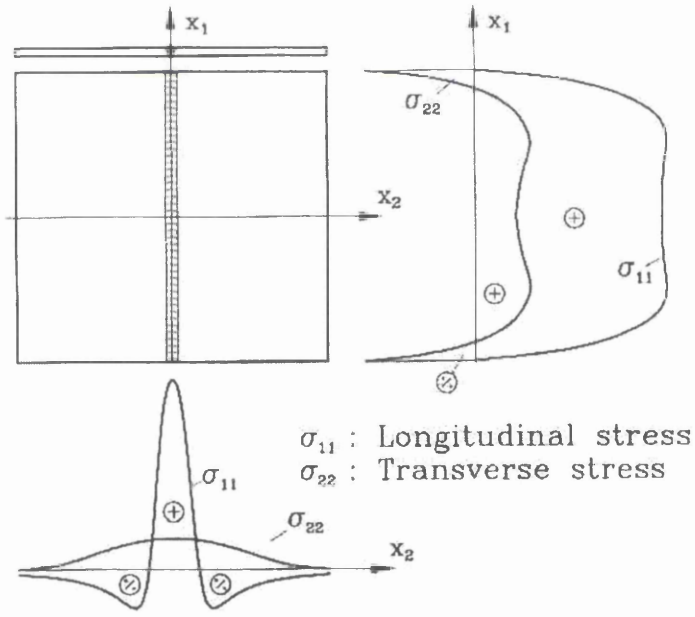

Figure 3.11 – *Longitudinal and transverse residual stress distribution in a butt weld*

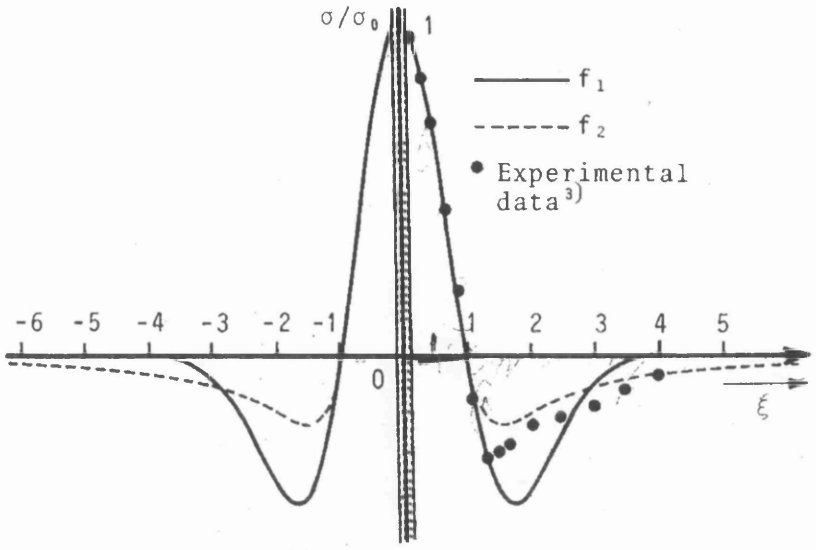

Figure 3.12 – *Residual stress fields by welding near a butt weld* (from Terada 1985)

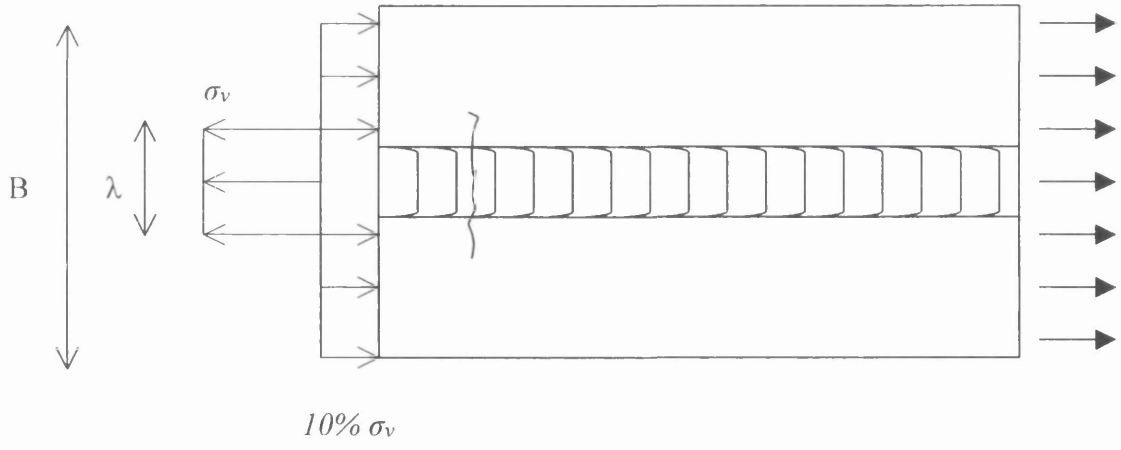

Figure 3.13 - *Simplified residual stress field in a butt weld*

CHAPTER 4

METHODOLOGY FOR FRACTURE ASSESSMENT AND CRACK GROWTH

4.1 Modes of Fracture

Fracture occurs when a crack that has grown to a certain length through fatigue, leads to failure of the structure. There are at least three distinctive types of fracture failure, each with different behavior, (Barsom 1987):

1. *Brittle fracture*, which is associated with cleavage on a micro-structural scale, and the body behaves in a linear elastic manner up to the point of final fracture, any plasticity that occurs is negligible. Brittle fracture gives little or no warning before fracture.

2. *Elastic-plastic fracture*, where the structure shows some plasticity, which although limited in extent has a significant impact on the toughness.

3. *Ductile fracture*, where the fracture is ductile in both microscopic and macroscopic sense. As the load increases and the net section ligament deforms plastically, the crack grows in a stable fashion, until a point is reached where the rate of reduction of load bearing capacity due to crack growth is equal to the rate of work hardening. At this point if the load is not dropped, the system will become unstable, and will fail under fracture and plastic collapse. Because of the plastic deformation that takes place, ductile fracture is preferable to brittle fracture since it can give some indication of a potential fracture.

There are several standardized methods for assessing the risk of fracture failure. If a component is likely to fail in a brittle fashion then the most appropriate method to calculate when fracture will occur is the linear elastic fracture mechanics method (LEFM, section 4.6). However, ship steels display some degree of ductile behavior, and plastic regions form close to the crack tip. A different approach is then necessary to calculate the fracture resistance, as we shall see in section 4.9.

4.2 Fracture Mechanics as a Design Tool

Fracture mechanics allows the assessment of a damaged structure for both residual strength, in the presence of cracks (e.g. from a failure assessment diagram FAD), and for the rate at which cracks are growing under cyclic loads (e.g. from Paris' equation).

Figure 4.1 shows schematically two design approaches, namely the traditional approach and the fracture mechanics approach. In the traditional approach the design stress is compared with the stress the material can carry. A material is assumed to be safe if its strength is greater than the expected applied stress (usually multiplied by a safety factor). The fracture mechanics approach on the other hand, has three important variables, rather than two, the flaw size being the third variable and the fracture toughness replaces material property or provides an additional strength. For this assessment of failure there are several alternative approaches to fracture analysis that include elastic/elasto-plastic, energy criterion, the stress intensity and the crack opening approaches.

Since it is impossible to prevent cracks being built into a structure, fracture control should be used to minimise the risk of failure. This is particularly important where fatigue is likely to make the cracks grow, or where very large strains are possible (e.g. if collision or earthquake are important design considerations). Fracture mechanics crack growth assessment assumes an initial crack and therefore an initiation period is not considered in the analysis. In welded structures this is a good assumption since welds contain many sorts of imperfections as discussed in chapter 1.

In fracture mechanics analysis it is necessary to distinguish between different types of crack deformation modes, (Broek 1989). These are shown in Figure 4.2.

The opening mode I, is associated with local displacement in which the crack surfaces move directly apart. The edge-sliding mode II is characterised by displacements in which the crack surfaces slide over one another with deformations in the plane of the plate. The tearing mode III finds the crack surfaces sliding with deformation out of the plane of the plate.

For ship structures, crack loading is mainly in modes I and II and crack growth tends to be dominated by mode I (SSC-402, SSC-393), so in this thesis only mode I is considered. One important finding is that if these loading modes are in phase then the crack will propagate under mode I only, and most of the combination cases will be reduced to this mode (98% of engineering problems). There are some other cases however which cannot be reduced to mode I, for example in the case when there is a direction in a material where the fracture resistance is low. The combined modes of fracture are more difficult and require more advanced analysis to deal with them, e.g. the energy criterion, (Broek 1989).

4.3 Stress and Displacement Fields at the Crack Tip

The distribution of stress in a body because of the presence of the crack, may be found by linear elastic stress analysis. A crack in a body is considered as a discontinuity, this gives rise to stress concentrations and complicated stress fields around the crack tip. Even if the stress is uniaxial throughout the body, the state of stress around the tip of a crack is at least biaxial. Because of the interruption of the material because of the crack, the load path will bypass the crack tip and will go *around* it. This gives rise to a second stress component, Figure 4.3. The surfaces of a crack are the dominating influence on the distribution of stresses near and around the crack tip since they are near the perpendicular-to-plate stress-free boundaries of the body.

Since the free surface carries no perpendicular stress, the state of stress will be plane stress. However, the free surface carries no shear as well, therefore it is a principal plane, with principal stress equal to zero. The state of stress where one of the three principal stresses is zero is a *plane stress*. A thin steel plate is under approximately plane stress conditions throughout its thickness.

In a thick material, because of the crack tip, at the notch the high σ_x and σ_y stresses will result in a negative strain in the Z-direction, which indicates a thinning of the material. These x and y stresses and z strains are high only near the notch root. Further way σ_x vanishes and σ_y is much lower. Therefore, it will be only a small part

of material close to the crack that undergoes large strains (contraction) in the Z-direction. However this contraction is constrained by the surrounding material, and this causes a tension σ_z in the Z-direction. At a crack tip in a piece of thick steel the constraint provided by the surrounding material results in zero strain in the z direction except near the plate surfaces. A state of stress where one principal strain is zero is a *plane strain*.

The most direct approach to the determination of the stress and displacement fields in the vicinity of the crack tip are based on the method of Westergaard's stress functions (Westergaard 1939). For a more detailed derivation of the relationships, the text books of Kanninen (1985) and Parker (1981) are more appropriate. The material is considered elastic, following Hooke's law. The body is assumed to have an arbitrary shape with a crack of arbitrary size, subjected to tension loading. This will make the results general.

The stress fields near the crack tip for mode I opening are obtained from (Tada *et al* 1973)

$$\sigma_x = \frac{K_I}{\sqrt{2\pi r}} cos\frac{\theta}{2}\left(1 - sin\frac{\theta}{2} sin\frac{3\theta}{2}\right) \qquad 4.1$$

$$\sigma_y = \frac{K_I}{\sqrt{2\pi r}} cos\frac{\theta}{2}\left(1 + sin\frac{\theta}{2} sin\frac{3\theta}{2}\right) \qquad 4.2$$

$$\sigma_{xy} = \frac{K_I}{\sqrt{2\pi r}} cos\frac{\theta}{2} sin\frac{\theta}{2} sin\frac{3\theta}{2} \qquad 4.3$$

and the near tip displacements are given as

$$u_x = \frac{K_I}{G^*}\left(\frac{r}{2\pi}\right)^{1/2} cos\frac{\theta}{2}\left\{\frac{1}{2}(k-1) + sin^2\frac{\theta}{2}\right\} \qquad 4.4$$

$$u_y = \frac{K_I}{G^*}\left(\frac{r}{2\pi}\right)^{1/2} sin\frac{\theta}{2}\left\{\frac{1}{2}(k+1) - cos^2\frac{\theta}{2}\right\} \qquad 4.5$$

In the case where θ equals zero, the functions of θ will be either 0 or 1. This leads to the following simpler expressions

$$\sigma_x = \frac{K_I}{\sqrt{2\pi r}} \qquad 4.6$$

$$\sigma_y = \frac{K_I}{\sqrt{2\pi r}} \qquad 4.7$$

$$\sigma_{xy} = 0 \qquad 4.8$$

where

r and θ are polar co-ordinates, $r = 0$ at the crack tip, θ is measured from the axis of the crack (Figure 4.5). G^* is the shear modulus. The parameter K_I is defined as the *stress intensity factor* (I denotes mode I opening). Similar solutions are available for the other two modes of fracture.

4.4 The Stress Intensity Factor Concept

Note that the stresses at the crack tip ($r = 0$ in equations 4.6 and 4.7), are all infinite but the stress, at some small distance from the crack tip, is proportional to the stress intensity factor 'K'. K must be proportional to the applied stress and the square root of the crack length for the isolated crack in an infinite plate, i.e.

$$\sigma_y \propto \frac{\sigma\sqrt{\alpha}}{\sqrt{2\pi r}} \qquad 4.9$$

The result that, at a small distance from the crack tip the stress is proportional to the K value, suggests that the toughness of the material might be related to a tensile capacity of the material near the crack tip. However, the toughness is usually considered in energy terms as discussed in the section 4.5.

For more general geometries, a dimensionless constant Y is introduced. We now have

$$\sigma_y = \frac{Y\sigma\sqrt{\pi \cdot \alpha}}{\sqrt{2\pi r}} \qquad 4.10$$

The stress intensity factor then is equal to

$$K = Y \cdot \sigma \cdot \sqrt{\pi\alpha} \qquad 4.11$$

For the simple case of a centre crack in a plate $Y = 1$.

The constant Y is called the *geometry factor*. It is a factor that depends on the configuration of the structure and crack geometry and has been the subject of extensive research. The geometry factor accounts for crack geometry, free surface effects, finite width and stress gradient effects (Broek 1989). Values of geometry factors for simple geometries are available in handbooks of stress intensity factors (e.g. Tada 1973, Sih 1973, Rooke & Cartwright 1976)

The geometry function, Y, may also be expressed as $Y = M_k\ Y_u$ where Y_u is the value of Y for the same crack geometry in plate with no weld, and Mk is a correction factor allowing for the weld, (Gurney 1979). Raju and Newman (1981) have developed parametric expressions for stress intensity factors for part through thickness cracks. In Almar-Naess (1985) a general method of calculating the stress intensity factors is described, for an arbitrary geometry by the means of a general relationship for the stress intensity given by

$$Y = Y_S \cdot Y_T \cdot Y_W \cdot Y_E \cdot Y_C \cdot Y_G \cdot Y_P \qquad 4.12$$

where

Y_S = free surface correction factor
Y_T = finite thickness correction factor
Y_W = finite width correction factor
Y_E = crack shape correction factor
Y_C = curvature correction factor
Y_G = non-uniform stress correction factor
Y_P = plasticity correction factor

The development of stress intensity factors for complex joint geometries, such as those found in ship structures is crucial for the calculation of the residual life of the cracked components. It is therefore important that the correct solutions are used for the particular details during the calculations. In this report the various geometry functions required for the analysis have been calculated using finite elements techniques. The analytical description of this work follows in chapter 5.

4.5 Induced Plastic Zone close to the Crack Tip

Equations 4.1 – 4.3 have two important limitations.

1. They are valid only for $r << a$ i.e. close to the crack tip, otherwise they suggest that far away from the crack tip the stresses will be zero.

However, as Figure 4.3b shows (for the special case when the applied stress is normal to the crack axis) the σy stresses far away from the crack tip should equal the applied stresses σ. In general, they should satisfy the Von-Mises criterion. The complete stress distribution solution should then be of the form (Broek 1989)

$$\sigma_y = \frac{K}{\sqrt{2\pi x}} + Ax^0 + Bx^{0.5} + Cx^1 + \ldots \qquad 4.13$$

So now for large x the second term will ensure that $\sigma_y = \sigma$, (if $A = \sigma$, and the rest coefficients B, C etc. are zero)

2. At the crack tip, where $x = 0$, the stresses become infinite.

This solution satisfies the theory of elasticity where there are no limitations on stress and strain. According to the Tresca yield criterion, yielding begins when the difference between the maximum and minimum principal stress is equal to the yield strength, (Broek 1989). For plane strain conditions and according to equations 4.6 and 4.7, ($\sigma_x = \sigma_y \rightarrow \sigma_z \approx 0.66\sigma_y$, v is the Poisson's ratio ≈ 0.33 for steel), in order for plastic deformation to occur, $\sigma_y - \sigma_z = \sigma_{yield} \rightarrow \sigma_y \approx 3\sigma_{yield}$.

For plane stress, where $\sigma_z = 0$, σ_y needs only to be equal to σ_{yield} for plastic deformation. Assuming that stresses cannot increase further than σ_y, the stress distributions will be as shown in Figure 4.6.

The curved part of the distribution is described from equation 4.2, but there will be some distance r_p from the crack tip where the plastic deformation takes place. This area is called the *plastic zone*. It follows from equation 4.7 that

$$\sigma_{yield} = \frac{K}{\sqrt{2\pi r^*}} \text{ , or } r^* = \frac{K^2}{2\pi\sigma_{yield}^2}, \text{ for plane stress} \qquad 4.14$$

and

$$3\sigma_{yield} = \frac{K}{\sqrt{2\pi r^*}}, \text{or } r^* = \frac{K^2}{18\pi\sigma_{yield}^2} \quad \text{for plane strain} \qquad 4.15$$

However, by limiting the crack tip stresses because of plastic deformation to σ_y, the dashed part of the stress distribution in Figure 4.6 was eliminated. This violates equilibrium. The dashed part the stress distribution represent a load that cannot be carried by the material in the plastic zone since that material capacity is limited by yielding. This means that yielding extends beyond r^* and the actual plastic zone is larger than that evaluated by equations 4.14 and 4.15. To evaluate the actual size of the plastic zone we need to shift the whole curve to the left, so that the shaded area is taken by the extra area (coloured) under the $\sigma_y = \sigma_{yield}$ curve, (Figure 4.6). The actual size of the plastic zone would be

$$r_p = \frac{K^2}{2\pi\sigma_{yield}^2} \quad \text{for plane stress,} \qquad 4.16$$

and

$$r_p = \frac{K^2}{6\pi\sigma_{yield}^2} \quad \text{for plane strain} \qquad 4.17$$

Note that r_p, represents the radius of the plastic zone, and that for the plane strain case the actual size of the plastic zone is 3 times greater than the one calculated from 4.15. The plastic zone in plane stress condition is larger than in plane strain.

4.6 Fracture Criterion in Elastic Materials

Consider a brittle plate under tension loading containing a crack. Fracture will occur when K exceeds the *toughness* of the plate, i.e. if

$$K = K_{material} \qquad 4.18$$

where K (calculated from 4.11) is the stress intensity due to the maximum applied stress at the crack tip (e.g. extreme stresses due to wave loading and residual stresses due to welding, if any).

How high this toughness is, depends on the material. Toughness is then called the value of the stress intensity factor at which fracture occurs. Section 4.7 deals with methods of measuring toughness.

Suppose that a thin plate (plane stress) and a thick plate (plane strain), both with cracks, are loaded so that both have identical stress intensity factors. In the case where this stress intensity factor is equal to the fracture toughness of the thick plate, fracture will occur. However, in the thin plate the stress distribution close to the crack would not be so severe (Figure 4.6), and it is anticipated that the stress intensity can increase further, i.e. toughness is higher in thin than in thick plates. Therefore, for the plate thicknesses of general interest for ship structures fracture toughness is not a material property but a property of the material in a specific thickness of plate.

In plates of intermediate thickness the state of stress changes gradually from plane stress to plane strain. The toughness will be higher at thinner plates (plane stress) and will decrease as thickness increases. Beyond a certain thickness, the fracture toughness will be of that of the plane strain conditions.

However, from the discussion of section 4.5, certain degree of plasticity forms close to the crack tip. If plastic deformations are too large and the stresses in the remaining

section exceed the flow stress of the material, (fracture) failure due to plastic collapse may occur before K reaches the toughness (Broek 1989). Which failure occurs first depends on the material properties. Between two competing failure modes, the one that first becomes possible will prevail.

Failure by plastic collapse will occur first when the toughness of the material is high, crack size is very small, or area of section is small. In such case, the fracture criterion of equation 4.18 is applicable to materials with high yield strength and low toughness. The concept of Elastic-Plastic Fracture Mechanics (EPFM) is necessary to characterize failure between the possibilities of plastic collapse and brittle fracture as will be discussed in section 4.8.

4.7 Fracture Toughness Testing and Measurement

Fracture testing methods have been developed during the past 50 years. This was the result, as mentioned in chapter 1, of the catastrophic failures in some Liberty ships and brittle fractures of high-strength materials in rocket motor cases, where conventional design methodology was found to be inadequate, (Barsom 1987).

Probably the first and most widely accepted technique for a qualitative assessment of fracture toughness, which considerably predates these failures, was the *Charpy V-notch* specimen test. This test was firstly introduced in 1905, and it is still used today by various branches of industry for determining the fracture toughness of steel, and its sensitivity to temperature. By using a notched test piece and impact loading, brittle fracture occurs in the test specimen and this gives good indication of the brittleness of the material.

Another fracture toughness test is the K_{IC} *test.* This is one of the standard methods for measuring critical stress intensity factors. A detailed review of the overall background and development of the method is given in Barsom 1999. Before the test, a fatigue crack is grown from the notch to a particular size, usually about half the thickness of the specimen. After that the test piece is loaded at a slow rate to avoid dynamic effects. By measuring the displacements across the notch it can be confirmed that the test piece behaves in a linear-elastic manner prior to fracture, and determine the load

at which fracture occurs. After testing, the crack length before failure is measured and under certain limitations for the test piece dimensions, and if all requirements of the standards are met, then a fracture toughness value is calculated.

For lower yield strength materials, the test-piece size requirements for a valid K_{IC} test become too large for practical use. In addition, modern type of structural steels at thicknesses less than 30 mm, fail in a ductile manner. The crack tip opening displacement *(CTOD),* test was developed from the Welding Institute in United Kingdom, to provide a more convenient test for lower strength, tougher materials, (e.g. marine structural steels), which behave in a ductile manner.

A test is performed on a small three-point bend specimen. Fracture takes place at a critical CTOD value defined as δ_{mat}, which is a material property characterizing fracture resistance, and as such, it provides information on the material's toughness. The CTOD value is converted to a fracture toughness value by

$$K_{mat} = \sqrt{\frac{1.6\sigma_f \delta_{mat} E}{(1-\nu^2)}} \qquad 4.19$$

where σ_f is the flow strength, ν the Poisson's ratio, and E is the modulus of elasticity. In some cases the critical strain energy release (G for elastic materials, J for non-linear) is available $J_{mat,}$ associated with elastic-plastic fracture mechanics, as it is shown in the next section. In this case the fracture toughness is calculated from

$$K_{mat} = \sqrt{\frac{J_{mat} E}{(1-\nu^2)}} \qquad \text{for plane strain} \qquad 4.20$$

and

$$K_{mat} = \sqrt{J_{mat} E} \qquad \text{for plane stress} \qquad 4.21$$

The CTOD method was introduced to measure toughness in the ductile-brittle transition zone, whereas the J value is a more used for materials behaving fully ductile, (SSC-402).

4.8 Elastic-Plastic Fracture Mechanics

It was discussed in earlier sections that Linear Elastic Fracture Mechanics are used when the material behaves in an elastic manner, and fracture occurs under the brittle mode. It was also discussed that structural steels (e.g. for marine applications typically less than 30 mm in thickness) induce some degree of plasticity close to the crack tip region, and fracture is not entirely brittle (nor fully ductile) but in some transitional region (i.e. elastic-plastic). For this transitional region Elastic-Plastic Fracture Mechanics have been developed, (e.g. Kanninen 1985 for detailed review).

In LEFM the stress intensity factor, based on the stress distribution of equations 4.1 to 4.3, fully described the crack driving force, and could be directly compared with the fracture toughness of the material e.g. using equation 4.18. However, when material is not perfectly elastic these stress distributions are not valid. In this case a parameter similar to the stress intensity for LEFM, is the strain energy release J which can be calculated using the energy criterion. The energy criterion can also be used to calculate the linear elastic strain energy release G, which can then give the stress intensity factor. The theory does not change, only the symbols.

4.8.1 The Energy Criterion for Elastic-Plastic Fracture

Griffith (1920) was first to put forward a rational theory of fracture mechanics concerned with the specific conditions under which a small, sharp crack in a stressed body becomes unstable. Griffith's approach to this problem was by way of energy, rather than the traditional force and stress method. Griffith regarded Inglis's stress concentration, (Inglis 1913) as a "mechanism for converting strain energy into fracture energy". Griffith assumed that incipient fracture in ideally brittle materials takes place when the magnitude of the elastic energy supplied at the crack tip, during an incremental increase in crack length, is equal or greater than the magnitude of the elastic energy required to create new crack surfaces. His analysis was based on a model in the form of an elliptical cut-out of length $2a$, where for a very small dimension and sharp corner radius, the cut-out resembles a typical crack geometry,

see Figure 4.7. There were some other conditions necessary for the analysis of the crack extension:

- The stresses acting ahead of the crack tip should reach a critical value.
- The total energy of the system should be reduced during crack propagation.

The basic idea in the Griffith theory of fracture is that there is a driving energy for crack propagation, resulting from the release of energy in the body, along with an inherent resistance to crack growth. By using the mathematical developments of Inglis, Griffith was able to formulate an energy balance approach. A good description of Griffith's theory is given by Rolfe and Barsom, (1987). For an elastic-brittle material such as glass, the energy criterion is given by

$$\frac{dU}{dA} = \frac{dW}{da} \quad \text{or} \quad \frac{Y^2\sigma^2\pi a}{E} = \frac{dW}{da} = G \qquad 4.22$$

which is the energy conservation law and states that fracture will occur over *da*, when enough energy can be delivered (*dU/da*), also denoted by *G*, to provide for the fracture energy (*dW/da*). The left hand side is called the strain energy release, and the right hand side the fracture resistance. A relationship between *G* and the stress intensity factor *K* (for LEFM) is

$$G = \left(1 - \nu^2\right)\frac{K^2}{E} \qquad \text{for plane strain} \qquad 4.23$$

$$G = \frac{K^2}{E} \qquad \text{for plane stress} \qquad 4.24$$

In the energy approach the crack extension occurs when the energy available for crack is sufficient to overcome the resistance of the material. The resistance of the material includes the surface energy, the plastic work or other type of energy dissipation with a propagating crack.

From equation 4.22 it was possible to determine equation 4.23/4.24, because the stress-strain relationship for an elastic material is known (Hooke's law). In the case of

elastic-plastic materials, the stress-strain relationship can be split to a linear and non-linear part. In this case, the energy criterion becomes

$$J_{el} + J_{pl} = J_R \qquad 4.25$$

where J_{el} is the strain release energy for the linear part and J_{pl} is the strain release energy for the plastic part. These can be further expanded to

$$\frac{Y^2\sigma^2\pi a}{E} + \frac{H\sigma^{n+1}a}{F} = J_R \qquad 4.26$$

The first term represents the elastic strain energy release. H is a non-dimensional parameter similar to Y for the linear stress intensity factor, and F is the plastic modulus. The second term, is related to a quantity known as *J-integral* which can be calculated using Finite Element Analysis, (see chapter 5). J_R is the fracture resistance, which is measured using test procedures as discussed in 4.7, (e.g. CTOD test). Similar expressions to 4.23 and 4.24 are obtained for the *J-integral*

$$K = \sqrt{\frac{JE}{(1-\nu^2)}} \qquad \text{for plane strain} \qquad 4.27$$

$$K = \sqrt{JE} \qquad \text{for plane stress} \qquad 4.28$$

The CTOD, δ, is related to the *J-integral* by the relationship

$$J = m \cdot \sigma_y \cdot \delta \qquad 4.29$$

where m is a constant in the range $1 < m < 2$.

EPFM have also limitations and assumptions built in. They are developed based on a non-linear-elastic stress-strain relationship, and not a true elastic-plastic. This puts restrictions on the unloading of the crack tip. The problem of stress singularity at the crack tip has not been solved and plastic collapse needs to be treated separately, as in LEFM. EPFM is still an area of research, and so far, it has not been proven that they provide more accurate results than LEFM (with some approximations), (Broek 1989, Barsom 1987).

4.9 Strength Assessment Method for Plates with Cracks in a Bulk Carrier

The purpose of a strength assessment of a structure with a crack, is to determine whether the structure will fail, either by fracture or plastic collapse. The criterion of failure depends on the mode of fracture (e.g. brittle, elastic-plastic) as it was discussed in sections 4.6 and 4.8.

For materials with low toughness and high stress concentrations, brittle fracture is of most importance because fracture (due to a defect) may occur at stress levels far less than the maximum yield stress of the material. Brittle fracture is important not only for primary members but for secondary members, since a fatigue crack from any small detail can grow to adjacent members without being arrested and eventually lead to terminal failure.

For high toughness materials, brittle fracture may not be a problem but plastic collapse is. Plastic collapse occurs when the stress, (because of the stress singularity at the crack tip, which gives rise to very high stresses), in the remaining ligament next to the crack exceeds the yield stress of the material. This is a local plastic collapse failure, and not an overall plastic collapse of the structure, but it can lead to structural failure if the collapsed member belongs to a non-redundant structure.

Between these two extreme cases, fracture can occur in a ductile way, or elastic-plastic way. In order to perform a strength assessment, a failure assessment diagram (FAD) is used. This indicates all possible failure combinations between brittle fracture and plastic collapse, for combinations of crack driving force K (for fracture), and net section stresses (for plastic collapse). The FAD consists of two axes; in the vertical axis is the ratio (K_r) of the crack driving force K to the materials fracture toughness K_{mat}. In the horizontal axis, we have the ratio (S_r) of the net section forces (σ_n) to the flow strength of the material (σ_f). There is the failure assessment curve, which separates the failure and safe regions. The use of the failure assessment diagram presupposes the calculation of both, K_r and S_r. With these two values, a point describing the state of the cracked component is calculated an if this point fails below

the assessment curve, the structure is safe. A point that falls on or above the curve represents failure, (Figure 4.9 shows a typical FAD).

Earlier, in section 4.6, a fracture criterion was described for linear elastic materials. Namely, fracture will occur when the stress intensity factor becomes equal to the fracture toughness of the material. In that case the FAD would be a square bounded by the $K_r = 1$ and $S_r = 1$ lines. The crack driving force would be given by equation 4.11, and the failure criterion would be as in equation 4.18 or 4.22.

However, as it was discussed in section 4.5, there is a plastic zone in front of the crack tip as a result of the stress singularity when $r=0$, (e.g. from equation 4.7 for σ_y). Taking account of the actual plastic zone requires a shift of the stress curve that amounts to the stress intensity factor K, being associated with $(a + r_p)$ so that K is now a function of $(a + r_p)$, and the effective crack driving force would be

$$K^* = Y^* \sigma \sqrt{\pi (a + r_p)} \qquad 4.30$$

where r_y is the plastic zones radius, from equation 4.16 or 4.17. Equation 4.26 is valid only if the applied stress does not exceed ~70% the material yield stress, otherwise it becomes inaccurate. Plastic zone correction becomes significant when the applied stress is about equal to half the yield stress. With the applied stress being equal to about 70% of the yield stress of the material, the effective crack driving force is about 18% larger than the linear elastic K, (Barsom 1999).

If the applied stresses are small, the size of this plastic zone is considerably small compared with the surrounding elastic material and can be estimated from equation 4.16/4.17 (for an 50 mm crack $r_p \approx 7$ mm when $\sigma = 70\% \sigma_y$). This is a condition of '*small scale yielding*'. Small scale yielding means that the non-linear effect at a crack tip is small compared to the region in which the elastic crack tip stress fields apply. Under these circumstances the non-linear or plastic zone may be regarded as embedded well within a surrounding elastic region. How small the plastic zone must be, compared to other dimensions, is dependent upon the accuracy desired. If the ratio r_p / a is small, the error in using a only in equation 4.30 will be small. The above criterion works well with materials having low toughness and high yield strength.

Should the plastic zone be large, then other terms of equation 4.13 are important and its size would also depend upon *A, B, C* etc. One alternative method would be to use EPFM and the corresponding criterion of failure, as discussed in 4.8. This would require a non-linear elastic analysis (usually a FEA) to calculate *J* or *CTOD* for a complex ship structural detail. This is a much more rigorous analysis compared with the LEFM method. Another solution is to use the failure criterion based on the '*strip yield*' plasticity model or *Dugdale* solution (Dugdale 1960).

4.9.1 The Strip-Yield (Dugdale) Plasticity Correction Model

The effective stress intensity factor is developed from the strip-yield solution for a cracked, infinite thin plate (i.e. plane stress) of an elastic-perfectly plastic material. The strip-yield plastic zone is modelled based on a crack of length $2a+2\rho$ where ρ is the length of the plastic zone (modelled as a thin strip), (Figure 4.8a). The closure stress at the plastic zone is equal to σ_a. The model approximates the elastic-plastic behavior as a through thickness crack under tension, (σ) and a through thickness crack with closure yield stresses (σ_a) at the tip, (i.e. there is no stress singularity at the tip). The physical crack is equal with the stress-free length.

The solution of this model results in the determination of the size of the plastic zone so that the stress intensity factors due to the tensile loading and the closure stress, cancel one another. The stress intensity due to closure is equal to (Anderson 1991)

$$K_{closure} = -2\sigma_a\sqrt{\frac{a+\rho}{\pi}}\int_a^{a+\rho}\frac{dx}{\sqrt{(a+\rho)^2 - x^2}} \qquad 4.31$$

solving the integral results in

$$K_{closure} = -2\,\sigma_a\sqrt{\frac{a+\rho}{\pi}}\cos^{-1}\left(\frac{a}{a+\rho}\right) \qquad 4.32$$

The stress intensity due to the tensile loading is equal to

$$K_{tensile} = \sigma\sqrt{\pi(a+\rho)} \qquad 4.33$$

By equating equations 4.28 and 4.29 results in

$$\frac{a+\rho}{a} = cos\left(\frac{\pi\sigma}{2\sigma_a}\right) \qquad 4.34$$

Burdekin and Stone (1966), applied the Westergaard (Westergaard 1939) stress functions to the strip-yield method, to derive an expression of the CTOD by superimposing a stress function for the closure yield stresses, (σ_a), on the crack faces. From their analysis, the expression for the displacement is given by

$$\delta = \frac{8\sigma_a\alpha}{\pi E} ln\left(\frac{1}{cos\left(\frac{\pi\sigma}{\sigma_a}\right)}\right) \qquad 4.35$$

Combining equations 4.35, 4.29 and 4.21, the effective stress intensity, which allows for the plastic zone correction is given by

$$K_{eff} = \sigma_a\sqrt{\pi a}\left[\frac{8}{\pi^2} ln\, sec\left(0.5\pi\frac{\sigma}{\sigma_a}\right)\right]^{1/2} \qquad 4.36$$

The strip-yield correction to the critical stress intensity for fracture is equivalent to an elastic-plastic (J-based) approach, for

4.9.2 FAD Based on Strip-Yield Model (PD 6493)

The U.K. Central Electricity Generating Board, CEGB first proposed a failure assessment diagram, based on the two criteria approach of Dowling and Townley (1975). The CEGB approach (in SSC 393) addressed post-yield fracture by an interpolation formula between two limiting cases, linear elastic brittle fracture and plastic collapse, (the R6 diagram).

To generalise the strip-yield model for a real structure some modifications were necessary. The compressive yield stresses (σ_α) at the plastic zone need to be replaced by the collapse load of the structure. For a structural member loaded in tension,

collapse occurs when the net section stresses on the remaining section reach the flow strength of the material. Flow strength depends on the tensile properties of the material and the flaw size relative to the total cross section of the member. The collapse ratio is defined as

$$S_r = \frac{\sigma_n}{\sigma_f} \qquad 4.37$$

where σ_n is the applied net section stress in the component. The σ_f term is the stress at plastic collapse of the cracked component and represents the flow strength of the material, assumed to be the average of the yield and tensile strength, with a maximum value of

$$\sigma_f = 1.2 \cdot \sigma_y \qquad 4.38$$

The definition of plastic collapse as discussed in 4.9 is a local collapse of the cross section next to the crack tip, and not an overall collapse of the structure. The cross section dimensions are not necessary since plastic collapse occurs in tension. If bending was assumed, then the sectional area would be necessary to define the stress distribution.

The ratio of the linear elastic stress intensity factor to the effective stress intensity factor, (K / K_{eff}) is the given by

$$K_r = \frac{S_r}{\sqrt{\frac{8}{\pi^2} ln[sec\, 0.5\pi S_r]}} \qquad 4.39$$

This ratio needs no information of the of the crack and represents the limiting curve in Figure 4.10. This is the limit bound between safe and failure regions. For example, a brittle material (i.e. with low toughness) will fail when $K_r = 1$, but a material with high toughness it will fail first be plastic collapse, i.e. when $S_r = 1$. This curve represents the strength capacity, and is the limit line between failure and safe region.

A point must be calculated, which represents the actual state of the cracked component. Both the applied K_r and S_r values must be determined and plotted on Figure 4.10. The applied fracture ratio K_r is defined as

$$K_r = \frac{K_{Total}}{K_{mat}} + \rho \qquad 4.40$$

With K_{mat} being the fracture toughness of the material based on the actual thickness of the plate (i.e. a K_C not a K_{IC} value as determined from tests described in 4.7), and K_{Total} being the total stress intensity factor, which comprises K due to external loading, and self equilibrating (e.g. thermal, residual stresses). The latter stresses cannot cause plastic collapse of the structure as a whole as discussed in 4.9, but if large and close to the crack tip, they can contribute to fracture.

ρ is a plasticity correction factor, which models the plastic interaction between the primary and the secondary stresses. It is plasticity correction factor, but for internal self-equilibrating stresses and is calculated based on work by Ainsworth (1984).

By evaluating K_r from equations 4.39 and 4.40 we can see if the point lies within or out of the safe region. The component lies in the safe region if

$$\frac{K_{Total}}{K_{mat}} + \rho\,(from\ eq.\ 4.40) < \frac{S_r}{\sqrt{\frac{8}{\pi^2} ln[sec\,0.5\pi S_r]}}\,(from\ eq.\ 4.39) \qquad 4.41$$

The above equation is a fundamental relationship, for the reliability analysis performed in this thesis, because it will be used as the Limit State Function necessary to evaluate the probability of fracture of a bulk carrier containing cracked members, (chapter 7).

The most widely acceptable FAD is found in PD6493: "Guidance on methods for assessing the acceptability of flaws in fusion welded structures", first published in 1980, and being revised in 1991. The 1980 version did not include the strip-yield based FAD, but it was part of the R6 document. In 1998, there was a draft version

available, but it has not yet been published. The 1991 edition is used in this thesis unless another revision is specifically referenced.

Equation 4.39 defines the FAC of level 2 approach stated in PD6493, shown in Figure 4.10. The main advantage of this method is that the calculations are still based on linear elastic fracture mechanics, but at the same time allows for the plastic zone correction. It is a very useful simplification in comparison with using EPFM which require the evaluation of the *J-Integral* or the CTOD, probably by using FEA. The method allows for the variation between brittle fracture and plastic collapse. For high toughness materials K_r is usually small and S_r high, which implies plastic collapse. For low toughness materials with high yield strength, S_r is small and K_r high, i.e. failure in brittle mode. For intermediate stages elastic-plastic fracture occurs.

It is interesting to note that plastic collapse strength is not reduced until K_r exceeds 0.4, because a small stable crack will cause negligible reduction of area and hence negligible loss of strength. The fracture strength is slightly reduced even at quite small value of S_r, through the effect of crack tip plasticity.

The level 2 method is suitable for low work hardening materials therefore suitable for welded steel structures. For high work hardening materials a level 3 method maybe required, since level 2 is not very accurate for high S_r values and does not permit σ_f to exceed 1.2 σ_y. Level 3 method are used in the nuclear industry and for the design of pressure vessels. Level 3 method is less important for low toughness steels, would need more data on ship steels since they are material specific (e.g. require stress-strain curve), and are still important area for future research.

There is also a level 1 curve which is consistent with the CTOD design curve of the 1980 version of PD 6493. Level 1 is more conservative than level 2 FAD, and is shown in Figure 4.9.

It must be noted that all FAD's consider fracture in mode I as described in section 4.2. Other limitations include the absence of buckling mode of collapse, which is common in ship structures. In applying the method, one assumes that the applied stresses are well defined. However, certain stress re-distributions take place when a crack is

propagating and this effect is neglected, since it is difficult to determine the re-distribution of stresses. Even the use of finite element analysis would require a very complicated model. Therefore in a failure assessment analysis, the structural member is isolated from the other members and if failure occurs, it is then regarded as if this member is not present in the structure. However, this is not an important limitations since stress re-distributions are important only for very large cracks, relatively to the ship's width and height.

4.9.3 Stress Definitions

A member containing a crack, and subject to cyclic fatigue loading will have a strength that reduces with time. The crack will grow under the cyclic applied stress and at some time when the crack has grown to a limiting size, there will be a combination of applied stress and crack size that will exceed the residual strength of the member and fracture will occur. Residual strength assessment requires the **maximum** value of the net section stresses and of the crack driving force, that are probable during the period of interest.

For a ship being subjected to wave loading, stresses arise mainly from the cyclic wave action. But only the highest of these stresses will cause the member to fail. Discussion in chapter 3 for extreme loading explains the methods to determine these high stresses the ship will encounter. In addition to wave loading, still water loading is essential, since it adds to the stresses acting on the crack, and has effects on both S_r and K_r. Welding residual stresses have effect only on K_r since they add to the maximum stress intensity factor K_{max} used in K_r and contribute to fracture. They do not have a significant effect on the plastic collapse ratio since, they are self equilibrating and, with sufficiently large plastic strains would disappear ('shake down' as discussed in chapter 3)

Both ratios on the FAD depend on the applied stress. It is essential that correct stress components are used in the evaluation of K_r and S_r.

Stresses for S_r *(For use in equation 4.39)*

S_r is given from equation 4.37. The flow strength σ_f is easily calculated from

$$\sigma_f = \frac{\sigma_y + \sigma_t}{2} \qquad 4.42$$

with a limiting value given by equation 4.38.

The net section stresses for plastic collapse will be a combination of all possible loads acting on the member. These include,

- Maximum wave induced stress amplitudes (extreme loading)
- Still water bending stresses

Therefore

$$\sigma_n = \sigma_{max,wave\ amplitude} + \sigma_{swBM} \qquad 4.43$$

Stress Intensities for actual K_r *(For use in equation 4.40)*

The actual K_r is given by equation 4.40. The crack driving force K is a combination of the stress intensity factor because of extreme wave loading, still water bending stresses, and residual stresses. The stress intensity factor for extreme loading and still water bending are given by,

$$K_{extreme} = Y\sigma_{extreme}\sqrt{\pi a} \qquad 4.44$$

$$K_{swBM} = Y\sigma_{swBM}\sqrt{\pi a} \qquad 4.45$$

Still water bending stress is calculated from 3.39 and extreme stress amplitude from 3.29, for use in equations 4.43, 4.44 and 4.45. The total stress intensity factor required for residual strength assessment has three components, i.e. the stress intensity factor due to extreme loading, still water bending stresses and residual stresses. The residual stress intensity factor is calculated using the weight function technique as described in chapter 5. Given that the stress intensity factors are derived from linear elastic analysis, the principle of *superposition* applies to determine the total stress intensity

factor. This principle states that the stress intensity factor due to many loads acting on the system together is equal to the sum of stress intensity factors of the individual loads as if they were acting separately. Namely,

$$K_{Total} = K_{extreme} + K_{swBM} + K_{res} \qquad 4.46$$

4.10 Fatigue Crack Propagation

From an engineering point of view the fatigue life of a component or structure consists of three stages, (Barsom 1987):

- Crack initiation, which starts with the first load cycle and ends when a detectable crack is present
- Crack propagation, and
- Fracture

Depending on the type of component and on the intended application, the contribution to the total fatigue life of these three stages can consume widely different portions. For example, structural components that contain stress concentration or initial defects may be determined primarily by crack propagation stage. On the other hand, the fatigue of structural components intended for infinite life applications under constant fluctuation of low magnitude stress fields, may be governed by the fatigue initiation stage. The final stage, the fracture stage, represents the terminal conditions of the component's life, that is when the particular combination of stress, crack size and material fracture toughness leads to failure.

In general, a calculation method for fatigue life would have to include the first two stages. If is assumed that the appearance of cracks is indicative of failure, the calculation of crack initiation alone would be sufficient, (e.g. mechanical components required to survive for hundreds of millions of cycles). On the other hand, if cracks are present from the start, the calculation method for fatigue life can be restricted to the crack propagation stage only. In the case of welded structures, as in the case of

ship structures, where cracks or crack-like defects are present from the manufacturing stages onwards, the whole fatigue life consists of crack propagation alone.

Crack growth rate, usually denoted as $\frac{da}{dN}$, is the crack extension Δa, occurring per load cycle. Crack growth is a highly complicated phenomenon and depends on,

- The cyclic stress near the crack tip area
- Material properties
- Surface quality
- Crack size and crack front shape
- Environment

The prediction of crack growth from first principles is still a research area. To overcome such difficulties, practical methods are used which correlate the crack growth rates of *similar conditions*. In more detail, this means that for similar conditions (same environment, same material and same loading and crack size), the crack growth rates are similar. In section 4.4 it was discussed that the stress intensity factor K completely characterizes the local conditions near the crack tip area. The general expression for K is

$$K = Y\sigma\sqrt{\pi a} \qquad 4.47$$

So that a cyclic variation in stress σ will also cause a similar cyclic variation to K. The stress intensity range for a crack tip area will then be characterized by ΔK

$$\Delta K = K_{max} - K_{mn} = Y\Delta\sigma\sqrt{\pi a} \qquad 4.48$$

Equation 4.48 predicts that the stress intensity range for a small crack subjected to a large stress range and for a large crack subjected to a small stress range, will be the same, (Anderson 1991). Equation 4.48 is based on LEFM theory. The effect of the plastic zone in fatigue crack growth is not that important since the stress range levels

are relatively small and the size of the plastic zone is also very small. Hence, LEFM can be used to characterize the crack driving force (stress intensity range) necessary for crack growth predictions.

Crack growth rates are affected by the mean stress levels. If this is not the same in both cases, the crack growth rates will not be the same. Results from tests have indicated that crack growth with the same stress range, is lower when mean tensile stress is low or compressive and higher when mean stress is high. This is called the *mean stress* effect or *stress ratio* effect. We define stress ratio as

$$R = \frac{S_{min}}{S_{max}} = \frac{K_{min}}{K_{max}} \qquad 4.49$$

In the case of small surface cracks initiated at welds in a ship structure, they will be subjected to tensile residual stresses. In this case the stress ratio will be approximately one, as will be discussed in section 4.11. Hence stress ratio effect is not modelled in this thesis.

Given a crack in a particular material and environment the crack growth rate must be a function of stress intensity factor and stress ratio, i.e. $\frac{da}{dN} = f(\Delta K, R)$.

To determine crack growth rates, fatigue-testing experiments are carried out. Testing is conducted to specimens with cracks (edge crack specimens, center crack specimens, specimens with holes), for various load conditions (pure tension, pure bending, tension and bending) with constant amplitude stresses, and crack growth rates are recorded. Crack growth is measured visually or electrically, and the number of cycles counted. The stress intensity factors are computed for every crack increment and a $\frac{da}{dN} vs \Delta K$ curve is plotted, (Barsom 1999)

Figure 4.11 shows a schematic log-log plot of *da/dN* versus ΔK, which illustrates typical fatigue crack growth behaviour in metals. The sigmoidal curve contains three distinct regions.

Region I, where slow growth takes place, which diminishes with a decrease in ΔK. Eventually there will be a limit value of ΔK under which growth does not occur. This is called the stress intensity *threshold* value. Mean stress has a significant effect on growth in this region, (SSC-402).

Region II, where it can be assumed as a linear curve describing $\frac{da}{dN} vs \Delta K$, and mean stress effects have a less significant impact on growth, (SSC-402).

Region III, where crack growth increases rapidly with increase in ΔK. When ΔK exceeds a critical value (K_{IC}), the fracture toughness of the material, crack growth becomes unstable, until fracture occurs.

In this thesis, it will be assumed that crack growth mainly takes place in region two. Region I will only be modeled using a threshold factor which reduces the rate of crack growth, and not by considering some special crack growth relationship which accounts for this region.

4.10.1 Fatigue Crack Growth Equations

Crack growth equations are mainly empirical relationships deduced from test data. There are also some relationships which are semi-empirical based on physical considerations, but are valid only for specific applications and they are not general applicable. The applicability of the crack growth equations depends on over which region they are used. The most well-known and simplest equation is *Paris'* equation (Paris 1963)

$$\frac{da}{dN} = C\Delta K^m \qquad 4.50$$

where C and m are constants for a particular material and particular testing condition. This equation was developed from empirical results and has found wide application. The equation provides good accuracy in the intermediate region of fatigue crack growth, after the threshold region and before the fracture region. It is observed that if Paris' equation, with C and m values for region II, is used over region I it will provide

very conservative results, and if used over region *III* it will yield non-conservative results. However, because very little fatigue life is left when the crack enters region *III*, Paris' equation, with constant region II coefficients, will lead to conservative estimates, (Barsom 1999). Therefore, other forms have also been developed to provide estimates of the crack growth in the other regions. Klesnil and Lukas (1972) modified equation 4.50 to take into account the threshold effect in region I, to

$$\frac{da}{dN} = C(\Delta K^m - \Delta K_{th}^m) \qquad 4.51$$

where ΔK_{th} is the threshold stress intensity factor.

Walker (1970) suggested the introduction of the stress ratio R into the crack growth equation of 4.50

$$\frac{da}{dN} = C\left[\frac{\Delta K}{(1-R)^{1-n}}\right]^m \qquad 4.52$$

Where n is a constant depending on particular material.

Forman (1967) proposed the following equation to include the effect of rapid growth when entering region III

$$\frac{da}{dN} = \frac{C\Delta K^m}{(1-R)K_c - \Delta K} \qquad 4.53$$

where K_c is the fracture toughness of the material. Further improvement of this formula was made by Priddle (1976) to include the threshold effect

$$\frac{da}{dN} = \frac{C(\Delta K^m - \Delta K_{th}^m)}{(1-R)K_c - \Delta K} \qquad 4.54$$

Depending on which region the crack growth takes place, different models are available as shown above. In the middle region, which the relationship varies almost linearly, and is also called the stable crack growth region, a simple relationship to characterise the rate of crack growth is Paris' law and is given by equation 4.50. In

this thesis, Paris' equation is used to describe the crack growth in the middle region where the cracks spend most of their time, and has been found to give very good agreement with experiments if the appropriate material constants are used.

The crack growth in the first region is quite complicated phenomenon. In general, there is a value of stress intensity factor below of which there is no crack growth, called the stress intensity threshold factor. This stress threshold intensity value varies with crack size as well as material and loading. There are specific equations to account for the threshold effect e.g. equations 4.51 and 4.54, however a simple approach is to use a stress threshold intensity factor which reduces the rate of crack growth when the stress intensity fails below a threshold value. The modelling of the stress threshold intensity factor is discussed in 4.12.1 and is used in this thesis. An even simpler approach would be to have a cut off exactly at the stress threshold intensity value and assume there is no crack propagation at all and assuming a linear relationship down to this point, (which is not strictly correct since the rate of growth is reduced even before reaching the threshold value, due to the curved form of the relationship).

An opposite effect happens in region three, which is also called the unstable fracture region, and cracks grow uncontrollably when the stress intensity exceeds a critical value. An equation to describe crack growth in this region is equation 4.53. It is also possible to describe the crack growth in more than one regions or in all three, e.g. equation 4.54. Region III is not modelled in this report since very little fatigue life has been left when crack growth takes part in that region and failure occurs immediately.

4.10.2 Fatigue Life under Constant Amplitude Loading

In this report a one-dimensional fatigue crack growth model has been used to calculate the crack propagation. The basic equation used for the fracture mechanics model is Paris' law, given in equation 4.50.

where the stress range intensity factor is given by

$$\Delta K = Y(a) \cdot \Delta\sigma \cdot \sqrt{\pi \cdot a} \qquad (MPa\sqrt{m}) \qquad 4.55$$

Where C and m are material constants, $Y(a)$ is the geometry function (dependent on crack length), a is the crack length (m), and $\Delta\sigma$ is the stress range (MN/m^2).

The material constants are also dependent on the environment.

Substituting equation 4.55 into 4.50 and separating variables yields

$$\frac{da}{(Y(a)\sqrt{\pi a})^m} = C\Delta\sigma^m dN \qquad 4.56$$

Integration of equation 4.56 results to

$$\int_{a_o}^{a_N} \frac{da}{\left(Y(a)\cdot\sqrt{\pi\cdot a}\right)^m} = C\cdot\sum_{i=1}^{N}(\Delta\sigma_i)^m \qquad 4.57$$

But if $\Delta\sigma$ is constant

$$\sum_{i=1}^{N}(\Delta\sigma_i)^m = N\cdot\Delta\sigma^m \qquad 4.58$$

a_N is the crack size after N stress cycles, and a_o is the initial crack size. Substituting equation 4.58 into 4.57

$$\int_{a_o}^{a_N} \frac{da}{\left(Y(a)\cdot\sqrt{\pi\cdot a}\right)^m} = C\cdot N\cdot\Delta\sigma^m \qquad 4.59$$

The RHS of equation 4.59 is complicated by $\Delta\sigma$ not being a constant. However, as discussed in later sections the variability of $\Delta\sigma$ can be taken into account. The LHS of equation 4.59 however, is a more complicated term since the factor $Y(a)$ is dependent on crack size and the integral cannot usually be evaluated analytically, and numerical integration has to be used. In the case of a very simple geometry and with $Y(a)$ = constant ,solving for final crack length a_N, equation 4.59 takes the form

$$a_N = \left[\left\{\left(\frac{2-m}{2}\right)\cdot C\cdot N\cdot\Delta\sigma^m\cdot Y^m\pi^{m/2}\right\} + a_o^{\frac{2-m}{2}}\right]^{\frac{2}{2-m}} \qquad 4.60$$

4.10.3 Fatigue Crack Growth under Variable Loading

Under random loading the stress range will not be constant. For fracture mechanics calculations the sum of the *m'th* order of stress ranges is of particular importance, as it is shown from equation 4.57.

There are two approaches accounting for variable amplitude loading.

4.10.3.1 Equivalent Block Loading Approach

In this approach the purpose is to group all stress ranges with the same amplitude, for a specific time-history, to a finite number of *blocks*. The stress cycles in each block are assumed to be constant. Hence, the actual variable amplitude loading is reduced to an equivalent block loading. Having obtained the stress probability density function for a single response spectrum, the stress ranges are transformed into a block loading.

Assuming that the block loading has N_L number of blocks each with width dS_n where $dS_n = S_{n+1} - S_n$, and each block represents a constant amplitude stress S_n ,with $n(S_n)$ stress cycles, from the probability density function of the stress range distribution we can find the probability $f(S_n)$ of a stress range, falling in one of the blocks.

$$p(S_n)\, dS_n = f(S_n)\, dS_n \qquad 4.61$$

The number of stress cycles $n(S_n)$, for a stress range S_n in each block is equal to the probability of the stress range $p(S_n)$, times the rate of peaks in the process v_p, times the time of duration of the time-history t, times dS_n. Therefore,

$$n(S_n) = f(S_n) \times v_p \times t \times dS_n \qquad 4.62$$

The total number of cycles N in all blocks is equal to

$$N = \sum_{j=1}^{N_L} n(S_n)_j = \sum_{j=1}^{N_L} f(S_n)_j \times v_{p_j} \times t_j \times dS_n \qquad 4.63$$

The expected cumulative loading for all blocks is equal to

$$\sum_{i=1}^{N} S_i^m = \sum_{j=1}^{N_L} f(S_n)_j \times v_{p_j} \times t_j \times dS_n \times S_{nj} \qquad 4.64$$

If more than one sea state is considered, then the same procedure is followed but allowing for the probability of occurrence of each sea state. This is a useful approach when stress data in the form of a stress history is available. Then the stress history can be decomposed in a series of equivalent stress blocks and crack growth analysis for each block can be performed. In this method the stress blocks can be applied in any order, e.g. high-low, low-high-low, so that the effect of sequence in loading is studied.

4.10.3.2 Equivalent Stress Range Approach

The calculation of crack growth under variable loading can be considerably simplified if certain assumptions are made. If sequence and interaction effects are ignored, (discussed in section 4.10.5), then a weighted average stress range may be calculated to determine an equivalent stress range for cycle by cycle integration with the crack growth equation.

Each individual stress range and hence the sum of the stress ranges is a random process. However, in a fatigue analysis, if the number of cycles is large, the randomness of the sum is small and can be ignored (SSC-386). In this case the sum of the *m 'th* order can be expressed as the expected value. Namely

$$\sum_{i=1}^{N} \Delta\sigma_i^m \approx N\, E[\Delta\sigma^m] \qquad 4.65$$

with N being the total number of stress cycles in the process which is given by

$$N = v_0 \rho T \qquad 4.66$$

where v_0 is the zero crossing rate, given by equation 3.12, ρ is the fraction of time spent in sea, and T is the time which the ship is exposed under the specified loading.

In this approach, an equivalent constant amplitude stress is considered to replace the actual variable amplitude loading. The equivalent stress range is defined as an imaginary constant amplitude stress range that would cause the same amount of

fatigue damage as the total linearly accumulated damage caused by the actual random amplitude loading, (Barltrop 1991). It is calculated from

$$\Delta\sigma_{eq} = \left[\frac{\sum_{j=1}^{N} \Delta\sigma_j^m}{N}\right]^{\frac{1}{m}} \qquad 4.67$$

Using equation 4.65

$$\Delta\sigma_{eq} = \left[E\left(\Delta\sigma^m\right)\right]^{1/m} \qquad 4.68$$

Consequently an equivalent stress intensity factor is evaluated,

$$\Delta K_{eq} = Y\Delta\sigma_{eq}\sqrt{\pi a} \qquad 4.69$$

This approach is preferred for its simplicity and for its accuracy since it has shown reasonably good agreement with experimental works. It is also more suited for long-term fatigue and crack growth analysis and is therefore used in this thesis.

Using the discussion in sections 3.4.1 ad 3.4.2 for the short-term and long-term stress range distribution, the expected value for a short-term stress range distribution following a Rayleigh distribution is,

$$E[\sigma^m] = \left(2\sqrt{2}\ \sigma_\sigma\right)^m \Gamma\left(1+\frac{m}{2}\right) \qquad 4.70$$

where σ_σ is the standard deviation of the distribution. The long-term distribution is given by the weighted average of all short-term responses, using equation 3.15. Assuming a Weibull distribution for the long-term stress ranges with shape and scale parameters, B and A respectively, then

$$E[\sigma^m] = \int_0^\infty \sigma^m f_s(\sigma) d\sigma = \int_0^\infty \sigma^m \frac{B\sigma^{B-1}}{A^B} e^{-\left(\frac{\sigma}{A}\right)^B} d\sigma$$
$$= A^m \Gamma\left(1 + \frac{m}{B}\right) \qquad 4.71$$

4.10.4 Other Equivalent Stress Range Models

Many models have been proposed in the literature, using the assumption of the narrow band, stationery, Gaussian process. In such a case the stress distribution follows a Rayleigh distribution and the expected value given by equation 4.70.

It was mentioned in section 3.4.2 that using the Rayleigh model, stress ranges are overestimated and hence fatigue damage over predicted. When the process is not narrow banded the stress range probability distribution will not be as equation 3.13. Wirsching and Light (1980) have proposed a correction factor λ, which is based on simulation results from a rainflow analysis, that relates the damage rate by rainflow analysis to the damage rate by the Rayleigh, narrow band approximation, so that

$$E[\sigma^m] = \left(2\sqrt{2}\ \sigma_\sigma\right)^m \left[\lambda \Gamma\left(1 + \frac{m}{2}\right)\right] \qquad 4.72$$

$$\lambda = \frac{Damage\ rate\ from\ rainflow\ analysis}{Damage\ rate\ from\ Rayleigh\ approximation} \qquad 4.73$$

Using regression analysis, Wirsching proposed the following expression for λ

$$\lambda = a + (1-a)(1-\varepsilon)^b \qquad 4.74$$

with a = 0.926 – 0.033m and b = 1.587m – 2.323, where m is the exponent in Paris' equation. Typical values for λ for a bulk carrier are in the range of 0.9 ~ 1, (SSC-386).

Another model introduced by Chaudhury and Dover (1985) based on the assumption that the equivalent stress range solution will lie always between the narrow and wide band approximation, combined the Gaussian (for wide band) and the Rayleigh (for narrow band) probability distributions of the peak stresses to obtain

$$E[\sigma^m] = \left(2\sqrt{2}\,\sigma_\sigma\right)^m \left[\frac{\varepsilon^{m+2}}{2\sqrt{\pi}}\Gamma\left(1+\frac{m}{2}\right)+0.75\gamma\Gamma\left(1+\frac{m}{2}\right)\right] \qquad 4.75$$

where γ is called the irregularity factor defined as

$$\gamma = \frac{\nu_0}{\nu_p} \qquad 4.76$$

where ν_0, is given from equations 3.12.

$$\nu_p = \frac{1}{2\pi}\sqrt{\frac{m_4}{m_2}} \qquad 4.77$$

Another equation proposed by Hancock (1986) incorporates curve fitting parameters of the Weibull distribution, and has the form

$$E[\sigma^m] = (\alpha\sigma_\sigma)^m \Gamma\left(1+\frac{m}{\beta}\right) \qquad 4.78$$

with

$$\alpha = \sqrt{2}\sigma_\sigma\left(2-\varepsilon^2\right) \qquad 4.79$$

$$\beta = 2-\varepsilon^2 \qquad 4.80$$

A modified model of equation 4.78 was developed by Kam and Dover (1988) by introducing an error function *erf(x)* for each set of bandwidth parameters, γ and ε. This procedure improves the equivalent stress range in both narrow band and wide band stress spectra. This version has the form

$$E[\sigma^m] = \left(2\sqrt{2}\sigma_\sigma\right)^m \left\{\frac{\varepsilon^{m+2}}{2\sqrt{\pi}}\Gamma\left(1+\frac{m}{2}\right)+\left[\left(1+erf(\varepsilon,m)\right)\frac{\gamma}{2}\Gamma\left(1+\frac{m}{2}\right)\right]\right\} \qquad 4.81$$

In 1980 Wirsching has presented various stress spectra which are typical of offshore structures, subjected to random loading. These spectra were used by Zhao (1989) who

used the method of autoregressive simulation and rainflow counting method, to calculate an equivalent stress range.

Compared with these models the Rayleigh model (assumed in this thesis), using the narrow band assumption, is in the conservative side. However, the error is reduced when calculating the cumulative loading because of the large number of stress cycles which are assumed to be equal with the expected number of zero crossings; the other models use the expected number of peaks to equal the stress cycles.

4.10.5 Variable Amplitude Loading Effects and Assumptions for Ship Structures

When a structure is subjected to variable loading, cracks in structural components will experience changing stress amplitude. Cycle-by-cycle variations of stress ranges can produce *interaction effects* such as crack growth retardation or acceleration. When a high stress range is applied, (the stress range must be much bigger than the *usual* stress ranges in the stress history), then *crack closure* (crack retardation) is possible, or even crack arrest. Reasons for that effect include: a compressive plastic region being present ahead of the crack tip, crack branching, oxide-induced and/or roughness-induced crack closure, (Dominguez 1994).

The process of stress interaction is complex and although different models have been developed they only give an approximate correlation with the real physics of the phenomenon. Models that take into account stress interaction effects, fall into two categories:

Yield zone models, such as the models proposed by Willenborg *et al* (1971) and Wheeler (1972), which explain crack growth delays caused by overloads.

Wheeler's model includes a parameter φ, such that

$$\frac{da}{dN} = \varphi \cdot f(\Delta K) \qquad 4.82$$

Where φ varies between 0 and 1. The determination of φ is based on evaluating the size of the plastic zone near the crack tip and experimental results are required.

Willemborg, uses the concept of an effective stress intensity required to cancel out the effect of the plastic zone created by the overload. The model assumes the occurrence of compressive residual stress field due to the overload, which reduces the stress intensity factor and hence crack growth retardation. The Willemborg model does not require any experimental work.

Crack Closure models, which are based on the phenomenon of plasticity-induced crack closure. Here Elber's crack closure concept, (Elber 1970} is used i.e. the effective stress intensity factor. In an ideal crack, the crack faces close when the load is completely removed, and crack faces open at the time the load is applied. Elber suggested that cracks close before the load is completely removed, and cracks do not open until a certain level of stress has been reached. He proposed therefore

$$\Delta\sigma_{eff} = \sigma_{max} - \sigma_{op} \qquad 4.83$$

Where σ_{op} is the stress at which the crack starts to open. The concept of the effective stress intensity is illustrated in Figure 4.12.

In some cases (e.g. for some aluminium alloys in aircraft structures) the sequential order the load is applied is very important because of retardation effects, crack closure etc. However, Kam and Dover (1988), found that interaction effects cancel out under the assumptions of stationary, narrow-banded, long-term load responses, typical for marine structures. Hence, plasticity induced crack closure is not considered further in the analysis.

4.11 Effect of Residual Stresses on Fatigue Crack Growth

In the presence of residual stresses, the actual stress intensity factor, SIF, differs significantly from the stress intensity factor due to external load only. The actual SIF is not only a function of the residual stress field and the external applied stress field but it is a function of the crack geometry as well. The crack geometry has a significant

role on the SIF since, as discussed in section 4.10.5, crack closure due to plasticity requires the evaluation of an effective stress intensity factor, K_{eff}, which generally retards the crack growth.

Under these considerations, there are three distinct situations to examine,

(1). The crack remains fully open

(2). The crack tip is open while some part of the crack surfaces are closed

(3). The crack remains closed

The three cases are shown in Figure 4.13.

In the first case, when the crack remains fully open, the actual SIF due to external load and residual stress field can be calculated using the *principle of superposition*, as the algebraic sum of the two different contributions

$$K_{actual} = K_{ext} + K_{res} \qquad 4.84$$

During a stress cycle, the crack must remain open not only at the maximum stress intensity but at the minimum stress intensity as well.

The range of stress intensity factor, to be used in the crack growth equation is then given by

$$\Delta K_{actual} = (K_{max} + K_{res}) - (K_{min} + K_{res}) = K_{max} - K_{min} \qquad 4.85$$

i.e. the range of stress intensity factor is ***not*** affected by the residual stress intensity factor. Therefore, the residual stress field does not affect crack growth. This is true if the crack growth equation follows Paris' law, and the stress intensity range characterizes fully the crack propagation process.

When the crack faces are not fully open during a stress cycle, the superposition principle is not valid, since when crack surfaces 'touch', non-linear effects take place and numerical techniques are used to calculate the actual SIF. In addition to the

external and residual stress SIF, when crack surfaces close, a third component due to contact must be included i.e. the SIF due to contact or crack closure.

The actual range of stress intensity must then be calculated considering the non-linear contact effects. At maximum load the crack surfaces remain open, and the maximum stress intensity can be calculated using equation 4.84. At minimum load, crack surface closure is expected, and the minimum stress intensity must be calculated by the following two different cases,

(1). For cracks partially closed at minimum load

$$\Delta K_{actual} = (K_{max} + K_{res}) - K_{min} \qquad 4.86$$

(2). For crack fully closed at minimum load,

$$\Delta K_{actual} = (K_{max} + K_{res}) \qquad 4.87$$

Generally, for small cracks the crack surfaces remain fully open even at minimum load, therefore ΔK is calculated using 4.84. Larger cracks require analysis using the other two cases as well, since it is possible for the crack surfaces to be partially or fully closed.

Under static tensile residual stresses small cracks tend to remain open, therefore residual stresses enhance the effect of fatigue cyclic loading. On the other hand, compressive residual stresses tend to close the crack front, and reduce the fatigue effect of cyclic loading.

Under the assumption of Paris' law with small cracks, propagating within a tensile residual stress field, crack surfaces remain open even at minimum load and residual stress intensity has no effect on the stress intensity range used in Paris' law to calculate the crack propagation. The assumption is true for small cracks initiated from welds in a ship structure which are inside tensile residual fields. No adjustment is therefore needed on the crack growth model used in this thesis (Paris' law) because of residual stress.

4.12 Fatigue Crack Growth Modelling

Following the earlier discussion in section 3.6.3 the stress range distribution may be approximated as a Weibull distribution. The Weibull probability function has the form:

$$F(\sigma)=1-e^{-\left(\frac{\sigma}{A}\right)^{B}} \qquad 4.88$$

and the density function the form

$$f(\sigma)=\frac{B}{A}\cdot\left(\frac{\sigma}{A}\right)^{B-1}\cdot e^{-\left(\frac{\sigma}{A}\right)^{B}} \qquad 4.89$$

with expected value

$$E[\sigma]=A\cdot\Gamma\left[\frac{1}{B}+1\right] \qquad 4.90$$

and the m'th moment of the stress range is equal to

$$E[\sigma^{m}]=A^{m}\cdot\Gamma\left[\frac{m}{B}+1\right] \qquad 4.91$$

Where A is the scale and B is the shape parameter of the Weibull distribution and $\Gamma[...]$ is the gamma function.

If the *equivalent constant amplitude stress range approach*, is used the crack growth equation for variable amplitude loading becomes

$$\int_{a_0}^{a_N}\frac{da}{\left(Y(a)\cdot\sqrt{\pi\cdot a}\right)^{m}}=C\cdot N\cdot A^{m}\cdot\Gamma\left[\frac{m}{B}+1\right] \qquad 4.92$$

4.12.1 Modelling of Stress Threshold Effect

If the stress intensity threshold effect is to be considered, then only the damaging part of the stress ranges need to be considered in the crack growth analysis. Namely

$$E\left[\Delta\sigma^{m}\right]\cdot G(a) \qquad 4.93$$

Where $G(a)$ is the stress threshold factor. The stress threshold factor is expressed as

$$G(a)=\frac{E_{dam}[\Delta\sigma^{m}]|_{th}^{\infty}}{E[\Delta\sigma^{m}]} \qquad 4.94$$

$$G(a)=1-\frac{E_{dam}[\Delta\sigma^{m}]|_{0}^{th}}{E[\Delta\sigma^{m}]} \qquad 4.95$$

where

$$E_{dam}[\Delta\sigma^{m}]|_{0}^{th}=A^{m}\cdot\Gamma\left[1+\frac{m}{B};\left(\frac{\Delta\sigma_{th}}{A}\right)^{B}\right] \qquad 4.96$$

Where $\Gamma[...;...]$ is the incomplete gamma function. Clearly as $\Delta\sigma_{th} \rightarrow 0$, $G(a) \rightarrow 1$ with $0 \leq G(a) \leq 1$.

Where

$$\Delta\sigma_{th}=\frac{\Delta K_{th}}{Y(a)\sqrt{\pi a}} \qquad 4.97$$

Note that as $\Delta\sigma_{th}$ is function of crack length and changes as crack grows. The purpose of the stress intensity threshold factor is to filter-out the non-damaging stress cycles from the total stress range distribution.

The equation for crack propagation then becomes

$$\int_{a_o}^{a_N}\frac{da}{\left(Y(a)\cdot\sqrt{\pi\cdot a}\right)^{m}G(a)}=C\cdot N\cdot A^{m}\cdot\Gamma\left[\frac{m}{B}+1\right] \qquad 4.98$$

4.12.2 Modelling of Corrosion Effect on Crack Growth

The effect of corrosion increasing with time also needs to be considered. Corrosion in general was discussed in chapter 1. In this section the modelling of the corrosion rate is considered.

Corrosion affects the Paris law coefficients C and m, threshold value and stress (through thickness loss). In the present study, the relative increase in stress level over time, because of the thickness reduction, is calculated from the following expression:

$$S_{cor} = \frac{z}{z - k_{cor} \cdot T} \qquad 4.99$$

Where

z : Is the thickness of the material

k_{cor} : Is the corrosion rate

T : Is the time

In such a case the $\sum_{i=1}^{N} (\Delta\sigma_i)^m$ term in crack growth equation becomes, $\sum_{i=1}^{N} (\Delta\sigma_i \cdot S_{cor})^m$, and approximation being given by, (SSC-386)

$$\sum_{i=1}^{N} (\Delta\sigma_i \cdot S_{cor})^m \approx N \cdot E[\Delta\sigma^m] \cdot B_{cor} \qquad 4.100$$

where

$$B_{cor} = \frac{z}{k_{cor} \cdot T \cdot (m-1)} \cdot \left\{ \left(\frac{z}{z - k_{cor} \cdot T} \right)^{(m-1)} - 1 \right\} \qquad 4.101$$

B_{cor} : Is the corrosion factor

Including 4.101 in equation 4.98, yields

$$\int_{a_o}^{a_N} \frac{da}{\left(Y(a) \cdot \sqrt{\pi \cdot a}\right)^m \cdot G(a)} = C \cdot N \cdot A^m \cdot \Gamma\left[\frac{m}{B} + 1\right] \cdot B_{cor} \qquad 4.102$$

Another model, introduced by Paik (1998), considers also the time before the coating breaks down and is given by,

$$r = c_1 T_o^{c_2} \qquad 4.103$$

where r is the reduction in thickness, c_1 is the annual corrosion rate, c_2 is about 1/3, T_o is the elapsed time after coating breakdown $T_o = T\text{-}T_a$, T represents the age of the vessel, T_a is the life of the coating.

4.13 Crack Growth Example

Equation 4.102 is the basic equation that will be used in this thesis to calculate the crack extension from an initial value a_o to a value a_N after N cycles. The LHS of this equation represents the total fatigue damage accumulated in N cycles. The RHS is the loading term obtained as a summation of all the individual stress ranges acting over N cycles.

Using equation 4.102 we can calculate the crack increase with respect to time, or in this case with respect to stress cycles. This form of the equation is usually more suitable to solve if both the initial and final cracks are known. In such a case, the integral is solved, usually numerically because of the complexity of its form, and the stress cycles required to propagate the crack from the initial value to the final value are evaluated, assuming all other parameters are known. The stress cycles can be related to number of years, if the number of stress cycles in one year is known.

In this report, a fracture assessment analysis is used which requires the crack size with respect to time (stress cycles), and therefore equation 4.102 has to be used to evaluate crack size with respect of time and not number of stress cycles. Usually the crack growth is calculated on a year by year basis, which means N represents the number of cycles in one year, which is determined from the spectral fatigue analysis performed.

The problem that arises is to solve the integral in equation 4.102 for the final crack size, i.e. the crack size after one year or N cycles (where N: number of stress cycles in one year). Since the final crack size is not known, the $G(a)$ and $Y(a)$ parameters which

are a function of a, are not known, and the integral cannot be solved. A different technique must be used than the one described above, i.e when the final crack size is known. This method involves the crack propagation of an initial crack to a known final crack, in very small increments and the corresponding stress cycles for each crack increment evaluated. A crack size versus stress cycles graph can then be plotted. From the actual initial crack and with the number of stress cycles in one year, the final crack size after one year can be determined. The graph must be produced with the same parameters as in the actual case i.e. stress range, material constants etc. The method is illustrated in Figure 4.14.

The first step is to produce a crack advance curve i.e. a plot that relates the crack sizes to the number of stress cycles as shown in Table 4.2. By solving equation 4.102 for the number of stress cycles N we have the necessary relationship between crack sizes and stress cycles is found, i.e.

$$N = \frac{\int_{a_o}^{a_N} \frac{da}{\left(Y(a)\cdot\sqrt{\pi\cdot a}\right)^m \cdot G(a)}}{C\cdot A^m \cdot \Gamma\left[\frac{m}{B}+1\right]\cdot B_{cor}} \qquad 4.104$$

Using equation 4.104 with the crack sizes in Table 4.3 and the input data in Table 4.2 the number of stress cycles it is required to grow the crack from one crack size to another is determined.

With the crack growth curve determined, the initial crack a_o is plotted, as shown in Figure 4.14, and the value N_o read. Then the number of stress cycles in one year N,is added to the value read from the graph and N_n is obtained. A line is drawn from this point to the curve, and the value of the new crack size a_n is read. The procedure follows the direction of the arrows on the figure.

4.13.1 Numerical Example on Crack Growth Analysis

In actual structures, through thickness cracks usually have an irregular curved crack front. Also, surface and embedded cracks have irregular shapes. For fracture mechanics analysis, it is common practice to assume that through thickness cracks

have straight fronts and only the average crack growth along the front line is predicted. An embedded crack is idealised as an elliptical flaw whereas the surface crack is idealised as a semi-elliptical flaw.

Consider a surface crack in a plate, that grows in the thickness direction as shown in Figure 4.15. The crack that grows into the thickness direction is denoted by *a*, whereas the crack that grows in the surface is denoted by *c*.

The stress intensity threshold value is set to zero for simplicity of the calculations. The integral in equation 4.104 is evaluated numerically using the trapezoidal rule. Table 4.6 shows the calculation of the number of stress cycles for the corresponding crack sizes i.e. from an initial value of 0 mm up to a value of 24 mm.

The first column in Table 4.6 represents the crack increments. The smaller the crack increments the more accurate the results, will be. The second column represents the geometry factor values for a surface crack. These values were evaluated using the solution for a semi elliptical surface crack in a plate, from PD6493. The third column is the value of the integral in equation 4.104. For example the first and the second values of the third column are given by,

$$I_1 = 0.5 \cdot (1-0) \cdot \left(\frac{1}{0.9631^3 \cdot \left(\sqrt{\pi \cdot 1}\right)^3} \right) = 0.1005 \qquad 4.105$$

$$I_2 = 0.5 \cdot (1.5-1) \cdot \left(\frac{1}{0.8708^3 \cdot \left(\sqrt{\pi \cdot 1.5}\right)^3} - \frac{1}{0.9631^3 \cdot \left(\sqrt{\pi \cdot 1}\right)^3} \right) + I_1 \qquad 4.106$$

$$I_2 = 0.1878$$

The third column is determined by equation 4.104, and it is a simple division of the values of the third column by the product of the terms in the numerator.

In this case

$$\left[C \cdot A^m \cdot \Gamma\left(1 + \frac{m}{B}\right) \cdot B_{cor} \right]^{-1} = \left[6.91E-13 \cdot 8^3 \cdot \Gamma\left(1 + \frac{3}{0.842}\right) \cdot 1.0 \right]^{-1} = 219217303.7$$

so the second entry in the fourth column is equal to,

$N_1 = I_1 \cdot 219217303.7 \approx 22034636$ cycles. B_{cor} comes from equation 4.127 for T=1 and z = 25 mm.

Dividing this number by the number of stress cycles in one year, i.e. N = 3884938, we obtain the number of years (fifth column) required for the crack to grow from the initial size (0 mm) to the final size (1 mm) is obtained. Figure 4.16 shows the final crack growth curve.

Unfortunately, the calculations must be repeated every year because the variables change, i.e. the stress levels increase because of the reduction in thickness and B_{cor} must be calculated every year, and the stress intensity threshold also changes with time and must be re-calculated.

Once the crack growth curve is established, crack growth analysis can be performed. An initial value is assumed. In this case the initial value assumed is 0.5 mm.

The number of stress cycles that correspond to a crack of 0.5 mm should be determined from the graph or from Table 4.6. If the crack size increment used for the numerical integration is very small, the crack growth rate is approximately constant in each band of 'a'. If the values of Table 4.6 are used, a linear interpolation gives a value that corresponds to a = 0.5mm. This is found to be, $N_{0.5}$ = 11017318 cycles. The number of cycles in one year should be added to this value, giving

$$N_f = 11017318 + 3884938 = 14902256 \text{ cycles}$$

Again an interpolation is necessary to find the crack length that corresponds to this number. This turns out to be between 0mm and 1mm and the corresponding crack length is

$$a_f = 0.676\text{mm}$$

This means that the crack has grown from an initial value of 0.5 mm to 0.676 mm in one year. If the variables used in the crack propagation equation do not change, the

same crack growth curve can be used to calculate the growth for the next year as well. Otherwise, the crack growth curve should be re-evaluated with the new parameters.

REFERENCES

- Almar-Naess A., 'Fatigue handbook', Offshore Steel Structures, Tapir, 1985
- Anderson T. L., 'Fracture mechanics, fundamentals and applications', CRC Press, 1991
- Ainsworth R. A., 'The treatment of thermal and residual stresses in fracture assessments', CEGB Report TPRD/0479/N84, 1984
- Barltrop N. P. D., Adams A. J., 'Dynamics of fixed marine structures', Butterworth-Heinemann, 3rd Edition, London 1991
- Barsom J. M., Rolfe S. T., 'Fracture and fatigue control in structures', Prentice-Hall, 2nd edition, 1987
- Barsom J. M., Rolfe S. T., 'Fracture and fatigue control in structures: applications of fracture mechanics', Butterworth-Heinemann, 3d edition, 1999
- Broberg B. K., 'Cracks and fracture', Academic Press, 1999
- Broek D. 'The practical use of fracture mechanics' ,1989
- BSI, PD6493, 'Guidance on methods for assessing the acceptability of flaws in fusion welded structures', 1991
- Burdekin F. M., Stone D. E. W., 'The crack opening displacement approach to fracture mechanics in yielding materials', Journal of Strain Analysis, Vol. 1, 1966
- Choudhury G., Dover W. D., 'Fatigue analysis of offshore platforms subjected to sea wave loads', International Journal of Fatigue, Vol. 7, 1985
- Dominguez J., 'Fatigue crack growth under variable amplitude loading', Handbook of Fatigue Crack Propagation in Metallic Structures, Andrea Carpinteri (Editor), 1994

- Dowling A. R., Townley C. H. A., 'The effects of defects on structural failure: a two-criteria approach', International Journal of Pressure Vessels and Piping, Vol. 3, 1975

- Dugdale D. S., 'Yielding of steel sheets containing slits', Journal of Mech. Phys. Solids, Vol. 8, 1960

- Elber W., 'Fatigue crack closure under cyclic tension', Engineering Fracture Mechanics, Vol. 2, 1970

- Forman R. G., Keary V. E., Engle R. M., 'Numerical analysis of crack propagation in cyclic-loaded structures', Journal of Basic Engineering, Vol. 89, 1967

- Griffith A. A., 'The phenomena of rupture and flow in solids', Philosophical Transactions, Series A, Vol. 21, 1920

- Gurney T. R., 'A revised analysis of the influence of toe defects on the fatigue strength of transverse non-load-carrying fillet welds', Welding Research International, Vol. 9, No. 3, 1979

- Gurney T. R., 'Fatigue of welded structures', Cambridge University Press, 2nd edition, 1979

- Hancock J. W., Gall D. S., Huang X., 'Fatigue crack growth due to random loading', Proceedings in Fatigue and Crack Growth in Offshore Structures, IME, 1986

- Inglis C. E., 'Stresses in a plate due to the presence of cracks and sharp corners', Transactions of Institution of Naval Architects, Vol. 55, 1913

- Irwin G. R., 'Fracture dynamics', Fracturing of Metals, ASME, 1948

- Kam J. C. P., Dover W. D., 'Fast fatigue assessment procedures for offshore structures under random stress history', Proceedings of ICE, Vol. 85, 1988

- Kanninen M. F., Popelar C. H., 'Advanced fracture mechanics', Oxford University Press, 1985

- Klesnil M., Lucas P., 'Influence of strength and stress history on growth and stabilisation of fatigue cracks', Engineering Fracture Mechanics, Vol. 4, 1972

- Maddox S. J., 'Fatigue strength of welded structures', Abington Press, 2nd edition, 1991

- Miner M. A., 'Cumulative damage in fatigue", Journal of Applied Mechanics, Vol. 12, Trans. of ASME, vol. 67, pp A159-A164, 1945

- Osgood C., 'Fatigue design', Pergamon press, 2nd edition, 1982

- Paik J. K. , Thayamballi A. , Kim S. K. , Yang S. H. , 'Ship hull ultimate strength reliability considering corrosion', Journal of ship research, Vol. 42, No. 2, June 1998

- Paris P. C., Erdogan F., 'A critical analysis of crack propagation laws' Journal of Basic Engineering December 1963, pp. 528-534

- Parker A. P., 'The mechanics of fracture and fatigue', E.& F.N. SPON LTD, 1981

- Priddle E. K., 'High cycle fatigue crack propagation under random and constant amplitude loadings', Int. J. Pres. Ves. & Piping, Vol. 4, 1976

- Raju I., Newman J., 'An empirical stress intensity factor equation for the surface crack', Engineering Fracture Mechanics, Vol. 15, 1981

- Reemsnyder H. S., 'Fatigue and fracture of ship structures', in Symposium and Workshop on the Prevention of Fracture in Ship Structure, NRC, 1997

- Rooke D. P., Cartwright D. J., 'Compendium of stress intensity factors', Her Majesty's Stationery Office, 1976

- Schijve J., 'Four lectures on fatigue crack growth', Engineering Fracture Mechanics, Vol. 11, 1979

- Sih G. C., 'Handbook of stress intensity factors', Lehigh University Press, 1973

- SSC-369, 'Reduction of S-N curves for Ship Structural Details', Ship Structure Committee, 1993

- SSC-381, 'Residual strength of damaged marine structures', Ship Structures Committee report, 1995

- SSC-386, 'Ship's maintenance project', Ship Structures Committee report, 1995

- SSC-393, 'Evaluation of ductile fracture models', Ship Structures Committee report, 1997

- SSC-402, 'Guide to damage tolerance analysis of marine structures', Ship Structures Committee report, 1997

- Tada H., Paris P. C., Irwin G. R., 'The stress analysis of cracks, handbook', Del Research Corporation, 1973

- Tait & Garret, 'Fracture and fracture mechanics-case studies', 1984

- Thayamballi A., Chen Y. K., Donald L., 'Fracture mechanics based assessment of fatigue reliability in ship structures', SNAME, in Ship Structures Symposium 1984

- Tetelman A. S., 'Fracture of structural materials', 1967

- Tomita Y., Toyosada M., Sumi Y., Kumano A., 'Fatigue crack propagation in ship structures', Handbook of Fatigue Crack Propagation in Metallic Structures, Andrea Carpinteri (Editor), 1994

- Walker E. K., 'The effect of stress ratio during crack propagation and fatigue for 2024-T3 and 7065-T6 aluminium', ASTM, STP-462, 1970

- Westergaard H. M., 'Bearing pressures and cracks', Journal of Applied Mechanics, Series A, Vol. 66, 1939

- Wheeler O. E., 'Spectrum loading and crack growth', Journal of Basic Engineering, Vol. 94, 1972

- Willenborg J. D., Engle R. M., Wood H. A., 'A crack growth retardation model using an effective stress concept', AFFDL-TM-FBR-71-1, Air Force Flight Dynamics Lab., 1971

- Wirsching P. H., Light M. C., 'Fatigue under wide band random stresses', Journal of Structural, Division, ASCE, 106(ST7), 1980

- Zhao W., 'Reliability analysis of fatigue and fracture under random loading', PhD Thesis, Dept. of Civil Eng., Imperial College London, 1989

Initial crack size	a_o	known
Stress range	$\Delta\sigma$	known
Number of stress cycles	N	known
Material constants	C & m	known
Final crack size	a	uknown

Table 4.1 – *Table of input variables*

Crack size increment	Stress cycles
a0	*N0*
a1	*N1*
a2	*N2*
a3	*N3*
a4	*N4*
a5	*N5*
a6	*N6*
a7	*N7*
a8	*N8*
a9	*N9*
a10	*N10*

Table 4.2 - *Crack sizes vs. stress cycles*

Initial crack size	*ao*	*0.500*	mm
Material constant	*C*	*6.91E-13*	for □K in Mpa-m $^{0.5}$
Material constant	*m*	*3.00*	-
Thickness	t	*25*	mm
Weibull scale parameter	*A*	*8.00*	-
Weibull shape parameter,	*B*	*0.842*	-
Stress cycles in one year	*N*	*3884938*	cycles
Stress intensity threshold	$\square K_{th}$	*0.00*	Mpa-m$^{0.5}$
Corrosion rate	K_{cor}	*0.25*	mm/year

Table 4.3 – *Input variables for crack growth example*

Crack sizes (mm)	Y	I	Stress cycles	Years
0	0	0	0	0
1	0,9631	0,1005	22034636	5,67
1,5	0,8708	0,1878	41165260	10,60
2	0,8313	0,2524	55335764	14,24
2,5	0,8021	0,3021	66217929	17,04
3	0,7793	0,3423	75045054	19,32
3,5	0,7606	0,3762	82463220	21,23
4	0,7451	0,4053	88853335	22,87
4,5	0,7319	0,4309	94457200	24,31
5	0,7201	0,4536	99444486	25,60
6	0,7016	0,4928	108037687	27,81
7	0,6866	0,5255	115199521	29,65
8	0,6745	0,5534	121318116	31,23
9	0,6648	0,5777	126634348	32,60
10	0,6567	0,5990	131313626	33,80
12	0,6441	0,6352	139253738	35,84
14	0,6352	0,6648	145730361	37,51
16	0,6283	0,6895	151142881	38,90
18	0,6226	0,7105	155759042	40,09
20	0,6172	0,7288	159767196	41,12
22	0,6114	0,7450	163308609	42,04
24	0,6046	0,7595	166492986	42,86

Table 4.4 - *Calculation of crack sizes vs. stress cycles*

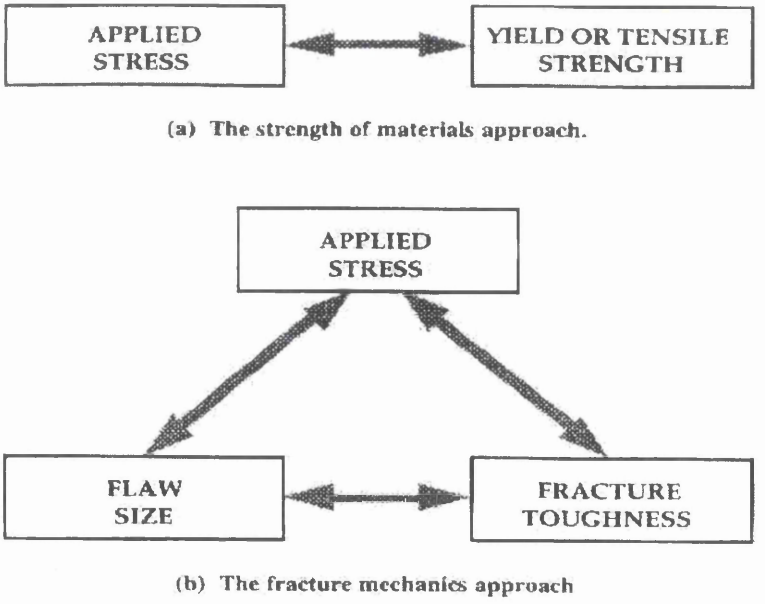

Figure 4.1 – *Traditional approach versus Fracture Mechanics approach* (Anderson 1991)

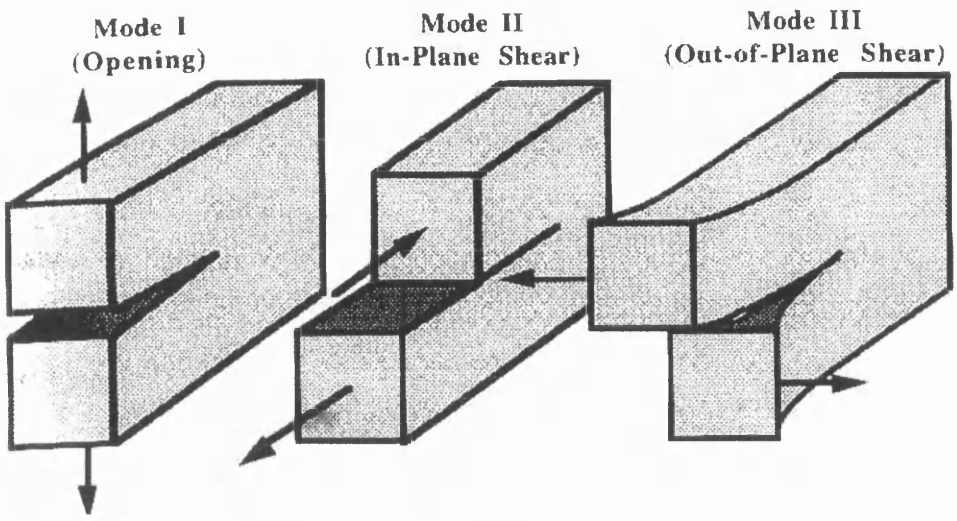

Figure 4.2 - *Modes of fracture* (Broek 1989)

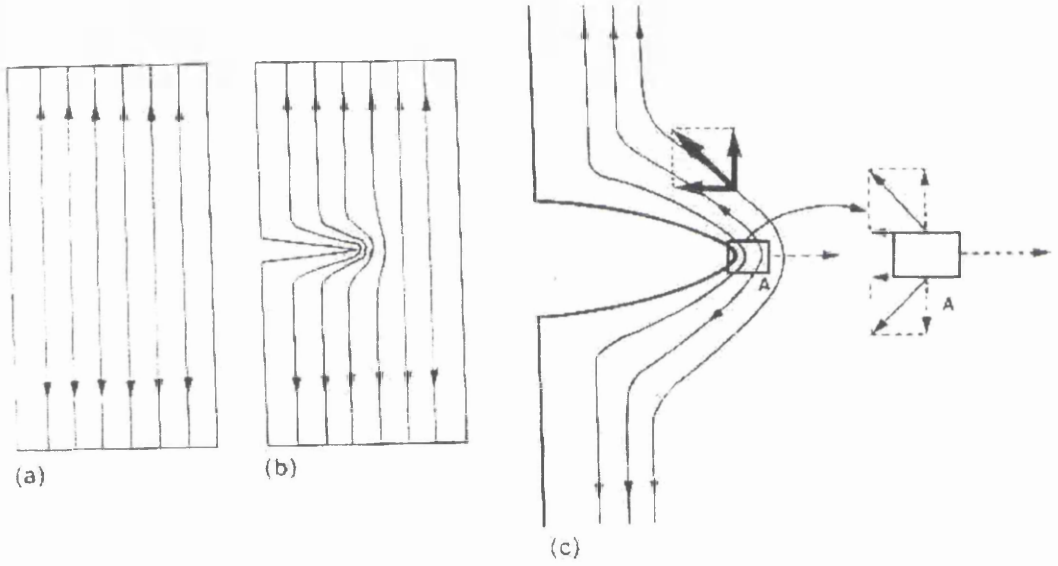

Figure 4.3 – *Load redistribution due to cracked ligament* (Broek 1989)

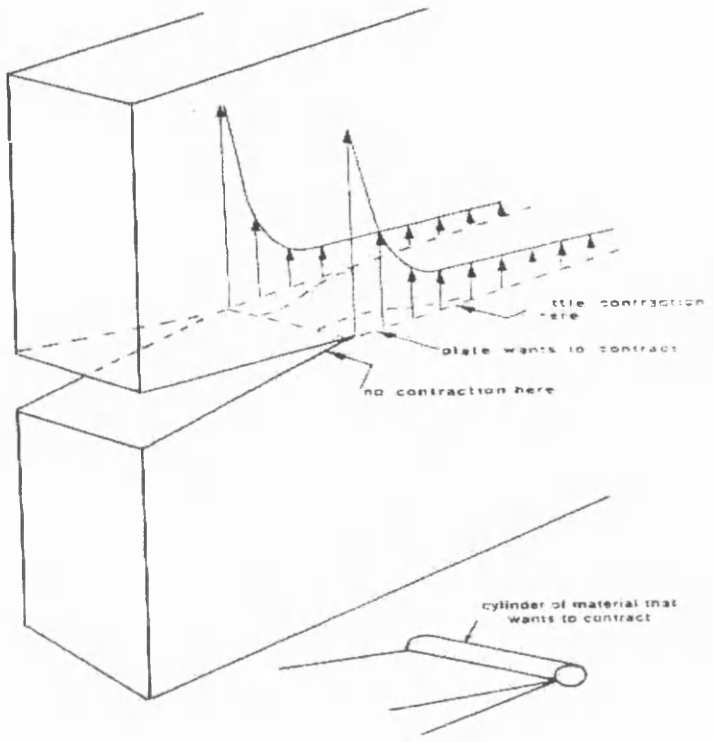

Figure 4.4 – *Effect of thickness on stress distribution close to crack tip* (Broek 1989)

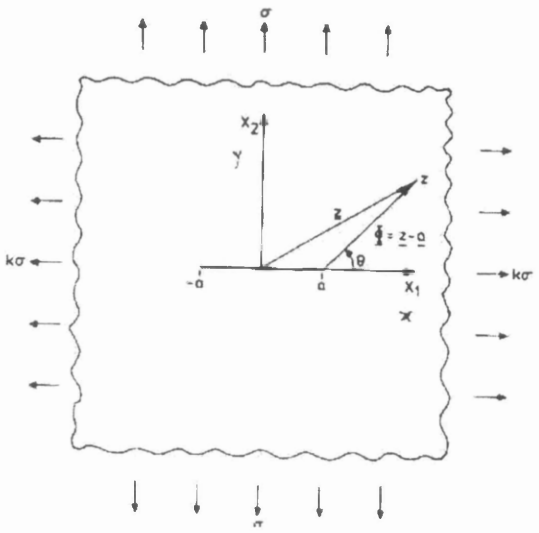

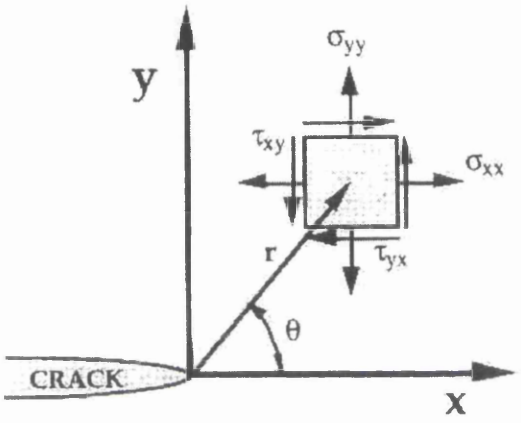

$$\sigma_{xx} = \frac{K_I}{\sqrt{2\pi r}} \cos\left(\frac{\theta}{2}\right)\left[1 - \sin\left(\frac{\theta}{2}\right)\sin\left(\frac{3\theta}{2}\right)\right]$$

$$\sigma_{yy} = \frac{K_I}{\sqrt{2\pi r}} \cos\left(\frac{\theta}{2}\right)\left[1 + \sin\left(\frac{\theta}{2}\right)\sin\left(\frac{3\theta}{2}\right)\right]$$

$$\tau_{xy} = \frac{K_I}{\sqrt{2\pi r}} \cos\left(\frac{\theta}{2}\right)\sin\left(\frac{\theta}{2}\right)\cos\left(\frac{3\theta}{2}\right)$$

Figure 4.5 – *Stress field equations near crack tip* (Anderson 1991)

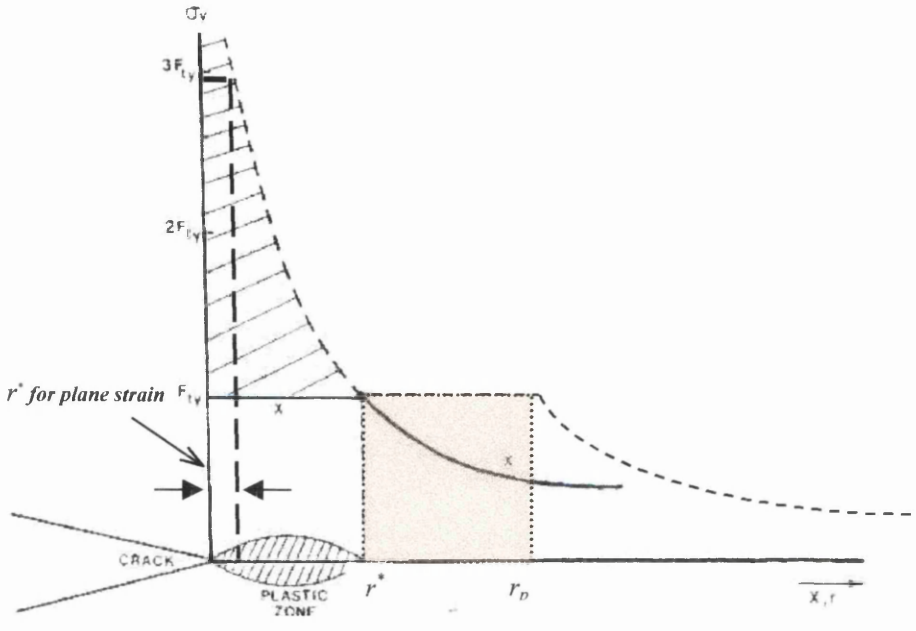

Figure 4.6 – *Plastic region close to crack tip* (Broek 1989)

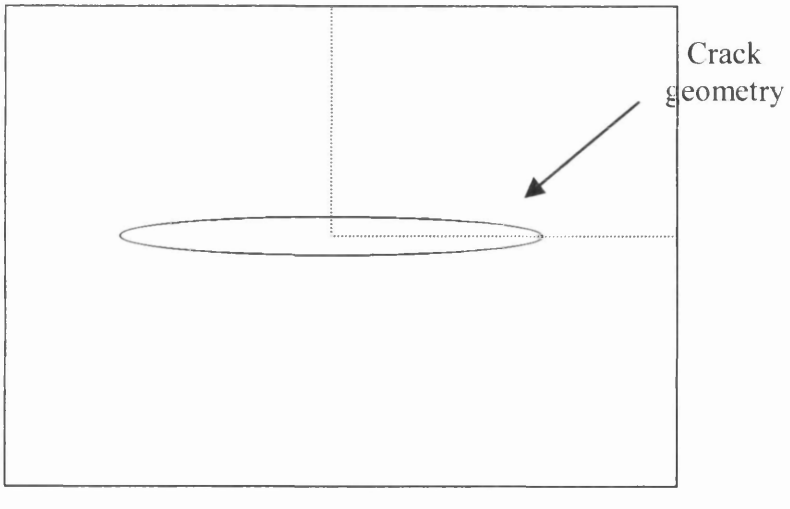

Figure 4.7 – *Cracked geometry*

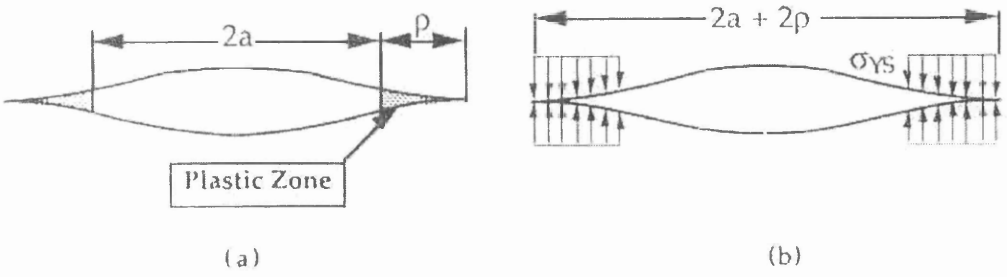

Figure 4.8 – *The strip-yield model* (Anderson 1991)

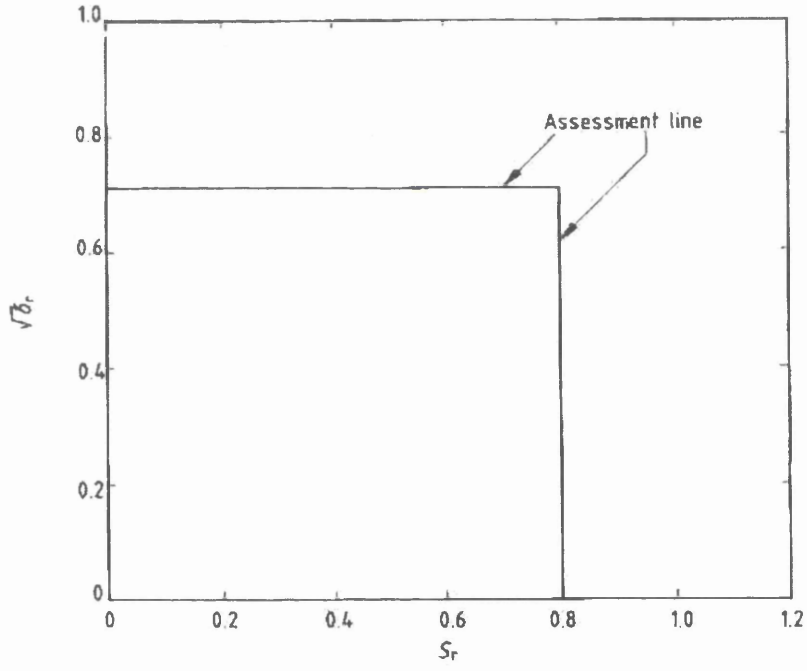

Figure 4.9 – *Level 1 failure assessment diagram* (PD 6493)

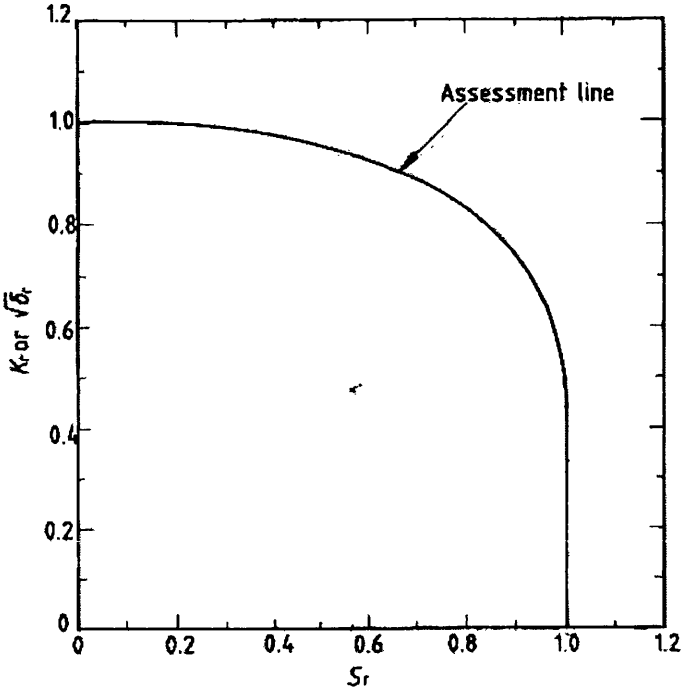

NOTE. The line is derived from the following equation

$$K_r \text{ or } \sqrt{\delta_r} = S_r \left[\frac{8}{\pi^2} \ln \sec \left(\frac{\pi}{2} S_r \right) \right]^{-0.5}$$

Figure 4.10 - *Level 2 failure assessment curve* (PD 6493)

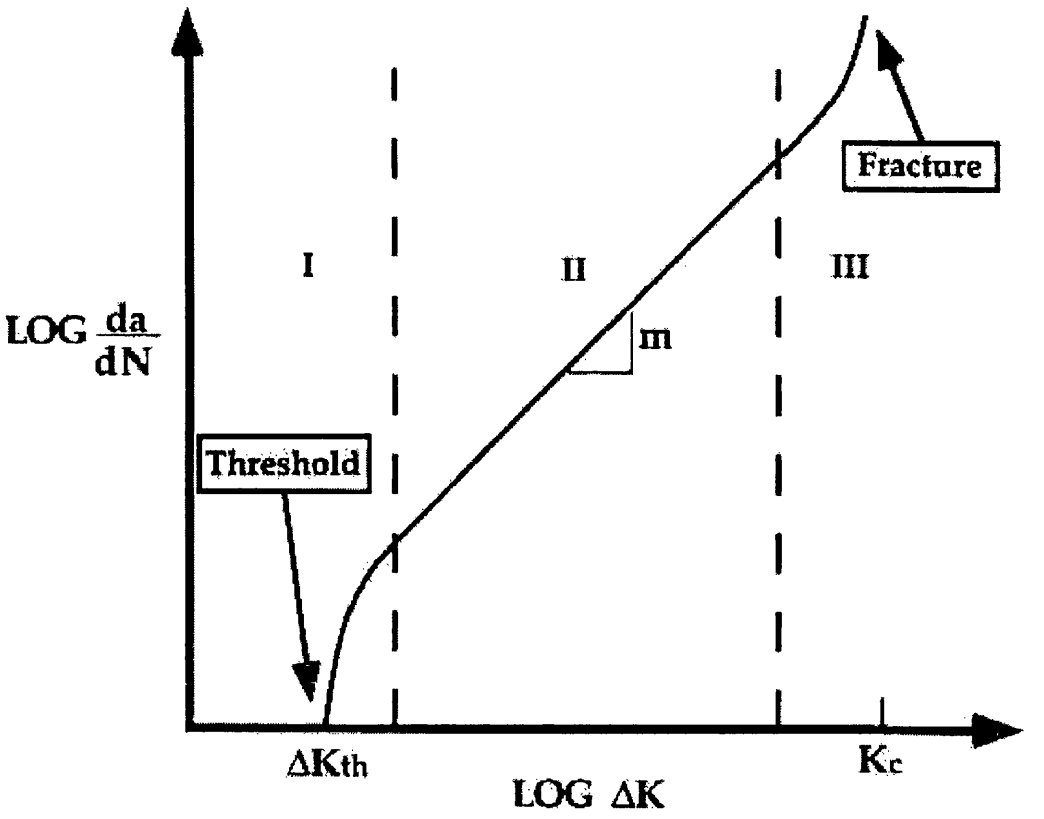

Figure 4.11 – *Crack growth curve* (Anderson 1991)

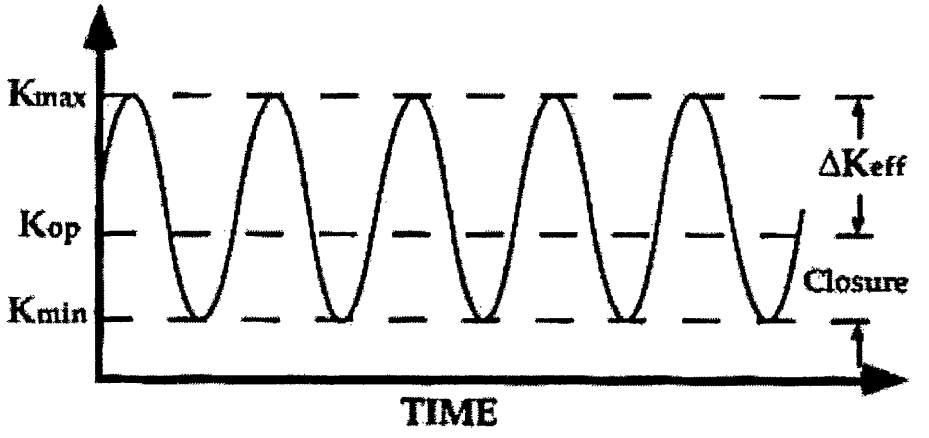

Figure 4.12 – *Effective stress intensity* (Anderson 1991)

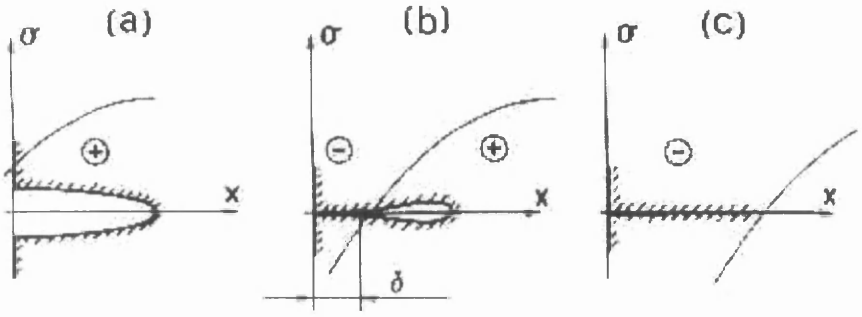

Figure 4.13 – *Crack fully open; crack partially closed; crack fully closed*

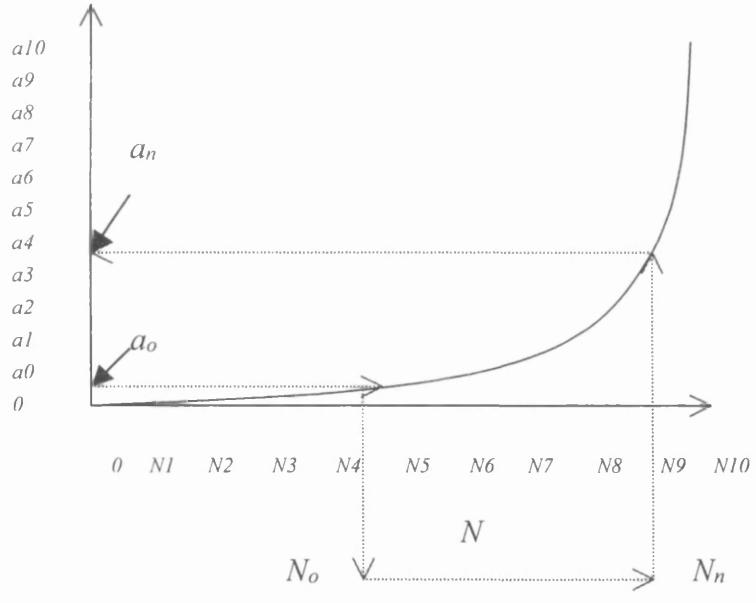

Figure 4.14 – *Schematic illustration of crack propagation*

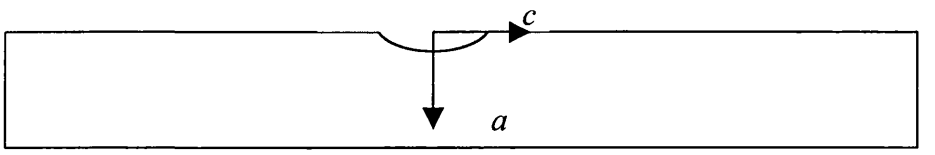

Figure 4.15 – *Surface crack in a plate, growing into the thickness*

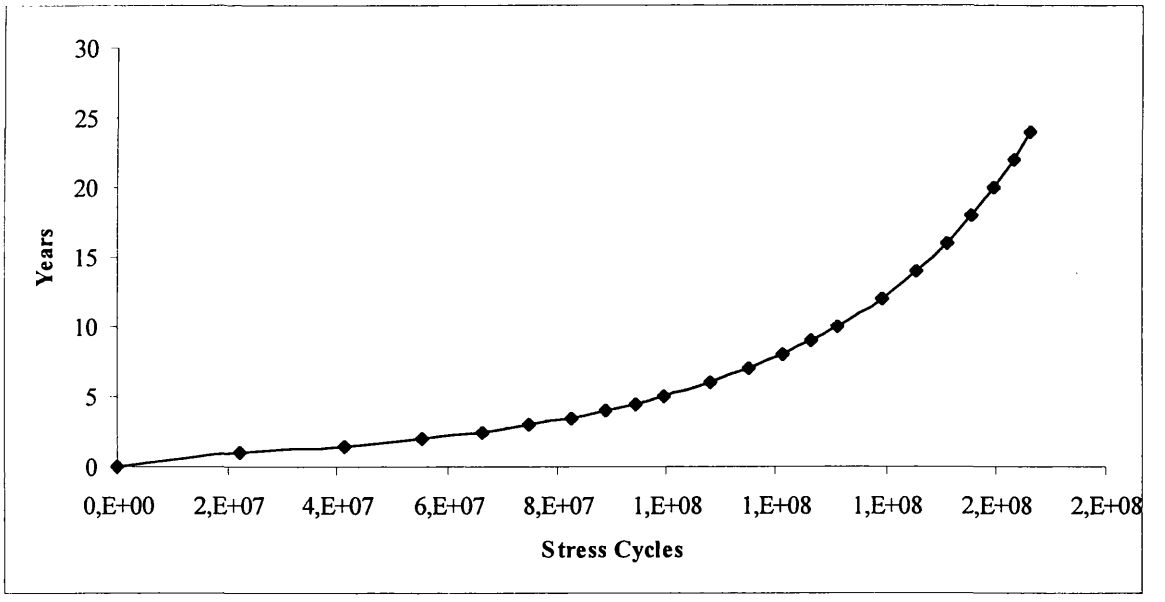

Figure 4.16 – *Crack growth versus time (in cycles) curve*

CHAPTER 5

STRESS INTENSITY FACTORS FOR BULK CARRIER DETAILS

5.1 Introduction

Fracture assessment and fatigue crack growth analysis (both discussed in chapter 4) require the computation of the stress intensity factor or range. The stress intensity factor is calculated from

$$K = Y \cdot \sigma \cdot \sqrt{\pi \cdot a} \qquad 5.1$$

and the stress range intensity factor

$$\Delta K = Y \cdot \Delta\sigma \cdot \sqrt{\pi \cdot a} \qquad 5.2$$

They both require the '*geometry factor*', Y, to be known. It was discussed in section 4.4, that Y is a factor that depends on the crack geometry, crack size, loading and other factors. It is because Y depends on crack size, the integral in equation 4.102 cannot be solved analytically, and has to be solved numerically.

There are three principal techniques that can be used to estimate Y:

1. Use of published solution
2. The weight function method
3. Numerical methods

All three methods have been used in this thesis to determine the geometry factor for various cracked geometries, which will be used for the reliability analysis. A general description of the three techniques follows.

5.2 Published Solutions

These are available in special text books or handbooks and include stress intensity factor solutions for simple geometries, loading and boundary conditions. The solutions are therefore correct for the particular model they represent, and care should be given when using these solutions, so that they represent well the actual model.

They are represented either from graphical representation or by using simple mathematical formulae with some coefficients. Some important sources for these solutions are written by Tada 1973, Sih 1973, Rooke & Cartwright 1976.

Published solutions are also presented in PD 6493, for many surface and through thickness cracks near welds, and are used in this report.

It is also possible to use these solutions by combining/superimposing individual solutions (e.g. for one loading case), to obtain a solution for a cracked geometry if more than one loadings are applied. In this report, published solutions have been used to calculate the geometry factor of simple cracked geometries found in ship structures (e.g. a centre crack in an infinite plate). Also, to calculate the SIF for surface cracks near welds (from PD 6493, presented in section B.4 of appendix B).

5.3 The Weight Function Method

The weight function method, (Bueckner 1958), is an economical way to determine stress intensity factor solutions to complicated geometries. The weight function represents a self-equilibrating stress field which does not produce any body forces. They are used to represent the stress field near the crack. Once the equation for the stress field is obtained, the stress intensity factor can be estimated, using the superposition principle. In an uncracked plate under external loading, the weight function is superimposed to represent the stress fields that would have been created by the presence of the crack. The external forces are the forces applied to the uncracked plate, Figure 5.12.

Weight functions are independent of loading and boundary conditions, and depend only on the geometry of the cracked body. The stress intensity factor is given by

$$K = \int \sigma(x) \cdot m(x) dx \qquad 5.3$$

where $\sigma(x)$ is the stress field applied on the crack faces, and $m(x)$ is the weight function. The integration must be carried over the crack face.

Weight functions exist for 2D as well as 3D problems. They can also introduce self-equilibrating stresses at the crack faces (e.g. thermal, residual stresses), and calculate the stress intensity factor due to these stresses. The weight function is used in this report to calculate the stress intensity factor due to tensile residual stresses (section 5.6).

An interesting technique, which is an extension of the weight function method, is the line spring method. The line spring method (Rice 1972), provides an inexpensive solution for stress intensity factors of surface cracks. It provides a method of estimating weight functions for a general cracked elastic component but also provides a rational method for extending the analysis in the presence of large amounts of plasticity.

5.4 Numerical Methods for SIF Evaluation

Accurate analytical determination of the crack tip stress intensity factor requires an exact solution of the elasticity problem formulated for the cracked structure. In most cases exact solutions to actual cracked geometries are very difficult if not impossible to obtain. The existing theoretical solutions for stress intensity factors are the result of highly sophisticated mathematical analysis for idealised model configuration and loading conditions.

It is well known that in many real cases an exact solution does not exist, and such theoretical results do not provide good estimates of the stress intensity factors. Therefore, there is a need for a relatively straightforward numerical method that enables the estimation of the stress intensity factor. The finite element method is often the best method of obtaining approximate stress intensity factors, whenever exact solutions are not available.

There are several general approaches that can be used in finite element for the determination of stress intensity factors. The ones used more often are

1. The Contour Integral

2. Energy Release Rate Methods

3. Crack Tip Elements

5.4.1 Selection of the Finite Element Method

The difficulty that the finite element method faces is to model the stress singularity at the crack tip. The earlier attempts used simply a very large number of conventional elements, and it was demonstrated that the accuracy achieved was not better than 5%, (Aliabadi 1991). This method was the abandoned for a more attractive method, that would not require a very fine mesh and it would give results that are more accurate.

To model the stress singularity at the crack tip, special elements have been created. Accurate solutions are obtained when these elements are positioned at the crack tip. Although the mesh near to the crack tip still needs to be fine, a coarser mesh of the surrounding model is possible. One simple way to achieve the stress singularity is to use a 6-noded triangular element and place the 'mid' side nodes at the quarter points. Another advantage is that they provide a direct estimate of the stress intensity factor without further analysis. Although crack tip elements were available in the finite element package used for the analysis, there is one reason that they were not selected. To model the crack growth, the crack tip element had to be moved and positioned at the new crack tip. However, it is not only the crack tip element that has to be moved but all the (very fine) mesh which models the crack tip area. The procedure would require re-meshing of the model, every time the crack propagated. This is very time consuming. Although there are special techniques that can be used to automatically re-mesh the model, still this is a very complicated method, and was not preferred, especially when there were other simpler methods available to use.

The method which was used in this thesis, is based on the *J-Integral* evaluation. The *J-Integral* is evaluated using the finite element code, and then related to the stress intensity using the relationships given in chapter 4, section 4.8.1. A technique to model crack growth is described in appendix B, and was available in the finite element code (ABAQUS). The basis of the *J-Integral* is discussed in the following section.

Another method is based on strain energy evaluation for two different crack lengths a and $a + da$. The difference in the strain energy, determines the energy release rate, which is then used to determine the stress intensity factor. This method has the advantage that it does not require a very fine mesh, however it requires two separate solutions for the determination of K, and although this can be done very efficiently using a substructure containing the crack tip and only moving the crack tip nodes, it involves re-meshing the model for each change of crack tip position.

5.4.2 The Contour Integral (*J-Integral*) Method

In section 4.8.1, it was discussed that the energy release rate (for elastic and non-linear stress-strain curves) is equal to a path independent integral, called the *J-Integral*. This integral can be related to the stress intensity factor and the CTOD for use in a fracture assessment analysis. The derivation of the path independent integral is attributed to Rice (1968). With reference to Figure 5.1a it can be shown that the principle of energy conservation, i.e. the work done in a body by an external force must be stored as strain energy, is written as

$$\Pi = \int_A \int W dx dy - \int_\Gamma F \cdot u \cdot ds = 0 \qquad 5.4$$

where the first term represents the stored strain energy inside the contour Γ and the second term represents the work done by the external forces (acting on the surface of the contour). Consider now a cracked plate, Figure 5.1b. Equation 5.4 still holds. The change in the total energy resulting from the crack extending by da, is given by

$$\frac{d\Pi}{da} = \int_A \int \frac{dW}{da} dx dy - \int_\Gamma F \cdot \frac{du}{da} \cdot ds \qquad 5.5$$

If we consider a co-ordinate system that moves with the crack tip, $X = x - a$ the derivative with respect to a is given by

$$\frac{d}{da} = \frac{\partial}{\partial a} + \frac{\partial X}{\partial a}\frac{\partial}{\partial X} = \frac{\partial}{\partial a} - \frac{\partial}{\partial X} = \frac{\partial}{\partial a} - \frac{\partial}{\partial x} \qquad 5.6$$

since $\frac{\partial}{\partial X} = \frac{\partial}{\partial x}$ and $\frac{\partial X}{\partial a} = -1$

so that

$$\frac{d\Pi}{da} = \iint_A \left(\frac{\partial W}{\partial a} - \frac{\partial W}{\partial x}\right) dxdy - \int_\Gamma F \cdot \left(\frac{\partial u}{\partial a} - \frac{\partial u}{\partial x}\right) \cdot ds \qquad 5.7$$

From the principal of virtual work

$$\iint_A \frac{\partial W}{\partial a} dxdy = \int_\Gamma F \cdot \frac{\partial u}{\partial a} \cdot ds \qquad 5.8$$

Substituting 5.8 in 5.7 results in

$$\frac{d\Pi}{da} = \iint_A \frac{\partial W}{\partial x} dxdy - \int_\Gamma F \cdot \frac{\partial u}{\partial x} \cdot ds \qquad 5.9$$

or using Green's theorem (Anderson 1991)

$$-\frac{d\Pi}{da} = \int_\Gamma \left(Wdy - F\frac{\partial u}{\partial x} ds\right) \qquad 5.10$$

which is called the *J-Integral*, and is equal to the energy release rate.

The strain energy changes within the contour of the *J-Integral* equal i) the energy changes caused by forces and deflections on the contour + ii) the energy changes caused by forces and deflections on the crack tip. (Note the contour starts and stops at the crack surfaces and does not run around them.) The *J-Integral* is a method of calculating the second energy term described above as a difference between the strain and contour energies. These energy changes are easily written in terms of *d/da* e.g. equation 5.5, and computational methods exist to calculate them by changing *a*. But the *J-Integral* cleverly uses ∂/∂x instead because this avoids the need to change the crack length in the calculation.

A physical explanation of the change from differentiating with respect to a in equation 5.5 to differentiating with respect to x in equation 5.9 in *J-Integral* is to split *d/da* in two partials (Figure 5.2)

a) $\frac{\partial}{\partial a}$ which represents the crack extending and the contour moving with the crack tip.

b) $\frac{\partial}{\partial x}\left(=\frac{\partial}{\partial X}\right)$ which moves the contour back. This represents the contour moving relative to a fixed crack tip.

Although $\frac{\partial}{\partial a}$ represents the contour moving with the crack tip as it extends, this is analogous to a crack that is not extending but is subject to a changing set of forces on the contour and with no forces applied to the crack surfaces (Figure 5.3i). Therefore the strain energy internal to the contour and the contour energies are equal and cancel out in the *J-Integral* equation (e.g. equation 5.8).

The $-\frac{\partial}{\partial x}$ partial derivative term represents the contour moving towards the crack tip (Figure 5.3ii). This is equivalent to a crack which is retreating relative to a fixed contour, and this is mathematically equivalent to the geometry not changing but crack surface forces being applied to hold some length of the crack closed and then released to allow it to extend. The crack surface energy change when the crack opens is the difference between the energy change on the contour and the energy change in the material.

The *J-Integral* is also path independent.

A closed contour is formed as seen in Figure 5.3. Equation 5.4 consists now of four different parts e.g.

$$\int_{\Gamma_1}+\int_{\Gamma_2}+\int_{\Gamma_3}+\int_{\Gamma_4}=0 \qquad 5.11$$

However, $F=0$ along Γ_2 and Γ_4 since there are no traction forces on the crack surface, and also $dy = 0$. Hence, Γ_2 and Γ_4 have no contribution and

$$\int_{\Gamma_1} = \int_{\Gamma_3} \qquad 5.12$$

Equation 5.12 proves that the line integral is path independent. By numerically evaluating the *J-Integral* for the finite element solution over a path surrounding the crack tip, an estimate of the stress intensity factor can be made by use of the equations of section 4.8.1.

Since the finite element solution is only approximate, the values of J calculated over various paths surrounding the crack tip will vary somewhat. Its accuracy is not as dependent on mesh size at the crack tip as the other methods. It is limited, however, to two-dimensional, mode I problems, and as such is restricted for application to practical problems.

5.5 Stress Intensity Factors Calculated by FEA

Two details have been selected for numerical analysis. A hatch corner subjected to multi-axial loading (tension and compression), and a stiffened panel (subjected to axial and pressure loading).

5.5.1 Description of the Finite Element Models

The rounded hatch corner detail is shown in Figure 5.5, which also indicates the overall nature of the finite element mesh. The mesh shown is not the actual mesh used, as this would have been difficult to show, because of the fine mesh, especially close to the crack.

The loading and boundary conditions are shown in Figure 5.6. For the this detail a combined loading was introduced: σy to take into account the dynamic wave loading due to wave pressure acting at the sides of the ship structure, and σx to account for the primary longitudinal bending stress. The boundary conditions are set as follows: along the edge1-2 the model is prevented from moving in the x-direction or rotating

about the z-axis. Along the edge 3-4 the model is prevented from moving in the y-direction or rotating about the z-axis. At the points 1 through 5 the movement in the z-direction was prevented. Therefore, boundaries 1-2 and 3-4 were treated as symmetric.

The next model that was analyzed is shown in Figure 5.7 and is a plate containing three longitudinal stiffeners and one transverse stiffener. This configuration can be found at the bottom and deck structure of a bulk carrier. The geometry consists of a square bottom plating of width of 1,500 mm and thickness of 20 mm. The longitudinal stiffeners have a height of 250 mm and thickness 35 mm and are flat bars. With this model the effect of the stiffeners on the stress intensity factor is investigated as the crack grows in the plate, in a direction normal to the stiffeners.

The loading for this model is defined by pressure acting on the bottom of the plate and is the result of the dynamic wave pressure acting at the keel structure of the ship. The primary longitudinal stress due to global bending moment is also introduced in the loading and this stress acts on the edge of the plating and on the edges of the longitudinal stiffeners, Figure 5.8. Fixed supports were assumed along all the edges of the plate except edge 1 where axial tensile loading was applied and simply supported conditions where assumed.

5.5.2 Crack Growth Using ABAQUS

The modeling of crack growth is achieved by the de-bonding of nodes. The advantage of this technique lies in the fact that no special elements are required or sub-blocks, and no re-meshing of the model. It is however, only applicable to 2D models and the crack path must be assumed by the user. But because only mode I crack growth is assumed, the crack path follows a line normal to the maximum applied stress, and hence it can be deduced. The model needs to be meshed only once with normal elements, and the crack tip growth is simulated by the de-bonding of two adjacent elements. A time history can be given as input to specify when the elements will de-bond, and therefore the SIF can be calculated for various crack lengths. From the analysis, the *J-Integral* is calculated by the finite element code, and it is then used to determine the SIF, using the equations given in section 4.8.1.

Appendix B presents analytically the method and the commands used for the crack growth simulation. The FE code used is called ABAQUS, together with a pre-processor called MSC Patran, where all the results where processed.

A typical example is shown in Figures 5.9-5.11. The model is an inverted T-joint of a plate with a stiffener jointed together by a fully penetrated weld. The crack (a surface defect) grows from the weld toe towards the thickness of the plating. Uni-axial stress acts at the edges of the plate, and the crack is assumed to grow normal to the direction of the stress. Figure 5.9 shows the initial defect, in the deformed state. Large crack increments are shown in this example so that the crack propagation would be visible, and a very coarse mesh to show the de-bonding of the elements. Figure 5.10 shows the average x-direction stress components with the plastic region at the crack tip. As the crack grows, the crack tip moves along the specified path, and re-distribution of stresses occurs.

At every crack length specified during the analysis, ABAQUS calculates the *J*-integral and hence the SIF.

The same procedure was followed for the two structural details of concern i.e. the hatch corner and the stiffened panel. However, because of the finer mesh it is not possible to see from the figures the crack path. Also because of some problems with the software availability it is not possible to show a complete set of figures showing crack growth and stress redistribution. The results (geometry factors) though are being presented in appendix B.

5.6 Stress Intensity Factors in Residual Stress Fields

There are many weight functions available for different cracked geometries inside residual stress fields. Terada (1976 & 1985), provides such a solution for a crack approaching a longitudinal weld. Wu (1984), provides also solutions for half-elliptical cracks in residual stress fields in butt welds for which and thin plates. In many cases because of the complexity of the weight function, the integral in equation 5.3 must be evaluated numerically.

5.6.1 K_{res} for a Through Thickness Crack Approaching a Butt Weld

A crack located close to a weld line is an interesting case since these types of welds account for many thousands of meters in a ship structure and defects are very likely to be present. It is a case which is important for the residual strength assessment and it will be considered in this thesis. Figure 5.13 illustrates this case.

The residual stress field for the above case can be seen in Figure 3.11.

Residual stress distributions were discussed in section 3.8 in chapter 3. The co-ordinate system is shown in Figure 5.14, where $\xi=x / d$ and d is the length of the tensile region in *mm* and corresponds to $\xi=1$.

Using equation 5.3 we have

$$K_{Res} = \int_{-a}^{a} \sigma_{res}(\xi) m(\xi) d\xi \qquad 5.13$$

where

$$\sigma_{res}(\xi) = \begin{Bmatrix} F_1(\xi) \\ or \\ F_2(\xi) \end{Bmatrix} \qquad 5.14$$

with

$$F_1(\xi) = \sigma_o e^{-0.5(\xi+L)}\left(1-(\xi+\lambda)^2\right) \qquad \text{(Terada)} \qquad 5.15$$

$$F_2(\xi) = \sigma_o\left[\frac{\left(1-(\xi+\lambda)^2\right)}{\left(1+(\xi+\lambda)^4\right)}\right] \qquad \text{(Tada \& Paris)} \qquad 5.16$$

where λ is the normalised distance ($\lambda = x / d$) between the centre of the crack and the weld line, σ_o is the maximum stress at the center of the weld (usually $\sigma_o = \sigma_y$) and ξ is the normalized distance from the weld center, $\xi = 1$ is the distance where the residual stress distribution becomes zero, i.e. it changes from tension to compression. These

equations are similar to 3.42 and 3.43 but include the eccentricity λ, when the crack center does not coincide with the welding line, and can be seen in Figure 3.12.

The weight function is given by

$$m(\xi)_{\pm a} = \frac{1}{\sqrt{\pi\alpha}} \frac{\sqrt{\alpha \pm \xi}}{\sqrt{\alpha \mp \xi}} \qquad 5.17$$

where in this case α is the normalised crack length with respect to d, $(\alpha = x / d)$.

It then follows that

$$K_{Res,\pm a} = \frac{1}{\sqrt{\pi\alpha}} \int_{-a}^{a} F_i(\xi) \frac{\sqrt{\alpha \pm \xi}}{\sqrt{\alpha \mp \xi}} d\xi \qquad 5.18$$

Terada (1985) gives an approximation to the integral in equation 5.18 as

$$\int_{-a}^{a} F_i(\xi) \frac{\sqrt{\alpha + \xi}}{\sqrt{\alpha - \xi}} d\xi = 2\alpha \sum_{j=1}^{N} w_j F_i(y_j), \quad (i = 1 \text{ or } 2) \qquad 5.19$$

where

$$\left\{ \begin{array}{l} y_j = -\alpha(1 - 2x_j) \\ x_j = \cos^2\left(\dfrac{(2j-1)\pi}{2(2N+1)} \right) \\ w_j = \dfrac{2\pi x_j}{(2N+1)} \end{array} \right\} \qquad 5.20$$

The case of interest in this report is when the crack propagates from the weld to the plate, e.g. from an initial defect within the weld. In this case $\lambda=0$. Table 5.1 shows $K_{Res} / \sigma_o \sqrt{\pi\alpha}$ values (i.e. geometry factors) for a crack propagating from the weld to the plate, for the two different residual stress distributions, i.e. $F_1(\xi)$ and $F_2(\xi)$. In the case of $F_1(\xi)$, the values become negative from about $a=2$ (a is the non dimensional crack length), as a result of the larger compressive residual stress region (Figure 3.12). However, negative values have no physical meaning (it means that the crack surfaces

overlap each other), unless some additional tensile loading is applied. This means that when tensile loading is applied, a reduction of the stress intensity value will be achieved when the crack enters the compressive residual stress field, and this becomes beneficial for fatigue (as the stress intensity range is reducing) and fracture (as the total stress intensity decreases).

Table 5.3 shows stress intensity factors and the corresponding geometry factor for a through thickness crack propagating away from the welding line, for the residual stress distribution given by Terada (i.e. $F_1(\xi)$). Values from this table are used to determine the residual stress intensity factor which will contribute to the total stress intensity factor that will be checked against fracture (equation 4.46).

5.6.2 K_{res} for a Surface Crack Perpendicular to a Weld

Wu (1984) have studied stress intensity factors for surface cracks (half elliptical) perpendicular to the welding line in thick (t > 25 mm) and thin plate calculated by FEM for 2D and 3D configurations. For thin plates, the distribution of residual stress across the thickness can be assumed constant. Wu also assumed a constant profile for the transverse residual stress distributions with a value equal to 20% of the maximum longitudinal residual stress at the centre of the weld.

The residual stress intensity factor is given by

$$K_{res} = M \cdot \frac{\sigma_o \cdot \sqrt{\pi a}}{\Phi} \qquad 5.21$$

where σ_o is equal to the yield stress, M is a correction factor and Φ is given by

$$\Phi = \left[1 + 1.464 \left(\frac{a}{c} \right)^{1.65} \right]^{1/2} \qquad 5.22$$

where c is the half-length of the crack (at the surface). Values for the M factor can be seen in table 5.3 for various crack depths and crack lengths.

Figure 5.15 shows K_{Res} values for a point on the surface ($\theta=90^o$) and for the deepest point ($\theta=0^0$) and for a through thickness crack (2D). It is interesting to note that the stress intensities for the surface crack at the surface point and for the through

thickness crack increase up to a maximum value and then start to decrease, while the stress intensity for the surface crack at the deepest point always increases. This means that a surface crack will grow faster through the thickness than it will grow at the surface.

REFERENCES

- ABAQUS Version 5.5, User's Manual

- Aliabadi M. H., Rooke D. P., 'Numerical fracture mechanics', Kluwer Academic, 1991

- BSI, PD6493, 'Guidance on methods for assessing the acceptability of flaws in fusion welded structures', 1991

- Bueckner H. F., 'The propagation of cracks and the energy of elastic deformation', Transactions of ASME, Vol. 80, 1958

- Gurney T. R., 'A revised analysis of the influence of toe defects on the fatigue strength of transverse non-load-carrying fillet welds', Welding Research International, Vol. 9, No. 3, 1979

- Rooke D. P., Cartwright D. J., 'Compendium of stress intensity factors', Her Majesty's Stationery Office, 1976

- Sih G. C., 'Handbook of stress intensity factors', Lehigh University Press, 1973

- Smith E., 'The stress intensity factor for a crack perpendicular to a longitudinal weld in a large plate', International Journal of Fracture, Vol. 27, pp. 75-79, 1985

- Tada H., Paris P. C., Irwin G. R., 'The stress analysis of cracks, handbook', Del Research Corporation, 1973

- Terada H., 'An analysis of the stress intensity factor of a crack perpendicular to the welding bead', Engineering Fracture Mechanics, Vol. 8, 1976

- Terada H., Nakajima T., 'Analysis of stress intensity factor of a crack approaching welding bead', International Journal of Fracture, Vol. 27, 1985

- Wu X. R., Carlsson J., 'Welding residual stress intensity factors for half-elliptical surface cracks in thin and thick plates', Engineering Fracture Mechanics, Vol. 19, 1984

L	σ_{res}	$a = 0$	0.5	1	2	3	4	5
0	F1	1	0,8265	0,4446	-0,0499	-0,0555	-0,0190	-0,0080
	F2	1	0,8572	0,4551	0,0851	0,0260	0,0110	0,0060

Table 5.1 - $K_{res}/\sigma_o Y\sqrt{\pi a}$ (Terada 1985)

a	K	Y
0.0	0.0000	1.0000
0.1	0.5563	0.9925
0.2	0.7692	0.9704
0.4	0.9930	0.8858
0.6	1.0412	0.7584
0.8	0.9592	0.6051
1.0	0.7880	0.4446
1.2	0.5701	0.2936
1.4	0.3451	0.1646
1.6	0.1437	0.0641
1.8	-0.0154	-0.0065
2.0	-0.1252	-0.0499
2.5	-0.2160	-0.0771
3.0	-0.1705	-0.0555
3.5	-0.1084	-0.0327
4.0	-0.0674	-0.0190

Table 5.2 – *Residual stress intensity factor and the corresponding geometry factor* (Terada 1976)

	a/t	2ψ/π	c/ℓ 0.	0.2	0.4	0.6	0.8	1.0	1.5	2.0
		0.	1.194	1.190	1.180	1.165	1.147	1.131	1.045	.978
		0.125	1.181	1.175	1.158	1.133	1.105	1.078	.927	.798
		0.25	1.145	1.132	1.097	1.046	.988	.932	.631	.394
		0.375	1.084	1.063	1.005	.920	.823	.731	.290	.014
	.25	0.5	1.001	.973	.893	.778	.646	.521	.022	- .203
		0.625	.896	.863	.771	.636	.484	.338	-.124	-.267
		0.75	.776	.743	.649	.512	.357	.209	-.167	- .247
		0.875	.647	.617	.531	.407	.267	.132	-.158	-.204
		1.0	.592	.563	.483	.365	.232	.105	-.152	- .187
		0	1.418	1.412	1.395	1.371	1.343	1.316	1.182	1.081
		0.125	1.402	1.394	1.370	1.335	1.296	1.258	1.058	.896
		0.25	1.353	1.338	1.296	1.234	1.165	1.098	.747	.476
		0.375	1.273	1.250	1.184	1.089	.981	.877	.386	.078
(a)	.5	0.5	1.168	1.137	1.051	.925	.782	.645	.099	-.155
		0.625	1.043	1.008	.909	.765	.601	.445	-.061	-.230
		0.75	.912	.876	.776	.630	.464	.306	-.132	- .215
		0.875	.776	.743	.652	.519	.368	.223	- .108	- .176
		1.0	.726	.693	.605	.478	.334	.196	-.104	-.161
		0	1.622	1.614	1.591	1.558	1.520	1.484	1.304	1.171
		0.125	1.613	1.602	1.572	1.528	1.479	1.431	1.183	.988
		0.25	1.562	1.545	1.496	1.426	1.346	1.269	.870	.569
		0.375	1.470	1.446	1.380	1.283	1.174	1.069	.498	.164
	.75	0.5	1.383	1.349	1.254	1.115	.958	.808	.201	- .091
		0.625	1.202	1.164	1.058	.904	.729	.562	.008	- .187
		0.75	1.074	1.035	.927	.770	.591	.420	-.051	- .182
		0.875	.916	.881	.782	.639	.477	.321	-.055	- .147
		1.0	.882	.848	.752	.613	.455	.304	-.047	-.132

Table 5.3 - *M factors for surface crack perpendicular to the weld in thin plate a) for a/c 0.2 b) a/c =0.5 c) a/c = 0.8* (Wu 1984)

	a/t	2c/t	0.	0.2	0.4	0.6	0.8	1.0	1.5	2.0
		0.	1.131	1.126	1.111	1.090	1.065	1.042	.926	.841
		0.125	1.123	1.116	1.096	1.067	1.034	1.003	.840	.709
		0.25	1.107	1.095	1.060	1.009	.952	.897	.621	.406
		0.375	1.082	1.043	.991	.916	.830	.748	.356	.107
	.25	0.5	1.014	.989	.919	.816	.700	.589	.136	-.085
		0.625	.959	.929	.844	.721	.582	.448	-.004	-.179
		0.75	.908	.875	.781	.645	.491	.344	-.074	-.193
		0.875	.873	.838	.740	.598	.436	.282	-.101	-.195
		1.0	.869	.833	.732	.586	.420	.261	-.114	-.200
		0.	1.241	1.234	1.215	1.188	1.157	1.127	.983	.882
		0.125	1.234	1.225	1.201	1.167	1.127	1.089	.897	.748
		0.25	1.214	1.200	1.163	1.107	1.045	.985	.676	.445
		0.375	1.181	1.161	1.104	1.022	.928	.839	.415	.147
(b)	.5	0.5	1.138	1.111	1.036	.927	.803	.684	.197	-.044
		0.625	1.089	1.057	.967	.836	.688	.546	.058	-.128
		0.75	1.046	1.011	.912	.768	.604	.448	-.008	-.150
		0.875	1.022	.985	.881	.730	.598	.384	-.031	-.149
		1.0	1.035	.997	.889	.732	.555	.385	-.036	-.149
		0.	1.315	1.307	1.286	1.254	1.219	1.185	1.020	.928
		0.125	1.315	1.305	1.279	1.240	1.195	1.153	.939	.777
		0.25	1.301	1.286	1.246	1.187	1.119	1.055	.729	.488
		0.375	1.280	1.270	1.213	1.131	1.038	.949	.485	.205
	.75	0.5	1.262	1.234	1.157	1.045	.917	.795	.275	.015
		0.625	1.222	1.186	1.093	.955	.799	.649	.136	-.082
		0.75	1.218	1.180	1.074	.919	.744	.576	.071	-.099
		0.875	1.212	1.172	1.060	.897	.712	.535	.057	-.093
		1.0	1.261	1.219	1.102	.931	.737	.552	.066	-.085
		0.	1.101	1.096	1.080	1.058	1.032	1.008	.892	.809
		0.125	1.098	1.091	1.071	1.042	1.009	.978	.818	.694
		0.25	1.090	1.078	1.046	.999	.945	.894	.629	.427
		0.375	1.077	1.059	1.009	.937	.855	.776	.399	.157
	.25	0.5	1.064	1.040	.971	.871	.757	.649	.201	-.025
		0.625	1.054	1.023	.938	.813	.672	.537	.067	-.114
		0.75	1.055	1.020	.920	.776	.611	.456	-.004	-.147
		0.875	1.066	1.027	.919	.761	.581	.410	-.033	-.155
		1.0	1.166	1.123	1.003	.829	.631	.441	-.029	-.164
		0.	1.155	1.149	1.131	1.106	1.077	1.050	.919	.829
		0.125	1.153	1.145	1.123	1.091	1.055	1.020	.846	.714
		0.25	1.149	1.137	1.102	1.051	.994	.939	.658	.447
		0.375	1.142	1.123	1.071	.994	.908	.825	.431	.179
(c)	.5	0.5	1.137	1.111	1.040	.935	.817	.704	.236	.028
		0.625	1.137	1.105	1.016	.887	.740	.599	.108	-.080
		0.75	1.150	1.113	1.010	.860	.699	.527	.043	-.115
		0.875	1.175	1.135	1.022	.858	.671	.493	.020	-.119
		1.0	1.302	1.257	1.132	.949	.741	.543	.037	-.119
		0.	1.173	1.168	1.154	1.134	1.112	1.090	.936	.852
		0.125	1.176	1.169	1.150	1.123	1.092	1.062	.864	.739
		0.25	1.177	1.166	1.134	1.087	1.034	.984	.682	.474
		0.375	1.200	1.181	1.128	1.051	.965	.879	.482	.212
	.75	0.5	1.225	1.199	1.126	1.020	.899	.784	.305	.055
		0.625	1.248	1.214	1.120	.983	.828	.679	.155	-.057
		0.75	1.261	1.223	1.115	.959	.782	.612	.098	-.076
		0.875	1.320	1.278	1.159	.985	.789	.601	.089	-.073
		1.0	1.492	1.444	1.311	1.116	.896	.685	.127	-.058

Table 5.3 - *Continued*

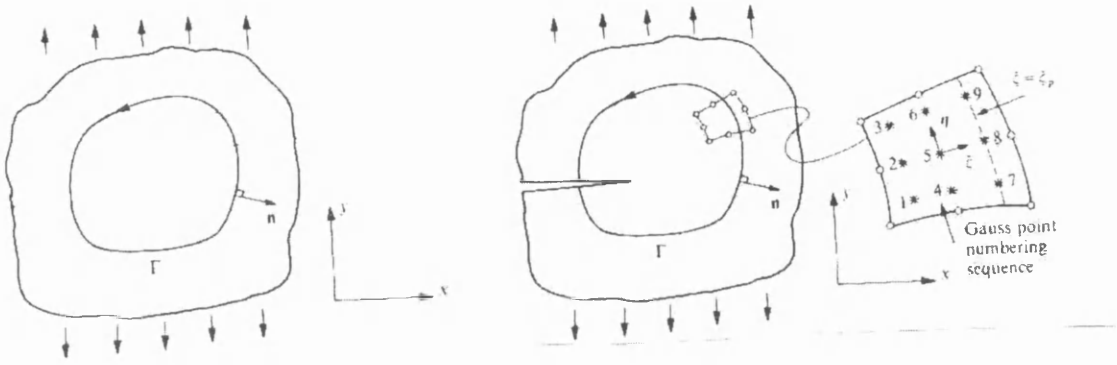

a) b)

Figure 5.1 – *a) closed contour in a plate b) closed contour in a cracked plate*

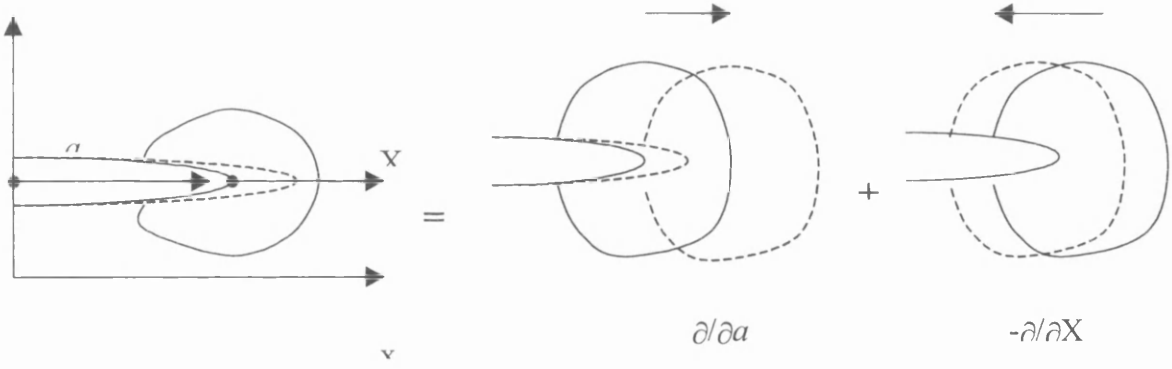

i) *ii)* *iii)*

Figure 5.2 *i) Original crack tip and contour, ii) Contour moving with crack tip, iii) Contour moving back, crack tip remaining at the extended position.*

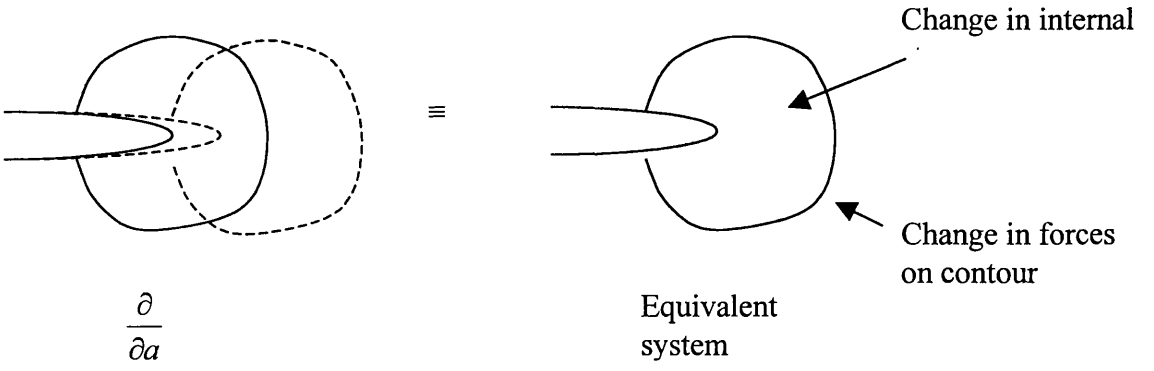

i)

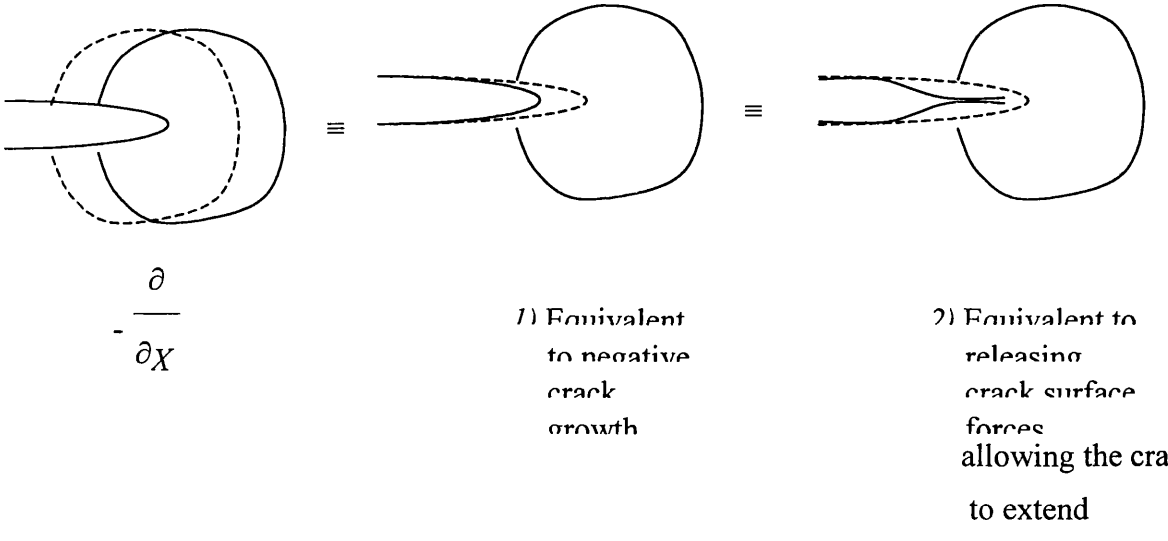

ii)

Figure 5.3 – *The two components of the partial derivative necessary to derive the J-Integral*

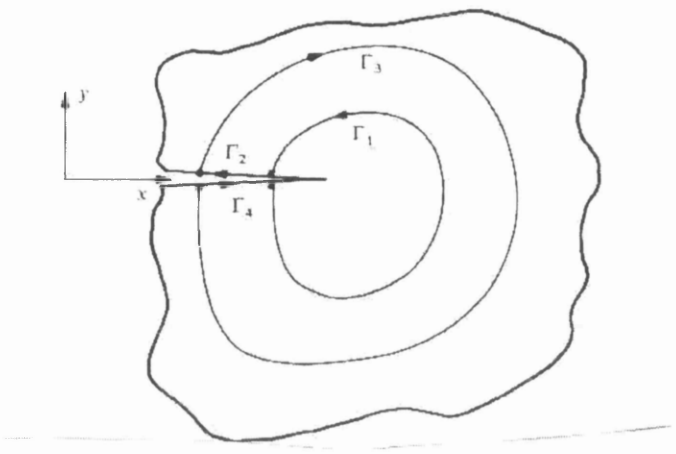

Figure 5.4 - *Different contour paths for proof of J integral's path independence*

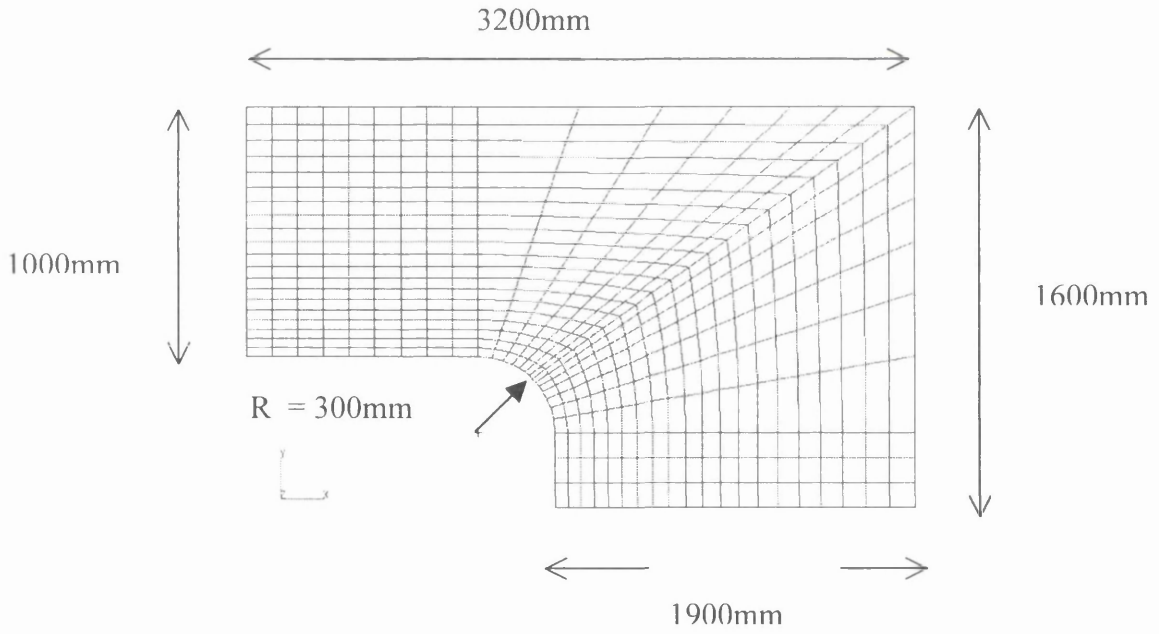

Figure 5.5 - *Geometric and finite element model for the hatch corner model*

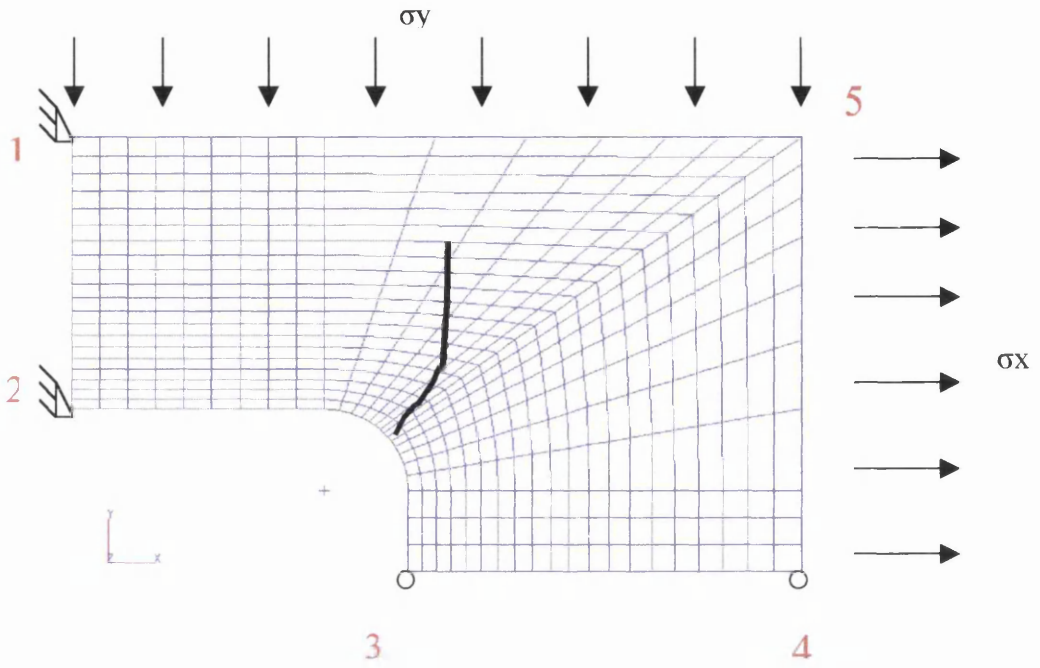

Figure 5.6 - *Boundary and loading conditions for the hatch corner model*

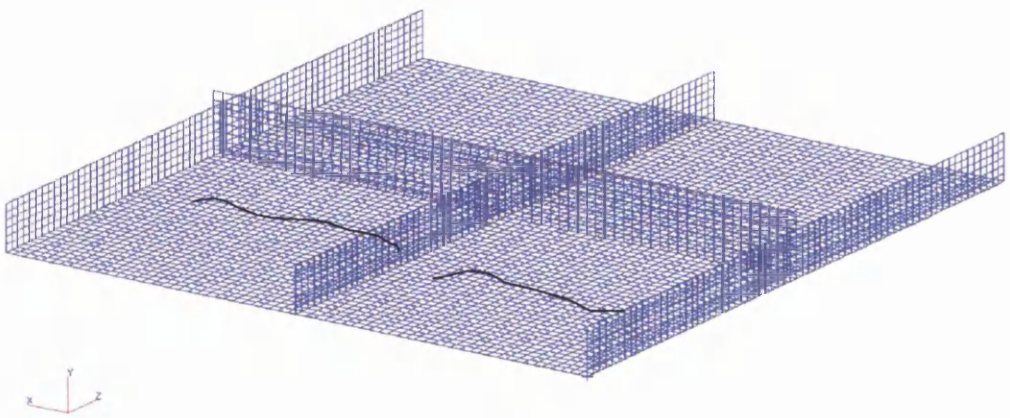

Figure 5.7 – *Stiffened plate model*

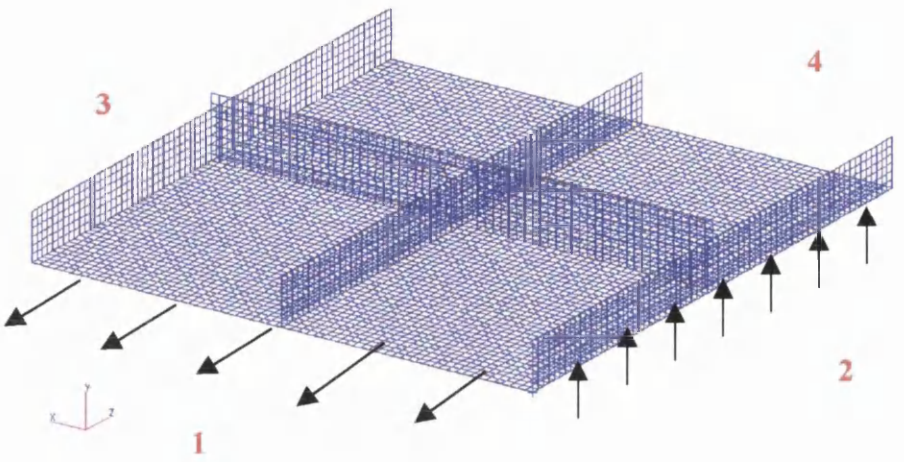

Figure 5.8 – *Boundary and loading conditions for plate with stiffeners model*

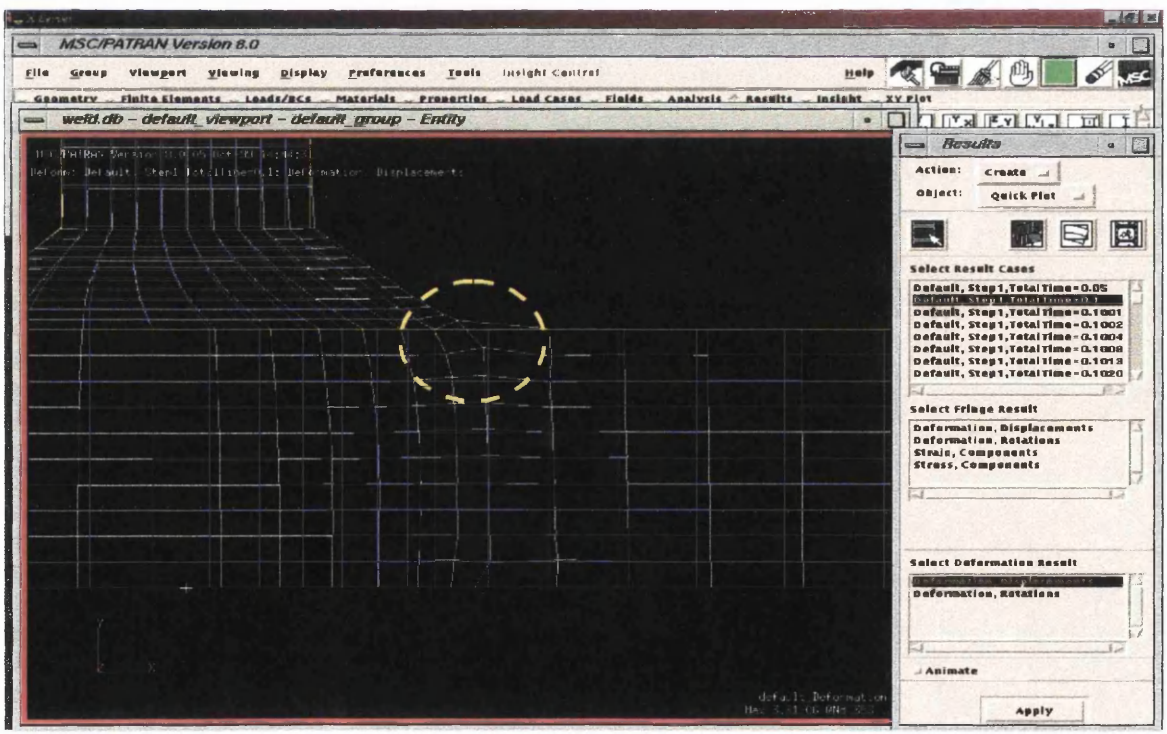

Figure 5.9 – *Initial defect at the toe of the weld*

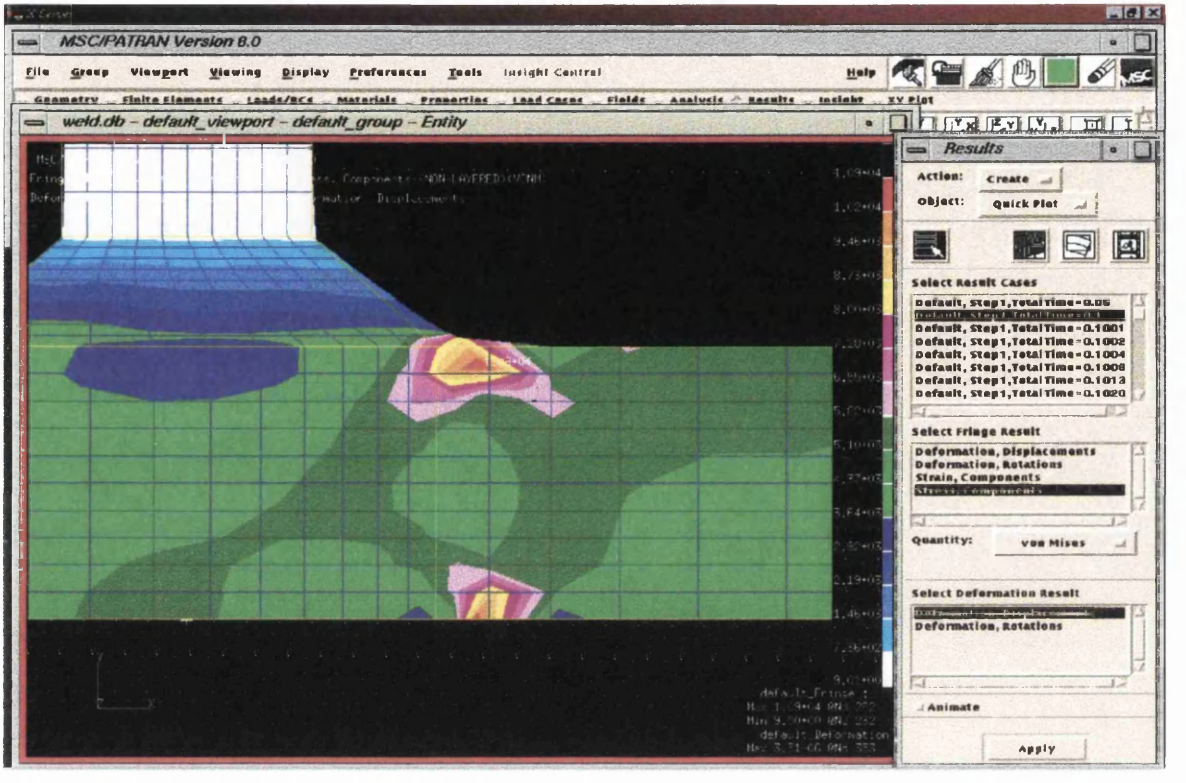

Figure 5.10 – *Average x-direction stress components, showing plastic region close to crack tip*

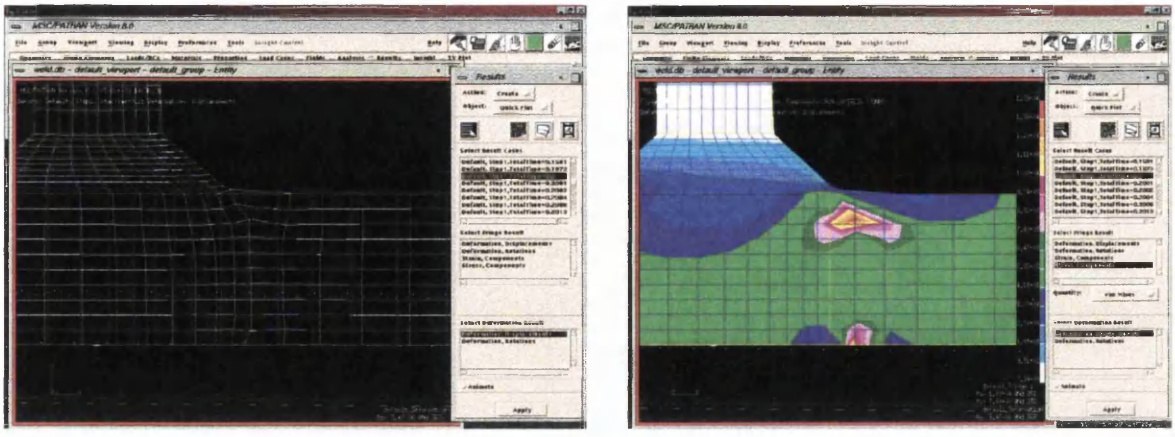

a

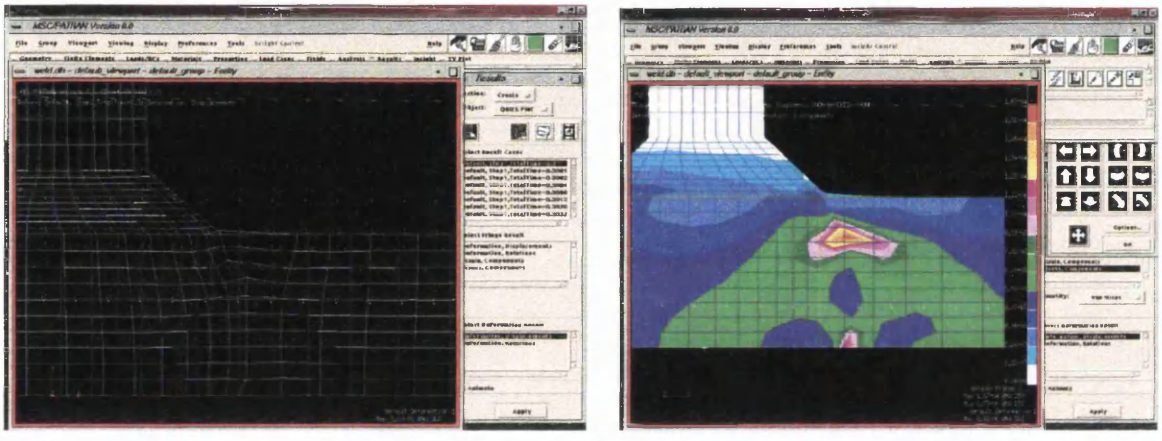

b

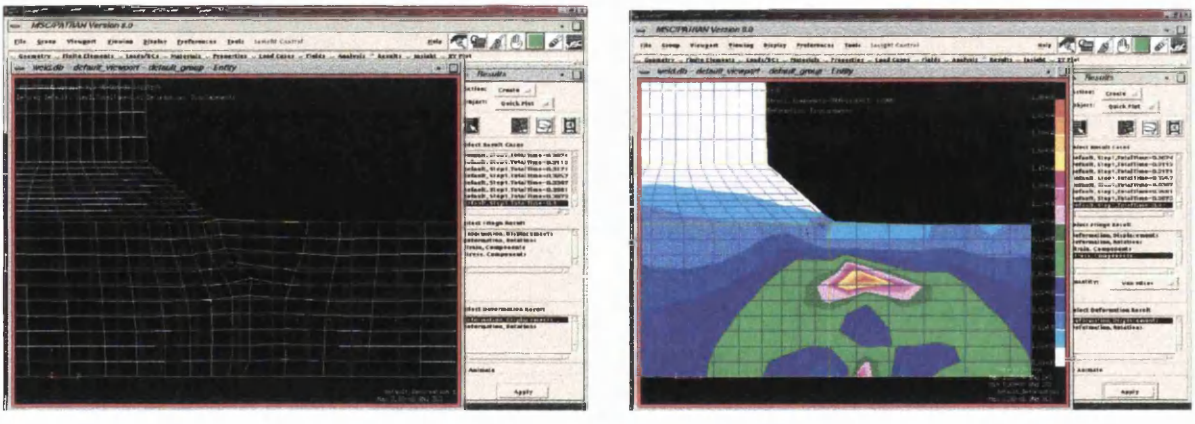

c

Figure 5.11 a,b,c – *Crack propagation and de-bonding of elements, and corresponding stress re-distribution*

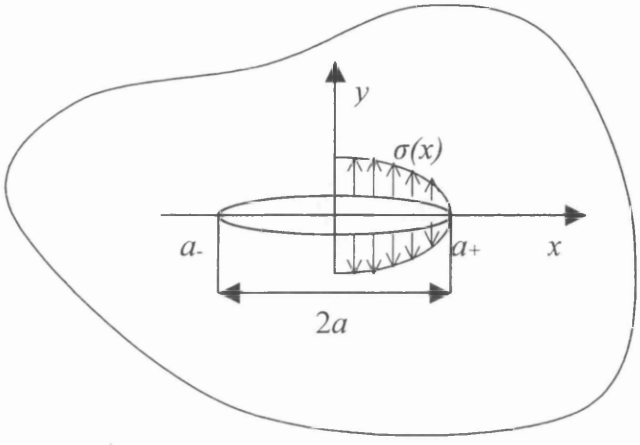

Figure 5.12 - *Arbitrary stress field acting on the crack tip*

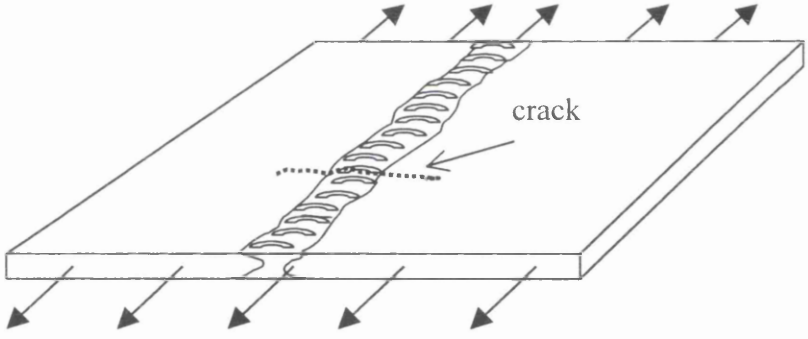

Figure 5.13 – *Through thickness crack perpendicular to a weld line*

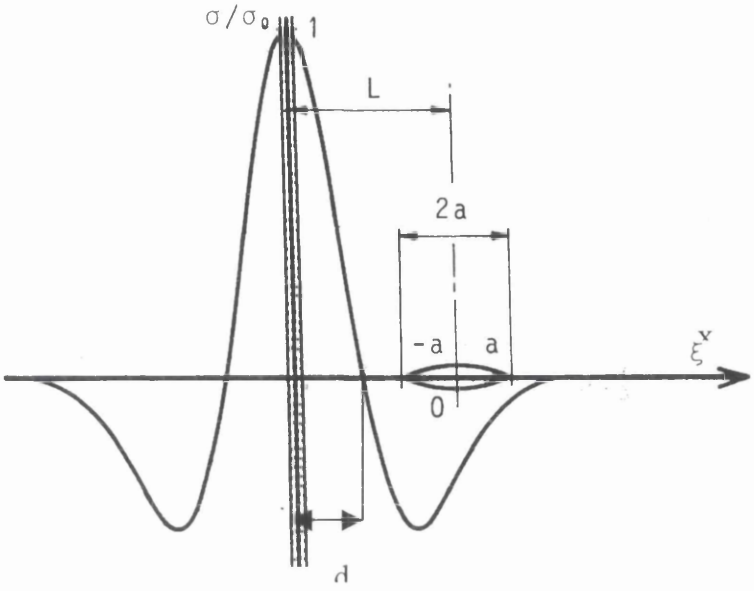

Figure 5.14 – *Co-ordinate system of residual stress field near butt weld*

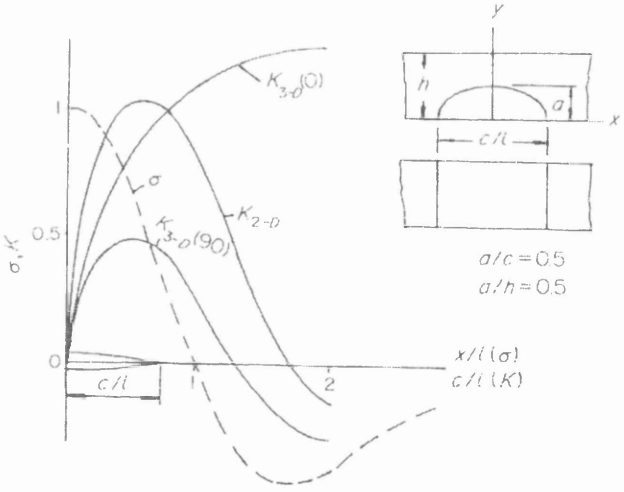

Figure 5.15 – *Comparison between K for a surface crack (θ=0° deepest point, θ=90° surface) and a through thickness crack (2D)* (Wu 1984)

CHAPTER 6

REVIEW AND ESTIMATION OF THE INPUT PARAMETERS

6.1 General Characterisation of the Input Data

The work reported in this thesis has concentrated on methodology and not on the required input data. However, data acquisition is perhaps one of the most important tasks in a reliability analysis. Since reliability analysis, by itself, estimates the risk of failure based on the uncertainties that govern the basic variables of the limit state function. The more reliable the data on the basic variables, the more reliable the estimate from the reliability analysis. Hence, for a more realistic estimate of the probability of failure of a structure it is necessary that the most accurate data is used.

There are many sources of uncertainties, which were described in chapter 2, for the basic variables. In this chapter, effort is put to describe the variability of each parameter after reviewing many references and sources of information and the best possible description is chosen giving the reasons for the choice.

In a reliability analysis, the basic variables can either be *deterministic* or *random.* Deterministic variables are those whose value is known exactly. Random variables possess uncertainty and their value is not known exactly. Random variables may be described in two categories for the purpose of this thesis

Category A – The random variable does not change value with time, but its value is only known through a statistical distribution which describes the degree of the uncertainty, e.g. the yield stress of the material.

Category B – Under this category, the value of the variable changes with time and is described by a probability distribution which characterises the variability with time. For example, fatigue loading is described by the Weibull distribution having scale and shape parameters. The scale and shape parameters have also statistical uncertainty and are described by probability distributions.

An overall review of the reliability method was given in chapter 1. Here, to understand better the role of each variable the input parameters have been split into two different groups. In the first group are the parameters necessary for the

probabilistic crack growth analysis and in the second group belong the parameters necessary for the probabilistic fracture analysis.

6.2 Parameters Necessary for the Probabilistic Crack Growth Analysis

6.2.1 *Paris' Law Material Constants C and m*

The crack propagation parameters C and m, defined in Paris' law determine the rate of crack growth under certain conditions. These parameters are affected by the material environment, applied loading intensity and the mean stress. They are measured using regression analysis of da/dN vs. ΔK plots. Virkler et al (1979), have shown that a large degree of scatter exists in the measurement of the crack growth rate, which suggests a probabilistic modelling of these parameters is required. Virkler believes that the reason for this scatter is because the material is not homogeneous continuum when considered in a microscopic scale.

Gurney (1979), has proved that strong correlation between C and m exists, equation 6.1a. Equation 6.1a best fits published data for parent and weld metals for structural and high strength steels. This correlation is not linked to a physical property of the material, but rather from the mathematical expression of Paris' law. In order to access the mean value of C one can refer to experimental results that have been carried out to standard specimens. For example Bokalrud and Karlsen (1981) state that DnV have carried out approximately 2900 crack growth measurements (da/dN vs. ΔK) for various steels and the results are shown in Table 6.1a.

An empirical relationship relating C and m has been introduced by Gurney (1979), equation 6.1b, which shows the negative correlation between C and m.

$$C = \frac{1.315 \times 10^{-4}}{895.4^{m}} \qquad \text{for } \Delta K \text{ in } MNm^{-3/2} \qquad 6.1a$$

$$C = \frac{1.315 \times 10^{-7}}{28.31^{m}} \qquad \text{for } \Delta K \text{ in } MPa\sqrt{m} \qquad 6.1b$$

A summary of mean values for C and m for steels in air and steels in a corrosive environment is given in Table 6.1b. It is clear that huge scatter exists between the available data.

To justify the selection of crack growth parameters, it is necessary to calibrate the results of a probabilistic fracture mechanics analysis with standard S-N curves. For example, the mean line S-N curve has a probability of failure 50%, and the mean minus two standard deviations curve has a probability of failure of about 2.3%. Mean S-N curves for different weld details can be seen in Figure 6.2. On the same figure the corresponding mean curve of stress range versus cycles using the C *and* m values from Yazdani (1989), is shown. An edge crack geometry was chosen, subjected to constant stress ranges, and the time period that had a probability of failure equal to 50% was read from the simulation results. The mean fatigue lives of the standard S-N curves can be seen in Table 6.7, and also the time period that has a probability of failure equal to 50%, as calculated from the probabilistic fracture mechanics analysis. Using these results we can see that the C and m values suggested by Yazdani, for a corrosive environment, produce fatigue lives between a class E and F2 mean S-N curve with a different slope since the S-N curves assume m equal to 3 where Yazdani takes m equal to 3.279. The same analysis but using C and m values from the other sources produced S-N curves which gave very small fatigue lives, even smaller than the worst S-N class (W).

A comparison was made between the crack growth rates for C and m values obtained from Gurney's equation, using a simple deterministic calculation. Table 6.2 presents the results for values in air. The last column presents the ratio of the crack growth rates. The values in bold are the values used in the report. For smaller cracks, there is a big difference in the results whereas for large ΔK or large crack sizes the crack growth rates are similar. Therefore, for small ΔK values which are important in this analysis the values for C and m given by Yazdani, (both for steels in air and in corrosive environments), were chosen.

In this thesis the parameter m is considered as a deterministic variable and only C is allowed to vary, a simple assumption which gives good results. The Paris' constant C

is assumed to be lognormally distributed with coefficient of variation up to 20%. The lognormal distribution to model the variability in C is used by DnV, and by many other studies. The effect of this variability comes from the fact that even identical details will be cracked to a different extent after the same amount of time and applied load. Such differences may be due to variability in the material, variability in the experimental processes measuring the crack growth rate, presence of residual stresses, environmental conditions, and load sequence effects. Virkler *et al* (1979), have shown this variability of crack growth data on identical specimens, as shown in Figure 6.1. Ostergaard *et al* (1983), have further analysed the data by Virkler and have shown that the error in reproducing crack growth rates from the finite integral method was always less than 20% when compared when the actual data. Johnston (1983) using Gurney's equation, 6.1a, and using a value of m equal to 3, has shown that the coefficient of variation of C is about 21%.

6.2.2 *The Stress Intensity Threshold, ΔK_{th}*

The crack growth threshold stress intensity is also another important parameter in the crack propagation analysis. According to many experimental observations, crack growth does not occur below a threshold stress intensity value, ΔK_{th}. Many experimental results however have shown a large degree of scatter in the evaluation of ΔK_{th}. In a study of Shetty and Baker (1991), ΔK_{th} for a BS 4360: grade 50D steel, a mean value of 7.60 MPa$\sqrt{m}$ is reported, assuming a lognormal distribution. In his book, Barsom (1987), has found a lower bound for ΔK_{th} in air, as a function of stress ratio R, indicating the strong dependence of ΔK_{th} and R. The relationship is expressed as

$$\Delta K_{th} = 221(1 - 0.85\,R), \quad R \geq 0.1 \qquad \Delta K_{th} \text{ in MPa}\sqrt{mm}$$

$$= 190 \qquad R < 0.1 \qquad 6.2$$

A study from Hadrboletz *et al* (1994) , is indicating that due to the many factors affecting the threshold stress intensity, a simple expression reducing the number of parameters is given by

$$\Delta K_{th,eff} = K_{th,max} - K_{closure} \qquad 6.3$$

where $K_{th,maxf}$ is the maximum stress intensity *and* $K_{closure}$ is the stress intensity at crack closure. $\Delta K_{th,eff}$ is obtained from experiments and the values range from 2.4 to 2.6 MPa $m^{1/2}$ for steels.

Another important source of information about threshold stress intensities comes from the study of Tanaka et al (1990), where six grades of steel were tested with yield stress ranging from 163 to 888 MPa, under various stress ratios and the threshold stress intensity was the same for all the steels with a value of 3.45 MPa $m^{1/2}$, which is outside the range given by Hadrboletz.

ASM, presents typical ΔK_{th} values for mild steel. These values are reported as 4 MPa$\sqrt{m}$ in vacuum and 2.8 MPa$\sqrt{m}$ in air, which compare well with Hadrboletz. In this report a mean value of 2.5 MPa$\sqrt{m}$ is assumed for the fatigue stress intensity and is assumed as a deterministic quantity. To examine the sensitivity of the stress threshold on the reliability results, a parametric study is the best method. From this study it is seen that stress threshold has very little effect on the reliability results. When the stress threshold is significant, the cracks are very small and hardly cause any fracture. When cracks are large and the failure probability increases, the stress intensity threshold has diminished.

Since, stress intensity threshold decreases with increase in crack length, a simple linear model was assumed to decrease ΔK_{th} with increase in crack length. To include the effect of stress intensity threshold, a threshold factor *G(a)* was introduced in the crack propagation law, as was described in section 4.9.1.

6.2.3 *Corrosion Rates*

Environmental effects also have a role on crack growth, since many environments can produce a profound increase in crack growth rates. For ship structures, corrosion significantly increases crack growth rate by reducing material thickness hence increasing stress levels as well as altering crack growth parameters C and m. The interactions that give rise to corrosion are very complex phenomena, and a small discussion was given in chapter 1. In some cases, the effect of corrosion fatigue is taken into account directly in the Paris' constant C, from experimental results carried

out in a corrosive environment. In this thesis corrosion is assumed to increase the stress levels by a factor of

$$S_{cor}(t) = \frac{t}{t - k_{cor} \cdot T} \qquad 6.4$$

where

t : Thickness of material

k_{cor} : Corrosion rate

T: Time

$S_{cor}(t)$: Corrosion factor

Corrosion rates at particular points in ship hulls vary greatly from ship to ship due to the combined effect of different routes and cargoes. A thorough statistical study done by Valsgard *et al* (1998), proves the complexity and the peculiarity of the problem since in most of the locations studied the standard deviation is almost as large as the corrosion rate and in some cases it is greater. Indicative values for corrosion rates have been published in a report by the Tanker Structure Co-operative Forum and can be seen in Table 6.3, for various locations for oil tankers and OBO carriers. In this project the rates for unprotected steel are used since, they are only slightly greater than the corrosion rates published by the Tanker Structure Co-operative Forum, taking into consideration the standard deviation. Corrosion rates may change with time, and it has been shown that corrosion rates generally increase with time, as shown in SSC-397. To allow this increase of corrosion rates with time a linear model is assumed which increases the rate of corrosion with time. Table 6.4 presents indicative mean corrosion rates for various locations along the ship, for unprotected steels taken from Valsgard. Also typical corrosion rates for oil tankers and OBO carriers are given in Table 6.5.

Corrosion rates for bulk carriers are also given by Paik *et al* (1998). In this study corrosion rates for various parts of a bulk carrier are given as can be seen in Figure 6.3.

In this work the corrosion rate factor was modelled as a deterministic variable which changes with time according to equation 6.5. This allows the sensitivity to corrosion to be determined from a parametric study of the probabilistic crack growth analysis. This showed that corrosion rate variability had a small effect on the results, a 100% on the corrosion rate only increased the failure probability by 0.5%. This is perhaps as a result of the inspections which were allowed every 3 years and the loss of thickness due to corrosion was not significant.

6.2.4 *Geometry Factor*

The evaluation of the stress intensity factor is a complex process, and many papers have been published concerning the accuracy and applicability of different techniques predicting the stress intensity factor. Chapter 5 is devoted entirely to this matter. The finite element method was used in this report to obtain the stress intensities for various geometric configurations that are commonly found in ship structures. The results from the finite element analysis were then compared with standard solutions if available. Stress intensity factors can be calculated accurately, even for complicated geometries and loading conditions using the finite element method, which is difficult to do using analytical methods. Furthermore, crack growth simulation is possible, hence stress intensities can be directly calculated with varying crack size taking into account stress re-distribution.

Since stress intensity does not remain constant but changes with crack length, it cannot be modelled probabilistically. But because crack size is a random variable, for every crack size generated from the defect distribution, the corresponding geometry factor is calculated from the data obtained from the finite element analysis for various crack geometries, which is given in appendix B.

6.2.5 *Initial Defect Distribution*

A ship structure contains many kilometres of welds. The potential of defects being present is very high, even from the fabrication stage. Generally, defects are the product of poor welding quality, which results in undercuts, porosity, lack of fusion, incomplete penetration, depending on the welding technique. Defects can be internal i.e. embedded or surface type. For welded structures, due to the large uncertainty on the crack initiation stage, the conservative assumption of pre-existing flaws in the structure is made.

Not every defect necessarily develops into a sharp crack. This will depend on many reasons but the most important are, whether or not they are within a high stress field zone, the type of joint, the direction of the loading and the finishing process. The presence of cracks usually signifies high local stress fields, geometric stress concentrations and repetitive cyclic loading.

Crack sizes and occurrence rates are very random. There are very limited reports on crack size measurements and defect occurrences for ship structures. Maddox (1974), reports that in fillet welds, undercuts and slag inclusions range from 0.1 to 0.5 mm. Kountouris and Baker (1989), report initial defect depths for a TLP structure, with mean of 0.73mm and standard deviation of 0.78mm following a lognormal distribution.

For ship structures a study from Bokalrud and Karlsen (1981), is more appropriate. A distribution of internal defects was established based on random measurements made on 3,200 m out of 40,000 m of butt welds, which revealed 327 defects. The histogram of internal defects that was obtained was fitted to one-sided normal distribution. Measurements were also made for undercuts i.e. surface defects and the distribution was based on 20 m of metal arc welds where 325 undercuts were found. The distribution fitted has the exponential form and is shown in Figure 6.4.

Another method of evaluating the initial crack size distribution is to work backwards from the failure data. This requires knowledge of the S-N data, of the member. The distribution of stress cycles can then be found by normalising the stress data to a

stress range. A lognormal distribution was found by Connolly and Hudak (1993), to give good fit of the fatigue lives

$$f(N) = \left(\frac{1}{\zeta N\sqrt{2\pi}}\right) exp\left[-0.5\left(\frac{ln(N)-\lambda}{\zeta}\right)^2\right] \qquad 6.5$$

where

λ and ζ are the mean and standard deviation of the lognormal distribution and N is the number of stress cycles. Integrating Paris' law we obtain a relationship to relate stress cycles and initial defect size assuming a constant geometry factor. This yields to

$$N = R \cdot a_{in}^{-m/2} \cdot \left(a_f - a_i\right) \qquad 6.6$$

where $R = 1/\left[C\left(Y\Delta\sigma\sqrt{\pi}\right)^m\right]$ and a_i is the initial crack size and a_f is the final crack at failure. The initial crack size distribution can be calculated by using equations 6.5 and 6.6 using the relationship $\int_0^{N_{failure}} f(N)dN = \int_{a_0}^{\infty} f_{init}(a_i)da_i$ which yields

$$f_{init}(a_i) = \frac{1}{R \cdot a_{in}^{-m/2} \cdot \left(a_f - a_i\right) \cdot \sigma \cdot \sqrt{2\pi}} exp\left[-0.5\left(\frac{ln(R \cdot a_{in}^{-m/2} \cdot \left(a_f - a_i\right)) - \mu}{\sigma}\right)^2\right] \qquad 6.7$$

where the mean value, μ, and standard deviation σ are obtained from fatigue tests (S-N data). Unfortunately there are no such values available for ship structure details, but only for tubular joints. Hence, a direct comparison of this distribution with actual data is not possible.

This method to evaluate the initial defect distribution produces a distribution that is somewhat larger than the actual defect distribution, since the S-N curves used are a lower bound of the actual data. However, the distribution of equation 6.7 represents the distribution of the largest cracks in the population which produce failure, whereas the actual distribution represents the size of all cracks found during inspection. Equation 6.7 also assumes that all variability is in the crack size whereas a

considerable part will be in the material constants C and m. Equation 6.7 should therefore represent an upper bound to the actual measured distributions of the largest crack sizes.

It has been recognised that the initial defect size distribution is the parameter with the highest level of uncertainty in a fatigue reliability analysis. There are many factors that affect the crack size distribution that makes it very difficult to find a unique form. Since, most of the defects are present in the welds, the welding quality and procedure is one of the factors affecting the distribution. The quality of the crack detection technique used in the shipyard is also another factor, (when the cracks are found and repaired).

Cracks can also originate from bad design of local details. The type of the geometry of the structural detail has a significant impact on the defect distribution. For different types of details, the defect size distribution is not the same. A detailed design for the local connections may have important effect on the distribution as well. A recent study concerning fracturing in tankers, 'Prevention of fractures in ship structure' (NRC 1997 report), states that most fractures in ships classed with high strength steels (A, B, and D) occurred in mild steel components, despite the concern of the use of high strength steels, which produces larger stresses because of reduced scantlings. It was concluded that the problem was therefore related to design rather than material. However, the use of high tensile steel will generally make fatigue cracking worse and may increase stress ranges in mild steel components.

The exponential distribution fitted to actual crack size measurement by Bokalrud and Karlsen, shown in Figure 6.4, is believed to represent more closely the initial crack size distribution for ship structures and is adopted in this thesis. It is difficult to know exactly the statistical parameters of this distribution because of the high variability in this parameter, which depends on, welding quality and technique, position along the ship, and type of detail. Truly speaking this is the distribution of the detectable crack sizes, but it is believed the distribution describes well the crack sizes which are important for the fracture analysis, since the very small crack sizes being undetected will not contribute to the probability of failure due to fracture.

The distribution is chosen to represent the uncertainty in crack sizes for the whole ship, and the same distribution is used for each crack location assumed.

6.2.6 *Fatigue Loading and Stress Cycles*

Under random loading the long-term stress history is described with appropriate probability distributions as discussed in chapter 3, section 3.6.3. The Weibull distribution has proved to give good fit to actual stress data as discussed in chapter 3. The Weibull distribution has the form

$$F(\sigma) = 1 - exp\left[-\left(\frac{\sigma}{A}\right)^{B}\right] \qquad 6.8$$

In order to estimate the mean values of the scale and shape parameters of the Weibull long-term stress range distribution, a complete fatigue analysis was performed as part of this thesis, described in detail in appendix A. Several different locations along the ship were chosen for the fatigue analysis. For each detail the long-term stress range distribution was estimated as explained in chapter 3. The Weibull distribution is only a theoretical distribution that has been proven to fit quite well the actual stress history. Therefore, it needs to be fitted to the actual data and the parameters to be estimated. The least squares fitting technique was used to fit the Weibull distribution to the stress history obtained from the spectral analysis. This is described in detail in chapter 3, section 3.7. The results of the least squares fitting can be seen in Table A1 in appendix A, for different locations along the ship and different loading conditions.

To take into account the uncertainty in the environmental loading the scale and shape parameters, A and B respectively, can be treated as random variables. For the purpose of this report the scale and shape parameters are assumed to follow a normal distribution. The degree of variability is of major importance, especially for the shape parameter, therefore an estimation of the variance of the shape parameter has to be made.

An estimation of the variability of the shape and scale parameters is possible using special statistical subroutines available in the *Microsoft Developer Studio,* FORTRAN

library. This analysis yields an approximate coefficient of variation for the scale parameter of about 10% and a coefficient of variation for the shape parameter of about 3%.

Another parameter that is modelled probabilistically is the annual number of stress cycles, *N*. The uncertainty in this parameter arises from the randomness of the waves and in particular the sea state the vessel is facing every time. Several sea states were modelled in the dynamic response analysis, and the weighted response was calculated, taking into account the relative time the ship spends in each of the sea states, and the frequency of occurrence. The mean value of the total number of stress cycles at a particular point on the ship is evaluated using the average time the ship spends in every sea state. To account for the variability of the number of cycles in a year and for the percentage of time spent at sea a lognormal distribution is chosen with a cov of 20%.

6.3 Parameters Necessary for the Probabilistic Fracture Analysis

6.3.1 *Extreme Wave Loading*

Extreme loading will be responsible for the fracture of the vessel, when applied to a crack which will then grow unsteady. Extreme stress amplitudes were calculated using spectral analysis, and the stress amplitude response spectrum combining all sea states was fitted to a Weibull distribution with scale and shape parameters, as was described in chapter 3. The Weibull distribution parameters were modelled as random variables following a normal distribution, to account for the variability which arises from the fitting of the distribution. As in the case of fatigue loading, the scale parameter has a cov of 10% and the shape parameter a cov of 5%. Mean values for the scale and shape parameters of the Weibull distribution of stress amplitudes are given in Table A2 in appendix A.

6.3.2 *Still Water Vertical Bending Moment*

The still water bending moment is a basic variable with additional uncertainty with time and position, since its mean value may change because of ballast shift, fuel consumption, and cargo transfers. Much remains to be done in this subject. Values of still water bending moment can be obtained from the trim and stability book of the vessel for several loading conditions. Although this value does not remain the same during the ship's voyage, it is very difficult to find a mathematical model describing the still water bending moment with time, and position. However, the mean value of the bending moment is reported by Guedes Soares (1996), to be normally distributed with a cov of about 20%. A simple linear model is assumed to describe the variability of the still water bending moment with position, which may be not true but for the purpose of a comparative analysis can be justified. A typical still water bending moment distribution can be seen in Figure 6.5 for a particular loading condition. Similar still water bending moment distributions are available from the trim and stability book of the vessel for the other loading conditions assumed in this report. From these distributions the mean value of the still water bending moment is determined for different sections along the length of the vessel, and is used for the reliability analysis of the ship as a system, described in the next chapter.

6.3.3 *Residual Stresses*

Residual stresses and their modelling have been discussed in chapter 3 and 4. Their value has been modelled deterministically and has not been assigned a probability distribution because very little data exists on residual stress measurements. However, they are allowed to 'shake down' with time, i.e. reduce their magnitude because of the reasons stated at chapter 3.

6.3.4 *Fracture Toughness*

Fracture toughness is an important parameter for the fracture analysis since it represents the strength of the metal to fracture. Fracture toughness is inherently a probabilistic variable, since even under identical test procedures there is considerable scatter in the measurements. Fracture toughness apart from the statistical variability,

varies also with temperature. Hence, all the measurements are for various temperatures. During, a ship's voyage it is likely that changes in temperatures occur, which suggests that fracture toughness should be modelled as a function of temperature. This would require also a temperature distribution with time and accordingly a joint distribution of time and fracture toughness, to sample values for fracture toughness. Another suggestion would be to run the analysis for different fracture toughness distributions and see the effect fracture toughness has on the results. There is also likely to be some correlation of temperature and hence fracture toughness with the wind and hence wave environment. However, this was not taken into account in this thesis.

DERA have produced a report which presents information on fracture toughness values and distributions for various metals, temperatures and loading rates. As a more valid source of information, the values presented by this report have been selected in this thesis. The fracture toughness is modelled using the two-parameter Weibull distribution with scale and shape parameters. A shift of the Weibull distribution is applied to fit the distribution to the cumulative probability points below a value of 200 MPa$\sqrt{m}$, but this results in conservative values. A cut off value is introduced so that many low unrealistic values are neglected. A summary of Weibull scale and shape parameters from this report is available in Table 6.6 and they are values for a slow loading rate with stress intensities less than 100 MPa$\sqrt{m}$/sec typical of normal wave loading in deck structures. The FATT temperature results were chosen for this work (the 27 Joule temperature values are more conservative).

There is a huge amount of scatter in the FATT temperatures. For a 25 mm thick plate one reference measures the FATT temperature about –20 °C and another reference about +30 °C (Figure 6.6). A mean FATT temperature is then assumed for the transition temperature (i.e. approximately +10 °C) which is relatively high. That means that the steel behaviour will be more brittle rather than ductile. The Weibull distribution for the +10 FATT temperature was selected. The Weibull scale parameter is approximately similar to the –10 FATT temperature curve. However the larger shape factor allows for a bigger variability in fracture toughness. Because, it was decided that only one distribution of fracture toughness will be used to represent the

variability in the whole ship structure, and not consider variability with temperature as discussed above, the distribution with the greater variability was selected. For environments with very low ambient temperature the FATT or the –10 FATT distributions would be more appropriate.

6.3.5 *Yield Stress and Ultimate Strength*

Yield stress value of mild steel is well documented and is used in this thesis with a mean value of 245 N/mm^2 and a cov of 8% being lognormally distributed. The ultimate strength takes a value of 420 N/mm^2 and is a deterministic parameter. A bias is also included in the yield strength modelling but this is normally small for modern steels.

6.4 Inspection Modelling

There is no standard procedure to assess the quality of an inspection or the chance of finding a crack. The basic variables that affect the inspection quality, apart from the variables already mentioned (size of ships, access to spaces), are

- The experience of the inspector or inspection team. Studies have shown that there is a high degree of variability between results from different inspection teams.

- Another variable is the environment. Lightning conditions inside the ship are often poor with little other than assisting the inspector to find his way around. The inspections are usually carried out with a flashlight.

- Available time is also a factor. The 'time is money' concept is perhaps the biggest principle in the operation of large merchant ships. The more time the ship spends in the dry dock the more prohibitive the costs involved.

With the above factors in mind, a way must be found to model the inspection quality, namely the probability of detecting a crack. Probabilistic methods are applied together with extensive experimental trials to model inspection quality. Usually inspection quality is represented by the Probability Of Detection (POD) curve. POD curves show the probability of a crack been detected against the crack size. A perfect POD curve

would equal to one, but because of the reasons mentioned before inspections are not perfect.

Different inspection techniques have different POD curves. POD curves are different even among different inspection teams. POD curves also depend on the location of the cracks i.e. areas with no good access will have lower detection probabilities. It is vital that the appropriate POD curve is used for the inspection carried out.

The POD curve indicates the proportion of cracks that will be detected by a non-destructive evaluation (NDE) technique when applied by inspectors to a population of structural elements. However, POD curves depend on many factors such as the quality of the NDE technique, the ability of the inspectors, the geometry and material of the structure, the environment in which the inspection takes place and location, orientation and size of the flaw. All of the above dependencies are modelled through the POD curve as the probability as a function of crack length.

In practice the true probability of detection will never be known. POD curves are constructed from experiments in which representative structures with known crack lengths are inspected and the POD is constructed by the observed percentage of correct findings. Statistical analysis is then performed to evaluate confidence limits and to account for the finite sample size.

There are different POD curves for different NDE techniques. For visual inspections in ship structures the following POD curve is representative

$$POD(a) = 1 - e^{-\left(\frac{a}{a^*}\right)} \qquad 6.9$$

where a is the crack length and a^* is a crack length value which accounts for the quality of inspection. For a close visual inspection in a ship structure this value takes values from 30 mm up to 150 mm depending on experience of inspector and location, whereas for visual inspection of a plate in a laboratory it can be as low as 5 mm. Figure 6.7 shows a POD curve with a^* equal to100 mm.

One POD curve has been used in this thesis to model visual inspection. During the reliability analysis the quality of the inspection is investigated by a parametric study

(chapter 7). A value of 100 mm and a value of 50 mm is used. For different locations, e.g. ballast tanks, cargo spaces, different POD curves can be used, but as a simplifying assumption only one POD curve has been used in this thesis.

References

- ABS, 'Guide for dynamic based design & evaluation of bulk carrier structures', March 1995

- ASM, 'Fatigue mechanism, crack growth and testing'

- Barsom J. M. , Rolfe S. T. , 'Fracture and fatigue control in structures', Prentice Hall, Englewood Cliffs, New Jersey, 1987

- Bokalrud T, Karlsen A, "Probabilistic fracture mechanics evaluation of fatigue failure from weld defects in butt welded joints", in proceedings, International conference on fitness for purpose validation of welded constructions, The welding institute, London 1981.

- Connolly M. P. , Hudak Jr S. J. ., 'A simple reliability model for the fatigue failure of repairable offshore structures', Fatigue Fract. Engng Mater. Struct. Vol. 16, No. 2, 1993

- DERA Report, DERA/MSS2/CR990041/1.0, 'Toughness probability distributions for ship steels & weld', Feb. 1999

- DnV, Recommended Practice, D404, 'Unstable Fracture', August 1988

- Guedes Soares C. , Garbatov Y. , 'Influence of inspection and repair on the fatigue reliability of oil tankers', Proceedings of OMAE 1996, Volume II

- Gurney T. R., 'Fatigue of welded structures', Cambridge University Press, 1979

- Hadrboletz A. , Weiss B. , Strickler R. , 'Fatigue thresholds of metallic materials – A review', Handbook of Fatigue Crack Propagation in Metallic Structures, pp. 847-882, 1994

- Johnston G. O., 'Statistical scatter in fracture toughness and fatigue crack growth rate data', Probabilistic Fracture Mechanics and Fatigue Methods, ASTM, STP 798, 1983

- Kountouris I. S. , Baker M. J. , 'Defect assessment analysis of defects detected by MPI in an offshore structure', CESLIC report No. OR6, Dept. of Civil Engineering, Imperial College, London, UK

- Maddox S. J., 'Fatigue crack propagation data obtained from parent plate, weld metal and HAZ in structural steels', Welding Research International, Vol. 4, 1974

- NRC, Symposium and Workshop on, 'Prevention of fracture in ship structures', Ship Structure Committee, SR-1363, February 1997

- Ostergaard D. F., Hillberry B. M., 'Characterization of the variability in fatigue crack propagation data', Probabilistic Fracture Mechanics and Fatigue Methods, ASTM, STP 798, 1983

- Paik J. K. , Thayamballi A. , Kim S. K. , Yang S. H. , 'Ship hull ultimate strength reliability considering corrosion', Journal of ship research, Vol. 42, No. 2, June 1998

- Shetty N. K. , Baker M. J. , 'Fatigue reliability of tubular joints in offshore structures: reliability analysis', Proceedings of OMAE 1990, Vol. II

- SSC-397, 'Commercial ship design and fabrication for corrosion control, Ship Structure Committee Report, 1997

- Tanaka Y., Soya I. , 'Metallurgical and mechanical factors affecting crack propagation and crack closure in various structural steels', Proceedings of 4th International Conference on Fatigue and Fatigue Thresholds, Vol. II, pp. 1143-1148, 1990

- Tanker Structure Co-operative Forum, 'Condition evaluation and maintenance of tanker structures', Witherby, 1992

- Valsgard S. , Andreassen E. , Kim S. K. , 'Development of ultimate hull girder capacity', Proceedings of the conference design & operation of bulk carriers, London, 1998

- Virkler D. A. , Hillberry B. M., Goel P. K. , 'The statistical nature of fatigue crack propagation', Transactions of ASME, vol 101, April 1979

- Yazdani N. , Albrecht P. , 'Crack growth rates of structural steels in air and aqueous environments', Engineering fracture mechanics, Vol. 32, No. 6, 1989

Environment	m	ln C (for ΔK in $Nmm^{-1.5}$)
Non-corrosive	3.1	-28.84
Corrosive	3.3	-28.89

Table 6.1a – *C and m values from DnV tests*

Steels in air			
C in $Nmm^{-3/2}$	**m**	**Steel**	**Reference**
4.92E-13	3	ferritic - pearlitic	Ship Structure Committee report 402
3.00E-13	3	ferritic - pearlitic	PD6493
1.10E-13	3.1	upper bound	DnV, D404 1988
$1.315e\text{-}4 / 895.4^{m}$		best fit to data	Gurney
2.99E-13	3.1		Bokalrud & Karlsen 1981
1.48E-14	3.344	mild & HSLA	Yazdani, 1989
Steels in corrosive environment			
2.30E-12	3	upper bound	PD6493
3.40E-14	3.5		DnV,D404 1988
2.84E-13	3.3		Bokalrud & Karlsen 1981
5.02E-14	3.279	mild & HSLA	Yazdani, 1989

Table 6.1b – *Summary of C and m values from various sources*

$\Delta\sigma$ = 20 *Nmm^-2*

Set	*C*	*m*
1	1.832E-13	3.000
2	9.283E-14	3.100
3	1.768E-14	3.344

a (mm)	*ΔK (Nmm^1.5)*	*da/dN*	Ratio
0.25	17.72	1.020E-09	1.000
		6.891E-10	0.676
		2.646E-10	**0.259**
25	177.25	1.020E-06	1.000
		8.675E-07	0.850
		5.843E-07	**0.573**
250	560.50	3.226E-05	1.000
		3.078E-05	1.000
		2.745E-05	**1.000**

Table 6.2 – Comparison between *C* and *m* values from Gurney equation (in air) and the corresponding crack growth rates. At high ΔK values crack growth rates are very similar. Bolded values are values used in thesis.

$\Delta\sigma$ = 20 *Nmm^-2*

Set	*C*	*m*
1	1.832E-13	3.000
2	2.384E-14	3.300
3	6.122E-15	3.5

a (mm)	*ΔK (Nmm^1.5)*	*da/dN*	Ratio
0.25	17.72	1.020E-09	1.000
		3.145E-10	0.308
		1.435E-10	**0.141**
25	177.25	1.020E-06	1.000
		6.274E-07	0.615
		4.538E-07	**0.445**
250	560.50	3.226E-05	1.000
		2.803E-05	1.000
		2.552E-05	**1.000**

Table 6.3 – Same calculations as in table 6.2 but values for a corrosive environment.

Condition	Corrosion rate
Immersed in still water	0.15 mm/year
Splash zone	0.5 mm/year
Immersed in fast flowing water	0.8 mm/year
Ballast tanks	0.2-0.4 mm/year

Table 6.4 – *Corrosion rates for bulk carriers under different environments from DnV*

CARGO/CLEAN BALLAST TANK CORROSION RATE (MM/YY)

Location	Side	General	Pit/Groove	Remark
1. Longitudinal elements:				
a. Deck Plating	1	0.05 - 0.30		Uncoated
Deck Longitudinals (Web)	2	0.05 - 0.30		Uncoated
Deck Longitudinals (Face Plate)	2			
b. Side Shell Plating	1	0.05 - 0.10	0.20 - 1.50	Uncoated
Side Shell Longitudinals (Web)	1	0.05 - 0.10	0.20 - 1.50	Uncoated
Side Shell Longitudinals (Face Plate)	2			
c. Bottom Shell Plating	1	0.05 - 0.25	1.00 - 2.00	Uncoated
			1.00 - 3.00	Coated
Bottom Shell Longitudinals (Web)	2	0.05 - 0.10		Uncoated
Bottom Shell Longs (Face Plate)	2			
d. Longitudinal Bulkhead Plating	1	0.10 - 0.50	0.20 - 1.50	Uncoated
Long. Bulkhead Longs (Web)	1	0.10 - 0.50	0.20 - 1.50	Uncoated
Long. Bulkhead Longs (Face Plate)	2			
2. Transverse Web Frames:				
a. Deck Transverse Web Plating	2	0.05 - 0.30		Uncoated
Deck Transverse Ring Face Plate	2			
b. Horizontal Tie Beam Web Plating	2			
Horizontal Tie Beam Ring Face Plate	2			
c. Bottom Transverse Web Plating	2	0.10 - 0.30	1.00 - 2.00	Uncoated
Bottom Transverse Ring Face Plate	2			
d. Side Shell Transverse Web Plating	2	0.10 - 0.30	1.00 - 2.00	Uncoated
Side Shell Transverse Ring Face Plate	2			
e. Long. Bhd Transverse Web Plating	2	0.10 - 0.30	1.00 - 2.00	Uncoated
Long. Bhd Transverse Ring Face Plate	2			
3. Transverse Bulkheads:				
a. Tran. Bhd Plating	1	0.05 - 0.10	0.20 - 1.50	Uncoated
Tran. Bhd Vertical Stiffener (Web)	2	0.05 - 0.10		
Tran. Bhd Vertical Stiffener (Face Plate)	2			
b. Tran. Bhd Horizontal Stringer Web Plating	1	0.15 - 0.70	1.00 - 2.00	Uncoated
c. Tran. Bhd Vertical Girder Web Plating	2	0.05 - 0.10		
4. Swash Bulkheads:				
a. Swash Bhd Web Plating	2	0.10 - 0.50	1.50 - 2.00	Uncoated
b. Swash Bhd Horizontal Stringer Web Plating	1	0.15 - 0.70	1.00 - 2.00	Uncoated
c. Swash Bhd Vertical Girder Web Plating	2	0.10 - 0.50		Uncoated

CARGO OIL TANK CORROSION RATE (MM/YY)

Location	Side	General	Pit/Groove	Remark
1. Longitudinal elements:				
a. Deck Plating	1	0.03 - 0.10		Uncoated
Deck Longitudinals (Web)	2	0.03 - 0.10		Uncoated
Deck Longitudinals (Face Plate)	2			
b. Side Shell Plating	1	0.03		Uncoated
Side Shell Longitudinals (Web)	1	0.03		Uncoated
Side Shell Longitudinals (Face Plate)	2			
c. Bottom Shell Plating	1	0.04 - 0.10		Uncoated
			1.00 - 2.00	Coated
Bottom Shell Longitudinals (Web)	2	0.03		Uncoated
Bottom Shell Longs (Face Plate)	2			
d. Longitudinal Bulkhead Plating	1	0.03		Uncoated
Long. Bulkhead Longs (Web)	1	0.03		Uncoated
Long. Bulkhead Longs (Face Plate)	2			
2. Transverse Web Frames:				
a. Deck Transverse Web Plating	2	0.04 - 0.10		Uncoated
Deck Transverse Ring Face Plate	2			
b. Horizontal Tie Beam Web Plating	2			
Horizontal Tie Beam Ring Face Plate	2			
c. Bottom Transverse Web Plating	2	0.03		Uncoated
Bottom Transverse Ring Face Plate	2			
d. Side Shell Transverse Web Plating	2	0.03		Uncoated
Side Shell Transverse Ring Face Plate	2			
e. Long. Bhd Transverse Web Plating	2	0.03		Uncoated
Long. Bhd Transverse Ring Face Plate	2			
3. Transverse Bulkheads:				
a. Tran. Bhd Plating	1	0.03		Uncoated
Tran. Bhd Vertical Stiffener (Web)	2	0.03		Uncoated
Tran. Bhd Vertical Stiffener (Face Plate)	2			
b. Tran. Bhd Horizontal Stringer Web Plating	1	0.06 - 0.10		Uncoated
c. Tran. Bhd Vertical Girder Web Plating	2	0.03		Uncoated
4. Swash Bulkheads:				
a. Swash Bhd Web Plating	2	0.03		Uncoated
b. Swash Bhd Horizontal Stringer Web Plating	1	0.06 - 0.10		Uncoated
c. Swash Bhd Vertical Girder Web Plating	2	0.03		Uncoated

Table 6.5 – *Average corrosion rates for oil tankers and OBO carriers (Tanker Structure Co-operative Forum)*

K MPam$^{1/2}$			
27 Joule temperature	scale	shape	mean
above 27 Joule	358	2.601	318
-10 below 27 Joule	290	2.961	259
-20 below 27 Joule	296	3.291	266
FATT	scale	shape	mean
+10 above FATT	273	6.711	255
FATT	311	3.506	280
-20 below FATT	281	2.589	250

Table 6.6 – *Scale and shape parameters of the Weibull distributed fracture toughness taken from the DERA report.*

	Mean S-N curve			
Stress Range	E	F	F2	Prob. Fract. Mech
20	142.4	74.7	53.3	160.0
30	31.2	16.3	11.7	25.0
40	13.1	6.9	4.9	7.5
50	6.7	3.5	2.5	3.2

Table 6.7 – *Fatigue lives for different mean S-N curves and from probabilistic fracture mechanics*

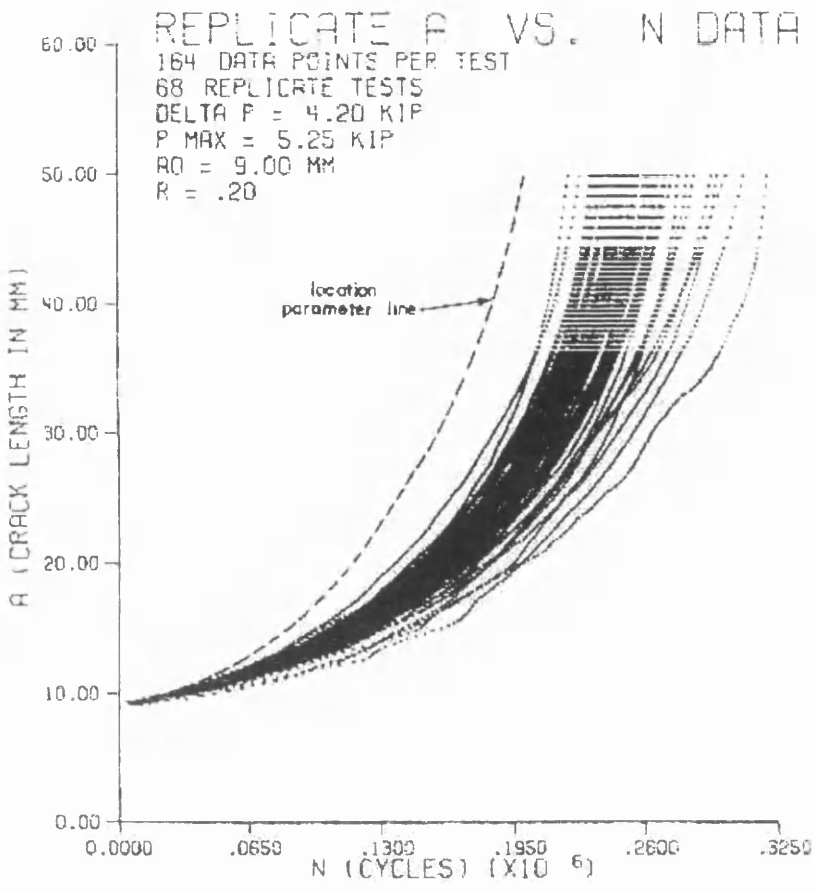

Figure 6.1 – *Variability on C and m parameters on fatigue crack growth (Vickler 1979)*

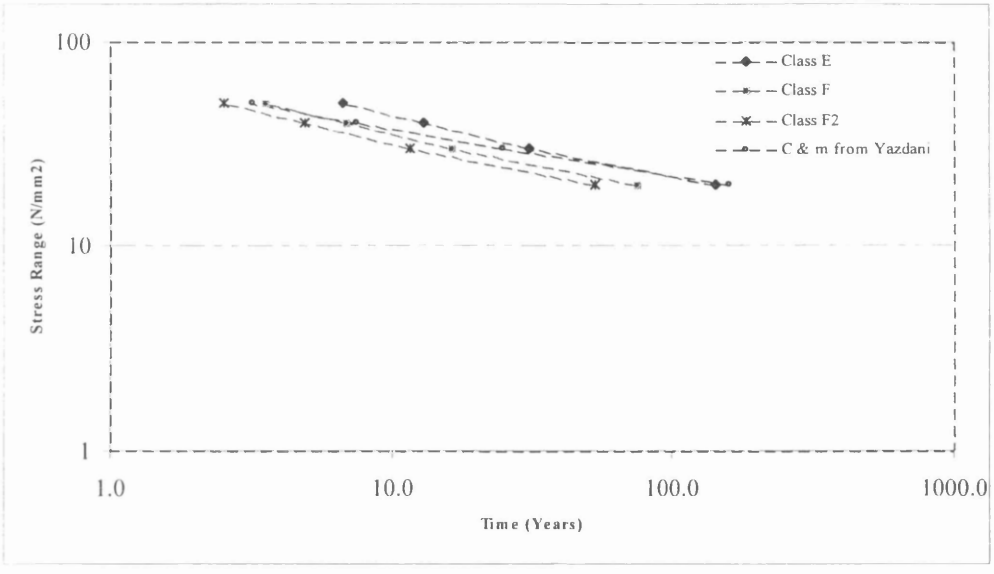

Figure 6.2 – *Mean standard S-N curves and S-N curve obtained from probabilistic fracture mechanics*

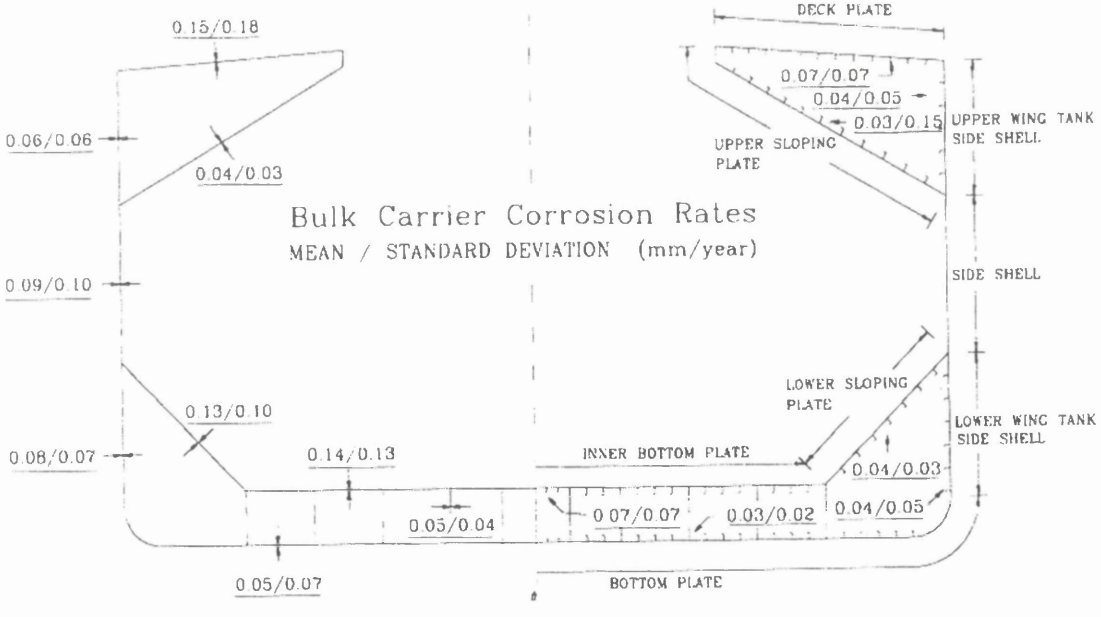

Figure 6.3 – Corrosion rates for various different locations along a ship's section

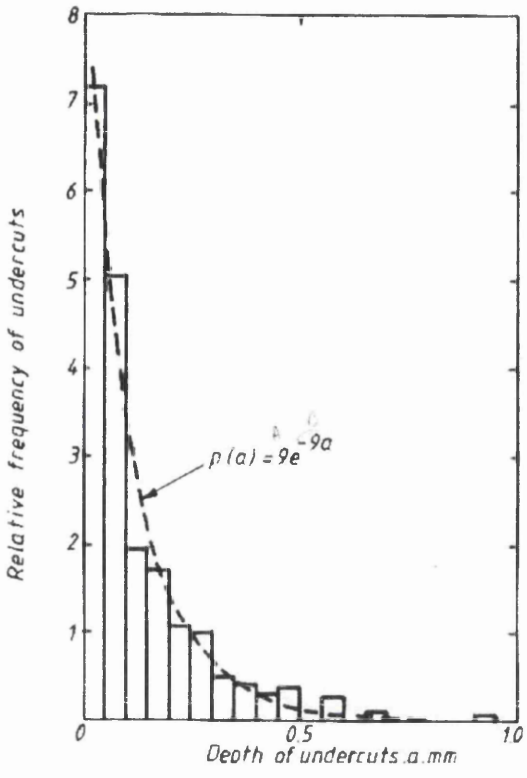

Figure 6.4 – *Initial crack size distribution (undercuts)*

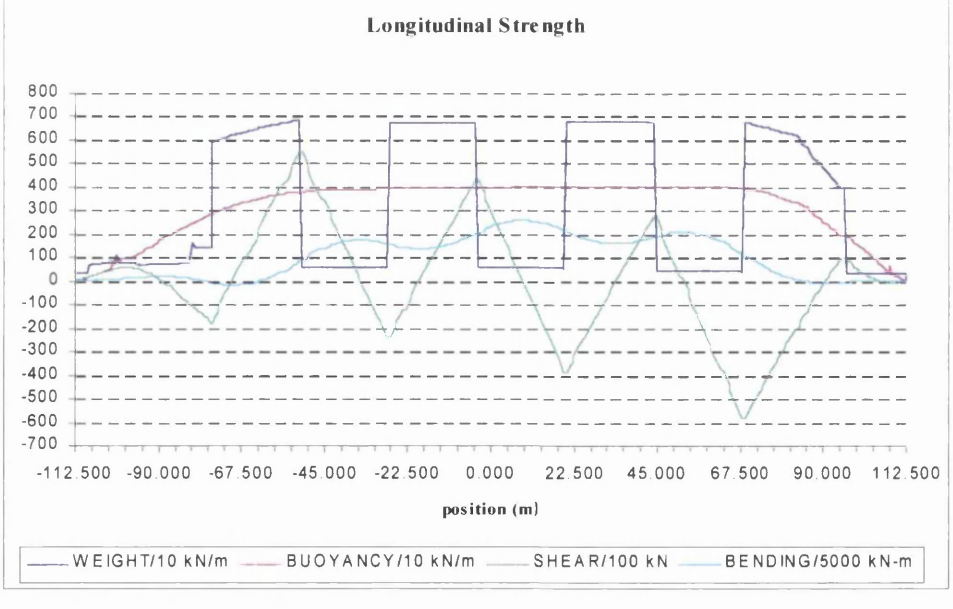

Figure 6.5 – *Typical Still Water Bending Moment Distribution*

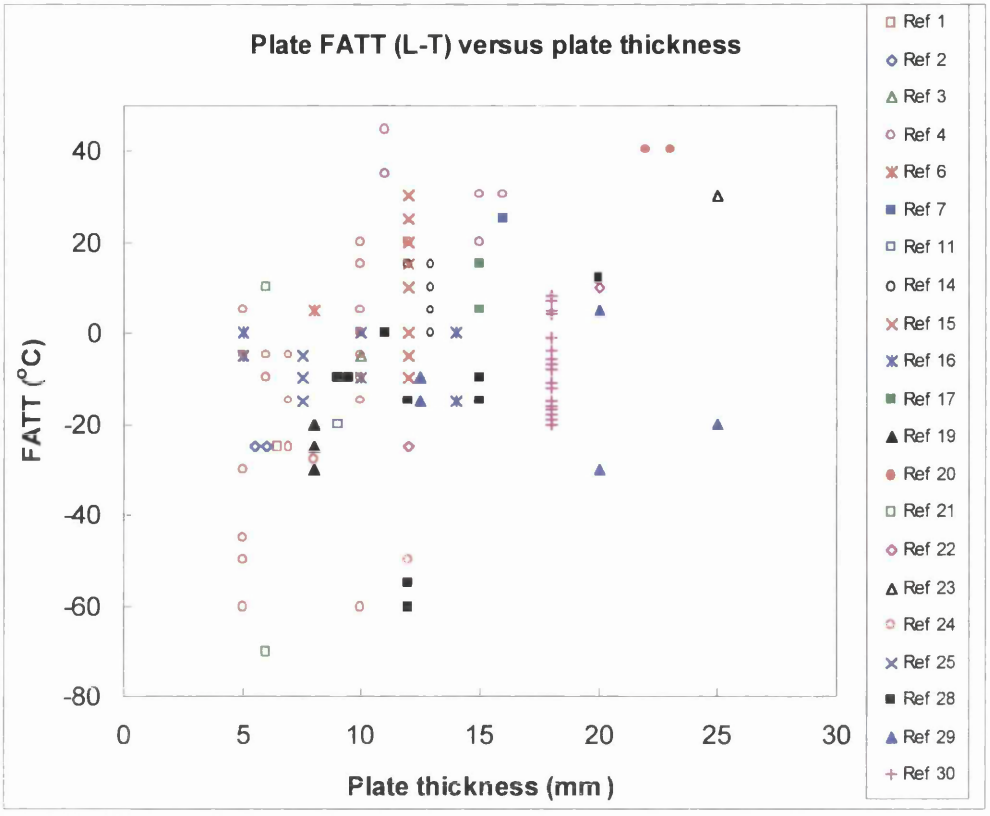

Figure 6.6 – *FATT temperature with thickness* (DERA report)

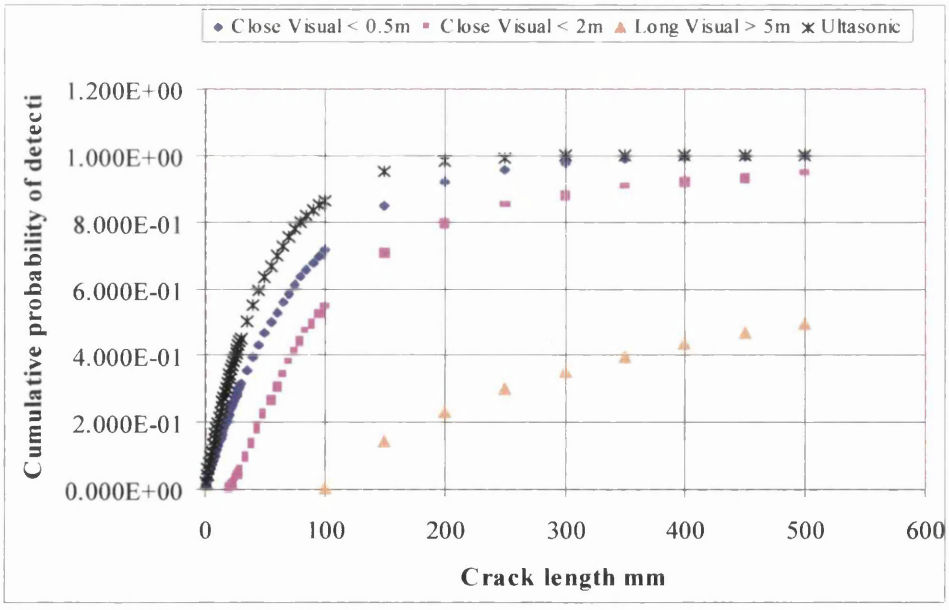

Figure 6.7 – *Probability of detection curves for close visual and ultrasonic inspections*

CHAPTER 7

RELIABILITY ANALYSIS OF A BULK CARRIER CONTAINING CRACKS

7.1 A Method to Estimate the Probability of Failure Due to Fracture

In chapter 1 the problem of cracks in ship structures was discussed. In section 1.1.3 there was a brief introduction of a method to analyse and investigate the failure probability of a vessel containing cracks, and the various tasks necessary for the analysis. In section 1.6 a very short introduction to method was given, and how to combine all the tasks together to perform the reliability analysis.

It is now appropriate to elaborate in the method and describe in detail all the components, and how to put them together in order to undertake a reliability analysis of a ship containing many crack locations, and estimate the failure probability by considering all the cracks at the same time and not individually.

This chapter explains the theory and application of a computer program that can handle multiple crack locations on a ship structure. However, the computer time required to analyse all possible failure locations is impractically large and so simplified techniques are developed for the whole ship problem.

There is no doubt that a ship structure contains cracks, even from the construction stage, and the reasons were discussed in 1.3. When the ship enters service, some of the defects inherited during the construction for the various reasons discussed in 1.3.2, will start to grow under the repetitive loading mainly caused due to waves, which is called fatigue loading and was discussed in 3.1.1. Calculation of fatigue loading was discussed in 3.3 and requires information about the ship's service profile, and use of response analysis, if actual stress records are not available.

The rate of crack growth will not be the same for each defect, some cracks for example will grow faster than others. Crack growth rate depends on the environment, (e.g. a corrosive environment will increase the rate of growth), applied load (higher stress ranges obviously will grow the crack faster), material properties (these are related with constants used in the crack growth equation) and crack orientation. A

physical model is also needed to relate the crack size with time. Section 4.7 has more on this subject.

During the ships' voyage there will be a possibility to face a severe sea condition which will produce stresses much higher than the normal operating stresses, and in some cases higher than the design stresses. Discussion on these high stresses caused by waves, called extreme stresses was given in 3.6. The value of the extreme stresses depends mainly on the geographical area the ship operates, since they are related to the wave statistical data (i.e. wave height and period) which is different for each geographical location. Calculation of extreme stresses usually requires knowledge of the wave statistics and use of extreme statistics theory, discussed in section 3.6.4.

When an extreme load is applied to the ship, due to big waves there is a possibility that fracture will occur. This means that a combination of crack size and load has produced some force which has exceeded the strength of the material to prevent fracture. The strength of the material to fracture is called fracture toughness and is a material property which depends also on temperature. There is at this point the need to be able to evaluate when failure occurs, due to a combination of load (crack size and extreme load) and strength (fracture toughness). A physical model for this task is described in 4.6.3 and is called the failure assessment diagram (FAD). It requires information on the loading, the crack sizes and strength mainly as a function of fracture toughness and plastic capacity.

To determine the probability of failure because of uncertainties in the input parameters it is necessary to adopt a probabilistic approach. There are many methods to carry out a probabilistic analysis and the basic methods were described in 2.3. In this thesis, the simulation method was chosen to perform the analysis, which is discussed in detail in 7.6.3.

When it is required to investigate the failure probability of a ship containing multiple defects, the probability of failure of each defect must be calculated and then the individual failure probabilities are combined together to determine the probability of failure of all the defects. This requires an analysis suitable to take into consideration all defects and the contribution to the overall failure probability (system probability of

failure) of all members (defects) of the system. Another important consideration is the definition of failure of a system. A system may have many failure paths, i.e. ways to fail. The various structural failure modes were described in 4.6.1. Depending also on the degree of redundancy, a system may require more than one member to fail before the system fails. The two simplest forms of a system failure are the series and the parallel systems, which were described in 2.5. In a series system failure occurs when any member fails, hence it is also called a weakest link system. A parallel system requires all members to fail before system failure occurs. The system modelling of a ship having cracks is discussed in 7.6.

System considerations require also the assignment of correlation between members. When the parameters of one member are related in some way to the parameters of another member, then these parameters are correlated. In the case where there is no correlation, the parameters are said to be independent. The concept of correlation is discussed in 2.5. As it is shown later in section 7.5, there is difference in the failure probability of an independent and a correlated system.

In the next section each component necessary for the reliability analysis of a ship containing cracks is discussed and a flowchart of the method is presented to give a clearer picture of each task and where it is used.

7.2 The Components of the Reliability Analysis

In section 1.1.3 a brief discussion of all the necessary tasks for the reliability analysis concerning fracture was given. Generally, a probabilistic approach for the reliability analysis of a ship structure to calculate the risk of failure because of cracks requires a lot of input, and many separate analyses put together. A diagram showing all the parts of the analysis is given in Figure 7.1. This thesis combines developments in each field of the analysis to calculate the reliability of the vessel with respect to fracture. A simple split would be to have three components;

- The crack growth analysis, using fracture mechanics
- The fracture assessment, using the failure assessment diagram (FAD)

- The treatment of both the above analyses in a probabilistic manner, using reliability methods to calculate the probability of failure

The first two components were discussed in detail in chapter 4 and the reliability method in chapter 2.

7.2.1 *Probabilistic Treatment of the Method*

If all parameters were known exactly, the analysis would be described as deterministic, and the answer would be that the structure was either safe or not. With the modelling of the uncertainties of the various parameters we can calculate the probability of failure of the structure at any given time.

In order to do this it is necessary to perform a reliability analysis. There are various methods to perform reliability analysis, some described in chapter 2. In this thesis, the simulation method is chosen to calculate the probability of failure of the structure, which is was described in 2.4, and the reasons for the choice are given in the next section.

With information on the uncertainty of each variable, described by a probability distribution, and the use of a reliability method it is possible to estimate the risk of failure of the structure. Figure 7.1 shows graphically the process, by using the probability distributions of each variable, and combining together crack growth analysis and fracture assessment. The reliability method chosen and a more detailed description of how it works follows in the next section.

7.3 Use of Monte Carlo Simulation to Estimate the Failure Probability

The Monte Carlo simulation technique is adopted, which is the simplest form of simulation available. The basis of the method was described in section 2.4 together with the advantages and disadvantages. One of the reasons why Monte Carlo simulation was chosen is that it copes well with the complexity of the analysis. It was shown earlier in the chapter, that fracture analysis requires crack growth calculations

and fracture assessment. This is because some parameters change with time, and their estimation requires a separate analysis (e.g. crack size estimation, requires use of fracture mechanics). This is easily dealt with, when Monte Carlo simulation is used, but may not be possible if another reliability method was chosen. Monte Carlo simulation can be used to simulate, the crack growth analysis (i.e. a time dependent analysis), the fracture analysis and at the same time provide an estimate of the probability of failure. The simulation method is the most flexible method to perform very complicated analyses like in this case. Especially the agility of the Monte Carlo method to combine in one computer code all the required individual assessments was the primary reason it was chosen for the reliability analysis in this thesis.

Another reason for using Monte Carlo is because it uses only statistical information for variables in the form of the probability distributions, to generate sample values for the variables, and not to estimate directly the failure probability. For example, the crack size distribution changes shape as well as parameters (mean value, standard deviation) with time, and it is very difficult to describe its shape with some known analytical distribution. However, in Monte Carlo only the samples are used to determine the failure probability and not the shape and form of the probability distributions. It uses therefore less information, compared with other reliability methods.

Monte Carlo simulation provides also flexibility to do some realistic comparisons. For example, it allows for the natural variability in loading to be accounted for by re-sampling for its value at every time interval separately, and not only using the mean value and standard deviation as other methods would do, and which would not be possible to see the difference. On the other hand, material properties do not change value with time (e.g. yield stress), therefore it is possible to sample for these parameters only once and use the same values throughout the analysis.

Monte Carlo is also very useful when system effects are analysed where the definition of failure is important (e.g. series/parallel system) and there is also correlation between the parameters. It is possible to calculate the failure probability of an independent system, whether it is in series, parallel or a combination of the two by

appropriately defining system failure. However, when a system is correlated extra information on the joint probability distributions is necessary. For a correlated system equation 2.23 gives an exact solution for the failure probability, albeit it is difficult to use. The reason is that they include terms which require the estimation of joint probabilities and these terms cannot be estimated, therefore only bounds for the failure probability can be estimated, as discussed in section 2.5.

The method of estimation of the probability of failure using Monte Carlo simulation hardly changes whether the system is independent or correlated. Exactly the same equation is used. However, there is a need to model correlation if correlation should be used, and a method to consider different systems i.e. series or parallel.

A method to account for correlation in Monte Carlo simulation is to control the way the samples are generated. As in every simulation technique samples are generated for every basic variable. A uniform distribution is used to generate pseudo random deviates (u, between zero and one) and these are then used to generate samples according to other probability distribution, a technique described in 2.4.1. If samples are generated, even for different probability distributions, but using the same random deviate from the uniform distribution, then they are fully positively correlated. By this technique, it is then possible to generate correlated samples during the simulation.

Modelling of a series system using Monte Carlo requires the following technique. During each simulation, samples are drawn for every member of the system and then an assessment is made of whether the member fails or not. Suppose that in a single simulation more than one members fail; this will be counted however as one failure and not as multiple failures since it only needs one member to fail for the whole system to fail, and in particular only the first failures are counted. A more detailed discussion on this subject is given in section 7.7, where the technique is used to calculate the failure probability of a system of cracks in a ship structure. In contrast, a parallel system requires the failure of all members before system failure occurs, so that when counting number of member failures, the number of times that all members have failed is counted.

There are however, some disadvantages associated with the method, the principal one being the time required to run the analysis. When the overall probability of failure is relatively small, (e.g. less than 10^{-4}) the amount of simulations required to estimate the failure probability and the result having low coefficient of variation, is large (probably exceeding 10^6, depending also on the number of members in the system). This inevitably, will take time even when the fastest of the systems is used. Another problem which is associated with the Monte Carlo simulation is the large amount of memory it needs when a complicated system is simulated, and it may be impossible to analyse a real system where thousands of members are present (e.g. all cracks in a ship).

A computer code is necessary, to perform the reliability calculations this is described in the next section.

7.4 Code Development for the Reliability Calculations

There are many general-purpose codes for reliability analysis including system effects. They offer also the option to calculate the failure probability using various reliability methods, e.g. FORM, SORM, simulation. However, the reliability analysis which needs to be performed for this thesis includes a further complication. This is the time dependent crack growth analysis, which is used to update the crack size distribution at every time interval, necessary to calculate the probability of failure of the ship structure with respect to time. Generally, this could not be analysed with the general-purpose codes.

A computer code was therefore written and used to perform the reliability analysis described in 7.2. A flowchart of the code is given in appendix D, the code was written in Fortran.

It is important that system (i.e. multiple location) calculations can be performed, hence the system must be defined first. The system is subdivided into groups, and each group into individual members, as shown in Figure 7.2. Variables between groups can vary, but within each group variables remain the same. Input data consists of general information, such as total time period, number of simulations, inspection

interval, number of groups and number of members in each group, which are the control variables. Then information for each group must be specified which mainly includes information of the basic variables of each group, their mean value and standard deviation as well as the probability distribution of each basic variable, i.e. data necessary for the crack growth analysis, the fracture assessment and finally the reliability calculations. Within the group input data, the geometry of the crack is specified and its location. Also, whether the basic variables are correlated between groups and whether to sample each year or once. A typical input file can be seen in Table 7.1. Other input data includes, the quality of inspection, corrosion rate, crack size after inspection, position of neutral axis, and information about residual stresses.

When all necessary data is given, the simulation runs and calculates the probability of failure of the specified system, for every time interval defined. The code also calculates the individual failure probability of each member of each group. It also calculates for each member (crack) the mean value and standard deviation of the crack size distribution, so that comparison can be made with other members and see which member (crack) grows faster. The number of failures of each member is also given, distinguishing the reason of failure i.e. brittle fracture or plastic collapse, so that an indication of what causes the failures is possible. One extra information provided is the number of cracks repaired, so when there is an increase in the reliability of the structure to see whether it happened because of the repairing action. There is an option to perform inspection only periodically every some specified time period, or perform inspection every time interval and repair cracks that are large enough. Results of the code are explained better with some examples later in this chapter. Output files from the code can be seen in appendix C.

Monte Carlo simulation calculates the failure probability using equation 2.17. Therefore, many simulations must be carried out and the number of failures during each simulation must be counted. By dividing the number of simulations that have failed with the total number of simulations performed, an estimate of the probability of failure is possible.

When a simulation has failed, it is not allowed to continue in the next time interval. This reduces the number of simulations with time, and it may produce strange results (e.g. failure probability reducing with time because of lack of number of simulations). This problem is discussed in section 7.6.

This is how the code works, explaining it in a simplified way. A better description of how it can be used to analyse the whole ship, is given in section 7.6.

7.5 Example Calculations for a Single Member and a Small System

Before analysing a complete system, it is a good practice to perform simplified calculations for only a single member. It is also easier to make comparisons between various cases, and understand the differences. In this section a single crack is examined, and the failure probability is calculated. Various cases have been run, to examine the effects of different parameters, e.g. effect of corrosion, inspection quality, and initial crack size distribution.

One of the reasons to perform this analysis was to examine the crack size distribution and how it changes with time.

The crack type that is selected for checking purposes is a centre crack in a finite plate. The geometry is shown in Figure 7.3. It is also assumed that this crack is at the deck structure, so that loading for that part of the ship is used. Tensile residual stresses are assumed to be present. A list of the input data is given in Table 7.2. The number of stress cycles for this example is about ten times higher than the actual number of stress cycles calculated from spectral analysis, this is to increase crack propagation and hence the failure probability. Otherwise, because the failure probability for a single crack is very small, the Monte Carlo simulation would yield no failing with a reasonable amount of computer time. It is for this reason that even in this example with increased number of cycles, at earlier stages the failure probability is zero. Inspection is occurring every 5 years.

Figure 7.4 shows the crack size distribution at various times, starting from an initial exponential distribution. It is clear that as cracks start to grow they move towards the tail end of the distribution and at the same time, they shift the standard deviation. As a comparison the actual histogram is plotted together with a lognormal distribution having the same mean and standard deviation, shown in Figure 7.5. It is clear that there is no agreement at all. This is the problem faced by simplified reliability methods, i.e. it is very difficult to make assumptions for the probability distribution of the crack size distribution without introducing errors, and it is clear from Figure 7.4 and Figure 7.5 that the crack size distribution is very difficult to estimate. However, this is not a problem for the simulation method because it uses every sample of the distribution.

The distribution of crack sizes that cause failure and the complete crack size distribution at various times, for this example, can be seen in Figure 7.6. Both axes are plotted in a logarithmic scale so that the distribution of cracks that causes failure can be seen clearly. Although the initial crack size distribution has a very small mean value (of 0.11 mm and the same standard deviation), we can see that some very big cracks develop over the years which cause fracture. A separate figure shows the distribution of cracks that cause failure at various times, Figure 7.7. The discontinuity in the actual crack size distribution comes from the change in geometry of the crack type. It starts as a surface crack growing in the direction of the thickness, but when it reaches the thickness it becomes a through thickness crack with a ratio of crack depth to crack length of 2:1.

Initially, the large cracks that cause failure (at earlier stages) come from the tail end of the complete initial crack size distribution and in combination with fatigue loading and corrosion have grown to large sizes, as can be seen from the spread of the crack size distribution at failure. Figure 7.8 the size of the initial defects that cause failure as a proportion of the complete initial crack size distribution. At earlier stages, only a small part of the tail end distribution contributes to failure, but as cracks grow because of fatigue more and more cracks from the tail end contribute to failure. However, it is cracks only from the tail end that cause failure and in particularly in the region between 3 to 7 mm. This is because the mean value of the distribution is very small.

In Figure 7.9 a logarithmic initial defect distribution has been used with a mean value of 10mm and st. dev. of 5mm, the other input data remained the same. Here it is more obvious that the failures initially occurred because of cracks of the tail end (e.g. year 5 and year 10), but as time passed more and more cracks also from the middle part of the distribution caused failures (e.g. year 20 and year 30).

The distribution of fracture toughness values at failure is shown in Figure 7.10, and there is a tendency for the distribution to move to the left with respect to time which indicates a reduction of the fracture toughness value at failure, as a result of the crack sizes growing bigger with time.

Reliability results from this simple example are shown in Figure 7.12. The effect of corrosion on the failure probability is most noticeable, it produces the higher failure probability curve. Corrosion, increases the stress levels and hence accelerates crack growth, the probability of failure increases. The effect of having a different initial crack size distribution is shown also in the figure. One case assumes the exponential form, determined from actual measurements in production welds, which was discussed in 6.2.6, the other case assumes a lognormal type having the same mean and standard deviation. It is not clear from the figure, but when comparing the failure probabilities between these two cases, the exponential distribution produces slightly bigger failure probabilities. The reason for that is that it has more cracks, at the tail end which produces more failures than the lognormal distribution. Residual stresses also tend to increase the failure probability.

An interesting comparison is made for results where inspection and repair is done. In Figure 7.12 we can see the failure probability when inspection is carried out every 5 years. The change of the crack size distribution because of inspection and repair can be seen in Figure 7.11. Initially, inspection has no significant effect on the crack size distribution since cracks are small and cannot be detected easily. But in later stages where cracks have grown larger, the change in the distribution is more evident and it has visible effect on the failure probability curve. Even when we perform inspection (and repair), the failure probability increases, although not as fast as with no

inspection. The reason is because the inspection is not perfect, i.e. not every crack is found, and even when cracks are repaired, new cracks may initiate from the repairs.

It is now a good opportunity to make comparisons between results of a single member and a small system, and validate the results of a system with the existing relationships. For example, it is possible to calculate the failure probability of an independent system using equation 2.27, when the individual member failure probabilities are known. This can then be checked against results from the Monte Carlo simulation. A case where all parameters are fully correlated (except crack sizes), is also studied to examine the effect of correlation.

In this example we will assume that all members of the system are subjected to the same input parameters, but members are independent. Table 7.3 presents the results of this calculation. For an independent system we can see that the results from the Monte Carlo simulation agree well with the results from theory (i.e. equation 2.27), columns 3 and 4.

Further examination of the results shows, as expected, that the probability of failure is less in a correlated system than in an independent system. If all parameters are fully correlated then all failures will occur at the same time and the probability of system failure in any year is the same as the probability of any one crack site failing. As correlation reduces, the failure probability increases to the uncorrelated value.

7.6 Reliability Analysis of a Ship Structure

7.6.1 *Definition of Failure*

A ship structure containing cracks is a system. The members of the system are all the cracks that are present in the structure. When examining the failure probability of the system, it is very important to define the failure path, i.e. the way failure occurs. Ships are very complicated structures, with a lot of redundancy in their strength. However, the degree of redundancy depends on what failure mode is examined. If for instance buckling collapse is considered as the failure mode, before system failure occurs, it would require the buckling collapse of many members, e.g. plates with stiffeners and

columns together. In that case, the system probably needs to be modelled as a combination of members, some in series and others in parallel.

In this thesis, however, fracture of the structure is considered due to the presence of cracks. Failure because of cracks, can be assumed in various ways. For example, a crack that has grown through the thickness of the material can be considered as a failure, especially when leakage of oil in the sea water occurs (because of the strict regulations in today's rules, due to environmental concerns). Another way to define failure due to cracks is when considering the serviceability of the vessel. In this case, members that have failed due to cracks need to be replaced and although their failure does not cause total loss of the structure, the service is interrupted.

However, the most serious failure by far, due to cracks, would be the total loss of the structure because of fracture, and possibly loss of lives. Under this failure mode, it is possible that even a single crack can cause the total loss of the structure. As an example, even though it was not a ship structure but an offshore platform, we can mention the loss of the Alexander Kieland platform, discussed in chapter 1, due to a single fatigue crack. Another unfortunate incident was the 'Kurdistan', in which the bow cracked off in cold weather due to crack in the bilge keel. Losses of ships, especially bulk carriers, due to fatigue cracks, do occur even today as it can be seen from statistical information on bulk carrier losses, (discussed in chapter 8). Therefore, it would be more appropriate to model the risk of fracture failure because of cracks as a series system. In that case, system failure is defined as the first (earliest) failure that occurs by any member. This is an important assumption when performing reliability calculations using the Monte Carlo method. This is also the failure path assumed in this thesis.

7.6.2 *Some Considerations for Cracks in a Real Ship*

Before analysing the system, it is necessary to make some assumptions regarding the behaviour of its members. One such assumption must be made for the various parameters of the analysis, which are associated with each member (crack). Cracks can be anywhere in the ship, so that members are in different locations. This means that the input data for each crack may not be the same. For example loading will not

be the same for cracks at the deck and cracks at the side structure or at the keel. For this reason, stress analysis was performed for various locations along the ship and the loading was defined, from the spectral analysis done and presented in appendix A. Therefore, appropriate loading is used for the different crack locations.

Crack geometry may also differ, i.e. crack type. It is then important for the crack growth analysis, that appropriate geometric factors are used to calculate the stress intensity factors and then the crack propagation. For this reason various geometric factors for different crack geometries have been established and used as a databank in the code.

Another possibility is that because cracks are in different locations, the local environment may change. For example, cracks at the keel or side structure may be subjected to corrosion, whereas cracks at the deck are not. This requires the use of appropriate crack growth constants in the crack propagation analysis, for each crack.

Apart from establishing the values of the different parameters it is also important to describe any degree of correlation that exists between the input parameters. Correlation between parameters is important for system considerations. It is necessary again at this point to distinguish between different types of correlation

Type A – Here correlation exists between the same parameters of different members of the same system. For example, loading is a parameter that is likely to be correlated in a ship (system). The correlation arises from the fact that if one location in the ship sees a high load, it is likely that other locations as well will be subjected to high loads. This is positive correlation.

Type B – Correlation between parameters of different systems. For example, the mean and standard deviation of initial crack sizes maybe correlated between two ships, (if both were constructed by the same shipyard, using same welding techniques, it is possible that both ships will have similar defect sizes). However, the size of the individual defects between different parts of the same ship can be independent.

In this thesis, positive correlation is assumed in the loading (and still water bending moment), as being a more realistic assumption than assuming independence. This applies to both, fatigue and extreme wave loading. On the other hand, material properties (e.g. yield stress, fracture toughness, crack growth constant and initial crack size) are assumed independent variables.

7.6.3 *Reliability Calculations Using the Monte Carlo Method*

The system is subdivided as shown in Figure 7.2, and a description of the input was given in 7.4. Briefly explaining the method, the ship is subdivided into groups of identical details with uncorrelated material properties subject to identical loading and each group into members. The simulation runs for each member of each group. First samples are drawn from the probability distribution of each random variable. For every sample drawn from the initial crack size distribution, a crack growth analysis is performed and at the end of each time interval a fracture assessment. When a sample fails, the time of failure is recorded. This is repeated for all the members and all groups.

Finally, at each time interval, the number of failures of each member is counted and the probability of failure of that member calculated, by dividing the number of failures of the individual members by the total number of simulations in that time interval. The probability of failure of the system, however, is found by counting at each time interval only the first failures, and dividing by the number of simulations in that time interval. By this way the system is modelled as a series system.

When dividing the number of first failure by the total number of simulations at each time interval, this gives the probability of failure at that time interval exactly. However, there are some problems associated with the simulation which can yield some peculiar results. For instance, when a simulation fails it is not allowed to continue to the next time interval, (e.g. when failure has occurred it is assumed that the system has failed and it will not be present in the next time interval). This results in reducing the number of simulations with time. It is possible that after some period all simulations have failed which means that the probability of failure thereafter is

zero. Or that the probability of failure is reducing after some period if it is not zero, because of the same problem (lack of simulations or samples left).

However, this may not be as strange as it seems. The probability of failure calculated is the probability of the structure failing at a particular time interval. When the ship is new, the probability of failure is low. But as the structure degrades with time due to fatigue, there is an increasing probability of failure. When the probability of failure starts to drop after some time, this means that there is less chance that the ship will survive up to that time or even further. An example is shown in Figure 7.13. Here, the probability of failure pf_1, is increasing up to about year 24, but starts to drop thereafter. This means that because there is higher probability for the ship to have failed at previous years, the probability to fail in later stages is reducing.

This is a perfectly satisfactory definition of failure probability however from a personnel safety viewpoint a more useful measure for the probability of failure would be the probability of failure at a particular year, considering that the ship has survived the previous year. The difference would be that, the second failure probability value takes into consideration the survival probability of the structure as well. The two failure probabilities are calculated by

$$pf_1 = \frac{Number\ of\ failures\ at\ any\ time}{Total\ number\ of\ simulations\ at\ that\ time} \qquad 7.1$$

$$= failure\ probability\ in\ a\ year\ given\ existence\ of\ ship\ at\ year\ 0$$

$$pf_2 = \frac{pf_1}{1 - (cumulative\ failure\ probability\ up\ to\ that\ time)} \qquad 7.2$$

$$= failure\ probability\ in\ a\ year\ given\ existence\ of\ ship\ at\ beginning\ of\ that\ year$$

As a more useful measure of the failure probability of the system pf_2, will be the failure probability discussed thereafter in this thesis, unless specific reference is made to pf_1. The difference between these two can be seen in Figure 7.13.

In case inspection is carried out, cracks are detected according to a probability of detection curve (POD), as described in 6.4. When a crack is detected it is

automatically repaired. However, there is always the probability that new cracks are initiated at the repairs, therefore any crack that is repaired takes a value again from the initial distribution of crack sizes used to initialise the analysis.

Monte Carlo simulation offers flexibility and copes very well with the complications of the analysis as we have discussed. There are however, some problems associated with the method. One obvious problem is the time required to run the analysis, since for every crack location a separate simulation must be run, and the problem arises when there is the need to investigate a real ship case where perhaps thousands of cracks are present. The other major problem is associated with the memory it needs to run, and again with increasing number of members the need for memory increases. Finally, for very low probabilities of failure (less than 10^{-4}) the amount of simulations needed, (see section 2.4), for an accurate estimate of the probability of failure is prohibitive for a PC.

Therefore a simpler approach is required in order to tackle a real ship. In section 7.7, a method is discussed which uses results from the Monte Carlo simulation, and then by the use of statistics offers a very simple, flexible and quick way to estimate the probability of failure of the system.

Because of the limitations of the Monte Carlo simulation, the maximum number of members in the system that can be examined at the same time is about 100. This allows the performance of reliability calculations only for a small section of the ship. However, these results can be used to verify results of a method used later to calculate the reliability of the whole ship.

7.7 Reliability Calculations Using the Convolution Integral Method

This section considers an approximate method for the analysis of a complete ship. In section 2.2 the basic problem in structural reliability is discussed. Namely, in the most simple case, when the load applied exceeds the strength offered by the structure, the structure fails. In a probabilistic treatment of the above problem, it is necessary to

consider all possible values that the load and the strength can take, and then calculate the probability of failure, using equation 2.8. It may usually be assumed that load and resistance are both statistically independent. This simple case is illustrated in Figure 7.14.

When we want to generalise the above method, it is necessary to consider system effects. Namely, each member will be subjected to a load distribution, and has its own strength distribution. First, the load and strength distributions for each member must be defined, and second a way must be found to combine the individual distributions of all the members into one overall distribution for the system. Instead of having for example as many distributions for load and strength as the members of the system, a single distribution for the load and the strength should be found for the whole system.

7.7.1 *The Load Distribution*

The load that causes failure is the extreme load applied and in particular the extreme wave loading, defined in section 3.6. For each member, the extreme load has exactly the same distribution i.e. the extreme type I, but with different parameters (mean value and standard deviation). However, if we normalise the distribution by its mean value, then the normalised load distribution will be similar for every member in the system, and will also equal the load distribution for the whole system, assuming the loading is fully correlated. For example, Figure 7.15 shows load distributions for two different locations, one at the deck and one at the keel. The actual distributions have the same shape since both follow the extreme type I, but because extreme load is not the same at these two locations they have different parameters (mean value and standard deviation). The normalised load distributions (normalised by the mean of the distribution), however, are very closely matched. The same approximation is made for all the members of the system, therefore the overall load distribution of the system will have the same normalised distribution as any member does.

7.7.2 *The Strength Distribution*

The strength distribution is related to the limit state function. Load and strength should have the same units before the convolution integral can be used. It is therefore

necessary to re-arrange the limit state function and relate it to the normalised wave load. At this point it is important to note that the limit state used in this thesis involves two failure modes; brittle fracture and plastic collapse.

The strength distribution for plastic collapse is calculated from the plastic collapse ratio S_r, defined in Equation 4.37. Failure for plastic collapse is defined when $S_r \geq 1$. This is conveniently written in terms of the resistance to extreme wave load

$$\frac{\sigma_n}{\sigma_f} \leq 1 \quad \text{or} \quad \sigma_f - \sigma_n \leq 0, \Rightarrow \sigma_f - \sigma_{still,water} - \sigma_{extreme,wav} \qquad 7.3$$

$$\sigma_{extreme,wave} = \sigma_f - \sigma_{still,water} \qquad 7.4$$

Equation 7.4 gives the plastic strength to extreme wave loading, reduced to account for the still water bending stress.

The strength to brittle fracture is deduced from the fracture ratio K_r, given in 4.49. Again, we need to solve this expression for the extreme wave loading.

$$K_r = \frac{K_{Total}}{K_{mat}} + \rho \qquad 7.5$$

This is also written in terms of the resistance to extreme wave load

$$(K_r - \rho) \cdot K_{mat} - (K_{res} + K_{swBM} + K_{extreme}) = 0 \qquad 7.6$$

is solved for extreme stress amplitude

$$\sigma_{extreme} = \frac{(K_r - \rho) \cdot K_{mat} - (K_{res} + K_{swBM})}{Y\sqrt{\pi a}} \qquad 7.7$$

which calculates the strength distribution for brittle fracture, and accounts the reductions due to still water bending load and residual stresses.

The distribution of plastic strength changes with time as a result of corrosion, even if extreme loading and still water bending moment remain constant. Brittle strength also changes with time, and in particular reduces with time as crack size increases due to

fatigue. It is possible to combine these two distributions in one, so that a total strength distribution is calculated. The strength distribution also needs to be normalised with the mean value of the load distribution at the same location, before using the convolution integral so that the units are consistent.

Both load and strength distributions are determined using the Monte Carlo simulation code. Figure 7.16 shows the total strength distribution at various times, with the plastic strength component being the peak distribution at the left and the brittle strength distribution being the one with the larger spread. However, as cracks propagate with time the fracture strength distribution moves to the left i.e. reducing but the plastic strength remains the same (assuming extreme load and still water bending moment do not change). From results in later sections we can say that, initially there is a probability of failure due to plastic collapse which remains the same every year, but there is little contribution from fractures. As time passes, the fracture strength reduces due to fatigue degradation, and it contributes more and more to the failure probability.

7.7.3 *Determination of Strength Distribution for the Ship System*

As discussed in 7.6.1 the ship system is assumed as a series system. There are two cases to be considered now. When the strength distribution between the members is independent and when the strength distribution has some degree of correlation. Plastic strength does depend on still water bending moment which can be correlated. Brittle strength depends on crack size, which depends on fatigue load, and fatigue load can be correlated. In both cases, the total strength distribution can be estimated using extreme statistics. However, only when strengths are independent the method is exact.

If we assume that the strength distribution for a single member is the parent distribution, then the combined strength distribution for the first member failure would follow the extreme smallest value distribution. This is because in our definition of failure of the system, the earliest failures are important, which are caused by the tail end of the smallest strength values in the strength distribution. As the number of highly loaded members increase so does the probability of the smallest values in the total strength distribution. (Note members that are lightly loaded will have a small

probability of failure and will not have a significant effect on the overall probability of structural system failure). In Figure 7.17, we see the strength distributions determined from Monte Carlo simulation for a single member, for a system with 5 members and for a system with 15 members, all at the same time. Clearly, as the number of members increases, the strength distribution moves towards the left hand side, i.e. towards the tail of the smallest values of the parent distribution.

The probability that a value, A, will be exceeded by a sample, x_1, of the distribution is

$$P(x_1 > A) = 1 - Q(A) \qquad 7.8$$

where Q(x) is the cumulative distribution function of the distribution of the value.

The probability that value A will be exceeded by another sample, x_2, is

$$P(x_2 > A) = 1 - Q(A) \qquad 7.9$$

The probability that, A, will be exceeded by both x_1 and x_2 is

$$P(x_1 > A) \cdot P(x_2 > A) = [1 - Q(A)] \cdot [1 - Q(A)] \qquad 7.10$$

if x_1 and x_2 are statistically independent. The distribution function of A, will then be

$$P(x > A, in \text{ k samples}) = 1 - [1 - Q(A)]^k \qquad 7.11$$

Equations 7.10 and 7.11 are used to calculate the total strength distribution for the ship and are exact only when strengths are independent, and represent the extreme smallest value distribution of the strength.

Figure 7.19, shows the parent strength distribution (i.e. for one member) and the extreme value distribution (which represents the total strength distribution of the system) for $k = 10$. In the figure two extreme distributions are shown, the actual as determined from the Monte Carlo simulation (with 10 members in the system) and the one calculated from equation 7.11. The system is independent, and the actual and calculated distributions agree well.

In Figure 7.20 the parent distribution is shown and the extreme value distributions as calculated from Monte Carlo simulation and using equation 7.11. In this case loading was assumed correlated, therefore the strength distributions of the members possess some degree of correlation, hence equation 7.11 will not calculate exactly the extreme strength distribution. The actual distribution has a small shift to the right, therefore using the calculated distribution of strength will produce slightly conservative results. The effect is examined better in the next section with some example cases.

If the parent distributions could be fitted to an analytical distribution (e.g. to a Gaussian) then the extreme value distribution could be found and integrated in the convolution integral using analytical methods. For example in Figure 7.20, at T = 0, the strength distribution resembles the normal distribution. In Figure 7.21 we can see that the parent distribution fits a normal distribution although the actual is a little bit shifted to the right. However, the actual extreme and the extreme of a normal as a parent, seen in the same figure, do not fit very well. And it is particular important that the tail end of the smallest values is very well fitted, before it can be used to calculate the convolution integral, since it is this part of the distribution that contributes to the failure probability.

In Figure 7.20 we also see the parent strength distribution as it changes with time. Although the initial distribution resembles the normal distribution, at later stages, the distribution is very difficult to describe. For this reason, it is chosen in this thesis to work with the actual numerical distributions as determined from the simulation. The extreme value distributions are then obtained using equation 7.11, and we can see from Figure 7.22, that a very good agreement is achieved between the actual extreme (from the simulation) and the calculated one using the actual numerical parent distribution and equation 7.11, assuming the system is independent. The corresponding extreme value distribution of a normal parent distribution, is not a good fit to the actual distribution.

7.7.4 *A Hybrid Method to Calculate the Failure Probability of the Ship*

In the this section an example follows, which is used to validate results from the convolution integral method, when compared with results from the Monte Carlo simulation. It was discussed earlier that Monte Carlo simulation can be used to perform system reliability analysis, but it has limitations on the number of crack sites that can be assumed and it needs a lot of computational time. Using the theory of extreme statistics, and the convolution integral a simple approach to estimate the failure probability of the ship can be formed.

Monte Carlo simulation is used to obtain the parent strength distribution for a single crack site. Cracks can be in different locations in the ship, and their strength distribution depends on loading and material properties which are likely to change between different locations. Therefore each crack location has its own strength distribution, which is estimated by the Monte Carlo simulation. The strength distribution needs also to be estimated with time since it reduces as cracks grow. Hence, a databank of strength distributions can be established for various locations along the ship, and different crack geometries.

To estimate the total strength distribution for the system, extreme statistics are used, and in particular the theory described in the previous section. Therefore, for a cluster of cracks at the same locations, subjected to the same loading and having identical material properties, equation 7.11 can be used to determine the strength distribution, since all cracks will have exactly the same parent strength distribution.

However, when cracks or cluster of cracks are in different locations, they will not have the same strength distribution as a parent. In this case the general form of equation 7.11 must be used, which is equation 7.10 (for as many member the system has).

The calculation of the total strength distribution is illustrated in Figure 7.23. This method of combining the individual strength distributions and calculating the strength distribution for the system is valid when the strength distributions are independent.

When we introduce correlation in loading, this affects also the strength distributions and they are no longer independent. This effect is studied in the next section with an example case, to examine the error if there is a correlation in strengths.

The load distributions for each location are as well calculated from the Monte Carlo simulation. Because, the loading distribution comes from the extreme wave loading distribution, it has the same form for every location, although the parameters of the distribution change (since loading is location dependent). After normalising the distributions with their corresponding mean values, the normalised distributions are the same for every location as was illustrated in section 7.7.1, therefore the total load distribution for the system will also be the same. Since, loading is assumed constant with time, the distribution will not change with time.

Because load distribution is normalised by its mean value, in order to use the convolution integral, the strength distributions are also normalised, using the mean value of the loading distribution.

An efficient method of calculating the failure probability of a system with many members is established using simulation methods and theory of extreme statistics. Simulation is used to obtain the individual parent strength distributions for every location considered in the ship, and extreme statistics to obtain the total strength distribution of the system. The convolution integral can then be solved to calculate the probability of failure of the system. The method is time efficient since requires only the parent distributions for different locations, and then use the statistics of extremes to account for the large number of members. In the case of a ship structure containing cracks, each crack is considered a member and there can be thousands of cracks in a ship. The above method is capable of dealing with the large number of cracks, whereas if only simulation was used, there would be limitations.

7.8 Comparison between Monte Carlo and Convolution Integral Results

The convolution integral method is used to estimate the integral given in equation 2.8. Even when both distributions are known analytically, the integral is difficult to solve in a closed form. An additional reason for not solving the integral analytically is because the load and strength distributions are defined numerically. The only option available to solve the integral is to use numerical integration. When the interval for numerical integration is small, even simple techniques produce accurate results. Melchers 1999, reports that an integration interval of 0.2 σ provides good accuracy even using the trapezoidal rule, with an integration range of $\pm 5\sigma$.

In this example a ship section is considered, with three different crack locations, and each location containing 10 cracks. The crack locations are shown Figure 7.24 .Two cases are considered: *a)* when loading is independent, and *b)* when loading is fully correlated (positively). The results are shown in Table 7.4.

When the failure probabilities are relatively large, the results from the Monte Carlo simulation and the convolution integral have a significant difference for the load correlated system, as we can see from Table 7.4 (e.g. from T = 24 and beyond), which indicates that as failure probabilities increase, correlation effects are important. For an independent system though good agreement is achieved, between the two methods as a result of the assumption made i.e. assuming that strengths are independent. However, the difference is large for large values of failure probabilities (approx. $Pf > 10^{-1}$), which in this case are possible because inspections are not performed.

However, when the probabilities of failure are low, as in the case where inspection is carried out (in this case every 5 years), the results from the convolution integral are much closer to the Monte Carlo simulation even for a correlated system, as we can see from Table 7.5. The results are also shown in Figure 7.26. Where there is a difference is probably because of the random variation of the Monte Carlo results due to limited samples used, (in this case 100,000) where for accurate estimate for low probabilities of failure much more simulations are needed.

It is then possible to use the convolution integral method, to calculate the failure probability of a system even when correlation effects are present, and at low failure probabilities the results will compare well with the actual values (but unfortunately it is impossible to use Monte Carlo to check the results for an actual ship case). The results will only have a significant difference, when the failure probabilities are very large, in the range of 10^{-1} and higher.

7.9 Case Study – Application of Methodology to a Real Bulk Carrier

An example case now follows, which puts together every part of the analysis, and the probability of a bulk carrier failing because of fracture is calculated.

A bulk carrier was selected for this analysis, and was used throughout this report to determine all the necessary input. A table of the main characteristics of the vessel is given in Table A.4 in appendix A.

Before the analysis is run, certain simplifications and assumptions must be made. These regard the

- Geometric definition of the ship
- Loading distribution along the vessel
- Distribution of cracks in the structure
- Inspection quality
- Local environment

7.9.1 *Defining the Vessel Geometry*

A typical bulk carrier is shown in Figure 7.27. Cracks are likely to be present in every welded connection along the structure. However, only the cracks that are subjected to large loads will cause failure. The section of the ship that is subjected to large loads is the main part of the hull structure that contains the cargo holds. The bow and the stern

section are subjected to relatively low global stresses. Therefore, only the main part of the hull is considered in the analysis.

Every location along the hull has its own loading characteristics (wave loading, still water loading) and material properties (steel thickness, section modulus), and hence its own strength capacity. However, considering every location along the ship would require a different load and stress analysis. For this reason, the vessel is split into sections and within each section the loading and strength characteristics are assumed constant. For this analysis each section contains one cargo hold, i.e. there are seven sections in total, the length of each section therefore is about 27 m. This means that load and strength characteristics remain constant for every 27 m of the structure. Note however, within each section loading is also fully correlated whereas strengths are independent. This is only a simplification used in this thesis, but for calculations that are more exact, many more sections can be used if loading is known exactly.

7.9.2 *Loading Definition along the Vessel*

Loading varies with position, and in this case study loading varies with section. There are three types of loading which must be defined. Wave global loading, wave pressure loading and still water bending moment.

- Wave loading is assumed to vary sinusoidally along the length of the ship, with the maximum value at the mid point, as shown in Figure 7.22. For the main part of the structure considered, the section can be assumed to remain constant, therefore the section modulus also. Hence, any variation in global stress arises from the wave loading only. Global wave loading (i.e. stress ranges and extreme stress amplitudes) have been calculated for the midship section, an analysis presented in appendix A. For other sections, values are scaled according to the wave distribution.

- Wave pressure at the side of the vessel, is assumed to be constant. This assumption is probably conservative, since wave pressure is high at the fore part of the ship i.e. ship usually turns into the weather, which results in increased pressure at the fore) as shown in Figure 7.22, taken from Barltrop

(1998). However, during the response analysis, pressure was calculated accounting for equal probability for each wave heading and averaging over all the wave headings. Therefore, a constant pressure profile is assumed for this case study.

- Still water bending moment is very difficult to describe, because its variation depends on the cargo distribution. Nevertheless, when we consider the distribution of still water bending moment over a large period (i.e. one year), we can assume it varies linearly as shown in Figure 7.22. This is a rough assumption, which is only made to demonstrate results from this case study. A better approximation would be to use information from the vessel's trading conditions and bending moment distributions given in the trim and stability booklet.

The cracks will also be subjected to residual stresses because of the weld. The effect of residual stresses on crack growth was discussed in 4.11. Tensile residual stresses equal to yield stress are assumed to act over the weld, with compressive residual stresses of lower magnitude over the rest of the section. If the crack lies within the tensile residual stress zone, then the whole stress range is assumed to be tensile. When the crack enters the compressive residual stress zone some reduction in the stress intensity occurs. The initial residual stresses are allowed to 'shake down' with time, which decreases their magnitude, as discussed in section 3.8.2.

7.9.3 *Crack Type, Location, and Number*

Cracks can initiate at various locations in the structure. However, most cracks are initiated at welded connections and begin as surface cracks which first grow through the thickness of the material (therefore stress intensity factors for surface cracks are initially used in the crack growth analysis), and then become through thickness cracks and are considered as centre cracks in a finite plate (i.e. the stress intensity factor for a centre crack in a plate is now used). The surface crack is assumed to be of elliptical form, and the crack depth to crack length ratio for the surface crack is assumed 0.5, i.e. the crack grows at the surface twice as it grows in depth.

Another type of crack that can be used is a crack that initiates at locations with high stress concentrations, e.g. cracks at the hatch openings. These cracks however, may be highly visible and in this thesis it is assumed they are repaired before they grow to a critical size.

Three different locations have been considered for this analysis

- Deck structure, where cracks initiate from longitudinal stiffeners and then grow under the action of global bending stresses, (vertical and horizontal), and this detail is shown in Figure A.2, (Detail 7), in appendix A.

- Side structure, where cracks grow mainly because of the local wave pressure forces. There are two critical crack configurations as shown in Figure A.2. Detail 5, a crack growing parallel to the welding connection between the frame and the hopper tank plating, and results in detaching the frame from the hopper tank and then from the side structure. However, this type of crack is a result of bad detail design, and new designs have been developed to avoid this problem, although it may still be a problem for the existing ships. The other crack configuration, grows first through the thickness of the side shell plating, and then propagates along the side of the vessel. This crack is assumed in the following analysis

- Keel structure, where cracks here grow from bottom longitudinal stiffeners across the bottom structure. Global stresses here are lower than the deck structure, because of the neutral axis position which is closer at the keel, however, local pressure and acceleration loads due to liquid cargo do contribute to the crack growth. The location considered is the Detail 2 shown in Figure A.2.

For cracks in other positions in the deck and keel, loading will be different. For this analysis the cracks chosen are subjected to the maximum global loading, (vertical bending does not change very much since the difference in the vertical position is small, but horizontal bending varies with the transverse coordinate), because horizontal bending stresses are largest at the location furthest from the centreline. For

other cracks on the deck or at the keel the same loading has been used, which is a conservative assumption.

7.9.3.1 Estimation of Number of Cracks in the Ship Structure

A rough estimation of the number of crack sizes is needed, to calculate the failure probability of the ship. We have to refer to a study by Bokalrud and Karlsen (1981) (referenced in chapter 6), where they have measured cracks from actual production welds of a shipyard. In their paper it is stated that a total of 327 cracks were found out of 3,200 m of butt welds. This approximately rounds to one crack every 10 meters of weld.

An approximate estimation of the meters of weld leads to the following estimation:

The length of each section is 27 m. The longitudinal stiffener spacing is 0.8 m, taken from the ship's midship section drawings. The effective length at the deck is about 16 m accounting for the breadth of the hatch openings. For the side structure, the height between the hopper tank and the wing tank (i.e. the length of the weld of the frame to the side structure) is about 5 m. The breadth at the keel is 32.2 m. Welds in meters, for each location, is then equal to

Keel : $32.2 \div 0.8 \times 27 \approx 1087$ m of weld i.e. approx. 109 cracks

Deck : $16 \div 0.8 \times 27 \approx 540$ m of weld i.e. approx. 54 cracks

Side : $27 \div 0.8 \times 5 \times 2$ (two sides) ≈ 340 m of weld i.e. approx. 34 cracks

Total 197 cracks in each section.

The total number of cracks in the ship is then

$N_{cracks} = 197 \times 7 = 1379$ cracks

There may actually be many more cracks in the ship, but the above estimation was based on the distribution of the smallest detectable cracks, which accounts only for the cracks that were found, and not for the very small cracks that escaped detection.

7.9.4 *Inspection Quality*

When performing inspection, in the probability of detecting a crack, among other factors discussed in 1.6.3, location plays an important role. In this case study, the same probability of detection curve is used everywhere, but it is also possible to use different ones for different locations.

7.9.5 *Local Environment*

The local environment in a bulk carrier changes, mainly due to the cargo that occupies the space where the cracks are. Local environment, mainly affects, in this analysis, the crack propagation constants. For example, cracks at the deck structure are subjected to very little corrosion, therefore the material constants do not account for corrosion, at the side shell and keel though corrosion is more significant, and as a result, cracks grow faster. The material constants used for cracks at the side shell and keel structure need to account for corrosion.

7.9.6 *Results from the Analysis*

The table of the input parameters is shown in Table C.1. First Monte Carlo simulation is used to determine the strength and load distributions for each location and at every section, for only one crack at each point. The analysis was run for a period of 40 years, with time interval of 1 year. Inspection (and repair) occurred every 3 years, but in one case annual inspections were also carried out and cracks were repaired if they were exceeding a specified value.

The simulation was run using a sample size of 500,000. Material properties, (fracture toughness, yield stress, crack growth constant C), were sampled for each location from the same distribution having the same mean value and standard deviation, assuming a correlation in their mean value. This means that for all the ship, material properties are sampled from the same distribution. Material properties are also sampled once in a lifetime, i.e. at the initial time ($T = 0$) and were kept the same throughout the time because material properties do not change with time, and it is not

correct to resample them every year. Material properties are also assumed statistically independent.

The results from the Monte Carlo runs are given in appendix C, in Tables C.1 to C.4, for each section of the ship and for two different cases: *a)*when inspection is occurring only every three years, *b)*when inspection occurs every three years, and also additional annual inspection which repairs cracks that are larger than 200 mm, with a probability of detection of 50%.

In the results, we can see the annual failure probability and its coefficient of variation for each crack location individually, the mean value and standard deviation of the crack size distribution of each location, the type and number of failure (i.e. plastic or brittle), the sample size left at each time interval, and the number of cracks repaired. From this information we can see, which location contributes more to the failures, what type of failure occurs, and how fast the cracks grow. The system annual failure probability and cumulative failure probabilities are also given below the information for each member.

The strength and load distributions are stored in different files, which are used by the convolution integral method. A separate code is used to solve the convolution integral. The input to this code is the number of sections along the ship, the number of different crack locations in each section, and the number of cracks at each location.

Results can be presented separately for each section, to see the contribution to the ship failure probability of each section, and within each section the contribution of each location.

The following results were obtained for the first case, (i.e. inspecting only every three years), assuming the number of cracks for each location as they were estimated in section 7.9.3.1. In Figure 7.28 we see the failure probability of sections 1 to 4 (5 to 7 are identical to 1 to 3, because of similarity in loading). In the first two sections the contribution from the side shell cracks is the main contributor to the total failure probability, because pressure was assumed constant throughout the sections, but global loading is reducing towards the fore and aft sections. As we move towards the

midships, deck and keel structure contribute more to the failure probability. In section 4 for example, which is in the middle of the ship, cracks at keel contribute the most (mainly because of the assumption made here for the number of cracks at the keel, which is much larger than the deck and side). The numerical results are presented in Table 7.6.

The total failure probability can be seen in Figure 7.29 and the failure probability values in Table 7.7. There is a small difference between the two cases, and in particular in case *b* where repairing is done every year, the failure probability of the ship can be kept constant with time, (e.g. it does not exceed the 10^{-2} failure probability), whereas with inspection occurring only every three years, the failure probability curve is always increasing. The second case may be more realistic, since classification societies have a scheme for annual inspections, and although not complete any large cracks found will be repaired.

It is clear from the graph in Figure 7.29 that the failure probability of the vessel until about year 15 is very low, and inspections do not have any effect on the failure probability. But as fatigue cracks grow larger, it is then necessary to perform inspections to maintain the failure probability to low levels (below 10^{-2}). The results obtained in this example, represent the estimate of the failure probability of the vessel (a bulk carrier) for the loading and material properties specified, which again represent the most realistic guesses for the various parameters. It is very difficult to verify the results with another method.

Some indication of whether these results are reasonable or not, is obtained by comparison with the statistical analysis for the losses of bulk carriers which is the subject of the next chapter. Note however that the data used for the above analysis is somewhat simplified so the comparison cannot be regarded as a verification.

References

- R.E. Melchers, 'Structural reliability analysis and prediction', second edition, John Wiley & sons, 1999

- N. D. P. Barltrop, 'Floating structures, a guide for design and analysis', BMP/OPL, 1998

- Ang A. H. S., Tang W. H., 'Probability concepts in engineering planning and design', Vol. 2, John Wiley, 1984

```
*CONTROL PARAMETERS
  GROUPS   NJOINT     NVAR  NSAMPLE
     3       1        12    500000
*INFORMATION OF JOINT (ID: 1, STIF.PLATE; 2, HATCH; 3, CENTER; 4, EDGE; 5, SEMI-ELLIPTICAL SURFACE )
*                6, SEMI-ELLIPTICAL SURFACE NEAR WELD, 7, SEMI-ELLIPTICAL AT T-JOINT)
*                8, CONSTANT TO BE GIVEN AS INPUT )
 GROUP NO      ID    THICKNESS       WIDTH       VERTICAL POSITION
     1         7       25.0          5000.0      17384.0
     2         7       25.0          5000.0       2460.0
     3         7       25.0          5000.0       7250.0
*IDENTIFICATION OF BASIC VARIABLES ID: ( 0, CONSTANT; 1, LOGNORMAL; 2, NORMAL; 3, WEIBULL
*                        4, EXTREME TYPE I; 5, EXPONENTIAL )
 ICOR: ( 0, FULLY CORRELATED; 1, INDEPENDENT )
*              SAMPLING FACTOR: ( 0, SAMPLE ONCE; 1, SAMPLE EVERY YEAR )
     NO.      ID      ICOR                          SAMPLING FACTOR
      1       1       1                             0
      2       3       1                             0
      3       5       1                             0
      4       1       0                             1
      5       2       0                             1
      6       2       0                             1
      7       2       0                             1
      8       2       0                             1
      9       1       1     0
     10       0       1     0
     11       2       0     1
     12       0       1     0
*MEAN VALUE OF BASIC VARIABLES
* 1: PARIS' C, 2: FRACTURE TOUGHNESS, 3: INITIAL CRACK SIZE, 4: STRESS CYCLES, 5: WEIBULL SHAPE PAR (DS)
* 6: WEIBULL SCALE PAR (DS) 7: WEIBULL SHAPE PAR (AMPL) 8: WEIBULL SCALE PAR (AMPL) 9: YIELD STRESS 10: ULTIMATE STRESS
* 11: STILL WATER B.M. 12: SECOND MOMENT OF AREA ABOUT N.A.
* FOR WEIBULL DISTR, MEAN: SCALE PAR, ST.DEV: SHAPE PAR, FOR EXPONENTIAL MEAN: FACTOR
GROUP     C      KMAT              AN      CN      B      A      B1  A1          SY          ST      BM      Iyy
1  1.481E-14   273.0     9.0 2887611.0   0.842   9.96   0.858   5.32  345.0   420.0  861652.0  1.884E14
2  5.020E-14   273.0     9.0 2879928.0   0.858   7.56   0.825   3.61  345.0   420.0  861652.0  1.884E14
3  5.020E-14   273.0     9.0 3071540.0   0.921   8.36   0.800   2.98  345.0   420.0  861652.0  1.884E14
*STANDARD DEVIATION OF VARIABLES
1  4.443E-15   6.   0.02     0.5    17.0     0.0  107706.5     0.0
2  1.506E-14   6.   0.02     0.5    17.0     0.0  107706.5     0.0
3  1.506E-14   6.   0.02     0.5    17.0     0.0  107706.5     0.0
*NUMBER OF YEARS, INSP.INTERVAL, CRACK SIZE AFTER INSPECTION, ST. DEV,  INSP. QUALITY
 40,          3,          9.0,                          50
*PARIS EXPONENT M, STRESS INTENSITY THRESHOLD (MPA-M*0.5), CORROSION RATE
 3.3,         2.5,                        0.25
*RESIDUAL STRESS FACTOR (0: NO EFFECT, 1: NO SHAKE DOWN, 2: WITH SHAKE DOWN)
                2
*CRACK DEPTH TO CRACK LENGTH RATIO (a/c) FOR SURFACE CRACKS (should be less or equal to 1)
              0.5
* POSITION OF NEUTRAL AXIS FROM KEEL
             7506
* SCALING FACTORS FOR LOADING (STILL WATER B.M.; WAVE B.M.; WAVE PRESSURE)
0.25, 0.38, 1.0
* ENABLE ANNUAL INSPECTION AND REPAIR OF CRACKS BIGGER THAN A CRITICAL SIZE
 ACCORDING TO A PROBABILITY OF DETECTION
 ENABLE : AI = 1, DISABLE: AI = 0 ; CRIT_CRK : CRACK SIZE ; POD : ANNUAL CRACK DETECTION PROBABILITY
   AI        CRIT_CRK        POD
    1,         500.,         0.6
```

Table 7.1 - *Typical input file for the Monte Carlo code*

Description	Variable	Distribution	Mean Value	Cov %	Units
Initial crack size	a_o	Exponential	0.11	100%	mm
Paris' constant	C	Lognormal	1.48E-14	20%	-
Paris' constant	m	Constant	3.3		-
Fracture toughness	K_{mat}	Weibull	sc(273), sh(6.711)	-	Mpa $m^{0.5}$
Material thickness	t	Constant	25		mm
Weibull scale ($\delta\sigma$)	A	Normal	9.96	10%	-
Weibull shape ($\delta\sigma$)	B	Normal	0.842	5%	-
Weibull scale (am)	α	Normal	5.32	10%	-
Weibull shape (am)	β	Normal	0.858	5%	-
Stress cycles	N	Lognormal	9884938	20%	cycles
Stress threshold	ΔK_{th}	Constant	2.5		Mpa $m^{0.5}$
Corrosion rate	K_{cor}	Constant	0.25		mm/year
Still water bending mnt	M_{still}	Normal	1077065	25%	KN m

Table 7.2 – *Input data for single crack problem*

Year/Members	Independent			Correlated
	1	10	10	10
	MC	MC	From 2.[]	MC
0	1.00E-05	0.00E+00	1.00E-04	1.00E-05
1	0.00E+00	2.00E-05	0.00E+00	0.00E+00
2	0.00E+00	1.00E-05	0.00E+00	0.00E+00
3	1.00E-05	1.00E-05	1.00E-04	2.00E-05
4	0.00E+00	0.00E+00	0.00E+00	0.00E+00
5	0.00E+00	2.00E-05	0.00E+00	0.00E+00
6	0.00E+00	1.00E-05	0.00E+00	1.00E-05
7	0.00E+00	0.00E+00	0.00E+00	1.00E-05
8	0.00E+00	1.00E-05	0.00E+00	2.00E-05
9	0.00E+00	1.00E-05	0.00E+00	3.00E-05
10	0.00E+00	0.00E+00	0.00E+00	0.00E+00
11	0.00E+00	1.00E-05	0.00E+00	1.00E-05
12	1.00E-05	1.00E-05	1.00E-04	3.00E-05
13	0.00E+00	1.10E-04	0.00E+00	3.00E-05
14	5.00E-05	2.10E-04	5.00E-04	2.30E-04
15	4.00E-05	4.20E-04	4.00E-04	4.30E-04
16	1.30E-04	9.71E-04	1.30E-03	7.71E-04
17	1.90E-04	1.81E-03	1.90E-03	1.63E-03
18	3.00E-04	3.04E-03	3.00E-03	2.94E-03
19	5.30E-04	5.86E-03	5.29E-03	4.91E-03
20	8.11E-04	8.63E-03	8.08E-03	8.50E-03
21	1.34E-03	1.28E-02	1.33E-02	1.27E-02
22	1.85E-03	1.80E-02	1.83E-02	1.84E-02
23	2.44E-03	2.53E-02	2.42E-02	2.53E-02
24	3.48E-03	3.33E-02	3.42E-02	3.14E-02
25	4.48E-03	4.43E-02	4.39E-02	4.39E-02
26	6.07E-03	5.49E-02	5.91E-02	5.41E-02
27	7.46E-03	7.09E-02	7.22E-02	6.83E-02
28	9.24E-03	8.66E-02	8.86E-02	8.40E-02
29	1.06E-02	1.03E-01	1.01E-01	1.00E-01
30	1.26E-02	1.20E-01	1.19E-01	1.12E-01
31	1.50E-02	1.38E-01	1.40E-01	1.29E-01
32	1.61E-02	1.57E-01	1.50E-01	1.52E-01
33	1.90E-02	1.76E-01	1.75E-01	1.72E-01
34	2.16E-02	1.95E-01	1.96E-01	1.97E-01
35	2.39E-02	2.19E-01	2.15E-01	2.17E-01
36	2.63E-02	2.37E-01	2.34E-01	2.31E-01
37	2.94E-02	2.55E-01	2.58E-01	2.46E-01
38	3.13E-02	2.75E-01	2.73E-01	2.68E-01
39	3.32E-02	2.95E-01	2.86E-01	2.78E-01
40	3.57E-02	3.08E-01	3.05E-01	3.01E-01

First and second columns are results from Monte Carlo sim for one and 10 cracks (independent system) respectively. Third column results from convolution integral. Last column results for a correlated (in loading) system. Correlated system has lower failure probability as expected. Convolution integral results agree well for an independent system

Table 7.3 – *Comparison between an independent and a correlated system*

Locations:	3	3	3	3
Cracks in each location:	10	10	10	10
System:	independent	correlated	independent	correlated
Results from:	Mc	Mc	Ci	Ci
Time (Years)				
0	1.00E-05	2.00E-05	0.00E+00	0.00E+00
1	1.00E-05	0.00E+00	0.00E+00	0.00E+00
2	0.00E+00	0.00E+00	0.00E+00	0.00E+00
3	0.00E+00	0.00E+00	0.00E+00	0.00E+00
4	1.00E-05	0.00E+00	2.01E-09	0.00E+00
5	0.00E+00	0.00E+00	2.01E-09	0.00E+00
6	0.00E+00	0.00E+00	1.30E-08	0.00E+00
7	0.00E+00	0.00E+00	1.10E-07	0.00E+00
8	0.00E+00	0.00E+00	2.65E-07	1.00E-09
9	1.00E-05	0.00E+00	2.73E-07	2.31E-06
10	1.00E-05	0.00E+00	2.32E-06	1.00E-04
11	1.00E-05	1.00E-05	6.95E-05	9.44E-05
12	6.00E-05	3.00E-05	1.06E-04	1.00E-04
13	1.70E-04	8.00E-05	2.43E-04	2.41E-04
14	4.40E-04	3.30E-04	4.12E-04	3.51E-04
15	9.21E-04	6.30E-04	9.01E-04	1.10E-03
16	2.77E-03	1.59E-03	2.35E-03	2.18E-03
17	5.16E-03	3.57E-03	3.80E-03	5.28E-03
18	9.89E-03	6.26E-03	9.18E-03	8.94E-03
19	1.94E-02	1.12E-02	1.73E-02	1.73E-02
20	3.29E-02	2.03E-02	2.92E-02	3.02E-02
21	5.40E-02	3.12E-02	4.89E-02	4.74E-02
22	8.21E-02	4.97E-02	7.68E-02	7.63E-02
23	1.20E-01	7.05E-02	1.12E-01	1.08E-01
24	1.73E-01	9.75E-02	1.57E-01	1.56E-01
25	2.26E-01	1.30E-01	2.16E-01	2.20E-01
26	2.99E-01	1.69E-01	2.83E-01	2.73E-01
27	3.71E-01	2.07E-01	3.49E-01	3.50E-01
28	4.52E-01	2.54E-01	4.20E-01	4.24E-01
29	5.26E-01	3.01E-01	4.97E-01	4.96E-01
30	6.08E-01	3.45E-01	5.81E-01	5.79E-01
31	6.73E-01	4.06E-01	6.45E-01	6.49E-01
32	7.34E-01	4.48E-01	7.25E-01	7.09E-01
33	8.15E-01	5.01E-01	7.73E-01	7.72E-01
34	8.18E-01	5.36E-01	8.18E-01	8.19E-01
35	8.33E-01	5.82E-01	8.64E-01	8.64E-01
36	0.00E+00	6.36E-01	8.94E-01	8.96E-01
37	0.00E+00	6.83E-01	9.20E-01	9.21E-01
38	0.00E+00	6.79E-01	9.41E-01	9.40E-01
39	0.00E+00	8.24E-01	9.57E-01	9.58E-01
40	0.00E+00	0.00E+00	9.70E-01	9.68E-01

Table 7.4 – *Comparison between MC and CI (no inspection)*

First two columns results from Monte Carlo for independent and correlated (in loading) system. Last two columns results from convolution integral. For an independent system Monte Carlo and convolution integral agree well. For a correlated system there is a significant difference specially at large failure probability values. This is because of the assumption of strengths being independent. This is also the reason why the results from convolution integral are very similar (i.e. between the independent and correlated system)

Locations:	3	3	3	3
Cracks in each location:	10	10	10	10
System:	independent	correlated	independent	correlated
Results from:	Mc	Mc	Ci	Ci
Time (Years)				
Inspection	Yes	Yes	Yes	Yes
0	0.00E+00	1.00E-05	0.00E+00	1.08E-07
1	0.00E+00	0.00E+00	0.00E+00	2.01E-09
2	0.00E+00	0.00E+00	0.00E+00	1.00E-08
3	0.00E+00	0.00E+00	0.00E+00	2.01E-09
4	0.00E+00	0.00E+00	0.00E+00	7.01E-09
5	**0.00E+00**	**0.00E+00**	**0.00E+00**	**2.90E-08**
6	0.00E+00	2.00E-05	0.00E+00	2.90E-08
7	0.00E+00	0.00E+00	0.00E+00	2.63E-07
8	0.00E+00	0.00E+00	0.00E+00	1.50E-06
9	0.00E+00	0.00E+00	1.00E-09	1.50E-06
10	**2.00E-05**	**0.00E+00**	**0.00E+00**	**7.38E-06**
11	0.00E+00	0.00E+00	1.00E-09	2.74E-05
12	1.00E-05	2.00E-05	0.00E+00	0.00E+00
13	2.00E-05	6.00E-05	3.01E-09	6.81E-05
14	1.20E-04	7.00E-05	2.28E-07	6.05E-04
15	**2.00E-05**	**3.00E-05**	**3.61E-08**	**2.01E-09**
16	9.00E-05	6.00E-05	2.36E-04	1.01E-04
17	5.20E-04	6.60E-04	6.54E-04	2.91E-04
18	1.03E-03	1.43E-03	1.05E-03	1.27E-03
19	2.80E-03	3.10E-03	2.81E-03	3.18E-03
20	**1.21E-04**	**1.21E-04**	**9.43E-06**	**6.44E-05**
21	1.20E-03	1.13E-03	1.10E-03	8.41E-04
22	5.54E-03	5.58E-03	5.64E-03	5.27E-03
23	1.19E-02	1.19E-02	1.23E-02	1.20E-02
24	2.01E-02	1.91E-02	1.85E-02	1.86E-02
25	**4.07E-04**	**3.76E-04**	**3.36E-04**	**5.76E-04**
26	4.58E-03	4.21E-03	4.79E-03	3.68E-03
27	2.10E-02	1.88E-02	2.08E-02	1.83E-02
28	4.20E-02	4.07E-02	4.12E-02	3.89E-02
29	6.53E-02	6.23E-02	6.31E-02	5.94E-02
30	**9.46E-04**	**8.08E-04**	**7.56E-04**	**5.37E-04**
31	1.02E-02	8.66E-03	7.13E-03	6.59E-03
32	4.10E-02	4.08E-02	3.92E-02	3.77E-02
33	8.60E-02	8.01E-02	7.62E-02	7.96E-02
34	1.29E-01	1.16E-01	1.23E-01	1.20E-01
35	**1.57E-03**	**1.60E-03**	**9.40E-04**	**6.48E-04**
36	1.32E-02	1.26E-02	9.84E-03	9.73E-03
37	5.96E-02	5.44E-02	5.27E-02	5.14E-02
38	1.23E-01	1.13E-01	1.12E-01	1.08E-01
39	1.82E-01	1.64E-01	1.66E-01	1.72E-01
40	**1.91E-03**	**1.72E-03**	**6.84E-04**	**1.00E-03**

Table 7.5 - *Comparison between MC and CI (with inspection)*

Because of inspection failure probabilities are kept low. In this case good agreement is achieved between the Monte Carlo results and convolution integral for a correlated system (columns 2 and 4 respectively)

Time	Section 1 Total Pf	Deck Pf	Side Pf	Keel Pf	Section 2 Total Pf	Deck Pf	Side Pf	Keel Pf
0	1.09E-08	1.73E-09	1.09E-08	0.00E+00	5.10E-08	8.64E-10	5.10E-08	0.00E+00
1	0.00E+00	0.00E+00	0.00E+00	0.00E+00	2.72E-09	0.00E+00	2.72E-09	0.00E+00
2	0.00E+00	0.00E+00	0.00E+00	0.00E+00	5.96E-09	0.00E+00	5.96E-09	0.00E+00
3	0.00E+00	0.00E+00	0.00E+00	0.00E+00	2.61E-08	0.00E+00	2.61E-08	0.00E+00
4	0.00E+00	0.00E+00	0.00E+00	0.00E+00	3.58E-08	0.00E+00	3.58E-08	0.00E+00
5	5.44E-10	0.00E+00	5.44E-10	0.00E+00	5.10E-08	0.00E+00	5.10E-08	0.00E+00
6	5.44E-10	0.00E+00	5.44E-10	0.00E+00	7.99E-08	0.00E+00	7.99E-08	0.00E+00
7	1.09E-09	0.00E+00	1.09E-09	0.00E+00	1.23E-07	0.00E+00	1.23E-07	0.00E+00
8	1.63E-09	0.00E+00	1.63E-09	0.00E+00	2.93E-07	0.00E+00	2.93E-07	0.00E+00
9	2.17E-09	0.00E+00	2.17E-09	0.00E+00	4.62E-07	0.00E+00	4.62E-07	0.00E+00
10	3.78E-09	0.00E+00	3.78E-09	0.00E+00	7.14E-07	0.00E+00	7.14E-07	0.00E+00
11	4.35E-09	0.00E+00	3.78E-09	0.00E+00	4.13E-06	8.64E-10	4.13E-06	0.00E+00
12	5.96E-09	0.00E+00	5.96E-09	0.00E+00	6.18E-06	8.64E-10	6.18E-06	0.00E+00
13	1.09E-08	0.00E+00	1.09E-08	0.00E+00	1.35E-05	8.64E-10	1.35E-05	0.00E+00
14	1.79E-08	0.00E+00	1.79E-08	0.00E+00	1.95E-05	8.64E-10	1.95E-05	0.00E+00
15	2.55E-08	0.00E+00	2.55E-08	0.00E+00	1.09E-09	8.64E-10	1.09E-09	0.00E+00
16	1.79E-08	0.00E+00	1.79E-08	0.00E+00	1.63E-09	8.64E-10	1.63E-09	0.00E+00
17	1.09E-08	0.00E+00	1.09E-08	0.00E+00	1.35E-05	2.59E-09	1.35E-05	0.00E+00
18	1.79E-08	0.00E+00	1.79E-08	0.00E+00	2.17E-09	1.73E-09	2.17E-09	0.00E+00
19	2.55E-08	0.00E+00	2.55E-08	0.00E+00	1.63E-09	1.73E-09	1.63E-09	0.00E+00
20	3.69E-08	0.00E+00	3.69E-08	0.00E+00	7.17E-07	2.59E-09	7.17E-07	0.00E+00
21	7.99E-08	0.00E+00	7.99E-08	0.00E+00	1.30E-08	2.59E-09	1.30E-08	0.00E+00
22	8.15E-08	0.00E+00	8.15E-08	0.00E+00	2.50E-08	3.45E-09	2.50E-08	0.00E+00
23	2.52E-04	0.00E+00	2.52E-04	0.00E+00	1.45E-04	2.59E-09	1.45E-04	0.00E+00
24	5.52E-07	0.00E+00	5.52E-07	0.00E+00	1.40E-07	6.01E-09	1.40E-07	0.00E+00
25	5.61E-05	0.00E+00	5.61E-05	0.00E+00	1.38E-06	6.01E-09	1.38E-06	0.00E+00
26	2.07E-04	0.00E+00	2.07E-04	0.00E+00	7.72E-05	6.01E-09	7.72E-05	0.00E+00
27	2.18E-06	0.00E+00	2.18E-06	0.00E+00	7.12E-07	9.46E-09	7.12E-07	0.00E+00
28	8.40E-06	0.00E+00	8.40E-06	0.00E+00	8.15E-05	9.46E-09	8.15E-05	0.00E+00
29	3.16E-04	0.00E+00	3.16E-04	0.00E+00	3.02E-04	9.46E-09	3.02E-04	0.00E+00
30	1.46E-05	0.00E+00	1.46E-05	0.00E+00	2.51E-05	2.84E-08	2.51E-05	0.00E+00
31	2.05E-04	0.00E+00	2.05E-04	0.00E+00	3.18E-04	2.84E-08	3.18E-04	0.00E+00
32	9.68E-04	0.00E+00	9.68E-04	0.00E+00	9.30E-04	1.72E-08	9.30E-04	8.18E-08
33	8.47E-05	0.00E+00	8.47E-05	0.00E+00	1.70E-04	4.05E-08	1.70E-04	8.18E-08
34	1.70E-04	0.00E+00	1.70E-04	0.00E+00	1.16E-04	4.05E-08	1.16E-04	1.11E-07
35	1.74E-03	0.00E+00	1.74E-03	0.00E+00	1.40E-03	5.52E-08	1.40E-03	1.58E-07
36	3.62E-04	0.00E+00	3.62E-04	0.00E+00	1.76E-04	4.05E-08	1.76E-04	1.58E-07
37	4.86E-04	0.00E+00	4.86E-04	0.00E+00	2.02E-04	5.52E-08	2.02E-04	1.58E-07
38	1.63E-03	0.00E+00	1.63E-03	0.00E+00	1.28E-03	5.52E-08	1.28E-03	2.58E-07
39	1.78E-04	0.00E+00	1.78E-04	0.00E+00	2.08E-04	1.27E-07	2.08E-04	2.58E-07
40	3.13E-04	0.00E+00	3.13E-04	0.00E+00	3.48E-04	7.85E-08	3.48E-04	3.97E-07

Time	Section 3 Total Pf	Deck Pf	Side Pf	Keel Pf	Section 4 Total Pf	Deck Pf	Side Pf	Keel Pf
0	1.09E-08	0.00E+00	1.09E-08	0.00E+00	5.51E-06	0.00E+00	0.00E+00	5.51E-06
1	5.44E-10	0.00E+00	5.44E-10	0.00E+00	1.11E-07	0.00E+00	0.00E+00	1.11E-07
2	5.44E-10	0.00E+00	5.44E-10	0.00E+00	3.94E-07	0.00E+00	0.00E+00	3.94E-07
3	5.44E-10	0.00E+00	5.44E-10	0.00E+00	1.48E-06	0.00E+00	0.00E+00	1.48E-06
4	1.09E-09	0.00E+00	1.09E-09	0.00E+00	3.58E-06	0.00E+00	0.00E+00	3.58E-06
5	1.09E-09	0.00E+00	1.09E-09	0.00E+00	3.58E-06	0.00E+00	0.00E+00	3.58E-06
6	1.63E-09	0.00E+00	1.63E-09	0.00E+00	1.48E-06	0.00E+00	0.00E+00	1.48E-06
7	1.63E-09	0.00E+00	1.63E-09	0.00E+00	1.48E-06	0.00E+00	0.00E+00	1.48E-06
8	3.78E-09	0.00E+00	3.78E-09	0.00E+00	1.48E-06	0.00E+00	0.00E+00	1.48E-06
9	3.78E-09	0.00E+00	3.78E-09	0.00E+00	3.58E-06	0.00E+00	0.00E+00	3.58E-06
10	5.96E-09	0.00E+00	5.96E-09	0.00E+00	5.51E-06	0.00E+00	0.00E+00	5.51E-06
11	1.09E-08	0.00E+00	1.09E-08	0.00E+00	3.58E-06	0.00E+00	0.00E+00	3.58E-06
12	1.79E-08	0.00E+00	1.79E-08	0.00E+00	1.32E-05	0.00E+00	0.00E+00	1.32E-05
13	3.47E-08	0.00E+00	3.47E-08	0.00E+00	1.32E-05	0.00E+00	0.00E+00	1.32E-05
14	4.94E-08	0.00E+00	4.94E-08	0.00E+00	1.98E-05	0.00E+00	0.00E+00	1.98E-05
15	4.94E-08	0.00E+00	4.94E-08	0.00E+00	1.98E-05	9.46E-09	0.00E+00	1.98E-05
16	8.04E-08	0.00E+00	8.04E-08	0.00E+00	4.34E-05	7.73E-09	0.00E+00	4.34E-05
17	1.24E-07	0.00E+00	1.24E-07	0.00E+00	8.79E-05	4.31E-09	0.00E+00	8.79E-05
18	1.64E-07	0.00E+00	1.64E-07	0.00E+00	1.20E-04	8.11E-08	0.00E+00	1.20E-04
19	1.26E-06	0.00E+00	1.26E-06	0.00E+00	1.59E-04	2.06E-07	0.00E+00	1.59E-04
20	9.47E-06	0.00E+00	9.47E-06	0.00E+00	2.13E-04	2.74E-06	2.70E-06	2.08E-04
21	1.36E-04	0.00E+00	1.36E-04	0.00E+00	3.63E-04	3.18E-07	6.37E-05	2.99E-04
22	5.25E-06	0.00E+00	5.25E-06	0.00E+00	3.19E-06	1.19E-06	1.58E-06	4.13E-07
23	2.31E-04	0.00E+00	2.31E-04	0.00E+00	5.47E-04	2.81E-06	4.18E-05	5.02E-04
24	1.36E-04	0.00E+00	1.36E-04	0.00E+00	1.71E-04	4.58E-06	8.79E-08	1.66E-04
25	1.40E-04	0.00E+00	1.40E-04	0.00E+00	6.68E-04	2.19E-05	1.36E-04	5.10E-04
26	1.40E-04	0.00E+00	1.40E-04	0.00E+00	2.51E-03	1.25E-04	2.81E-04	2.11E-03
27	1.59E-05	0.00E+00	1.58E-05	5.23E-09	6.14E-05	2.76E-06	2.86E-05	3.00E-05
28	1.76E-04	0.00E+00	5.61E-05	1.20E-04	4.67E-04	1.85E-06	1.27E-05	4.52E-04
29	4.36E-04	0.00E+00	4.33E-04	2.96E-06	2.78E-03	1.47E-05	3.81E-04	2.39E-03
30	1.06E-05	0.00E+00	1.00E-05	6.08E-07	1.93E-04	6.81E-08	1.47E-04	4.61E-05
31	1.52E-04	0.00E+00	1.52E-04	6.94E-07	2.58E-04	1.41E-07	1.62E-04	9.58E-05
32	2.03E-04	1.73E-09	1.89E-04	1.36E-05	5.71E-03	8.14E-05	5.07E-04	5.13E-03
33	1.19E-04	1.73E-09	1.12E-04	7.24E-06	2.11E-04	8.03E-05	7.62E-05	5.44E-05
34	4.40E-04	3.45E-09	2.68E-04	1.72E-04	1.12E-03	1.52E-05	1.48E-04	9.55E-04
35	1.18E-03	2.59E-09	6.37E-04	5.47E-04	8.08E-03	6.54E-04	6.27E-04	6.81E-03
36	5.56E-04	2.07E-08	5.56E-04	1.41E-07	2.71E-04	8.21E-05	1.69E-05	1.72E-04
37	6.04E-04	1.35E-07	6.03E-04	1.19E-06	1.22E-03	4.97E-05	1.63E-04	1.01E-03
38	2.17E-03	3.18E-07	1.63E-03	5.42E-04	6.60E-03	1.19E-04	1.06E-03	5.42E-03
39	5.33E-04	2.67E-08	3.68E-04	1.65E-04	1.01E-03	1.32E-04	4.11E-05	8.33E-04
40	6.57E-04	8.45E-08	3.15E-05	6.25E-04	1.07E-03	3.87E-04	1.35E-04	5.49E-04

Table 7.6 – *Table of numerical results for failure probabilities of each section and location*

	Case a		Case b	
Time(years)	Pf	Cf	Pf	Cf
0	5.66E-06	5.66E-06	6.50E-04	6.50E-04
1	1.18E-07	5.78E-06	6.15E-08	6.50E-04
2	4.07E-07	6.19E-06	8.45E-08	6.50E-04
3	1.53E-06	7.72E-06	1.60E-07	6.50E-04
4	3.65E-06	1.14E-05	1.19E-07	6.50E-04
5	3.68E-06	1.50E-05	2.67E-07	6.51E-04
6	1.64E-06	1.67E-05	2.78E-07	6.51E-04
7	1.73E-06	1.84E-05	4.63E-07	6.51E-04
8	2.08E-06	2.05E-05	6.75E-07	6.52E-04
9	4.51E-06	2.50E-05	2.39E-06	6.54E-04
10	6.96E-06	3.20E-05	2.46E-06	6.57E-04
11	8.82E-04	9.14E-04	1.73E-06	6.59E-04
12	2.56E-05	9.40E-04	4.45E-06	6.63E-04
13	4.04E-05	9.80E-04	9.56E-06	6.73E-04
14	5.90E-05	1.04E-03	7.86E-06	6.80E-04
15	2.00E-05	1.06E-03	1.66E-05	6.97E-04
16	4.36E-05	1.10E-03	1.66E-05	7.14E-04
17	1.15E-04	1.22E-03	1.65E-04	8.79E-04
18	1.21E-04	1.34E-03	2.07E-04	1.09E-03
19	1.62E-04	1.50E-03	1.62E-04	1.25E-03
20	2.34E-04	1.73E-03	8.18E-04	2.06E-03
21	1.39E-05	1.75E-03	7.56E-06	2.07E-03
22	6.36E-04	2.38E-03	5.97E-05	2.13E-03
23	1.80E-03	4.18E-03	7.43E-04	2.87E-03
24	4.44E-04	4.63E-03	8.46E-04	3.72E-03
25	1.06E-03	5.69E-03	6.24E-04	4.34E-03
26	3.36E-03	9.05E-03	2.42E-03	6.75E-03
27	9.89E-05	9.15E-03	1.65E-03	8.39E-03
28	9.99E-04	1.01E-02	1.22E-03	9.60E-03
29	4.89E-03	1.50E-02	2.80E-03	1.24E-02
30	2.94E-04	1.53E-02	1.46E-03	1.38E-02
31	1.61E-03	1.69E-02	1.48E-03	1.53E-02
32	9.88E-03	2.68E-02	6.06E-03	2.13E-02
33	9.56E-04	2.78E-02	2.58E-03	2.38E-02
34	2.56E-03	3.03E-02	2.66E-03	2.64E-02
35	1.66E-02	4.69E-02	8.31E-03	3.45E-02
36	2.45E-03	4.94E-02	1.02E-03	3.54E-02
37	3.80E-03	5.32E-02	4.12E-03	3.94E-02
38	1.66E-02	6.98E-02	9.35E-03	4.84E-02
39	2.84E-03	7.26E-02	3.37E-03	5.16E-02
40	3.70E-03	7.63E-02	4.52E-03	5.59E-02

Table 7.7 – *Failure and cumulative total failure probability for the two cases; a) Inspecting every 3 years, b) Inspecting annually*

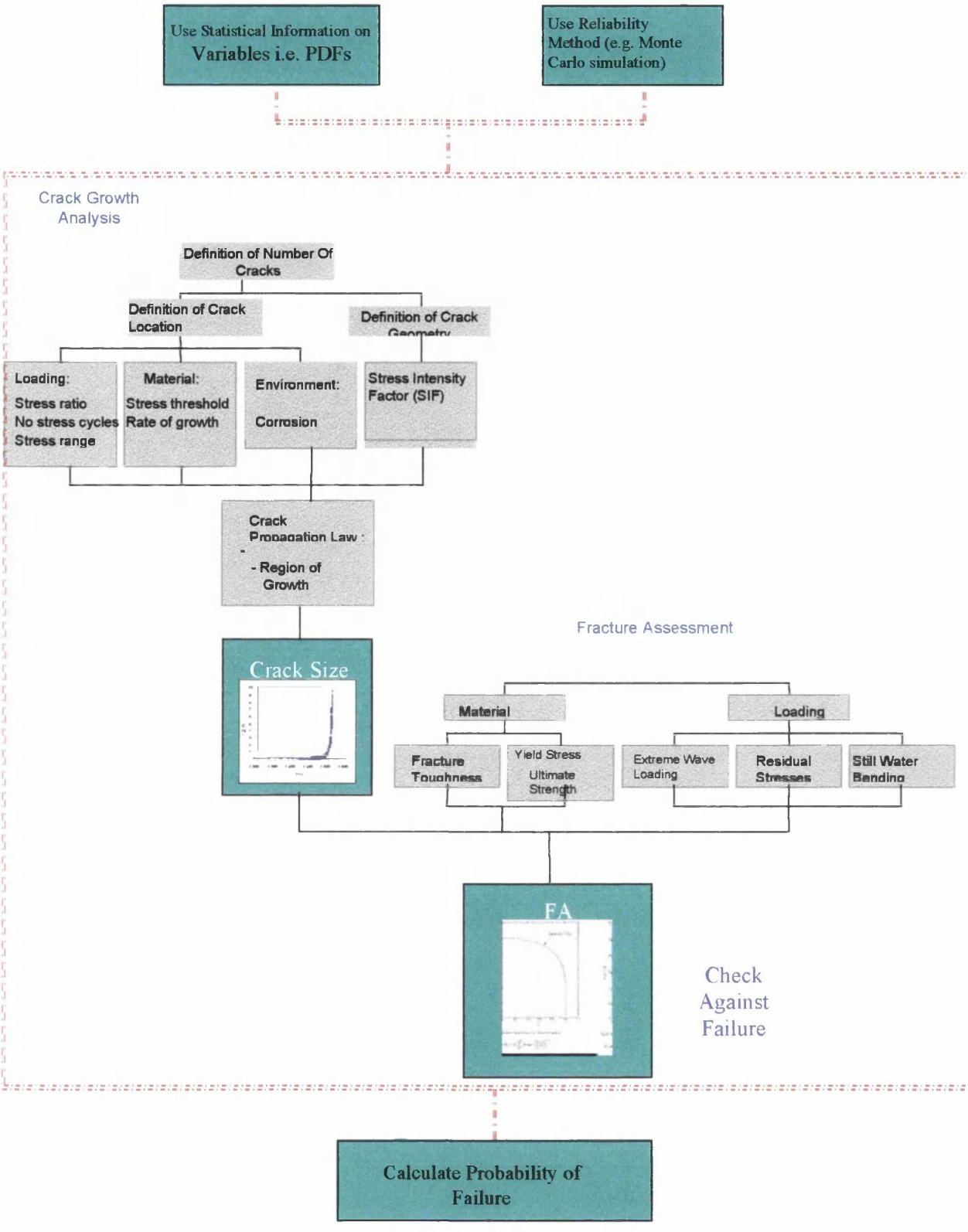

Figure 7.1 – *The components of the reliability analysis*

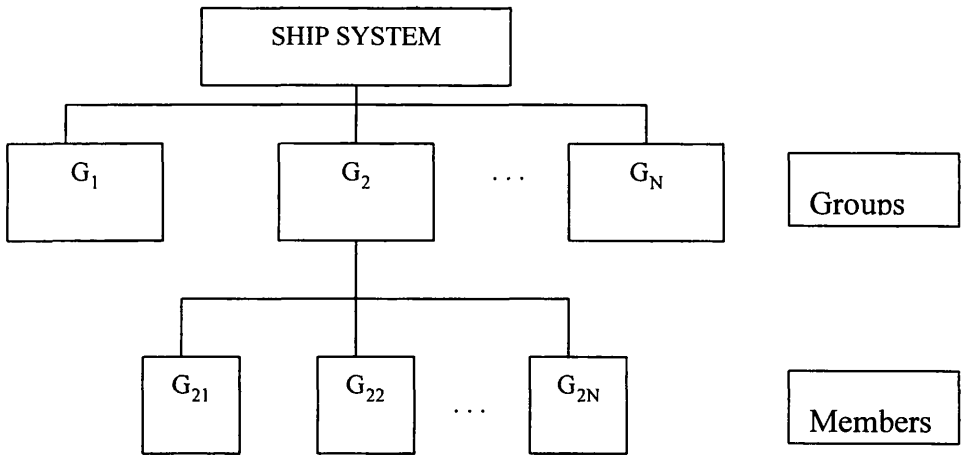

Figure 7.2 – *System subdivision into groups and members*

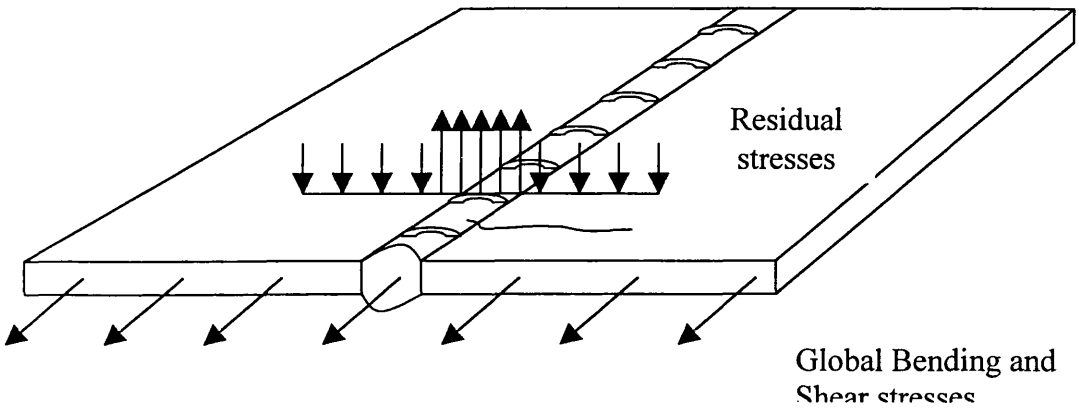

Figure 7.3 – *Crack in a finite plate at the deck structure inside tensile residual stress field*

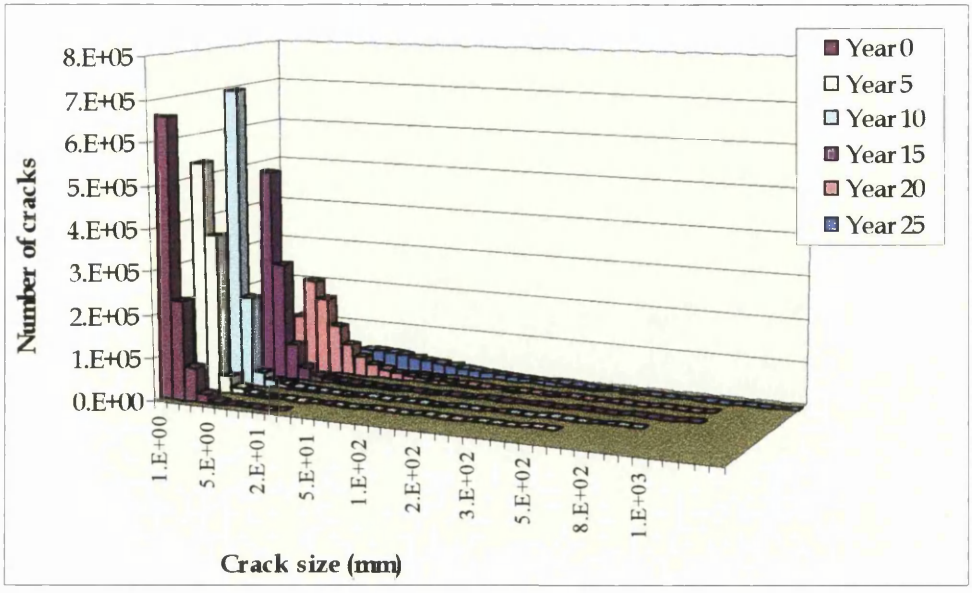

Figure 7.4 – *Crack size histogram at various times. Distribution spreads out with the passage of time as cracks grow larger and larger*

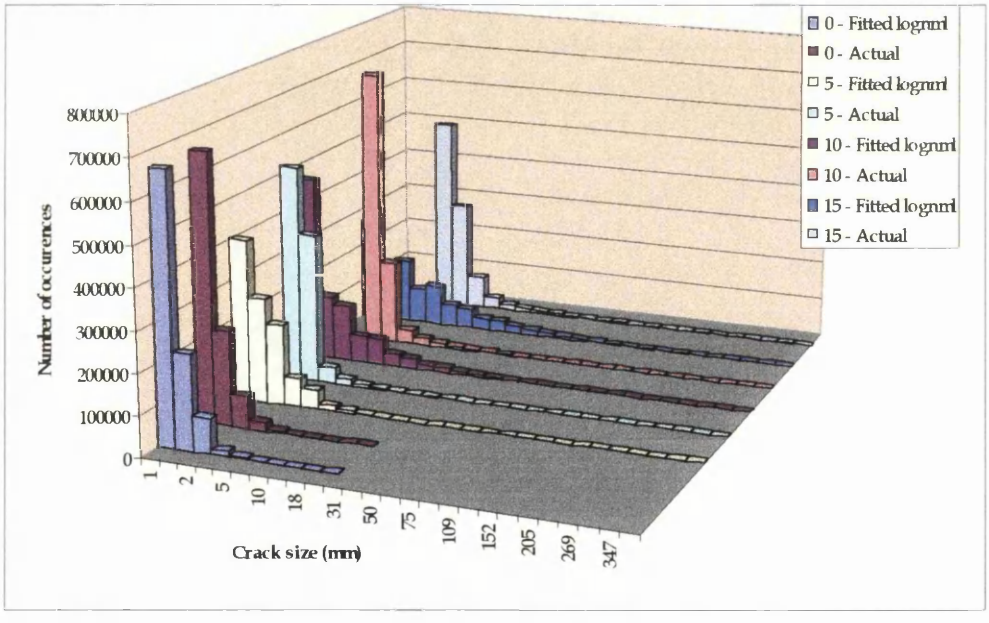

Figure 7.5 – *Actual crack size histogram and fitted lognormal distribution. There is no good agreement. It proved difficult to find a theoretical distribution to fit to the actual crack size distribution. Hence, the actual numerical distribution was used in the analysis*

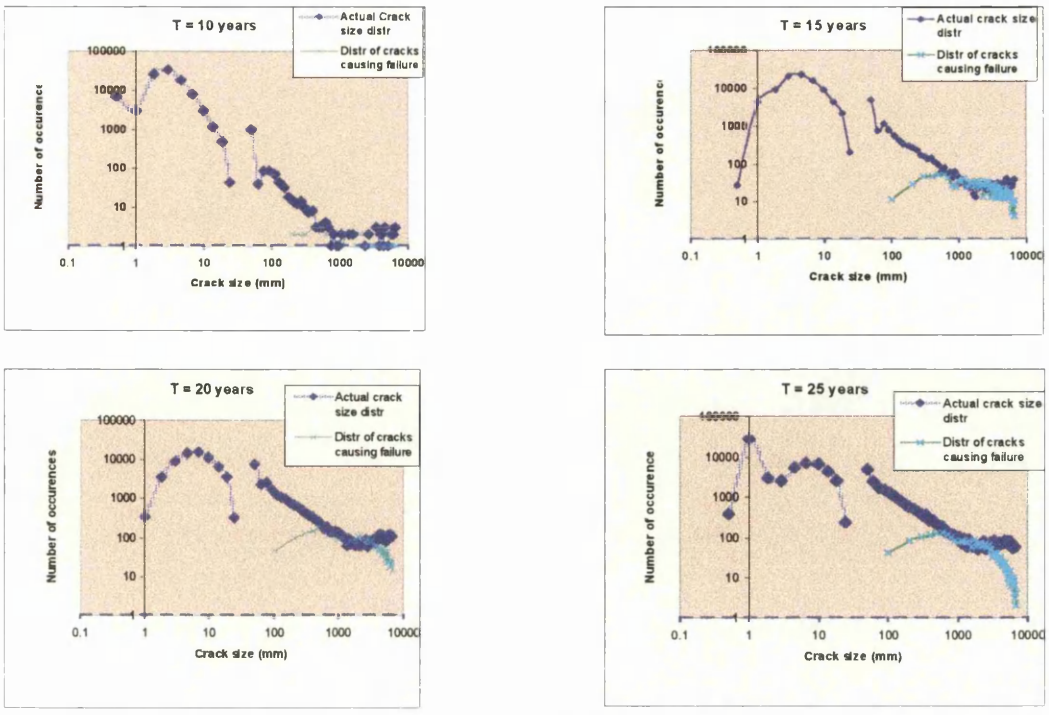

Figure 7.6 – *Complete crack size distribution and distribution of cracks causing failure at various times plotted together in logarithmic scale for both axes. Discontinuity is because of the change of crack geometry (Sample size 100,000)*

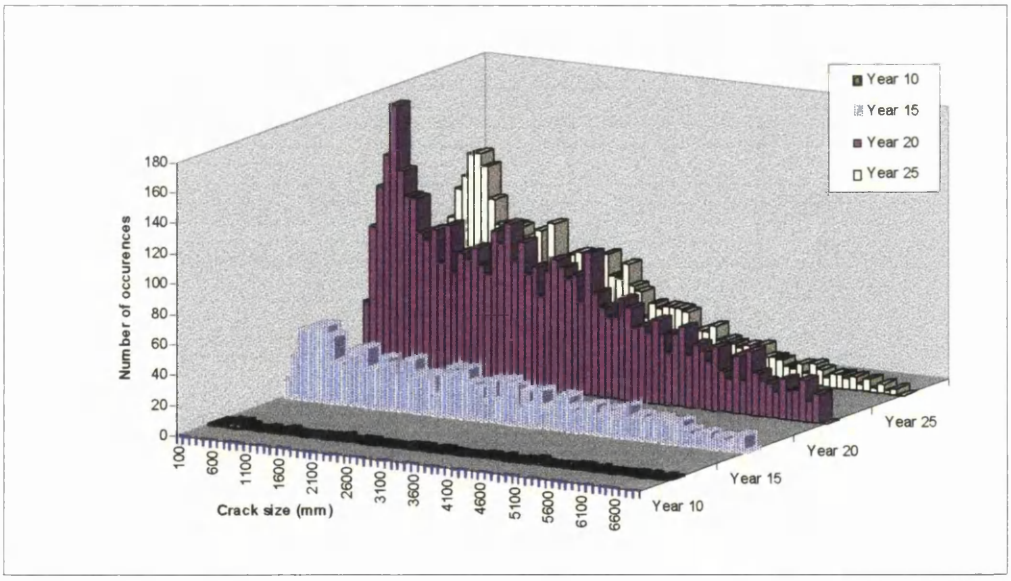

Figure 7.8 – *Crack size distributions that caused failure at various times plotted together. As time passes by, distribution spreads out. Inspection occurs every 5 years.*

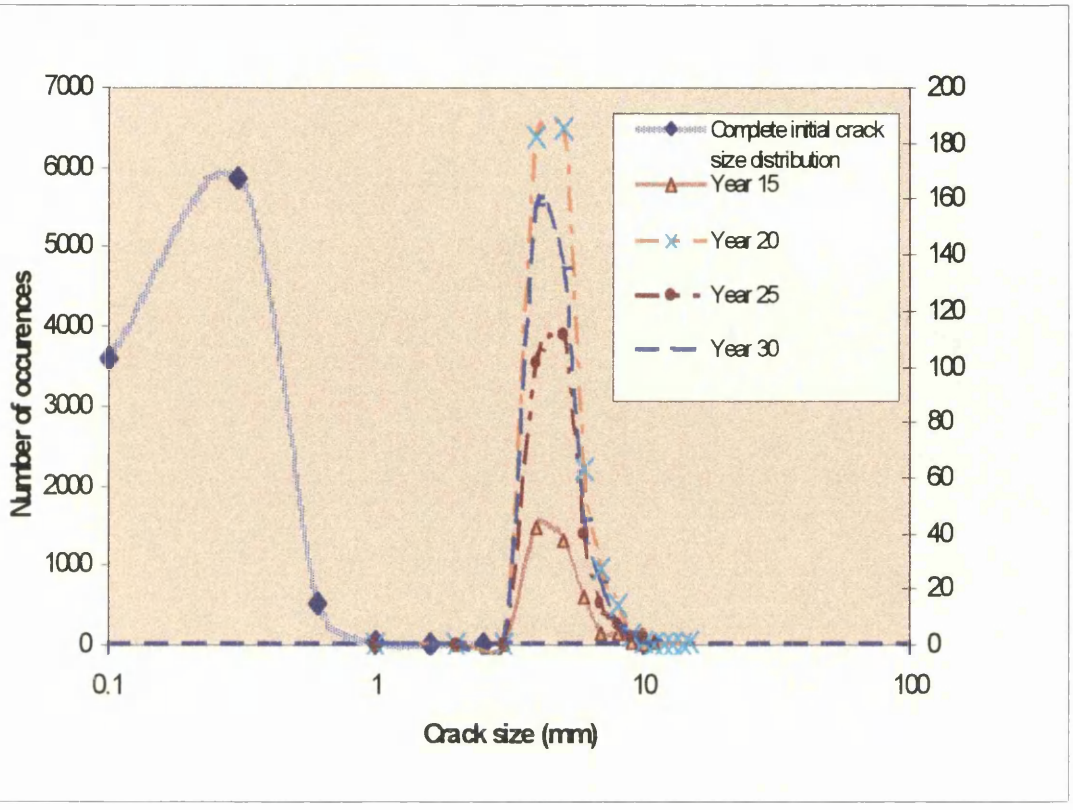

Figure 7.8 – *Initial crack size distribution and distribution of initial cracks that caused failure with respect to time. It is clearly seen that only cracks from the tail end, and in particular between 3 and 7 mm, cause all the failures. This is because the mean value of the distribution is very small and the small cracks do not grow to large dimensions even with fatigue*

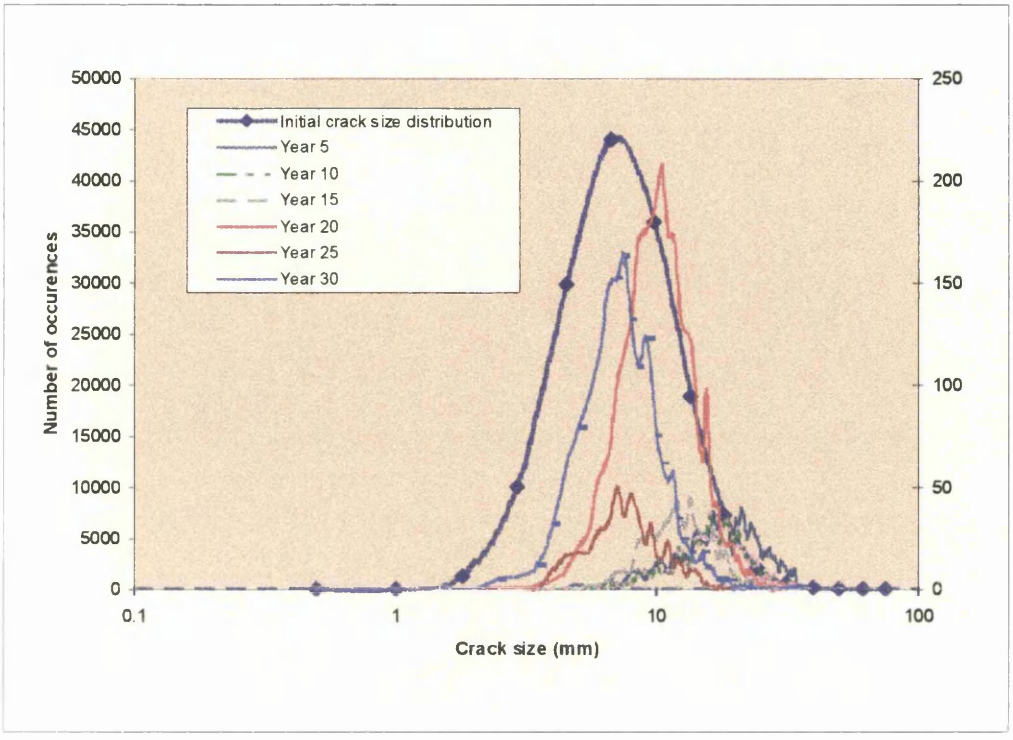

Figure 7.9 – *Same figure as Figure 7.8 but with a logarithmic initial crack size distribution with a mean value of 10mm and st. dev. of 5mm. Other input remained the same as in Table 7.2. Here we can see more clearly that at earlier stages only the large cracks of the initial crack size distribution cause failure, but with time smaller initial cracks have grown large and they cause failure as well. This is why the distribution of initial cracks that cause failure started at the tail end but the moves to the right. Vertical axis in logarithmic scale. Number of cracks that caused failure is read in the right vertical axis*

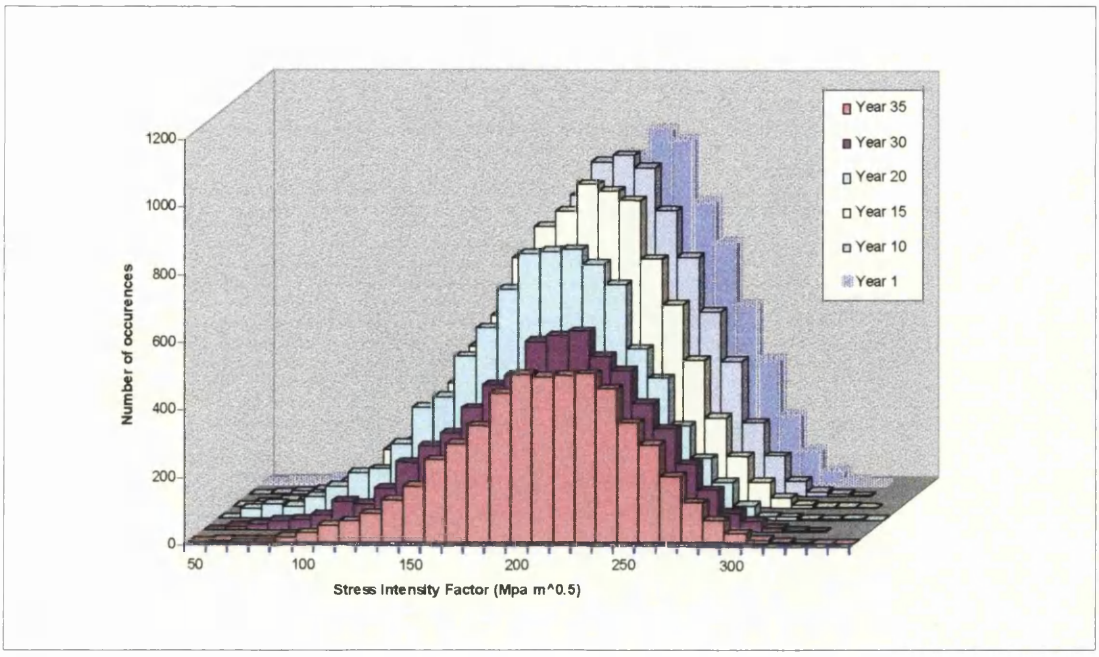

Figure 7.10 – *Stress intensity factor (SIF) distribution at failure w.r.t. time. With the passage of time, and because cracks grow larger, smaller SIF values are required for failure. Hence, the distributions shifts to the left*

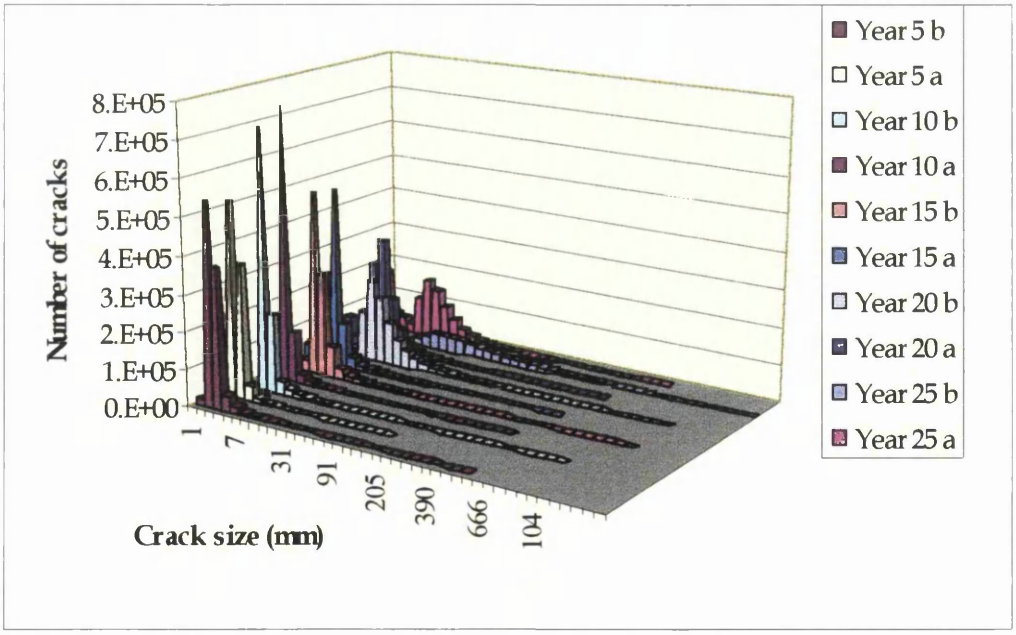

Figure 7.11 – *Effect of inspection on the crack size distribution (b: before inspection, a: after inspection)*

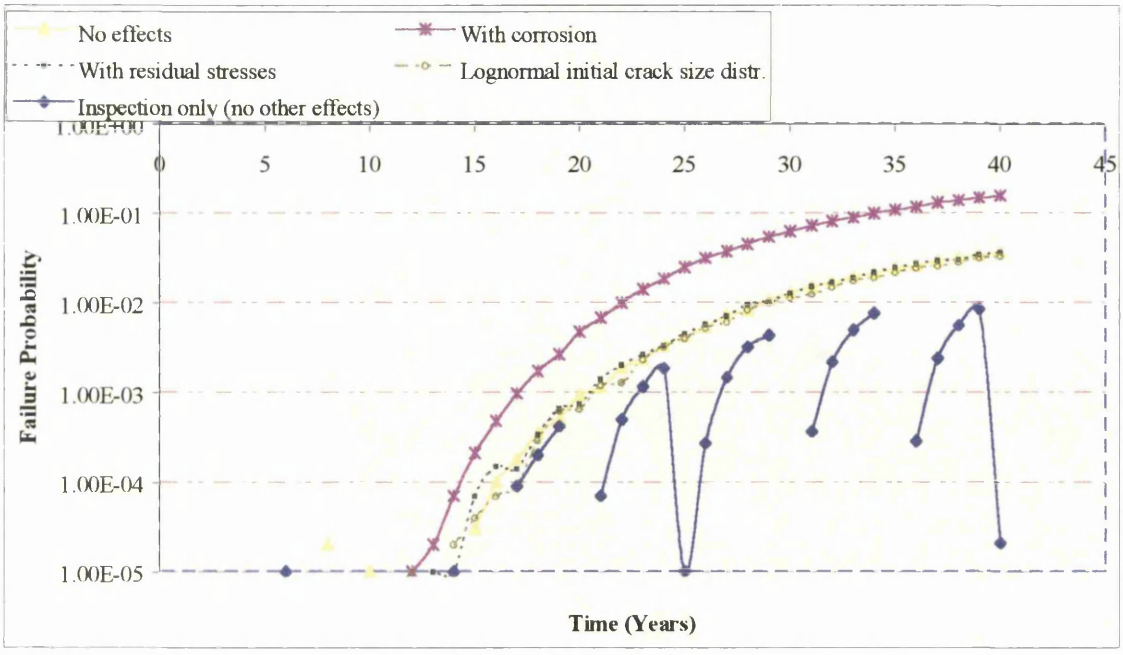

Figure 7.12 – *Results from Monte Carlo simulation. Probability of failure vs. time for various cases*

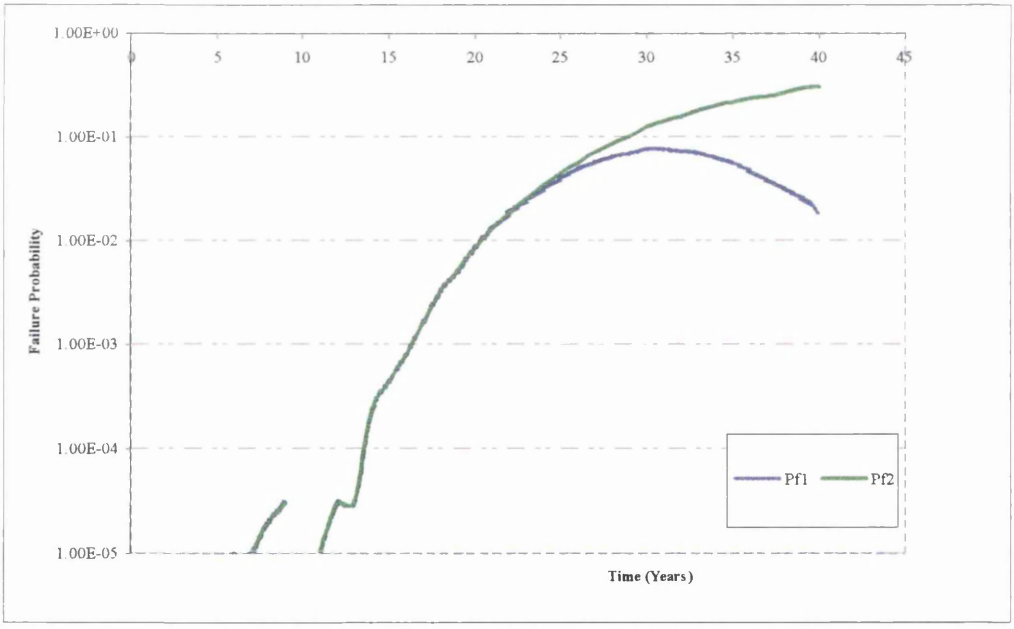

Figure 7.13 – *Pf_1 versus Pf_2 with time. The difference in the probability of failure between the case of the ship existing at year 0 (Pf_1) and the ship existing at the beginning of that year (Pf_2)*

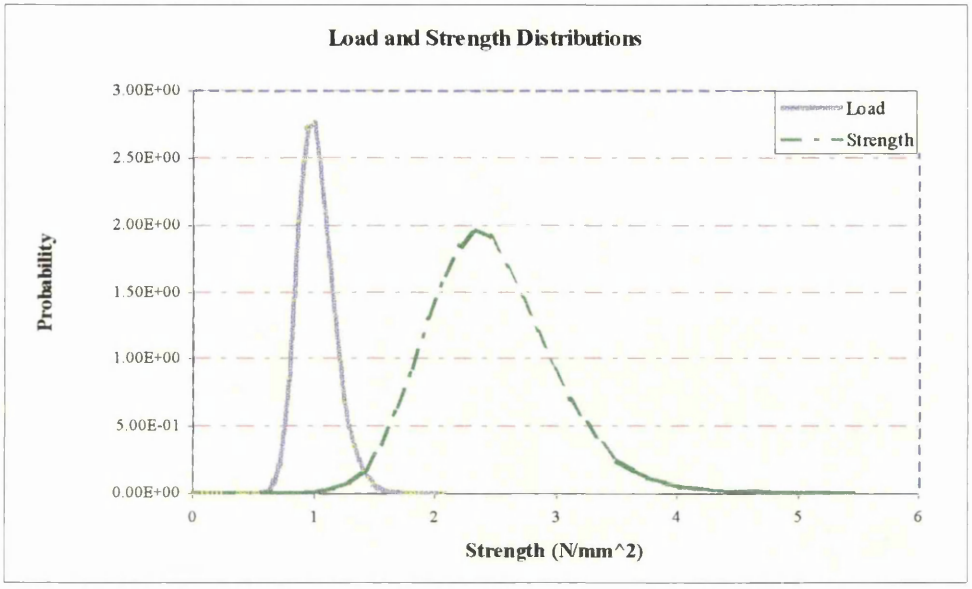

Figure 7.14 – *Normalised load and strength distributions. Convolution integral calculates the probability of failure that strength is less than the load. Mean value for load distribution 109 Nmm-^{2}.*

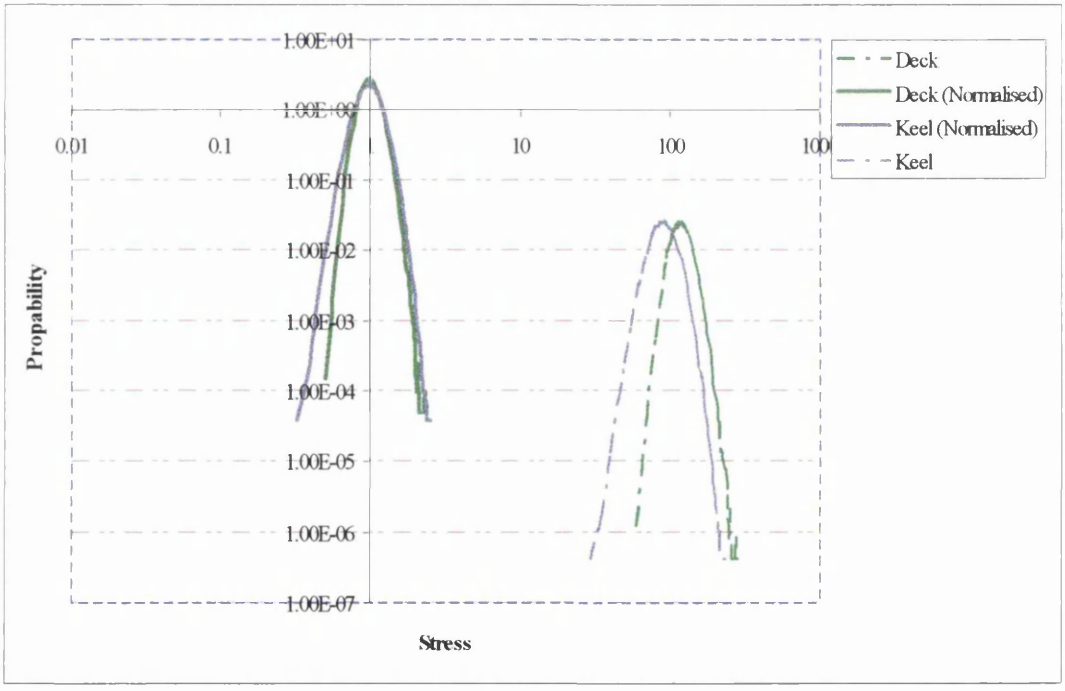

Figure 7.15 – *Actual and normalised load distributions for two locations in log-log plot*

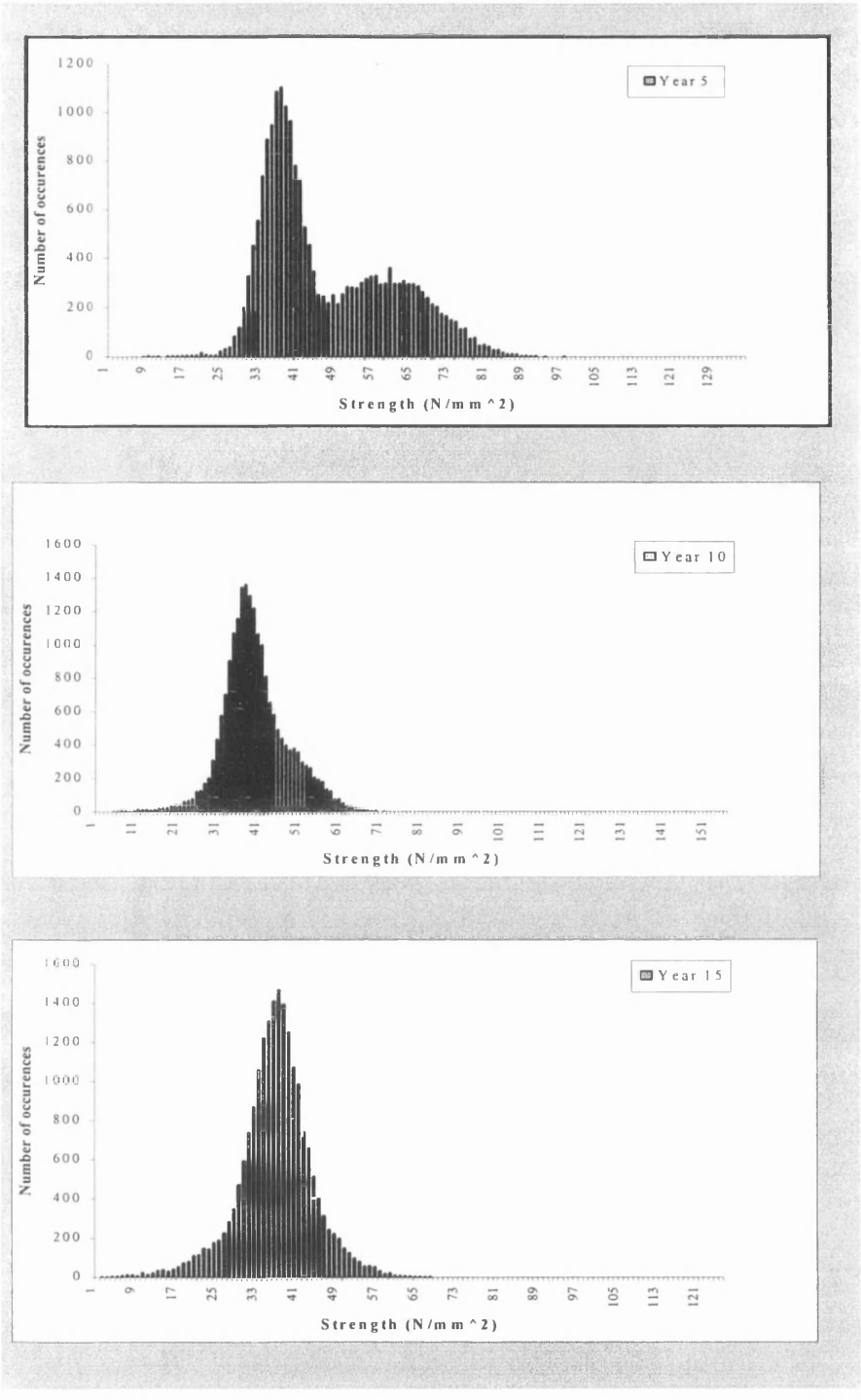

Figure 7.16 – *Total strength distribution, with fracture strength distribution reducing with time and plastic (large peak) remaining approximately constant. Note actual strength values in x-axis are ×5.*

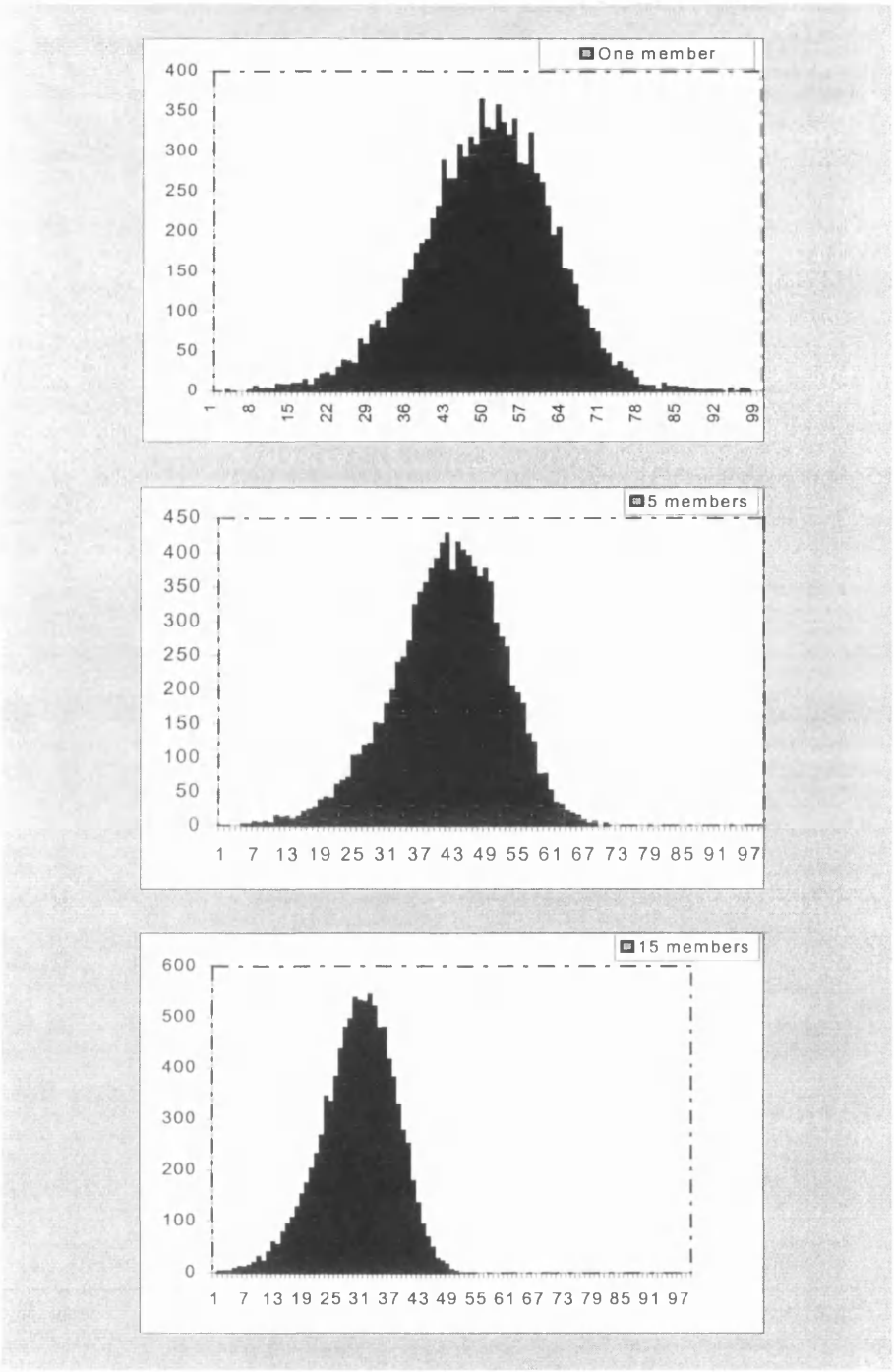

Figure 7.17 – *Strength distributions for different systems (different number of members) at the same time interval. Values in Y-axis are number of occurrences, values in X-axis are strength in N/mm^2 ×5.*

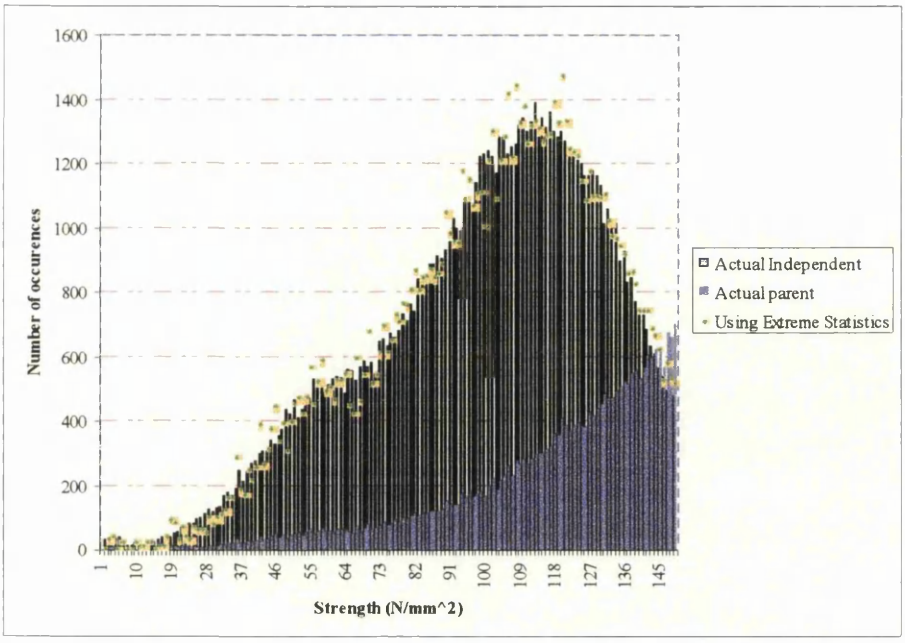

Figure 7.18 – *Actual and calculated extreme strength distribution for an independent system of 10 members (actual strength values ×5)*

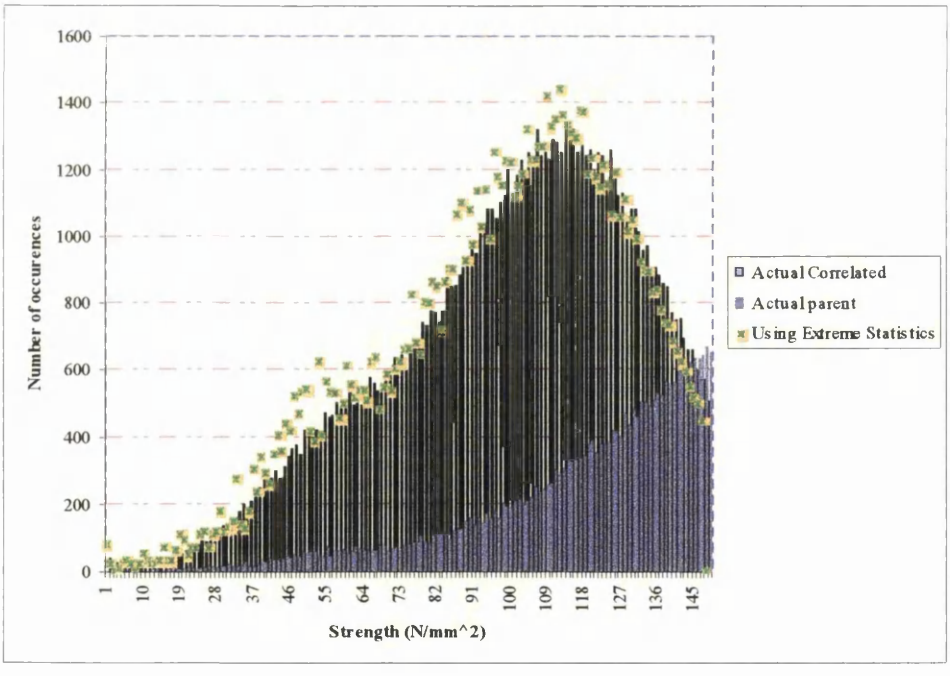

Figure 7.19 – *Actual and calculated extreme strength distribution for a correlated system of 10 members (actual strength values ×5)*

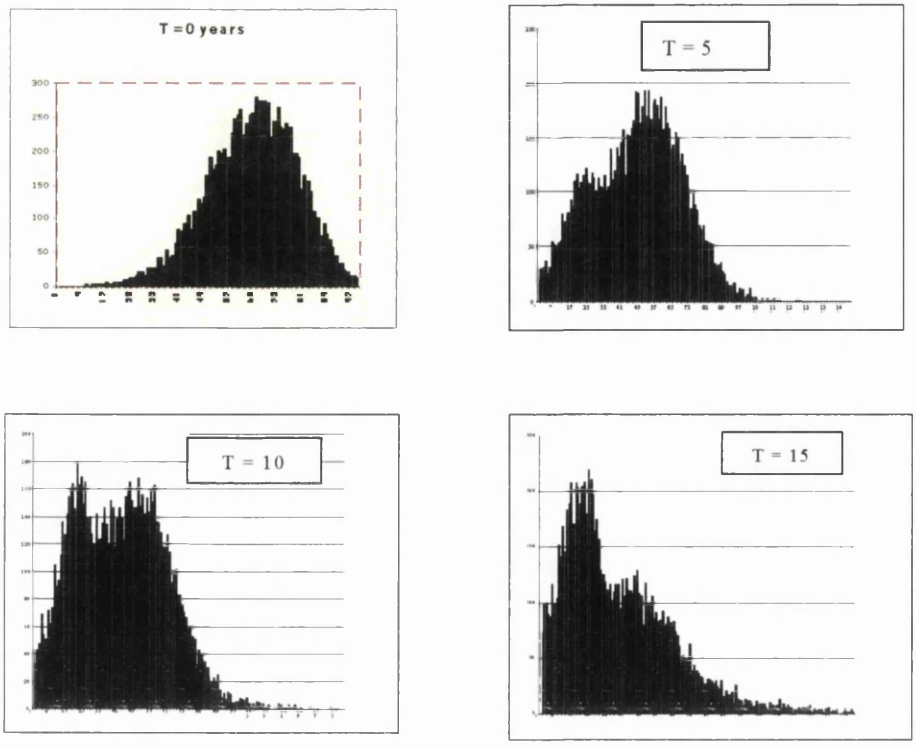

Figure 7.20 – Strength distribution at various times (T years), shape does not remain constant as a result of fatigue and corrosion

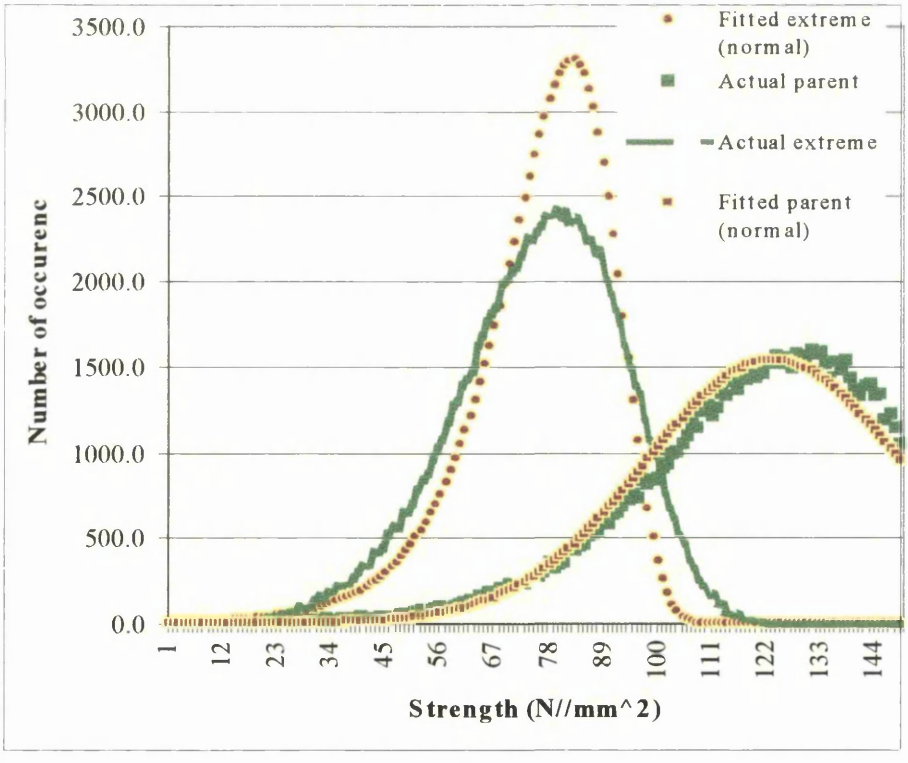

Figure 7.21 – *Actual and fitted, parent and extreme smallest strength distributions using the normal distribution (actual strength values x5)*

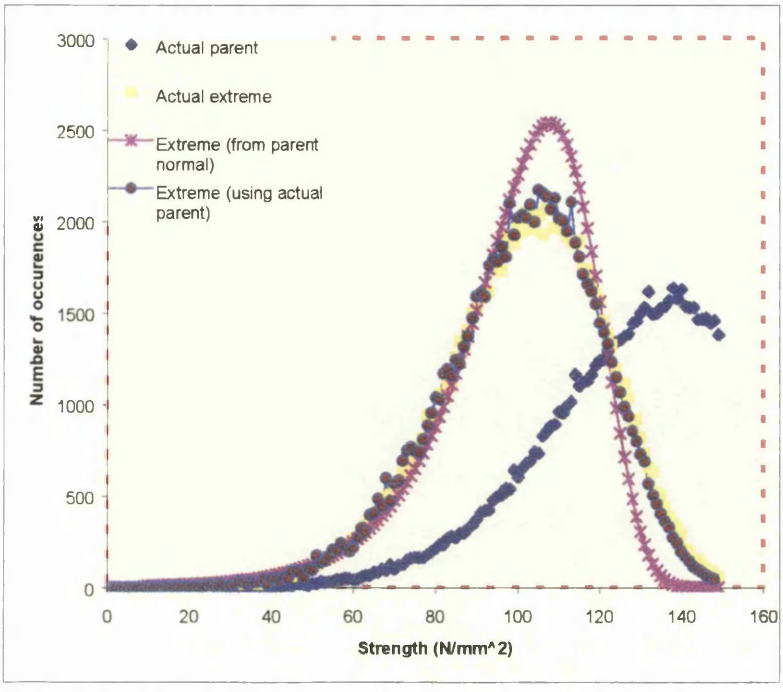

Figure 7.22 – *Actual and fitted extreme minimum strength from actual numerical distribution (actual strength values x5)*

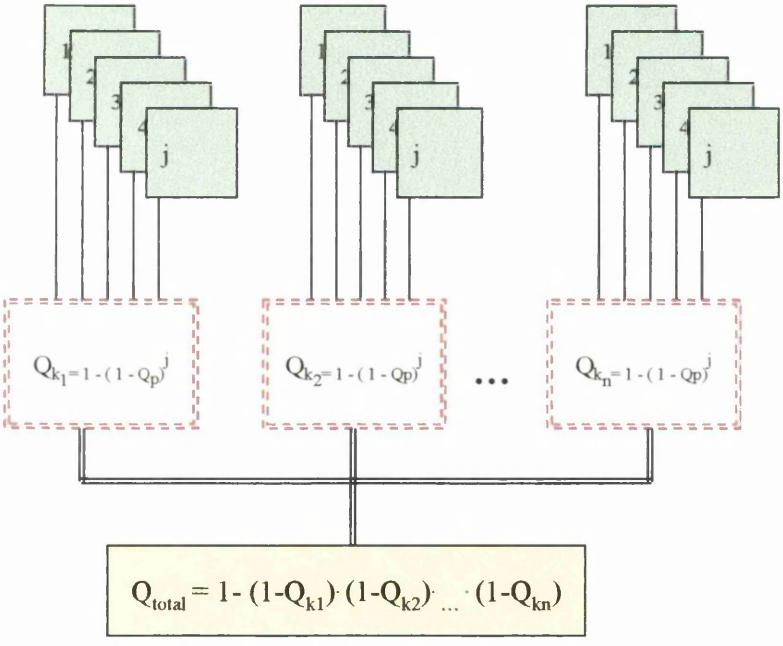

Figure 7.23 – *Total strength distribution calculation for the system*

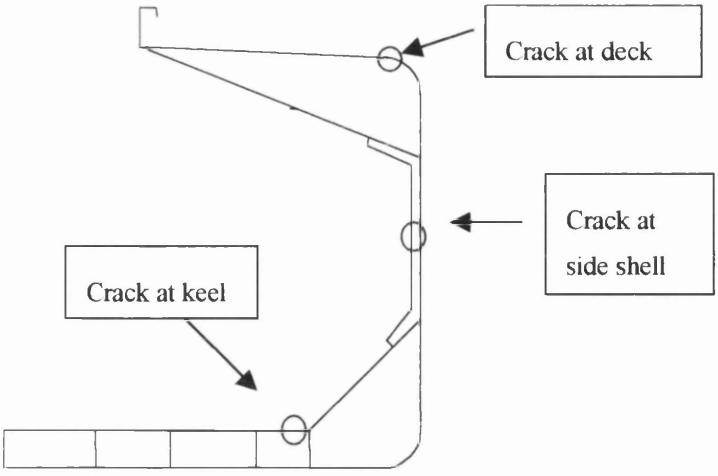

Figure 7.24 – *Crack locations for example case*

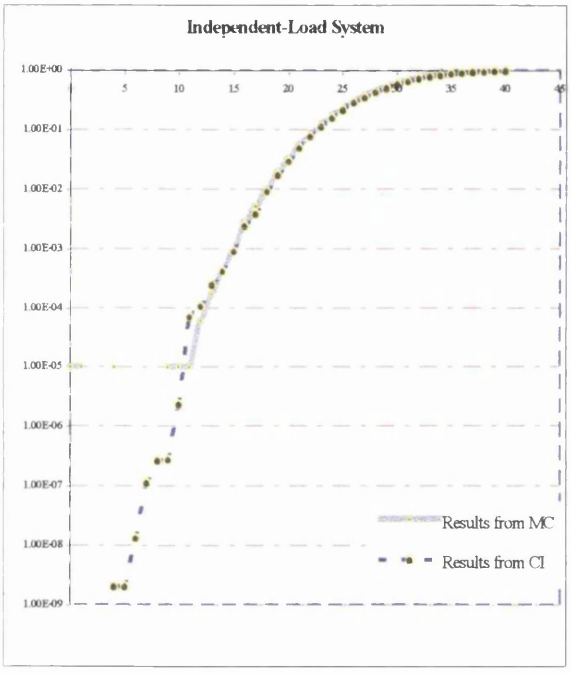

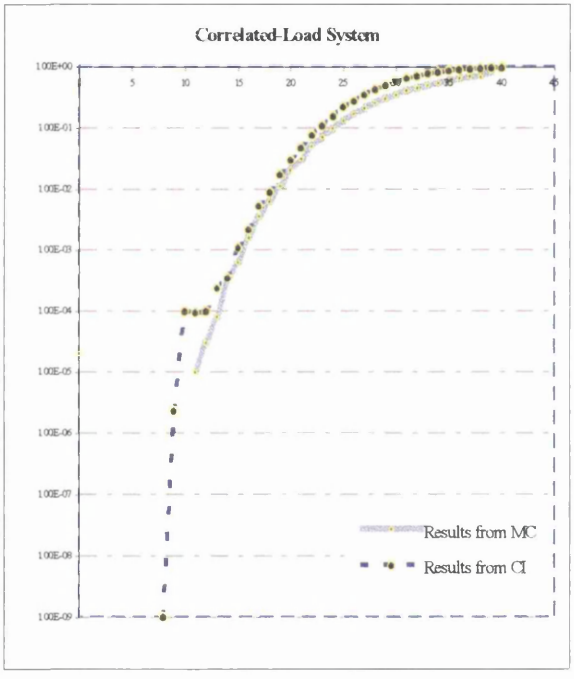

Figure 7.25 – *Comparisons Monte Carlo and Convolution Integral methods for independent and correlated (in load) systems of 10 identical locations (no inspection)*

Note: Y-axis is probability of failure (logarithmic scale), X-axis is time in years

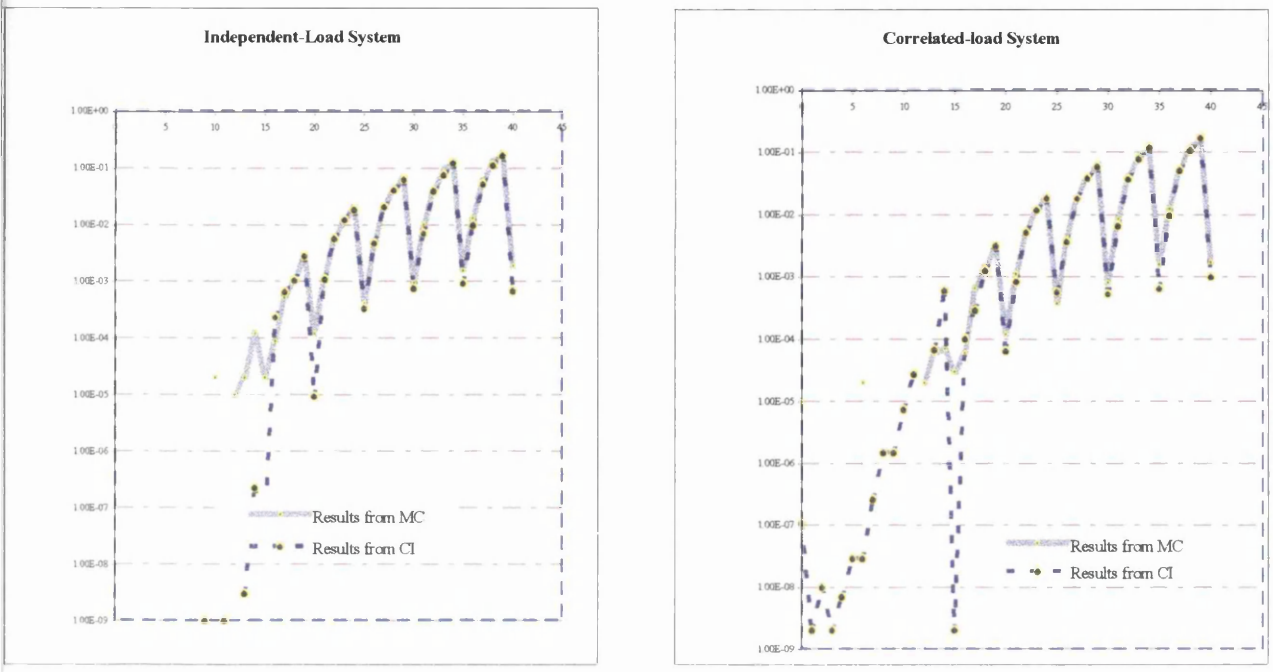

Figure 7.26 - *Comparisons between Monte Carlo and Convolution Integral methods for independent and correlated systems (with inspection)*

Note: Y-axis is probability of failure (logarithmic scale), X-axis is time in years

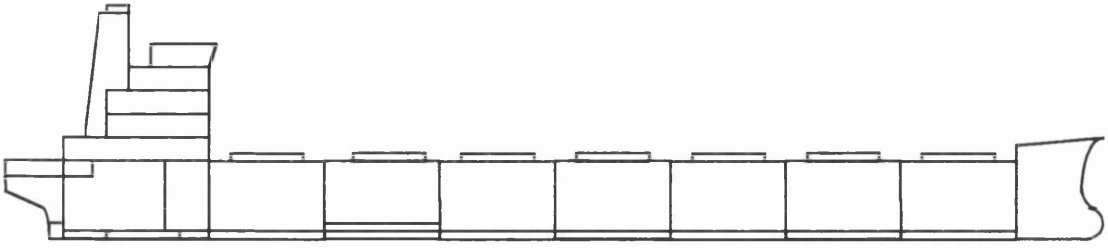

a) Actual ship

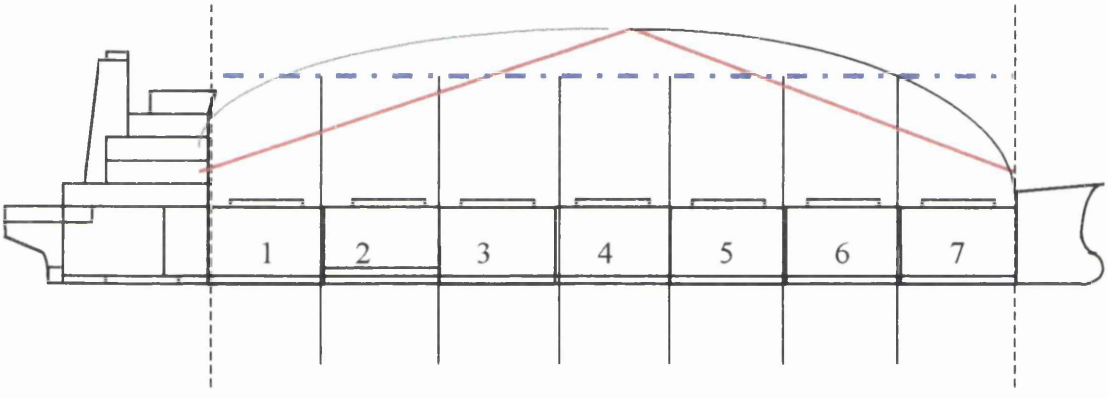

b) Idealised ship modelling

——— : *Wave global loading*

——— : *Still water bending moment*

– – – : *Wave pressure distribution at side shell*

Figure 7.27 – *Typical bulk carrier vessel*

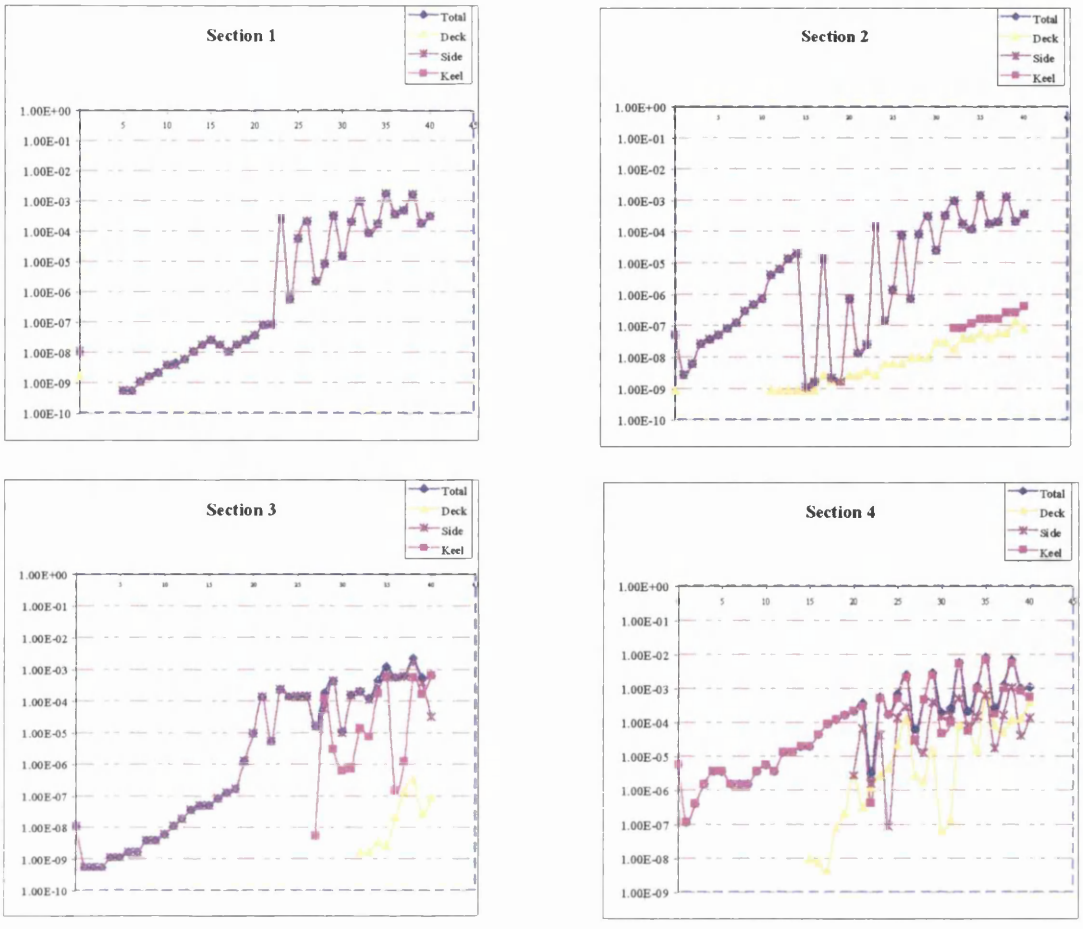

Figure 7.28 – *Probabilities of failure of sections 1-4 for cracks in deck, side and keel for case a (inspecting every 3 years)*

Note: Y-axis is probability of failure (logarithmic scale), X-axis is time in years

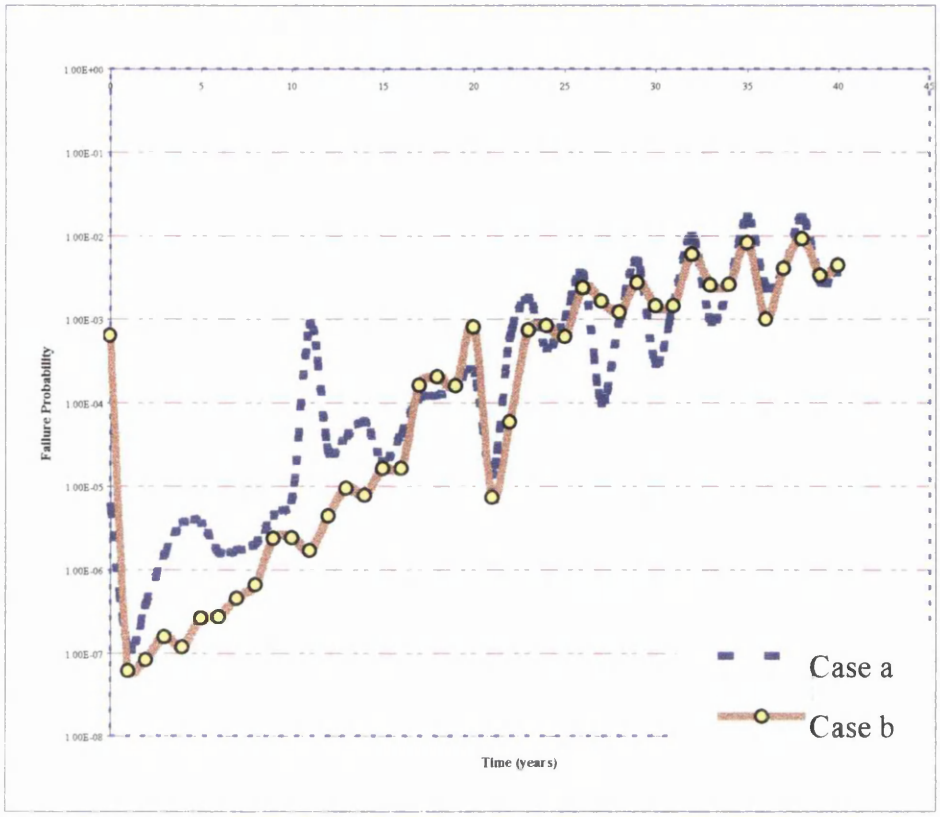

Figure 7.29 – *Total failure probability of ship, for both cases a and b*

a) Inspecting every 3 years

b) Detailed inspection every 3 years and annual repairing of cracks larger then 200 mm found with a POD of 50%

Note: Y-axis is probability of failure (logarithmic scale), X-axis is time in years

CHAPTER 8

STATISTICAL INFORMATION ON BULK CARRIER LOSSES

8.1 Statistics on Bulk Carrier Fleet

In the period 1980 to 1996 the average life expectancy for a bulk carrier was 23.3 years (from report 1). Figure 8.1 shows that in the same period the average age of bulk carriers (10,000dwt – 80,000dwt), i.e. the majority of the fleet, has been increasing. Consequently, the risk of failure due to structural failure increased as well. In 1998 bulk carriers constituted approximately 30% of world's gross tonnage of ships 100GT and over. Bulk carriers are the second largest group of ship type in terms of gross tonnage (oil tankers are first), and the third largest in terms of numbers (general cargo and oil tankers are first and second respectively). The total number of bulk carriers in 1998 was 6,413 with a total bulk of 158.6mGT, the average life was 23 years, (Lloyd's Register 'World Fleet Statistics 1997/98').

In the period 1991 to 2000 the average bulk carrier life was 20.3 years, (Intercargo 2000). At the start of 2000 the number of bulk carriers was 5513, and the average life of the fleet was 20.4 years. This is therefore at present an indicator of increased scrapping and a lower average age. Hopefully this will result in reduced losses.

8.2 Statistics on Bulk Carrier Losses and Causes of Loss

Many bulk carriers built during the early 1970s, are still trading today, far beyond their initial design life. Although several factors are related to the losses of the bulk carriers, there is an increased tendency for serious accidents to occur as the age of the vessel rises, (OECD report, Intercargo 2000 report). Generally as it is shown in Table 8.1, the number of ships lost (all merchant vessels) increase with age.

From Figure 8.2 it is evident that the number of ship losses (all ships) increased with age.

Specifically for bulk carriers, Table 8.2 presents ships lost between 1988 and 2000 and states also the causes of failure. Many of these ships were lost because of hull cracking. Table 8.3 presents data from bulk carrier losses due to structural failure only. 44 out of 109 bulk carrier losses were due to cracks. Analysis on IACS data reveals that from 1978 to 1998, 74% of all bulk carriers (larger than 20,000dwt) casualties were attributed to structural failure, and the average age of the ships was more than 17 years. Table 8.4 shows the number of bulk carriers lost stating also the

cause, for the period 1960 to 1998. Structural failure amounts for the larger number of losses, approximately 25% of all losses. Structural failure was also the primary reason of failure during the period 1991-2000 as shown also in Table 8.5, and Figure 8.3. Figure 8.4 shows the total number of losses and the number of losses due to structural failure, for bulk carriers between 1991 and 2000.

Structural failures do occur, as is evident from the data presented, and a large proportion of these structural failures can be attributed to cracking and eventual fracture of the vessel (data presented in Tables 8.2 and 8.3 demonstrates this).

8.3 Verification of Reliability Results with Real Data

By analysing the data of bulk carrier losses, it is believed that some comparisons can be made with the results of the reliability analysis.

Figure 8.5 shows the number of bulk carrier structural losses during the period 1980 and 1997, with years 1990 and 1991 particularly bad as they have the most casualties. Greater effort for improving safety by major classification societies and IMO, saw the number of failures dropping in 1992 and 1993 but in 1994 casualties rose again. However we cannot use, information of such type to make comparisons, since the failure probability calculated in this report is a function of bulk carrier age.

A better presentation of the data would be to relate ship losses with ship age, as shown in Figures 8.6 to 8.8. Then we can relate the findings of this report to actual data.

A general trend of the results is that the number of losses of bulk carriers, increases with age of vessel up to a certain point, and then drops again, e.g. from Figure 8.6 we see that losses increase up to vessels being 18 years and then start to drop for older vessels. This means that vessels around 17 to 18 years old have higher probability of failing than older vessels. However, it does not mean that older vessels are safer, but that there are not many vessels left beyond that age (either because they have failed already, or they are being scrapped hence limited number of vessels), as we can also see from the number of vessels in service by age (the dotted line in the same Figure). Figure 8.2 shows as well that ages 15-19 and 20-24 have higher probabilities of failure than the 25+.

This trend was also obtained also in this thesis, e.g. Figure 7.8 shows exactly the same trend (for Pf_1, a result that seemed strange at that point), there is a drop of the failure probability after some time, as in the actual data.

Another interesting observation that can be made from the actual statistical data of bulk carrier losses regards the age of the ships that posses the higher risk of failing. Figures 8.6 and 8.8 show that there is a considerable risk for ships over 15 years old. Intercargo, Lloyd's and IACS, all state that the average age of bulk carriers lost is about or exceeding 20 years, much higher than the average age of the world fleet. For example, Lloyd's data shows that between 1993 and 1998, 56 bulk carriers were lost due to structural failure, 73% of the ships lost were ships over 20 years. IACS data shows that from 1983 to 1997, 73 bulk carriers were lost due to structural failure, 70% of the ships were over 18 years old.

This agrees well with findings from the analysis of this thesis. For example, Figure 7.24 shows the failure probability (due to fracture) for a bulk carrier vessel, calculated with the input data collected in this thesis and described in chapter 6 (with the values being used, assumed to represent reality as accurate as possible). The failure probability increases significantly after year 20, and increases again with a slower rate afterwards mainly because of the repairing action. In Figure 8.6, we also witness a significant rise of the number of losses at about year 15 with the number of losses at later stages increasing but with a lower rate. After year 25, the number of losses is very much reduced, since the number of vessels beyond 25 years old is very small.

From the reliability analysis, the failure probability for the vessel after year 20 is in the range of 10^{-3} and 10^{-2}, with ups and downs due to the inspections carried out, and which they maintain the probability levels in that range. From Figure 8.6 a rough estimation allows us to verify the results of the reliability analysis. Assuming that the number of bulk carriers in the fleet remains constant from year to year (approximately 5000), the failure probability from approximately year 15 to 25, is in the range of 10^{-3} to 10^{-2} as well, (for example at year 18 $20 / 5000 = 4 \cdot 10^{-3}$).

REFERENCES

- OECD Report, 'The cost to users of substandard shipping', January 2001
- Lloyd's Register, 'World Fleet Statistics 1997/98'
- Lloyd's Register, 'Bulk carriers – an update', March 1998
- Intercargo, 'Bulk carrier casualty report: 2000 and the previous ten years (1991-2000)', Jan 2001
- Intercargo, 'Bulk carrier casualty report: Analysis of total loss and fatality statistics for dry bulk carriers, 1990-1997', Sept. 1998
- Keith Brook, 'The electronic future for managing ship condition data', Lloyd's Register of Shipping, 1997

Merchant Vessel Total Losses (All Ship Types) 1989-98

Vessel age (years):

	0-4		5-9		10-14		15-19		20-24		25 & over		GRAND TOTAL	
	No.	000 GT	No.	000 GT	No.	000 GT	No.	000 GT	No.	000 GT	No.	000 GT	No.	000 GT
1989	9	14	18	185	23	140	42	224	29	200	24	71	145	814
1990	2	21	8	72	21	237	60	708	37	260	3	100	121	1,398
1991	4	8	8	121	21	176	48	617	54	597	39	182	174	1,700
1992	3	58	6	14	19	105	39	477	41	371	30	112	137	1,138
1993	3	4	3	7	15	87	36	336	50	396	37	107	144	918
1994	1	1	2	2	17	106	24	466	48	651	30	196	122	1,421
1995	1	16	4	154	17	156	26	121	36	251	30	65	113	762
1996	1	17	2	3	9	30	26	298	28	212	47	201	113	701
1997	3	13	3	10	5	24	16	126	30	440	39	209	96	819
1998	1	19	6	34	6	64	13	33	31	225	39	173	96	547

Preliminary data for latest years.

Includes absolute total losses and constructive total losses.

Source: Institute of London Underwriters.

Table 8.1 – *Number of total ship losses between 1989 and 1998, (OCDE 2001 report)*

Dec- 90 Elounda Day 38,350 1973 17 PAN Bulk carrier Sunk Sank in heavy seas off Hawaii during laden voyage from west coast Canada, carrying potash.
Aug- 90 Corazon 28,757 1972 18 MLT Bulk carrier Sunk Sank off Cape Cod in Hurricane Bertha, while on cement- carrying coastal voyage.
Aug- 90 Silimna 69,165 1978 12 LBR Bulk carrier Sunk Sustained crack in hull, 5/ 90, and sank while in tow to Aden, laden with iron ore from India.
May- 90 Tao Yuan Hai 126,579 1977 13 TWN Bulk carrier Sank Sustained hull damage in heavy weather on voyage carrying iron ore from Port Kembla. Presumed sunk.
Mar- 90 Alexandre P 94,351 1967 23 PAN Bulk carrier Sank Sank on voyage from West Australia to Spain, while carrying iron ore.
Mar- 90 Azalea 78,571 1969 21 KOR Bulk carrier Sank Sank off Sweden while in tow after hull was holed on iron ore voyage from Norway to Germany.
Jan- 90 Orient Pioneer 108,504 1971 19 LBR Bulk carrier Sank Damaged in heavy weather carrying iron ore from Brazil to Taiwan. Sank in Indian Ocean.
Dec- 89 Vulca 42,245 1968 22 CYP Bulk carrier Sank Foundered in Pacific Ocean on laden voyage from New York to South Korea, carrying scrap iron.
Feb- 90 Walter Leonhardt 42,805 1966 24 CYP Bulk carrier Sank Sustained hull damage and sank in Atlantic, on voyage from Florida to Antwerp, carrying phosrock.
Jan- 90 Charlie 29,246 1975 15 CYP Bulk carrier Sank Presumed sunk in heavy seas in north Atlantic on voyage from EC Canada to Mozambique, carrying grain.
Feb- 91 C. Eregli 16,635 1974 17 TUR Bulk carrier Sank Sank off Yemen after collision with tanker "Mendana Spirit" while carrying Indian iron ore to Turkey.
Jan- 91 Continental Lotus 54,202 1967 24 IND Bulk carrier Sank Hull cracked in heavy weather off Malta and sank while carrying iron ore from India to Italy.
Jan- 91 Demetra Beauty 11,972 1974 17 CYP Bulk carrier Sank Explosion in engine room amid heavy seas in Gulf of Oman and sank, carrying tar from Germany to Iran.
Feb- 91 Fairwind 25,505 1967 24 MLT Bulk carrier Sank Sank in Red Sea after hitting submerged object while laden with Russian pig iron.
Sep- 90 Gallant Dragon 123,126 1976 15 PAN Bulk carrier Sank Struck submerged object off Tubarao in Brazil, after loading iron ore for Japan. Scuttled.
Jan- 91 Protektor 80,184 1967 24 SGP Bulk carrier Sank Missing, presumed sunk, in heavy weather off Newfoundland, carrying iron ore from Canada to Sweden.
Feb- 91 Salvia 153,256 1970 21 KOR Bulk carrier Sank Hull cracked on laden voyage carrying iron ore from Chile to South Korea. Sank in Pacific Ocean.
Feb- 91 Sanko Harvest 33,022 1985 6 PAN Bulk carrier Sank Stranded on reef on voyage from Florida to West Australia, carrying fertilisers. Broke in two & sank.
Oct- 89 Pan Dynasty 36,650 1968 21 Bulk carrier Sank Received hull damage in heavy weather in Atlantic while carrying phosphate rock & later sank.
Oct- 89 Porn Udom 16,504 1969 20 Bulk carrier Sank Sprang leak off Taiwan in Typhoon Angela and seemingly foundered.
May- 89 Huron 16,895 1972 17 Bulk carrier Sank Foundered in heavy weather in Indian Ocean, carrying timber, steel & scrap from South Africa to Taiwan.
Iran Fateh 16,894 1968 21 Bulk carrier Sank
Jan- 89 Kronos 19,392 1973 16 Bulk carrier Sank Presumed sunk in heavy seas on laden voyage from Belgium to Greece while carrying steel products.
Oltul 26,857 1967 22 Bulk carrier Sank
Apr- 89 Sevasti 15,167 1971 18 Bulk carrier Sank Foundered off Namibia as cargo of timber shifted in heavy seas on voyage from West Africa.
Apr- 89 Star of Alexandria 35,967 1966 23 Bulk carrier Sank Sank in heavy weather off US east coast while carrying cement from Piraeus to New York.
Jan- 89 Kumanovo 39,674 1966 23 Bulk carrier Sank In collision with ship off Gibraltar while carrying coal from Philadelphia. Sank under tow.
Dec- 88 Mega Taurus 30,413 1980 9 Bulk carrier Sank Believed to have sunk in rough seas on voyage from Taiwan to Japan carrying nickel ore.
Apr- 91 Mineral Diamond 141,028 1982 9 HKG Bulk carrier Sank Presumed sunk in Indian Ocean in Cyclone Fifi, carrying iron ore fines from W. Australia to Holland.
Jul- 91 Manila Transporter 115,960 1976 15 PHL Bulk carrier Sank Developed crack in hull while carrying iron ore from West Australia to UK. Sank in Indian Ocean.
Apr- 91 Starfish 56,277 1970 21 PAN Bulk carrier Sank Sustained crack in cargo hold on voyage from W. Australia to Poland, and sank off Mauritius.
Apr- 91 Vasso 68,490 1967 24 BHS Bulk carrier Sank Hull plating cracked on iron ore voyage from Saldhana Bay and sank off Durban.
Aug- 91 Melete 72,063 1975 16 GRC Bulk carrier Sank Hull cracked in heavy seas, carrying iron ore from West Australia to UK. Sank in Indian Ocean.
Oct- 91 Erato 29,098 1968 23 MLT Bulk carrier Sank Sank in heavy seas on laden voyage carrying phosphates from Israel to France.
Jul- 91 Sunset 20,932 1970 21 CYP Bulk carrier Sank Sank off Yemen as cargo shifted on voyage carrying steel products from Poland to Taiwan.
Nov- 91 Sonata 79,681 1969 22 PAN Bulk carrier Sank Flooded in heavy seas on voyage carrying iron ore pellets from Sweden to Germany. Sank under tow.
Nov- 91 Hanjin Karachi 18,888 1973 18 KOR Bulk carrier Sank Sank on ballast voyage as engine room flooded when ship hit submerged object off Philippines.
Dec- 91 Entrust Faith 63,533 1973 18 GRC Bulk carrier Sank Sustained heavy weather damage while carrying iron ore from Venezuela to Germany. Sank.
Jan- 92 Arisan 135,748 1974 18 PAN Bulk carrier Sank Engine failed on voyage from Narvik to Ymuiden carrying iron ore. Stranded off Sweden & broke in two.
Apr- 90 Frotanorte 25,231 1969 22 BRA Bulk carrier Sank Stranded off Belem on Brazilian coastal voyage, carrying grain. Broke in two under tow and sank.
May- 92 Great Eagle 65,230 1968 24 PAN Bulk carrier Sank Hull cracked in heavy seas in Indian Ocean, on iron ore voyage from South Africa to China. Sank.
Mar- 92 Karadeniz S 115,280 1969 23 TUR Bulk carrier Sank Engine room flooded in heavy seas on iron ore voyage from Brazil to Spain. Broke in two & sank.
Oct- 92 Daeyang Honey 123,744 1970 22 KOR Bulk carrier Sank Presumed sank on iron ore voyage from Yampi Sound to Japan, in Typhoon Colleen.
Korean Star 30,900 1984 4 Bulk carrier Sank Broke in two following damage sustained during Hurricane at Cape Cuvier, W. Australia.
Singa Sea 26,586 1976 12 Bulk carrier Sank Broke in two and sank on laden voyage from W. Australia to Rotterdam carrying mineral sands/ copper ore.
Nov- 92 Pegasus 23,423 1972 20 PAN Bulk carrier Sank Engine trouble off Taiwan, on Indonesia- S. Korea voyage, carrying wheat pellets. Broke in two & sank.
Mar- 93 Gold Bond Conveyor 26,549 1974 19 LBR Bulk carrier Sank Sank in heavy seas off east coast Canada on voyage from Halifax to Tampa, carrying gypsum.
Apr- 93 Atlas 18,915 1977 16 PHL Bulk carrier Sank Sank in S. China Sea after fire in engine room on voyage from Thailand to South Korea, carrying tapioca
May- 93 Nagos 74,596 1969 24 MLT Bulk carrier Sank Took water and sank in storm off South Africa on coal voyage from Richards Bay to Antwerp. Sank.
Sep- 93 Anderson 12,051 1975 18 MLT Bulk carrier Sank Sank off Hong Kong in Typhoon Becky, on voyage from Russia to Guangzhou, carrying iron.
Aug- 91 Petchomphoo 17,214 1969 24 THA Bulk carrier Sank Presumed foundered as No. 1 hold flooded on voyage from Nakhodka to Bangkok carrying steel.
Jun- 92 Flying Falcon 41,300 1970 23 MLT Bulk carrier Sank Wrecked. Stranded in heavy seas in Gulf of Aden on voyage from Bangkok to Ghent carrying animal feed.
Feb- 94 Christinaki 26,510 1973 21 MLT Bulk carrier Sank Sank in storm in North Atlantic, on laden voyage from UK to Vera Cruz, carrying scrap.
Jun- 93 Protoklitos 4 121,820 1974 20 CYP Bulk carrier Sank Scuttled off Brazil after grounding on laden voyage carrying iron ore to China.
Jun- 94 Apollo Sea 131,260 1973 21 PAN Bulk carrier Sank Sank 40 nm NW of Cape Town after loading iron ore at Saldanha Bay.
Jun- 94 Kamari 127,283 1973 21 CYP Bulk carrier Sank Sank off Brazil, following severe weather damage sustained on iron ore voyage Venezuela to China.
May- 94 Jag Shanti 27,071 1972 22 IND Bulk carrier Sank Sank after engine room flooded off New Mangalore in laden voyage from India to Turkey, carrying iron ore pel lets.
Iron Antonis 93,355 1968 26 CYP Bulk carrier Sank Sank in S. Atlantic carrying iron ore from Brazil to PRC. Owner reported this was final voyage prior to scrapping.
Colmena 28,620 1968 26 VCT Bulk carrier Sank

Table 8.2 – *Bulk Carrier total losses, 1988 – 2000, (OECD report)*

Lorenzo 45,499 1969 25 CYP Bulk carrier Sank
Ocean Lucky 27,447 1971 23 VCT Bulk carrier Sank Broke in two off Taiwan
Wellborn 26,450 1971 23 LBR Bulk carrier Sank Broke in two off Madagascar. Oil spillage occurred
Nov- 94 Golden Chariot 22,076 1972 22 PAN Bulk carrier Sank Sank in South Atlantic, while carrying grain from US Gulf to Africa.
Paris 25,957 1971 24 MLT Bulk carrier Sank Struck breakwater and sank in storm at Constantza Roads. Unladen.
You Xiu 26,600 1992 3 HKG Bulk carrier Sank Struck breakwater and sank in storm at Constantza Roads. Unladen.
Sun River II 11,784 1976 19 PAN Bulk carrier Sank Sank off Japan in heavy weather
Jun- 95 Mineral Dampier 170,968 1985 10 LBR Bulk carrier Sank Sank in East China Sea after collision with Hanjin Madras, while carrying iron ore from Brazil to S. Korea.
Aug- 95 Iron Baron 37,557 1985 10 AUS Bulk carrier Sank Scuttled off Tasmanian coast after going aground.
Feb- 96 Seafaith 68,275 1973 23 MLT Bulk carrier Sank Sank in bad weather north of Taiwan. Eleven of the 30 crew rescued. Laden with 59, 000t iron ore.
Anna Spiratou 26,098 1978 18 CYP Bulk carrier Sank Sank off S. Korea after collision with bulk carrier Polydefkis P.
Feb- 96 Innovator 20,009 1973 23 VCT Bulk carrier Sank Sank in 18 08 N 108 35.
Jun- 96 Million Hope 26,847 1972 24 CYP Bulk carrier Sank Grounded on coral reefs near Sharm el- Sheikh. Vessel ripped apart and lying partially submerged on reef.
Aug- 96 Al Hadi 16,659 1968 28 VCT Bulk carrier Sank Sank 5km off Mumbai Harbour, due to crack in shell plating.
Sep- 96 Iolcos Victory 132,597 1980 16 CYP Bulk carrier Sank Sank off S. Africa whilst laden with iron ore on voyage from Brazil- China
Feb- 97 Leros Strength 21,673 1976 21 CYP Bulk carrier Sank Sank 30 miles west of Stavanger, laden with apatite from Murmansk to Poland. 20 crew lost.
Mar- 77 Albion Two 29,676 1976 21 CYP Bulk carrier Sank Sank carrying steel products from Antwerp to Jamaica. Wreck found off Brittanny. 25 crew missing.
Sep- 97 ICL Vikraman 55,879 1979 18 IND Bulk carrier Sank Sank after collision in Malacca Strait with OBO "Mount I" while carrying steel to Singapore.
Oct- 97 Black Sea T 10,157 1969 28 VCT Bulk carrier Sank Sank off Hios (Aegean Sea). One crew member missing
Oct- 97 Corriente 158,178 1989 8 HKG Bulk carrier Sank Sank in typhoon having previously grounded at Okinotorishima, Japan. Crew rescued, Pollution.
Jan- 96 Flare 29,222 1975 23 CYP Bulk carrier Sank Stern sank in bad weather with the loss of 21 crew, four crew members rescued.
Feb- 96 Fei Cui Hai 32,818 1973 25 CHN Bulk carrier Sank Sank in abt 09 31 N 110 33 E, 31 crew lost, 3 rescued. Vessel on voyage New Mangalore- Nanjing
Apr- 98 Chian Mariner 35,224 1974 24 LBR Bulk carrier Sank Sank off Angola. Vessel on route from Takoradi for Jubail with a cargo of 25, 500t of manganese ore.
Jul- 98 Osool 19,427 1974 24 BLZ Bulk carri er Sank Sank 230 miles off Ratnagiri coast after water ingress into engine room and No1 hold. Al l crew rescued.
Jun- 98 Golden Harvest 20,203 1975 23 VCT Bulk carri er Sank Reported sunk, off Porbandar
Aug- 98 Sea Prospect 21,297 1996 2 PAN Bulk carri er Sank Capsi zed and sank in 24 29 N 130 37 E. 11 of the 21 crew rescued.
Aug- 98 Asean Carrier 16,873 1969 29 PAN Bulk carri er Sank Vessel abandoned in Arabian Sea due to listing after flooding in two cargo holds. Crew rescued. Presumed sunk.
Jan- 99 Peace 64,912 1971 28 BLZ Bulk carri er Sank Had Leakage through crack in hull and sank about 32 miles off Colombo. Al l crew safe.
Jul- 99 Maritime Fidelity 25,406 1984 15 PAN Bulk carrier Sank Sank after collision with m. t. New Venture off Horsburgh Light.
Aug- 99 Meliksah 17, 677 1977 22 TUR Bulk carri er Sank Sank off southern coast of Sri Lanka, en route from China to Russi a carrying fertil iser. 27 crew rescued.
Sep- 99 Well Speeder 26, 587 1976 23 VCT Bulk carri er Sank Sank after water ingress into holds 1 & 2 in heavy weather.
Jan- 00 J. Marion Sky 42,258 1991 9 SGP Bulk carri er Sank Sankaf ter col lision in the western Caribbean - Two missi ng
Dec- 99 Xin Zhu Jiang 35,500 1976 23 CHN Bulk carri er Sank Sank after water ingress into a cargo hold resulting in a list. Crew rescued - master missing.
Mar- 00 Leader L 69,120 1977 23 PAN Bulk carrier Sank Sank after collapse of No. 4 hatch.
May- 00 Evelyn 22,546 1979 21 MLT Bulk carri er Sank Caught f ire onBlack Sea- Malaysi a voyage, laden with f ertili ser. Later sank in the Gul f of Aden. All crew rescued.
Jun- 00 Treasure 143,731 1983 17 PAN Bulk carrier Sank No. 4 hatch flooded, taken in tow and later sank off Cape Town. All crew rescued.
Jun- 00 Kastor Too 17,666 1977 23 CYP Bulk carri er Sank Sank on voyage Aqaba- India.
Sep- 00 Eurobulker X 35,264 1974 26 KHM Bulk carri er Sank Broke in two whi le loading cement in vi cinity of Lefkanti. Sank two days l ater.
Sep- 00 Madona 33,037 1982 18 LBR Bulk carri er Sank Took on water in cargo hold, reported sunk.
Jul- 90 Petingo 80,580 1967 23 VUT Bulk carri er Sank Sank off Sal dhana Bay after sustai ning heavy weather damage while carrying iron ore.
Aug- 90 Pasi thea 155, 407 1971 19 GRC Combined carri er Sank Sank off Japan in Typhoon Vernon whil e carryi ng West Australi an iron ore to Wakayama.
Sep- 90 Algarrobo 169,623 1971 19 LBR Combined carri er Sank Missi ng, presumed sunk, on voyage from Chile to Japan, carrying iron ore.
Dec- 92 Aegean Sea 114, 036 1973 19 GRC Combined carri er Sank Ran aground in heavy seas off Cadiz, carryi ng Norwegian crude to Spain,. Broke in two and sank.
Jan- 94 Marika 169,140 1973 21 LBR Combined carri er Sank Sank in storm in North Atlantic on laden voyage, carrying iron ore, from Canada to Netherlands.
Nov- 94 Trade Daring 145,053 1972 22 CYP Combined carrier Sank Vessel's back broken whi lst loading iron ore at Ponta de Madeira.
Jun- 91 ABT Summer 267,801 1974 17 LBR Tanker Sank Explosion & fi re 500 mil es off Angola, carryi ng crude oil f rom Kharg Island to Rotterdam. Sank.
Ain Zalah 36,330 1972 19 IRQ Tanker Sank Sank off Mina Abdullah, Kuwait during Gul f war, 1q91. Unl aden.
Al Fao 89,188 1969 22 Tanker Sank Gulf war casualty, 1q91.
Amuriyah 155,211 1977 14 Tanker Sank Sank at Mina al Bakr, Iraq, duri ng Gulf war, 1q91. Apparently unladen.
Apr- 91 Haven 232,163 1973 18 CYP Tanker Sank Sank off Genoa after explosion and fi re aboard, while laden wi th crude oil .
Jul- 91 Blue River 16,800 1973 18 CYP Tanker Sank Capsi zed, broke in two and sank in Typhoon Amy, carryi ng molasses from Thailand to Taiwan.
Dec- 90 Bow Reidun 31,501 1975 15 NOR Chemical tanker Sank Sank off Taiwan after explosion duri ng laden voyage from Japan to Singapore, carryi ng chemicals.
Sep- 90 Caribica 31,185 1975 15 PAN Tanker Sank Sank off Malaysia after explosion duri ng ball ast voyage from Singapore.
Jan- 90 Raad Al Bakry VIII 21,032 1960 30 SAU Tanker Sank Experienced explosion and f ire off Port Sudan, on ballast voyage from Jeddah. Broke in two and sank.
Nov- 91 Svangen 17,610 1968 23 PAN Tanker Sank Sank on ballast voyage from Caen to Pi raeus after developing leak in engine room.
Alina P 53,003 1965 26 Tanker Sank Experienced explosion off Brazi l duri ng laden coastal voyage. Broke in two.
Apr- 92 Katina P 69,992 1966 26 MLT Tanker Sank Damaged in heavy weather off Mozambique on laden voyage from Fujairah. Broke i n two & sank under tow.

Table 8.2 – (*Continued*)

Mabrouk 63,132 1965 27 Tanker Sank
Mar- 89 Maasgusar 38,679 1984 5 Chemical tanker Sank Sank off Japan after explosion in engine room, whi le carrying chemicals.
Feb- 89 Maassluis 37,440 1982 7 Tanker Sank Struck breakwater and sank in heavy weather at Ski kda, whil e i n ballast condition.
Jan- 89 Sagheera 36,380 1961 28 Tanker Sank Sank after striking mine in Strait of Hormuz, while in ballast condition.
Apr- 88 Athenian Venture 30,526 1975 13 Tanker Sank Vessel exploded and broke in two off Nova Scotia whil e carrying gasoline from Amsterdam to New York.
Nov- 88 Oriental Phoenix 138, 392 1971 17 Tanker Sank Broke in two amid heavy seas in north Atlantic on crude oil voyage from UK North Sea to Canada.
Jan- 93 Braer 89,730 1975 18 LBR Tanker Sank Engine f ail ed off Shetland Is. i n heavy seas, on Norway- Canada crude voyage. Stranded & broke in two.
Run 11,660 1955 34 Tanker Sank
Sep- 93 Altair 20,848 1982 11 PAN Tanker Sank Broke in two and sank off Malaysi a f ollowing explosion duri ng tank cleaning.
Aug- 92 Borburata 30, 500 1981 12 VEN Tanker Sank Wrecked. Fire in pump room & engine room on bal last voyage f rom Curacao to Punta Cardon.Jan- 94 Cosmas A 27,643 1974 20 MLT Tanker Sank Sank in South China Sea after explosion during laden crude oil voyage from Dumai to Shanghai.
Feb- 94 Albinoni 16,900 1976 18 BHS Tanker Sank Broke in two after explosion during ballast voyage from Dominican Republic to Venezuela,.
Sep- 94 Burak M 132,250 1976 18 TUR Tanker Sank Sank off Sierra Leone on ballast voyage from Turkey to West Africa.
Oct- 94 Thanassis A 38,263 1976 18 MLT Tanker Sank Broke in two and sank in heavy weather in South China Sea on laden voyage from Nakhodka to Singapore.
Dec- 95 Sea 1 275,782 1990 5 CYP Tanker Sank Grounded off southern coast of South Korea. Declared total loss. Later sank under tow to Subic Bay.
Nakhodka 20,471 1970 27 RUS Tanker Sank Stern sank after vessel broke in two 110 km north east of Oki Islands in the Sea of Japan
Dec- 99 Erika 37,283 1975 24 MLT Tanker Sank Broke in two in Bay of Biscay and sank.

Table 8.2 – (*Continued*)

Ship Age Type Cargo Case date Deadweight Heavy Casualty details
No. Range Weather
1000 tonnes Recorded

1 15 Bulk Grain Jan 90 20–25 Yes * Missing
2 19 Bulk Iron Ore Jan 90 100–110 Yes * Hull damage. Holds flooded
3 17 Bulk Coal Jan 90 65–70 Yes Side shell lost No. 1 hold
4 19 OBO Iron Pellets Jan 90 85–90 Yes Heavy weather damage
5 9 Bulk Iron Ore Feb 90 120–130 Yes No. 8 side shell lost
6 24 Bulk Phosphate Feb 90 40–45 * Damage in No. 2 hold (flooded)
7 20 Bulk Ballast Feb 90 40–45 Yes Fracture No. 1 hold
8 23 Ore Iron Ore Mar 90 90–100 * Foundered
9 21 Ore Iron Ore Mar 90 75–80 * Ballast tank leak
10 22 Bulk Barytes Apr 90 55–60 2 m fracture in No. 6 hold
11 13 Bulk Iron Ore May 90 120–130 * Hull damage. Flooded
12 12 Bulk Iron Ore May 90 65–70 Yes * Fractures in holds 2 & 3
13 23 Bulk Iron Ore Jul 90 80–85 Yes * No 3 hold flooded
14 18 Bulk Cement Jul 90 25–30 Yes * Bow lost & keel fractured
15 9 Bulk Coal Aug 90 140–150 Side shell damage
16 17 OO Iron Ore Sep 90 130–140 * Missing
17 19 OO Iron Ore Oct 90 150–160 Yes * Presumed to have foundered
18 14 Bulk Iron Ore Oct 90 120–130 Fractured side shell
19 17 Bulk Iron Ore Oct 90 120–130 Wasted side shell framing in No. 3 hold
20 21 Bulk Bauxite Nov 90 35–40 Yes Fractures in holds 2, 3 & 6
21 19 Bulk Ballast Nov 90 65–70 Yes 12 m fracture in No. 5 hold
22 14 OBO Iron Ore? Nov 90 110–120 Yes Heavy weather damage – sent to scrap
23 18 Bulk Iron Ore? Dec 90 120–130 Yes Bulkhead frames loosened
24 17 Bulk Potash Dec 90 35–40 Yes * Fractures in No. 2 hold
25 18 Bulk Iron Ore Jan 91 65–70 Yes Damage to frames in No. 1 hold
26 24 Bulk Iron Ore Jan 91 80–85 Yes * No. 2 & 4 holds flooded
27 19 Bulk Iron Ore Jan 91 75–80 Yes Fractures & detached frames in two holds
28 24 Bulk Iron Ore Jan 91 50–55 Yes * Fracture in No. 5 hold. Flooded
29 21 OBO Iron Ore Feb 91 150–160 * Fracture in No. 1 hold
30 14 Bulk Ballast Feb 91 25–30 Fractures in No. 3 WB hold
31 24 Bulk Pig Iron Feb 91 25–30 * Took water after striking object
32 17 Bulk ? Mar 91 110–120 Frames detached from No. 6 hold
33 24 Bulk Iron Ore Apr 91 55–60 * No. 1 hold flooded
34 21 Bulk Iron Ore Apr 91 55–60 * Fracture in No. 4 hold. Flooded
35 9 Bulk Iron Ore Apr 91 140–150 Yes * Missing
36 16 Bulk Iron Ore May 91 150–160 Fracture in No. 1 hold
37 16 OO Iron Ore May 91 130–140 Yes Fracture in hull below waterline
38 15 Bulk Iron Ore Jul 91 110–120 * No. 3 hold flooded
39 21 Bulk Steel Aug 91 20–25 * Grounded No. 1 hold flooded
40 21 Bulk Iron Ore Aug 91 140–150 Severe crack No. 7 hold
41 16 Bulk Iron Ore Aug 91 70–75 * Ingress of water No. 1 or 2 hold
42 12 Bulk ? Aug 91 35–40 Shell fracture frames detached No. 3 hold
43 14 Bulk Steel Aug 91 35–40 Yes Heavy weather frames cracked
44 23 Bulk ? Aug 91 50–55 Disabled towed to safety
45 24 Bulk ? Aug 91 65–70 No. 5 hold frames fractured
46 18 OO Crude Oil Aug. 91 250–260 Hull frames
47 18 OO Oil? Sep 91 75–80 Shell fracture oil leakage
48 23 Bulk Phosphate Oct 91 25–30 Yes * Sank in mediterranean
49 18 Bulk To Load? Oct 91 120–130 Fractures in deck
50 14 Bulk Loaded Nov 91 35–40 Extensive corrosion of shell plating
51 25 Ore Iron Ore Nov 91 75–80 Yes * Leakage in heavy weather
52 18 Bulk Steel/Mcy Nov 91 25–30 No. 2 hold flooded rip in side
53 18 Bulk Iron Ore Nov 91 60–65 Yes * Cracks in side shell most holds
54 20 Bulk Iron Ore Dec 91 120–130 Side shell fracture
55 26 Bulk ? Jan 92 25–30 Hull leaks when on voyage to breakers

* = missing/sinking

Table 8.3 – *Bulk carrier losses (over 20,000dwt) due to structural failure, 1990-1998 (Lloyd's Register)*

Ship No. Age Type Cargo 1000 tonnes Case date Range Deadweight Recorded Heavy Weather Casualty details

56 25 Bulk Calc Nitrate Jan 92 25–30 Leakage into fore peak and double bottom
57 21 Bulk Coal Jan 92 130–140 Detained for extensive repairs
58 18 Bulk Grain Feb 92 65–70 Yes Upper deck fracture heavy weather
59 23 OBO Iron Ore Mar 92 110–120 * Engine room flooded
60 24 Bulk Iron Ore May 92 65–70 * Side shell fracture and progressive flooding
61 20 Bulk Iron Ore Aug 92 100–110 Bulkhead between holds 8/9 collapsed
62 19 OO Iron Ore Aug 92 220–230 Damage to side shell P & S
63 22 Ore Iron Ore Oct 92 120–130 Yes * Missing in typhoon
64 18 Bulk ? Oct 92 45–50 No 5 hold side frames adrift
65 19 Bulk Coal Nov 92 65–70 Severe structural wastage to topside tanks, fractures, etc.
66 20 Bulk Coal Nov 92 110–120 Structural cracking
67 16 Bulk Iron Ore Dec 92 120–130 Taking water No. 1 hold, hull fractures
68 19 Bulk Gypsum Mar 93 25–30 Yes * Sank in heavy weather
69 24 Bulk Coal May 93 70–75 Yes * Sank after loss of hatch cover
70 19 OBO Iron Ore Jun 93 120–130 Damage frames in No. 3
71 19 Bulk Steel Jul 93 25–30 No. 4 hold internals adrift and buckled
72 19 Bulk Iron Ore Jul 93 130–140 No. 5 hold framing damaged
73 25 Bulk Phosphate Nov 93 55–60 Hole 12 m x 6 m in No. 1 hold P & S
74 21 OBO Iron Ore Dec 93 100–110 No. 2 hold side shell leak
75 13 Bulk Wheat Dec 93 25–30 Took water in Nos. 1 & 7 holds
76 21 OO Iron Ore Jan 94 160–170 Yes * Sank in North Atlantic
77 24 Bulk Scrap Feb 94 25–30 Yes * Reported water in No. 1 hold
78 21 Bulk Mn Ore Mar 94 120–130 * Cargo damage, sailed with incomplete repairs class deleted, sank June
79 18 Bulk Ballast Mar 94 130–140 Yes No. 4 hold side shell and framing damage
80 20 Bulk Iron Ore Mar 94 130–140 Yes Heavy weather damage to hull
81 13 Bulk Iron Ore Jun 94 130–140 47 m crack in topside tank
82 13 Bulk Iron Ore Jun 94 120–130 No. 1 side shell holed
83 21 Bulk Iron Ore Jun 94 130–140 Yes * Disappeared
84 23 Bulk Mn Ore Aug 94 25–30 Side shell fracture
85 26 Ore Iron Ore Sep 94 90–100 Yes * Crack on starboard side and water ingress
86 22 OBO Iron Ore Nov 94 130–140 * Broke back while loading
87 22 Bulk Grain Nov 94 20–25 * Sank North of Guyana
88 20 Bulk Cu Ore Nov 94 25–30 Yes No. 3 hold crack, 2 holds flooded, heavy weather
89 12 Ore Iron Ore Dec 94 260–270 Yes Buckling of cross deck strips, typhoon
90 20 Bulk Iron Ore Mar 95 120–130 § Cracks in shell/frames refuge
91 22 Bulk Potash Apr 95 25–30 Shell fracture
92 22 OBO Ballast Jul 95 160–170 Yes Cracks in bow sector
93 21 Bulk Iron Ore Nov 95 80–85 Yes Deck fracture
94 17 Bulk Ballast Dec 95 50–55 Yes No. 5 hold fracture
95 17 Bulk Soda ash/steel Dec 95 35–40 Yes * Cracks, 3,4,5 holds sank
96 18 Bulk Steel Jan 96 25–30 Yes Water in 1 & 2 holds via vents
97 26 Bulk ? Jan 96 25–30 Yes Water in holds via hatch covers
98 23 Bulk Gypsum Feb 96 20–25 Yes * Sank in heavy weather
99 20 Bulk Rice Feb 96 25–30 80 cm hull fracture, cargo damage
100 23 Bulk Iron Ore Feb 96 65–70 Yes * Sank in heavy weather
101 26 Bulk Coal Feb 96 50–55 Yes Took water in holds
102 26 Bulk Coal Feb 96 50–55 Yes Took water in holds
103 16 Bulk Iron Ore Sep 96 130–140 Yes * Took water in Nos. 1, 2 & 3 holds
104 16 Bulk Ballast Nov 96 140–150 Ballast hold bulkhead collapse
105 21 Bulk Apatite Feb 97 20–25 Yes * Bow damage
106 21 Bulk Steel Mar 97 25–30 Yes * Missing in heavy weather
107 26 Bulk Ballast Jan 98 25–30 Yes * Broke in two in heavy weather
108 13 Bulk ? Jan 98 45–50 Yes No. 1 hold flooded, shell fractures
109 25 Bulk Iron Ore Feb 98 30–35 * Sank no details

* = missing/sinking

Table 8.3 (*Continued*)

Total built since 1960	6586	
Building or on order	342	
Total losses - all causes	303	
Summary of total losses	**Number of ships**	**Percentage of total losses**
losses by fire and explosion	56	18.5
war casualties	29	9.6
wrecked or stranded	76	25.1
collision or contact with a submerged object	27	8.9
cargo shift	4	1.3
engine room flooding	8	2.6
machinery damage	13	4.3
known or possible hull damage	76	25.1
missing unexplained	14	4.6

Table 8.4 – Total losses of bulk carriers since 1960 (Lloyd's Register)

Cause of incident	**Losses (1991-2000)**
Contact grounding	30
Structural	29
Machinery fire / explosion	20
Flooding	15
Contact collision	15
Disappearance / unknown	10
Machinery failure	7
Cargo loading / unloading	3
Contact object	2
Cargo fire / explosion	2
Capsize / cargo shift	1

Table 8.5 – *Bulk carrier losses between 1991 and 2000 (Intercargo)*

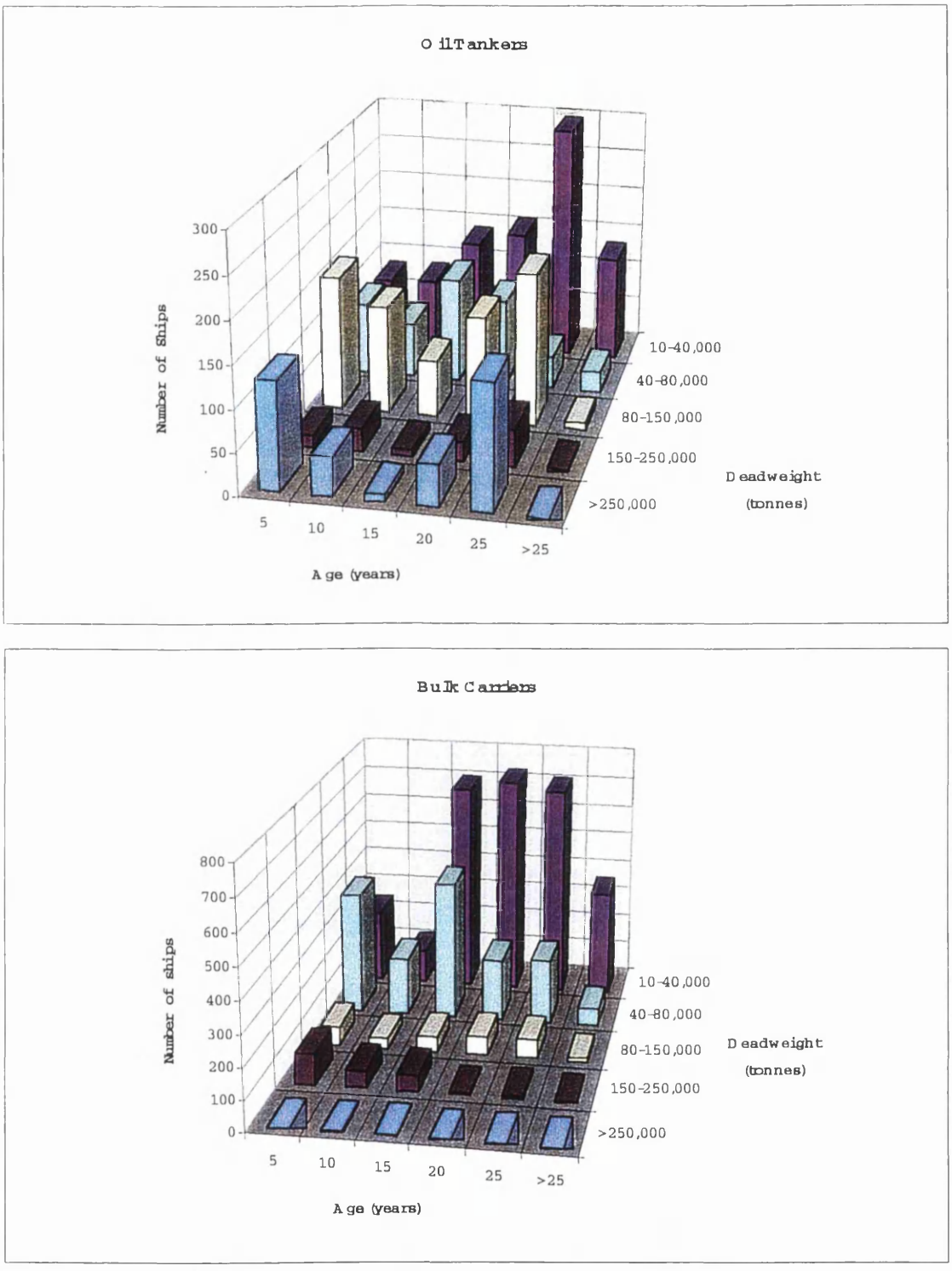

Figure 8.1 – *Age of oil tanker and bulk carrier fleet (over 10,000dwt), in 1997, (Keith 1997)*

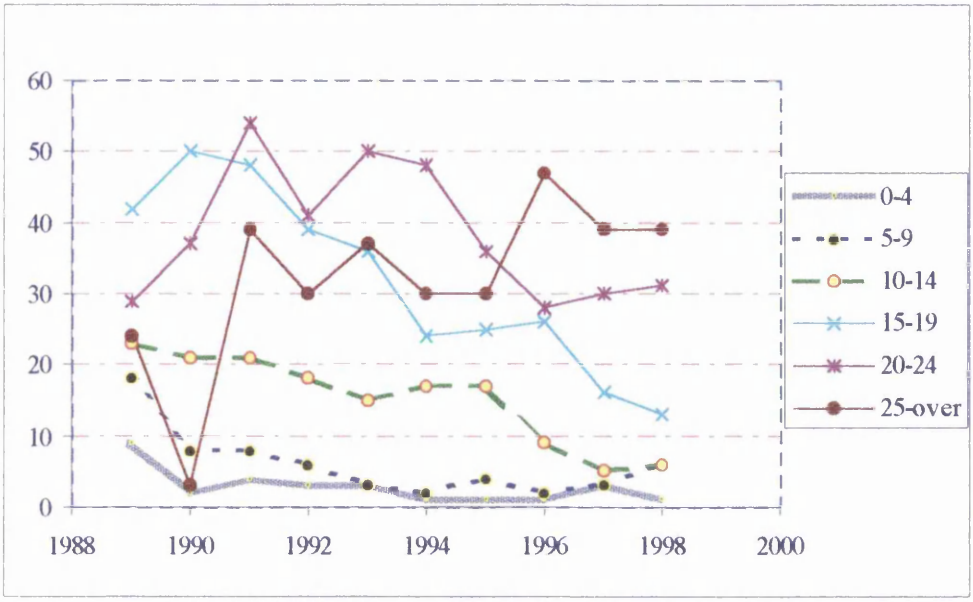

Figure 8.2 – *Number of ship losses by age, (Intercargo)*

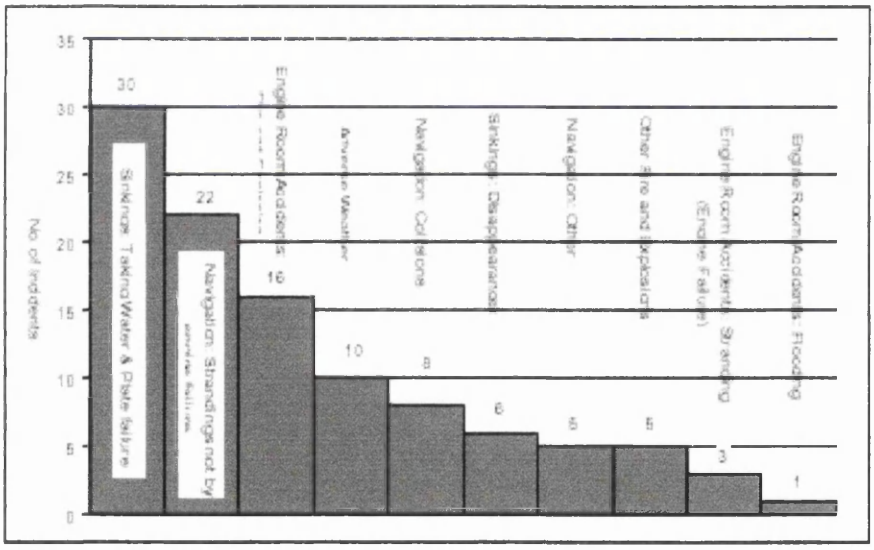

Figure 8.3 – *Bulk carrier losses by cause, 1990-1997 (Intercargo)*

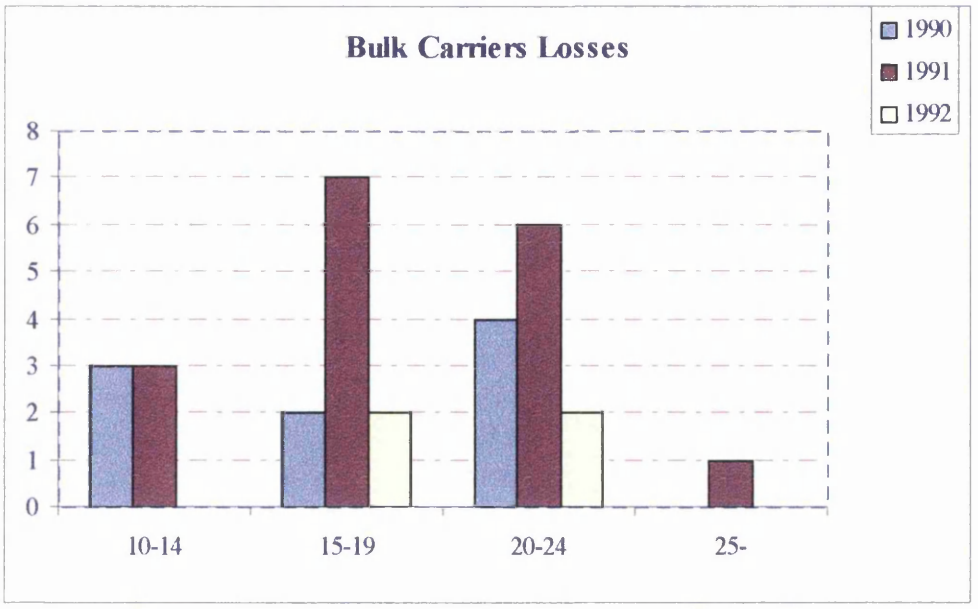

Figure 8.7 – *Bulk carrier losses due to fracturing during the period 1990 and 1992, (Lloyd's Register)*

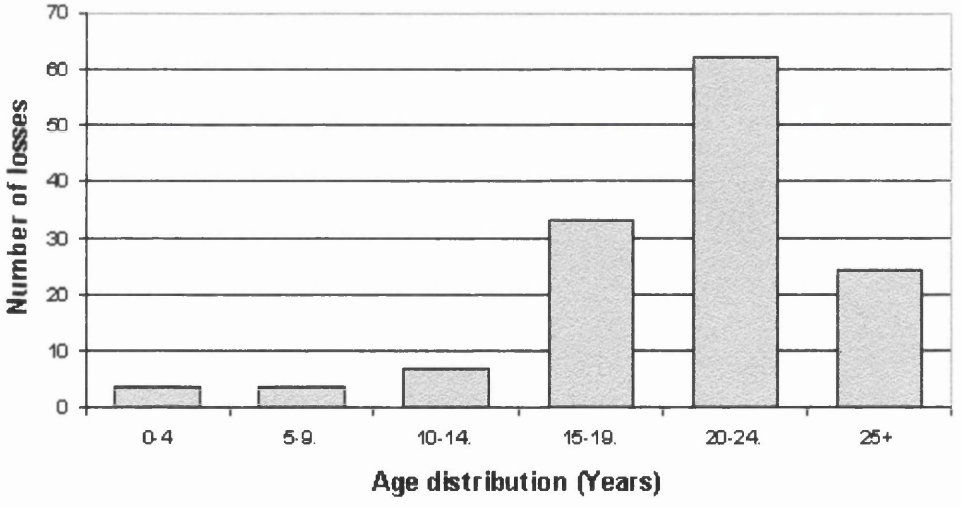

Figure 8.8 – *Bulk carrier losses by age, 1991-2000 (Intercargo)*

CHAPTER 9

SUMMARY & CONCLUSIONS

9.1. Review of the Main Assumptions and the Work

9.1.1. Review of the Work

In this thesis, the aim was to establish a methodology to calculate the failure probability of a complete ship structure, in particular a bulk carrier, because of fracture. The work undertaken in this thesis can be split into two parts

i) One first part that contains the analysis

ii) A second part that contains the developments of the study

The first part includes all the analytical work that was carried out during this study and involved the combination of advances in many engineering fields so that the aim of this thesis could be achieved.

Load determination was one of these tasks. Fatigue and extreme load in several different locations of the ship had to be calculated. Response analysis was first performed using strip theory and then used first principles stress analysis to translate the loads into stresses.

The modelling of the crack growth phenomenon and accounting for all the other complex phenomena that occur together with crack propagation (e.g. the threshold region, crack inside residual stress field, corrosion, and retardation effects) was another task of the thesis. This involved the use of fracture mechanics.

Another important part of the analysis was to model when fracture occurs. This involved the use of advanced fracture mechanics theories such as the use of the strip yield plasticity correction model, instead of using the more rigorous elastic-plastic fracture mechanics theory.

Finite element analysis was needed to determine stress intensity factor solutions for complicated ship structural details. This also involved modelling the crack growth process with the finite element code. Stress intensity factors were then obtained for real ship structural details that were not available in the literature, (e.g. a stiffened panel).

Finding an appropriate method to undertake reliability calculations was also important. Two general-purpose reliability codes were tried, for the reliability

analysis. However, because of the complex limit state function neither code was capable of solving this problem. The only method that produced results was the simulation method used in a special purpose code which was written as part of this PhD work. Hence the simulation method had to be adopted.

There are other reasons however, why these general purpose codes could not be used. First the reliability calculations for this analysis are time dependent, since crack size increases with time. And although reliability calculations were possible using the codes, crack growth calculations could not be performed.

The general codes also could not deal well with system effects (e.g. multiple crack sites, correlation). And since the aim of this project was to determine the reliability of a ship structure as a whole, which contains many thousands of cracked members, a special purpose code had to be written.

Techniques to improve the efficiency of the simulation method were also tried, e.g. variance reduction techniques (importance sampling using an adaptive search algorithm) but these failed because of the complexity of the limit state function. It was found that only the simplest of simulation methods could provide reliable results (in particularly the Monte Carlo method).

For the development part of the thesis, one of the main tasks was to write a computer code that performed crack growth and reliability calculations simultaneously. In addition system effects are incorporated, hence many cracks can be investigated at the same time. Each crack has its own input data, to model the fact that cracks are in different locations along the vessel. It is then possible to study which cracks contribute the most to the failure probability. Correlation between members can also be studied, e.g. the fact that basic variables between members are not independent as is the case in loading.

This special purpose code is capable of performing time dependent reliability calculations of a system of cracks. However, because of limitations in hardware, this code could not be used to calculate the reliability of a whole ship structure. A real ship structure contains thousands of cracks, and the computer memory was not sufficient to account for all these members. Furthermore, the computational time required would be prohibitive for such big runs.

The need for a simpler approach was evident. This approach was developed as part of the thesis. It reduces the complicated case of a system of cracks in a ship structure to a very simple case. A case where only two variables must be determined: The load and strength parameters for the whole ship structure. The probability of failure can then be calculated using a method called the convolution integral, which simply calculates the probability that the load exceeds the strength of the structure.

However, to calculate the load and strength distributions for the whole ship structure, information on the load and strength distributions for individual cracks is necessary, and this is obtained from the sophisticated special purpose computer code written in this thesis. Another, simpler computer code was then written to use this information and calculate the convolution integral and hence the failure probability of the ship structure. The key feature of this simplified method is that it uses information only for a few individual cracked members and calculates the failure probability of the ship structure in a very time efficient manner.

Some comparisons were made for simple systems between results from the sophisticated computer code and the convolution integral method and these agreed reasonably.

In general, it has been shown in this thesis, how a very complex problem can be reduced to a simpler problem if the appropriate assumptions are made. It is also shown that the assumptions associated with the method (i.e. assuming independence when there is some correlation and using the same load distribution for every location) work well and do not negate the results of the simplified method when compared with simulation results.

9.1.2. Review of the Main Assumptions

It was decided that for the input data used, simplified assumptions must be made. Input data is used in order to demonstrate the methodology, and not to analyse a specific bulk carrier. By providing and demonstrating the method, it is then feasible to perform fracture assessment for a specific vessel, if appropriate data is available.

It has been shown from chapters 1 to 7 that probabilistic fracture assessment requires bringing together many different parts. The various parts can be summarized below

- Load estimation
- Stress analysis
- Short and long term statistical analysis
- Crack propagation
- Fracture assessment
- Reliability analysis

Every part has assumptions associated with it in order to justify its use in the thesis.

Load estimation was done using linear strip theory. It has been proved that for box shaped structures (e.g. bulk carriers, oil tankers) it provides good results for low and medium sea states (especially for head and beam seas). It is hence appropriate to calculate fatigue loads which are induced by the low frequency wave forces acting on the ship, particularly in medium sea states. Where non-linear effects are important e.g. pressure distribution at the side shell due to dynamic wave loading in extreme sea states then 3D diffraction theory can be used. It is also possible to use linear strip theory with corrections based on 3D analysis.

First principles based on beam theory are used to translate loads in stresses for simple structural details. This method is also suggested as an alternative by classification societies in their strength assessment rules. The other more advanced method is to use FEA to evaluate local stresses. However, this involves the creation of a global model of the vessel and very good modelling of the local structural details. Of particular importance is the correct assignment of external loads and boundary conditions. FEM are used when very accurate stress analysis is required for a particular detail i.e. in order to improve the design to reduce SCF or any hot spot stresses. In this thesis the objective is to estimate stresses at a more general level so that they can be used at many locations along the vessel by using appropriate scaling factors.

The description of the sea state is important when predictions are made for the extreme and the fatigue loads. One fundamental assumption used in this thesis is that the sea state can be described by the Rayleigh distribution. This presupposes that the wave environment is narrow banded. The narrow band assumption produces slightly conservative results. Correction factors can be introduced for a wide band process.

The narrow band assumption is valid for an irregularity factor ε less than 0.6. From the spectral analysis it was calculated that the irregularity factor is always below 0.6, and hence no correction was applied.

When more than one sea state is considered, which is the case in this report, the probability distribution for the combined sea state no longer follows a Rayleigh distribution. A good description is achieved when using the Weibull distribution, which is used in this thesis. The Weibull distribution properties are used to determine the mean value of the fatigue loads. The extreme wave induced stresses, are determined by applying the theory of extreme statistics to the parent distribution of stress amplitudes, which is again assumed to follow the Weibull distribution. The extreme stress used in this thesis represents the extreme stress the vessel will see in one year, since the analysis is performed on a year by year basis.

Fatigue loads need to be determined for crack growth analysis. Every stress cycle causes the crack to grow. Ideally, each stress range in the stress history must be considered. However, stress history is not always available, and when it is, stress ranges must be extracted and this is time consuming. A simpler approach calculates an equivalent stress range, which would cause the same amount of crack growth as the actual stress range history. This is also the best available method to perform long-term fatigue and crack growth analysis.

Another assumption used in order to simplify the analysis is that each wave heading has equal probability of occurrence. If a specific vessel was considered then there would be more information about her sea route and a better estimation of the wave headings would be possible. In some cases though (depending on the route and master's decision) the vessel is preferred to face head waves which do not introduce torsional loads, and cargo shifts (which result in impact loads at the side structure). The probability of sea state occurrence is calculated from the sea scatter diagram for selected areas of the Atlantic Ocean. A simplified spectral analysis is carried out which combines all sea states and calculates fatigue lives for selected structural details.

Crack growth calculations are performed using linear elastic fracture mechanics. Paris' law is adopted which is simple to use and provides good estimates for the

middle region of the crack growth curve where cracks spent most of their time. By appropriately selecting material constants, the effect of corrosion and stress threshold can be taken into account. Other forms of crack growth laws are available but require more information on material properties and loading, e.g. stress ratio, fracture toughness, effective stress intensity factor. Crack closure has not been considered because of the presence of the residual stresses.

Fracture assessment is based on a FAD. Because of the plastic zone in front of the crack tip, linear elastic fracture mechanics cannot be used to describe the failure condition. The plasticity correction is taken into account by using the strip yield fracture criterion which is a simpler way to evaluate the fracture strength and is using the linear elastic stress intensity factor rather than the *J-integral* approach which requires a non-linear analysis. This approach was developed for materials exhibiting elastic-plastic behaviour i.e. a region between brittle and ductile modes of failure. It is justified for ship steels, which exhibit some ductility.

Most of the parameters are treated as random variables to account for their uncertainty. The uncertainty is modelled through a probability distribution defined by a mean value, a standard deviation and a distribution type. In the distribution of the fracture toughness a lower cut-off value has been introduced so that very low value with an unrealistic high probability are ignored.

Reliability analysis is performed using simulation techniques. This method is suitable for very complicated analysis and can be used also for time dependent assessments. The main limitation is the time it requires to produce acceptable results (i.e. with low coefficient of variation), and storage space (computer memory). An attempt to use variance reduction techniques (importance sampling) was not successful for many reasons. First the shape and type of the crack size distribution with time was not easy to determine, and a numerical distribution had to be used. This involved a separate simulation. Secondly, the joint p.d.f. which is required to evaluate the failure probability cannot be determined in the case when members are correlated. Therefore correlation effects could not be studied. Thirdly, because of the very non-linear limit state function, the search algorithm used with the importance sampling to improve its efficiency could not establish an approximate design point because of the many local minima close to the origin.

Although it is feasible to account for system effects using Monte Carlo simulation, it is not possible to consider many members (crack sites) in the system (maximum members approximately 100), whereas an actual ship may have thousands of cracks.

A simplified method has been developed that allows the evaluation of the failure probability of a ship structure containing a large number of cracks. Although simulation technique is not used to calculate the failure probability of the complete structure, it provides the basis. Using the theory of extreme statistics, it is possible to reduce the problem to its basic form with only two variables, i.e. the probability that the load applied will exceed the strength of the structure. This can be solved by evaluating the convolution integral.

There are two parameters to determine, the load and strength probability distributions. Load and strength distributions change with location. First, the load and strength distributions at each location must be determined. These are obtained for single crack sites from the simulation method as numerical distributions.

By normalising the load distribution for each location by its own mean value, it is shown that every distribution is approximately the same with each other in the normalised co-ordinate system. That means that the total load distribution will also be the same with any load distribution. This assumption is also supported by the fact that loading is assumed fully correlated, and loading distributions have the same form. If different shapes are required then a more complicated procedure will also be necessary. Load is assumed constant (i.e. its mean value stays the same with time) and only natural variability is taken into account by re-sampling. The effect of different sea routes can be an interesting case for study.

The total strength distribution is determined using the smallest extreme value distribution of all the individual strength distributions. An attempt was made to fit to the (numerical) parent strength distribution an analytical distribution. That would allow easier evaluation of the minimum extreme value distribution and easier evaluation of the convolution integral (e.g. by using the extreme type I distribution which is the extreme value distribution for parent distributions having an exponential decaying tail). However, fitting an analytical distribution to the (numerical) parent distribution did not yield good results (when compared with simulation results). The

extreme value distribution determined from the fitted parent distribution and from the actual numerical distribution were different. A solution would be to fit an analytical distribution only to the tail end of the parent that is important and not to the full distribution.

The total minimum value distribution is obtained assuming all strength distributions of members are independent of each other. This is not true since there will always be some degree of correlation between the strengths of different locations because loading is assumed correlated, and this inevitably introduces some correlation in the strengths as well. However, when the failure probabilities are small the effect of correlation is also small, as it has been shown in the example case studied in this thesis.

Because strength reduces with time (due to fatigue cracks growing larger with time and corrosion), strength must be determined with respect to time. Hence, new simulations are performed at every time interval. It would be very interesting if a model could be established to evaluate the strength distribution without the need to perform simulations at every time interval, which is very time consuming. Finding a probability distribution that could fit the strength data would be a nice solution to the problem. That would allow rapid calculations to be performed.

9.2. Significance and Application of the Work

It was shown in chapter 8 that even today ships are lost because of fractures. The problem is more serious in bulk carriers for a combination of reasons. The increased average age of the bulk carrier fleet is one. The structural strength of the vessel reduces with time because of corrosion and fatigue. Ageing together with improper maintenance creates a high risk of failure.

The other reason is the cargo. The majority of the bulk carrier losses due to fracture were attributed to vessels carrying iron ore. This is one of the highest density cargoes and results in a highly stressed structure. This, in combination with reduced strength due to large fatigue cracks and corrosion is likely to result in fracture.

Many ship owners will want to extend the operational life of the vessel subject to regular inspections and maintenance. The methodology developed in this thesis

allows a check against fracture failure of the vessel. It is also possible to determine inspection intervals so that the reliability is maintained to a specified target value and hence decide whether it would be economical and safe to the ship.

For better estimates from the reliability calculations actual data on loading can be used, taken from stress records of the real ship e.g. from readings of stress measuring devices placed on board the vessel at important locations at the deck, side shell and/or bottom structure. This would allow also the calculation of the probability of failure for shorter time intervals e.g. a month or a week i.e. a typical duration of a voyage. That would prove particularly interesting to the ship owner, since by knowing the structural condition of the vessel before the voyage, and by specifying the load on a week by week or even a day by day basis, it would be possible to estimate the failure probability at the end of the trip. A decision can then be made of whether or not it is safe to allow the vessel to sail, (or perform an inspection before).

Information available on board of the vessel e.g. loading, crack sizes, crack locations could be used to update the estimates of the method. E.g. by sending this information from the vessel to the head office, the calculations can be performed and then inform back the ship's master for the up to date condition of the vessel.

The methodology can also be used by classification societies to calibrate their safety factors of their rule-based designs. This can result in reduction of the safety factors if it can be proved that the design is very conservative (very safe because of very low failure probability). Reduction in safety factors results in reduction in scantlings and therefore more economical designs.

9.3. Conclusions

- A special purpose code performing time dependent reliability calculations had to be written, because general purpose reliability programs failed to produce results
- The simulation method (Monte Carlo) was found to be the best way to carry out the complicated analysis required for this work. Methods to improve the efficiency of the simulation method (variance reduction techniques) did not

work because of the complex limit state function. Also it proved difficult to incorporate system effects with the variance reduction techniques

- Because of limitations in computer memory and speed, the simulation method could not be used for a real ship study, which contains thousands of cracks
- A new methodology to calculate the probability of failure because of fracture of a whole ship structure containing multiple crack sites has been developed based on the convolution integral method
- The results from the simulations and the simplified method agreed reasonably well for simplified systems and checked against theoretical solutions. The results are only used to demonstrate the methodology
- Better data representation would produce more accurate results that can be used in a design analysis, (e.g. more accurate crack growth data, load estimation for specific details, fracture toughness modeling with temperature, bending moment that varies with time and location). Results from this analysis can also be used to calibrate existing safety factors in deterministic codes
- Results from this analysis were checked against bulk carrier losses due to fracture, and the trends agreed well (e.g. high risk of failure for older vessels, reducing the risk by inspecting regularly)
- Fracture mechanics theory was used for crack growth analysis, accounting for corrosion, residual stresses and threshold effects. Retardation effects were not considered because of the presence of the tensile residual stress field
- Fracture assessment was based on the strip yield plasticity correction model which accounts for the plastic zone in front of the crack tip. Hence, the need to perform rigorous elastic-plastic fracture mechanics calculations (probably using finite elements) was avoided
- Stress intensity factor solutions for real ship structural details which were not available in literature (from stress intensity factor handbooks) were established using finite element analysis (e.g. stiffened panel)

- A spectral fatigue analysis was performed to obtain the long-term stress range distribution which was fitted to a Weibull distribution. The Weibull distribution shape factors agreed well with what classification societies suggest

9.4. Recommendations for Further Research

Reliability analysis deals with uncertainties. The more reliable the data, the better the estimate of the analysis. One of the areas for future work is the collection of data. Important data for the analysis is related to material properties. Parameters that affect the results of the analysis are the crack growth constants used in Paris' law. Most of the data comes from testing on laboratory specimens. These hardly represent the real cracked components. Testing of real ship structural details is needed for a better estimation of the crack growth, including also the effect of corrosion.

Better data on the initial crack size distribution is also needed. Collecting data from measurements in production welds, or from measurements during inspection of ship structures can improve the data. Also crack distribution and number of cracks in ships requires more attention. By studying the crack distribution in a vessel it would be possible to see which parts of the structure are more critical.

Fracture toughness varies with temperature. It could therefore been modelled with respect to sea route (i.e. temperature). A joint distribution for fracture toughness and temperature would be required.

Physical models also need further improvements. A better representation of the long-term fatigue loading can be based on actual stress records instead of mathematical models describing the sea states. This would allow the calculations to be performed for shorter time intervals as well as long-term periods. Sequence effects could also be studied, and see whether any crack retardation is possible.

Crack growth calculations are based on Paris' law which is an empirical formula and is very much dependent on material constants. Better models might become available which would deal better with crack tip plasticity and threshold effects.

A further improvement would be to model the effect of inspection dependent on location, therefore accounting for difficult to reach areas, low lightning conditions and dirty areas.

A more efficient way to perform the reliability calculations will also be needed in the future, as the simple Monte Carlo simulation requires a lot of computer space and time. Variance reduction techniques can be used for that reason. However, they must be combined together with a time-dependent (crack growth) analysis very carefully so that they can use the up to date information for the distribution of the crack sizes (i.e. the time-dependent distribution).

Other parameters could also be modelled as time-dependent variables when a model is known to describe their variability with time (e.g. fracture toughness, bending moment, fatigue and extreme loading).

Of course, it is very difficult to check reliability analysis results with exact figures from actual data, since results from the reliability analysis are only an estimate which takes into account various uncertainties. The reliability results were obtained using many samples from probability distributions. For exact estimate of the failure probability from the real data, many more ships (samples) would be needed.

However, it is encouraging that using reliability analysis we can determine the trend of the failure probability of a ship structure (a bulk carrier in this example). Although, the absolute values may not be exactly the same (due to the many uncertainties involved), the proposed methodology should be able to provide guidance on inspection scheduling and make the vessel operation more efficient and safe.

APPENDIX A

MULTIAXIAL FATIGUE ANALYSIS USING FIRST PRINCIPLES

A.1 INTRODUCTION

This is a brief study into the simplified fatigue analysis of a bulk carrier. It is intended

1) to help understand the complex behaviour that would usually be studied using finite element analysis

2) to provide a fatigue analysis suitable for the use with the reliability analysis in this thesis.

It is not intended as a suitable methodology for assessment purposes.

This work was undertaken together with Jason Lambos, also as part of his M.Sc. thesis.

A.2 LITERATURE SURVEY

In this study, the fatigue behaviour of certain structural details is investigated. The most important aspect in a fatigue analysis is the determination of the fatigue loading and from there the stress distribution. DnV, [1], provides method of calculation stress distribution, and methods of performing fatigue analysis, mainly concentrating on mobile offshore units. Barltrop, [2], provides very useful information on fatigue analysis methods and methods for predicting wave loads.

For certain connections of a ship structure, (e.g. frame stiffeners), particular importance plays the wave pressure distribution at the side of the vessel. Because this pressure is not linearly varying with wave height, spectral analysis is not accurate for predicting the response to this loading. Barltrop, [2], describes several methods for calculating the response to this wave pressure by considering, a) the pressure profile into four regions, and b) by considering the cubic weighted wave pressure.

The method of spectral analysis is also well presented by Cronin, [11]. Cronin describes the full spectral analysis together with an useful example of a steel jacket. The fatigue behaviour of longitudinal stiffeners of an oil tanker and a containership subjected to dynamic loads is analysed by Xue, Pittaluga, and Cervetto in [20], again

applying spectral analysis, and including the pressure distribution at the sides of the ships.

Xu, [19], summarises the work of a five year research program on fatigue and fracture reliability that was conducted in University of California. In the paper presents an example fatigue damage calculation and the recommendation for a better design for the fatigue strength.

The presence of corrosion in ballast and cargo tanks results in a reduction of the fatigue life. Ref.[8], contains useful corrosion data for welded marine steels and details. It is also a very useful reference for fatigue and fracture methodologies.

Fatigue cracking of structural details due to cyclic loading has been a very serious concern in the operation of ships. This is a common problem for ships subjected to wave loads, which induce fatigue damage, especially in structural details with high stress concentrations. Although this damage is not responsible for the loss of the ship, it is often the cause of costly repairs and replacements of part of the hull structure, which greatly influence the serviceability and operational economy.

Since higher tensile steels have been used extensively, for reducing ship steel weight, ship classification societies, designers, and builders have devoted more consideration to fatigue behavior. This is due to the fact that high tensile steel structures have higher operational stress level but no improvement in fatigue properties compared with that of mild steel structures.

One problem for ship structures when performing a fatigue analysis is the number and variability of structural elements to be considered. Another difficulty is the determination of the stress ranges considering the complexity of the load components acting on these locations.

A.3 ENVIRONMENTAL MODEL & SERVICE PROFILE

The surface of the sea is subdivided into regions called Marsden zones, [13]. Each of these zones covers a geographic area over which the wave statistics have been estimated, i.e. the significant wave height, wave period, frequency of occurrence. For

this report, 4 different zones, (6, 7, 10 and 11) have been selected, and the corresponding scatter diagram was calculated and can be seen below

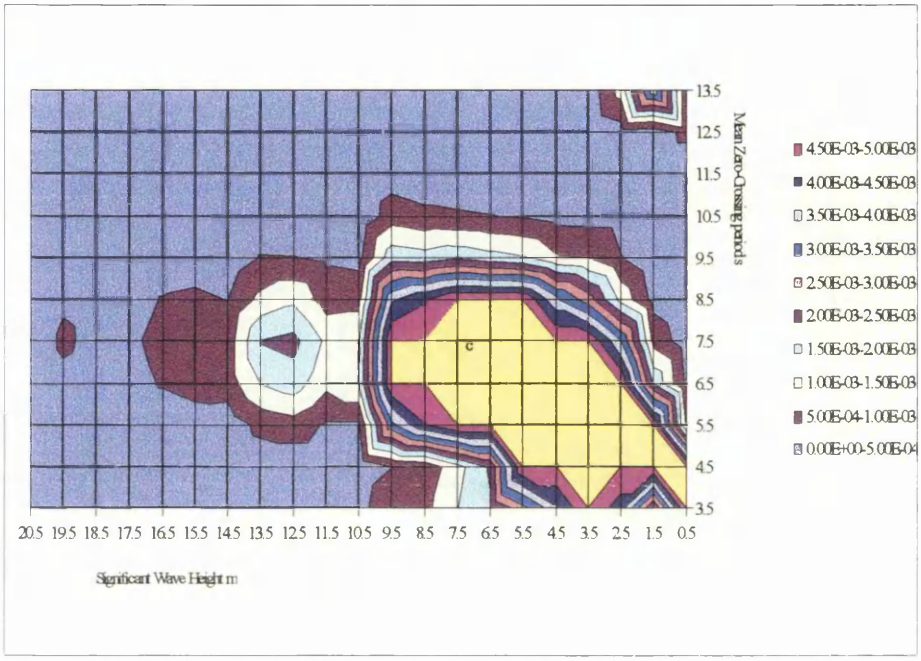

Figure A.1 – Sea scatter diagram for the selected regions in the Atlantic Ocean

For this study the ship speed has been kept constant at the service speed (15 knots). The wave headings that have been used for the analysis are *0,30,60,90,120,150,180* degrees. In addition three different loading conditions were selected, a ballast, a full load (ore) and a half load (grain condition). The fatigue damage calculations therefore have to be performed for three different cases, i.e. for the three loading conditions.

A.4 WAVE SPECTRUM

The wave spectrum defines the distribution of energy among the different hypothetical regular wave components, having various frequencies and directions. The wave spectrum that was chosen for this study is the I.S.S.C. (a special case to Pierson-Moskowitz) wave spectrum, which permits wave period and significant wave height to be assigned separately, ref. [4]. It has the form:

$$S(\omega) = \frac{0.11 \cdot Hs^2}{\omega_1} \cdot \left(\frac{\omega}{\omega_1}\right)^{-5} \cdot e^{\left\{-0.44 \cdot \left(\frac{\omega}{\omega_1}\right)^{-4}\right\}} \qquad \text{A.4.1}$$

Where

ω_1: $\omega_1 = \frac{2 \cdot \pi}{T}$

ω: Wave frequency

H_s: Significant wave height

T: mean zero-crossing rate

A.5 RESPONSE SPECTRUM

The response spectrum is a combination of the transfer function and the wave spectrum. The response spectrum is equal to:

$$RS = \text{Wave spectrum} \cdot \text{Transfer function}^2 \qquad \text{A.5.1}$$

From the response spectrum, we calculate the response statistics, such as the area under the response spectrum curve which is denoted by 'm_o' and defines the standard deviation of the response. The response statistics are used to calculate the fatigue damage of the structural details in concern.

A.6 FATIGUE DAMAGE MODEL

Fatigue damage is usually determined by the 'Miner-Palmgren' [15] accumulated damage rule which is also more often found in codes of practice. By the Miner hypothesis, it is assumed that one cycle of randomly varying stress, having amplitude 's_i', causes an amount of fatigue damage in the following proportion:

$$\delta D_i = \frac{1}{N_i} \qquad \text{A.6.1}$$

Here 'N_I' is the number of cycles of a sinusoidal varying stress of amplitude 's_i' required to cause failure. The cumulative damage due to fatigue during exposure to the random stress environment will then be given by:

$$\delta D_i = \sum_i \frac{n_i}{N_i} \qquad \text{A.6.2}$$

Here, 'n_i' is the number of stress cycles of level 's_i', during the period of exposure and the summation is taken over all levels of stress experienced during the period of time consideration. Failure of the structure is then presumed to occur when the length of exposure is sufficient for this sum to equal unity, i.e. when D = 1.

Assuming that the basic fatigue design curve has the form:

$$N \cdot \sigma^m = K \qquad \text{A.6.3}$$

Then the fatigue damage becomes:

$$D = \frac{n}{K} \cdot \overline{\sigma}^m \qquad \text{A.6.4}$$

where 'n' is the total number of cycles, '$\overline{\sigma}^m$' is the mean value of 'σ^m' and 'σ' is a random variable denoting fatigue stress occurring for 'n' cycles, 'K' is a constant which depends on the welding classification.

Equation (A.6.4) is valid for a non-stationery as well as a stationery process. If the is assumed to be a stationery narrow band Gaussian process, it follows a Rayleigh distribution and equation (A.6.4) can be expressed as:

$$D = \left(\frac{n}{K}\right) \cdot \left(2 \cdot \sqrt{2} \cdot \sigma\right)^m \cdot \Gamma\left(\frac{m}{2} + 1\right) \qquad \text{A.6.5}$$

where σ is the root mean square, (rms) of the process and '$\Gamma(...)$', is the gamma function.

The long term process with 'n_i' sea states can usually be described as 'n_i' stationery processes, for each one assuming 'f_i' is the zero crossing rate:

$$f_i = 2 \cdot \pi \cdot \sqrt{\frac{m_2}{m_0}} \qquad \text{A.6.6}$$

Or

$$f_i = \frac{1}{Tz} \qquad \text{A.6.7}$$

Where 'Tz' is the average response period.

If we assume that 'T' is the time over which the fatigue damage is calculated, the damage then in the 'i-th' sea state is written as:

$$D_i = \left(\frac{n_i}{K}\right) \cdot \left(2 \cdot \sqrt{2} \cdot \sigma_i\right)^m \cdot \Gamma\left(\frac{m}{2}+1\right) \qquad \text{A.6.8}$$

Where 'σ_i' is the rms stress in the 'i-th' sea state and

$$n_i = \gamma_i \cdot f_i \cdot T \qquad \text{A.6.9}$$

Where

γ_i : is the percentage of time in the 'i-th' sea state. This is the frequency of occurrence of each sea state

f_i : is the zero crossing rate as defined in equation (A.6.6)

The total fatigue damage then becomes:

$$D = \left(\frac{\left(2 \cdot \sqrt{2}\right)}{K}\right) \cdot \Gamma\left(\frac{m}{2}+1\right) \cdot T \cdot \sum_{i=1}^{x} \left\{\gamma_i \cdot f_i \cdot \sigma_i^m \right. \qquad \text{A.6.10}$$

Equation (A.6.10) is the basic equation used in this study to calculate the fatigue damage.

In the special case where corrosion is included in the fatigue damage the equation becomes:

$$D = \left(\frac{\left(2\cdot\sqrt{2}\right)}{K}\right)\cdot\Gamma\left(\frac{m}{2}+1\right)\cdot T\cdot\sum_{i=1}^{x}\{\gamma_i\cdot f_i\cdot(\sigma_i\cdot S_{cor}(t))^m \qquad \text{A.6.11}$$

A.7 STRESS ANALYSIS

A.7.1 Details Considered for Fatigue Analysis

In a ship structure there may be many hundreds of different structural details that consist a particular section of the ship. The case becomes even more complicated when we are considering a bulk carrier. For the purpose of a fatigue analysis, it is almost impossible to consider all these details. The current practice suggests that only the details that are the more important need to be considered in a fatigue analysis. The selection of these details depends mainly on judgement guided by experience. Many classification societies provide design rules and guidance on the selection of these details. Another complexity comes from the fact that for every detail a separate stress analysis has to be performed to calculate the stresses from the loads acting on each detail. These loads need not be the same, as the location from detail to detail changes, and different factors and geometries have to be considered every time.

For the purpose of this study eight different details have been selected as can be seen in Figure A.2. These details are typical for the section considered, and are the detail that experience shows they are the most prone to fatigue, for various reasons as explained in the rest of the section. Many of these details may suffer severe fatigue damage in just one trip.

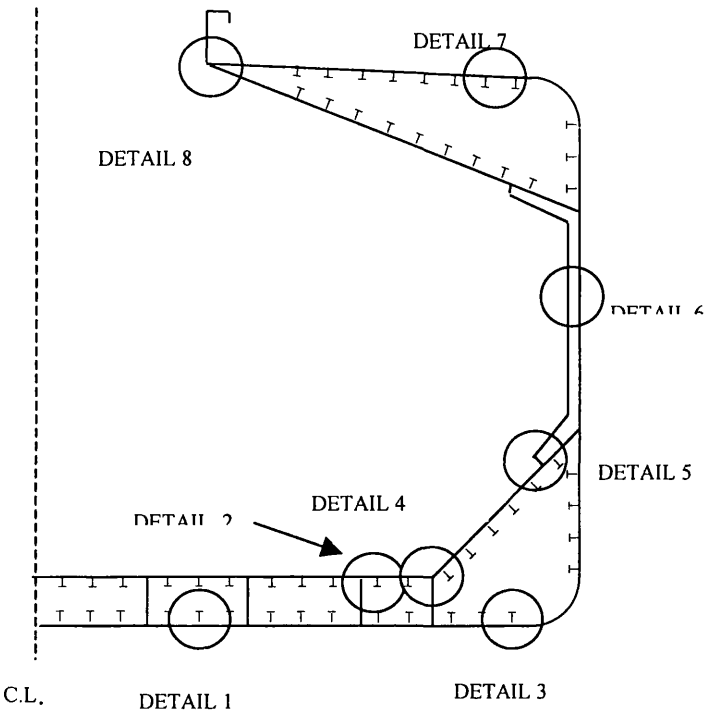

Figure A.2 - The midship section of the vessel and the details considered.

A.7.2 Keel Longitudinal (DETAIL 1)

The welding connection between the keel plating and the longitudinal stiffener (Fig. A.3) suffers with respect to fatigue from global stresses in the longitudinal direction and water pressure stresses in the transverse direction.

Two cracks were considered, each one affected by different stresses. The first crack propagates in a direction normal to the longitudinal axis of the ship. The stresses that cause this crack to propagate are due to global bending moments and shear forces (Fig. A.4). The second crack experiences stresses due to water pressure at the bottom shell plating. The crack initiates at the edge of the weld and propagates through the thickness of the plating (Fig. A.5).

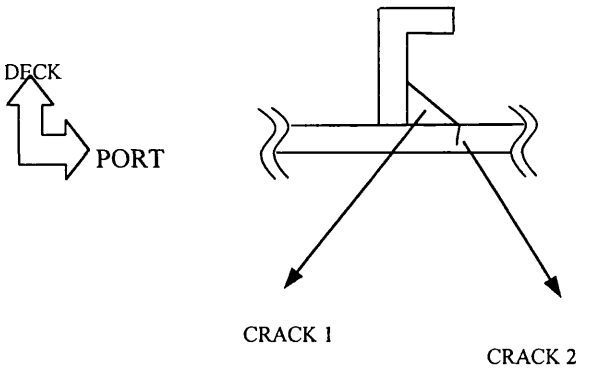

Figure A.3 - Most probable cracks at the keel plating/stiffener connection.

Crack1

The equation used to determine the stress range for crack 1 is:

$$\sigma_{\varphi} = \sigma_x \cdot \cos^2\theta + \tau \cdot \sin 2\theta \qquad \text{A.7.1}$$

Where σx : is the global bending stress

τ : is the global shear stress

The S-N curve used is class E

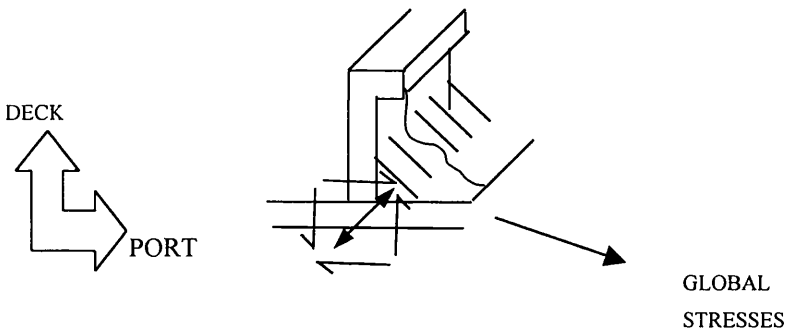

Figure A.4 - Direction of global stresses acting on the weld

Crack 2

The equations used to determine the stress range for crack 2 are:

$$M = \frac{wl^2}{12} \qquad \text{A.7.2}$$

$$\sigma_p = \frac{M}{z} \qquad \text{A.7.3}$$

The S-N curve used is again class F

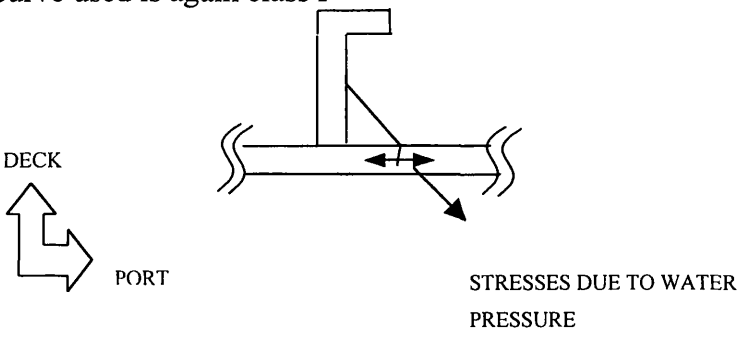

Figure A.5 – Direction of stresses due to water pressure acting on the weld.

A.7.3 Bottom Longitudinal (DETAIL 2)

The double bottom longitudinals are likely to suffer fatigue damage from global or local loading (Fig. A.6). The local loading that causes fatigue damage is due to cargo accelerations in the hold.

The first crack considered suffers from global loading (Fig. A.7). The second crack is influenced by the acceleration of the cargo stored in the hold. The procedure to calculate the stresses acting on the crack starts by calculating the acceleration of a strip of the cargo and therefore the distributed loading on the plate. The plate is considered as fixed ended.

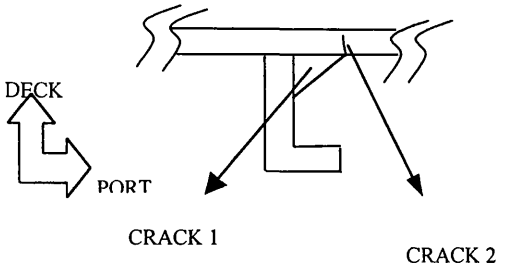

Figure A.6 – Most probable cracks at the bottom plating/stiffener connection.

Crack1

The equation used to determine the stress range for crack 1 is:

$$\sigma_{\varphi} = \sigma_x \cdot \cos^2 \theta + \tau \cdot \sin 2\theta \qquad \text{A.7.4}$$

Were σx : is the global bending stress

τ : is the global shear stress

The S-N curve used is class F

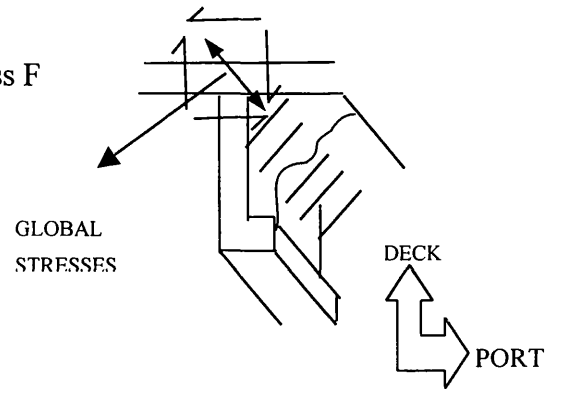

Figure A.7 - Direction of global stresses affecting the weld.

Crack 2

The equations used to determine the stress range for crack 2 are:

$$M = \frac{wl^2}{12} \qquad \text{A.7.5}$$

$$\sigma_p = \frac{M}{z} \qquad \text{A.7.6}$$

Where z : section modulus of the local section

The S-N curve used is class F

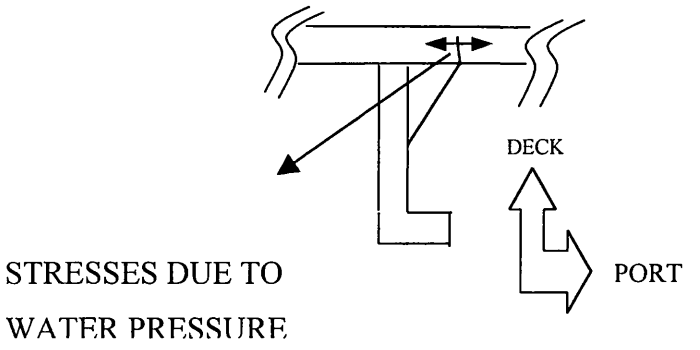

Figure A.8 - Direction of stresses due to water pressure affecting the weld.

A.7.4 Hopper Longitudinal (DETAIL 3)

The third detail is a longitudinal stiffener inside the hopper tank welded to the bottom plating. The weld is a butt weld and the main stresses arise form global as well as local bending. The global stresses due to global bending moments and shear forces cause crack one to propagate in a direction normal to the longitudinal axis of the ship and normal to the weld, (Fig A.9). The local bending stresses arise from the local bending, between the two adjacent stiffeners, caused by the water pressure at the bottom of the plating. These stresses cause crack two to propagate through the thickness of the bottom plate, (Fig A.10).

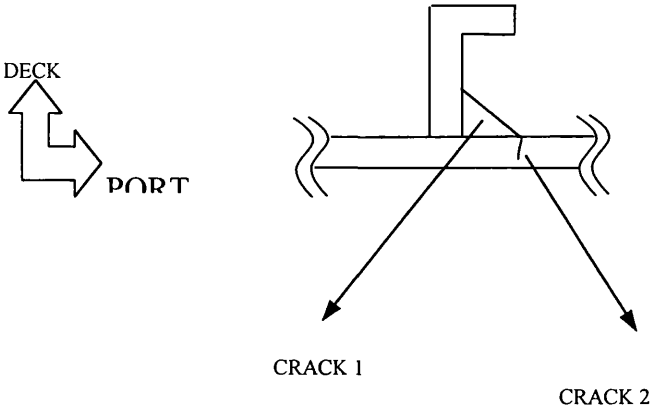

Figure A.9 - Most probable cracks at the keel plating/stiffener connection.

Crack1

The equation used to determine the stress range for crack 1 is:

$$\sigma_{\varphi} = \sigma_x \cdot \cos^2\theta + \tau \cdot \sin 2\theta \qquad \text{A.7.7}$$

Were σ_x : is the global bending stress

τ : is the global shear stress

The S-N curve used is class F

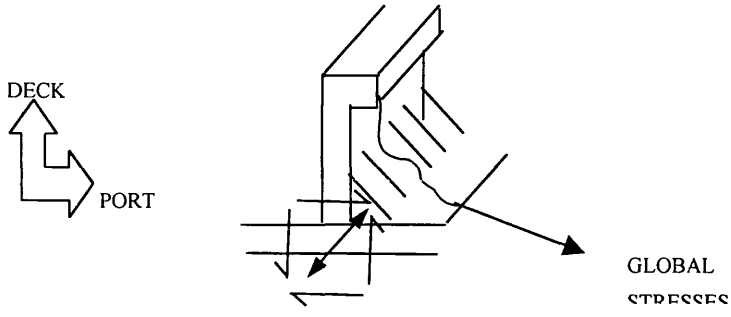

Figure A.10 - Direction of global stresses acting on the weld.

Crack 2

The equations used to determine the stress range for crack 2 are:

$$M = \frac{wl^2}{12} \qquad \text{A.7.7}$$

$$\sigma_p = \frac{M}{z} \qquad \text{A.7.8}$$

Where z : section modulus of the local section

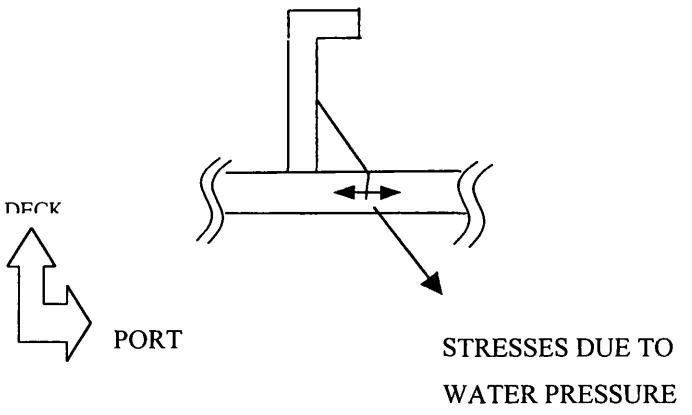

Figure A.11 - Direction of stresses due to water pressure acting on the weld.

A.7.5 Hopper Tank Corner (DETAIL 4)

The fourth detail describes the connection between the hopper tank and the double bottom. This detail is prone to fatigue damage and therefore was selected for the fatigue analysis calculations. The particular detail requires very complicated analysis to determine exactly the stress ranges. Perhaps the most accurate method would be to perform a finite element analysis. For this study a simpler analysis, based on first principles was adopted. The main stresses present at this location come from the water pressure forces below and around the hopper tank.

Two cracks are important at this location, (Fig. A.15). The first crack is propagating because of the global bending and shear stresses, and the second crack because of the local bending caused by the water pressure and cargo acceleration forces.

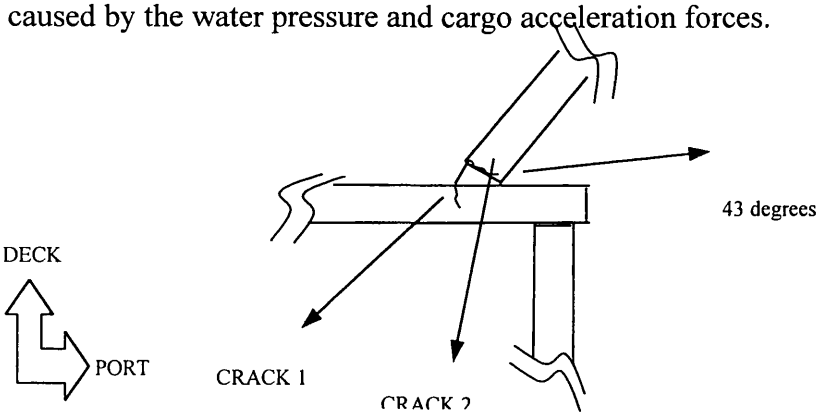

Figure A.12 - Most probable cracks at the hopper corner.

A small finite elemant model was setup to determine the stresses due to dynamic water pressure at this location, (Fig. A.12). The area that the water pressure acts, is subdivided into two regions. The first region is under the keel plate; the second region is around the hopper tank.

The stiffness matrix for the finite element model was created comprising the torsional stiffness of the hopper and the bending stiffness of the double bottom. The effect of the transverse bulkheads was incporparated in the model by multiplying the moment matrix with reduction factors. At the bulkheads, the moment was zero, and reaching maximum value at one third of the distance between the two bulkheads, constant for one third then reducing to zero. Although this reduction on the applied moment does not fully simulate the stiffer structural components closer to the transverse bulkheads it was considered adequate.

The matrix moment comprises the moment due to water pressure forces underneath the double bottom. The matrix was multiplied by the inverse of the total stiffness matrix to give us the rotations at the ends of the double bottom to cause equilibrium at that point of the structure. The total moment used to calculate the stress from the water pressure was calculated by adding the moment to cause equilibrium, with the moment acting on the hopper due to the wave pressure and then subtracting the the moment caused by the wave pressure underneath the double bottom.

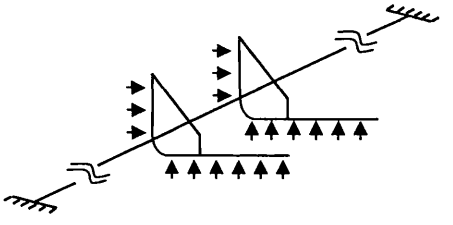

Figure A.13 - Graphic representation of the finite element model

he moment to cause rotation at the hopper A.7.9

$\frac{\mathfrak{o} \cdot B^2}{12}$ F.E. moment caused by pressure underneath the double bottom A.7.10

$$K_M = \begin{bmatrix} \frac{E \cdot I}{b} & 0 & \dots & 0 \\ 0 & \frac{E \cdot I}{b} & \dots & 0 \\ \dots & \dots & \dots & 0 \\ 0 & 0 & 0 & \frac{E \cdot I}{b} \end{bmatrix}$$ Stiffness matrix of double bottom A.7.11

$$M = \begin{bmatrix} r_1 \cdot \frac{\omega \cdot B^2}{12} \\ r_2 \cdot \frac{\omega \cdot B^2}{12} \\ \dots \\ r_{30} \cdot \frac{\omega \cdot B^2}{12} \end{bmatrix}$$ Moment underneath the double bottom A.7.12

$$K_T = \begin{bmatrix} \frac{G \cdot J}{L} & -\frac{G \cdot J}{L} & \dots & 0 \\ -\frac{G \cdot J}{L} & 2 \cdot \frac{G \cdot J}{L} & \dots & 0 \\ \dots & \dots & \dots & -\frac{G \cdot J}{L} \\ 0 & 0 & -\frac{G \cdot J}{L} & \frac{G \cdot J}{L} \end{bmatrix}$$ Stiffness matrix of hopper tank A.7.13

$K = K_T + K_M$ Total stiffness matrix A.7.14

$X = K^{-1} \cdot M$ Rotation at the hopper corner A.7.15

$M_R = X \cdot \frac{E \cdot I}{B}$ Moment to cause equilibrium A.7.16

$$M = M_P + M_R - M_L \qquad \text{Total moment} \qquad \text{A.7.17}$$

$$\sigma_p = \frac{M}{z} \qquad \text{Stress at the hopper corner} \qquad \text{A.7.18}$$

Crack 1

The equation used to determine the stress range for crack 1 is:

$$\sigma_\varphi = 1.1 \cdot \sigma_x \cdot \cos^2\theta + \sigma_p \cdot \sin^2\vartheta + 1.1 \cdot \tau \cdot \sin 2\theta \qquad \text{A.7.19}$$

Where, σx : is the global stress

σp : is the stress due to water pressure

τ : is the global shear stress

The S-N curve used is class F

A magnification factors was used for the global stresses to incorporate the difference between the F and F2 class.

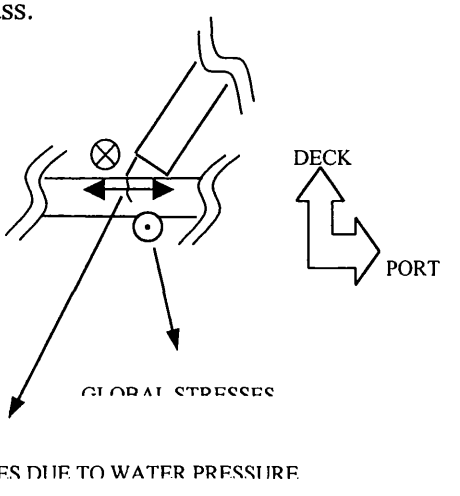

Figure A.14 - Stresses affecting crack 1 at hopper corner

Crack 2

The equation used to determine the stress range for crack 2 is:

$$\sigma_{\varphi} = 1.1 \cdot \sigma_x \cdot \cos^2\theta + \sigma_{pl} \cdot \sin^2\vartheta + 1.1 \cdot \tau \cdot \sin 2\theta \qquad \text{A.7.20}$$

$$\sigma_{pl} = \sigma_p \cdot \frac{t_h}{t_d} \cdot \frac{1}{\cos 43} \qquad \text{A.7.21}$$

The stress due to wave pressure was transformed to the plane that is perpendicular to the direction of the crack and the difference in thickness between the plate of the double bottom and the hopper plate was taken into consideration.

The SN curve used is class F2

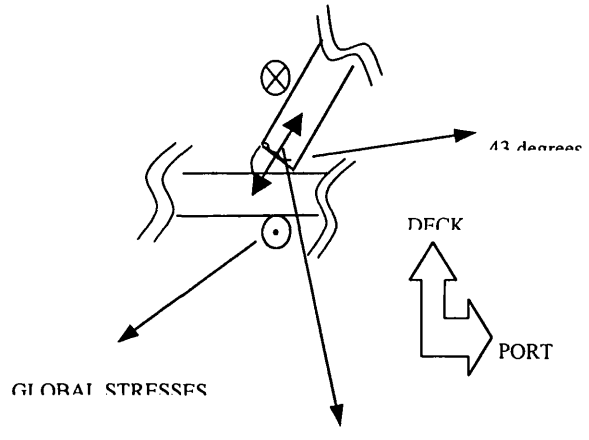

Figure A.15 - Stresses affecting crack 2 at the hopper corner

A.7.6 Side Frame (DETAIL 5)

The weld connecting the side frame with the hopper tank top plate suffers through its life largely from stresses due to water pressure at the side of the ship and also from accidental loading during loading and unloading procedures which indirectly affect the fatigue life of the detail (Fig. A.16). Four possible cracks were considered. The first one starts from the weld and propagates through the frame thickness (Fig. A.17).

The second one propagates inside the weld (Fig. A.18) and the third one starts from the weld and propagates in the hopper plating (Fig. A.22).

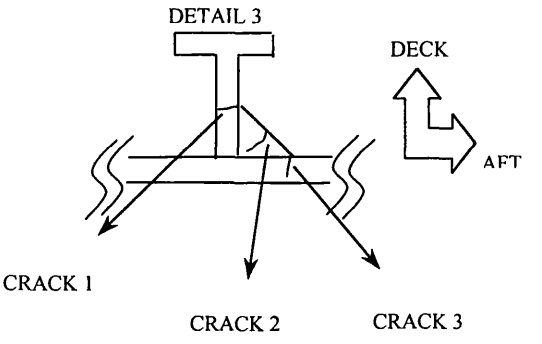

Figure A.16 - Most probable cracks at the connection of the side bracket with the upper hopper plating (The drawing is inclined by 47 degrees)

The methodology used to calculate the stresses is the following. The distributed loading was considered according to the pressure profile. The side bracket was modeled as a beam since an effective breadth was included in the calculations. The area that the bracket should be able to support was considered as having the height of the distance between the hopper tank and the upper wing tank and the breadth of the spacing of the brackets. The fixed end moments and the forces at the supports were calculated and the stresses were calculated by introducing a cut at the foot of the bracket and then calculating the properties (inertia, etc.) (Fig A.17).

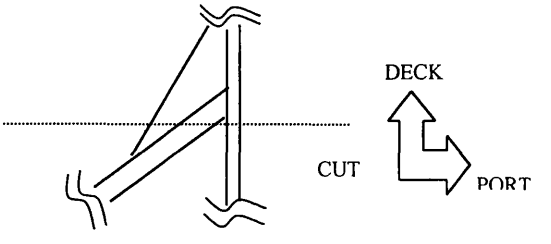

Figure A.17 - The position of the 'cut' to calculate structural properties

The stresses calculated are parallel to the side shell plating and perpendicular to the bottom plating. The welding and so the possible cracks have an angle of 47 degrees with the side shell plating. The stresses calculated had to be transformed into a direction perpendicular to the welding.

$$\sigma = \frac{M}{z} \qquad \text{A.7.22}$$

$$\tau = \frac{ShearForce}{SectionArea} \qquad \text{A.7.23}$$

Crack 1

Stresses due to water pressure

S-N Curve is class F2

$$\sigma_0 = \sigma_p \cdot \cos^2\theta + \tau_p \cdot \sin 2\theta \qquad \text{A.7.24}$$

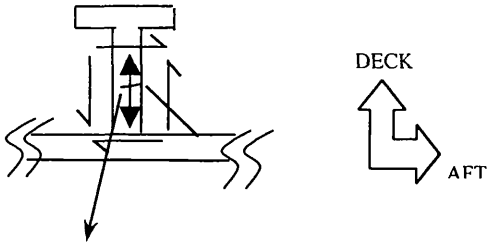

STRESSES DUE TO WATER PRESSURE

Figure A.18 - Stresses affecting crack 1 at the upper hopper plate and side bracket connection.

Crack 2

Stresses due to water pressure two different S-N curves used for the two different planes

First plane due to water pressure S-N curves class W

$$\sigma_\theta = \sqrt{(\sigma_{wp})^2 + (\tau_{wp})^2} \qquad \text{A.7.25}$$

Where

$$\tau_{wp} = \tau_p \cdot \frac{t_{foot}}{2 \cdot t_{weld}} \qquad \text{A.7.26}$$

$$\sigma_{wp} = \sigma_p \cdot \frac{t_{foot}}{2 \cdot t_{weld}} \qquad \text{A.7.27}$$

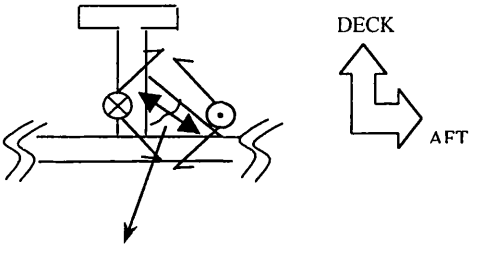

STRESSES DUE TO WATER PRESSURE

Figure A.19 - Stresses affecting crack 2 at the upper hopper plate and side bracket connection.

Second plane due to shear force caused by water pressure S-N curve class D

$$\sigma_\theta = \sigma_{90} \cdot \cos^2\theta + \tau_{90} \cdot \sin 2\theta \qquad \text{A.7.28}$$

Where

$$\tau_{90} = \frac{1}{2} \cdot \sigma \cdot \sin 86 - \tau \cdot \cos 86 \qquad \text{A.7.29}$$

And

$$\sigma_{90} = \sigma \cdot \sin^2(43+90) + \tau \cdot \sin(43+90) \qquad \text{A.7.30}$$

Crack 3

Stresses due to global bending

S-N Curve used class F

$$\sigma_\theta = \sigma_x \cdot \cos^2\theta + \tau \cdot \sin 2\theta \qquad \text{A.7.31}$$

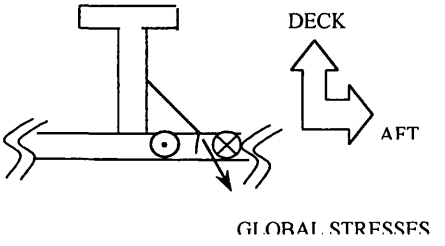

Figure A.20 - Global stresses affecting crack 3 at the upper hopper plate and side bracket connection.

A.7.7 Transverse Stiffener (DETAIL 6)

The welding connecting the side bracket with the side plate may suffer also from fatigue damage (Fig. A.21). The crack considered starts from the weld and propagates in the plate (Fig. A.22).

The weld suffers from mainly wave induced stresses but also there is some contribution from global stresses. The wave-induced stresses were calculated using the pressure profile as loading. The plate between the side brackets was considered which is bended by the loading. The bending will induce moments and forces at the supports and so stresses. The procedure included the calculation of a certain point at

which the fatigue analysis would be done. The criterion for selecting the point was the dynamic water pressure.

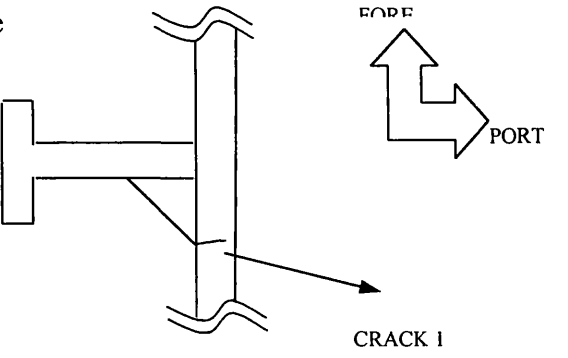

Figure A.21 - Most probable crack at the side stiffener/side plate connection

$$\sigma_p = \frac{M}{z} \qquad \text{A.7.32}$$

$$\tau_p = \frac{R}{A} \qquad \text{A.7.33}$$

$$\sigma_\vartheta = (\sigma_x + \sigma_p)\cdot\cos^2\theta + (\tau + \tau_p)\cdot\sin 2\theta \qquad \text{A.7.34}$$

Where, σx : is the global stress

σp : is the stress due to water pressure

τ : is the global shear stress

τp : is the shear stress due to water pressure

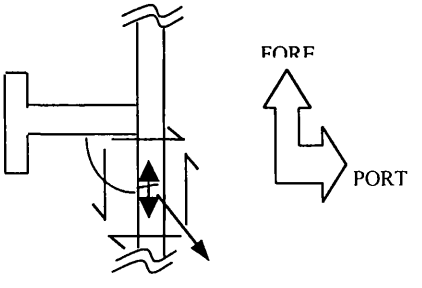

STRESSES DUE TO WATER PRESSURE AND GLOBAL

Figure A.22 - The direction of global and water pressure stresses at the crack considered.

A.7.8 Upper Wing Tank Longitudinal (DETAIL 7)

Generally all deck structural components suffer under the global stresses and especially those induced by global vertical bending moment because of the distance from the neutral axis. A welding detail inside the upper wing tank is considered were a longitudinal stiffener is connected to the deck plating (Fig. A.23)

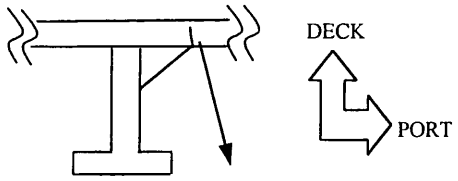

Figure A.23 - Most probable crack at the deck plate/longitudinal stiffener connection

Global stresses were considered for a crack starting from the weld and propagating in the deck plating (Fig A.24). The global stresses and shear stresses were combined to calculate the overall stress in the area.

Crack 1

The stress equation combines the global stresses and shear stresses

$$\sigma_{\varphi} = \sigma_{x} \cdot \cos^2 \theta + \tau \cdot \sin 2\theta \qquad \text{A.7.35}$$

The S-N curve used is class F

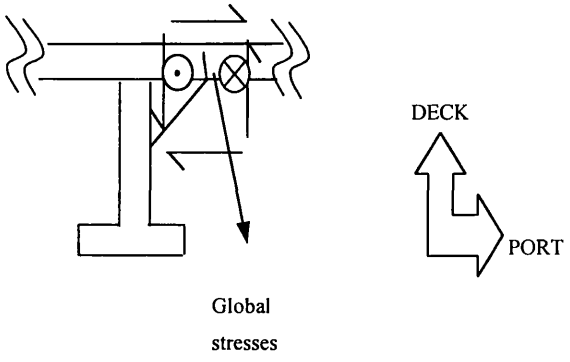

Figure A.24 - The direction of the global stresses affecting the crack.

A.7.9 Hatch Corner (DETAIL 8)

The hatch corner is a crucial detail because the maximum vertical bending moment stresses are combined with high compressive stresses due to wave pressure at the side plates. There are also the large openings of the hatch that introduce high stress concentration factors.

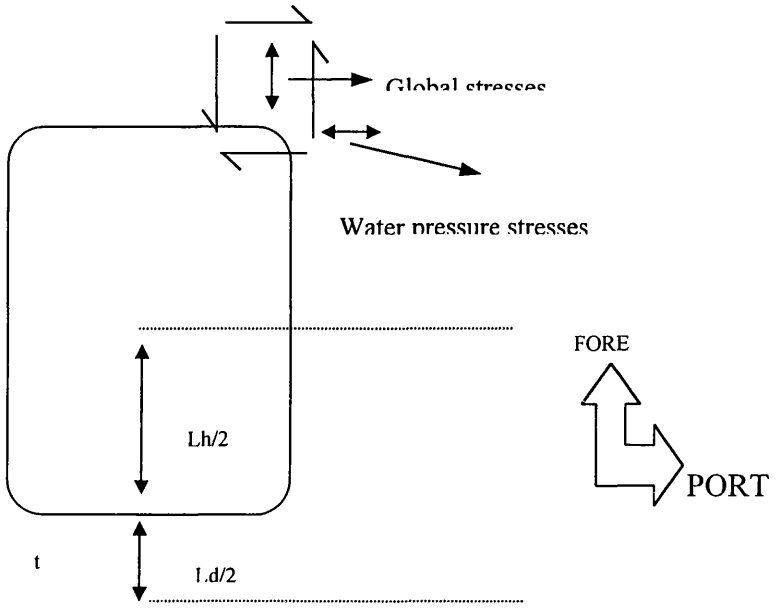

Figure A.25 - The direction of stresses at the hatch corner.

The assumption made here for the load distribution is that the deck structure carries one third of the load acting on the side of the vessel. The global bending and local compressive stresses were combined using the stress transformation equations.

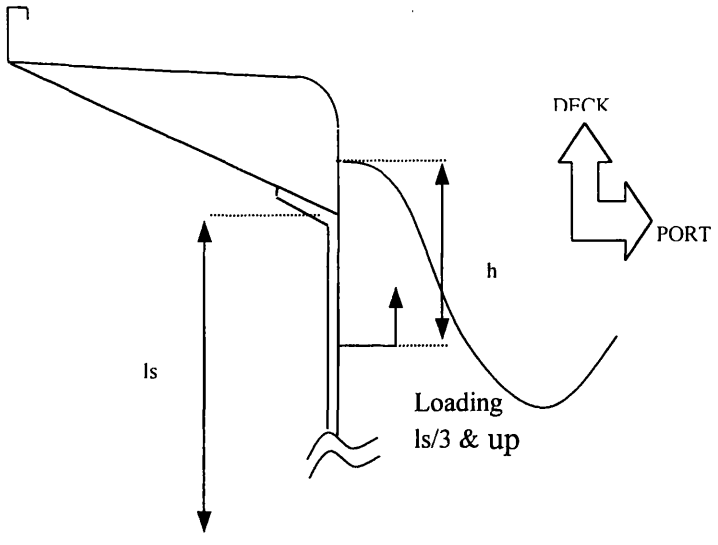

Figure A.26 - The hydrodynamic loading model used to calculate the water pressure stresses affecting the hatch corner.

$$\sigma_{\varphi} = SCF_1 \cdot \sigma_x \cdot \cos^2\theta + SCF_2 \cdot \sigma_p \cdot \sin^2\vartheta + \tau \cdot \sin 2\theta \qquad \text{A.7.36}$$

where σ_x : is the global bending stress

σ_p : is the stress due to water pressure

τ : is the global shear stress

$$\sigma_p = \frac{(\frac{Ld}{2} + \frac{Lh}{2})}{\frac{Ld}{2} \cdot t} \cdot \int Pdh \qquad \text{A.7.37}$$

The stress concentration factors SCF_1 and SCF_2 are a function of the geometry of the hatch opening and were calculated according to Brock [7].

$SCF_1 = 3.62$

$SCF_2 = 3.8$

A.8 References

1. "Fatigue Strenght Analysis for Mobile Offshore Units", (1984), Classification notes #30.2, Det norske Veritas

2. "Guide For \Dynamic Based Design and Evaluation of Bulk Carrier Structures", March 1995., American Bureau of Shipping

3. Barltrop N.D.P.,(1998), 'Floating Structures: a Guide for Design and Analysis'

4. Barltrop N.D.P.,Adams A.J.,(1991),Dynamics of Fixed Marine Structures, London, Butterworth-Heinemann, 3rd Edition

5. Borse G.J.,(1991), Fortran 77 and Numerical Methods for Engineers,Boston, PWS-KEN 2nd Edition

6. Braidwood I.T. ,Zhu Z.Y. ,Buxton I. L.,Hills W.,Marshall P. W.,Stevens P. ,White N.,(1998), Bulk Carrier Structural Integrity: Predicting Fatigue Life with Inluence Functions., Proceedings of the Conference Design and Operation of Bulk Carriers, London

7. Brock J. S., (1958), The Stresses Aroun Square Holes with Rounded Corners, Journal of Ship Research, vol 2, pp37

8. Burnside O.H., Hudak S. J., Oelkers E., Chan K., Dexter J.,(1984), Long –Term Corrosio Fatigue of Welded Marine Steels, (SSC-326)

9. Chan H.S., (1992) ,Dynamic Structural Responses of a Mono-hull Vaessel to Regular Waves., Int. Shipbuild. Progr., 39, # 419, pp 287

10. Cramer E.H.,Shulte-Strauthaus R.,Bea R.G.(1995), Ship Maintenance Project (Fatigue Damage Evaluation),(SSC-386)

11. Cronin D. J.,Godfey P.S.,Spaectral Fatigue Analysis of Offshore Structures

12. Faltinsen O.M.(1990),Sea Loads on Ships and Offshore Structures, Cambridge, Cambridge University Press.

Cambridge University Press.

13. Hogben, H. and Lumb, F.E. , (1976), Ocean Wave Statistics, Glasgow University Main Library.

14. Mansour A., Thayamballi A., (1993),Probability Based Ship Design Loads and Load Combinations,(SSC-373),

15. Miner, M.A., (1945), Cumulative Damage in Fatigue, Journal of Applied Mechanics, paper 12, Trans. Of ASME, vol 67, pp A159

16. Parente J.,Daidola J.,Nedret S., Basar S., Rodi R.C.(1997),Commercial Ship design for Corrosion Control, (SSC-397)

17. Rawson K. J.,Tupper E. C.,(1994),Basic Ship Theory,Essex,Longman Scientific & Technical, 4th Edition, Vol 1+2

18. Salvensen, N., Tuck, E.O., Faltinsen, O., (1970), Ship Motions and Sea Loads ,SNAME Trans. Vol. 78

19. Valsgard, S., Andreassen E., Kim S.K., (1998), Development of ultimate Hull girder Capacity, Proceedings of the Conference Design and Operation of Bulk Carriers, London

20. Xu T.,Fatigue of Ship Structural Details – Technical Development and Problems, (1997),Journal of Ship Research,Vol 41, # 4 ,pp318

21. Xue J.,Pittaluga A. ,Cervetto D.,Faigue Damage Calculation for Oil Tanker and Containe Ship Structures, (1993),Marine Structures, vol 7,pp499

22. Young C.W., (1989), Roark's Formulas for Stress & Strain,New York, McGraw-Hill, 6th edition

DECK LONGITUDINAL

Loading Condition	*Stress range (Spectral)*	*Stress range (Weibull)*	*Weibull scale parameter*	*Weibull shape parameter*	*Stress cycles*
Heavy ballast	24.11	24.63	10.13	0.822	3687492
Grain arrival	22.22	23.03	9.91	0.844	3868252
Ore arrival	22.11	22.90	9.80	0.841	3850498
Combined	22.81	23.25	9.96	0.842	3802081

HATCH COAMING

Loading Condition	*Stress range (Spectral)*	*Stress range (Weibull)*	*Weibull scale parameter*	*Weibull shape parameter*	*Stress cycles*
Heavy ballast	24.48	26.97	10.93	0.815	3609368
Grain arrival	24.39	24.93	10.24	0.821	3656138
Ore arrival	24.31	24.83	10.17	0.82	3652444
Combined	24.40	25.43	10.49	0.823	3639317

HATCH CORNER

Loading Condition	*Stress range (Spectral)*	*Stress range (Weibull)*	*Weibull scale parameter*	*Weibull shape parameter*	*Stress cycles*
Heavy ballast	26.53	27.13	11.12	0.82	3664290
Grain arrival	24.45	25.08	10.43	0.827	3717519
Ore arrival	24.37	24.97	10.36	0.826	3713550
Combined	25.12	25.48	10.55	0.825	3698453

Table A.1 – Summary of Weibull scale and shape parameters of the long-term stress range distribution.

HOPPER PLATING & BOTTOM PLATING

Loading Condition	*Stress range (Spectral)*	*Stress range (Weibull)*	*Weibull scale parameter*	*Weibull shape parameter*	*Stress cycles*
Heavy ballast	20.69	21.56	10.50	0.914	4485926
Grain arrival	20.94	21.49	12.05	1.015	4580167
Ore arrival	20.77	21.77	12.35	1.033	4589721
Combined	20.80	22.13	12.19	1.001	4551938

KEEL LONGITUDINAL

Loading Condition	*Stress range (Spectral)*	*Stress range (Weibull)*	*Weibull scale parameter*	*Weibull shape parameter*	*Stress cycles*
Heavy ballast	18.44	18.85	7.98	0.836	3718178
Grain arrival	17.14	18.02	8.00	0.86	3910471
Ore arrival	17.06	17.78	7.86	0.858	3891047
Combined	17.54	17.84	7.56	0.836	3839899

SIDE FRAME & HOPPER PLATING

Loading Condition	*Stress range (Spectral)*	*Stress range (Weibull)*	*Weibull scale parameter*	*Weibull shape parameter*	*Stress cycles*
Heavy ballast	12.63	13.61	7.32	0.982	4189336
Grain arrival	13.94	14.73	7.40	0.934	4178237
Ore arrival	14.06	14.82	7.43	0.932	4161534
Combined	13.54	14.21	7.24	0.943	4176369

SIDE PLATE & SIDE FRAME

Loading Condition	*Stress range (Spectral)*	*Stress range (Weibull)*	*Weibull scale parameter*	*Weibull shape parameter*	*Stress cycles*
Heavy ballast	16.61	17.30	8.65	0.931	4064733
Grain arrival	16.52	17.19	8.34	0.911	4111053
Ore arrival	16.22	16.80	7.92	0.845	4110359
Combined	16.45	16.96	8.36	0.921	4095382

Table A.1 - (*Continued*)

DECK LONGITUDINAL

Loading Condition	Weibull scale parameter	Weibull shape parameter
Heavy ballast	5.92	0.877
Grain arrival	5.04	0.853
Ore arrival	5.01	0.852
Combined	5.32	0.858

HATCH COAMING

Loading Condition	Weibull scale parameter	Weibull shape parameter
Heavy ballast	6.87	0.895
Grain arrival	6.05	0.879
Ore arrival	6.03	0.879
Combined	6.29	0.881

HATCH CORNER

Loading Condition	Weibull scale parameter	Weibull shape parameter
Heavy ballast	6.88	0.895
Grain arrival	6.08	0.88
Ore arrival	6.04	0.879
Combined	6.30	0.881

HOPPER PLATING & BOTTOM PLATING

Loading Condition	Weibull scale parameter	Weibull shape parameter
Heavy ballast	2.46	0.706
Grain arrival	2.24	0.683
Ore arrival	2.16	0.678
Combined	2.26	0.687

KEEL LONGITUDINAL

Loading Condition	Weibull scale parameter	Weibull shape parameter
Heavy ballast	3.76	0.825
Grain arrival	3.75	0.844
Ore arrival	3.75	0.845
Combined	3.61	0.825

SIDE FRAME & HOPPER PLATING

Loading Condition	Weibull scale parameter	Weibull shape parameter
Heavy ballast	4.16	0.946
Grain arrival	3.42	0.867
Ore arrival	3.36	0.861
Combined	3.32	0.863

SIDE PLATE & SIDE FRAME

Loading Condition	Weibull scale parameter	Weibull shape parameter
Heavy ballast	3.04	0.802
Grain arrival	2.97	0.798
Ore arrival	2.95	0.800
Combined	2.98	0.800

Table A.2 – Summary of Weibull scale and shape parameters for the extreme value distribution

CRACK 1

	SN Class D		
COR. RATE	0	0.15	0.5
ORE	31.0	30.6	29.0
GRAIN	30.6	30.0	28.7
BALLAST	25.0	24.5	23.0
COMBINED	**28.9**	**28.4**	**27.1**

DETAIL 2 BOTTOM LONGITUDINAL

CRACK 1

	SN Class F		
COR. RATE	0	0.1	0.4
ORE			
GRAIN	103.5	102	97
BALLAST	52.83	52	50
COMBINED	**52.11**	**51.33**	**49.00**

CRACK 2

	SN Class F		
COR. RATE	0	0.1	0.4
ORE	350	345	343
GRAIN	2531	2491	2374
BALLAST	2074	2042	2026
COMBINED	**2478**	**2439**	**2372**

DETAIL 3 HOPPER LONGITUDINAL

CRACK 1

	SN Class D		
COR. RATE	0	0.15	0.5
ORE	32.4	31.8	30.4
GRAIN	30.8	30.3	28.9
BALLAST	25.5	25.00	24.00
COMBINED	**29.57**	**29.03**	**27.77**

Table A.3 – *Fatigue lives for the structural details chosen for the analysis*

DETAIL 4 HOPPER CORNER

CRACK 1

	SN Class F2		SN Class F	
COR. RATE	0	0.15	0	0.15
ORE	2.2	2.1	3.2	3.1
GRAIN	2.2	2.1	3.2	3.1
BALLAST	3.3	3.2	4.8	4.7
COMBINED	**2.57**	**2.47**	**3.73**	**3.63**

CRACK 2

	SN Class F2		SN Class F	
COR. RATE	0	0.15	0	0.15
ORE	0.63	0.61	0.92	0.89
GRAIN	0.63	0.61	0.92	0.89
BALLAST	1.03	1.00	1.50	1.45
COMBINED	**0.76**	**0.74**	**1.11**	**1.08**

DETAIL 5 SIDE FRAME AND HOPPER CONECTION

CRACK 1

	SN Class F2		SN Class F	
COR. RATE	0	0.15	0	0.15
ORE	8.49	8.15	12.44	11.94
GRAIN	10.56	10.13	15.47	14.84
BALLAST	1.71	1.64	2.51	2.41
COMBINED	**6.92**	**6.64**	**10.14**	**9.73**

CRACK 2

	SN Class W	
COR. RATE	0	0.15
ORE	6.36	6.1
GRAIN	8.15	7.83
BALLAST	1.16	1.17
COMBINED	**5.22**	**5.03**

CRACK 3

	SN Class D	
COR. RATE	0	0.15
ORE	66.53	63.84
GRAIN	87.22	83.7
BALLAST	23.46	22.51
COMBINED	**59.07**	**56.68**

CRACK 4

	SN Class E	
COR. RATE	0	0.15
ORE	306	298
GRAIN	194	191
BALLAST	142	140
COMBINED	**214.00**	**209.67**

Table A.3 – (*Continued*)

DETAIL 6 TRANSVERSE FRAME STIFFENER

CRACK 1

	SN Class F2		SN Class F	
COR. RATE	0	0.15	0	0.15
ORE	8.2	7.9	12.00	11.5
GRAIN	10.4	10	15.3	14.6
BALLAST	9.2	9	13.5	13.2
COMBINED	**9.27**	**8.97**	**13.60**	**13.10**

DETAIL 7 DECK LONGITUDINAL

CRACK 1

	SN Class E		
COR. RATE	0	0.2	0.4
ORE	19.4	19.0	18.4
GRAIN	14.7	14.4	14.1
BALLAST	15.0	14.7	14.3
COMBINED	**16.37**	**16.03**	**15.60**

DETAIL 8 HATCH CORNER

CRACK 1

	SN Class D			SN Class C		
COR. RATE	0	0.15	0.5	0	0.15	0.5
ORE	1.3	1.23	1.12	3.17	3.04	2.75
GRAIN	1.25	1.2	1.08	3.05	2.9	2.6
BALLAST	0.98	0.94	0.86	2.3	2.2	1.97
COMBINED	**1.18**	**1.12**	**1.02**	**2.84**	**2.71**	**2.44**

Table A.3 – (*Continued*)

General

Operator:	Endeavour Shipping CO. S.A.
Port of registry:	MONROVIA, LIBERIA
Kind of ship:	Bulk carrier
Keel laid:	25th JAN. 1976
Launched:	23rd JULY 1976
Delivered:	15th NOV. 1976
Shipyard:	HITACHI, SAKAI SHIPYARD
Yard number:	4461

Principal dimensions

Length, over all:	225.000 m
Length, registered:	216.761 m
Length, between perpendiculars:	215.000 m
Breadth, moulded:	32.200 m
Depth, moulded:	17.800 m
Designed load draft, moulded:	12.400 m
Scantling draft, moulded:	12.400 m
Summer freeboard (from deck mark:	4.487 m
Summer load draft, extreme:	12.450 m

Table A.4 – *Principal characteristics of the vessel*

Corresponding full load displacement:	72,981 kt (71,828 L.T.)
Block coefficient at full load draft:	0.8249
Prismatic coefficient at full load draft:	0.8304
Water plane coefficient at full load draft:	0.8875
Midship section coefficient at full load draft:	0.9934

Classification and Regulations

Classification:	American Bureau of Shipping + A1 E, "Bulk Carrier", "Strengthened for the Carriage of Ore Cargoes-Holds No.2, 4 &6 may be empty", + AMS and + ACCU
Regulations:	International Convention for the Safety of Life at Sea, 1960. International Load Line Convention, 1960. Liberian Maritime Laws and Regulations. Tonnage Regulations.

International Tele-communication Convention, 1967.

Suez and Panama Canal Rules Including Tonnage Measurements.

Speed

Maximum. trial speed at ballast condition of displacement (45% full) and at maximum continuous output of the main engine.
17.639 knots
Sea speed at full-loaded condition and at continuous service output of the main engine with 15% of sea margin. 15.300 knots

Type of ship

Type of ship:	Single deck type bulk carrier with F'cle deck.
Stem:	Bulbous type.
Stern:	Transom type.

Tonnage

Gross tonnage:	30592.2 t (Liberia)
Net tonnage:	23585 t (Liberia)

Dead-weight

Light weight:	11,607 kt (11,424 L.T.)
Dead-weight:	61,374 kt (60,404 L.T.)

Table A.4 – (*Continued*)

Complement

Officer:	12 persons
Crew:	27 persons
Other:	2 persons
Total:	41 persons

Propelling machinery

Main engine:	Hitachi Sulzer 8rind
	Vertical, 2-stroke, single acting, direct reversible, crosshead type, turbo- charged, welded design.
Propeller:	Aerofoil solid type 1set
	Material: Manganese bronze
	Diameter: 6,000 mm
	Pitch: 4,125 mm
	Pitch ratio: 0.6875
	Exp. area ratio: 0.6417

Table A.4 – (*Continued*)

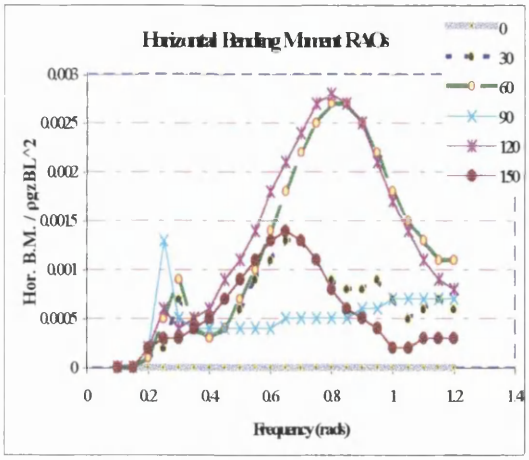

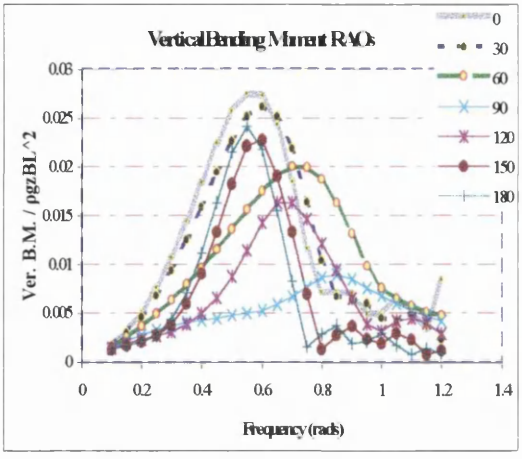

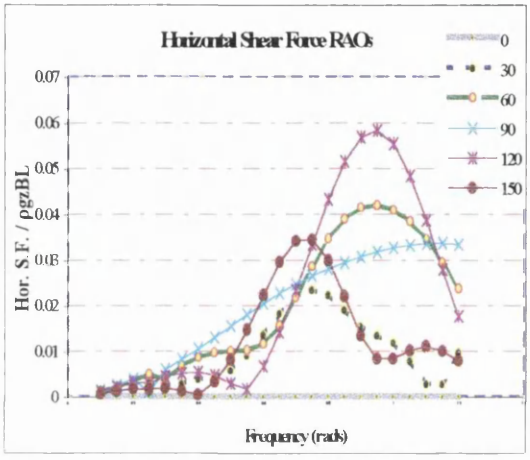

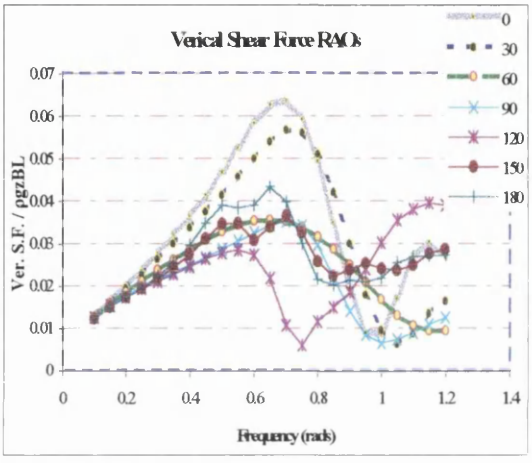

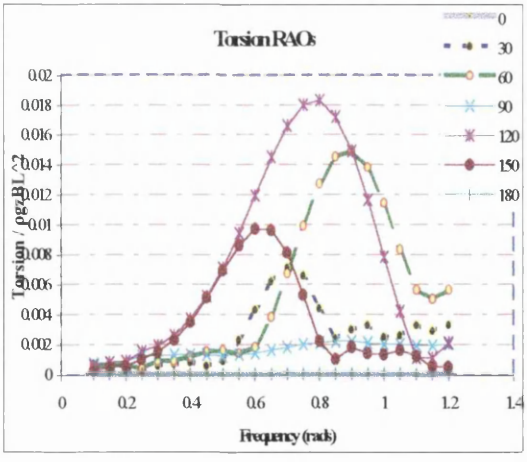

Figure A.27 – *RAOs for Ballast loading condition*

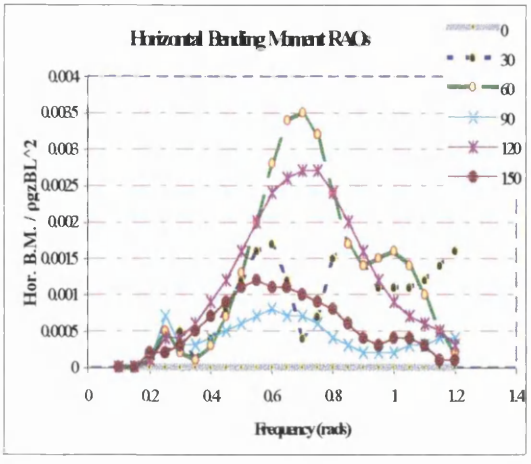

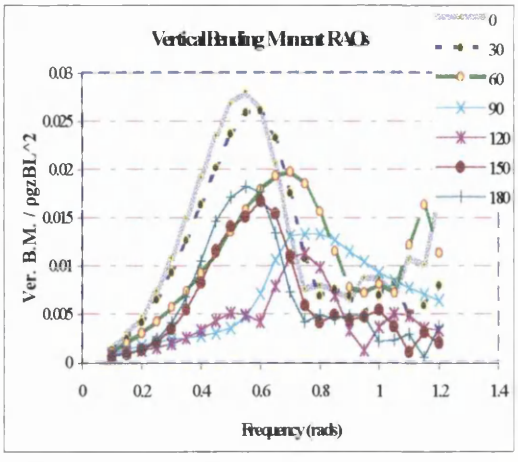

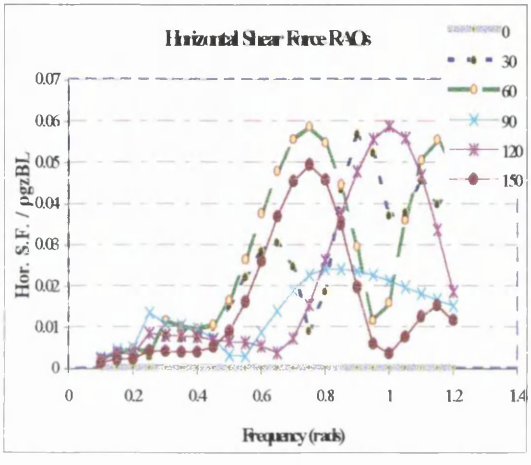

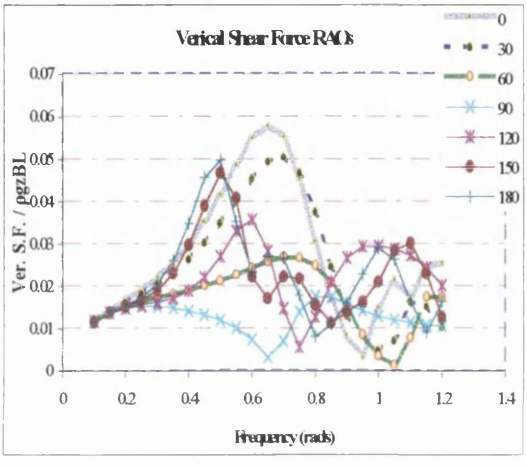

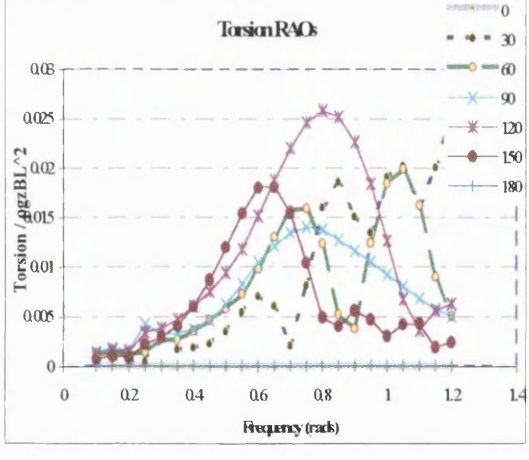

Figure A.28 – *RAOs for Grain loading condition*

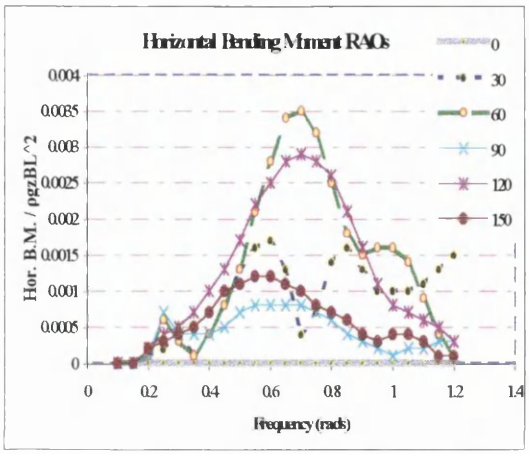

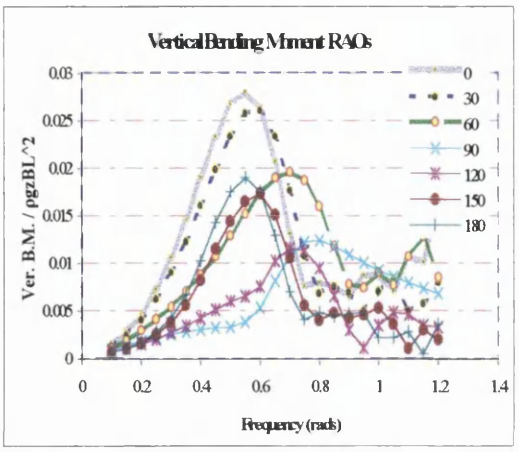

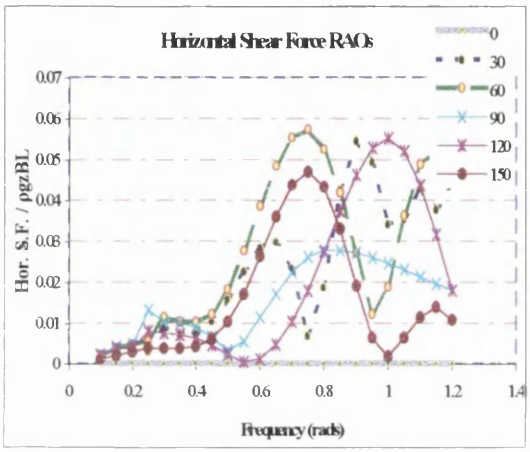

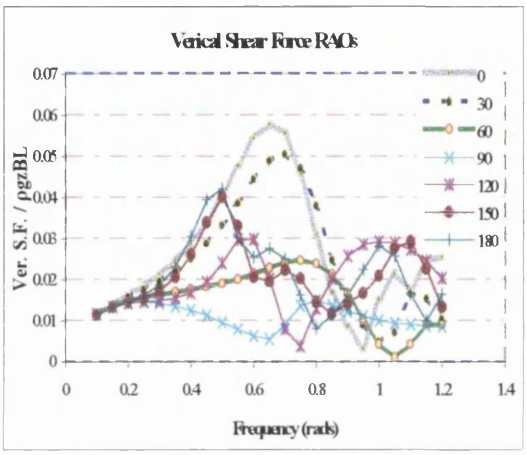

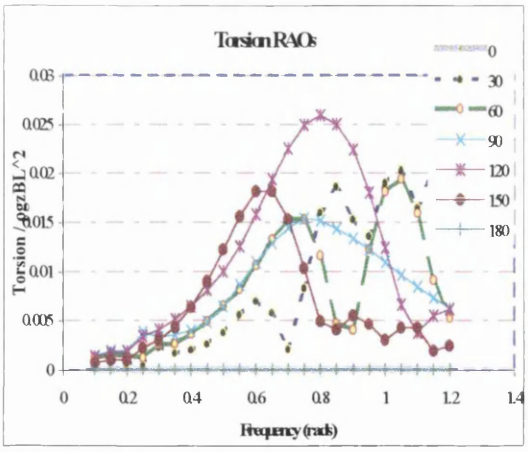

Figure A.29 – *RAOs for Ore loading condition*

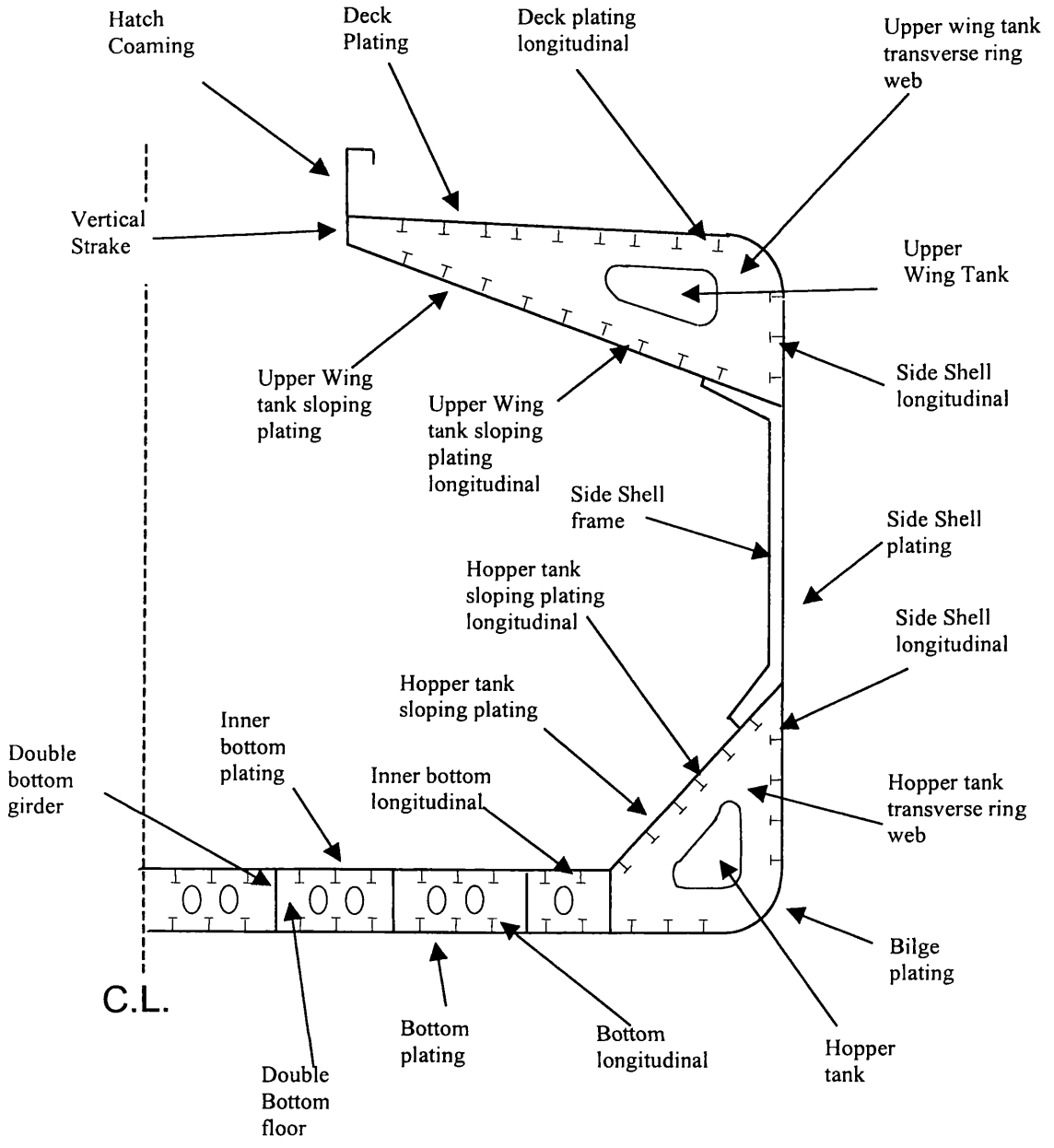

Figure A.30 - *Midship section*

APPENDIX B

CRACK PROPAGATION IN ABAQUS

&

STRESS INTENSITY FACTOR SOLUTIONS

B.1 Crack Propagation in ABAQUS

The crack propagation facility of ABAQUS allows the estimation of the stress intensity factors of a propagating crack.

First the crack and the assumed crack path must be specified. This is done by creating the crack surface. The crack surface defines the crack path and final crack length. The crack surface is created by two different surfaces: the slave and the master contact surfaces. These two surfaces must be joined along the crack surface. That is, they must have identical nodes at the crack surface.

Consider a simple plate with an edge crack. Assuming the crack propagates along the plate in a normal direction to the applied stress.

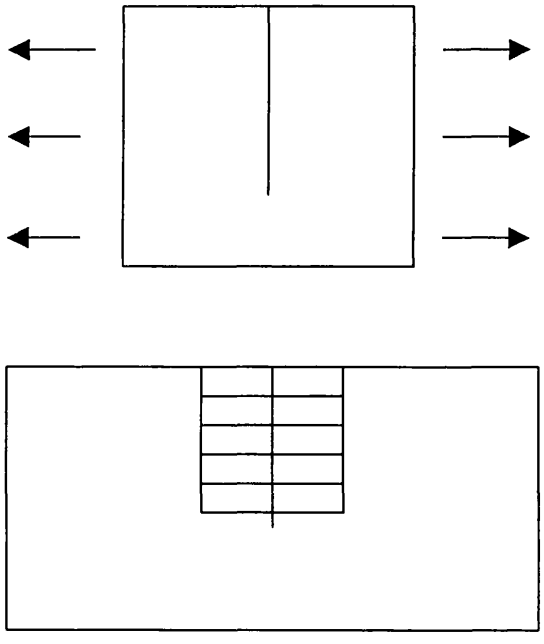

Figure B.1 – *Crack modelling (Plate with edge crack)*

The crack is defined by the nodes along the assumed crack, namely, the straight line. These nodes must be duplicates, because the slave and the master surfaces must not have any nodes in common. The slave surface can include all the elements along the crack, that is elements 1 to 5. To do this you use the surface definition command line in the input file.

The command line is, (see example input in B.2):

*SURFACE DEFINITION, NAME=SLAVE

SET1, S2

The elements that consist the surface, 3,9...57 consist the set1 element set, defined in the previous line.

The s2 term in the input defines which side of the elements is on the crack surface. In this case the s2 side of the slave, and s4 side of the master surface form the crack surface.

To create the master surface you use the elements along the other side of the crack, namely elements 4,10... 58. The command line is the same.

The surface interaction line is used to define the thickness of the crack.

The nodes that are on the crack are specified next, using

*NSET, NSET=BNODES, GENERATE

500,509,1

4,67,7

All nodes that form the crack. In this case nodes 500 to 509 are on the slave surface, and nodes 4,11,...,67 are on the master surface.

The other necessary command input line is the

*CONTACT PAIR, INTERACTION=SET1

SLAVE,MASTER

Here we define which is the slave and which is the master surfaces for ABAQUS. It is very important that first the slave and then the master surface is written in the command line.

Next the initial conditions command line must be specified, defining first the slave surface, the master surface, and the nodes that form the crack.

*INITIAL CONDITIONS, TYPE=CONTACT, NORMAL

SLAVE, MASTER, BNODES

The technique that ABAQUS is using for crack propagation is based on the debonding of the initially bonded nodes along the crack. The two important command lines are

*DEBOND, SLAVE=SLAVE, MASTER=MASTER, TIME INCREMENT=0.0001, OUTPUT=BOTH,

FREQUENCY=1

0.0, 1.0

0.005, 0.0

In the command line again the name of the slave and the name of the master surfaces is specified with some optional parameters, output, frequency etc. In the data line you must specify the traction force between the nodes before debonding and after. In this case, at time = 0 the traction force is 100% between the nodes. At time = 0.005 the traction is zero. If required a more accurate traction force can be specified by adding more data lines.

The next step is to specify a fracture criterion. This can be the CTOD criterion, the critical stress or the crack versus time criterion. The last is the one chosen here. For this criterion a crack length versus time relationship must be specified, so that crack propagates according to this relationship. The command line has the form,

*FRACTURE CRITERION, TYPE=CRACK LENGTH, NSET=REF, TOLERANCE=0.01

1.000001, 0.000000001

1.05, 0.20

1.1, 0.400

1.15, 0.54

1.2, 0.700

1.3, 0.850

1.4, 1.280

1.5, 1.340

1.65, 1.450

1.8, 1.530

2.0, 1.700

The required parameter is the, Type=(name of the criterion) which specify the criterion that ABAQUS will use for the analysis. For this criterion another necessary parameter is the reference point, defined by NSET= (reference node) which ABAQUS will use to estimate the crack propagation. In this case the reference node is node 510,

*NODE, NSET=REF

510, 0.0, 2.00000001

The next step is to specify the output requests that is the stress intensity factors. ABAQUS cannot calculate, using this method, the stress intensity factors and first the J-integral must be evaluated using the CONTOUR INTEGRAL command line. The relationship between J-integral and stress intensity factor, for plane strain and mode I crack propagation is given in chapter 4.

The command line for the J-integral evaluation is

*CONTOUR INTEGRAL, CONTOURS=4, OUTPUT=BOTH

TIP1,0,-1

Where you specify how many contours to be evaluated, usually more than 2, and in the data line the parameters are

The crack tip, TIP1, which is the initial crack tip in this case, and for more crack tips this command line must be repeated specifying all the crack tips i.e. all the nodes that form the crack.

The direction cosine of the crack, 270^{o} i.e. cos270=0

and direction sine, sin270=-1

B.2 Example Input (Plate with Edge Crack)

*HEADING, SPARSE
ABAQUS job created on 20-Sep-99 at 14:46:20
**

```
*NODE
    1,      -0.5,        0.
    2,  -0.333333,       0.
    3,  -0.166667,       0.
    4,        0.,        0.
    5,   0.166667,       0.
    6,   0.333333,       0.
    7,       0.5,        0.
    8,      -0.5,       0.2
    9,  -0.333333,       0.2
   10,  -0.166667,       0.2
   11,        0.,       0.2
   12,   0.166667,       0.2
   13,   0.333333,       0.2
   14,       0.5,       0.2
   15,      -0.5,       0.4
   16,  -0.333333,       0.4
   17,  -0.166667,       0.4
   18,        0.,       0.4
   19,   0.166667,       0.4
   20,   0.333333,       0.4
   21,       0.5,       0.4
   22,      -0.5,       0.6
   23,  -0.333333,       0.6
   24,  -0.166667,       0.6
   25,  2.77556E-17,     0.6
   26,   0.166667,       0.6
   27,   0.333333,       0.6
   28,       0.5,       0.6
   29,      -0.5,       0.8
   30,  -0.333333,       0.8
   31,  -0.166667,       0.8
   32,        0.,       0.8
   33,   0.166667,       0.8
   34,   0.333333,       0.8
   35,       0.5,       0.8
   36,      -0.5,        1.
   37,  -0.333333,       1.
   38,  -0.166667,       1.
   39,        0.,        1.
   40,   0.166667,       1.
   41,   0.333333,       1.
   42,       0.5,        1.
   43,      -0.5,       1.2
   44,  -0.333333,       1.2
   45,  -0.166667,       1.2
   46,        0.,       1.2
   47,   0.166667,       1.2
   48,   0.333333,       1.2
   49,       0.5,       1.2
   50,      -0.5,       1.4
   51,  -0.333333,       1.4
   52,  -0.166667,       1.4
   53, -2.77556E-17,     1.4
   54,   0.166667,       1.4
   55,   0.333333,       1.4
   56,       0.5,       1.4
   57,      -0.5,       1.6
   58,  -0.333333,       1.6
   59,  -0.166667,       1.6
   60,        0.,       1.6
   61,   0.166667,       1.6
   62,   0.333333,       1.6
   63,       0.5,       1.6
   64,      -0.5,       1.8
   65,  -0.333333,       1.8
   66,  -0.166667,       1.8
   67,  5.55112E-17,     1.8
   68,   0.166667,       1.8
   69,   0.333333,       1.8
   70,       0.5,       1.8
   71,      -0.5,        2.
   72,  -0.333333,       2.
```

```
    73,   -0.166667,        2.
    74,        0.,        2.
    75,    0.166667,        2.
    76,    0.333333,        2.
    77,         0.5,        2.
    500, 0.0, 0.0
    501, 0.0, 0.2
    502, 0.0, 0.4
    503, 0.0, 0.6
    504, 0.0, 0.8
    505, 0.0, 1.0
    506, 0.0, 1.2
    507, 0.0, 1.4
    508, 0.0, 1.6
    509, 0.0, 1.8
    510, 0.0, 2.0
**
**
*ELEMENT, TYPE=CPE4, ELSET=PLATE
     1,     1,     2,     9,     8
     2,     2,     3,    10,     9
     3,     3,   500,   501,    10
     4,     4,     5,    12,    11
     5,     5,     6,    13,    12
     6,     6,     7,    14,    13
     7,     8,     9,    16,    15
     8,     9,    10,    17,    16
     9,    10,   501,   502,    17
    10,    11,    12,    19,    18
    11,    12,    13,    20,    19
    12,    13,    14,    21,    20
    13,    15,    16,    23,    22
    14,    16,    17,    24,    23
    15,    17,   502,   503,    24
    16,    18,    19,    26,    25
    17,    19,    20,    27,    26
    18,    20,    21,    28,    27
    19,    22,    23,    30,    29
    20,    23,    24,    31,    30
    21,    24,   503,   504,    31
    22,    25,    26,    33,    32
    23,    26,    27,    34,    33
    24,    27,    28,    35,    34
    25,    29,    30,    37,    36
    26,    30,    31,    38,    37
    27,    31,   504,   505,    38
    28,    32,    33,    40,    39
    29,    33,    34,    41,    40
    30,    34,    35,    42,    41
    31,    36,    37,    44,    43
    32,    37,    38,    45,    44
    33,    38,   505,   506,    45
    34,    39,    40,    47,    46
    35,    40,    41,    48,    47
    36,    41,    42,    49,    48
    37,    43,    44,    51,    50
    38,    44,    45,    52,    51
    39,    45,   506,   507,    52
    40,    46,    47,    54,    53
    41,    47,    48,    55,    54
    42,    48,    49,    56,    55
    43,    50,    51,    58,    57
    44,    51,    52,    59,    58
    45,    52,   507,   508,    59
    46,    53,    54,    61,    60
    47,    54,    55,    62,    61
    48,    55,    56,    63,    62
    49,    57,    58,    65,    64
    50,    58,    59,    66,    65
    51,    59,   508,   509,    66
    52,    60,    61,    68,    67
    53,    61,    62,    69,    68
    54,    62,    63,    70,    69
```

```
    55,    64,    65,    72,    71
    56,    65,    66,    73,    72
    57,    66,    509,   510,   73
    58,    67,    68,    75,    74
    59,    68,    69,    76,    75
    60,    69,    70,    77,    76
**
** plate
**
*SOLID SECTION, ELSET=PLATE, MATERIAL=STEEL
0.025
**
** steel
** Date: 13-Sep-99        Time: 12:40:38
**
*MATERIAL, NAME=STEEL
**
*ELASTIC, TYPE=ISO
  207000.,      0.3
**
** bound
**
*BOUNDARY, OP=NEW
    2, 2,,      0.
    3, 2,,      0.
    4, 2,,      0.
    5, 2,,      0.
    6, 2,,      0.
**
** bound2
**
*BOUNDARY, OP=NEW
    1, 1,,      0.
    1, 2,,      0.
    7, 1,,      0.
    7, 2,,      0.
**

*ELSET, ELSET=SET1, GENERATE
3,57,6
*SURFACE DEFINITION, NAME=SLAVE
SET1, S2
*ELSET, ELSET=SET2, GENERATE
4,58,6
*SURFACE DEFINITION, NAME=MASTER
SET2, S4
*SURFACE INTERACTION, NAME=SET1
0.025
**
*NSET, NSET=BNODES, GENERATE
500,509,1
4,67,7
**
*CONTACT PAIR, INTERACTION=SET1
SLAVE,MASTER
**
*INITIAL CONDITIONS, TYPE=CONTACT, NORMAL
SLAVE, MASTER, BNODES
**
*NODE, NSET=REF
510, 0.0, 2.00000001
** Step 1, Default Static Step
** LoadCase, Default
**
*STEP, AMPLITUDE=RAMP
**
This load case is the default load case that always appears
**
*STATIC
0.05, 5.0, 0.00001, 0.5
**
*DEBOND, SLAVE=SLAVE, MASTER=MASTER, TIME INCREMENT=0.001, OUTPUT=BOTH,
FREQUENCY=1
```

```
0.0, 1.0
0.005, 0.0
**
*FRACTURE CRITERION, TYPE=COD, TOLERANCE=0.01, DISTANCE=0.1, SYMMETRY
0.1, 0.02
**
*NSET, NSET=F1
     7,    14,    21,    28,    35,    42,    49,    56,
    63,    70,    77
*NSET, NSET=F2
     1,     8,    15,    22,    29,    36,    43,    50,
    57,    64,    71
** f1
*CLOAD, OP=NEW
F1, 1,       10.
**
** f2
*CLOAD, OP=NEW
F2, 1,      -10.
*DLOAD, OP=NEW
*TEMPERATURE, OP=NEW
*NODE PRINT, FREQ=1
U,
*NODE FILE, FREQ=1
U,
*EL PRINT, POS=INTEG, FREQ=1
S,
E,
*EL PRINT, POS=INTEG, FREQ=1, ELSET=PLATE
  2  3  4
S,
E,
*EL FILE,  POS=INTEG, FREQ=1
S,
E,
*EL FILE,  POS=INTEG, FREQ=1, ELSET=PLATE
  2  3  4
S,
E,
*EL PRINT, POS=NODES, FREQ=0
*EL FILE,  POS=NODES, FREQ=0
*EL PRINT, POS=CENTR, FREQ=0
*EL FILE,  POS=CENTR, FREQ=0
*EL PRINT, POS=AVERAGE, FREQ=0
*EL FILE,  POS=AVERAGE, FREQ=0
*MODAL PRINT, FREQ=99999
*MODAL FILE, FREQ=99999
*ENERGY PRINT, FREQ=0
*ENERGY FILE, FREQ=0
*PRINT, FREQ=1
*END STEP
```

B.3 Table of Stress Intensity Factors from the FEA

Hatch corner

a/W	0	0.001	0.002	0.003	0.004
	0.005	0.006	0.007	0.008	0.009
0.1	1.897	1.892	1.886	1.881	1.876
	1.872	1.867	1.862	1.857	1.853
0.11	1.848	1.844	1.839	1.835	1.83
	1.826	1.822	1.818	1.814	1.81
0.12	1.806	1.802	1.798	1.794	1.79
	1.786	1.783	1.779	1.776	1.772
0.13	1.768	1.765	1.762	1.758	1.755
	1.752	1.748	1.745	1.742	1.739
0.14	1.736	1.733	1.73	1.727	1.724
	1.721	1.718	1.715	1.712	1.709
0.15	1.707	1.704	1.701	1.699	1.696
	1.694	1.691	1.688	1.686	1.684
0.16	1.681	1.679	1.676	1.674	1.672
	1.669	1.667	1.665	1.663	1.661
0.17	1.659	1.656	1.654	1.652	1.65
	1.648	1.646	1.644	1.642	1.64
0.18	1.639	1.637	1.635	1.633	1.631
	1.629	1.628	1.626	1.624	1.623
0.19	1.621	1.619	1.618	1.616	1.614
	1.613	1.611	1.61	1.608	1.607
0.2	1.605	1.604	1.602	1.601	1.6
	1.598	1.597	1.596	1.594	1.593
0.21	1.592	1.59	1.589	1.588	1.587
	1.586	1.584	1.583	1.582	1.581
0.22	1.58	1.579	1.578	1.577	1.576
	1.574	1.573	1.572	1.571	1.57
0.23	1.57	1.569	1.568	1.567	1.566
	1.565	1.564	1.563	1.562	1.562
0.24	1.561	1.56	1.559	1.558	1.558
	1.557	1.556	1.555	1.555	1.554
0.25	1.553	1.553	1.552	1.551	1.551
	1.55	1.549	1.549	1.548	1.548
0.26	1.547	1.546	1.546	1.545	1.545
	1.544	1.544	1.543	1.543	1.542
0.27	1.542	1.542	1.541	1.541	1.54
	1.54	1.54	1.539	1.539	1.539
0 28	1.538	1.538	1.538	1.537	1.537
	1.537	1.536	1.536	1.536	1.536
0 29	1.535	1.535	1.535	1.535	1.535
	1.534	1.534	1.534	1.534	1.534
0.3	1.534	1.534	1.533	1.533	1.533
	1.533	1.533	1.533	1.533	1.533
0.31	1.533	1.533	1.533	1.533	1.533
	1.533	1.533	1.533	1.533	1.533
0.32	1.533	1.533	1.533	1.533	1.533
	1.534	1.534	1.534	1.534	1.534
0.33	1.534	1.534	1.535	1.535	1.535
	1.535	1.535	1.536	1.536	1.536

a/W	0	0.001	0.002	0.003	0.004
	0.005	0.006	0.007	0.008	0.009
0.34	1.536	1.537	1.537	1.537	1.537
	1.538	1.538	1.538	1.539	1.539
0.35	1.539	1.54	1.54	1.54	1.541
	1.541	1.541	1.542	1.542	1.543
0.36	1.543	1.543	1.544	1.544	1.545
	1.545	1.546	1.546	1.547	1.547
0.37	1.548	1.548	1.549	1.549	1.55
	1.55	1.551	1.552	1.552	1.553
0.38	1.553	1.554	1.555	1.555	1.556
	1.557	1.557	1.558	1.559	1.559
0.39	1.56	1.561	1.561	1.562	1.563

Table B.1 - *Geometry factors for hatch corner detail*

	1.563	1.564	1.565	1.566	1.566
0.4	1.567	1.568	1.569	1.57	1.57
	1.571	1.572	1.573	1.574	1.575
0.41	1.576	1.576	1.577	1.578	1.579
	1.58	1.581	1.582	1.583	1.584
0.42	1.585	1.586	1.587	1.588	1.589
	1.59	1.591	1.592	1.593	1.594
0.43	1.595	1.596	1.597	1.598	1.599
	1.601	1.602	1.603	1.604	1.605
0.44	1.606	1.607	1.609	1.61	1.611
	1.612	1.613	1.615	1.616	1.617
0.45	1.618	1.62	1.621	1.622	1.624
	1.625	1.626	1.628	1.629	1.63
0.46	1.632	1.633	1.635	1.636	1.637
	1.639	1.64	1.642	1.643	1.645
0.47	1.646	1.648	1.649	1.651	1.652
	1.654	1.655	1.657	1.659	1.66
0.48	1.662	1.663	1.665	1.667	1.668
	1.67	1.672	1.673	1.675	1.677
0.49	1.679	1.68	1.682	1.684	1.686
	1.687	1.689	1.691	1.693	1.695
0.5	1.697	1.699	1.7	1.702	1.704
	1.706	1.708	1.71	1.712	1.714
0.51	1.716	1.718	1.72	1.722	1.724
	1.727	1.729	1.731	1.733	1.735
0.52	1.737	1.739	1.742	1.744	1.746
	1.748	1.751	1.753	1.755	1.758
0.53	1.76	1.762	1.765	1.767	1.769
	1.772	1.774	1.777	1.779	1.782
0.54	1.784	1.787	1.789	1.792	1.795
	1.797	1.8	1.802	1.805	1.808
0.55	1.81	1.813	1.816	1.819	1.822
	1.824	1.827	1.83	1.833	1.836
0.56	1.839	1.842	1.845	1.848	1.851
	1.854	1.857	1.86	1.863	1.866
0.57	1.869	1.873	1.876	1.879	1.882
	1.885	1.889	1.892	1.896	1.899
0.58	1.902	1.906	1.909	1.913	1.916
	1.92	1.923	1.927	1.931	1.934
0.59	1.938	1.942	1.946	1.949	1.953
	1.957	1.961	1.965	1.969	1.973

a/W					
	0	0.001	0.002	0.003	0.004
	0.005	0.006	0.007	0.008	0.009
0.6	1.977	1.981	1.985	1.989	1.993
	1.997	2.002	2.006	2.01	2.015
0.61	2.019	2.023	2.028	2.032	2.037
	2.041	2.046	2.051	2.055	2.06
0.62	2.065	2.07	2.075	2.079	2.084
	2.089	2.094	2.1	2.105	2.11
0.63	2.115	2.12	2.126	2.131	2.137
	2.142	2.148	2.153	2.159	2.165
0.64	2.17	2.176	2.182	2.188	2.194
	2.2	2.206	2.212	2.218	2.225
0.65	2.231	2.238	2.244	2.251	2.257
	2.264	2.271	2.278	2.285	2.292
0.66	2.299	2.306	2.313	2.32	2.328
	2.335	2.343	2.35	2.358	2.366
0.67	2.374	2.382	2.39	2.398	2.406
	2.415	2.423	2.432	2.441	2.449
0.68	2.458	2.467	2.476	2.486	2.495
	2.504	2.514	2.524	2.534	2.544
0.69	2.554	2.564	2.574	2.585	2.595
	2.606	2.617	2.628	2.64	2.651
0.7	2.663	2.674	2.686	2.698	2.711
	2.723	2.736	2.749	2.762	2.775
0.71	2.788	2.802	2.816	2.83	2.844
	2.859	2.874	2.889	2.904	2.919
0.72	2.935	2.951	2.968	2.984	3.001

Table B.1 - *Continued*

	3.019	3.036	3.054	3.072	3.091
0.73	3.11	3.129	3.149	3.169	3.189
	3.21	3.231	3.253	3.275	3.298
0.74	3.321	3.345	3.369	3.394	3.419
	3.445	3.472	3.499	3.527	3.555
0.75	3.584	3.614	3.645	3.677	3.709
	3.742	3.776	3.812	3.848	3.885
0.76	3.923	3.963	4.003	4.045	4.089
	4.133	4.179	4.227	4.277	4.328
0.77	4.381	4.436	4.493	4.552	4.614
	4.678	4.745	4.815	4.888	4.965
0.78	5.045	5.129	5.217	5.31	5.408
	5.511	5.62	5.736	5.859	5.99
0.79	6.13	6.281	6.442	6.616	6.804
	7.009	7.232	7.478	7.749	8.051
0.8	8.39	8.773	9.212	9.72	10.32
	11.04	11.92	13.04	14.53	16.63
0.81	19.94	26.26			
0.82					

Table B.1 – ***Continued***

Stiffened panel

a/W	0
	0.05
0.05	
	1.359
0.1	1.3494
	1.3398
0.15	1.3296
	1.3212
0.2	1.3122
	1.305
0.24	1.296
	1.2882
0.25	1.2816
	1.2744
0.26	1.2678
	1.2612
0.27	1.2558
	1.2492
0.28	1.2438
	1.2384
0.29	1.2336
	1.2282
0.3	1.224
	1.221
0.31	1.2162
	1.212
0.32	1.209
	1.2054
0.33	1.2024
	1.2
0.34	1.197
	1.1946
0.35	1.1922
	1.1904
0.36	1.1892
	1.1868
0.37	1.1856
	1.1856
0.38	1.185

Table B.2 – *Geometry factors for stiffened panel*

0.39	1.1838
	1.1838
0.4	1.1826
	1.1826
0.41	1.1814
	1.1814
0.42	1.1814
	1.1814
0.43	1.1814
	1.1814
------- -	1.1814

------- -	
a/W	----------

0.44	----------
	1.113636
0.45	1.092583
	1.072727
0.46	1.052631
	1.033492
0.47	1.014832
	0.996172
0.48	0.978708
	1.064641
0.49	1.10064
	1.138075
0.5	1.177028
	1.34892
0.51	1.395748
	1.444178
0.52	1.49469
	1.547412
0.53	1.602021
	1.65957
0.54	1.719266
	1.607724
0.55	1.504886
	1.408304
0.56	1.318449
	1.234449
0.57	1.155925
	1.08252
0.58	1.014244
	1.108187
0.59	1.093033
	1.078636
0.6	1.064997
	1.051736
0.61	1.18368
	1.169424
0.62	1.1556
	1.142208
0.63	1.128816
	1.116288
0.64	1.104192
	1.092528
0.65	1.080864
	1.069632
0.66	1.058832
	1.048464
0.67	1.03896
	1.029888
0.68	1.020384
	1.011744
0.69	1.003104
	0.994464

Table B.2 – *Continued*

0.7	----------
	0.978708
0.71	0.996172
	1.014832
0.72	1.033492
	1.052631
0.73	1.064641
	1.072727
0.74	1.092583
	1.113636
0.75	1.134688
	1.155741
0.76	1.176794
	1.197846
0.77	1.218899
	1.239952
0.78	1.261004
	1.282057
0.79	1.303109
	1.324162
0.8	1.345215
	1.366267

Table B.2 - *Continued*

B.4 Stress Intensity Factor Solutions for Surface Cracks near Welds (Taken from PD 6493)

E.1 General

This appendix contains stress intensity factor solutions for most of the types of flaw which are likely to arise in welded joints. They are recommended as the best available at present, based on consideration of accuracy, range of applicability and convenience. However, additional cases and improved solutions are likely to be produced in future, particularly for 3-D cases such as semi-elliptical cracks at weld toes and toe cracks in tubular joints, and these will be introduced in future updates of this document.

E.2 Embedded or surface elliptical cracks

E.2.1 ***General***

The solutions given in **E.2.2** and **E.2.3** are applicable to planar flaws or cracks of the types shown in figure 30(a) and (b).

In general,

$$K = \left\{\frac{(M_m\sigma_m + M_b\sigma_b)}{\Phi}\right\}(\pi a)^{0.5} \qquad \text{(E1)}$$

where

σ_m is the membrane stress component;

σ_b is the bending stress component;

a is the crack depth, as defined in figure 30;

M is the correction function dependent on crack size and shape, proximity of the crack tip to free surfaces and loading. Suffix 'm' refers to membrane and suffix 'b' to bending loading;

Φ is the complete elliptic integral of the second kind.

Φ may be obtained from standard tables, figure 7 or for convenience in calculations, the following approximate solution is sufficiently accurate (see reference 84):

$$\Phi = \{1.0 + 1.464\,(a/c)^{1.65}\}^{0.5} \quad \text{for } a/c \le 1 \qquad \text{(E2)}$$
$$\Phi = \{1.0 + 1.464\,(c/a)^{1.65}\}^{0.5} \quad \text{for } 1 < a/c \le 2$$

where c is the crack length, as defined in figure 30.

The values of M are given in **E.2.2** and **E.2.3**.

E.2.2 ***Embedded elliptical cracks***

NOTE. See figure 30(a).

E.2.2.1 *Membrane loading*

NOTE. See reference 84.

E.2.2.1.1 *Conditions*

The conditions for membrane loading are as follows:

$0 \le a/2c \le 1.0$; $2c/W < 0.5$; $-\pi \le \theta \le \pi$;

and $a/B < 0.625(a/c + 0.6)$ for $0 \le a/2c \le 0.1$

$a/B < 0.5$ for $0.1 \le a/2c \le 1.0$

E.2.2.1.2 *Solution*

The solution for the conditions given in **E.2.2.1.1** is as follows:

$$M_m = \{M_1 + M_2(2a/B')^2 + M_3(2a/B')^4\}\, gf_\theta f_w \qquad \text{(E3)}$$

where $B' = 2a + 2p$, the effective thickness.

$M_1 = 1$ for $a/2c \leq 0.5$

$M_1 = (c/a)^{0.5}$ for $0.5 < a/2c \leq 1.0$

$$M_2 = \frac{0.05}{0.11 + (a/c)^{1.5}}$$

$$M_3 = \frac{0.29}{0.23 + (a/c)^{1.5}}$$

$$g = 1 - \left[\frac{(2a/B')^4 \{2.6 - (4a/B')\}^{0.5}}{1 + 4(a/c)}\right] |\cos \theta|$$

$f_\theta = \{(a/c)^2 \cos^2 \theta + \sin^2 \theta\}^{0.25}$ for $a/2c \leq 0.5$

$f_\theta = \{(c/a)^2 \sin^2 \theta + \cos^2 \theta\}^{0.25}$ for $0.5 < a/2c \leq 1.0$

$f_w = \{\sec(\pi c/W)(2a/B')^{0.5}\}^{0.5}$

E.2.2.1.3 *Simplifications*

The following simplifications may be used.

(a) At the point on the crack front closest to the material surface, $\theta = \pi/2$ so that $g = f_\theta = 1$.

(b) At the ends of the crack, $\theta = 0$ so that

$$g = 1 - \left[\frac{(2a/B')^4 \{2.6 - (4a/B')\}^{0.5}}{1 + 4(a/c)}\right]$$

and $f_\theta = (a/c)^{0.5}$ for $a/2c \leq 0.5$

$f_\theta = 1.0$ for $0.5 < a/2c \leq 1.0$

(c) If $W \geq 20c$ it can be assumed that $c/W = 0$, so that $f_w = 1$.

(d) If $a/2c > 1.0$, use solution for $a/2c = 1.0$.

E.2.2.2 *Bending loading*

E.2.2.2.1 *Conditions*

The conditions for bending loading are as follows:

$0 \leq a/2c \leq 0.5$; $\theta = \pi/2$ (i.e. solution only refers to the ends of the minor axis of the elliptical crack).

E.2.2.2.2 *Solution*

The solution for the conditions given in **E.2.2.2.1** is as follows:

$M_b = A_1 + A_2(p/B) + A_3(a/B) + A_4(pa/B^2)$ (E4)[1)]

where

for $p/B \leq 0.1841$; $A_1 = 1.044$; $A_2 = -2.44$; $A_3 = 0$; $A_4 = -3.166$

for $p/B > 0.1841$ and $a/B \leq 0.125$; $A_1 = 0.94$; $A_2 = -1.875$; $A_3 = -0.1146$; $A_4 = -1.844$

for $p/B > 0.1841$ and $a/B > 0.125$; $A_1 = 1.06$; $A_2 = -2.20$; $A_3 = A_4 = -0.6666$.

E.2.3 *Semi-elliptical surface cracks*

NOTE. See figure 30(b).

E.2.3.1 *Membrane loading*

NOTE. See reference 84.

E.2.3.1.1 *Conditions*

The conditions for membrane loading are as follows:

$$0 \le a/2c \le 1.0;\ 2c/W < 0.5;\ 0 \le \phi \le \pi;$$

and $a/B < 1.25\,(a/c + 0.6)$ for $0 \le a/2c \le 0.1$

$a/B < 1.0$ for $0.1 \le a/2c \le 1.0$

E.2.3.1.2 *Solution*

The solution for the conditions given in **E.2.3.1.1** is as follows:

$$M_m = \{M_1 + M_2(a/B)^2 + M_3(a/B)^4\}\, g f_\phi f_w$$

where

$M_1 = 1.13 - 0.09\,(a/c)$ for $a/2c \le 0.5$

$M_1 = (c/a)^{0.5}\{1 + 0.04(c/a)\}$ for $0.5 < a/2c \le 1.0$

$$M_2 = \frac{0.89}{0.2 + (a/c)} - 0.54 \quad \text{for } a/2c \le 0.5$$

$M_2 = 0.2(c/a)^4$ for $0.5 < a/2c \le 1.0$

$$M_3 = 0.5 - \frac{1}{0.65 + (a/c)} + 14\,\{1 - (a/c)\}^{24} \quad \text{for } a/2c \le 0.5$$

$M_3 = -0.11\,(c/a)^4$ for $0.5 < a/2c \le 1.0$

$g = 1 + \{0.1 + 0.35(a/B)^2\}\,(1 - \sin\phi)^2$ for $a/2c \le 0.5$

$g = 1 + \{0.1 + 0.35(c/a)(a/B)^2\}\,(1 - \sin\phi)^2$ for $0.5 < a/2c \le 1.0$

$f_\phi = \{(a/c)^2 \cos^2\phi + \sin^2\phi\}^{0.25}$ for $a/2c \le 0.5$

$f_\phi = \{(c/a)^2 \sin^2\phi + \cos^2\phi\}^{0.25}$ for $0.5 < a/2c \le 1.0$

$f_w = \{\sec\,(\pi c/W)(a/B)^{0.5}\}^{0.5}$

E.2.3.1.3 *Simplifications*

The following simplifications may be used.

(a) At the deepest point on the crack front, $\phi = \pi/2$ so that $g = f_\phi = 1$.

(b) At the ends of the crack, $\phi = 0$, so that

$g = 1.1 + 0.35(a/B)^2$ for $a/2c \le 0.5$

$g = 1.1 + 0.35(c/a)(a/B)^2$ for $0.5 < a/2c \le 1.0$

and $f_\phi = (a/c)^{0.5}$ for $a/2c \le 0.5$

$f_\phi = 1.0$ for $0.5 < a/2c \le 1.0$

(c) If $W \ge 20c$, it can be assumed that $c/W = 0$, so that $f_w = 1$.

(d) If $a/2c > 1.0$, use solution for $a/2c = 1.0$.

E.2.3.2 *Bending loading*

NOTE. See reference 84.

E.2.3.2.1 *Conditions*

The conditions for bending loading are as given in **E.2.3.1.1**.

E.2.3.2.2 *Solution*

The solution for the conditions given in **E.2.3.2.1** is as follows:

$M_b = HM_m$

where

M_m is given by equation (E5)

$H = H_1 + (H_2 - H_1)\sin^q\theta$

where

$q = 0.2 + (a/c) + 0.6(a/B)$ for $a/2c \leq 0.5$

$q = 0.2 + (c/a) + 0.6(a/B)$ for $0.5 < a/2c \leq 1.0$

$H_1 = 1 - 0.34(a/B) - 0.11(a/c)(a/B)$ for $a/2c \leq 0.5$

$H_1 = 1 - \{0.04 + 0.41(c/a)\}(a/B) + \{0.55 - 1.93(c/a)^{0.75} + 1.38(c/a)^{1.5}\}(a/B)^2$ for $0.5 < a/2c \leq 1.0$

$H_2 = 1 + G_1(a/B) + G_2(a/B)^2$

where

$G_1 = -1.22 - 0.12(a/c)$ for $a/2c \leq 0.5$

$G_1 = -2.11 + 0.77(c/a)$ for $0.5 < a/2c \leq 1.0$

$G_2 = 0.55 - 1.05(a/c)^{0.75} + 0.47(a/c)^{1.5}$ for $a/2c \leq 0.5$

$G_2 = 0.55 - 0.72(c/a)^{0.75} + 0.14(c/a)^{1.5}$ for $0.5 < a/2c \leq 1.0$

E.2.3.2.3 *Simplifications*

The following simplifications may be used.

(a) At the deepest point on the crack front, $\theta = \pi/2$ so that $g = f_\theta = \sin^q\theta = 1$ and $H = H_2$.

(b) At the ends of the crack, $\theta = 0$, so that

$g = 1.1 + 0.35(a/B)^2$ for $a/2c \leq 0.5$

$g = 1.1 + 0.35(c/a)(a/B)^2$ for $0.5 < a/2c \leq 1.0$

$f_\theta = (a/c)^{0.5}$ for $a/2c \leq 0.5$

$f_\theta = 1.0$ for $0.5 < a/2c \leq 1.0$

and $H = H_1$

(c) If $W \geq 20c$, it can be assumed that $c/W = 0$, so that $f_w = 1$.

(d) If $a/2c > 1.0$, use solution for $a/2c = 1.0$.

E.3 Surface cracks at weld toes

NOTE. See figures 30(c) to (e).

E.3.1 ***General***

When a flaw or crack is situated in a region of local stress concentration, such as the weld toe, it is necessary to include the effect of the field of stress concentration when calculating K. This approach contrasts with that used in the application of the fatigue design rules (e.g. BS 5400 : Part 10), where the design data, obtained from fatigue tests on welded specimens, already incorporate the influence of the weld stress concentration factor and are therefore used in conjunction with the nominal stress range near the weld. Unless the K solution being used already incorporates the influence of the stress concentration, it is necessary to introduce the correction factor M_k, which is a function of crack size, geometry and loading. In general,

$$M_k = \frac{K \text{ for crack in material with stress concentration}}{K \text{ for same crack in material without stress concentration}}$$

Thus, M_k normally decreases with increase in crack depth, from a value equal to the stress concentration factor in the absence of a crack down to unity at crack depths of typically 30 % of material thickness.

The resulting stress intensity factor is:

$$K = \frac{(M_{km}M_m\sigma_m + M_{kb}M_b\sigma_b)}{\Phi}\sqrt{(\pi a)} \qquad \text{(E7)}$$

where M_m and M_b are as given in **E.2.3** and M_{km} and M_{kb} are M_k values for membrane and bending loading respectively.

For transverse butt welds, cruciform joints and members with fillet welded attachments, M_k has been found to be a function of a, B and L, where L is the overall length of the 'attachment' measured from weld toe to weld toe (see reference 85), as illustrated in figure 30(c) to (e). The resulting relationships are given in **E.3.2.**

If the equations given for cruciform joints are applied to T-joints the resulting values for tension will overestimate the stress intensity factor, whereas for bending there are some cases where the cruciform results underestimate the T-joint behaviour.

E.3.2 ***Membrane loading***

E.3.2.1 *Conditions*

M_k decreases to unity as a/B increases. For greater values of a/B, assume $M_k = 1$.

M_k has been calculated by 2-D finite element analysis for profiles representing sections of the welded joint geometry. Thus, M_k is directly applicable to the case of a straight-fronted weld toe crack (i.e. $a/2c = 0$). However, experience indicates that it can also be applied to semi-elliptical cracks ($0 < a/2c \leq 0.5$). The nature of the finite element model used to calculate M_k is such that the solutions produced are not applicable for $a = 0$. Thus, for a semi-elliptical crack they do not apply to the ends of the crack, at the surface. Experience indicates that it is reasonable to assume M_k is equal to the elastic stress concentration factor at the weld toe, or to adopt the value of M_k corresponding to a very small crack, such as $a = 0.15$ mm. The latter approach is compatible with the fact that in steels there are inherent crack-like flaws of this order of depth at all weld toes.

The solutions presented apply for 45° weld profiles. M_k is slightly lower for lower angles and vice versa.

E.3.2.2 *Solution*

In general,

$$M_k = v(a/B)^w, \text{ down to } M_k = 1 \qquad \text{(E8)}$$

where v and w have the values given in table 16.

Table 16. Values of v and w for axial and bending loading

Loading mode	L/B	a/B	v	w
Axial	≤ 2	≤ 0.05 $(L/B)^{0.55}$	0.51 $(L/B)^{0.27}$	−0.31
		> 0.05 $(L/B)^{0.55}$	0.83	$-0.15(L/B)^{0.46}$
	> 2	≤ 0.073	0.615	−0.31
		> 0.073	0.83	−0.20
Bending	≤ 1	≤ 0.03 $(L/B)^{0.55}$	0.45 $(L/B)^{0.21}$	−0.31
		> 0.03 $(L/B)^{0.55}$	0.68	$-0.19\ (L/B)^{0.21}$
	> 1	≤ 0.03	0.45	−0.31
		> 0.03	0.68	−0.19

E.4 Weld root crack in cruciform joint

NOTE. See figure 31.

E.4.1 *Conditions*

The solution was derived for tension loading but it is conservative to apply it for bending.

Also,

$0.2 \leq h/B \leq 1.2;\ 0 \leq 2a/W \leq 0.7$

E.4.2 *Solution*

NOTE. See reference 86.

The solution for the conditions given in **E.4.1** is as follows:

$$K = M_k \sigma_m [\pi a \sec(\pi a/W)]^{0.5} \qquad \text{(E9)}$$

where

$$M_k = \frac{A_1 + A_2\,(2a/W)}{1 + (2h/B)}$$

σ_m is the membrane stress in loaded member;

$A_1 = 0.528 + 3.287(h/B) - 4.361(h/B)^2 + 3.696(h/B)^3 - 1.875(h/B)^4 + 0.415(h/B)^5$

$A_2 = 0.218 + 2.717(h/B) - 10.171(h/B)^2 + 13.122(h/B)^3 - 7.755(h/B)^4 + 1.783(h/B)^5$

and dimensions are indicated in figure 31.

In this case M_k is always less than unity and its value may increase or decrease with crack size, depending on the value of h/B.

APPENDIX C

RESULTS FROM MONTE CARLO SIMULATION

Table C.1 – *Results from Monte Carlo simulation for first section*

```
========== CONTROL PARAMETER ==========
NUMBER OF GROUPS              :        3
NUMBER OF JOINTS              :        1
NUMBER OF BASIC VARIABLE IN LSF  :        12
SAMPLING SIZE IN MONTE CARLO SIM.  :      500000

NUMBER OF YEARS               :       40
INSPECTION INTERVAL           :        3
INSPECTION QUALITY            :       50.
CRACK GROWTH CONSTANT m       :      3.3
CORROSION RATE                :      0.3
STRESS THRESHOLD              :      2.5

========== INFORMATION OF JOINT ==========
    NO.    ID.   THICKNESS     REF_LEN     POSITION

     1      7       25.0       5000.0      17384.0
     2      7       25.0       5000.0       2460.0
     3      7       25.0       5000.0       7250.0
==== IDENTIFICATION OF BASIC VARIABLES ====
    NO.    ID.

     1      1      1      0
     2      3      1      0
     3      5      1      0
     4      1      0      1
     5      2      0      1
     6      2      0      1
     7      2      0      1
     8      2      0      1
     9      1      1      0
    10      0      1      0
    11      2      0      1
    12      0      1      0
====== MEAN VALUE OF BASIC VARIABLES =====
GROUP     C  KMAT    AN      CN    B    A     B1   A1    SY     ST      BM       Iyy

 1 0.148E-13  273.0  9.000 2887611.0  0.842  9.960  0.858  5.320  345.000  420.000  861652.000
0.188E+15
 2 0.502E-13  273.0  9.000 2879928.0  0.858  7.560  0.825  3.610  345.000  420.000  861652.000
0.188E+15
 3 0.502E-13  273.0  9.000 3071540.0  0.921  8.360  0.800  2.980  345.000  420.000  861652.000
0.188E+15
== STANDARD DEVIATION OF BASIC VARIABLES =
GROUP     C  KMAT    AN      CN    B    A     B1   A1    SY     ST      BM       Iyy

 1 0.444E-14  6.7  0.000 285049.8  0.020  1.000  0.020  0.500  17.000  0.000  107706.500 0.000E+00
 2 0.151E-13  6.7  0.000 283990.0  0.020  1.000  0.020  0.500  17.000  0.000  107706.500 0.000E+00
 3 0.151E-13  6.7  0.000 309538.2  0.020  1.000  0.020  0.500  17.000  0.000  107706.500 0.000E+00
==========================================
     END OF INPUT PARAMETERS
==========================================

 Program started at :
 DAY / MONTH / YEAR
 17    6    2001
 HOUR:MIMUTE:SECOND
 23    19    42
==========================================
          RESULTS
==========================================
```

Year	joint	Pf	Cov	CPf	a	sa	Brittle failures	Plastic failures	Sample left	Cracks Repaired
0	1	0.000E+00	0.000E+00	0.000E+00	0.3552	0.1111	0	0	250000	0
0	2	0.000E+00	0.000E+00	0.000E+00	0.3552	0.1113	0	0	250000	0
0	3	0.000E+00	0.000E+00	0.000E+00	0.3553	0.1109	0	0	250000	0

PROBABILITY OF FAILURE OF SYSTEM

CASE1	CASE2	CASE3
0.000E+00	0.000E+00	0.000E+00

CUMULATIVE PROBABILITY OF FAILURE OF SYSTEM

CASE1	CASE2	CASE3
0.000E+00	0.000E+00	0.000E+00

Year	joint	Pf	Cov	CPf	a	sa	Brittle failures	Plastic failures	Sample left	Cracks Repaired
1	1	0.000E+00	0.000E+00	0.000E+00	0.3578	0.1111	0	0	250000	0
1	2	0.000E+00	0.000E+00	0.000E+00	0.3575	0.1114	0	0	250000	0
1	3	0.000E+00	0.000E+00	0.000E+00	0.4636	0.1269	0	0	250000	0

PROBABILITY OF FAILURE OF SYSTEM

CASE1	CASE2	CASE3
0.000E+00	0.000E+00	0.000E+00

CUMULATIVE PROBABILITY OF FAILURE OF SYSTEM

CASE1	CASE2	CASE3
0.000E+00	0.000E+00	0.000E+00

Year	joint	Pf	Cov	CPf	a	sa	Brittle failures	Plastic failures	Sample left	Cracks Repaired
2	1	0.000E+00	0.000E+00	0.000E+00	0.3587	0.1113	0	0	250000	0
2	2	0.000E+00	0.000E+00	0.000E+00	0.3579	0.1115	0	0	250000	0
2	3	0.000E+00	0.000E+00	0.000E+00	0.5399	0.1437	0	0	250000	0

PROBABILITY OF FAILURE OF SYSTEM

CASE1	CASE2	CASE3
0.000E+00	0.000E+00	0.000E+00

CUMULATIVE PROBABILITY OF FAILURE OF SYSTEM

CASE1	CASE2	CASE3

0.000E+00 0.000E+00 0.000E+00

Year	joint	Pf	Cov	CPf	a	sa	Brittle failures	Plastic failures	Sample left	Cracks Repaired
3	1	0.000E+00	0.000E+00	0.000E+00	0.3610	0.1112	0	0	250000	1775
3	2	0.000E+00	0.000E+00	0.000E+00	0.3599	0.1114	0	0	250000	1753
3	3	0.000E+00	0.000E+00	0.000E+00	0.6479	0.1667	0	0	250000	3273

PROBABILITY OF FAILURE OF SYSTEM

CASE1 CASE2 CASE3

0.000E+00 0.000E+00 0.000E+00

CUMULATIVE PROBABILITY OF FAILURE OF SYSTEM

CASE1 CASE2 CASE3

0.000E+00 0.000E+00 0.000E+00

Year	joint	Pf	Cov	CPf	a	sa	Brittle failures	Plastic failures	Sample left	Cracks Repaired
4	1	0.000E+00	0.000E+00	0.000E+00	0.3637	0.1113	0	0	250000	0
4	2	0.000E+00	0.000E+00	0.000E+00	0.3622	0.1116	0	0	250000	0
4	3	0.000E+00	0.000E+00	0.000E+00	0.7536	0.1818	0	0	250000	0

PROBABILITY OF FAILURE OF SYSTEM

CASE1 CASE2 CASE3

0.000E+00 0.000E+00 0.000E+00

CUMULATIVE PROBABILITY OF FAILURE OF SYSTEM

CASE1 CASE2 CASE3

0.000E+00 0.000E+00 0.000E+00

Year	joint	Pf	Cov	CPf	a	sa	Brittle failures	Plastic failures	Sample left	Cracks Repaired
5	1	0.000E+00	0.000E+00	0.000E+00	0.3645	0.1114	0	0	250000	0
5	2	0.000E+00	0.000E+00	0.000E+00	0.3626	0.1117	0	0	250000	0
5	3	0.000E+00	0.000E+00	0.000E+00	0.8287	0.1914	0	0	250000	0

PROBABILITY OF FAILURE OF SYSTEM

CASE1 CASE2 CASE3

0.000E+00 0.000E+00 0.000E+00

CUMULATIVE PROBABILITY OF FAILURE OF SYSTEM

CASE1 CASE2 CASE3

0.000E+00 0.000E+00 0.000E+00

Year	joint	Pf	Cov	CPf	a	sa	Brittle failures	Plastic failures	Sample left	Cracks Repaired
6	1	0.000E+00	0.000E+00	0.000E+00	0.3669	0.1113	0	0	250000	1798
6	2	0.000E+00	0.000E+00	0.000E+00	0.3646	0.1116	0	0	250000	1782
6	3	0.000E+00	0.000E+00	0.000E+00	0.9138	0.2104	0	0	250000	4594

PROBABILITY OF FAILURE OF SYSTEM

CASE1 CASE2 CASE3

0.000E+00 0.000E+00 0.000E+00

CUMULATIVE PROBABILITY OF FAILURE OF SYSTEM

CASE1 CASE2 CASE3

0.000E+00 0.000E+00 0.000E+00

Year	joint	Pf	Cov	CPf	a	sa	Brittle failures	Plastic failures	Sample left	Cracks Repaired
7	1	0.000E+00	0.000E+00	0.000E+00	0.3695	0.1114	0	0	250000	0
7	2	0.000E+00	0.000E+00	0.000E+00	0.3669	0.1118	0	0	250000	0
7	3	0.000E+00	0.000E+00	0.000E+00	0.9993	0.2136	0	0	250000	0

PROBABILITY OF FAILURE OF SYSTEM

CASE1 CASE2 CASE3

0.000E+00 0.000E+00 0.000E+00

CUMULATIVE PROBABILITY OF FAILURE OF SYSTEM

CASE1 CASE2 CASE3

0.000E+00 0.000E+00 0.000E+00

Year	joint	Pf	Cov	CPf	a	sa	Brittle failures	Plastic failures	Sample left	Cracks Repaired
8	1	0.000E+00	0.000E+00	0.000E+00	0.3704	0.1115	0	0	250000	0
8	2	0.000E+00	0.000E+00	0.000E+00	0.3673	0.1119	0	0	250000	0
8	3	0.400E-05	0.100E+01	0.400E-05	1.0608	0.2204	1	0	249999	0

PROBABILITY OF FAILURE OF SYSTEM

CASE1 CASE2 CASE3

0.133E-05 0.400E-05 0.399E-05

CUMULATIVE PROBABILITY OF FAILURE OF SYSTEM

CASE1 CASE2 CASE3

0.133E-05 0.400E-05 0.399E-05

Year	joint	Pf	Cov	CPf	a	sa	Brittle failures	Plastic failures	Sample left	Cracks Repaired
9	1	0.000E+00	0.000E+00	0.000E+00	0.3727	0.1114	0	0	250000	1861
9	2	0.000E+00	0.000E+00	0.000E+00	0.3693	0.1117	0	0	250000	1809
9	3	0.000E+00	0.000E+00	0.400E-05	1.1202	0.2575	0	0	249999	5632

PROBABILITY OF FAILURE OF SYSTEM

CASE1 CASE2 CASE3

0.000E+00 0.000E+00 0.000E+00

CUMULATIVE PROBABILITY OF FAILURE OF SYSTEM

CASE1 CASE2 CASE3

0.133E-05 0.400E-05 0.399E-05

Year	joint	Pf	Cov	CPf	a	sa	Brittle failures	Plastic failures	Sample left	Cracks Repaired
10	1	0.000E+00	0.000E+00	0.000E+00	0.3754	0.1115	0	0	250000	0
10	2	0.000E+00	0.000E+00	0.000E+00	0.3716	0.1120	0	0	250000	0
10	3	0.000E+00	0.000E+00	0.400E-05	1.1941	0.2708	0	0	249999	0

PROBABILITY OF FAILURE OF SYSTEM

CASE1 CASE2 CASE3

0.000E+00 0.000E+00 0.000E+00

CUMULATIVE PROBABILITY OF FAILURE OF SYSTEM

CASE1 CASE2 CASE3

0.133E-05 0.400E-05 0.399E-05

Year	joint	Pf	Cov	CPf	a	sa	Brittle failures	Plastic failures	Sample left	Cracks Repaired
11	1	0.000E+00	0.000E+00	0.000E+00	0.3763	0.1117	0	0	250000	0
11	2	0.000E+00	0.000E+00	0.000E+00	0.3720	0.1121	0	0	250000	0
11	3	0.000E+00	0.000E+00	0.400E-05	1.2525	0.2897	0	0	249999	0

PROBABILITY OF FAILURE OF SYSTEM

CASE1 CASE2 CASE3

0.000E+00 0.000E+00 0.000E+00

CUMULATIVE PROBABILITY OF FAILURE OF SYSTEM

CASE1 CASE2 CASE3

0.133E-05 0.400E-05 0.399E-05

Year	joint	Pf	Cov	CPf	a	sa	Brittle failures	Plastic failures	Sample left	Cracks Repaired
12	1	0.000E+00	0.000E+00	0.000E+00	0.3786	0.1117	0	0	250000	1890
12	2	0.000E+00	0.000E+00	0.000E+00	0.3740	0.1120	0	0	250000	1911
12	3	0.000E+00	0.000E+00	0.400E-05	1.3018	0.3491	0	0	249999	6558

PROBABILITY OF FAILURE OF SYSTEM

CASE1 CASE2 CASE3

0.000E+00 0.000E+00 0.000E+00

CUMULATIVE PROBABILITY OF FAILURE OF SYSTEM

CASE1 CASE2 CASE3

0.133E-05 0.400E-05 0.399E-05

Year	joint	Pf	Cov	CPf	a	sa	Brittle failures	Plastic failures	Sample left	Cracks Repaired
13	1	0.000E+00	0.000E+00	0.000E+00	0.3812	0.1119	0	0	250000	0
13	2	0.000E+00	0.000E+00	0.000E+00	0.3763	0.1123	0	0	250000	0
13	3	0.000E+00	0.000E+00	0.400E-05	1.3790	0.3771	0	0	249999	0

PROBABILITY OF FAILURE OF SYSTEM

CASE1 CASE2 CASE3

0.000E+00 0.000E+00 0.000E+00

CUMULATIVE PROBABILITY OF FAILURE OF SYSTEM

CASE1 CASE2 CASE3

0.133E-05 0.400E-05 0.399E-05

Year	joint	Pf	Cov	CPf	a	sa	Brittle failures	Plastic failures	Sample left	Cracks Repaired
14	1	0.000E+00	0.000E+00	0.000E+00	0.3821	0.1120	0	0	250000	0
14	2	0.000E+00	0.000E+00	0.000E+00	0.3767	0.1124	0	0	250000	0
14	3	0.000E+00	0.000E+00	0.400E-05	1.4439	0.4110	0	0	249999	0

PROBABILITY OF FAILURE OF SYSTEM

CASE1 CASE2 CASE3

0.000E+00 0.000E+00 0.000E+00

CUMULATIVE PROBABILITY OF FAILURE OF SYSTEM

CASE1 CASE2 CASE3

0.133E-05 0.400E-05 0.399E-05

Year	joint	Pf	Cov	CPf	a	sa	Brittle failures	Plastic failures	Sample left	Cracks Repaired
15	1	0.000E+00	0.000E+00	0.000E+00	0.3844	0.1120	0	0	250000	1921
15	2	0.000E+00	0.000E+00	0.000E+00	0.3787	0.1124	0	0	250000	1876
15	3	0.000E+00	0.000E+00	0.400E-05	1.4902	0.4882	0	0	249999	7555

PROBABILITY OF FAILURE OF SYSTEM

CASE1 CASE2 CASE3

0.000E+00 0.000E+00 0.000E+00

CUMULATIVE PROBABILITY OF FAILURE OF SYSTEM

CASE1 CASE2 CASE3

0.133E-05 0.400E-05 0.399E-05

Year	joint	Pf	Cov	CPf	a	sa	Brittle failures	Plastic failures	Sample left	Cracks Repaired
16	1	0.000E+00	0.000E+00	0.000E+00	0.3871	0.1122	0	0	250000	0
16	2	0.000E+00	0.000E+00	0.000E+00	0.3811	0.1126	0	0	250000	0
16	3	0.000E+00	0.000E+00	0.400E-05	1.5782	0.5345	0	0	249999	0

PROBABILITY OF FAILURE OF SYSTEM

CASE1 CASE2 CASE3

0.000E+00 0.000E+00 0.000E+00

CUMULATIVE PROBABILITY OF FAILURE OF SYSTEM

CASE1 CASE2 CASE3

0.133E-05 0.400E-05 0.399E-05

Year	joint	Pf	Cov	CPf	a	sa	Brittle failures	Plastic failures	Sample left	Cracks Repaired
17	1	0.000E+00	0.000E+00	0.000E+00	0.3880	0.1123	0	0	250000	0
17	2	0.000E+00	0.000E+00	0.000E+00	0.3815	0.1127	0	0	250000	0

17	3	0.000E+00	0.000E+00	0.400E-05	1.6550	0.6051	0	0	249999	0

PROBABILITY OF FAILURE OF SYSTEM

CASE1 CASE2 CASE3

0.000E+00 0.000E+00 0.000E+00

CUMULATIVE PROBABILITY OF FAILURE OF SYSTEM

CASE1 CASE2 CASE3

0.133E-05 0.400E-05 0.399E-05

Year	joint	Pf	Cov	CPf	a	sa	Brittle failures	Plastic failures	Sample left	Cracks Repaired
18	1	0.000E+00	0.000E+00	0.000E+00	0.3902	0.1123	0	0	250000	1877
18	2	0.000E+00	0.000E+00	0.000E+00	0.3834	0.1127	0	0	250000	1951
18	3	0.000E+00	0.000E+00	0.400E-05	1.6994	0.7288	0	0	249999	8655

PROBABILITY OF FAILURE OF SYSTEM

CASE1 CASE2 CASE3

0.000E+00 0.000E+00 0.000E+00

CUMULATIVE PROBABILITY OF FAILURE OF SYSTEM

CASE1 CASE2 CASE3

0.133E-05 0.400E-05 0.399E-05

Year	joint	Pf	Cov	CPf	a	sa	Brittle failures	Plastic failures	Sample left	Cracks Repaired
19	1	0.000E+00	0.000E+00	0.000E+00	0.3929	0.1124	0	0	250000	0
19	2	0.000E+00	0.000E+00	0.000E+00	0.3858	0.1129	0	0	250000	0
19	3	0.000E+00	0.000E+00	0.400E-05	1.8027	0.8794	0	0	249999	0

PROBABILITY OF FAILURE OF SYSTEM

CASE1 CASE2 CASE3

0.000E+00 0.000E+00 0.000E+00

CUMULATIVE PROBABILITY OF FAILURE OF SYSTEM

CASE1 CASE2 CASE3

0.133E-05 0.400E-05 0.399E-05

Year	joint	Pf	Cov	CPf	a	sa	Brittle failures	Plastic failures	Sample left	Cracks Repaired

20	1	0.000E+00	0.000E+00	0.000E+00	0.3938	0.1126	0	0	250000	0
20	2	0.000E+00	0.000E+00	0.000E+00	0.3862	0.1130	0	0	250000	0
20	3	0.000E+00	0.000E+00	0.400E-05	1.8971	1.2077	0	0	249999	0

PROBABILITY OF FAILURE OF SYSTEM

CASE1	CASE2	CASE3
0.000E+00	0.000E+00	0.000E+00

CUMULATIVE PROBABILITY OF FAILURE OF SYSTEM

CASE1	CASE2	CASE3
0.133E-05	0.400E-05	0.399E-05

Year	joint	Pf	Cov	CPf	a	sa	Brittle failures	Plastic failures	Sample left	Cracks Repaired
21	1	0.000E+00	0.000E+00	0.000E+00	0.3959	0.1125	0	0	250000	2055
21	2	0.000E+00	0.000E+00	0.000E+00	0.3881	0.1130	0	0	250000	1940
21	3	0.000E+00	0.000E+00	0.400E-05	1.9309	1.1209	0	0	249999	9740

PROBABILITY OF FAILURE OF SYSTEM

CASE1	CASE2	CASE3
0.000E+00	0.000E+00	0.000E+00

CUMULATIVE PROBABILITY OF FAILURE OF SYSTEM

CASE1	CASE2	CASE3
0.133E-05	0.400E-05	0.399E-05

Year	joint	Pf	Cov	CPf	a	sa	Brittle failures	Plastic failures	Sample left	Cracks Repaired
22	1	0.000E+00	0.000E+00	0.000E+00	0.3986	0.1126	0	0	250000	0
22	2	0.000E+00	0.000E+00	0.000E+00	0.3904	0.1132	0	0	250000	0
22	3	0.000E+00	0.000E+00	0.400E-05	2.0608	3.8765	0	0	249999	0

PROBABILITY OF FAILURE OF SYSTEM

CASE1	CASE2	CASE3
0.000E+00	0.000E+00	0.000E+00

CUMULATIVE PROBABILITY OF FAILURE OF SYSTEM

CASE1	CASE2	CASE3
0.133E-05	0.400E-05	0.399E-05

Year	joint	Pf	Cov	CPf	a	sa	Brittle failures	Plastic failures	Sample left	Cracks Repaired
23	1	0.000E+00	0.000E+00	0.000E+00	0.3995	0.1128	0	0	250000	0
23	2	0.000E+00	0.000E+00	0.000E+00	0.3908	0.1133	0	0	250000	0
23	3	0.800E-05	0.707E+00	0.120E-04	2.2327	23.1557	2	0	249997	0

PROBABILITY OF FAILURE OF SYSTEM

CASE1	CASE2	CASE3
0.267E-05	0.800E-05	0.799E-05

CUMULATIVE PROBABILITY OF FAILURE OF SYSTEM

CASE1	CASE2	CASE3
0.400E-05	0.120E-04	0.120E-04

Year	joint	Pf	Cov	CPf	a	sa	Brittle failures	Plastic failures	Sample left	Cracks Repaired
24	1	0.000E+00	0.000E+00	0.000E+00	0.4016	0.1129	0	0	250000	2019
24	2	0.000E+00	0.000E+00	0.000E+00	0.3927	0.1133	0	0	250000	1965
24	3	0.000E+00	0.000E+00	0.120E-04	2.1861	1.5855	0	0	249997	11164

PROBABILITY OF FAILURE OF SYSTEM

CASE1	CASE2	CASE3
0.000E+00	0.000E+00	0.000E+00

CUMULATIVE PROBABILITY OF FAILURE OF SYSTEM

CASE1	CASE2	CASE3
0.400E-05	0.120E-04	0.120E-04

Year	joint	Pf	Cov	CPf	a	sa	Brittle failures	Plastic failures	Sample left	Cracks Repaired
25	1	0.000E+00	0.000E+00	0.000E+00	0.4043	0.1131	0	0	250000	0
25	2	0.000E+00	0.000E+00	0.000E+00	0.3950	0.1135	0	0	250000	0
25	3	0.000E+00	0.000E+00	0.120E-04	2.3370	2.2206	0	0	249997	0

PROBABILITY OF FAILURE OF SYSTEM

CASE1	CASE2	CASE3
0.000E+00	0.000E+00	0.000E+00

CUMULATIVE PROBABILITY OF FAILURE OF SYSTEM

CASE1 CASE2 CASE3

0.400E-05 0.120E-04 0.120E-04

Year	joint	Pf	Cov	CPf	a	sa	Brittle failures	Plastic failures	Sample left	Cracks Repaired
26	1	0.000E+00	0.000E+00	0.000E+00	0.4052	0.1132	0	0	250000	0
26	2	0.000E+00	0.000E+00	0.000E+00	0.3954	0.1136	0	0	250000	0
26	3	0.400E-05	0.100E+01	0.160E-04	2.5210	10.5506	1	0	249996	0

PROBABILITY OF FAILURE OF SYSTEM

CASE1 CASE2 CASE3

0.133E-05 0.400E-05 0.399E-05

CUMULATIVE PROBABILITY OF FAILURE OF SYSTEM

CASE1 CASE2 CASE3

0.533E-05 0.160E-04 0.160E-04

Year	joint	Pf	Cov	CPf	a	sa	Brittle failures	Plastic failures	Sample left	Cracks Repaired
27	1	0.000E+00	0.000E+00	0.000E+00	0.4074	0.1133	0	0	250000	1981
27	2	0.000E+00	0.000E+00	0.000E+00	0.3973	0.1136	0	0	250000	2008
27	3	0.400E-05	0.100E+01	0.200E-04	2.4582	2.2340	1	0	249995	12769

PROBABILITY OF FAILURE OF SYSTEM

CASE1 CASE2 CASE3

0.133E-05 0.400E-05 0.399E-05

CUMULATIVE PROBABILITY OF FAILURE OF SYSTEM

CASE1 CASE2 CASE3

0.667E-05 0.200E-04 0.200E-04

Year	joint	Pf	Cov	CPf	a	sa	Brittle failures	Plastic failures	Sample left	Cracks Repaired
28	1	0.000E+00	0.000E+00	0.000E+00	0.4100	0.1135	0	0	250000	0
28	2	0.000E+00	0.000E+00	0.000E+00	0.3996	0.1139	0	0	250000	0
28	3	0.400E-05	0.100E+01	0.240E-04	2.6515	3.5403	1	0	249994	0

PROBABILITY OF FAILURE OF SYSTEM

CASE1 CASE2 CASE3

0.133E-05 0.400E-05 0.399E-05

CUMULATIVE PROBABILITY OF FAILURE OF SYSTEM

CASE1 CASE2 CASE3

0.800E-05 0.240E-04 0.240E-04

Year	joint	Pf	Cov	CPf	a	sa	Brittle failures	Plastic failures	Sample left	Cracks Repaired
29	1	0.000E+00	0.000E+00	0.000E+00	0.4110	0.1136	0	0	250000	0
29	2	0.000E+00	0.000E+00	0.000E+00	0.4000	0.1140	0	0	250000	0
29	3	0.160E-04	0.500E+00	0.400E-04	2.9309	14.4655	4	0	249990	0

PROBABILITY OF FAILURE OF SYSTEM

CASE1 CASE2 CASE3

0.533E-05 0.160E-04 0.160E-04

CUMULATIVE PROBABILITY OF FAILURE OF SYSTEM

CASE1 CASE2 CASE3

0.133E-04 0.400E-04 0.399E-04

Year	joint	Pf	Cov	CPf	a	sa	Brittle failures	Plastic failures	Sample left	Cracks Repaired
30	1	0.000E+00	0.000E+00	0.000E+00	0.4130	0.1137	0	0	250000	2120
30	2	0.000E+00	0.000E+00	0.000E+00	0.4018	0.1139	0	0	250000	2042
30	3	0.000E+00	0.000E+00	0.400E-04	2.7455	2.9859	0	0	249990	14116

PROBABILITY OF FAILURE OF SYSTEM

CASE1 CASE2 CASE3

0.000E+00 0.000E+00 0.000E+00

CUMULATIVE PROBABILITY OF FAILURE OF SYSTEM

CASE1 CASE2 CASE3

0.133E-04 0.400E-04 0.399E-04

Year	joint	Pf	Cov	CPf	a	sa	Brittle failures	Plastic failures	Sample left	Cracks Repaired
31	1	0.000E+00	0.000E+00	0.000E+00	0.4157	0.1139	0	0	250000	0
31	2	0.000E+00	0.000E+00	0.000E+00	0.4042	0.1141	0	0	250000	0
31	3	0.000E+00	0.000E+00	0.400E-04	2.9892	4.3771	0	0	249990	0

PROBABILITY OF FAILURE OF SYSTEM

CASE1 CASE2 CASE3

0.000E+00 0.000E+00 0.000E+00

CUMULATIVE PROBABILITY OF FAILURE OF SYSTEM

CASE1 CASE2 CASE3

0.133E-04 0.400E-04 0.399E-04

Year	joint	Pf	Cov	CPf	a	sa	Brittle failures	Plastic failures	Sample left	Cracks Repaired
32	1	0.000E+00	0.000E+00	0.000E+00	0.4167	0.1140	0	0	250000	0
32	2	0.000E+00	0.000E+00	0.000E+00	0.4046	0.1142	0	0	250000	0
32	3	0.000E+00	0.000E+00	0.400E-04	3.3505	17.7380	0	0	249990	0

PROBABILITY OF FAILURE OF SYSTEM

CASE1 CASE2 CASE3

0.000E+00 0.000E+00 0.000E+00

CUMULATIVE PROBABILITY OF FAILURE OF SYSTEM

CASE1 CASE2 CASE3

0.133E-04 0.400E-04 0.399E-04

Year	joint	Pf	Cov	CPf	a	sa	Brittle failures	Plastic failures	Sample left	Cracks Repaired
33	1	0.000E+00	0.000E+00	0.000E+00	0.4187	0.1142	0	0	250000	2079
33	2	0.000E+00	0.000E+00	0.000E+00	0.4064	0.1144	0	0	250000	2001
33	3	0.000E+00	0.000E+00	0.400E-04	3.0407	4.1535	0	0	249990	16037

PROBABILITY OF FAILURE OF SYSTEM

CASE1 CASE2 CASE3

0.000E+00 0.000E+00 0.000E+00

CUMULATIVE PROBABILITY OF FAILURE OF SYSTEM

CASE1 CASE2 CASE3

0.133E-04 0.400E-04 0.399E-04

Year	joint	Pf	Cov	CPf	a	sa	Brittle failures	Plastic failures	Sample left	Cracks Repaired
34	1	0.000E+00	0.000E+00	0.000E+00	0.4214	0.1145	0	0	250000	0
34	2	0.000E+00	0.000E+00	0.000E+00	0.4087	0.1146	0	0	250000	0
34	3	0.000E+00	0.000E+00	0.400E-04	3.3785	8.6023	0	0	249990	0

PROBABILITY OF FAILURE OF SYSTEM

CASE1 CASE2 CASE3

0.000E+00 0.000E+00 0.000E+00

CUMULATIVE PROBABILITY OF FAILURE OF SYSTEM

CASE1 CASE2 CASE3

0.133E-04 0.400E-04 0.399E-04

Year	joint	Pf	Cov	CPf	a	sa	Brittle failures	Plastic failures	Sample left	Cracks Repaired
35	1	0.000E+00	0.000E+00	0.000E+00	0.4223	0.1146	0	0	250000	0
35	2	0.000E+00	0.000E+00	0.000E+00	0.4092	0.1147	0	0	250000	0
35	3	0.280E-04	0.378E+00	0.680E-04	4.0444	40.2758	7	0	249983	0

PROBABILITY OF FAILURE OF SYSTEM

CASE1 CASE2 CASE3

0.933E-05 0.280E-04 0.280E-04

CUMULATIVE PROBABILITY OF FAILURE OF SYSTEM

CASE1 CASE2 CASE3

0.227E-04 0.680E-04 0.679E-04

Year	joint	Pf	Cov	CPf	a	sa	Brittle failures	Plastic failures	Sample left	Cracks Repaired
36	1	0.000E+00	0.000E+00	0.000E+00	0.4243	0.1147	0	0	250000	2042
36	2	0.000E+00	0.000E+00	0.000E+00	0.4109	0.1148	0	0	250000	2047
36	3	0.000E+00	0.000E+00	0.680E-04	3.3082	5.1159	0	0	249983	17101

PROBABILITY OF FAILURE OF SYSTEM

CASE1 CASE2 CASE3

0.000E+00 0.000E+00 0.000E+00

CUMULATIVE PROBABILITY OF FAILURE OF SYSTEM

CASE1 CASE2 CASE3

0.227E-04 0.680E-04 0.679E-04

Year	joint	Pf	Cov	CPf	a	sa	Brittle failures	Plastic failures	Sample left	Cracks Repaired
37	1	0.000E+00	0.000E+00	0.000E+00	0.4270	0.1150	0	0	250000	0
37	2	0.000E+00	0.000E+00	0.000E+00	0.4133	0.1150	0	0	250000	0
37	3	0.000E+00	0.000E+00	0.680E-04	3.7072	10.5608	0	0	249983	0

PROBABILITY OF FAILURE OF SYSTEM

CASE1	CASE2	CASE3
0.000E+00	0.000E+00	0.000E+00

CUMULATIVE PROBABILITY OF FAILURE OF SYSTEM

CASE1	CASE2	CASE3
0.227E-04	0.680E-04	0.679E-04

Year	joint	Pf	Cov	CPf	a	sa	Brittle failures	Plastic failures	Sample left	Cracks Repaired
38	1	0.000E+00	0.000E+00	0.000E+00	0.4280	0.1152	0	0	250000	0
38	2	0.000E+00	0.000E+00	0.000E+00	0.4137	0.1151	0	0	250000	0
38	3	0.280E-04	0.378E+00	0.960E-04	4.4396	39.0108	7	0	249976	0

PROBABILITY OF FAILURE OF SYSTEM

CASE1	CASE2	CASE3
0.933E-05	0.280E-04	0.280E-04

CUMULATIVE PROBABILITY OF FAILURE OF SYSTEM

CASE1	CASE2	CASE3
0.320E-04	0.960E-04	0.960E-04

Year	joint	Pf	Cov	CPf	a	sa	Brittle failures	Plastic failures	Sample left	Cracks Repaired
39	1	0.000E+00	0.000E+00	0.000E+00	0.4299	0.1153	0	0	250000	2064
39	2	0.000E+00	0.000E+00	0.000E+00	0.4155	0.1153	0	0	250000	2027
39	3	0.000E+00	0.000E+00	0.960E-04	3.5297	5.9916	0	0	249976	18464

PROBABILITY OF FAILURE OF SYSTEM

CASE1	CASE2	CASE3
0.000E+00	0.000E+00	0.000E+00

CUMULATIVE PROBABILITY OF FAILURE OF SYSTEM

CASE1	CASE2	CASE3
0.320E-04	0.960E-04	0.960E-04

Year	joint	Pf	Cov	CPf	a	sa	Brittle failures	Plastic failures	Sample left	Cracks Repaired
40	1	0.000E+00	0.000E+00	0.000E+00	0.4326	0.1156	0	0	250000	0

40	2	0.000E+00	0.000E+00	0.000E+00	0.4179	0.1156	0	0	250000	0
40	3	0.000E+00	0.000E+00	0.960E-04	3.9814	10.4911	0	0	249976	0

PROBABILITY OF FAILURE OF SYSTEM

CASE1	CASE2	CASE3
0.000E+00	0.000E+00	0.000E+00

CUMULATIVE PROBABILITY OF FAILURE OF SYSTEM

CASE1	CASE2	CASE3
0.320E-04	0.960E-04	0.960E-04

Program finished at :
DAY / MONTH / YEAR
18 6 2001
HOUR:MIMUTE:SECOND
0 13 20

Table C.2 – *Results from Monte Carlo simulation for second section*

========== CONTROL PARAMETER ==========
NUMBER OF GROUPS : 3
NUMBER OF JOINTS : 1
NUMBER OF BASIC VARIABLE IN LSF : 12
SAMPLING SIZE IN MONTE CARLO SIM. : 250000

NUMBER OF YEARS : 40
INSPECTION INTERVAL : 3
INSPECTION QUALITY : 50.

CRACK GROWTH CONSTANT m : 3.3
CORROSION RATE : 0.3
STRESS THRESHOLD : 2.5

========== INFORMATION OF JOINT ==========

NO.	ID.	THICKNESS	REF_LEN	POSITION
1	7	25.0	5000.0	17384.0
2	7	25.0	5000.0	2460.0
3	7	25.0	5000.0	7250.0

==== IDENTIFICATION OF BASIC VARIABLES ====

NO.	ID.		
1	1	1	0
2	3	1	0
3	5	1	0
4	1	0	1
5	2	0	1
6	2	0	1
7	2	0	1
8	2	0	1
9	1	1	0
10	0	1	0
11	2	0	1
12	0	1	0

====== MEAN VALUE OF BASIC VARIABLES =====

GROUP	C	KMAT	AN	CN	B	A	B1	A1	SY	ST	BM	Iyy
1	0.148E-13	273.0	9.000	2887611.0	0.842	9.960	0.858	5.320	345.000	420.000	861652.000	0.188E+15
2	0.502E-13	273.0	9.000	2879928.0	0.858	7.560	0.825	3.610	345.000	420.000	861652.000	0.188E+15
3	0.502E-13	273.0	9.000	3071540.0	0.921	8.360	0.800	2.980	345.000	420.000	861652.000	0.188E+15

== STANDARD DEVIATION OF BASIC VARIABLES =

GROUP	C	KMAT	AN	CN	B	A	B1	A1	SY	ST	BM	Iyy
1	0.444E-14	6.7	0.000	285049.8	0.020	1.000	0.020	0.500	17.000	0.000	107706.500	0.000E+00
2	0.151E-13	6.7	0.000	283990.0	0.020	1.000	0.020	0.500	17.000	0.000	107706.500	0.000E+00
3	0.151E-13	6.7	0.000	309538.2	0.020	1.000	0.020	0.500	17.000	0.000	107706.500	0.000E+00

==========

END OF INPUT PARAMETERS

==========

Program started at :
DAY / MONTH / YEAR
18 6 2001
HOUR:MIMUTE:SECOND
0 13 20

==========

RESULTS

==========

Year	joint	Pf	Cov	CPf	a	sa	Brittle failures	Plastic failures	Sample left	Cracks Repaired
0	1	0.000E+00	0.000E+00	0.000E+00	0.3553	0.1110	0	0	250000	0
0	2	0.000E+00	0.000E+00	0.000E+00	0.3556	0.1113	0	0	250000	0
0	3	0.000E+00	0.000E+00	0.960E-04	0.3555	0.1114	0	0	250000	0

PROBABILITY OF FAILURE OF SYSTEM

CASE1 CASE2 CASE3

0.000E+00 0.000E+00 0.000E+00

CUMULATIVE PROBABILITY OF FAILURE OF SYSTEM

CASE1 CASE2 CASE3

0.000E+00 0.000E+00 0.000E+00

Year	joint	Pf	Cov	CPf	a	sa	Brittle failures	Plastic failures	Sample left	Cracks Repaired
1	1	0.000E+00	0.000E+00	0.000E+00	0.3829	0.1121	0	0	250000	0
1	2	0.000E+00	0.000E+00	0.000E+00	0.3868	0.1135	0	0	250000	0
1	3	0.000E+00	0.000E+00	0.960E-04	0.4638	0.1271	0	0	250000	0

PROBABILITY OF FAILURE OF SYSTEM

CASE1 CASE2 CASE3

0.000E+00 0.000E+00 0.000E+00

CUMULATIVE PROBABILITY OF FAILURE OF SYSTEM

CASE1 CASE2 CASE3

0.000E+00 0.000E+00 0.000E+00

Year	joint	Pf	Cov	CPf	a	sa	Brittle failures	Plastic failures	Sample left	Cracks Repaired
2	1	0.000E+00	0.000E+00	0.000E+00	0.4024	0.1139	0	0	250000	0
2	2	0.000E+00	0.000E+00	0.000E+00	0.4033	0.1159	0	0	250000	0
2	3	0.000E+00	0.000E+00	0.960E-04	0.5399	0.1440	0	0	250000	0

PROBABILITY OF FAILURE OF SYSTEM

CASE1 CASE2 CASE3

0.000E+00 0.000E+00 0.000E+00

CUMULATIVE PROBABILITY OF FAILURE OF SYSTEM

CASE1 CASE2 CASE3

0.000E+00 0.000E+00 0.000E+00

Year	joint	Pf	Cov	CPf	a	sa	Brittle failures	Plastic failures	Sample left	Cracks Repaired
3	1	0.000E+00	0.000E+00	0.000E+00	0.4303	0.1159	0	0	250000	2205
3	2	0.000E+00	0.000E+00	0.000E+00	0.4350	0.1192	0	0	250000	2172
3	3	0.000E+00	0.000E+00	0.960E-04	0.6481	0.1671	0	0	250000	3251

PROBABILITY OF FAILURE OF SYSTEM

CASE1 CASE2 CASE3

0.000E+00 0.000E+00 0.000E+00

CUMULATIVE PROBABILITY OF FAILURE OF SYSTEM

CASE1 CASE2 CASE3

0.000E+00 0.000E+00 0.000E+00

Year	joint	Pf	Cov	CPf	a	sa	Brittle failures	Plastic failures	Sample left	Cracks Repaired
4	1	0.000E+00	0.000E+00	0.000E+00	0.4581	0.1185	0	0	250000	0
4	2	0.000E+00	0.000E+00	0.000E+00	0.4668	0.1230	0	0	250000	0
4	3	0.000E+00	0.000E+00	0.960E-04	0.7538	0.1821	0	0	250000	0

PROBABILITY OF FAILURE OF SYSTEM

CASE1 CASE2 CASE3

0.000E+00 0.000E+00 0.000E+00

CUMULATIVE PROBABILITY OF FAILURE OF SYSTEM

CASE1 CASE2 CASE3

0.000E+00 0.000E+00 0.000E+00

Year	joint	Pf	Cov	CPf	a	sa	Brittle failures	Plastic failures	Sample left	Cracks Repaired
5	1	0.000E+00	0.000E+00	0.000E+00	0.4784	0.1212	0	0	250000	0
5	2	0.000E+00	0.000E+00	0.000E+00	0.4843	0.1262	0	0	250000	0
5	3	0.000E+00	0.000E+00	0.960E-04	0.8289	0.1917	0	0	250000	0

PROBABILITY OF FAILURE OF SYSTEM

CASE1 CASE2 CASE3

0.000E+00 0.000E+00 0.000E+00

CUMULATIVE PROBABILITY OF FAILURE OF SYSTEM

CASE1 CASE2 CASE3

0.000E+00 0.000E+00 0.000E+00

Year	joint	Pf	Cov	CPf	a	sa	Brittle failures	Plastic failures	Sample left	Cracks Repaired
6	1	0.000E+00	0.000E+00	0.000E+00	0.5054	0.1252	0	0	250000	2571
6	2	0.000E+00	0.000E+00	0.000E+00	0.5154	0.1316	0	0	250000	2630
6	3	0.000E+00	0.000E+00	0.960E-04	0.9142	0.2108	0	0	250000	4574

PROBABILITY OF FAILURE OF SYSTEM

CASE1 CASE2 CASE3

0.000E+00 0.000E+00 0.000E+00

CUMULATIVE PROBABILITY OF FAILURE OF SYSTEM

CASE1 CASE2 CASE3

0.000E+00 0.000E+00 0.000E+00

Year	joint	Pf	Cov	CPf	a	sa	Brittle failures	Plastic failures	Sample left	Cracks Repaired
7	1	0.000E+00	0.000E+00	0.000E+00	0.5334	0.1288	0	0	250000	0
7	2	0.000E+00	0.000E+00	0.000E+00	0.5476	0.1366	0	0	250000	0
7	3	0.000E+00	0.000E+00	0.960E-04	0.9998	0.2143	0	0	250000	0

PROBABILITY OF FAILURE OF SYSTEM

CASE1 CASE2 CASE3

0.000E+00 0.000E+00 0.000E+00

CUMULATIVE PROBABILITY OF FAILURE OF SYSTEM

CASE1 CASE2 CASE3

0.000E+00 0.000E+00 0.000E+00

Year	joint	Pf	Cov	CPf	a	sa	Brittle failures	Plastic failures	Sample left	Cracks Repaired
8	1	0.000E+00	0.000E+00	0.000E+00	0.5542	0.1324	0	0	250000	0
8	2	0.000E+00	0.000E+00	0.000E+00	0.5660	0.1404	0	0	250000	0
8	3	0.000E+00	0.100E+01	0.960E-04	1.0615	0.2212	0	0	250000	0

PROBABILITY OF FAILURE OF SYSTEM

CASE1 CASE2 CASE3

0.000E+00 0.000E+00 0.000E+00

CUMULATIVE PROBABILITY OF FAILURE OF SYSTEM

CASE1 CASE2 CASE3

0.000E+00 0.000E+00 0.000E+00

Year	joint	Pf	Cov	CPf	a	sa	Brittle failures	Plastic failures	Sample left	Cracks Repaired
9	1	0.000E+00	0.000E+00	0.000E+00	0.5801	0.1383	0	0	250000	2974

9	2	0.000E+00	0.000E+00	0.000E+00	0.5961	0.1476	0	0	250000	2902
9	3	0.000E+00	0.000E+00	0.960E-04	1.1212	0.2577	0	0	250000	5609

PROBABILITY OF FAILURE OF SYSTEM

CASE1	CASE2	CASE3
0.000E+00	0.000E+00	0.000E+00

CUMULATIVE PROBABILITY OF FAILURE OF SYSTEM

CASE1	CASE2	CASE3
0.000E+00	0.000E+00	0.000E+00

Year	joint	Pf	Cov	CPf	a	sa	Brittle failures	Plastic failures	Sample left	Cracks Repaired
10	1	0.000E+00	0.000E+00	0.000E+00	0.6081	0.1425	0	0	250000	0
10	2	0.000E+00	0.000E+00	0.000E+00	0.6282	0.1527	0	0	250000	0
10	3	0.000E+00	0.000E+00	0.960E-04	1.1952	0.2717	0	0	250000	0

PROBABILITY OF FAILURE OF SYSTEM

CASE1	CASE2	CASE3
0.000E+00	0.000E+00	0.000E+00

CUMULATIVE PROBABILITY OF FAILURE OF SYSTEM

CASE1	CASE2	CASE3
0.000E+00	0.000E+00	0.000E+00

Year	joint	Pf	Cov	CPf	a	sa	Brittle failures	Plastic failures	Sample left	Cracks Repaired
11	1	0.000E+00	0.000E+00	0.000E+00	0.6291	0.1462	0	0	250000	0
11	2	0.000E+00	0.000E+00	0.000E+00	0.6470	0.1565	0	0	250000	0
11	3	0.000E+00	0.000E+00	0.960E-04	1.2536	0.2908	0	0	250000	0

PROBABILITY OF FAILURE OF SYSTEM

CASE1	CASE2	CASE3
0.000E+00	0.000E+00	0.000E+00

CUMULATIVE PROBABILITY OF FAILURE OF SYSTEM

CASE1	CASE2	CASE3
0.000E+00	0.000E+00	0.000E+00

Year	joint	Pf	Cov	CPf	a	sa	Brittle failures	Plastic failures	Sample left	Cracks Repaired
12	1	0.000E+00	0.000E+00	0.000E+00	0.6534	0.1537	0	0	250000	3267
12	2	0.000E+00	0.000E+00	0.000E+00	0.6751	0.1650	0	0	250000	3402
12	3	0.000E+00	0.000E+00	0.960E-04	1.3030	0.3504	0	0	250000	6555

PROBABILITY OF FAILURE OF SYSTEM

CASE1	CASE2	CASE3
0.000E+00	0.000E+00	0.000E+00

CUMULATIVE PROBABILITY OF FAILURE OF SYSTEM

CASE1	CASE2	CASE3
0.000E+00	0.000E+00	0.000E+00

Year	joint	Pf	Cov	CPf	a	sa	Brittle failures	Plastic failures	Sample left	Cracks Repaired
13	1	0.000E+00	0.000E+00	0.000E+00	0.6810	0.1576	0	0	250000	0
13	2	0.000E+00	0.000E+00	0.000E+00	0.7068	0.1694	0	0	250000	0
13	3	0.000E+00	0.000E+00	0.960E-04	1.3803	0.3788	0	0	250000	0

PROBABILITY OF FAILURE OF SYSTEM

CASE1	CASE2	CASE3
0.000E+00	0.000E+00	0.000E+00

CUMULATIVE PROBABILITY OF FAILURE OF SYSTEM

CASE1	CASE2	CASE3
0.000E+00	0.000E+00	0.000E+00

Year	joint	Pf	Cov	CPf	a	sa	Brittle failures	Plastic failures	Sample left	Cracks Repaired
14	1	0.000E+00	0.000E+00	0.000E+00	0.7020	0.1609	0	0	250000	0
14	2	0.000E+00	0.000E+00	0.000E+00	0.7256	0.1726	0	0	250000	0
14	3	0.000E+00	0.000E+00	0.960E-04	1.4453	0.4138	0	0	250000	0

PROBABILITY OF FAILURE OF SYSTEM

CASE1	CASE2	CASE3
0.000E+00	0.000E+00	0.000E+00

CUMULATIVE PROBABILITY OF FAILURE OF SYSTEM

CASE1	CASE2	CASE3

0.000E+00 0.000E+00 0.000E+00

Year	joint	Pf	Cov	CPf	a	sa	Brittle failures	Plastic failures	Sample left	Cracks Repaired
15	1	0.000E+00	0.000E+00	0.000E+00	0.7241	0.1697	0	0	250000	3632
15	2	0.000E+00	0.000E+00	0.000E+00	0.7507	0.1823	0	0	250000	3923
15	3	0.000E+00	0.000E+00	0.960E-04	1.4920	0.4915	0	0	250000	7545

PROBABILITY OF FAILURE OF SYSTEM

CASE1 CASE2 CASE3

0.000E+00 0.000E+00 0.000E+00

CUMULATIVE PROBABILITY OF FAILURE OF SYSTEM

CASE1 CASE2 CASE3

0.000E+00 0.000E+00 0.000E+00

Year	joint	Pf	Cov	CPf	a	sa	Brittle failures	Plastic failures	Sample left	Cracks Repaired
16	1	0.000E+00	0.000E+00	0.000E+00	0.7509	0.1725	0	0	250000	0
16	2	0.000E+00	0.000E+00	0.000E+00	0.7812	0.1852	0	0	250000	0
16	3	0.000E+00	0.000E+00	0.960E-04	1.5801	0.5516	0	0	250000	0

PROBABILITY OF FAILURE OF SYSTEM

CASE1 CASE2 CASE3

0.000E+00 0.000E+00 0.000E+00

CUMULATIVE PROBABILITY OF FAILURE OF SYSTEM

CASE1 CASE2 CASE3

0.000E+00 0.000E+00 0.000E+00

Year	joint	Pf	Cov	CPf	a	sa	Brittle failures	Plastic failures	Sample left	Cracks Repaired
17	1	0.000E+00	0.000E+00	0.000E+00	0.7714	0.1750	0	0	250000	0
17	2	0.000E+00	0.000E+00	0.000E+00	0.7995	0.1874	0	0	250000	0
17	3	0.000E+00	0.000E+00	0.960E-04	1.6569	0.6372	0	0	250000	0

PROBABILITY OF FAILURE OF SYSTEM

CASE1 CASE2 CASE3

0.000E+00 0.000E+00 0.000E+00

CUMULATIVE PROBABILITY OF FAILURE OF SYSTEM

CASE1 CASE2 CASE3

0.000E+00 0.000E+00 0.000E+00

Year	joint	Pf	Cov	CPf	a	sa	Brittle failures	Plastic failures	Sample left	Cracks Repaired
18	1	0.000E+00	0.000E+00	0.000E+00	0.7909	0.1846	0	0	250000	3874
18	2	0.000E+00	0.000E+00	0.000E+00	0.8215	0.1980	0	0	250000	4108
18	3	0.000E+00	0.000E+00	0.960E-04	1.7013	0.7484	0	0	250000	8588

PROBABILITY OF FAILURE OF SYSTEM

CASE1 CASE2 CASE3

0.000E+00 0.000E+00 0.000E+00

CUMULATIVE PROBABILITY OF FAILURE OF SYSTEM

CASE1 CASE2 CASE3

0.000E+00 0.000E+00 0.000E+00

Year	joint	Pf	Cov	CPf	a	sa	Brittle failures	Plastic failures	Sample left	Cracks Repaired
19	1	0.000E+00	0.000E+00	0.000E+00	0.8164	0.1862	0	0	250000	0
19	2	0.000E+00	0.000E+00	0.000E+00	0.8502	0.1994	0	0	250000	0
19	3	0.000E+00	0.000E+00	0.960E-04	1.8073	2.0806	0	0	250000	0

PROBABILITY OF FAILURE OF SYSTEM

CASE1 CASE2 CASE3

0.000E+00 0.000E+00 0.000E+00

CUMULATIVE PROBABILITY OF FAILURE OF SYSTEM

CASE1 CASE2 CASE3

0.000E+00 0.000E+00 0.000E+00

Year	joint	Pf	Cov	CPf	a	sa	Brittle failures	Plastic failures	Sample left	Cracks Repaired
20	1	0.000E+00	0.000E+00	0.000E+00	0.8360	0.1877	0	0	250000	0
20	2	0.000E+00	0.000E+00	0.000E+00	0.8677	0.2008	0	0	250000	0
20	3	0.400E-05	0.100E+01	0.100E-03	1.9361	19.0693	1	0	249999	0

PROBABILITY OF FAILURE OF SYSTEM

CASE1 CASE2 CASE3

0.133E-05 0.400E-05 0.399E-05

CUMULATIVE PROBABILITY OF FAILURE OF SYSTEM

CASE1	CASE2	CASE3
0.133E-05	0.400E-05	0.399E-05

Year	joint	Pf	Cov	CPf	a	sa	Brittle failures	Plastic failures	Sample left	Cracks Repaired
21	1	0.000E+00	0.000E+00	0.000E+00	0.8522	0.1988	0	0	250000	4242
21	2	0.000E+00	0.000E+00	0.000E+00	0.8858	0.2130	0	0	250000	4478
21	3	0.000E+00	0.000E+00	0.100E-03	1.9331	1.0604	0	0	249999	9756

PROBABILITY OF FAILURE OF SYSTEM

CASE1	CASE2	CASE3
0.000E+00	0.000E+00	0.000E+00

CUMULATIVE PROBABILITY OF FAILURE OF SYSTEM

CASE1	CASE2	CASE3
0.133E-05	0.400E-05	0.399E-05

Year	joint	Pf	Cov	CPf	a	sa	Brittle failures	Plastic failures	Sample left	Cracks Repaired
22	1	0.000E+00	0.000E+00	0.000E+00	0.8762	0.1992	0	0	250000	0
22	2	0.000E+00	0.000E+00	0.000E+00	0.9127	0.2134	0	0	250000	0
22	3	0.000E+00	0.000E+00	0.100E-03	2.0561	1.3357	0	0	249999	0

PROBABILITY OF FAILURE OF SYSTEM

CASE1	CASE2	CASE3
0.000E+00	0.000E+00	0.000E+00

CUMULATIVE PROBABILITY OF FAILURE OF SYSTEM

CASE1	CASE2	CASE3
0.133E-05	0.400E-05	0.399E-05

Year	joint	Pf	Cov	CPf	a	sa	Brittle failures	Plastic failures	Sample left	Cracks Repaired
23	1	0.000E+00	0.000E+00	0.000E+00	0.8947	0.1999	0	0	250000	0
23	2	0.000E+00	0.000E+00	0.000E+00	0.9291	0.2144	0	0	250000	0
23	3	0.000E+00	0.707E+00	0.100E-03	2.1780	2.2708	0	0	249999	0

PROBABILITY OF FAILURE OF SYSTEM

CASE1	CASE2	CASE3

0.000E+00 0.000E+00 0.000E+00

CUMULATIVE PROBABILITY OF FAILURE OF SYSTEM

CASE1 CASE2 CASE3

0.133E-05 0.400E-05 0.399E-05

Year	joint	Pf	Cov	CPf	a	sa	Brittle failures	Plastic failures	Sample left	Cracks Repaired
24	1	0.000E+00	0.000E+00	0.000E+00	0.9072	0.2128	0	0	250000	4636
24	2	0.000E+00	0.000E+00	0.000E+00	0.9434	0.2284	0	0	250000	4760
24	3	0.000E+00	0.000E+00	0.100E-03	2.1855	1.4796	0	0	249999	11161

PROBABILITY OF FAILURE OF SYSTEM

CASE1 CASE2 CASE3

0.000E+00 0.000E+00 0.000E+00

CUMULATIVE PROBABILITY OF FAILURE OF SYSTEM

CASE1 CASE2 CASE3

0.133E-05 0.400E-05 0.399E-05

Year	joint	Pf	Cov	CPf	a	sa	Brittle failures	Plastic failures	Sample left	Cracks Repaired
25	1	0.000E+00	0.000E+00	0.000E+00	0.9297	0.2125	0	0	250000	0
25	2	0.000E+00	0.000E+00	0.000E+00	0.9687	0.2284	0	0	250000	0
25	3	0.000E+00	0.000E+00	0.100E-03	2.3393	2.2236	0	0	249999	0

PROBABILITY OF FAILURE OF SYSTEM

CASE1 CASE2 CASE3

0.000E+00 0.000E+00 0.000E+00

CUMULATIVE PROBABILITY OF FAILURE OF SYSTEM

CASE1 CASE2 CASE3

0.133E-05 0.400E-05 0.399E-05

Year	joint	Pf	Cov	CPf	a	sa	Brittle failures	Plastic failures	Sample left	Cracks Repaired
26	1	0.000E+00	0.000E+00	0.000E+00	0.9471	0.2129	0	0	250000	0
26	2	0.000E+00	0.000E+00	0.000E+00	0.9843	0.2294	0	0	250000	0
26	3	0.000E+00	0.100E+01	0.100E-03	2.5077	5.0068	0	0	249999	0

PROBABILITY OF FAILURE OF SYSTEM

CASE1 CASE2 CASE3

0.000E+00 0.000E+00 0.000E+00

CUMULATIVE PROBABILITY OF FAILURE OF SYSTEM

CASE1 CASE2 CASE3

0.133E-05 0.400E-05 0.399E-05

Year	joint	Pf	Cov	CPf	a	sa	Brittle failures	Plastic failures	Sample left	Cracks Repaired
27	1	0.000E+00	0.000E+00	0.000E+00	0.9572	0.2271	0	0	250000	4634
27	2	0.000E+00	0.000E+00	0.000E+00	0.9956	0.2457	0	0	250000	4952
27	3	0.400E-05	0.100E+01	0.104E-03	2.4626	2.3095	1	0	249998	12727

PROBABILITY OF FAILURE OF SYSTEM

CASE1 CASE2 CASE3

0.133E-05 0.400E-05 0.399E-05

CUMULATIVE PROBABILITY OF FAILURE OF SYSTEM

CASE1 CASE2 CASE3

0.267E-05 0.800E-05 0.799E-05

Year	joint	Pf	Cov	CPf	a	sa	Brittle failures	Plastic failures	Sample left	Cracks Repaired
28	1	0.000E+00	0.000E+00	0.000E+00	0.9784	0.2267	0	0	250000	0
28	2	0.000E+00	0.000E+00	0.000E+00	1.0196	0.2459	0	0	250000	0
28	3	0.400E-05	0.100E+01	0.108E-03	2.6670	4.8037	1	0	249997	0

PROBABILITY OF FAILURE OF SYSTEM

CASE1 CASE2 CASE3

0.133E-05 0.400E-05 0.399E-05

CUMULATIVE PROBABILITY OF FAILURE OF SYSTEM

CASE1 CASE2 CASE3

0.400E-05 0.120E-04 0.120E-04

Year	joint	Pf	Cov	CPf	a	sa	Brittle failures	Plastic failures	Sample left	Cracks Repaired
29	1	0.000E+00	0.000E+00	0.000E+00	0.9949	0.2269	0	0	250000	0
29	2	0.000E+00	0.000E+00	0.000E+00	1.0347	0.2472	0	0	250000	0

29 3 0.240E-04 0.408E+00 0.132E-03 3.0388 34.2617 6 0 249991 0

PROBABILITY OF FAILURE OF SYSTEM

CASE1 CASE2 CASE3

0.800E-05 0.240E-04 0.240E-04

CUMULATIVE PROBABILITY OF FAILURE OF SYSTEM

CASE1 CASE2 CASE3

0.120E-04 0.360E-04 0.360E-04

Year	joint	Pf	Cov	CPf	a	sa	Brittle failures	Plastic failures	Sample left	Cracks Repaired
30	1	0.000E+00	0.000E+00	0.000E+00	1.0018	0.2436	0	0	250000	5011
30	2	0.000E+00	0.000E+00	0.000E+00	1.0434	0.2654	0	0	250000	5110
30	3	0.000E+00	0.000E+00	0.132E-03	2.7419	2.9626	0	0	249991	14192

PROBABILITY OF FAILURE OF SYSTEM

CASE1 CASE2 CASE3

0.000E+00 0.000E+00 0.000E+00

CUMULATIVE PROBABILITY OF FAILURE OF SYSTEM

CASE1 CASE2 CASE3

0.120E-04 0.360E-04 0.360E-04

Year	joint	Pf	Cov	CPf	a	sa	Brittle failures	Plastic failures	Sample left	Cracks Repaired
31	1	0.000E+00	0.000E+00	0.000E+00	1.0221	0.2432	0	0	250000	0
31	2	0.400E-05	0.100E+01	0.400E-05	1.0667	0.2661	1	0	249999	0
31	3	0.120E-04	0.577E+00	0.144E-03	2.9882	4.6518	3	0	249988	0

PROBABILITY OF FAILURE OF SYSTEM

CASE1 CASE2 CASE3

0.533E-05 0.160E-04 0.160E-04

CUMULATIVE PROBABILITY OF FAILURE OF SYSTEM

CASE1 CASE2 CASE3

0.173E-04 0.520E-04 0.520E-04

Year	joint	Pf	Cov	CPf	a	sa	Brittle failures	Plastic failures	Sample left	Cracks Repaired

32	1	0.000E+00	0.000E+00	0.000E+00	1.0380	0.2439	0	0	250000	0
32	2	0.000E+00	0.000E+00	0.400E-05	1.0814	0.2679	0	0	249999	0
32	3	0.800E-05	0.707E+00	0.152E-03	3.3724	18.9107	2	0	249986	0

PROBABILITY OF FAILURE OF SYSTEM

CASE1 CASE2 CASE3

0.267E-05 0.800E-05 0.799E-05

CUMULATIVE PROBABILITY OF FAILURE OF SYSTEM

CASE1 CASE2 CASE3

0.200E-04 0.600E-04 0.600E-04

Year	joint	Pf	Cov	CPf	a	sa	Brittle failures	Plastic failures	Sample left	Cracks Repaired
33	1	0.000E+00	0.000E+00	0.000E+00	1.0429	0.2619	0	0	250000	5130
33	2	0.000E+00	0.000E+00	0.400E-05	1.0874	0.2882	0	0	249999	5396
33	3	0.000E+00	0.000E+00	0.152E-03	3.0298	4.1776	0	0	249986	16000

PROBABILITY OF FAILURE OF SYSTEM

CASE1 CASE2 CASE3

0.000E+00 0.000E+00 0.000E+00

CUMULATIVE PROBABILITY OF FAILURE OF SYSTEM

CASE1 CASE2 CASE3

0.200E-04 0.600E-04 0.600E-04

Year	joint	Pf	Cov	CPf	a	sa	Brittle failures	Plastic failures	Sample left	Cracks Repaired
34	1	0.000E+00	0.000E+00	0.000E+00	1.0625	0.2618	0	0	250000	0
34	2	0.000E+00	0.000E+00	0.400E-05	1.1104	0.2895	0	0	249999	0
34	3	0.000E+00	0.000E+00	0.152E-03	3.3528	7.6247	0	0	249986	0

PROBABILITY OF FAILURE OF SYSTEM

CASE1 CASE2 CASE3

0.000E+00 0.000E+00 0.000E+00

CUMULATIVE PROBABILITY OF FAILURE OF SYSTEM

CASE1 CASE2 CASE3

0.200E-04 0.600E-04 0.600E-04

Year	joint	Pf	Cov	CPf	a	sa	Brittle failures	Plastic failures	Sample left	Cracks Repaired
35	1	0.000E+00	0.000E+00	0.000E+00	1.0782	0.2627	0	0	250000	0
35	2	0.000E+00	0.000E+00	0.400E-05	1.1251	0.2918	0	0	249999	0
35	3	0.240E-04	0.408E+00	0.176E-03	3.9869	35.8440	6	0	249980	0

PROBABILITY OF FAILURE OF SYSTEM

CASE1	CASE2	CASE3
0.800E-05	0.240E-04	0.240E-04

CUMULATIVE PROBABILITY OF FAILURE OF SYSTEM

CASE1	CASE2	CASE3
0.280E-04	0.840E-04	0.840E-04

Year	joint	Pf	Cov	CPf	a	sa	Brittle failures	Plastic failures	Sample left	Cracks Repaired
36	1	0.000E+00	0.000E+00	0.000E+00	1.0809	0.2825	0	0	250000	5355
36	2	0.000E+00	0.000E+00	0.400E-05	1.1290	0.3140	0	0	249999	5662
36	3	0.120E-04	0.577E+00	0.188E-03	3.2945	4.8469	3	0	249977	17043

PROBABILITY OF FAILURE OF SYSTEM

CASE1	CASE2	CASE3
0.400E-05	0.120E-04	0.120E-04

CUMULATIVE PROBABILITY OF FAILURE OF SYSTEM

CASE1	CASE2	CASE3
0.320E-04	0.960E-04	0.960E-04

Year	joint	Pf	Cov	CPf	a	sa	Brittle failures	Plastic failures	Sample left	Cracks Repaired
37	1	0.000E+00	0.000E+00	0.000E+00	1.1003	0.2828	0	0	250000	0
37	2	0.000E+00	0.000E+00	0.400E-05	1.1519	0.3162	0	0	249999	0
37	3	0.400E-05	0.100E+01	0.192E-03	3.6785	8.1029	1	0	249976	0

PROBABILITY OF FAILURE OF SYSTEM

CASE1	CASE2	CASE3
0.133E-05	0.400E-05	0.399E-05

CUMULATIVE PROBABILITY OF FAILURE OF SYSTEM

CASE1 CASE2 CASE3

0.333E-04 0.100E-03 0.100E-03

Year	joint	Pf	Cov	CPf	a	sa	Brittle failures	Plastic failures	Sample left	Cracks Repaired
38	1	0.000E+00	0.000E+00	0.000E+00	1.1157	0.2842	0	0	250000	0
38	2	0.000E+00	0.000E+00	0.400E-05	1.1668	0.3192	0	0	249999	0
38	3	0.200E-04	0.447E+00	0.212E-03	4.2965	24.9823	5	0	249971	0

PROBABILITY OF FAILURE OF SYSTEM

CASE1 CASE2 CASE3

0.667E-05 0.200E-04 0.200E-04

CUMULATIVE PROBABILITY OF FAILURE OF SYSTEM

CASE1 CASE2 CASE3

0.400E-04 0.120E-03 0.120E-03

Year	joint	Pf	Cov	CPf	a	sa	Brittle failures	Plastic failures	Sample left	Cracks Repaired
39	1	0.000E+00	0.000E+00	0.000E+00	1.1167	0.3051	0	0	250000	5544
39	2	0.000E+00	0.000E+00	0.400E-05	1.1689	0.3430	0	0	249999	5848
39	3	0.120E-04	0.577E+00	0.224E-03	3.5312	5.8428	3	0	249968	18518

PROBABILITY OF FAILURE OF SYSTEM

CASE1 CASE2 CASE3

0.400E-05 0.120E-04 0.120E-04

CUMULATIVE PROBABILITY OF FAILURE OF SYSTEM

CASE1 CASE2 CASE3

0.440E-04 0.132E-03 0.132E-03

Year	joint	Pf	Cov	CPf	a	sa	Brittle failures	Plastic failures	Sample left	Cracks Repaired
40	1	0.000E+00	0.000E+00	0.000E+00	1.1361	0.3059	0	0	250000	0
40	2	0.000E+00	0.000E+00	0.400E-05	1.1921	0.3459	0	0	249999	0
40	3	0.400E-05	0.100E+01	0.228E-03	3.9748	9.0751	1	0	249967	0

PROBABILITY OF FAILURE OF SYSTEM

CASE1 CASE2 CASE3

0.133E-05 0.400E-05 0.399E-05

```
 CUMULATIVE PROBABILITY OF FAILURE OF SYSTEM
 -------------------------------------------

   CASE1       CASE2       CASE3

0.453E-04    0.136E-03    0.136E-03

Program finished at :
DAY / MONTH / YEAR
18    6    2001
HOUR:MIMUTE:SECOND
 1    20    48
```

Table C.3 – *Results from Monte Carlo simulation for third section*

```
========== CONTROL PARAMETER ==========
NUMBER OF GROUPS              :        3
NUMBER OF JOINTS              :        1
NUMBER OF BASIC VARIABLE IN  LSF  :       12
SAMPLING SIZE IN MONTE CARLO SIM.  :      250000

NUMBER OF YEARS               :       40
INSPECTION INTERVAL           :        3
INSPECTION QUALITY            :       50.
CRACK GROWTH CONSTANT m       :      3.3
CORROSION RATE                :      0.3
STRESS THRESHOLD              :      2.5

========== INFORMATION OF JOINT ==========
    NO.    ID.    THICKNESS     REF_LEN     POSITION

     1      7       25.0        5000.0      17384.0
     2      7       25.0        5000.0       2460.0
     3      7       25.0        5000.0       7250.0
==== IDENTIFICATION OF BASIC VARIABLES ====
    NO.    ID.

     1      1      1      0
     2      3      1      0
     3      5      1      0
     4      1      0      1
```

```
     5     2     0     1
     6     2     0     1
     7     2     0     1
     8     2     0     1
     9     1     1     0
    10     0     1     0
    11     2     0     1
    12     0     1     0
====== MEAN VALUE OF BASIC VARIABLES =====
GROUP    C  KMAT   AN     CN  B  A    B1  A1   SY   ST    BM      Iyy

 1 0.148E-13  273.0  9.000 2887611.0  0.842  9.960  0.858  5.320  345.000  420.000  861652.000
0.188E+15
 2 0.502E-13  273.0  9.000 2879928.0  0.858  7.560  0.825  3.610  345.000  420.000  861652.000
0.188E+15
 3 0.502E-13  273.0  9.000 3071540.0  0.921  8.360  0.800  2.980  345.000  420.000  861652.000
0.188E+15
== STANDARD DEVIATION OF BASIC VARIABLES =
GROUP    C  KMAT   AN     CN  B  A    B1  A1   SY   ST    BM      Iyy

 1 0.444E-14  6.7  0.000  285049.8  0.020  1.000  0.020  0.500  17.000  0.000  107706.500 0.000E+00
 2 0.151E-13  6.7  0.000  283990.0  0.020  1.000  0.020  0.500  17.000  0.000  107706.500 0.000E+00
 3 0.151E-13  6.7  0.000  309538.2  0.020  1.000  0.020  0.500  17.000  0.000  107706.500 0.000E+00
=============================================
     END OF INPUT PARAMETERS
=============================================

Program started at :
DAY / MONTH / YEAR
18    6    2001
HOUR:MIMUTE:SECOND
 1    20    49
=============================================
          RESULTS
=============================================

Year    joint      Pf        Cov       CPf       a        sa      Brittle failures  Plastic failures  Sample left  Cracks
Repaired

 0      1  0.000E+00  0.000E+00  0.000E+00   0.3550   0.1109      0          0        250000       0
 0      2  0.000E+00  0.000E+00  0.400E-05   0.3553   0.1117      0          0        250000       0
 0      3  0.000E+00  0.000E+00  0.228E-03   0.3554   0.1113      0          0        250000       0
-----------------------------------------
   PROBABILITY OF FAILURE OF SYSTEM
-----------------------------------------

   CASE1       CASE2       CASE3


0.000E+00    0.000E+00    0.000E+00

-------------------------------------------------
 CUMULATIVE PROBABILITY OF FAILURE OF SYSTEM
-------------------------------------------------

   CASE1       CASE2       CASE3


0.000E+00    0.000E+00    0.000E+00

Year    joint      Pf        Cov       CPf       a        sa      Brittle failures  Plastic failures  Sample left  Cracks
Repaired

 1      1  0.000E+00  0.000E+00  0.000E+00   0.4249   0.1164      0          0        250000       0
 1      2  0.000E+00  0.000E+00  0.400E-05   0.4381   0.1226      0          0        250000       0
 1      3  0.000E+00  0.000E+00  0.228E-03   0.4637   0.1274      0          0        250000       0
-----------------------------------------
```

PROBABILITY OF FAILURE OF SYSTEM

CASE1	CASE2	CASE3
0.000E+00	0.000E+00	0.000E+00

CUMULATIVE PROBABILITY OF FAILURE OF SYSTEM

CASE1	CASE2	CASE3
0.000E+00	0.000E+00	0.000E+00

Year	joint	Pf	Cov	CPf	a	sa	Brittle failures	Plastic failures	Sample left	Cracks Repaired
2	1	0.000E+00	0.000E+00	0.000E+00	0.4837	0.1248	0	0	250000	0
2	2	0.000E+00	0.000E+00	0.400E-05	0.4965	0.1344	0	0	250000	0
2	3	0.000E+00	0.000E+00	0.228E-03	0.5398	0.1443	0	0	250000	0

PROBABILITY OF FAILURE OF SYSTEM

CASE1	CASE2	CASE3
0.000E+00	0.000E+00	0.000E+00

CUMULATIVE PROBABILITY OF FAILURE OF SYSTEM

CASE1	CASE2	CASE3
0.000E+00	0.000E+00	0.000E+00

Year	joint	Pf	Cov	CPf	a	sa	Brittle failures	Plastic failures	Sample left	Cracks Repaired
3	1	0.000E+00	0.000E+00	0.000E+00	0.5537	0.1367	0	0	250000	2727
3	2	0.000E+00	0.000E+00	0.400E-05	0.5799	0.1512	0	0	250000	2877
3	3	0.000E+00	0.000E+00	0.228E-03	0.6480	0.1672	0	0	250000	3170

PROBABILITY OF FAILURE OF SYSTEM

CASE1	CASE2	CASE3
0.000E+00	0.000E+00	0.000E+00

CUMULATIVE PROBABILITY OF FAILURE OF SYSTEM

CASE1	CASE2	CASE3
0.000E+00	0.000E+00	0.000E+00

Year	joint	Pf	Cov	CPf	a	sa	Brittle failures	Plastic failures	Sample left	Cracks Repaired
4	1	0.000E+00	0.000E+00	0.000E+00	0.6235	0.1478	0	0	250000	0

4	2	0.000E+00	0.000E+00	0.400E-05	0.6630	0.1655	0	0	250000	0
4	3	0.000E+00	0.000E+00	0.228E-03	0.7537	0.1823	0	0	250000	0

PROBABILITY OF FAILURE OF SYSTEM

CASE1 CASE2 CASE3

0.000E+00 0.000E+00 0.000E+00

CUMULATIVE PROBABILITY OF FAILURE OF SYSTEM

CASE1 CASE2 CASE3

0.000E+00 0.000E+00 0.000E+00

Year	joint	Pf	Cov	CPf	a	sa	Brittle failures	Plastic failures	Sample left	Cracks Repaired
5	1	0.000E+00	0.000E+00	0.000E+00	0.6835	0.1583	0	0	250000	0
5	2	0.000E+00	0.000E+00	0.400E-05	0.7235	0.1763	0	0	250000	0
5	3	0.000E+00	0.000E+00	0.228E-03	0.8288	0.1919	0	0	250000	0

PROBABILITY OF FAILURE OF SYSTEM

CASE1 CASE2 CASE3

0.000E+00 0.000E+00 0.000E+00

CUMULATIVE PROBABILITY OF FAILURE OF SYSTEM

CASE1 CASE2 CASE3

0.000E+00 0.000E+00 0.000E+00

Year	joint	Pf	Cov	CPf	a	sa	Brittle failures	Plastic failures	Sample left	Cracks Repaired
6	1	0.000E+00	0.000E+00	0.000E+00	0.7468	0.1736	0	0	250000	3736
6	2	0.000E+00	0.000E+00	0.400E-05	0.7968	0.1929	0	0	250000	3982
6	3	0.000E+00	0.000E+00	0.228E-03	0.9139	0.2109	0	0	250000	4607

PROBABILITY OF FAILURE OF SYSTEM

CASE1 CASE2 CASE3

0.000E+00 0.000E+00 0.000E+00

CUMULATIVE PROBABILITY OF FAILURE OF SYSTEM

CASE1 CASE2 CASE3

0.000E+00 0.000E+00 0.000E+00

Year	joint	Pf	Cov	CPf	a	sa	Brittle failures	Plastic failures	Sample left	Cracks Repaired
7	1	0.000E+00	0.000E+00	0.000E+00	0.8118	0.1797	0	0	250000	0
7	2	0.000E+00	0.000E+00	0.400E-05	0.8711	0.1979	0	0	250000	0
7	3	0.000E+00	0.000E+00	0.228E-03	0.9994	0.2141	0	0	250000	0

PROBABILITY OF FAILURE OF SYSTEM

CASE1	CASE2	CASE3
0.000E+00	0.000E+00	0.000E+00

CUMULATIVE PROBABILITY OF FAILURE OF SYSTEM

CASE1	CASE2	CASE3
0.000E+00	0.000E+00	0.000E+00

Year	joint	Pf	Cov	CPf	a	sa	Brittle failures	Plastic failures	Sample left	Cracks Repaired
8	1	0.000E+00	0.000E+00	0.000E+00	0.8663	0.1840	0	0	250000	0
8	2	0.000E+00	0.000E+00	0.400E-05	0.9245	0.2018	0	0	250000	0
8	3	0.000E+00	0.100E+01	0.228E-03	1.0611	0.2208	0	0	250000	0

PROBABILITY OF FAILURE OF SYSTEM

CASE1	CASE2	CASE3
0.000E+00	0.000E+00	0.000E+00

CUMULATIVE PROBABILITY OF FAILURE OF SYSTEM

CASE1	CASE2	CASE3
0.000E+00	0.000E+00	0.000E+00

Year	joint	Pf	Cov	CPf	a	sa	Brittle failures	Plastic failures	Sample left	Cracks Repaired
9	1	0.000E+00	0.000E+00	0.000E+00	0.9155	0.2006	0	0	250000	4614
9	2	0.000E+00	0.000E+00	0.400E-05	0.9791	0.2219	0	0	250000	4899
9	3	0.000E+00	0.000E+00	0.228E-03	1.1208	0.2573	0	0	250000	5559

PROBABILITY OF FAILURE OF SYSTEM

CASE1	CASE2	CASE3
0.000E+00	0.000E+00	0.000E+00

CUMULATIVE PROBABILITY OF FAILURE OF SYSTEM

CASE1	CASE2	CASE3

0.000E+00 0.000E+00 0.000E+00

Year	joint	Pf	Cov	CPf	a	sa	Brittle failures	Plastic failures	Sample left	Cracks Repaired
10	1	0.000E+00	0.000E+00	0.000E+00	0.9704	0.2015	0	0	250000	0
10	2	0.000E+00	0.000E+00	0.400E-05	1.0410	0.2248	0	0	250000	0
10	3	0.000E+00	0.000E+00	0.228E-03	1.1948	0.2707	0	0	250000	0

PROBABILITY OF FAILURE OF SYSTEM

CASE1 CASE2 CASE3

0.000E+00 0.000E+00 0.000E+00

CUMULATIVE PROBABILITY OF FAILURE OF SYSTEM

CASE1 CASE2 CASE3

0.000E+00 0.000E+00 0.000E+00

Year	joint	Pf	Cov	CPf	a	sa	Brittle failures	Plastic failures	Sample left	Cracks Repaired
11	1	0.000E+00	0.000E+00	0.000E+00	1.0166	0.2036	0	0	250000	0
11	2	0.000E+00	0.000E+00	0.400E-05	1.0873	0.2308	0	0	250000	0
11	3	0.000E+00	0.000E+00	0.228E-03	1.2533	0.2895	0	0	250000	0

PROBABILITY OF FAILURE OF SYSTEM

CASE1 CASE2 CASE3

0.000E+00 0.000E+00 0.000E+00

CUMULATIVE PROBABILITY OF FAILURE OF SYSTEM

CASE1 CASE2 CASE3

0.000E+00 0.000E+00 0.000E+00

Year	joint	Pf	Cov	CPf	a	sa	Brittle failures	Plastic failures	Sample left	Cracks Repaired
12	1	0.000E+00	0.000E+00	0.000E+00	1.0517	0.2291	0	0	250000	5287
12	2	0.000E+00	0.000E+00	0.400E-05	1.1276	0.2651	0	0	250000	5656
12	3	0.000E+00	0.000E+00	0.228E-03	1.3024	0.3497	0	0	250000	6670

PROBABILITY OF FAILURE OF SYSTEM

CASE1 CASE2 CASE3

0.000E+00 0.000E+00 0.000E+00

CUMULATIVE PROBABILITY OF FAILURE OF SYSTEM

CASE1 CASE2 CASE3

0.000E+00 0.000E+00 0.000E+00

Year	joint	Pf	Cov	CPf	a	sa	Brittle failures	Plastic failures	Sample left	Cracks Repaired
13	1	0.000E+00	0.000E+00	0.000E+00	1.0996	0.2321	0	0	250000	0
13	2	0.000E+00	0.000E+00	0.400E-05	1.1844	0.2747	0	0	250000	0
13	3	0.000E+00	0.000E+00	0.228E-03	1.3798	0.3779	0	0	250000	0

PROBABILITY OF FAILURE OF SYSTEM

CASE1 CASE2 CASE3

0.000E+00 0.000E+00 0.000E+00

CUMULATIVE PROBABILITY OF FAILURE OF SYSTEM

CASE1 CASE2 CASE3

0.000E+00 0.000E+00 0.000E+00

Year	joint	Pf	Cov	CPf	a	sa	Brittle failures	Plastic failures	Sample left	Cracks Repaired
14	1	0.000E+00	0.000E+00	0.000E+00	1.1415	0.2379	0	0	250000	0
14	2	0.000E+00	0.000E+00	0.400E-05	1.2294	0.2876	0	0	250000	0
14	3	0.000E+00	0.000E+00	0.228E-03	1.4448	0.4111	0	0	250000	0

PROBABILITY OF FAILURE OF SYSTEM

CASE1 CASE2 CASE3

0.000E+00 0.000E+00 0.000E+00

CUMULATIVE PROBABILITY OF FAILURE OF SYSTEM

CASE1 CASE2 CASE3

0.000E+00 0.000E+00 0.000E+00

Year	joint	Pf	Cov	CPf	a	sa	Brittle failures	Plastic failures	Sample left	Cracks Repaired
15	1	0.000E+00	0.000E+00	0.000E+00	1.1684	0.2739	0	0	250000	5800
15	2	0.000E+00	0.000E+00	0.400E-05	1.2628	0.3351	0	0	250000	6302
15	3	0.000E+00	0.000E+00	0.228E-03	1.4913	0.4893	0	0	250000	7556

PROBABILITY OF FAILURE OF SYSTEM

CASE1 CASE2 CASE3

0.000E+00 0.000E+00 0.000E+00

CUMULATIVE PROBABILITY OF FAILURE OF SYSTEM

CASE1	CASE2	CASE3
0.000E+00	0.000E+00	0.000E+00

Year	joint	Pf	Cov	CPf	a	sa	Brittle failures	Plastic failures	Sample left	Cracks Repaired
16	1	0.000E+00	0.000E+00	0.000E+00	1.2146	0.2816	0	0	250000	0
16	2	0.000E+00	0.000E+00	0.400E-05	1.3212	0.3531	0	0	250000	0
16	3	0.000E+00	0.000E+00	0.228E-03	1.5792	0.5340	0	0	250000	0

PROBABILITY OF FAILURE OF SYSTEM

CASE1	CASE2	CASE3
0.000E+00	0.000E+00	0.000E+00

CUMULATIVE PROBABILITY OF FAILURE OF SYSTEM

CASE1	CASE2	CASE3
0.000E+00	0.000E+00	0.000E+00

Year	joint	Pf	Cov	CPf	a	sa	Brittle failures	Plastic failures	Sample left	Cracks Repaired
17	1	0.000E+00	0.000E+00	0.000E+00	1.2565	0.2924	0	0	250000	0
17	2	0.000E+00	0.000E+00	0.400E-05	1.3692	0.3738	0	0	250000	0
17	3	0.000E+00	0.000E+00	0.228E-03	1.6557	0.5871	0	0	250000	0

PROBABILITY OF FAILURE OF SYSTEM

CASE1	CASE2	CASE3
0.000E+00	0.000E+00	0.000E+00

CUMULATIVE PROBABILITY OF FAILURE OF SYSTEM

CASE1	CASE2	CASE3
0.000E+00	0.000E+00	0.000E+00

Year	joint	Pf	Cov	CPf	a	sa	Brittle failures	Plastic failures	Sample left	Cracks Repaired
18	1	0.000E+00	0.000E+00	0.000E+00	1.2783	0.3378	0	0	250000	6508
18	2	0.000E+00	0.000E+00	0.400E-05	1.3987	0.4320	0	0	250000	7052
18	3	0.000E+00	0.000E+00	0.228E-03	1.6993	0.6807	0	0	250000	8563

PROBABILITY OF FAILURE OF SYSTEM

CASE1	CASE2	CASE3

0.000E+00 0.000E+00 0.000E+00

CUMULATIVE PROBABILITY OF FAILURE OF SYSTEM

CASE1 CASE2 CASE3

0.000E+00 0.000E+00 0.000E+00

Year	joint	Pf	Cov	CPf	a	sa	Brittle failures	Plastic failures	Sample left	Cracks Repaired
19	1	0.000E+00	0.000E+00	0.000E+00	1.3263	0.3506	0	0	250000	0
19	2	0.000E+00	0.000E+00	0.400E-05	1.4622	0.4590	0	0	250000	0
19	3	0.000E+00	0.000E+00	0.228E-03	1.8020	0.7765	0	0	250000	0

PROBABILITY OF FAILURE OF SYSTEM

CASE1 CASE2 CASE3

0.000E+00 0.000E+00 0.000E+00

CUMULATIVE PROBABILITY OF FAILURE OF SYSTEM

CASE1 CASE2 CASE3

0.000E+00 0.000E+00 0.000E+00

Year	joint	Pf	Cov	CPf	a	sa	Brittle failures	Plastic failures	Sample left	Cracks Repaired
20	1	0.000E+00	0.000E+00	0.000E+00	1.3708	0.3662	0	0	250000	0
20	2	0.000E+00	0.000E+00	0.400E-05	1.5156	0.4894	0	0	250000	0
20	3	0.000E+00	0.100E+01	0.228E-03	1.8950	0.9683	0	0	250000	0

PROBABILITY OF FAILURE OF SYSTEM

CASE1 CASE2 CASE3

0.000E+00 0.000E+00 0.000E+00

CUMULATIVE PROBABILITY OF FAILURE OF SYSTEM

CASE1 CASE2 CASE3

0.000E+00 0.000E+00 0.000E+00

Year	joint	Pf	Cov	CPf	a	sa	Brittle failures	Plastic failures	Sample left	Cracks Repaired
21	1	0.000E+00	0.000E+00	0.000E+00	1.3893	0.4174	0	0	250000	7057
21	2	0.000E+00	0.000E+00	0.400E-05	1.5415	0.5551	0	0	250000	7822
21	3	0.400E-05	0.100E+01	0.232E-03	1.9308	1.0190	1	0	249999	9863

PROBABILITY OF FAILURE OF SYSTEM

CASE1 CASE2 CASE3

0.133E-05 0.400E-05 0.399E-05

CUMULATIVE PROBABILITY OF FAILURE OF SYSTEM

CASE1 CASE2 CASE3

0.133E-05 0.400E-05 0.399E-05

Year	joint	Pf	Cov	CPf	a	sa	Brittle failures	Plastic failures	Sample left	Cracks Repaired
22	1	0.000E+00	0.000E+00	0.000E+00	1.4409	0.4354	0	0	250000	0
22	2	0.000E+00	0.000E+00	0.400E-05	1.6119	0.5936	0	0	250000	0
22	3	0.000E+00	0.000E+00	0.232E-03	2.0538	1.3559	0	0	249999	0

PROBABILITY OF FAILURE OF SYSTEM

CASE1 CASE2 CASE3

0.000E+00 0.000E+00 0.000E+00

CUMULATIVE PROBABILITY OF FAILURE OF SYSTEM

CASE1 CASE2 CASE3

0.133E-05 0.400E-05 0.399E-05

Year	joint	Pf	Cov	CPf	a	sa	Brittle failures	Plastic failures	Sample left	Cracks Repaired
23	1	0.000E+00	0.000E+00	0.000E+00	1.4893	0.4565	0	0	250000	0
23	2	0.000E+00	0.000E+00	0.400E-05	1.6729	0.6485	0	0	250000	0
23	3	0.400E-05	0.100E+01	0.236E-03	2.2047	15.6960	1	0	249998	0

PROBABILITY OF FAILURE OF SYSTEM

CASE1 CASE2 CASE3

0.133E-05 0.400E-05 0.399E-05

CUMULATIVE PROBABILITY OF FAILURE OF SYSTEM

CASE1 CASE2 CASE3

0.267E-05 0.800E-05 0.799E-05

Year	joint	Pf	Cov	CPf	a	sa	Brittle failures	Plastic failures	Sample left	Cracks Repaired
24	1	0.000E+00	0.000E+00	0.000E+00	1.5049	0.5136	0	0	250000	7543
24	2	0.000E+00	0.000E+00	0.400E-05	1.6942	0.7432	0	0	250000	8723

24	3	0.400E-05	0.100E+01	0.240E-03	2.1867	1.7709	1	0	249997	11211

PROBABILITY OF FAILURE OF SYSTEM

CASE1	CASE2	CASE3
0.133E-05	0.400E-05	0.399E-05

CUMULATIVE PROBABILITY OF FAILURE OF SYSTEM

CASE1	CASE2	CASE3
0.400E-05	0.120E-04	0.120E-04

Year	joint	Pf	Cov	CPf	a	sa	Brittle failures	Plastic failures	Sample left	Cracks Repaired
25	1	0.000E+00	0.000E+00	0.000E+00	1.5610	0.5379	0	0	250000	0
25	2	0.000E+00	0.000E+00	0.400E-05	1.7736	0.8386	0	0	250000	0
25	3	0.400E-05	0.100E+01	0.244E-03	2.3799	20.8483	1	0	249996	0

PROBABILITY OF FAILURE OF SYSTEM

CASE1	CASE2	CASE3
0.133E-05	0.400E-05	0.399E-05

CUMULATIVE PROBABILITY OF FAILURE OF SYSTEM

CASE1	CASE2	CASE3
0.533E-05	0.160E-04	0.160E-04

Year	joint	Pf	Cov	CPf	a	sa	Brittle failures	Plastic failures	Sample left	Cracks Repaired
26	1	0.000E+00	0.000E+00	0.000E+00	1.6141	0.5663	0	0	250000	0
26	2	0.000E+00	0.000E+00	0.400E-05	1.8449	1.0818	0	0	250000	0
26	3	0.400E-05	0.100E+01	0.248E-03	2.5144	8.0332	1	0	249995	0

PROBABILITY OF FAILURE OF SYSTEM

CASE1	CASE2	CASE3
0.133E-05	0.400E-05	0.399E-05

CUMULATIVE PROBABILITY OF FAILURE OF SYSTEM

CASE1	CASE2	CASE3
0.667E-05	0.200E-04	0.200E-04

Year	joint	Pf	Cov	CPf	a	sa	Brittle failures	Plastic failures	Sample left	Cracks Repaired

27	1	0.000E+00	0.000E+00	0.000E+00	1.6238	0.6287	0	0	250000	8347
27	2	0.000E+00	0.000E+00	0.400E-05	1.8562	0.9721	0	0	250000	9398
27	3	0.000E+00	0.100E+01	0.248E-03	2.4600	2.2070	0	0	249995	12739

PROBABILITY OF FAILURE OF SYSTEM

CASE1 CASE2 CASE3

0.000E+00 0.000E+00 0.000E+00

CUMULATIVE PROBABILITY OF FAILURE OF SYSTEM

CASE1 CASE2 CASE3

0.667E-05 0.200E-04 0.200E-04

Year	joint	Pf	Cov	CPf	a	sa	Brittle failures	Plastic failures	Sample left	Cracks Repaired
28	1	0.000E+00	0.000E+00	0.000E+00	1.6850	0.6670	0	0	250000	0
28	2	0.000E+00	0.000E+00	0.400E-05	1.9458	1.1372	0	0	250000	0
28	3	0.000E+00	0.100E+01	0.248E-03	2.6561	3.8939	0	0	249995	0

PROBABILITY OF FAILURE OF SYSTEM

CASE1 CASE2 CASE3

0.000E+00 0.000E+00 0.000E+00

CUMULATIVE PROBABILITY OF FAILURE OF SYSTEM

CASE1 CASE2 CASE3

0.667E-05 0.200E-04 0.200E-04

Year	joint	Pf	Cov	CPf	a	sa	Brittle failures	Plastic failures	Sample left	Cracks Repaired
29	1	0.000E+00	0.000E+00	0.000E+00	1.7436	0.7121	0	0	250000	0
29	2	0.000E+00	0.000E+00	0.400E-05	2.0293	1.5046	0	0	250000	0
29	3	0.400E-05	0.100E+01	0.252E-03	2.9690	24.1307	1	0	249994	0

PROBABILITY OF FAILURE OF SYSTEM

CASE1 CASE2 CASE3

0.133E-05 0.400E-05 0.399E-05

CUMULATIVE PROBABILITY OF FAILURE OF SYSTEM

CASE1 CASE2 CASE3

0.800E-05 0.240E-04 0.240E-04

Year	joint	Pf	Cov	CPf	a	sa	Brittle failures	Plastic failures	Sample left	Cracks Repaired
30	1	0.000E+00	0.000E+00	0.000E+00	1.7483	0.7630	0	0	250000	8893
30	2	0.000E+00	0.000E+00	0.400E-05	2.0280	1.3010	0	0	250000	10263
30	3	0.000E+00	0.000E+00	0.252E-03	2.7446	3.1005	0	0	249994	14151

PROBABILITY OF FAILURE OF SYSTEM

CASE1	CASE2	CASE3
0.000E+00	0.000E+00	0.000E+00

CUMULATIVE PROBABILITY OF FAILURE OF SYSTEM

CASE1	CASE2	CASE3
0.800E-05	0.240E-04	0.240E-04

Year	joint	Pf	Cov	CPf	a	sa	Brittle failures	Plastic failures	Sample left	Cracks Repaired
31	1	0.000E+00	0.000E+00	0.000E+00	1.8153	0.8249	0	0	250000	0
31	2	0.000E+00	0.100E+01	0.400E-05	2.1311	1.6292	0	0	250000	0
31	3	0.400E-05	0.100E+01	0.256E-03	3.0156	12.6053	1	0	249993	0

PROBABILITY OF FAILURE OF SYSTEM

CASE1	CASE2	CASE3
0.133E-05	0.400E-05	0.399E-05

CUMULATIVE PROBABILITY OF FAILURE OF SYSTEM

CASE1	CASE2	CASE3
0.933E-05	0.280E-04	0.280E-04

Year	joint	Pf	Cov	CPf	a	sa	Brittle failures	Plastic failures	Sample left	Cracks Repaired
32	1	0.000E+00	0.000E+00	0.000E+00	1.8803	0.9163	0	0	250000	0
32	2	0.000E+00	0.000E+00	0.400E-05	2.2335	2.5909	0	0	250000	0
32	3	0.800E-05	0.707E+00	0.264E-03	3.3602	17.3028	2	0	249991	0

PROBABILITY OF FAILURE OF SYSTEM

CASE1	CASE2	CASE3
0.267E-05	0.800E-05	0.799E-05

CUMULATIVE PROBABILITY OF FAILURE OF SYSTEM

CASE1 CASE2 CASE3

0.120E-04 0.360E-04 0.359E-04

Year	joint	Pf	Cov	CPf	a	sa	Brittle failures	Plastic failures	Sample left	Cracks Repaired
33	1	0.000E+00	0.000E+00	0.000E+00	1.8783	0.9792	0	0	250000	9372
33	2	0.000E+00	0.000E+00	0.400E-05	2.2052	1.9520	0	0	250000	11390
33	3	0.000E+00	0.000E+00	0.264E-03	3.0336	4.0027	0	0	249991	15716

PROBABILITY OF FAILURE OF SYSTEM

CASE1 CASE2 CASE3

0.000E+00 0.000E+00 0.000E+00

CUMULATIVE PROBABILITY OF FAILURE OF SYSTEM

CASE1 CASE2 CASE3

0.120E-04 0.360E-04 0.359E-04

Year	joint	Pf	Cov	CPf	a	sa	Brittle failures	Plastic failures	Sample left	Cracks Repaired
34	1	0.000E+00	0.000E+00	0.000E+00	1.9520	1.1021	0	0	250000	0
34	2	0.400E-05	0.100E+01	0.800E-05	2.3320	4.1263	1	0	249999	0
34	3	0.800E-05	0.707E+00	0.272E-03	3.3512	6.8164	2	0	249989	0

PROBABILITY OF FAILURE OF SYSTEM

CASE1 CASE2 CASE3

0.400E-05 0.120E-04 0.120E-04

CUMULATIVE PROBABILITY OF FAILURE OF SYSTEM

CASE1 CASE2 CASE3

0.160E-04 0.480E-04 0.479E-04

Year	joint	Pf	Cov	CPf	a	sa	Brittle failures	Plastic failures	Sample left	Cracks Repaired
35	1	0.000E+00	0.000E+00	0.000E+00	2.0243	1.2898	0	0	250000	0
35	2	0.400E-05	0.100E+01	0.120E-04	2.4681	8.5052	1	0	249998	0
35	3	0.800E-05	0.707E+00	0.280E-03	3.8237	20.9768	2	0	249987	0

PROBABILITY OF FAILURE OF SYSTEM

CASE1 CASE2 CASE3

0.400E-05 0.120E-04 0.120E-04

CUMULATIVE PROBABILITY OF FAILURE OF SYSTEM

CASE1 CASE2 CASE3

0.200E-04 0.600E-04 0.599E-04

Year	joint	Pf	Cov	CPf	a	sa	Brittle failures	Plastic failures	Sample left	Cracks Repaired
36	1	0.000E+00	0.000E+00	0.000E+00	2.0068	1.1811	0	0	250000	10304
36	2	0.000E+00	0.000E+00	0.120E-04	2.3828	2.2040	0	0	249998	12100
36	3	0.120E-04	0.577E+00	0.292E-03	3.3115	5.1254	3	0	249984	17015

PROBABILITY OF FAILURE OF SYSTEM

CASE1 CASE2 CASE3

0.400E-05 0.120E-04 0.120E-04

CUMULATIVE PROBABILITY OF FAILURE OF SYSTEM

CASE1 CASE2 CASE3

0.240E-04 0.720E-04 0.719E-04

Year	joint	Pf	Cov	CPf	a	sa	Brittle failures	Plastic failures	Sample left	Cracks Repaired
37	1	0.000E+00	0.000E+00	0.000E+00	2.0880	1.3935	0	0	250000	0
37	2	0.000E+00	0.000E+00	0.120E-04	2.5231	3.0134	0	0	249998	0
37	3	0.120E-04	0.577E+00	0.304E-03	3.7135	11.2621	3	0	249981	0

PROBABILITY OF FAILURE OF SYSTEM

CASE1 CASE2 CASE3

0.400E-05 0.120E-04 0.120E-04

CUMULATIVE PROBABILITY OF FAILURE OF SYSTEM

CASE1 CASE2 CASE3

0.280E-04 0.840E-04 0.839E-04

Year	joint	Pf	Cov	CPf	a	sa	Brittle failures	Plastic failures	Sample left	Cracks Repaired
38	1	0.000E+00	0.000E+00	0.000E+00	2.1700	1.8909	0	0	250000	0
38	2	0.000E+00	0.000E+00	0.120E-04	2.6897	7.6914	0	0	249998	0
38	3	0.440E-04	0.302E+00	0.348E-03	4.4801	42.0600	11	0	249970	0

PROBABILITY OF FAILURE OF SYSTEM

CASE1 CASE2 CASE3

0.147E-04 0.440E-04 0.440E-04

CUMULATIVE PROBABILITY OF FAILURE OF SYSTEM

CASE1 CASE2 CASE3

0.427E-04 0.128E-03 0.128E-03

Year	joint	Pf	Cov	CPf	a	sa	Brittle failures	Plastic failures	Sample left	Cracks Repaired
39	1	0.000E+00	0.000E+00	0.000E+00	2.1418	1.5525	0	0	250000	10778
39	2	0.000E+00	0.000E+00	0.120E-04	2.5563	2.6442	0	0	249998	13185
39	3	0.800E-05	0.707E+00	0.356E-03	3.5352	5.8775	2	0	249968	18357

PROBABILITY OF FAILURE OF SYSTEM

CASE1 CASE2 CASE3

0.267E-05 0.800E-05 0.799E-05

CUMULATIVE PROBABILITY OF FAILURE OF SYSTEM

CASE1 CASE2 CASE3

0.453E-04 0.136E-03 0.136E-03

Year	joint	Pf	Cov	CPf	a	sa	Brittle failures	Plastic failures	Sample left	Cracks Repaired
40	1	0.000E+00	0.000E+00	0.000E+00	2.2337	2.0052	0	0	250000	0
40	2	0.400E-05	0.100E+01	0.160E-04	2.7192	3.6542	1	0	249997	0
40	3	0.000E+00	0.100E+01	0.356E-03	3.9868	10.1448	0	0	249968	0

PROBABILITY OF FAILURE OF SYSTEM

CASE1 CASE2 CASE3

0.133E-05 0.400E-05 0.399E-05

CUMULATIVE PROBABILITY OF FAILURE OF SYSTEM

CASE1 CASE2 CASE3

0.467E-04 0.140E-03 0.140E-03

Program finished at :
DAY / MONTH / YEAR
18 6 2001
HOUR:MIMUTE:SECOND
2 29 17

Table C.4 – *Results from Monte Carlo simulation for fourth section*

```
========== CONTROL PARAMETER ==========
NUMBER OF GROUPS              :        3
NUMBER OF JOINTS              :        1
NUMBER OF BASIC VARIABLE IN LSF  :        12
SAMPLING SIZE IN MONTE CARLO SIM.  :      250000

NUMBER OF YEARS               :       40
INSPECTION INTERVAL           :        3
INSPECTION QUALITY            :       50.
CRACK GROWTH CONSTANT m       :      3.3
CORROSION RATE                :      0.3
STRESS THRESHOLD              :      2.5

========== INFORMATION OF JOINT ==========
    NO.    ID.   THICKNESS     REF_LEN     POSITION

     1      7       25.0       5000.0      17384.0
     2      7       25.0       5000.0       2460.0
     3      7       25.0       5000.0       7250.0
==== IDENTIFICATION OF BASIC VARIABLES ====
    NO.    ID.

     1      1      1      0
     2      3      1      0
     3      5      1      0
     4      1      0      1
     5      2      0      1
     6      2      0      1
     7      2      0      1
     8      2      0      1
     9      1      1      0
    10      0      1      0
    11      2      0      1
    12      0      1      0
====== MEAN VALUE OF BASIC VARIABLES ======
GROUP     C  KMAT    AN      CN    B    A     B1   A1    SY     ST      BM       Iyy

 1 0.148E-13  273.0  9.000 2887611.0  0.842  9.960  0.858  5.320  345.000  420.000  861652.000
0.188E+15
```

2 0.502E-13 273.0 9.000 2879928.0 0.858 7.560 0.825 3.610 345.000 420.000 861652.000 0.188E+15
3 0.502E-13 273.0 9.000 3071540.0 0.921 8.360 0.800 2.980 345.000 420.000 861652.000 0.188E+15

== STANDARD DEVIATION OF BASIC VARIABLES =

GROUP	C	KMAT	AN	CN	B	A	B1	A1	SY	ST	BM	Iyy
1	0.444E-14	6.7	0.000	285049.8	0.020	1.000	0.020	0.500	17.000	0.000	107706.500	0.000E+00
2	0.151E-13	6.7	0.000	283990.0	0.020	1.000	0.020	0.500	17.000	0.000	107706.500	0.000E+00
3	0.151E-13	6.7	0.000	309538.2	0.020	1.000	0.020	0.500	17.000	0.000	107706.500	0.000E+00

END OF INPUT PARAMETERS

Program started at :
DAY / MONTH / YEAR
18 6 2001
HOUR:MIMUTE:SECOND
2 29 17

RESULTS

Year	joint	Pf	Cov	CPf	a	sa	Brittle failures	Plastic failures	Sample left	Cracks Repaired
0	1	0.000E+00	0.000E+00	0.000E+00	0.3548	0.1107	0	0	250000	0
0	2	0.000E+00	0.000E+00	0.160E-04	0.3551	0.1110	0	0	250000	0
0	3	0.000E+00	0.000E+00	0.356E-03	0.3558	0.1120	0	0	250000	0

PROBABILITY OF FAILURE OF SYSTEM

CASE1	CASE2	CASE3
0.000E+00	0.000E+00	0.000E+00

CUMULATIVE PROBABILITY OF FAILURE OF SYSTEM

CASE1	CASE2	CASE3
0.000E+00	0.000E+00	0.000E+00

Year	joint	Pf	Cov	CPf	a	sa	Brittle failures	Plastic failures	Sample left	Cracks Repaired
1	1	0.000E+00	0.000E+00	0.000E+00	0.4464	0.1198	0	0	250000	0
1	2	0.000E+00	0.000E+00	0.160E-04	0.4649	0.1292	0	0	250000	0
1	3	0.000E+00	0.000E+00	0.356E-03	0.4642	0.1277	0	0	250000	0

PROBABILITY OF FAILURE OF SYSTEM

CASE1	CASE2	CASE3
0.000E+00	0.000E+00	0.000E+00

CUMULATIVE PROBABILITY OF FAILURE OF SYSTEM

CASE1	CASE2	CASE3

0.000E+00 0.000E+00 0.000E+00

Year	joint	Pf	Cov	CPf	a	sa	Brittle failures	Plastic failures	Sample left	Cracks Repaired
2	1	0.000E+00	0.000E+00	0.000E+00	0.5263	0.1329	0	0	250000	0
2	2	0.000E+00	0.000E+00	0.160E-04	0.5474	0.1481	0	0	250000	0
2	3	0.000E+00	0.000E+00	0.356E-03	0.5404	0.1445	0	0	250000	0

PROBABILITY OF FAILURE OF SYSTEM

CASE1 CASE2 CASE3

0.000E+00 0.000E+00 0.000E+00

CUMULATIVE PROBABILITY OF FAILURE OF SYSTEM

CASE1 CASE2 CASE3

0.000E+00 0.000E+00 0.000E+00

Year	joint	Pf	Cov	CPf	a	sa	Brittle failures	Plastic failures	Sample left	Cracks Repaired
3	1	0.000E+00	0.000E+00	0.000E+00	0.6172	0.1511	0	0	250000	3065
3	2	0.000E+00	0.000E+00	0.160E-04	0.6559	0.1719	0	0	250000	3298
3	3	0.000E+00	0.000E+00	0.356E-03	0.6484	0.1677	0	0	250000	3263

PROBABILITY OF FAILURE OF SYSTEM

CASE1 CASE2 CASE3

0.000E+00 0.000E+00 0.000E+00

CUMULATIVE PROBABILITY OF FAILURE OF SYSTEM

CASE1 CASE2 CASE3

0.000E+00 0.000E+00 0.000E+00

Year	joint	Pf	Cov	CPf	a	sa	Brittle failures	Plastic failures	Sample left	Cracks Repaired
4	1	0.000E+00	0.000E+00	0.000E+00	0.7069	0.1647	0	0	250000	0
4	2	0.000E+00	0.000E+00	0.160E-04	0.7617	0.1870	0	0	250000	0
4	3	0.000E+00	0.000E+00	0.356E-03	0.7540	0.1827	0	0	250000	0

PROBABILITY OF FAILURE OF SYSTEM

CASE1 CASE2 CASE3

0.000E+00 0.000E+00 0.000E+00

CUMULATIVE PROBABILITY OF FAILURE OF SYSTEM

CASE1 CASE2 CASE3

0.000E+00 0.000E+00 0.000E+00

Year	joint	Pf	Cov	CPf	a	sa	Brittle failures	Plastic failures	Sample left	Cracks Repaired
5	1	0.000E+00	0.000E+00	0.000E+00	0.7848	0.1752	0	0	250000	0
5	2	0.000E+00	0.000E+00	0.160E-04	0.8407	0.1968	0	0	250000	0
5	3	0.000E+00	0.000E+00	0.356E-03	0.8289	0.1924	0	0	250000	0

PROBABILITY OF FAILURE OF SYSTEM

CASE1 CASE2 CASE3

0.000E+00 0.000E+00 0.000E+00

CUMULATIVE PROBABILITY OF FAILURE OF SYSTEM

CASE1 CASE2 CASE3

0.000E+00 0.000E+00 0.000E+00

Year	joint	Pf	Cov	CPf	a	sa	Brittle failures	Plastic failures	Sample left	Cracks Repaired
6	1	0.000E+00	0.000E+00	0.000E+00	0.8595	0.1930	0	0	250000	4369
6	2	0.000E+00	0.000E+00	0.160E-04	0.9249	0.2160	0	0	250000	4639
6	3	0.000E+00	0.000E+00	0.356E-03	0.9141	0.2112	0	0	250000	4588

PROBABILITY OF FAILURE OF SYSTEM

CASE1 CASE2 CASE3

0.000E+00 0.000E+00 0.000E+00

CUMULATIVE PROBABILITY OF FAILURE OF SYSTEM

CASE1 CASE2 CASE3

0.000E+00 0.000E+00 0.000E+00

Year	joint	Pf	Cov	CPf	a	sa	Brittle failures	Plastic failures	Sample left	Cracks Repaired
7	1	0.400E-05	0.100E+01	0.400E-05	0.9351	0.1954	0	1	249999	0
7	2	0.000E+00	0.000E+00	0.160E-04	1.0101	0.2198	0	0	250000	0
7	3	0.000E+00	0.000E+00	0.356E-03	0.9996	0.2147	0	0	250000	0

PROBABILITY OF FAILURE OF SYSTEM

CASE1 CASE2 CASE3

0.133E-05 0.400E-05 0.399E-05

CUMULATIVE PROBABILITY OF FAILURE OF SYSTEM

CASE1 CASE2 CASE3

0.133E-05 0.400E-05 0.399E-05

Year	joint	Pf	Cov	CPf	a	sa	Brittle failures	Plastic failures	Sample left	Cracks Repaired
8	1	0.000E+00	0.000E+00	0.400E-05	0.9988	0.1983	0	0	249999	0
8	2	0.000E+00	0.000E+00	0.160E-04	1.0747	0.2278	0	0	250000	0
8	3	0.000E+00	0.100E+01	0.356E-03	1.0613	0.2215	0	0	250000	0

PROBABILITY OF FAILURE OF SYSTEM

CASE1 CASE2 CASE3

0.000E+00 0.000E+00 0.000E+00

CUMULATIVE PROBABILITY OF FAILURE OF SYSTEM

CASE1 CASE2 CASE3

0.133E-05 0.400E-05 0.399E-05

Year	joint	Pf	Cov	CPf	a	sa	Brittle failures	Plastic failures	Sample left	Cracks Repaired
9	1	0.000E+00	0.000E+00	0.400E-05	1.0505	0.2253	0	0	249999	5198
9	2	0.000E+00	0.000E+00	0.160E-04	1.1339	0.2659	0	0	250000	5618
9	3	0.000E+00	0.000E+00	0.356E-03	1.1206	0.2583	0	0	250000	5668

PROBABILITY OF FAILURE OF SYSTEM

CASE1 CASE2 CASE3

0.000E+00 0.000E+00 0.000E+00

CUMULATIVE PROBABILITY OF FAILURE OF SYSTEM

CASE1 CASE2 CASE3

0.133E-05 0.400E-05 0.399E-05

Year	joint	Pf	Cov	CPf	a	sa	Brittle failures	Plastic failures	Sample left	Cracks Repaired
10	1	0.000E+00	0.000E+00	0.400E-05	1.1126	0.2301	0	0	249999	0
10	2	0.000E+00	0.000E+00	0.160E-04	1.2082	0.2810	0	0	250000	0
10	3	0.000E+00	0.000E+00	0.356E-03	1.1945	0.2718	0	0	250000	0

PROBABILITY OF FAILURE OF SYSTEM

CASE1 CASE2 CASE3

0.000E+00 0.000E+00 0.000E+00

CUMULATIVE PROBABILITY OF FAILURE OF SYSTEM

CASE1 CASE2 CASE3

0.133E-05 0.400E-05 0.399E-05

Year	joint	Pf	Cov	CPf	a	sa	Brittle failures	Plastic failures	Sample left	Cracks Repaired
11	1	0.000E+00	0.000E+00	0.400E-05	1.1680	0.2396	0	0	249999	0
11	2	0.000E+00	0.000E+00	0.160E-04	1.2700	0.3023	0	0	250000	0
11	3	0.000E+00	0.000E+00	0.356E-03	1.2529	0.2911	0	0	250000	0

PROBABILITY OF FAILURE OF SYSTEM

CASE1 CASE2 CASE3

0.000E+00 0.000E+00 0.000E+00

CUMULATIVE PROBABILITY OF FAILURE OF SYSTEM

CASE1 CASE2 CASE3

0.133E-05 0.400E-05 0.399E-05

Year	joint	Pf	Cov	CPf	a	sa	Brittle failures	Plastic failures	Sample left	Cracks Repaired
12	1	0.000E+00	0.000E+00	0.400E-05	1.2072	0.2844	0	0	249999	6003
12	2	0.000E+00	0.000E+00	0.160E-04	1.3194	0.3636	0	0	250000	6689
12	3	0.000E+00	0.000E+00	0.356E-03	1.3018	0.3522	0	0	250000	6771

PROBABILITY OF FAILURE OF SYSTEM

CASE1 CASE2 CASE3

0.000E+00 0.000E+00 0.000E+00

CUMULATIVE PROBABILITY OF FAILURE OF SYSTEM

CASE1 CASE2 CASE3

0.133E-05 0.400E-05 0.399E-05

Year	joint	Pf	Cov	CPf	a	sa	Brittle failures	Plastic failures	Sample left	Cracks Repaired
13	1	0.000E+00	0.000E+00	0.400E-05	1.2676	0.2983	0	0	249999	0
13	2	0.000E+00	0.000E+00	0.160E-04	1.3980	0.3940	0	0	250000	0
13	3	0.000E+00	0.000E+00	0.356E-03	1.3793	0.3915	0	0	250000	0

PROBABILITY OF FAILURE OF SYSTEM

CASE1 CASE2 CASE3

0.000E+00 0.000E+00 0.000E+00

CUMULATIVE PROBABILITY OF FAILURE OF SYSTEM

CASE1 CASE2 CASE3

0.133E-05 0.400E-05 0.399E-05

Year	joint	Pf	Cov	CPf	a	sa	Brittle failures	Plastic failures	Sample left	Cracks Repaired
14	1	0.000E+00	0.000E+00	0.400E-05	1.3243	0.3172	0	0	249999	0
14	2	0.000E+00	0.000E+00	0.160E-04	1.4669	0.4309	0	0	250000	0
14	3	0.000E+00	0.000E+00	0.356E-03	1.4446	0.4881	0	0	250000	0

PROBABILITY OF FAILURE OF SYSTEM

CASE1 CASE2 CASE3

0.000E+00 0.000E+00 0.000E+00

CUMULATIVE PROBABILITY OF FAILURE OF SYSTEM

CASE1 CASE2 CASE3

0.133E-05 0.400E-05 0.399E-05

Year	joint	Pf	Cov	CPf	a	sa	Brittle failures	Plastic failures	Sample left	Cracks Repaired
15	1	0.000E+00	0.000E+00	0.400E-05	1.3591	0.3752	0	0	249999	6718
15	2	0.000E+00	0.000E+00	0.160E-04	1.5137	0.5112	0	0	250000	7630
15	3	0.000E+00	0.000E+00	0.356E-03	1.4917	0.4915	0	0	250000	7398

PROBABILITY OF FAILURE OF SYSTEM

CASE1 CASE2 CASE3

0.000E+00 0.000E+00 0.000E+00

CUMULATIVE PROBABILITY OF FAILURE OF SYSTEM

CASE1 CASE2 CASE3

0.133E-05 0.400E-05 0.399E-05

Year	joint	Pf	Cov	CPf	a	sa	Brittle failures	Plastic failures	Sample left	Cracks Repaired
16	1	0.000E+00	0.000E+00	0.400E-05	1.4241	0.3988	0	0	249999	0
16	2	0.000E+00	0.000E+00	0.160E-04	1.6034	0.5676	0	0	250000	0

16	3	0.000E+00	0.000E+00	0.356E-03	1.5798	0.5534	0	0	250000	0

PROBABILITY OF FAILURE OF SYSTEM

CASE1 CASE2 CASE3

0.000E+00 0.000E+00 0.000E+00

CUMULATIVE PROBABILITY OF FAILURE OF SYSTEM

CASE1 CASE2 CASE3

0.133E-05 0.400E-05 0.399E-05

Year	joint	Pf	Cov	CPf	a	sa	Brittle failures	Plastic failures	Sample left	Cracks Repaired
17	1	0.000E+00	0.000E+00	0.400E-05	1.4870	0.4274	0	0	249999	0
17	2	0.000E+00	0.000E+00	0.160E-04	1.6850	0.6414	0	0	250000	0
17	3	0.000E+00	0.000E+00	0.356E-03	1.6567	0.6311	0	0	250000	0

PROBABILITY OF FAILURE OF SYSTEM

CASE1 CASE2 CASE3

0.000E+00 0.000E+00 0.000E+00

CUMULATIVE PROBABILITY OF FAILURE OF SYSTEM

CASE1 CASE2 CASE3

0.133E-05 0.400E-05 0.399E-05

Year	joint	Pf	Cov	CPf	a	sa	Brittle failures	Plastic failures	Sample left	Cracks Repaired
18	1	0.000E+00	0.000E+00	0.400E-05	1.5177	0.4990	0	0	249999	7736
18	2	0.000E+00	0.000E+00	0.160E-04	1.7278	0.7342	0	0	250000	8807
18	3	0.000E+00	0.000E+00	0.356E-03	1.6989	0.7182	0	0	250000	8723

PROBABILITY OF FAILURE OF SYSTEM

CASE1 CASE2 CASE3

0.000E+00 0.000E+00 0.000E+00

CUMULATIVE PROBABILITY OF FAILURE OF SYSTEM

CASE1 CASE2 CASE3

0.133E-05 0.400E-05 0.399E-05

Year	joint	Pf	Cov	CPf	a	sa	Brittle failures	Plastic failures	Sample left	Cracks Repaired

19	1	0.000E+00	0.000E+00	0.400E-05	1.5907	0.5416	0	0	249999	0
19	2	0.000E+00	0.000E+00	0.160E-04	1.8333	0.8636	0	0	250000	0
19	3	0.000E+00	0.000E+00	0.356E-03	1.8025	0.8835	0	0	250000	0

PROBABILITY OF FAILURE OF SYSTEM

CASE1	CASE2	CASE3
0.000E+00	0.000E+00	0.000E+00

CUMULATIVE PROBABILITY OF FAILURE OF SYSTEM

CASE1	CASE2	CASE3
0.133E-05	0.400E-05	0.399E-05

Year	joint	Pf	Cov	CPf	a	sa	Brittle failures	Plastic failures	Sample left	Cracks Repaired
20	1	0.000E+00	0.000E+00	0.400E-05	1.6619	0.6043	0	0	249999	0
20	2	0.000E+00	0.000E+00	0.160E-04	1.9334	1.2326	0	0	250000	0
20	3	0.000E+00	0.100E+01	0.356E-03	1.9056	4.7790	0	0	250000	0

PROBABILITY OF FAILURE OF SYSTEM

CASE1	CASE2	CASE3
0.000E+00	0.000E+00	0.000E+00

CUMULATIVE PROBABILITY OF FAILURE OF SYSTEM

CASE1	CASE2	CASE3
0.133E-05	0.400E-05	0.399E-05

Year	joint	Pf	Cov	CPf	a	sa	Brittle failures	Plastic failures	Sample left	Cracks Repaired
21	1	0.000E+00	0.000E+00	0.400E-05	1.6877	0.6575	0	0	249999	8562
21	2	0.400E-05	0.100E+01	0.200E-04	1.9657	1.1821	1	0	249999	10069
21	3	0.400E-05	0.100E+01	0.360E-03	1.9316	1.0502	1	0	249999	9674

PROBABILITY OF FAILURE OF SYSTEM

CASE1	CASE2	CASE3
0.267E-05	0.800E-05	0.799E-05

CUMULATIVE PROBABILITY OF FAILURE OF SYSTEM

CASE1	CASE2	CASE3
0.400E-05	0.120E-04	0.120E-04

Year	joint	Pf	Cov	CPf	a	sa	Brittle failures	Plastic failures	Sample left	Cracks Repaired
22	1	0.000E+00	0.000E+00	0.400E-05	1.7698	0.7111	0	0	249999	0
22	2	0.000E+00	0.000E+00	0.200E-04	2.0978	2.9635	0	0	249999	0
22	3	0.000E+00	0.000E+00	0.360E-03	2.0564	1.3857	0	0	249999	0

PROBABILITY OF FAILURE OF SYSTEM

CASE1	CASE2	CASE3
0.000E+00	0.000E+00	0.000E+00

CUMULATIVE PROBABILITY OF FAILURE OF SYSTEM

CASE1	CASE2	CASE3
0.400E-05	0.120E-04	0.120E-04

Year	joint	Pf	Cov	CPf	a	sa	Brittle failures	Plastic failures	Sample left	Cracks Repaired
23	1	0.000E+00	0.000E+00	0.400E-05	1.8514	0.7994	0	0	249999	0
23	2	0.000E+00	0.000E+00	0.200E-04	2.2491	9.9916	0	0	249999	0
23	3	0.000E+00	0.100E+01	0.360E-03	2.1762	1.9940	0	0	249999	0

PROBABILITY OF FAILURE OF SYSTEM

CASE1	CASE2	CASE3
0.000E+00	0.000E+00	0.000E+00

CUMULATIVE PROBABILITY OF FAILURE OF SYSTEM

CASE1	CASE2	CASE3
0.400E-05	0.120E-04	0.120E-04

Year	joint	Pf	Cov	CPf	a	sa	Brittle failures	Plastic failures	Sample left	Cracks Repaired
24	1	0.000E+00	0.000E+00	0.400E-05	1.8701	0.8672	0	0	249999	9529
24	2	0.000E+00	0.000E+00	0.200E-04	2.2287	1.7442	0	0	249999	11414
24	3	0.000E+00	0.100E+01	0.360E-03	2.1841	1.5732	0	0	249999	11124

PROBABILITY OF FAILURE OF SYSTEM

CASE1	CASE2	CASE3
0.000E+00	0.000E+00	0.000E+00

CUMULATIVE PROBABILITY OF FAILURE OF SYSTEM

CASE1 CASE2 CASE3

0.400E-05 0.120E-04 0.120E-04

Year	joint	Pf	Cov	CPf	a	sa	Brittle failures	Plastic failures	Sample left	Cracks Repaired
25	1	0.000E+00	0.000E+00	0.400E-05	1.9636	0.9908	0	0	249999	0
25	2	0.800E-05	0.707E+00	0.280E-04	2.3923	3.1993	2	0	249997	0
25	3	0.400E-05	0.100E+01	0.364E-03	2.3533	9.0741	1	0	249998	0

PROBABILITY OF FAILURE OF SYSTEM

CASE1 CASE2 CASE3

0.400E-05 0.120E-04 0.120E-04

CUMULATIVE PROBABILITY OF FAILURE OF SYSTEM

CASE1 CASE2 CASE3

0.800E-05 0.240E-04 0.240E-04

Year	joint	Pf	Cov	CPf	a	sa	Brittle failures	Plastic failures	Sample left	Cracks Repaired
26	1	0.400E-05	0.100E+01	0.800E-05	2.0576	1.1624	1	0	249998	0
26	2	0.200E-04	0.447E+00	0.480E-04	2.6547	21.5006	5	0	249992	0
26	3	0.800E-05	0.707E+00	0.372E-03	2.5568	23.2543	2	0	249996	0

PROBABILITY OF FAILURE OF SYSTEM

CASE1 CASE2 CASE3

0.107E-04 0.320E-04 0.320E-04

CUMULATIVE PROBABILITY OF FAILURE OF SYSTEM

CASE1 CASE2 CASE3

0.187E-04 0.560E-04 0.560E-04

Year	joint	Pf	Cov	CPf	a	sa	Brittle failures	Plastic failures	Sample left	Cracks Repaired
27	1	0.000E+00	0.000E+00	0.800E-05	2.0643	1.1832	0	0	249998	10484
27	2	0.000E+00	0.000E+00	0.480E-04	2.5026	2.3788	0	0	249992	12935
27	3	0.400E-05	0.100E+01	0.376E-03	2.4555	2.1181	1	0	249995	12507

PROBABILITY OF FAILURE OF SYSTEM

CASE1 CASE2 CASE3

0.133E-05 0.400E-05 0.399E-05

CUMULATIVE PROBABILITY OF FAILURE OF SYSTEM

CASE1 CASE2 CASE3

0.200E-04 0.600E-04 0.600E-04

Year	joint	Pf	Cov	CPf	a	sa	Brittle failures	Plastic failures	Sample left	Cracks Repaired
28	1	0.000E+00	0.000E+00	0.800E-05	2.1721	1.4109	0	0	249998	0
28	2	0.000E+00	0.000E+00	0.480E-04	2.7162	6.8559	0	0	249992	0
28	3	0.000E+00	0.100E+01	0.376E-03	2.6496	3.4560	0	0	249995	0

PROBABILITY OF FAILURE OF SYSTEM

CASE1 CASE2 CASE3

0.000E+00 0.000E+00 0.000E+00

CUMULATIVE PROBABILITY OF FAILURE OF SYSTEM

CASE1 CASE2 CASE3

0.200E-04 0.600E-04 0.600E-04

Year	joint	Pf	Cov	CPf	a	sa	Brittle failures	Plastic failures	Sample left	Cracks Repaired
29	1	0.400E-05	0.100E+01	0.120E-04	2.2846	1.8067	1	0	249997	0
29	2	0.200E-04	0.447E+00	0.680E-04	3.0741	31.8201	5	0	249987	0
29	3	0.120E-04	0.577E+00	0.388E-03	2.9225	15.4514	3	0	249992	0

PROBABILITY OF FAILURE OF SYSTEM

CASE1 CASE2 CASE3

0.120E-04 0.360E-04 0.360E-04

CUMULATIVE PROBABILITY OF FAILURE OF SYSTEM

CASE1 CASE2 CASE3

0.320E-04 0.960E-04 0.960E-04

Year	joint	Pf	Cov	CPf	a	sa	Brittle failures	Plastic failures	Sample left	Cracks Repaired
30	1	0.000E+00	0.000E+00	0.120E-04	2.2683	1.6928	0	0	249997	11751
30	2	0.000E+00	0.000E+00	0.680E-04	2.8053	3.2349	0	0	249987	14298
30	3	0.400E-05	0.100E+01	0.392E-03	2.7546	3.1609	1	0	249991	14234

PROBABILITY OF FAILURE OF SYSTEM

CASE1 CASE2 CASE3

0.133E-05 0.400E-05 0.399E-05

CUMULATIVE PROBABILITY OF FAILURE OF SYSTEM

CASE1	CASE2	CASE3
0.333E-04	0.100E-03	0.100E-03

Year	joint	Pf	Cov	CPf	a	sa	Brittle failures	Plastic failures	Sample left	Cracks Repaired
31	1	0.000E+00	0.000E+00	0.120E-04	2.3971	2.2282	0	0	249997	0
31	2	0.000E+00	0.100E+01	0.680E-04	3.0793	6.7628	0	0	249987	0
31	3	0.400E-05	0.100E+01	0.396E-03	3.0125	5.1604	1	0	249990	0

PROBABILITY OF FAILURE OF SYSTEM

CASE1	CASE2	CASE3
0.133E-05	0.400E-05	0.399E-05

CUMULATIVE PROBABILITY OF FAILURE OF SYSTEM

CASE1	CASE2	CASE3
0.347E-04	0.104E-03	0.104E-03

Year	joint	Pf	Cov	CPf	a	sa	Brittle failures	Plastic failures	Sample left	Cracks Repaired
32	1	0.400E-05	0.100E+01	0.160E-04	2.5437	3.9963	1	0	249996	0
32	2	0.440E-04	0.302E+00	0.112E-03	3.6649	42.6760	11	0	249976	0
32	3	0.120E-04	0.577E+00	0.408E-03	3.4644	28.6863	3	0	249987	0

PROBABILITY OF FAILURE OF SYSTEM

CASE1	CASE2	CASE3
0.200E-04	0.600E-04	0.600E-04

CUMULATIVE PROBABILITY OF FAILURE OF SYSTEM

CASE1	CASE2	CASE3
0.547E-04	0.164E-03	0.164E-03

Year	joint	Pf	Cov	CPf	a	sa	Brittle failures	Plastic failures	Sample left	Cracks Repaired
33	1	0.400E-05	0.100E+01	0.200E-04	2.4792	2.2967	1	0	249995	12730
33	2	0.000E+00	0.000E+00	0.112E-03	3.1005	4.2914	0	0	249976	16004
33	3	0.000E+00	0.000E+00	0.408E-03	3.0270	3.9994	0	0	249987	15812

PROBABILITY OF FAILURE OF SYSTEM

CASE1	CASE2	CASE3

0.133E-05 0.400E-05 0.399E-05

CUMULATIVE PROBABILITY OF FAILURE OF SYSTEM

CASE1 CASE2 CASE3

0.560E-04 0.168E-03 0.168E-03

Year	joint	Pf	Cov	CPf	a	sa	Brittle failures	Plastic failures	Sample left	Cracks Repaired
34	1	0.000E+00	0.000E+00	0.200E-04	2.6358	3.4809	0	0	249995	0
34	2	0.160E-04	0.500E+00	0.128E-03	3.4462	8.9852	4	0	249972	0
34	3	0.800E-05	0.707E+00	0.416E-03	3.3384	6.2631	2	0	249985	0

PROBABILITY OF FAILURE OF SYSTEM

CASE1 CASE2 CASE3

0.800E-05 0.240E-04 0.240E-04

CUMULATIVE PROBABILITY OF FAILURE OF SYSTEM

CASE1 CASE2 CASE3

0.640E-04 0.192E-03 0.192E-03

Year	joint	Pf	Cov	CPf	a	sa	Brittle failures	Plastic failures	Sample left	Cracks Repaired
35	1	0.160E-04	0.500E+00	0.360E-04	2.8441	15.1149	4	0	249991	0
35	2	0.640E-04	0.250E+00	0.192E-03	4.1125	35.6491	16	0	249956	0
35	3	0.160E-04	0.500E+00	0.432E-03	3.8854	28.8120	4	0	249981	0

PROBABILITY OF FAILURE OF SYSTEM

CASE1 CASE2 CASE3

0.320E-04 0.960E-04 0.960E-04

CUMULATIVE PROBABILITY OF FAILURE OF SYSTEM

CASE1 CASE2 CASE3

0.960E-04 0.288E-03 0.288E-03

Year	joint	Pf	Cov	CPf	a	sa	Brittle failures	Plastic failures	Sample left	Cracks Repaired
36	1	0.800E-05	0.707E+00	0.440E-04	2.6851	2.8837	2	0	249989	13844
36	2	0.000E+00	0.000E+00	0.192E-03	3.3766	5.2182	0	0	249956	17472
36	3	0.000E+00	0.577E+00	0.432E-03	3.2969	5.2092	0	0	249981	17086

PROBABILITY OF FAILURE OF SYSTEM

CASE1 CASE2 CASE3

0.267E-05 0.800E-05 0.799E-05

CUMULATIVE PROBABILITY OF FAILURE OF SYSTEM

CASE1 CASE2 CASE3

0.987E-04 0.296E-03 0.296E-03

Year	joint	Pf	Cov	CPf	a	sa	Brittle failures	Plastic failures	Sample left	Cracks Repaired
37	1	0.400E-05	0.100E+01	0.480E-04	2.8688	4.1290	1	0	249988	0
37	2	0.400E-05	0.100E+01	0.196E-03	3.7932	9.3527	1	0	249955	0
37	3	0.400E-05	0.100E+01	0.436E-03	3.6849	8.9519	1	0	249980	0

PROBABILITY OF FAILURE OF SYSTEM

CASE1 CASE2 CASE3

0.400E-05 0.120E-04 0.120E-04

CUMULATIVE PROBABILITY OF FAILURE OF SYSTEM

CASE1 CASE2 CASE3

0.103E-03 0.308E-03 0.308E-03

Year	joint	Pf	Cov	CPf	a	sa	Brittle failures	Plastic failures	Sample left	Cracks Repaired
38	1	0.800E-05	0.707E+00	0.560E-04	3.0905	6.8399	2	0	249986	0
38	2	0.440E-04	0.302E+00	0.240E-03	4.5265	34.9754	11	0	249944	0
38	3	0.200E-04	0.447E+00	0.456E-03	4.4124	35.5877	5	0	249975	0

PROBABILITY OF FAILURE OF SYSTEM

CASE1 CASE2 CASE3

0.240E-04 0.720E-04 0.720E-04

CUMULATIVE PROBABILITY OF FAILURE OF SYSTEM

CASE1 CASE2 CASE3

0.127E-03 0.380E-03 0.380E-03

Year	joint	Pf	Cov	CPf	a	sa	Brittle failures	Plastic failures	Sample left	Cracks Repaired
39	1	0.000E+00	0.000E+00	0.560E-04	2.8829	3.5220	0	0	249986	14658
39	2	0.800E-05	0.707E+00	0.248E-03	3.6346	6.4307	2	0	249942	18589
39	3	0.000E+00	0.707E+00	0.456E-03	3.5353	6.0811	0	0	249975	18411

PROBABILITY OF FAILURE OF SYSTEM

CASE1 CASE2 CASE3

0.267E-05 0.800E-05 0.799E-05

CUMULATIVE PROBABILITY OF FAILURE OF SYSTEM

CASE1 CASE2 CASE3

0.129E-03 0.388E-03 0.388E-03

Year	joint	Pf	Cov	CPf	a	sa	Brittle failures	Plastic failures	Sample left	Cracks Repaired
40	1	0.280E-04	0.378E+00	0.840E-04	3.1017	5.4998	7	0	249979	0
40	2	0.400E-05	0.100E+01	0.252E-03	4.1328	10.9124	1	0	249941	0
40	3	0.400E-05	0.100E+01	0.460E-03	4.0040	11.2689	1	0	249974	0

PROBABILITY OF FAILURE OF SYSTEM

CASE1 CASE2 CASE3

0.120E-04 0.360E-04 0.360E-04

CUMULATIVE PROBABILITY OF FAILURE OF SYSTEM

CASE1 CASE2 CASE3

0.141E-03 0.424E-03 0.424E-03

Program finished at :
DAY / MONTH / YEAR
18 6 2001
HOUR:MIMUTE:SECOND
3 38 7

APPENDIX D

FLOWCHART OF THE CODE

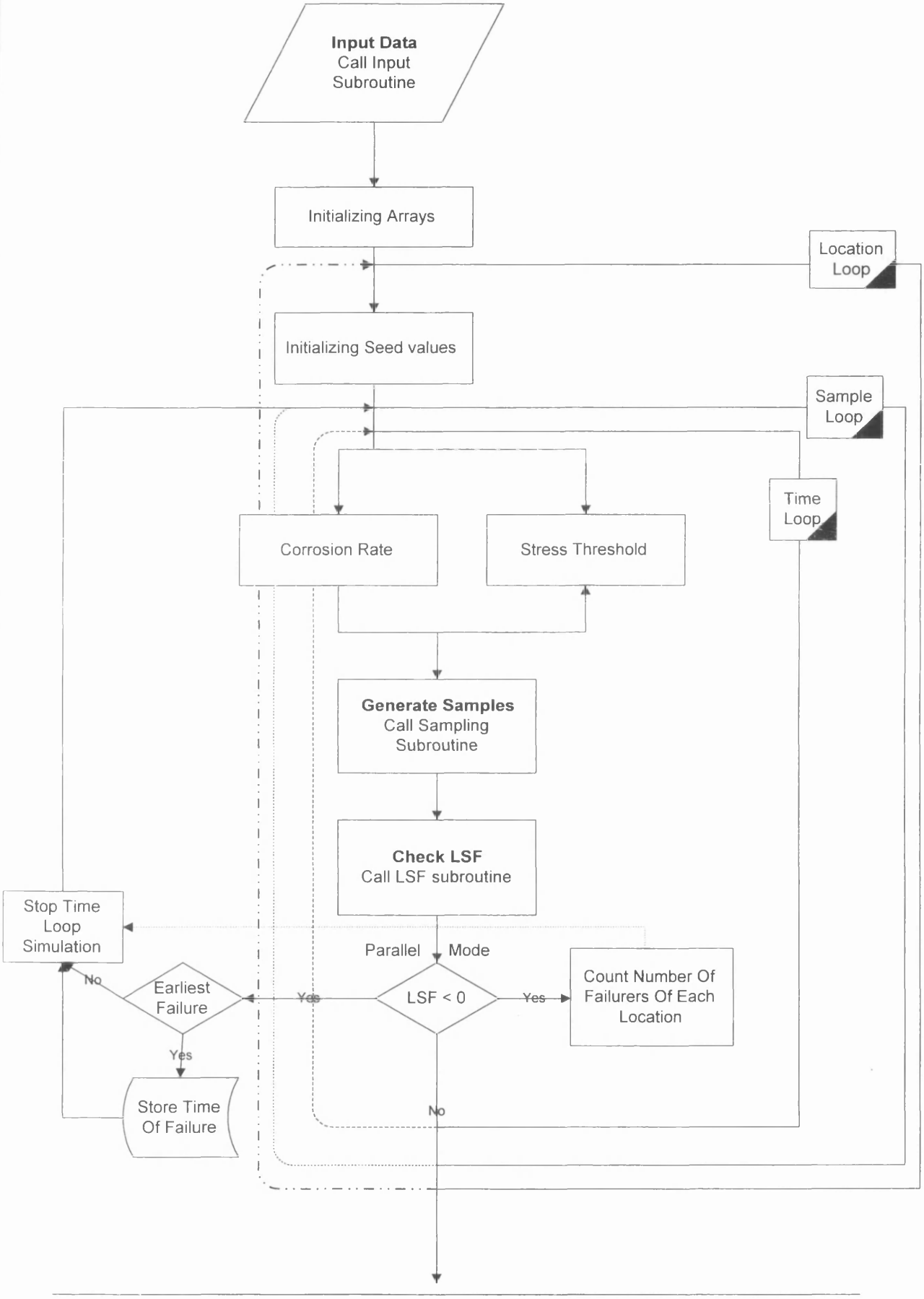
Input Data
Call Input Subroutine
Initializing Arrays
Location Loop
Initializing Seed values
Sample Loop
Time Loop
Corrosion Rate
Stress Threshold
Generate Samples
Call Sampling Subroutine
Check LSF
Call LSF subroutine
Stop Time Loop Simulation
Parallel
Mode
No
Earliest Failure
Yes
LSF < 0
Yes
Count Number Of Failurers Of Each Location
Yes
Store Time Of Failure
No

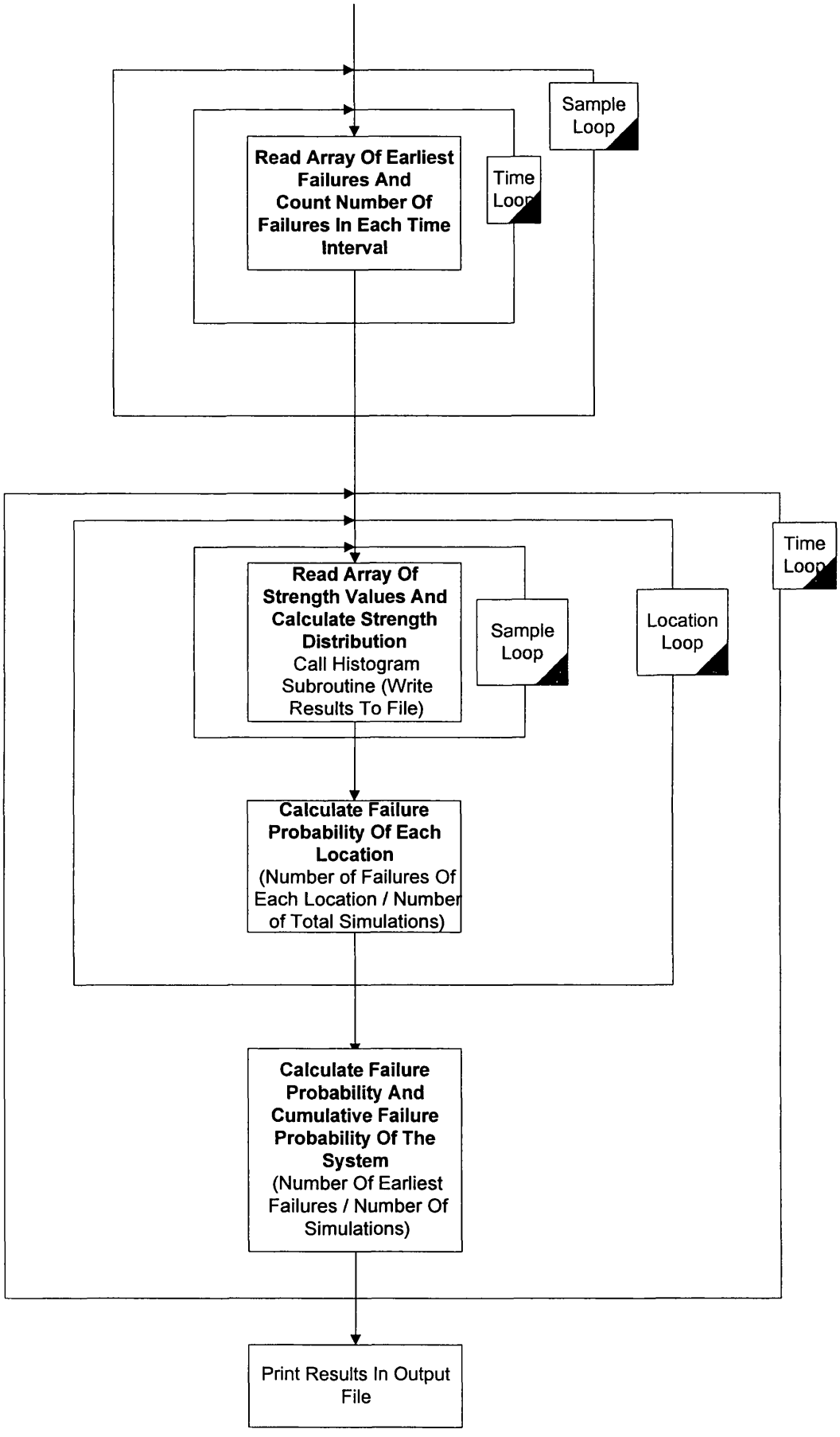
Sample Loop
Read Array Of Earliest Failures And Count Number Of Failures In Each Time Interval
Time Loop
Time Loop
Read Array Of Strength Values And Calculate Strength Distribution
Call Histogram Subroutine (Write Results To File)
Sample Loop
Location Loop
Calculate Failure Probability Of Each Location
(Number of Failures Of Each Location / Number of Total Simulations)
Calculate Failure Probability And Cumulative Failure Probability Of The System
(Number Of Earliest Failures / Number Of Simulations)
Print Results In Output File

SUBROUTINES

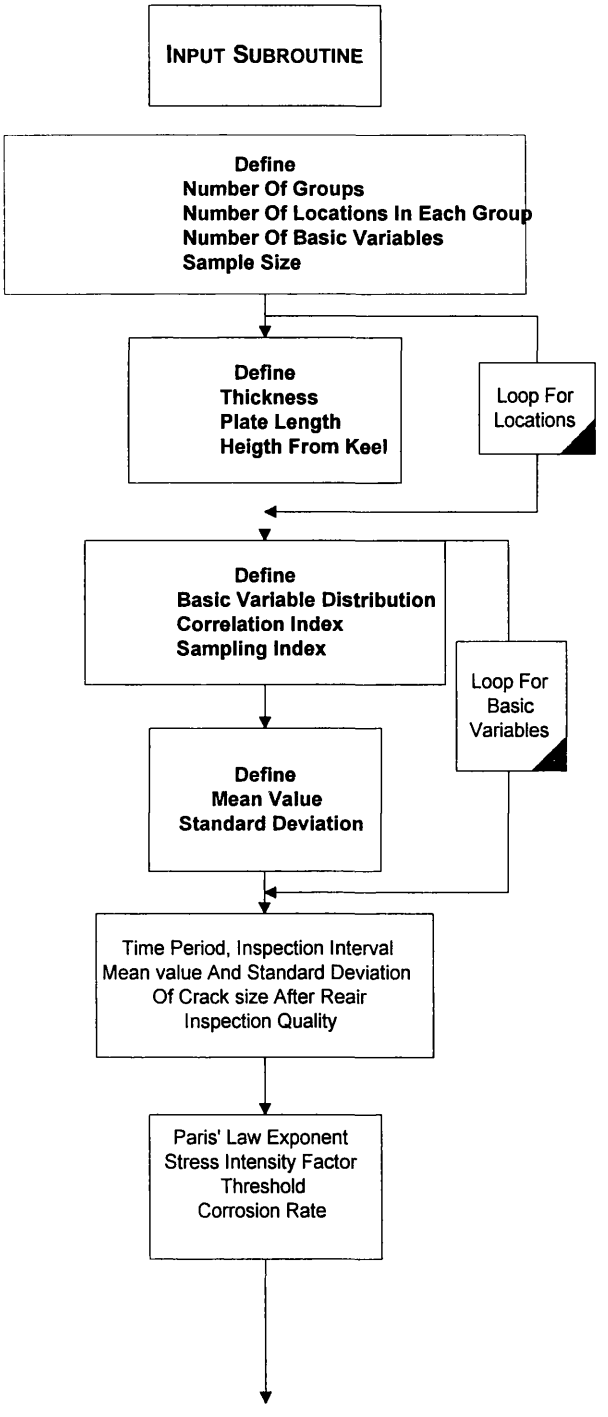

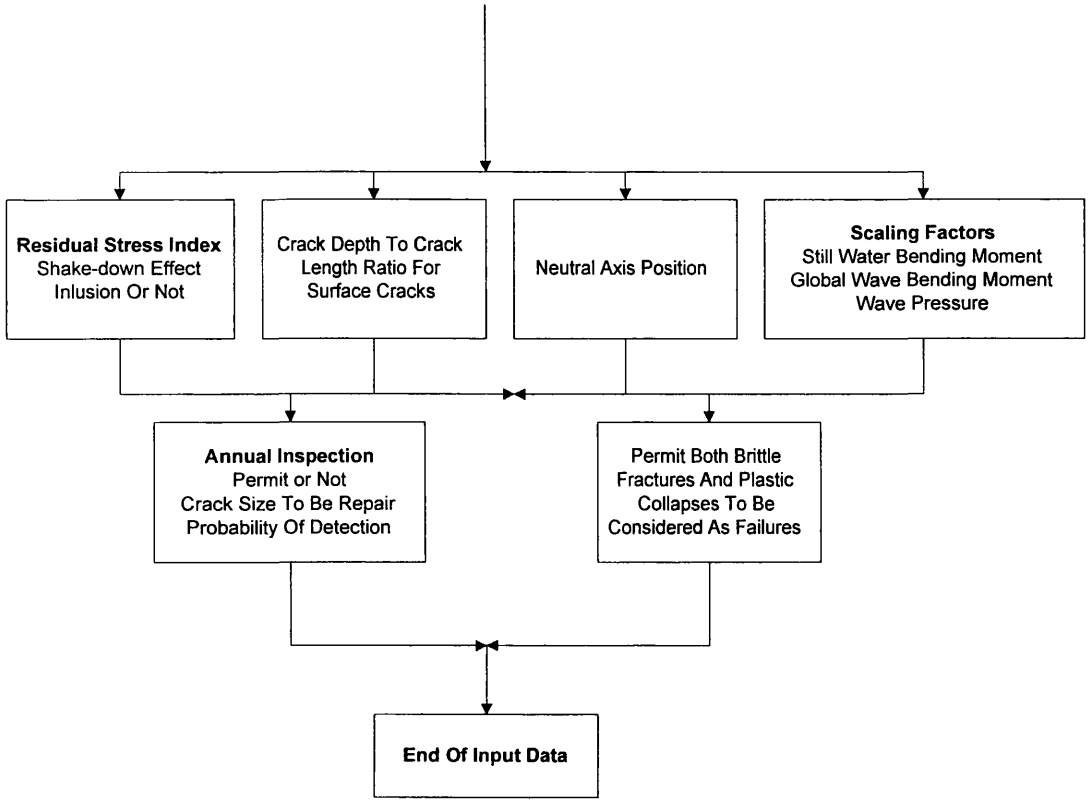
Residual Stress Index
Shake-down Effect
Inlusion Or Not
Crack Depth To Crack Length Ratio For Surface Cracks
Neutral Axis Position
Scaling Factors
Still Water Bending Moment
Global Wave Bending Moment
Wave Pressure
Annual Inspection
Permit or Not
Crack Size To Be Repair
Probability Of Detection
Permit Both Brittle Fractures And Plastic Collapses To Be Considered As Failures
End Of Input Data

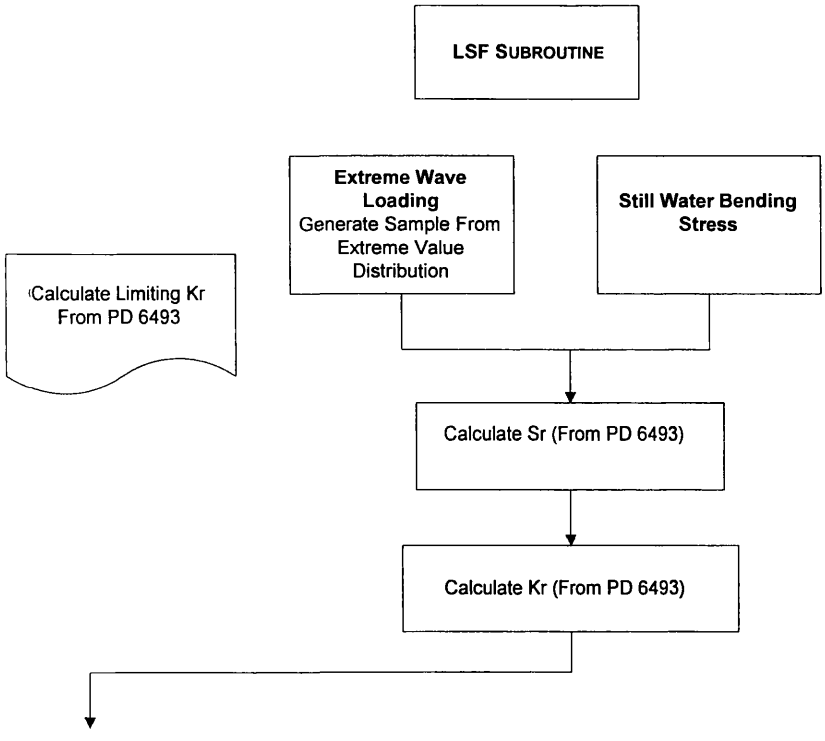
LSF SUBROUTINE
Extreme Wave Loading
Generate Sample From Extreme Value Distribution
Still Water Bending Stress
Calculate Limiting Kr From PD 6493
Calculate Sr (From PD 6493)
Calculate Kr (From PD 6493)

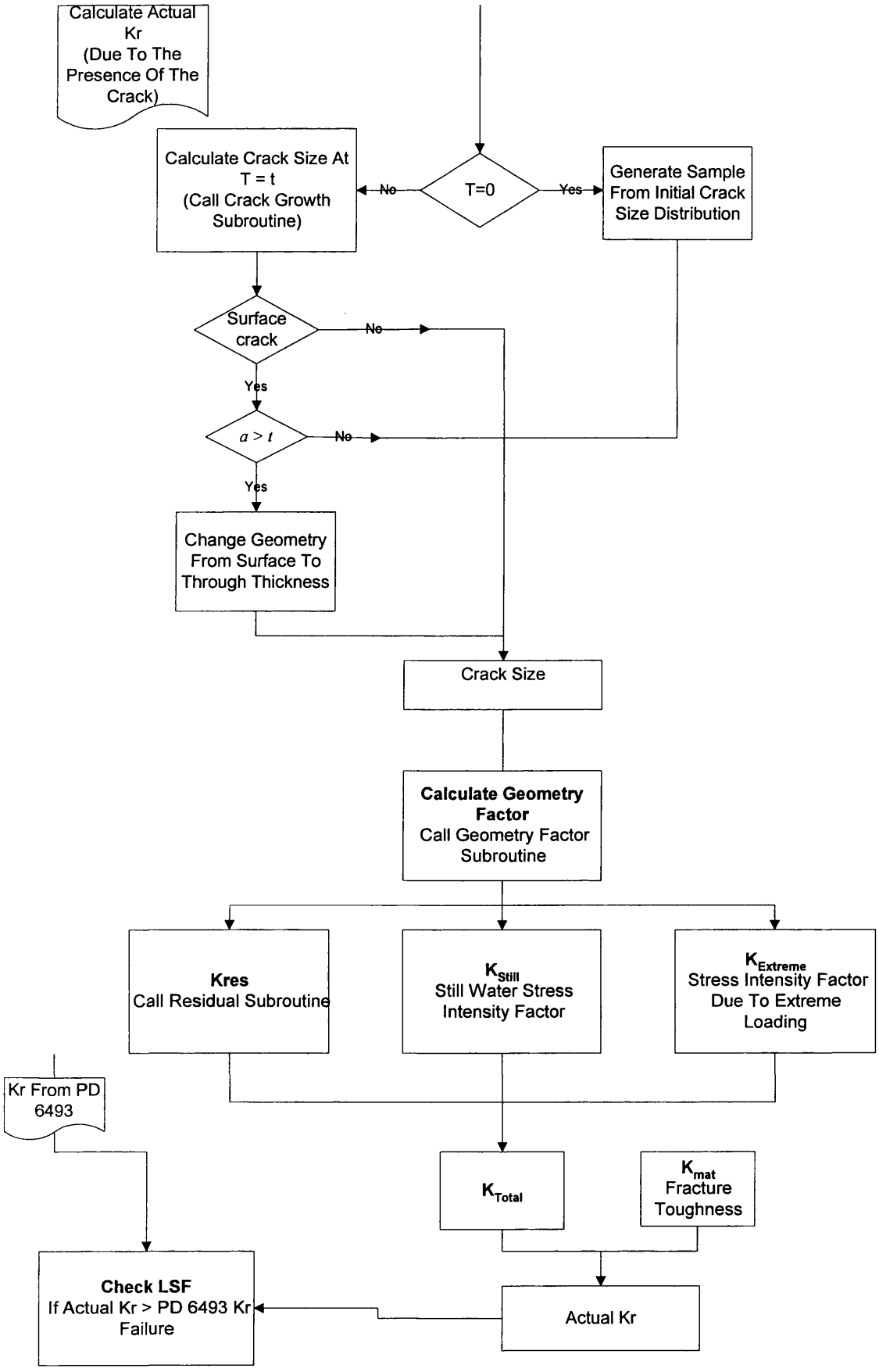
Calculate Actual Kr (Due To The Presence Of The Crack)
Calculate Crack Size At T = t (Call Crack Growth Subroutine)
No
T=0
Yes
Generate Sample From Initial Crack Size Distribution
Surface crack
No
Yes
a > t
No
Yes
Change Geometry From Surface To Through Thickness
Crack Size
Calculate Geometry Factor
Call Geometry Factor Subroutine
Kres
Call Residual Subroutine
K Still
Still Water Stress Intensity Factor
K Extreme
Stress Intensity Factor Due To Extreme Loading
Kr From PD 6493
K Total
K mat
Fracture Toughness
Check LSF
If Actual Kr > PD 6493 Kr
Failure
Actual Kr

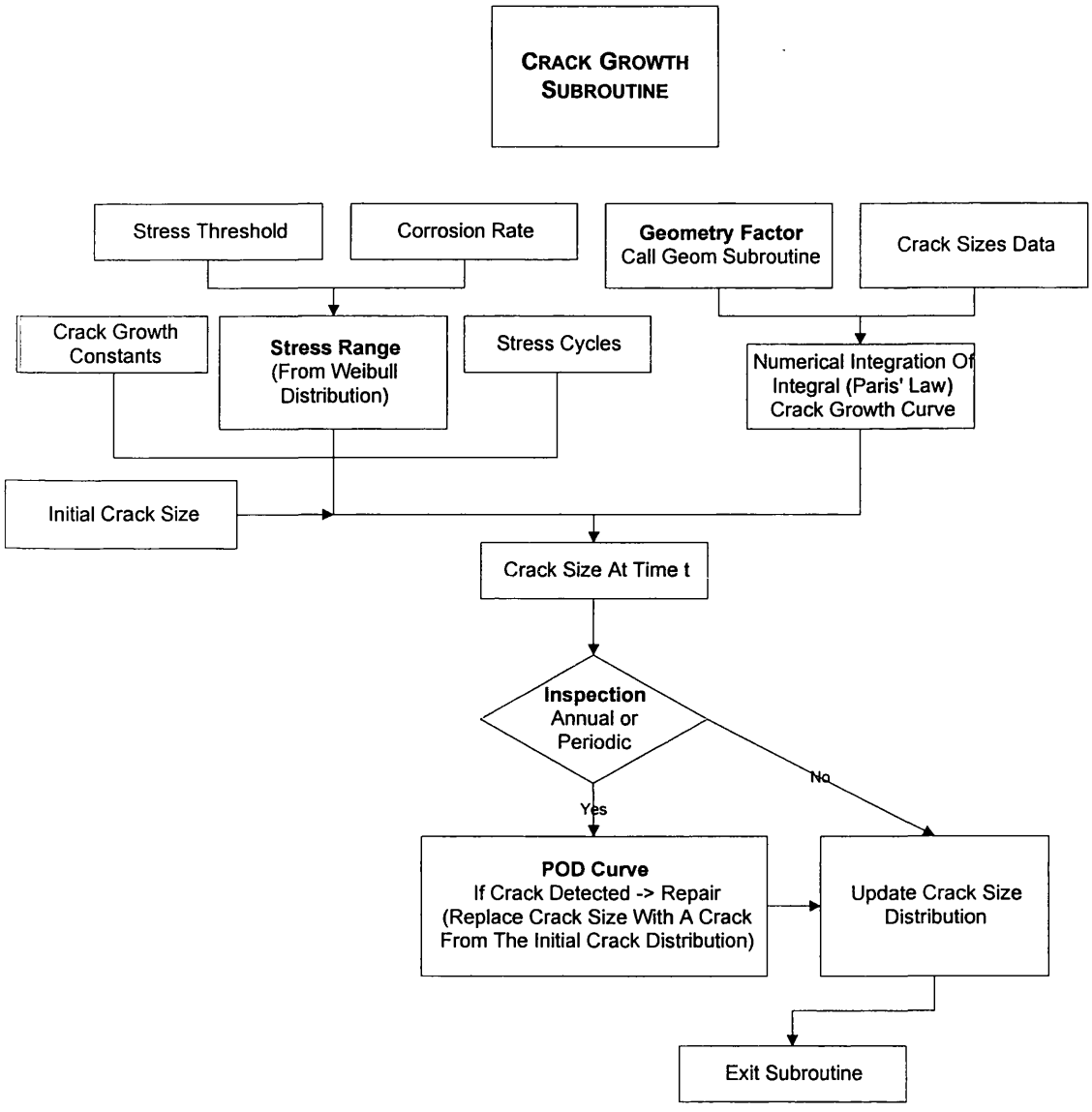
CRACK GROWTH SUBROUTINE
Stress Threshold
Corrosion Rate
Geometry Factor
Call Geom Subroutine
Crack Sizes Data
Crack Growth Constants
Stress Range
(From Weibull Distribution)
Stress Cycles
Numerical Integration Of Integral (Paris' Law) Crack Growth Curve
Initial Crack Size
Crack Size At Time t
Inspection
Annual or Periodic
No
Yes
POD Curve
If Crack Detected -> Repair
(Replace Crack Size With A Crack From The Initial Crack Distribution)
Update Crack Size Distribution
Exit Subroutine

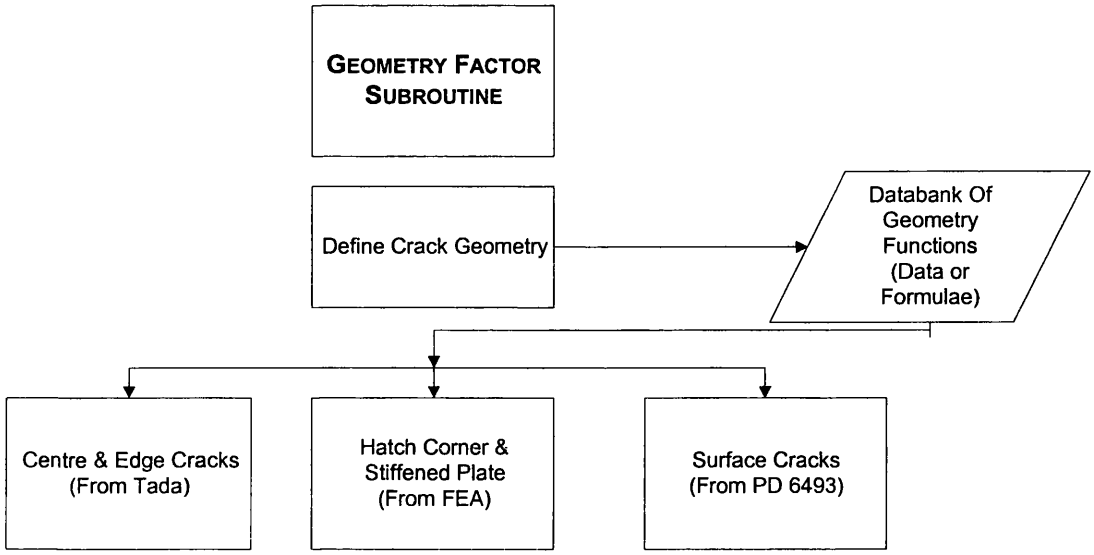
GEOMETRY FACTOR SUBROUTINE
Define Crack Geometry
Databank Of Geometry Functions (Data or Formulae)
Centre & Edge Cracks (From Tada)
Hatch Corner & Stiffened Plate (From FEA)
Surface Cracks (From PD 6493)

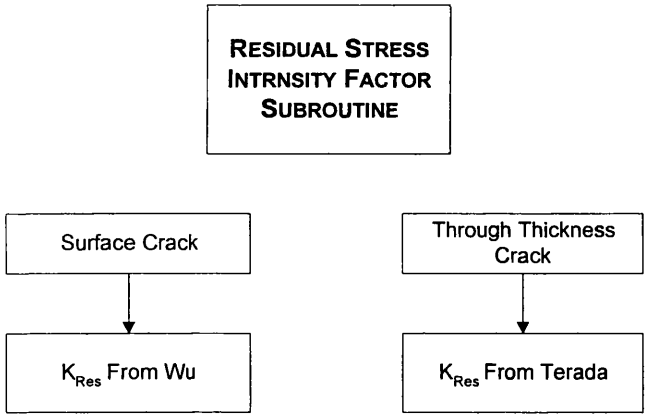
RESIDUAL STRESS INTRNSITY FACTOR SUBROUTINE
Surface Crack
Through Thickness Crack
K_{Res} From Wu
K_{Res} From Terada